Development of Bifunctional Degraders for Targeted Proteolysis of Histone Deacetylases

Dissertation

zur

Erlangung des Doktorgrades (Dr. rer. nat.)

der

Mathematisch-Naturwissenschaftlichen Fakultät

der

Rheinischen Friedrich-Wilhelms-Universität Bonn

vorgelegt von

Shiyang Zhai

aus

Shangrao, China

Bonn 2026

Angefertigt mit Genehmigung der Mathematisch-Naturwissenschaftlichen Fakultät

der Rheinischen Friedrich-Wilhelms-Universität Bonn

Gutachter und Betreuer: Prof. Dr. Finn K. Hansen

Gutachter: Prof. Dr. Michael Gütschow

Tag der Promotion: 18.03.2026

Erscheinungsjahr: 2026

Die vorliegende Arbeit wurde in der Zeit von Dezember 2021 bis Januar 2026 unter der Leitung von Herrn Prof. Dr. Finn K. Hansen am Pharmazeutischen Institut der Rheinischen Friedrich-Wilhelms-Universität Bonn angefertigt.

Table of Contents

List of Abbreviations ..... **VIII**

List of Appendices ..... **XI**

1 Introduction ..... **- 1 -**

1.1 Epigenetics and histone deacetylases ..... - 1 -

1.2 Classification, localization and the biological roles of HDACs ..... - 2 -

1.3 Zn^{2+}-dependent HDACs and cancer ..... - 4 -

1.3.1 Class I HDACs in cancer ..... - 5 -

1.3.2 Class IIa HDACs in cancer ..... - 5 -

1.3.3 Class IIb HDACs in cancer ..... - 6 -

1.3.4 Class IV HDACs in cancer ..... - 7 -

1.4 HDAC inhibitors in cancer therapy: progress and challenges ..... - 9 -

1.5 Targeted protein degradation: PROTACs and emerging strategies ..... - 11 -

1.5.1 Origins and evolution of PROTAC technology ..... - 11 -

1.5.2 Current landscape and therapeutic targets ..... - 13 -

1.5.3 E3 ligases utilized in PROTAC design and their ligands ..... - 14 -

1.5.4 Limitations and design challenges of PROTACs ..... - 16 -

1.5.5 Beyond PROTACs: alternative degradation technologies ..... - 17 -

1.6 HDAC PROTACs: a next-generation approach to HDAC modulation ..... - 19 -

1.6.1 Selective HDAC3 PROTACs ..... - 20 -

1.6.2 Selective HDAC4 PROTACs ..... - 20 -

1.6.3 Selective HDAC6 PROTACs ..... - 21 -

1.6.4 Selective HDAC7 PROTACs ..... - 23 -

1.6.5 Selective HDAC8 PROTACs ..... - 23 -

1.7 Scope of Thesis ..... - 25 -

2 Development and characterization of the first selective class IIb histone deacetylase degrade ..... **- 28 -**

2.1 Publication Summary ..... - 28 -

2.2 Author Contribution ..... - 31 -

3 Discovery of histone deacetylase 8 (HDAC8)-specific proteolysis-targeting chimeras with anti-cancer activity against hematological malignancies ..... **- 32 -**

3.1 Publication Summary ..... - 32 -

3.2 Author Contribution ..... - 34 -

4 Targeted histone deacetylase degradation via chemical induced proximity by direct recruitment of the CUL4 complex adaptor protein DDB1 ..... **- 35 -**

4.1 Publication Summary ..... - 35 -

4.2 Author Contribution ..... - 37 -

5 Summary ..... **- 38 -**

6 References ..... **- 43 -**

7 Appendix ..... **- 57 -**

List of Abbreviations

A	
AbTACs	Antibody-based PROTACs
AD	Alzheimer's disease
AhR	Arylhydrocarbon receptor
AR	Androgen receptor
B	
BCL-2	B-cell lymphoma 2
BCL-X_L	B-cell lymphoma-extra large
BCR-ABL	Breakpoint cluster region-abelson tyrosine kinase
BRD4	Bromodomain-containing protein 4
C	
CDK4/6	Cyclin-dependent kinase 4/6
C/EBPβ	CCAAT/enhancer-binding protein beta
c-Myc	Cellular myelocytomatosis proto-oncogene
CTCL	Cutaneous T-cell lymphoma
CUL4	Cullin 4
D	
DC_{50}	Half-maximal degradation concentration
DCAF11	DDB1 and CUL4 associated factor 11
DCAF16	DDB1 and CUL4 associated factor 16
DDB1	Damage-specific DNA binding protein 1
DFMO	Difluoromethyl-1,3,4-oxadiazole
DNA	Deoxyribonucleic acid
E	
EMT	Epithelial-mesenchymal transition
ER	Estrogen receptor
EZH2	Enhancer of zeste homolog 2
F	
FDA	U.S. Food and Drug Administration
FEM1B	Fem-1 homolog B
G	
GSPT1	G1 to S phase transition 1
H	
HA	Hydroxamic acid
HATs	Histone acetyltransferases
HD	Huntington's disease
HDAC(s)	Histone deacetylase(s)
HDACi	Histone deacetylase inhibitor
HSP90	Heat shock protein 90
I	
IL-10	Interleukin-10
IKZF1/3	Ikaros family zinc finger 1/3

IAPs	Inhibitor of apoptosis proteins
IC_{50}	Half-maximal inhibitory concentration
IMiD	Immunomodulatory drugs

K

KEAP1	Kelch-like ECH-associated protein 1
KRAS	Kirsten rat sarcoma viral oncogene homolog

L

LC3-I/II	Microtubule-associated protein 1 light chain 3-I/II
LSD1	Lysine-specific demethylase 1
LRRK2	Leucine-rich repeat kinase 2

M

MAGE	Melanoma antigen gene
MDM2	Mouse double minute 2 homolog
MEK	Mitogen-activated protein kinase
MEF2D	Myocyte enhancer factor 2D
MGs	Molecular glues
MM	Multiple myeloma

N

NAD^+	Nicotinamide adenine dinucleotide
NanoBRET	Nanoluciferase bioluminescence resonance energy transfer
NanoDSF	Nano differential scanning fluorimetry
NCoR	Nuclear receptor corepressor
NDA	New drug application
NEDD8	Neural precursor cell expressed, developmentally down-regulated 8
NR4A1	Nuclear receptor subfamily 4 group A member 1
Nur77	Orphan nuclear receptor Nur77

P

p53	Tumor protein p53
p62	Sequestosome 1
p300/CBP	E1A binding protein p300 /CREB-binding protein
PD	Parkinson's disease
PD-L1	Programmed death-ligand 1
PEG	Polyethylene glycol
PG	Phenylglutarimide
PGC1α	Peroxisome proliferator-activated receptor-γ coactivator 1-α
PKs	Pharmacokinetics
POI	Protein of interest
PROTAC(s)	PROteolysis-TArgeting Chimera(s)
PTCL	Peripheral T-cell lymphoma

R

RAB28	Ras-related protein Rab-28
RBX1	RING-box protein 1
RIRI	Renal ischemia–reperfusion injury
RNA	Ribonucleic acid
RNF4	Ring finger protein 4
RNF114	Ring finger protein 114
Ro5	Rule of 5
ROS	Reactive oxygen species

S

SAR	Structure-activity relationship
SIRT	Sirtuins
SMC3	Structural maintenance of chromosomes 3
STAT3	Signal transducer and activator of transcription 3

T

TFMO	Trifluoromethyl-1,2,4-oxadiazole
TFs	Transcription Factors
TPD	Targeted protein degradation
TR-FRET	Time-resolved fluorescence resonance energy transfer

U

UPS	Ubiquitin-proteasome system
USP28	Ubiquitin-specific peptidase 28

V

VHL	Von Hippel–Lindau

Y

YAP1	Yes-associated protein 1

Z

ZBG(s)	Zinc-binding group(s)
ZFP91	Zinc finger protein 91

List of Appendices

Appendix I	Python scripts used for data extraction and visualization of Figure 2	-57-
Appendix II	Publication I: Development and characterization of the first selective class IIb histone deacetylase degraders	-60-
Appendix III	Publication II: Discovery of histone deacetylase 8 (HDAC8)-specific proteolysis-targeting chimeras with anti-cancer activity against hematological malignancies	-125-
Appendix IV	Publication III: Targeted histone deacetylase degradation via chemical induced proximity by direct recruitment of the CUL4 complex adaptor protein DDB1	-185-

1 Introduction

1.1 Epigenetics and histone deacetylases

Epigenetics, firstly introduced by Conrad Waddington in 1942[1] to explain how environmental conditions during development influence gene expression and phenotype,[2] refers nowadays more narrowly to heritable changes in gene expression that occur without alterations in the underlying DNA sequence.[3] These modifications are critical for regulating chromatin structure and gene accessibility, thereby influencing a broad spectrum of biological processes such as development, differentiation, genome stability, and cellular responses to environmental stimuli.[4] Major epigenetic mechanisms include DNA methylation, post-translational histone modifications (such as acetylation, methylation, phosphorylation, and ubiquitination), chromatin remodeling, and regulation by non-coding RNAs.[2-5]

Among these mechanisms, histone acetylation is one of the most thoroughly studied and reversible epigenetic marks. It is governed by the opposing activities of two enzyme families: histone acetyltransferases (HATs), which catalyze the addition of acetyl groups to lysine residues on histone tails, and histone deacetylases (HDACs), which remove these acetyl groups (Figure 1).[6] Acetylation neutralizes the positive charge of lysines, loosening the interaction between histones and DNA, thereby leading to a more relaxed chromatin conformation that favors transcriptional activation. In contrast, HDACs restore the positive charge on lysines, promoting chromatin condensation and transcriptional repression by reducing the accessibility of DNA to transcriptional machinery.[6] HDACs thus serve as key transcriptional repressors and epigenetic regulators, helping to silence genes by compacting chromatin structure. Importantly, their activity extends beyond histones. HDACs also deacetylate numerous non-histone proteins,[7] including transcription factors,[8] chaperones,[9-11] signaling molecules,[12, 13] and structural proteins[14-16], which allows them to influence a wide range of cellular processes, such as cell cycle regulation, apoptosis, DNA repair, metabolism, differentiation, and immune responses.[17-20] The dynamic equilibrium between acetylation and deacetylation is essential for gene regulation and cellular homeostasis.

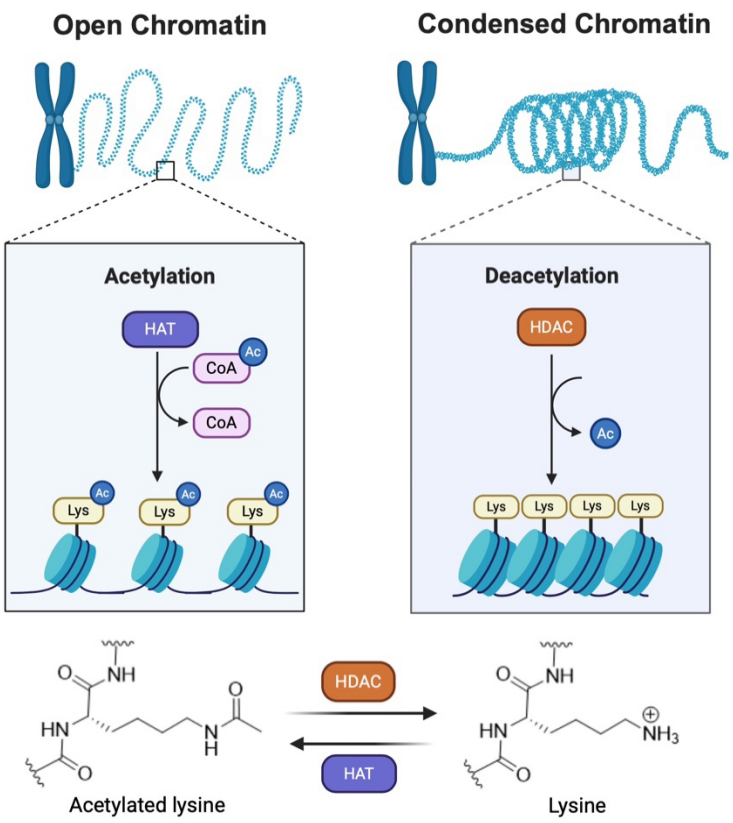

Figure 1. HATs and HDACs regulate gene transcription by adding or removing acetyl groups from lysine residues on histone N-terminal tails. Acetylation by HATs relaxes chromatin structure, while deacetylation by HDACs condenses it, thereby modulating transcriptional activity. Figure was created with Biorender.com.

1.2 Classification, localization and the biological roles of HDACs

Mammalian HDACs are classified into four major classes based on sequence similarity, subcellular localization, and cofactor dependency (Table 1). Among them, classes I (HDAC1, 2, 3, and 8), II (HDAC4, 5, 6, 7, 9, and 10), and IV (HDAC11) are Zn^{2+}-dependent, whereas class III HDACs (SIRT1–7) utilize NAD^+ as cofactor[21, 22]:

(1) Class I HDACs (HDAC1, 2, 3, 8) are mainly nuclear and ubiquitously expressed. They play essential roles in transcriptional repression through histone deacetylation, thereby regulating chromatin structure and gene expression.[23] These enzymes, normally acting *via*

multi-protein complexes, are critical for cell cycle progression, DNA damage repair, cell survival, and proliferation, and their dysregulation is often linked to tumorigenesis.[23-25]

(2) Class II HDACs are further divided into class IIa (HDAC4, 5, 7, 9) and class IIb (HDAC6, 10). Class IIa (HDAC4, 5, 7, 9) primarily act as transcriptional corepressors by recruiting other enzymatic partners rather than directly deacetylating histones. They are key regulators of muscle differentiation, cardiac hypertrophy, neuronal survival, and immune cell development, and their activity is often modulated by phosphorylation-dependent nuclear–cytoplasmic shuttling.[18] Class IIb (HDAC6, 10) possess unique structural features, including two catalytic deacetylase domains, and act mainly in the cytoplasm on non-histone substrates.[26] HDAC6 deacetylates α-tubulin, cortactin, and HSP90, thereby regulating cell motility, aggresome-mediated clearance of misfolded proteins, stress granule formation, and immune synapse function.[27] HDAC10, having acetylated polyamines as the main substrates,[28] is involved in lysosome-mediated autophagy, DNA damage repair, polyamine metabolism, cell survival under stress, and the development of chemotherapy resistance.[29-31]

(3) Class III HDACs, also known as sirtuins (SIRT1–7), are NAD^+-dependent enzymes that regulate a broad spectrum of biological processes, including energy metabolism, genomic stability, stress responses, circadian rhythm, and aging.[32, 33]

(4) Class IV is represented solely by HDAC11, which shares structural features with class I and II HDACs. Although less studied, emerging evidence suggests that HDAC11 modulates immune responses by regulating interleukin-10 expression[34] and controls metabolic homeostasis through fatty acid deacetylation.[35] It has been implicated in cancer progression, immune evasion, and inflammatory diseases, making it a potential target for therapeutic intervention.[35-37]

Table 1. Classification and localization of histone deacetylases.

Class	Members	Cofactor	Localization
I	HDAC1	Zn^{2+}	nucleus
	HDAC2		nucleus
	HDAC3		nucleus, cytoplasm
	HDAC8		nucleus, cytoplasm
IIa	HDAC4	Zn^{2+}	nucleus, cytoplasm
	HDAC5		nucleus, cytoplasm
	HDAC7		nucleus, cytoplasm
	HDAC9		nucleus, cytoplasm
IIb	HDAC6	Zn^{2+}	cytoplasm
	HDAC10		cytoplasm
III	SIRT1–7	NAD^{+}	nucleus, mitochondria, cytoplasm
IV	HDAC11	Zn^{2+}	nucleus, cytoplasm

1.3 Zn^{2+}-dependent HDACs and cancer

Aberrant HDAC expression or activity has been associated with various pathological conditions, such as neurodegenerative disorders[38] like Alzheimer's disease (AD)[39, 40], Parkinson's disease (PD)[41, 42], and Huntington's disease (HD)[43, 44], cardiovascular diseases[45, 46], inflammatory conditions[47, 48], as well as cancers.[19, 49] In cancer, HDACs can silence tumor suppressor genes, enhance oncogene expression, support tumor growth[50], and immune evasion[51]. Given their significant roles in tumor initiation and progression, HDACs have emerged as important targets in the past decades for cancer treatment. To better understand the roles of individual HDACs in specific cancer types, the following sections outline the cancer associations and functional implications of HDACs, categorized by their respective classes.

1.3.1 Class I HDACs in cancer

In cancer biology, class I HDACs are the most intensively studied group, with strong associations reported across a broad range of malignancies, including both solid tumors and hematological cancers.

HDAC1 is among the most frequently studied isoforms. It is implicated in breast cancer, leukemia, lung cancer, and liver cancer (Figure 2). In these malignancies, HDAC1 is often overexpressed and contributes to tumorigenesis by promoting cell proliferation, inhibiting apoptosis, and immunosuppression.[52-54] For example, in breast cancer, HDAC1 has been associated with poor prognosis.[55] In the initial stages of liver cancer development, the regulation of C/EBPβ-HDAC1 complexes is crucial for sustaining normal levels of p53, SIRT1, and PGC1α.[56] HDAC2 is prominently implicated in breast cancer, leukemia, and colorectal cancer (Figure 2). It plays a key oncogenic role by driving tumor cell proliferation, promoting cell cycle progression, and inhibiting apoptosis.[57] For instance, HDAC2 promotes cancer progression by enhancing lipid catabolism *via* YAP1 K280 deacetylation in colorectal cancer.[58] HDAC3 is highly expressed in several cancers, including breast cancer, leukemia, liver cancer, and colorectal cancer (Figure 2). It is a core component of the NCoR/SMRT co-repressor complex and is involved in the epigenetic silencing of tumor suppressors.[59] In leukemia, HDAC3 promotes chemotherapy resistance in acute myeloid leukemia by activating protein kinase B signaling, and its inhibition sensitizes leukemia cells to chemotherapy.[60] HDAC8, although less widely studied, is also of particular interest in breast cancer and leukemia (Figure 2). HDAC8 is involved in both histone and non-histone deacetylation (e.g., SMC3), thereby contributing to chromosomal stability and mitotic control.[61, 62] Notably, a recent study showed its overexpression has also been associated with advanced tumor stage and reduced differentiation in neuroblastoma.[63]

1.3.2 Class IIa HDACs in cancer

Class IIa HDACs shuttle between the nucleus and cytoplasm. Unlike class I HDACs, they have a low catalytic activity but influence transcription through interactions with transcription

factors and corepressors. Importantly, they are often tissue-specific and associated with certain cancers.[64-66]

HDAC4 has been studied in lung cancer, leukemia and breast cancers (Figure 2). In these tumors, HDAC4 modulates differentiation, apoptosis, and cell motility.[67] In non-small cell lung cancer, HDAC4 promotes tumor progression by deacetylating glutaminase at lysine 311, maintaining glutaminase activity and supporting cancer cell metabolism and growth.[68] HDAC5 is mainly implicated in breast cancer (Figure 2) and contributes to oncogenesis through promotion of epithelial-mesenchymal transition (EMT), inhibition of apoptosis, and enhancement of metastatic behavior.[69] In breast cancer, overexpression of HDAC5 can stabilize lysine-specific demethylase 1 (LSD1) protein through upregulation of USP28. Furthermore, the HDAC5-LSD1 axis promotes breast cancer development and progression.[70] HDAC7 plays a regulatory role in hematologic malignancies, particularly leukemia (Figure 2), and it can modulate T-cell survival and apoptosis by regulating the orphan receptor Nur77.[71] In infants with t(4;11) acute lymphoblastic leukemia, HDAC7 is markedly downregulated, and its reduced expression correlates with significantly worse clinical outcomes[72]; HDAC9 is mainly studied in breast, lung cancers, and leukemia (Figure 2) by playing an important role in regulating cellular proliferation, migration, and immune modulation.[73] In breast and lung cancers, high HDAC9 levels are associated with aggressive phenotypes and poor survival.[74, 75]

1.3.3 Class IIb HDACs in cancer

Class IIb HDACs differ from other HDAC subclasses in both structure and function. HDAC6 and HDAC10 are primarily localized in the cytoplasm and are involved in non-histone protein deacetylation, affecting processes such as protein trafficking, autophagy, and cellular stress responses.[22, 76, 77] Their cancer-related activities often extend beyond chromatin remodeling and include modulation of cytoskeletal dynamics[16], immune signaling[78, 79], and chemoresistance.[80, 81] HDAC6 is one of the best-characterized isoforms. It is mainly associated with leukemia, breast and lung cancers (Figure 2). Beyond histone protein deacetylation, HDAC6 deacetylates α-tubulin, HSP90, and other proteins to promote cell motility[82], protein aggregation clearance

(*via* the aggresome-autophagy pathway)[83], and immune checkpoint escape.[84] It also modulates STAT3 signaling and contributes to resistance to chemotherapeutics and proteasome inhibitors.[85] For example, in triple-negative breast cancer, HDAC6 is involved in its immune evasion *via* the HDAC6/STAT3/PD-L1 pathway[84]. In contrast, HDAC10 is comparatively understudied but has increasingly recognized roles in lung cancer, leukemia, and neuroblastoma (Figure 2). It influences autophagy and DNA repair, with recent evidence showing that HDAC10 inhibition enhances sensitivity to DNA-damaging agents.[31] Its immunosuppressive roles and regulation of lysosomal function are areas of growing interest.[81, 86]

1.3.4 Class IV HDACs in cancer

HDAC11 is the only member of class IV and has been implicated in breast and liver cancers (Figure 2). Its role in suppressing IL-10 production and modulating T-cell activation suggests an immunoregulatory function that may aid tumor immune escape.[34] Although mechanistic studies are still limited, HDAC11 is gaining attention as a potential target in cancer immunotherapy.[87]

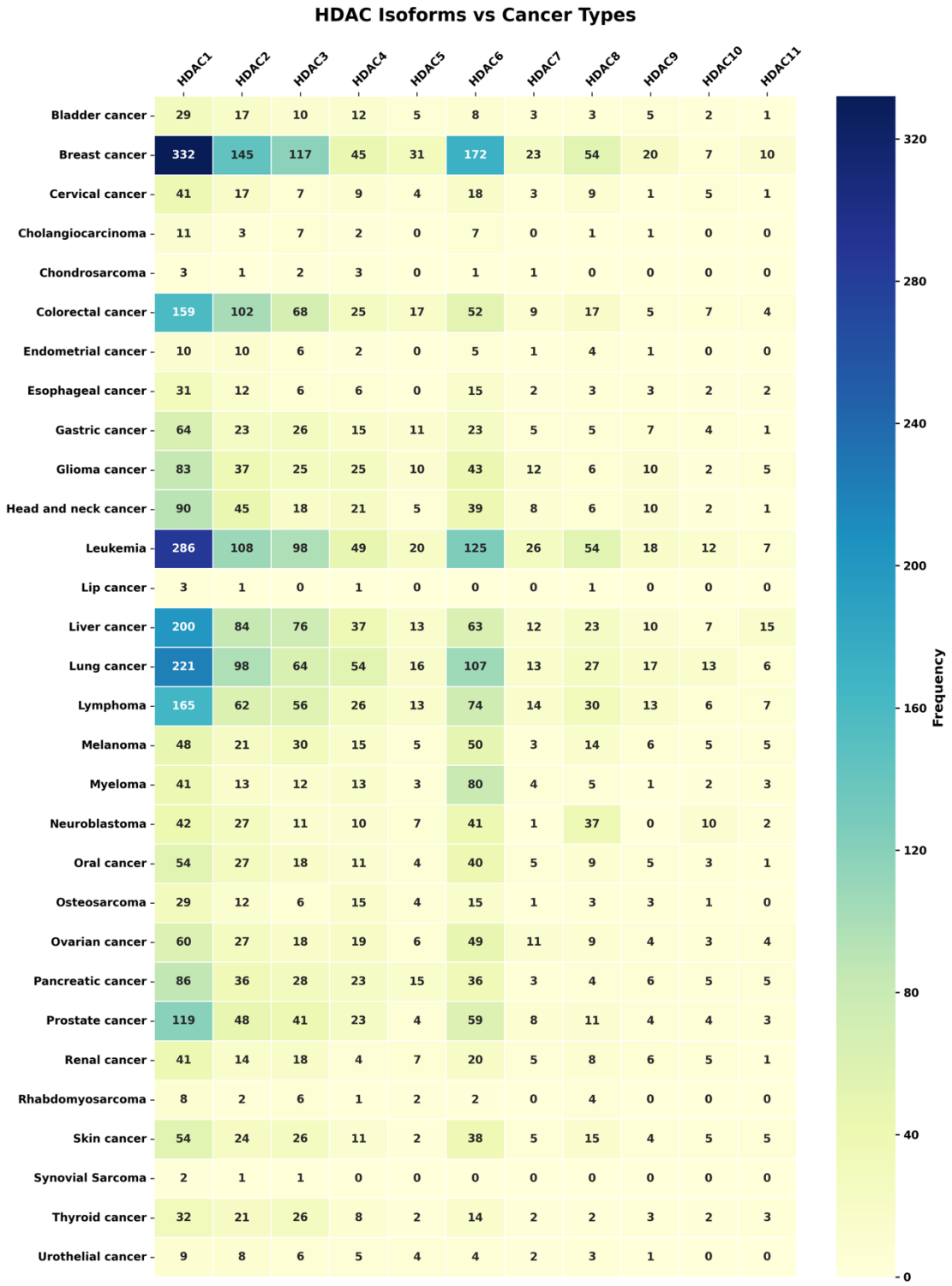

Figure 2. HDAC isoforms and related cancer types. Data (accessed on 15.12.2025) are derived from PubMed (https://pubmed.ncbi.nlm.nih.gov) using Python-based text mining, and the heatmap was generated with seaborn to visualize the frequency of HDAC-cancer associations. The scripts used for data extraction and visualization is provided in the Appendix I.

1.4 HDAC inhibitors in cancer therapy: progress and challenges

The recognition of HDACs as key players in cancer and other diseases has driven the development of histone deacetylase inhibitors (HDACis) in the past decades. HDACis are small molecules that block the enzymatic activity of HDACs, leading to increased acetylation of histones and reactivation of gene expression programs that are often silenced in cancer cells. In addition to modulating chromatin structure, HDACis can also affect numerous non-histone proteins, such as p53, α-tubulin, and HSP90, influencing diverse cellular processes including cell cycle progression, DNA repair, protein degradation, and immune signaling.[20, 88-91]

Trichostatin A, an antifungal compound originally isolated by Tsuji et al. from *Streptomyces hygroscopicus* in the 1970s,[92] was later identified in the 1990s as the first molecule exhibiting potent HDAC inhibitory activity.[93] In 1997, Jung et al.[94] designed a series of analogs by integrating pharmacophoric features from trichostatin A and trapoxin B, thereby proposing the first pharmacophore model for HDACis. This model, comprising three fundamental components, remains the basis for the structural design of most HDACis developed to date: a zinc-binding group (ZBG), which chelates the catalytic Zn^{2+} ion in the HDAC active site; a linker, which fits into the hydrophobic channel; and a surface recognition domain (cap group) that interacts with residues at the rim of the catalytic pocket (Figure 3).[94] Based on their chemical scaffolds, HDACis are roughly categorized into several classes, including hydroxamic acids (e.g., vorinostat, panobinostat), benzamides (e.g., tucidinostat, entinostat), cyclic peptides (e.g., romidepsin), aliphatic acids (e.g., valproic acid), and more recent hydrazide-based compounds (e.g., DS-103).[91, 95]

To date, several HDACis have gained clinical approval (Figure 3), primarily for the treatment of hematological malignancies. These agents are largely classified as pan-HDAC inhibitors that target multiple HDAC isoforms and have demonstrated antitumor activity through the induction of cell cycle arrest, apoptosis, and immune modulation.[96] The first HDACi approved by the U.S. Food and Drug Administration (FDA) was vorinostat (SAHA), a hydroxamic acid-based non-selective HDAC inhibitor, for the treatment of cutaneous T-cell lymphoma (CTCL) in 2006.

Vorinostat exerts its effects by increasing acetylation of histone and non-histone proteins, thereby restoring the expression of tumor suppressor genes and inducing apoptosis in malignant T cells.[97] Following vorinostat, several other HDACis have been approved[98]: Romidepsin, a cyclic peptide natural product and preferential inhibitor of class I HDACs, is approved for CTCL in 2009.[99] Belinostat, another non-selective HDAC inhibitor, has been approved for relapsed or refractory peripheral T-cell lymphoma (PTCL).[100] Tucidinostat, a benzamide-type HDACi with selective activity against HDAC1, 2, and 3, has been approved in China for PTCL in 2014.[101] Panobinostat, a potent pan-HDAC inhibitor with strong class I activity, is approved in combination with bortezomib and dexamethasone for the treatment of multiple myeloma in 2015.[102] Recently, in March 2024, the FDA approved givinostat as the first nonsteroidal, first-in-class therapy for all genetic variants of Duchenne muscular dystrophy.[103]

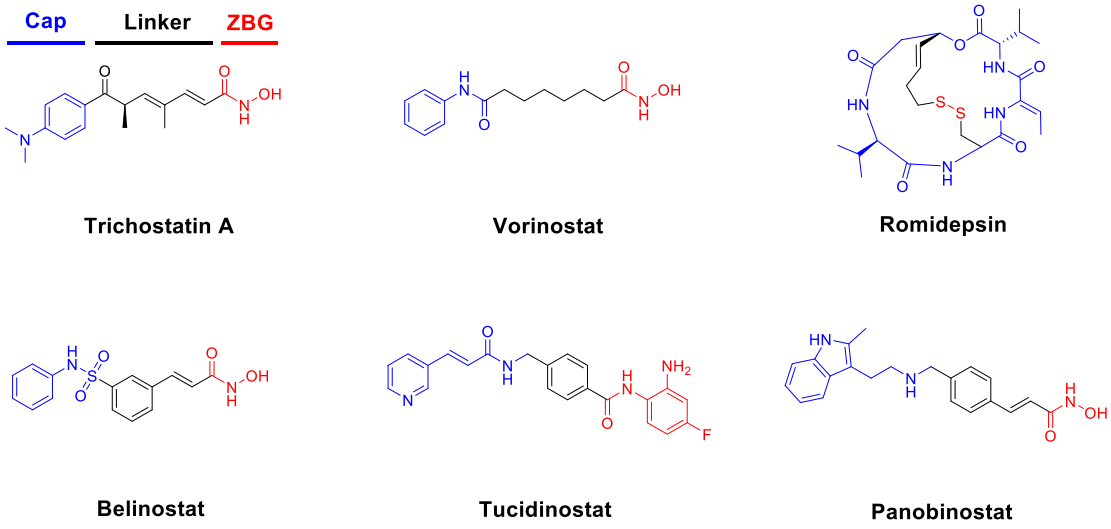

Figure 3. Structure of Trichostatin A and the approved HDACis for cancer treatment.

These agents have shown clinical benefits, particularly in T-cell lymphomas and multiple myeloma. However, their use is often limited by dose-limiting toxicities, such as fatigue, thrombocytopenia, and gastrointestinal effects, which are largely attributable to their non-selective inhibition of multiple HDAC isoforms.[104] Moreover, their efficacy in solid tumors remains modest, likely due to poor tumor penetration, resistance mechanisms, and context-dependent HDAC function.[105] In response to these limitations, researchers have developed

isoform-selective HDAC inhibitors to improve target specificity and reduce off-target effects.[106] While these selective agents have advanced our understanding of HDAC biology and offered modest improvements in safety profiles, they still rely on reversible inhibition and often fail to achieve complete and sustained silencing of respective HDAC subtypes. To overcome the intrinsic limitations of traditional HDAC inhibitors, targeted protein degradation technologies have emerged as a promising alternative. Among them, PROTACs (proteolysis-targeting chimeras) represent a novel therapeutic modality that leverages the ubiquitin-proteasome system to induce selective degradation of disease-relevant proteins, including HDACs.[107]

1.5 Targeted protein degradation: PROTACs and emerging strategies

1.5.1 Origins and evolution of PROTAC technology

Targeted protein degradation (TPD) has emerged as an innovative therapeutic strategy that addresses the limitations of traditional small-molecule inhibitors. The concept of PROTACs was first introduced by Sakamoto et al. in 2001, using a bifunctional peptide-based molecule that brought a target protein into proximity with an E3 ubiquitin ligase, leading to its polyubiquitination and proteasomal degradation.[108] Although these early constructs proved the feasibility of induced proximity–mediated degradation, they were limited by poor cell permeability, metabolic instability, and unfavorable pharmacokinetics.[109]

A major breakthrough came with the development of small molecule PROTACs, which overcame the shortcomings of peptide-based designs and greatly expanded the scope of druggable targets, enabling their widespread application in chemical biology and drug discovery. In 2008, Schneekloth A. R. et al. reported the first fully small-molecule PROTAC targeting the androgen receptor (AR), in which a hydroxyflutamide-derived AR ligand was conjugated to the MDM2 recruiter (nutlin-3[110]), enabling the degradation of AR in HeLa cells.[111] To date, PROTACs generally consist of three functional components (Figure 4): (1) a ligand that binds to the protein of interest (POI); (2) a ligand that recruits an E3 ubiquitin ligase; and (3) a linker that connects the two moieties and facilitates the formation of a productive

ternary complex. This modular design enables rational optimization of binding affinity, linker flexibility, and spatial orientation to promote efficient ubiquitination and degradation of the target proteins.[112]

Notably, beyond their modular architecture, PROTACs are fundamentally different from conventional inhibitors in how they exert their effects. Traditional small molecules follow an "occupancy-driven" model, where sustained binding to the target is required to maintain inhibition. In contrast, PROTACs act through an "event-driven" pharmacology (Figure 4): once a target protein is ubiquitinated and degraded, the PROTAC molecule can dissociate and engage additional targets in a catalytic manner. This distinction not only enables the removal of both catalytic and non-catalytic functions of the protein but also reduces the need for continuous target engagement, offering the potential to overcome resistance caused by overexpression or mutation.[112, 113]

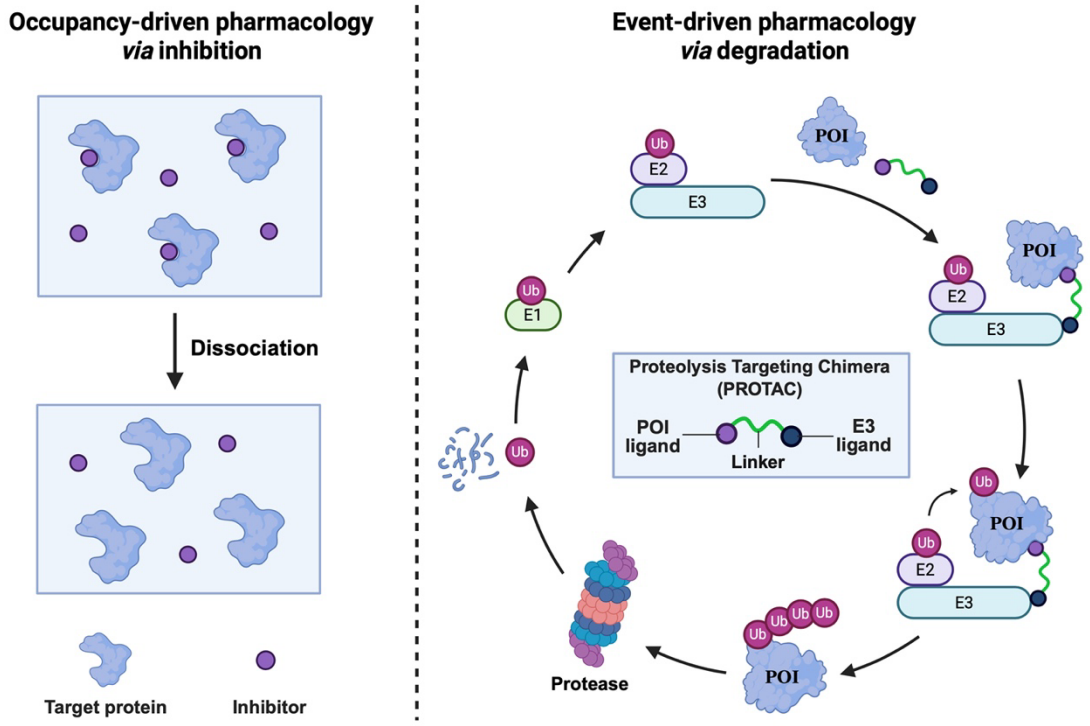

Figure 4. Mode of action for inhibitors and PROTACs, as well as PROTAC-mediated protein ubiquitination and subsequent proteasomal degradation. The figure was created with Biorender.com.

1.5.2 Current landscape and therapeutic targets

Since the introduction of small-molecule PROTACs, the field of targeted protein degradation has undergone rapid expansion. The scope of degradable proteins has extended far beyond enzymes with active sites to include non-enzymatic proteins such as scaffolding molecules, transcription factors, and chromatin regulators.[113] This broadened target space reflects a fundamental advantage of PROTACs over traditional inhibitors, enabling access to proteins that were previously considered "undruggable".

Currently, a wide variety of intracellular proteins have been successfully targeted for degradation in preclinical studies, including kinases (e.g., BTK, CDK4/6, BCR-ABL, LRRK2), transcription factors (e.g., STAT3, ER, AR, IKZF1/3), scaffold/signaling proteins (e.g., BCL-X_L, BCL-2), and epigenetic regulators (e.g., BRD4, EZH2, p300/CBP, HDACs).[114] Notably, several PROTAC candidates have progressed into clinical trials, underscoring their translational potential. Among these, degraders of the androgen receptor (ARV-110) and estrogen receptor (ARV-471) have shown promising results in early-phase studies, including favorable pharmacokinetics, efficient target knockdown, and preliminary antitumor activity in hormone-dependent cancers.[115, 116] Of note, after more than two decades of development, ARV-471 has become the first PROTAC to reach new drug application (NDA) submission, marking a milestone of the PROTAC technology maturation and clinical promise.[117] (Figure 5)

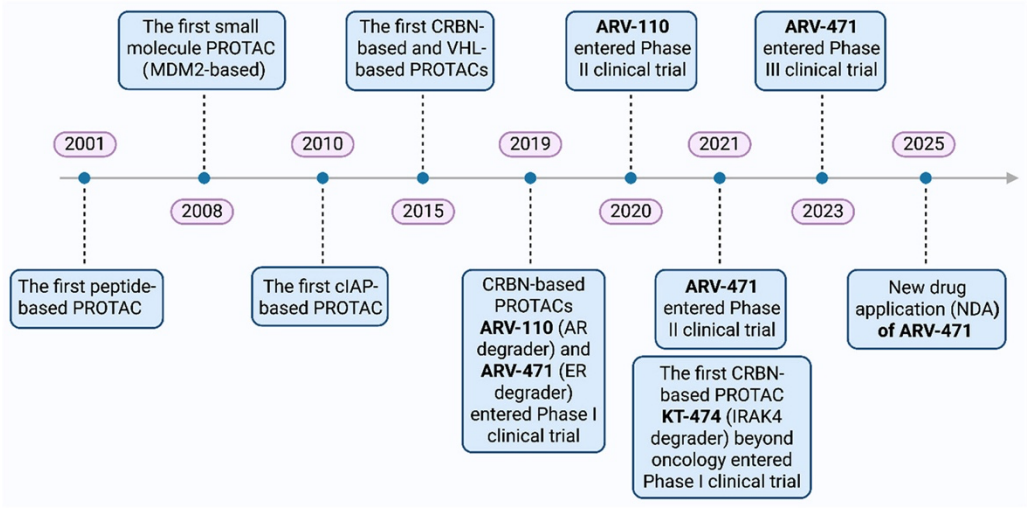

Figure 5. Timeline of PROTAC technology and the clinical progress. Figure reprinted from

Ma, Z.; Zhou, J. NDA Submission of Vepdegestrant (ARV-471) to U.S. FDA: The Beginning of a New Era of PROTAC Degraders. J. Med. Chem. 2025, 68, 14, 14129–14136.,[117] with the permission of American Chemical Society (License number 6083260478395). Copyright 2025 American Chemical Society.

Beyond oncology, PROTACs are also being explored in immunology[118], neurodegenerative diseases[119, 120], and infectious diseases[121, 122], with the aim of modulating abnormal signaling pathways, reducing toxic protein accumulation, or silencing host factors hijacked by pathogens. This expanding therapeutic landscape demonstrates the platform's broad application. Despite ongoing challenges in drug design and optimization, the current state of PROTAC development underscores its growing potential as a refined platform for both mechanistic studies and therapeutic intervention in a wide range of diseases. Continued innovation in target selection, linker chemistry, and E3 ligase engagement is expected to further expand the utility of this technology in the years to come.

1.5.3 E3 ligases utilized in PROTAC design and their ligands

A key component of PROTAC function is the recruitment of an E3 ubiquitin ligase to facilitate the ubiquitination and subsequently proteasomal degradation of the target protein. The human genome encodes over 600 E3 ligases, yet only a limited subset has been successfully exploited in PROTAC design. The choice of E3 ligase is a key determinant of degradation efficiency, tissue selectivity, and cellular activity, making it a critical consideration in rational degrader development.[123]

To date, the most widely used E3 ligases in PROTACs are cereblon (CRBN) and von Hippel–Lindau (VHL). These ligases have been favored due to the availability of well-characterized small-molecule ligands, broad tissue expression, and robust structural data that support ternary complex formation.[124] CRBN-based PROTACs often utilize thalidomide analogs as ligase-recruiting elements, whereas VHL-based PROTACs employ hydroxyproline derivatives that mimic native substrates. Both have demonstrated successful degradation across a wide range of targets and are featured prominently in clinical-stage degraders.[116] Notably, progress on the

simplified CRBN ligands has been made in recent years, such as phenylglutarimides[125]. In addition to CRBN and VHL, other E3 ligases have been explored, though with more limited success. For example, MDM2, which primarily regulates p53 turnover, has been employed in some early PROTACs but is constrained by oncogenic potential and context-specific activity.[126] Inhibitor of apoptosis proteins (IAPs) have also been investigated, particularly in SNIPER-type degraders, offering an alternative E3 ligase strategy but with less robust degradation profiles.[127] Moreover, an expanding numbers of recruited E3 ligases has been recently reported, including the arylhydrocarbon receptor (AhR)[128], DCAF11[129], DCAF16[130], FEM1B[131], RNF4[132], RNF114[133], KEAP1[134], as well as the melanoma antigen (MAGE) family[135]. A selection of representative ligands for the recruited E3 ligases is summarized in Figure 6.

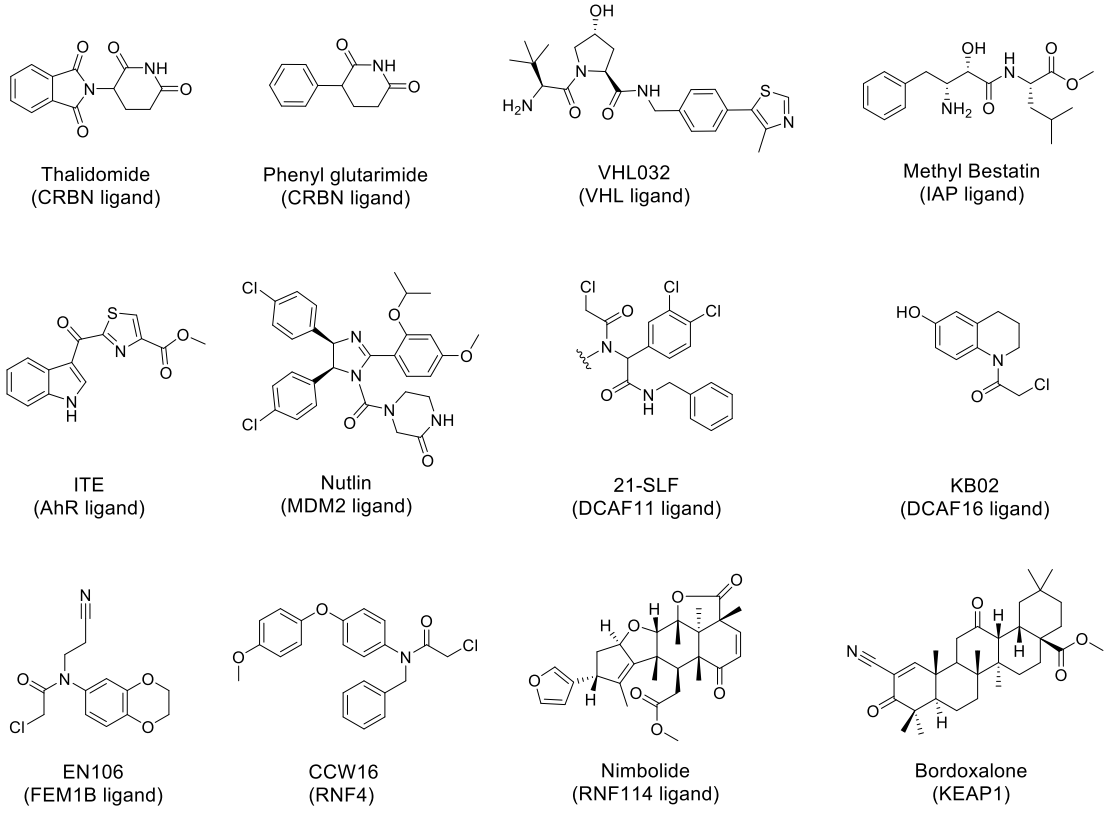

Figure 6. Representative ligands to recruit E3 ligases in the context of PROTACs.

The selection of an appropriate E3 ligase for PROTAC construction depends on multiple factors, including: (1) tissue distribution of the ligase, which influences degradation selectivity; (2) expression level and stability in target cells; (3) ability to form a productive ternary complex

with the target protein; (4) compatibility of the ligand with linker design; and (5) drug-like properties.[112, 113] Despite the theoretical abundance of > 600 E3 ligases, the field is currently constrained by the limited diversity of available ligase-binding ligands.[136] This bottleneck has sparked significant interest in ligand discovery for underexplored E3 ligases, including tissue-specific or inducible ligases that could offer more selective or conditional degradation. Moreover, advances in structural biology and computational modeling are accelerating the identification of novel E3 ligase–ligand pairs that may further expand the PROTAC toolbox.[116]

1.5.4 Limitations and design challenges of PROTACs

Despite their conceptual elegance and therapeutic promise, PROTACs face several significant limitations that currently restrict their broad clinical application. These challenges arise from both the physicochemical properties of PROTAC molecules themselves and the biological complexity of targeted protein degradation mechanisms.

One of the foremost issues lies in the large molecular size and structural complexity of PROTACs. Unlike traditional small molecule inhibitors, which typically adhere to Lipinski's rule of five (Ro5)[137], PROTACs are heterobifunctional and generally higher than 500 Da in molecular weight. This characteristic can lead to poor membrane permeability, low oral bioavailability, and unfavorable pharmacokinetics, limiting their *in vivo* efficacy.[138] While some orally bioavailable PROTACs have entered clinical trials, achieving favorable drug-like properties remains a central focus in PROTAC design optimization.

Another major challenge is the requirement for productive ternary complex formation between the target protein, PROTAC molecule, and E3 ligase. This process is highly dependent on the spatial and geometric compatibility of the three components.[113, 139] Even with strong binary affinities, an inefficient or unstable ternary complex can lead to poor degradation efficiency.[140] Factors such as linker length, flexibility, and composition profoundly influence complex stability, yet optimal configurations are often difficult to predict and must be determined experimentally.

Moreover, the limited pool of E3 ligases usable in PROTAC design presents a biological bottleneck, with most current PROTACs relying on CRBN or VHL. Despite that they are often successful in achieving potent target degradation, both ligases are ubiquitously expressed. While this broad distribution can be advantageous, it may also lead to lack of tissue selectivity and undesired off-target degradation in non-diseased cells.[123, 124] Thus, the discovery of tissue- or disease-specific E3 ligase and their recruiters remain a key, but underdeveloped, area of the field.

Furthermore, resistance mechanisms have also begun to emerge. In preclinical studies, prolonged PROTAC exposure has been shown to induce mutations or downregulation in the E3 ligase components[141, 142], as well as mutations in the target protein itself[143], thereby compromising degradation efficiency. Additionally, prolonged target depletion can trigger adaptive reprogramming of cellular protein homeostasis or activation of compensatory signaling pathways,[144] thereby diminishing the overall therapeutic efficacy.

In summary, although PROTACs represent a powerful new therapeutic modality, they are accompanied by a distinct set of design, delivery, and biological challenges. Addressing these limitations will require advances in chemical synthesis, predictive modeling, and mechanistic understanding of the ubiquitin–proteasome system. Continued progress in these areas will be crucial for fully realizing the clinical potential of targeted protein degradation.

1.5.5 Beyond PROTACs: alternative degradation technologies

To address the limitations of PROTACs and further expand the scope of targeted protein degradation, researchers have developed complementary strategies, including molecular glues (MGs), multitargeted PROTACs, antibody-based PROTACs (AbTACs), oligonucleotide-based PROTACs, bioPROTACs, pre-PROTACs, lysosome-mediated TPD and other novel concepts.[145] These concepts and applications are summarized in Table 2.

Table 2. Selected key emerging strategies in targeted protein degradation.

Technology	Key Idea	Main Targets/Notes
MGs[146]	Monovalent molecules induce target–E3 ligase proximity for UPS-dependent degradation.	Proven drugs in MM; rapid pipeline growth
Multitargeted PROTACs[147]	Degrade multiple proteins at once	Improved potency and PKs vs single-target versions
AbTACs[148]	Bispecific antibodies recruit E3 ligase to cell-surface proteins	Membrane proteins (e.g., PD-L1)
Oligonucleotide-PROTACs[149]	Oligonucleotide motif as warhead	RNA-binding proteins, TFs
BioPROTACs[150]	Engineered E3 ligases with new binding domains	c-Myc[151], KRAS[152]
Pre-PROTACs[153]	prodrug-like, activated by specific triggers	Light[154], ROS triggers[153], radiation[155]
Lysosome-mediated TPD[156]	Use lysosomal degradation instead of UPS	Extracellular, membrane proteins

Among the growing range of targeted protein degradation strategies, molecular glues (MGs) are small molecules that promote the interaction between an E3 ligase and a so-called neosubstrate, thereby triggering ubiquitin–proteasome–mediated degradation. Unlike bifunctional PROTACs, MGs generally have a lower molecular weight, more favorable pharmacokinetics, and superior tissue penetration. Well-known examples include thalidomide analogs such as lenalidomide and pomalidomide, which recruit CRBN to degrade IKZF1, IKZF3, and GSPT1.[146] Advances in structural biology and screening technologies have shifted MG discovery from serendipity to rational design, enabling the targeting of transcription factors[157], signaling proteins[158], and oncogenic drivers[159] once considered undruggable. With high cell permeability, oral bioavailability, broad tissue distribution, and the ability to cross the

blood–brain barrier, MGs can reach therapeutic sites that are challenging for PROTACs.[160] While identifying the optimal E3–target combinations remains a challenge, expanding the available ligase repertoire and combining MGs with other therapeutic modalities offer exciting opportunities.[160] Thanks to their unique mechanism and favorable drug-like properties, MGs are emerging as one of the most promising frontiers in the future of targeted protein degradation.

Taken together, these emerging platforms expand the capabilities of PROTACs by enabling the degradation of proteins located in diverse cellular compartments, thereby broadening the druggable proteome. Sustained innovation in this area will be essential for addressing current technological and biological challenges, and for realizing more precise, effective, and versatile protein modulation in both experimental research and clinical applications.

1.6 HDAC PROTACs: a next-generation approach to HDAC modulation

In light of the clinical challenges of conventional HDAC inhibitors, including limited isoform selectivity, systemic toxicity, and acquired resistance, the development of HDAC PROTACs has accelerated in recent years and offers significant advantages in overcoming these limitations.[161] By coupling an HDAC-binding ligand to an E3 ubiquitin ligase recruiter *via* a linker, these bifunctional molecules bring the targeted HDACs into polyubiquitination and trigger the subsequent degradation by 26S proteasome, which allows to eliminate all functions of the HDACs, including non-catalytic roles that are not inhibited by classical inhibitors. Over the past eight years, numerous HDAC-targeting PROTACs have been reported, demonstrating the degradation of HDAC1–4, HDAC6–8, and HDAC10, as confirmed by Western blotting. [82, 107, 162, 163] Among these cases, selective degradation of specific isoforms such as HDAC3, HDAC4, HDAC6, HDAC7, and HDAC8 has also been achieved (Figure 7-11). These findings underscore the feasibility of isoform-selective degradation within the HDAC family. The following sections highlight representative PROTACs that demonstrate selective degradation of HDAC isoforms.

1.6.1 Selective HDAC3 PROTACs

Selective degradation of HDAC3 has been demonstrated in two studies.[164, 165] Notably, both studies employed unconventional ligand ZBGs, hydrazides or *o*-aminoanilides, rather than the commonly used hydroxamic acid warhead (Figure 7). Compound **XZ9002**, which incorporates a hydrazide-based HDAC3 ligand and recruits VHL as the E3 ligase, demonstrated potent and selective degradation of HDAC3 in MDA-MB-468 cells, with a $DC_{50,\ 14\ h}$ value of 42 nM.[164] In contrast, compound **HD-TAC7**, utilizing an *o*-aminoanilide scaffold and a CRBN recruiter, achieved moderate degradation efficiency in RAW 264.7 macrophages, with a $DC_{50,\ 24\ h}$ value of 0.32 µM. These two studies indicate how variations in HDAC-binding moieties, E3 ligase recruitment, and cellular context collectively influence the degradation potency of HDAC3-targeting PROTACs.[165]

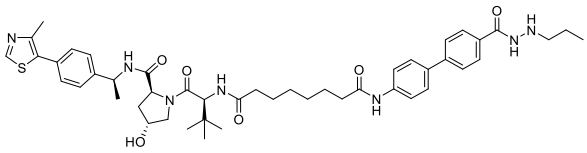

Compound **XZ9002**, 2020
$DC_{50,\ 14\ h}$ = 42 nM; D_{max}, 88%
MDA-MB-468 cells

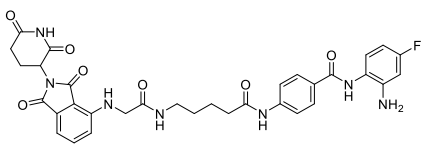

Compound **HD-TAC7**, 2020
$DC_{50,\ 24\ h}$ = 0.32 µM; D_{max}, not given
RAW 264.7 macrophages

Figure 7. Reported selective HDAC3 PROTACs and their potencies.

1.6.2 Selective HDAC4 PROTACs

Selective degradation of HDAC4 has been achieved for the first time by Macabuag *et al.*.[44] Notably, the two most potent degraders, compounds **7** and **11** (Figure 8), were derived from distinct inhibitor classes, hydroxamic acid (HA) and 1,2,4-trifluoromethyloxadiazole (TFMO), respectively, that linked to a VHL ligand *via* PEG linkers. Compound **11**, originating from the TFMO scaffold, exhibited superior potency in Jurkat E6-1 cells, with a $DC_{50,\ 24\ h}$ value of 4 nM, while compound **7**, from the HA series, achieved a $DC_{50,\ 24\ h}$ value of 37 nM. Both degraders demonstrated remarkable isoform selectivity, degrading HDAC4 without affecting other isoforms (HDAC1, 3, 5, 7, 9), despite different HDAC4 inhibition profiles. These findings reveal that chemically diverse HDAC4 ligands, when conjugated to a VHL-recruiting element,

can both drive efficient and selective degradation of HDAC4, emphasizing the flexibility of ligand choice in PROTAC design.

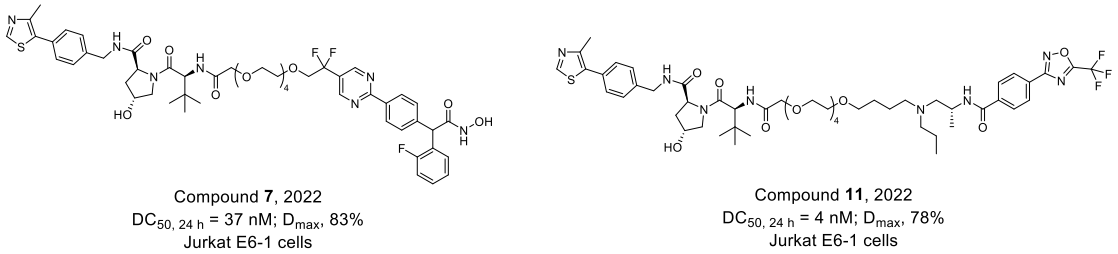

Figure 8. Reported selective HDAC4 PROTACs and their potencies.

1.6.3 Selective HDAC6 PROTACs

Among all HDAC isoforms, HDAC6 remains the most extensively studied subtype in the context of PROTAC development, mirroring its prominence in inhibitor research. To date, numerous HDAC6-targeting PROTACs have been reported (Figure 9), many of which exhibit high selectivity and potent degradation activity, with DC_{50} values frequently reaching the low nanomolar range. The majority of these degraders employ hydroxamic acid-based HDAC6 ligands as warheads and recruit either cereblon (CRBN)[166-173]or von Hippel–Lindau (VHL)[174] as E3 ubiquitin ligases.

The reported HDAC6 PROTACs have been constructed using a variety of HDAC ligands, including HDAC6-selective inhibitors such as Nexturastat A (in compounds **NP8**[167], **NH2**[169], **12d**[168], **3j**[174]), indirubin-based inhibitors (in compound **14a**[171]), and TO-317 (in compound **TO-1187**[173]); nonselective HDAC inhibitors such as crebinostat (in compound **9c**[166]) and vorinostat (in compound **A6**[172]). In addition to the conventional hydroxamic acid–based designs, the first non-hydroxamate HDAC6 degraders were reported in 2022. These compounds featured a difluoromethyl-1,3,4-oxadiazole (DFMO) zinc-binding moiety (in compound **1**) and achieved selective HDAC6 degradation *via* recruitment of either CRBN or VHL.[175] More recently, in 2025, a CRBN-recruiting HDAC6 degrader (compound **17c**) incorporating an ethyl hydrazide warhead was also disclosed.[176]

While most HDAC6 PROTACs have been developed for anticancer purposes, emerging studies suggest potential in non-oncological settings as well. A nexturastat A–based degrader has

demonstrated efficacy in a model of renal ischemia–reperfusion injury (RIRI),[177] while indirubin- and vorinostat-derived PROTACs have shown anti-inflammatory effects in preclinical studies.[171, 178] These findings expand the therapeutic scope of HDAC6 degraders and highlight their versatility across disease models.

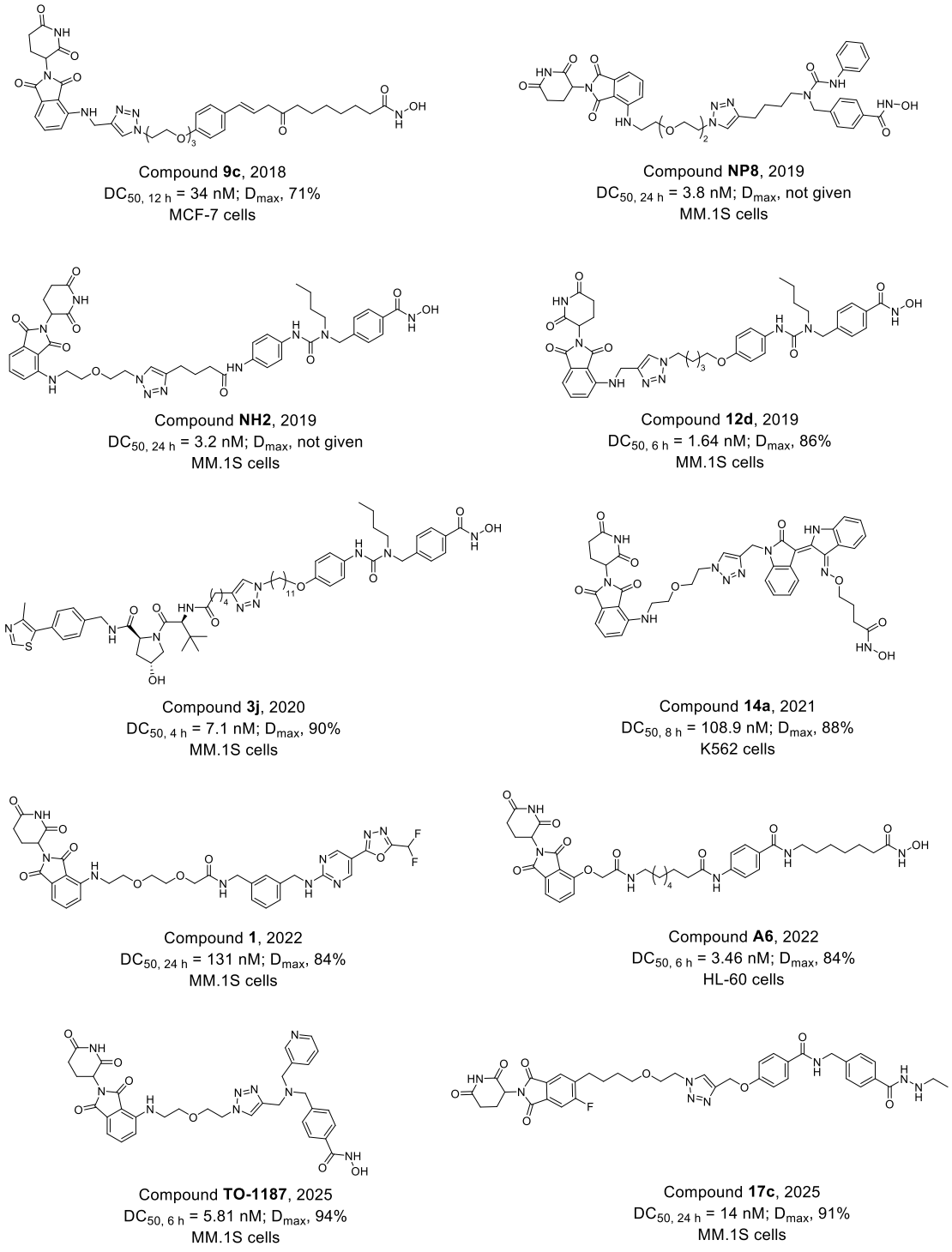

Figure 9. Reported selective HDAC6 PROTACs and their potencies.

1.6.4 Selective HDAC7 PROTACs

Although HDAC7 remains relatively underexplored compared to other isoforms, recent studies have shown that HDAC7 can be selectively and effectively targeted by PROTACs, with selective degraders showing promising results in cellular models (Figure 10). Utilizing a previously discovered class IIa HDAC inhibitor, **TMP269**[179], two independent studies demonstrated the selective degradation of HDAC7 in RAW264.7 cells and NB4 cells.[180, 181] In both cases, **TMP269** served as the HDAC-binding moiety, structurally modified by replacing its tetrahydropyran group with a piperidine ring to enable linker installation. Compound **B4**, incorporating a VHL ligand and a flexible polyethylene glycol (PEG) linker, displayed relatively low degradation potency in RAW264.7 cells, with a $DC_{50,\ 12\ h}$ value of 5 μM.[180] In contrast, compound **B14**, which utilizes a CRBN ligand and a more rigid linker structure, achieved markedly enhanced degradation efficiency in NB4 cells, yielding a $DC_{50,\ 12\ h}$ value of 25 nM.[181] The markedly enhanced activity of **B14** suggests that CRBN recruitment, in conjunction with increased linker rigidity, may better support the formation of a stable ternary complex with HDAC7 in this specific cellular context.

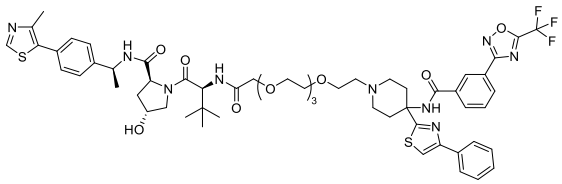

Compound **B4**, 2024
$DC_{50,\ 12\ h}$ = 5 μM; D_{max}, not given
RAW264.7 cells

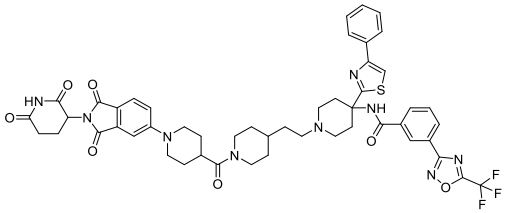

Compound **B14**, 2025
$DC_{50,\ 12\ h}$ = 25 nM; D_{max}, 90%
NB4 cells

Figure 10. Reported selective HDAC7 PROTACs and their potencies.

1.6.5 Selective HDAC8 PROTACs

Selective degradation of HDAC8 *via* PROTAC technology has gained increasing attention in recent years (Figure 11), offering a promising strategy to overcome the limitations of traditional HDAC8 inhibitors. The first selective HDAC8 PROTAC was reported by Chotitumnavee *et al.* in 2022,[182] in which a selective HDAC8 inhibitor was conjugated with pomalidomide to recruit CRBN, leading to efficient HDAC8 degradation in Jurkat cells with a $DC_{50,\ 24\ h}$ of 0.70 μM.

Since then, multiple selective HDAC8 degraders have been developed using diverse chemical scaffolds and E3 ligase ligands, primarily targeting CRBN or VHL.

Among hydroxamic acid–based PROTACs, compounds such as **ZQ-23**[183] and **16e**[184] have demonstrated sub-micromolar degradation potencies in various cancer cell lines. Additionally, **CRBN_1e**[185] has been reported as another selective HDAC8-targeting degrader. Notably, across the currently reported hydroxamate-based HDAC8 PROTACs, the observed degradation efficiency tends to fall within a moderate range. In contrast, hydrazide-based HDAC8 PROTACs have shown superior potency. This enhanced performance can be partly attributed to the stronger binding affinity of hydrazide-based ligands toward HDAC8, which facilitates more efficient recruitment and stabilization of the ternary complex. For example, **YX862**[186], a VHL-recruiting degrader, achieved >95% HDAC8 degradation in MDA-MB-231 cells and MCF-7 cells, with $DC_{50,\ 8\ h}$ values of 2.6 nM and 18 nM, respectively. Similarly, compound **Z16**[187], which incorporates a phenylglutarimide–based CRBN ligand, exhibited robust degradation across four cancer cell lines, with a minimum $DC_{50,\ 6\ h}$ of 0.27 nM in A549 cells.

Collectively, these studies highlight the growing success of selective HDAC8 PROTACs and emphasize the importance of ligand binding potency, warhead scaffold design, and E3 ligase pairing in achieving potent and selective degradation. Beyond their therapeutic potential, such molecules can also be used as valuable tools for probing HDAC8-specific biology in diverse disease models.

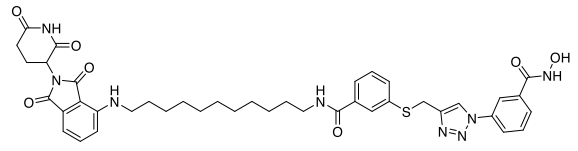

Compound **4c**, 2022
$DC_{50,\ 24\ h}$, 0.702 μM
Jurkat cells

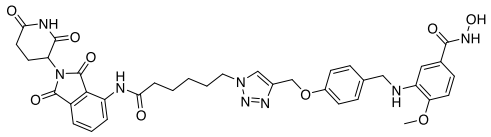

Compound **CRBN_1e**, 2022
DC_{50}, not given
SK-N-BE(2)-C cells

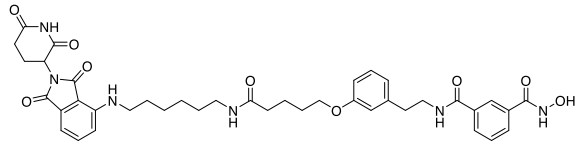

Compound **ZQ-23**, 2022
$DC_{50,\ 10\ h}$, 0.147 μM; D_{max}, 93%
HCT-116 cells

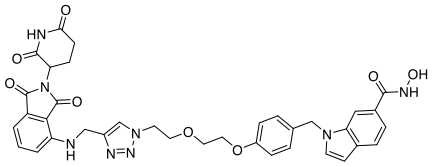

Compound **16e**, 2023
DC_{50}, 0.58 μM; D_{max}, >95%
A549 cells

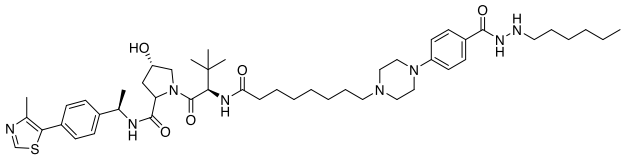

Compound **YX862**, 2024
$DC_{50,\ 8\ h}$, 2.6 nM; D_{max}, >95%, MDA-MB-231 cells
$DC_{50,\ 8\ h}$, 1.8 nM; D_{max}, >95%, MCF-7 cells

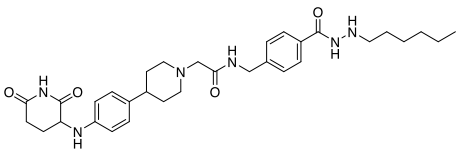

Compound **Z16**, 2024
$DC_{50,\ 6\ h}$, 0.32 nM; D_{max}, 97%, Jurkat cells
$DC_{50,\ 6\ h}$, 2.4 nM; D_{max}, 77%, HCT116 cells
$DC_{50,\ 6\ h}$, 3.1 nM; D_{max}, 92%, THP-1 cells
$DC_{50,\ 6\ h}$, 0.27 nM; D_{max}, 96%, A549 cells

Figure 11. Reported selective HDAC8 PROTACs and their potencies.

1.7 Scope of Thesis

In recent years, the development of PROTACs targeting HDAC has attracted growing attention as a strategy for achieving more precise epigenetic modulation beyond conventional inhibition by small molecules. Many HDAC-targeting PROTACs have been reported, primarily focusing on class I and II HDACs using well-characterized E3 ligases such as CRBN or VHL. These molecules have shown promising activity in degrading either multiple HDAC subtypes or specific isoforms, offering advantages such as sustained protein knockdown and a catalytic mechanism of action. However, challenges remain. Many existing HDAC PROTACs lack clear isoform selectivity, raising concerns about potential off-target effects and broad-spectrum HDAC depletion. Furthermore, the limited range of E3 ligases employed in HDAC PROTACs

may constrain their effectiveness in certain cellular contexts. In contrast, exploring alternative E3 ligases offers an opportunity to diversify degradation strategies and potentially enhance selectivity and/or efficiency. In this context, efforts to refine degradation selectivity and to explore new E3 ligase recruitment strategies represent promising directions for advancing the field. This thesis comprises three distinct yet related research projects aimed at developing PROTACs for selective degradation of HDACs, with particular focus on isoform or class selectivity and the use of novel E3 ligase complex recruitment strategies.

Chapter 2 focuses on the development and characterization of selective class IIb histone deacetylase (HDAC) degraders. Class IIb HDACs, comprising HDAC6 and HDAC10, share high structural homology and overlapping domain architectures. While HDAC6 has been extensively investigated as a therapeutic target, HDAC10 remains comparatively underexplored. This project aims to demonstrate that PROTACs designed to degrade HDAC6 can also concurrently target HDAC10 without affecting other HDAC subtypes. To verify this hypothesis, a previously reported selective HDAC6 inhibitor, Tubastatin A, and a ring-opened analog were used as warheads, while CRBN ligands served as E3 recruiters. The PROTAC design was guided by molecular docking analysis. After synthesis and characterization of the target compounds, the PROTACs were evaluated for target engagement, physicochemical properties, stability in human plasma, and cytotoxicity. Target degradation was assessed using Western blot analysis to examine HDAC6 and HDAC10 degradation, determine DC_{50} values, monitor time-dependent protein recovery, assess selectivity over other HDAC subtypes, evaluate effects on downstream substrates, elucidate the degradation mechanism, and to identify neosubstrate degradation. In addition, proteomics experiments were conducted to further confirm the degradation selectivity profiles. Finally, the effects of the lead compound on cell cycle arrest, autophagy, and cell migration were investigated.

Chapter 3 describes the discovery of HDAC8-specific PROTACs. As a member of class I HDACs, HDAC8 exhibits distinct biological roles and less homology with other class I HDACs and is known to play a crucial role in diverse biological processes, particularly in oncology. These features highlight the need for new PROTACs to achieve HDAC8-selective degradation.

This project aimed to develop selective HDAC8 degraders, addressing the moderate potency and limited selectivity observed in previously reported HDAC8 PROTACs. To achieve this goal, the selective HDAC8 ligand PCI-34051 was employed as the warhead, CRBN ligands were used as E3 recruiters, and flexible linkers were incorporated into the design. The PROTACs were synthesized and characterized, followed by evaluation of target engagement, physicochemical properties, and cytotoxicity. Additionally, degradation properties were examined using Western blot analysis, assessing HDAC8 degradation efficiency, DC_{50} values, selectivity over other HDAC subtypes, effects on downstream substrates, degradation mechanism, neosubstrates degradation, and long-term degradation stability. Proteomics experiments were further performed to confirm target degradation. Moreover, hit compounds were subsequently selected for further investigation of their anti-cancer potential.

Chapter 4 explores the development of HDAC degraders by the recruitment of the damage-specific DNA binding protein 1 (DDB1), a substrate adaptor within the CUL4-DDB1-RBX1 E3 ubiquitin ligase complex. In contrast to most reported HDAC PROTACs that employ well-established E3 ligases such as CRBN or VHL, this project investigates DDB1 as a novel ligase complex-recruitment element. By designing and synthesizing molecules that merge the pharmacophores of DDB1 recruiters and HDAC ligands, this work aims to expand the E3 ligase complex used in HDAC degraders, potentially improving degradation efficiency and isoform selectivity within the HDAC family. In this project, both reported covalent and non-covalent DDB1 recruiters were employed, together with vorinostat as the HDAC-binding moiety, to generate the HDAC degraders. Subsequently, HDAC subtype degradation was investigated for the synthesized compounds, followed by cell viability and HDAC enzyme inhibition assays. Additionally, nanoDSF DDB1 binding assays were also performed. Furthermore, the lead compound was investigated to determine its DC_{50} value, assess its effects on downstream substrates, elucidate its degradation mechanism, and evaluate its ability to induce apoptosis.

2 Development and characterization of the first selective class IIb histone deacetylase degrader

Shiyang Zhai, Irina Honin, Linda Schäker-Hübner, Maria Hanl, Lukas Jacobi, Finn Dressler, Dominika Ewa Pieńkowska, Philipp König, Jan Gerhartz, Rabea Voget, Gerd Bendas, Michael Gütschow, Felix Meissner, Bjoern B. Burckhardt, Radosław P. Nowak, Christian Steinebach, Finn K. Hansen.

J. Med. Chem. **2025**, 68, 13, 13793–13821.

https://doi.org/10.1021/acs.jmedchem.5c00674

Refer to Appendix II for the full text of the publication and supplementary information.

2.1 Publication Summary

Histone deacetylases (HDACs) regulate the acetylation status of histone and non-histone proteins, thereby influencing diverse processes such as gene transcription, protein stability, autophagy, and cell motility.[188] Within this family, the class IIb isoforms HDAC6 and HDAC10 share a highly similar structural organization, each containing two deacetylase domains and both are predominantly localized in the cytoplasm, where they act on non-histone substrates.[28, 189] HDAC6 is best known for deacetylating α-tubulin, regulating aggresome-mediated clearance of misfolded proteins, facilitating stress granule formation, and modulating cell migration and immune responses.[27] In contrast, HDAC10 is associated with autophagic flux, particularly lysosome-mediated autophagy, DNA damage repair, cell survival under stress, and the development of resistance to chemotherapy.[30, 190] Despite their structural similarity, these enzymes play distinct yet complementary roles in cancer-related pathways, making them both attractive therapeutic targets. In recent years, various potent and selective HDAC6 degraders have been developed using the PROTAC technology.[107] However, these efforts have focused solely on HDAC6, ignoring the potential impact on HDAC10 and failing to exploit the high degree of structural homology between the two enzymes to design dual-target degraders. The lack of chemical tools capable of simultaneously and selectively degrading both proteins,

together with this combination of structural and functional relationships, motivated the development of the first dual HDAC6/10 degraders to enable a comprehensive exploration of class IIb HDAC biology.

To achieve this, the design strategy began with the dual HDAC6/10 inhibitor tubastatin A, chosen due to its potency, available crystal structures, and ability to bind to both proteins. Molecular docking indicated that the tertiary amine in the tricyclic cap could serve as an optimal linker attachment point. Consequently, two warhead types, tubastatin A and a bicyclic derivative with higher HDAC10 selectivity, were coupled to cereblon (CRBN) ligands (either pomalidomide or a phenylglutarimide) *via* flexible alkyl linkers. A set of six initial degraders (**AP1**–**AP6**) was synthesized, along with follow-up analogs featuring rigid linkers or a fluorinated warhead (**AP7**–**AP10**) to explore structure–degradation relationships.

Subsequently, in biochemical assays, **AP1**–**AP6** inhibited HDAC6 and HDAC10 at low nanomolar IC_{50} values and showed micromolar-range CRBN engagement in NanoBRET assays. Physicochemical profiling revealed moderate lipophilicity, high polar surface area, and strong plasma protein binding, which is typical for PROTACs. Importantly, plasma stability studies identified **AP1** as the most stable compound, comparable to tubastatin A's stability.

In the next phase, Western blot analyses of MM.1S cell lysates demonstrated that **AP1**, **AP3**, **AP4**, and **AP6** robustly degraded both HDAC6 and HDAC10, with **AP1** achieving DC_{50} values of 13 nM and 29 nM respectively, no observable "hook effect," and no degradation of other HDAC isoforms (HDAC1, HDAC4, HDAC7, and HDAC8). Cellular target engagement studies showed that **AP1** treatment led to a marked increase in acetylated α-tubulin, a direct substrate of HDAC6, while levels of acetylated histone H3, primarily deacetylated by class I HDACs, remained unchanged. These results confirm the selectivity at the functional level. Furthermore, mechanistic rescue experiments with competing ligands (tubastatin A and pomalidomide), the non-degrading control **AP1-N**, the NEDD8-activating enzyme inhibitor MLN4924, and the proteasome inhibitor MG132, confirmed that **AP1** acts through CRBN binding and HDAC6/10 target engagement, as well as *via* neddylation- and proteasome-dependent degradation. Wash-out experiments showed sustained degradation for at least eight hours after compound removal.

To deepen the SAR understanding, analogs **AP7**–**AP10** were examined. **AP7** and **AP8** incorporated rigid linkers, which maintained potent HDAC6/10 degradation but also caused notable off-target HDAC8 depletion, indicating reduced selectivity. In the case of **AP9** and **AP10**, the basic nitrogen in the cap group was replaced by an amide linkage. This modification reduced the HDAC10 degradation while retaining HDAC6 activity, and also prevented the degradation of HDAC8. Moreover, fluorination of the warhead in **AP10** emerged as a potentially effective strategy for achieving HDAC6 preference. This comparison identified a flexible linker with a basic nitrogen anchor, as realized in **AP1**, as the best combination for balancing potency and selectivity for both class IIb enzymes.

To confirm the selectivity on a proteome-wide scale, quantitative proteomics in MM.1S and MOLT-4 cells revealed that **AP1** did not affect the protein levels of the other identified isoforms ((HDAC1-4, HDAC7, 8), but caused degradation of known CRBN neosubstrates (IKZF1, IKZF3, ZFP91, RAB28), consistent with the subsequent Western blot experiments investigating the degradation of IKZF1, IKZF3, and GSPT1. In contrast, phenylglutarimide-based analogs did not affect these neosubstrates in Western blot analyses. Moreover, additional immunoblot analyses verified that **AP1**-mediated neosubstrate degradation occurs *via* CRBN engagement rather than HDAC binding.

In terms of functional assays in MM.1S cells, **AP1** and related degraders produced minimal effects on proliferation despite maintaining HDAC6/10 knockdown for 72 hours, indicating that the absence of antiproliferative activity is not a result of instability of the degraders. Furthermore, additional studies revealed that **AP1** treatment significantly prolonged the G1-phase of the cell cycle, but had no measurable impact on the autophagy markers LC3-I/II or p62. In wound-healing assays using MDA-MB-231 breast cancer cells, **AP1** significantly impaired cell migration, whereas tubastatin A had no such effect.

In parallel, **AP1**–**AP6** were tested in MCF-7 breast cancer cells. Western blot analysis showed that **AP1**, **AP3**, **AP4**, and **AP6** effectively degraded both HDAC6 and HDAC10, whereas **AP2** and **AP5** were less active. Consistent with results in MM.1S cells, all six compounds exhibited low or negligible cytotoxicity, indicating that dual HDAC6/10 degradation does not affect cell viability in this solid tumor model.

In conclusion, by exploring different warhead, linker, and E3 ligand combinations, **AP1** was established as the first-in-class, highly selective, dual HDAC6/10 degrader. It combines nanomolar potency and strong class IIb selectivity with high plasma stability and an absence of off-target HDAC degradation. In addition, **AP1** demonstrated cellular effects on cell cycle and migration. Overall, **AP1** is a valuable chemical biology tool for investigating the function of class IIb HDACs, and represents a promising starting point for developing new therapeutic modalities that target HDAC6 and HDAC10.

2.2 Author Contribution

All numbers refer to the figure and table numbering within the publication. In this project, the conceptualization was carried out jointly by my supervisor and me. During the project, I performed the molecular docking analyses (Figure 2), and was responsible for the design, synthesis, and structural characterization of all the compounds (Figures 3, Schemes 1-2 and S1). In addition, I conducted all immunoblot experiments and data analyses presented in the paper (Figures 5-9, 10C, S1, S3, S5-S6, S8, and Table 2). Furthermore, I carried out the cell viability assays (Table S1 and Figure S4) and proteomics data analyses (Figure 10A-10B and S2). Finally, I prepared the original draft of both the main manuscript and the supplementary information.

3 Discovery of histone deacetylase 8 (HDAC8)-specific proteolysis-targeting chimeras with anti-cancer activity against hematological malignancies

Shiyang Zhai, Marie Kemkes, Cindy-Esther Kponomaizoun, Jan Gerhartz, Felix Feller, Jia-Wey Tu, Dominika Ewa Pieńkowska, Julian-Schliehe Diecks, Ina Dressel, Michael Gütschow, Radosław P. Nowak, Christian Steinebach, Sanil Bhatia, Finn K. Hansen.

J. Med. Chem. **2026**, 69, 2, 918-943.

https://doi.org/10.1021/acs.jmedchem.5c00939

Refer to Appendix III for the full text of the publication and supplementary information.

3.1 Publication Summary

Histone deacetylase 8 (HDAC8) is a class I zinc-dependent HDAC localized in both the nucleus and cytoplasm. It plays critical roles in regulating non-histone proteins such as SMC3.[191, 192] Beyond its enzymatic activity, HDAC8 functions as a scaffolding protein and interacts with transcription factors like STAT3, thereby influencing diverse cellular processes.[193] HDAC8 is implicated in hematological malignancies and solid tumors, with overexpression linked to leukemic stem cell maintenance and cancer progression.[192, 194] Existing HDAC8 inhibitors primarily target the catalytic function with limited selectivity,[195] highlighting the need for new strategies that eliminate both enzymatic and scaffolding functions.

This project aimed at the development of two series of CRBN-recruiting PROTACs to achieve selective HDAC8 degradation, using the selective inhibitor PCI-34051 as the warhead. Structural analysis identified the 4-methoxybenzyl group of PCI-34051 as solvent-exposed. Consequently, the *para*-position on the phenyl ring was selected for the linker attachment. Two classes of CRBN ligands – IMiD-based (pomalidomide or thalidomide) and phenylglutarimide (PG)-based – were connected to PCI-34051 *via* flexible alkyl and PEG linkers. Ten PROTACs (**BP1–BP5**, IMiD-based; **BP6–BP10**, PG-based) were synthesized utilizing either Cu(I)-catalyzed azide-alkyne cycloadditions or amide coupling reactions, followed by removing the

respective protecting groups to release the final compounds bearing a hydroxamic acid warhead as ZBG.

In vitro assays confirmed sub-micromolar HDAC8 inhibition for most compounds and verified CRBN engagement and cell permeability. Physicochemical profiling indicated generally higher lipophilicity for the IMiD-based PROTACs, compared to the PG-derived analogs. Plasma protein binding was generally high, with **BP1** and **BP6** slightly lower, presumably due to the incorporation of PEG linkers.

The subsequent functional evaluation in MM.1S cells identified **BP1** and **BP6** as the most potent HDAC8 degraders, achieving DC_{50} values of 20 nM and 81 nM, respectively, combined with high maximal degradation values. Further investigations showed that the IMiD-based PROTAC **BP1** induced degradation of CRBN neosubstrates such as IKZF1 and IKZF3, leading to potent cytotoxicity in MM.1S and HL60 cells, while the PG-based analog **BP6** displayed minimal cytotoxicity and no neosubstrate degradation. Rescue experiments confirmed that HDAC8 degradation was depended on HDAC8 and CRBN binding, as well as an active ubiquitin-proteasome system. Ternary complex modeling and TR-FRET assays validated the formation of productive HDAC8-PROTAC-CRBN complexes.

Selectivity profiling by quantitative proteomics and immunoblotting confirmed selective HDAC8 degradation without affecting other HDAC isoforms, including HDAC3. Both **BP1** and **BP6** increased the acetylation of the HDAC8 substrate SMC3 without affecting histone H3 or α-tubulin, confirming selective inactivation of HDAC8 enzymatic activity. Additional studies demonstrated durable HDAC8 degradation over 72 hours and effective activity in MDA-MB-231 breast cancer cells.

Furthermore, high-throughput screening of drug combinations revealed that pretreatment with **BP6** enhanced the sensitivity of leukemia cells to the mitogen-activated protein kinase (MEK) inhibitor cobimetinib. This treatment also stabilized p53 and significantly increased apoptosis when combined with the MDM2 antagonist idasanutlin.

In conclusion, two sets of selective HDAC8 PROTACs were developed. The IMiD-based **BP1** functions as a cytotoxic degrader that induces neosubstrate degradation, whereas the PG-based

BP6 acts as a selective and chemically stable degrader capable of modulating p53-dependent pathways, underscoring its potential for combinatorial therapeutic applications in leukemia.

3.2 Author Contribution

All numbers are referred to the numeration within the publication. In this project, the conceptualization was carried out jointly by my supervisor and me. During the project, I performed the molecular modeling analyses (Figures 2, 6A, S1, and S7A), and was responsible for the design, synthesis, and structural characterization of all compounds (Schemes 1-2, S1, and Figure 3). In addition, I conducted the immunoblot experiments and data analyses presented in Figures 4C-4D, Figure 5, and Figure S3. Furthermore, I carried out the proteomics data analyses (Figures 4E-4F). Finally, I prepared the original draft of both the main manuscript and the supplementary information.

4 Targeted histone deacetylase degradation via chemical induced proximity by direct recruitment of the CUL4 complex adaptor protein DDB1

Shiyang Zhai, Nicola Willemsen, Tao Sun, Mateo Malenica, Shixin Deng, Matthias Geyer, Finn K. Hansen

ACS Med. Chem. Lett. **2025**, 16, 2070–2077.

https://doi.org/10.1021/acsmedchemlett.5c00506

Refer to Appendix IV for the full text of the publication and supplementary information.

4.1 Publication Summary

Histone deacetylases (HDACs) are key epigenetic regulators that remove acetyl groups from histone and non-histone proteins, thereby controlling transcription, DNA repair, cell cycle, apoptosis, and immunity. Aberrant HDAC activity is associated with cancer progression, which has motivated the development of HDAC inhibitors for treating cancer.[22, 196] Although several inhibitors are FDA-approved, their use is limited by toxicity, narrow indications, and lack of first-line approval.[197] Recently, targeted protein degradation has emerged as an alternative approach, mostly relying on PROTACs that recruit CRBN or VHL. In contrast, DDB1, a core adaptor of the CUL4 E3 ligase complex, has been less explored despite its central role in ubiquitination. This study aims to develop HDAC degraders that induce HDAC degradation through direct recruitment of DDB1, thereby representing an alternative approach to classical E3 ligase recruitment strategies.

To realize this concept, a molecular hybridization approach was used by merging the pharmacophores of a reported, non-covalent DDB1 ligand,[198] the covalent DDB1 binder MM-02-57,[199] and the HDAC inhibitor vorinostat to generate three compounds: **SZ-1**, **SZ-2**, and **SZ-3**. Synthetic efforts yielded both noncovalent (**SZ-1**) and covalent (**SZ-2**, **SZ-3**) degraders.

The biological evaluations revealed that **SZ-1** retained strong HDAC inhibition but lacked degradation and antiproliferative effects, likely due to poor cell penetration. In contrast, **SZ-2**

emerged as a potent degrader and treatment of MM.1S multiple myeloma cells with 10 μM of **SZ-2** almost completely eliminated HDAC1 ($D_{max,\ 24\ h}$ = 99%). The subsequent analysis of the concentration-dependent degradation of HDAC1 provided a $DC_{50,\ 24\ h}$ value of 2.55 μM. In addition, **SZ-2** treatment (10 μM) strongly reduced the HDAC2 level ($D_{max,\ 24\ h}$ = 90%) in MM.1S cells with minimal effect on other isoforms, while compound **SZ-3** showed weaker degradation potency. In MCF-7 cells, **SZ-2** selectively degraded HDAC1 with moderate efficiency ($D_{max,\ 24\ h}$ = 38%). In parallel, viability assays revealed that **SZ-2** inhibited both MM.1S and MCF-7 cell growth with low IC_{50} values (3.28 and 3.46 μM), outperforming its covalent warhead and achieving comparable antiproliferative activity as ricolinostat. Biochemical enzyme inhibition assays revealed moderate direct inhibition of HDAC1/6 by **SZ-2**. However, cellular assays showed increased acetylation of histone H3 and α-tubulin, which is consistent with the results of dual HDAC1/2 degradation and HDAC6 inhibition.

Mechanistic experiments were performed to further characterize the mode of action of **SZ-2**. NanoDSF assays were carried out to investigate the thermal stability of DDB1ΔB in the presence and absence of **SZ-2**. These assays demonstrated thermal shifts of DDB1ΔB upon **SZ-2** treatment, indicating direct binding. A negative control (**SZ-2-N**), lacking the electrophilic chloroacetyl warhead, which is required for covalent binding, failed to induce HDAC1 degradation, confirming the importance of covalent DDB1 engagement. Functional assays demonstrated that **SZ-2** induced apoptosis in MM.1S cells at levels similar to ricolinostat and greater than its covalent warhead control, though less potent than vorinostat. Altogether, **SZ-2** acts as a bifunctional degrader that binds to DDB1, achieves selective degradation of HDAC1/2, promotes acetylation of histone and tubulin substrates, suppresses cancer cell proliferation, and induces cell apoptosis.

In conclusion, **SZ-2** represents the first example of a DDB1-recruiting HDAC degrader and highlights direct DDB1 recruitment as a viable alternative to CRBN/VHL-mediated degradation. By demonstrating selective knockdown of HDAC1/2 and potent anti-multiple myeloma activity, **SZ-2** expands the toolbox for HDAC degradation and offers a starting point for further optimization toward new anticancer agents.

4.2 Author Contribution

All numbers refer to the figure and table numbering within the publication. In this project, the conceptualization was carried out jointly by my supervisor and me. During the project, I designed, synthesized, and structurally characterized all compounds (Schemes 1-2 and S1-S2). In addition, I conducted all immunoblot experiments and data analyses presented in the paper (Figures 2, 4, S1-2, and the replicates provided in the supplementary information). Furthermore, I carried out the cell viability assays (Table 1 and Figure S3) and apoptosis induction analysis (Figure 5). Finally, I prepared the original draft of both the main manuscript and the supplementary information.

5 Summary

Selective degradation of individual HDAC isoforms has become an important strategy for improving therapeutic specificity and reducing unwanted side effects associated with unselective HDAC inhibition. Unlike selective inhibitors, isoform-targeted PROTACs enable more precise control of the enzymatic and/or non-enzymatic functions of HDACs, enabling targeted intervention in disease-relevant pathways while minimizing side effects. This selectivity can be achieved by using isoform-preferential warheads, the careful selection of E3 ligase recruiters, and the optimization of linker length, composition, and flexibility. In some cases, switching from traditional hydroxamic acid scaffolds to alkyl hydrazide or *o*-aminoanilide groups has markedly improved selectivity. Additionally, engaging DDB1 within the CUL4-DDB1 complex, rather than relying on conventional E3 ligases such as CRBN or VHL, may further improve degradation efficiency and target selectivity. As our understanding of the biology of HDAC isoforms and the design principles of PROTACs continues to expand, selective HDAC degraders show great promise as therapeutic agents and chemical biology tools for dissecting HDAC-specific functions in complex diseases.

The first project (chapter 2) focused on the design and characterization of the first selective dual HDAC6/10-selective degraders (Figure 12). Although the class IIb isoforms HDAC6 and HDAC10 share high structural homology, they have distinct roles in cancer biology. All existing PROTACs target HDAC6 exclusively, leaving the biology of HDAC10 unexplored. This work aimed to bridge the gap by creating degraders capable of simultaneously and selectively targeting both enzymes.

Starting from the dual HDAC6/10 inhibitor tubastatin A, two warhead types were coupled with CRBN ligands *via* alkyl linkers, resulting in the generation of **AP1**–**AP6**. In addition, **AP7**–**AP10** were designed to explore the effects of rigid linkers and warhead modifications. In biochemical assays, **AP1** inhibited HDAC6 and HDAC10 with low nanomolar IC_{50} values, demonstrated micromolar-range CRBN binding affinity in NanoBRET assays, and exhibited the highest plasma stability among all candidates. In MM.1S cells, **AP1** degraded HDAC6 and HDAC10 with $DC_{50,\,24\,h}$ values of 13 nM and 29 nM, respectively, showed no “hook effect”, and avoided degradation of other HDAC isoforms including HDAC1, HDAC4, HDAC7, and

HDAC8. Functionally, **AP1** increased the levels of acetylated α-tubulin without altering histone H3 acetylation, thereby confirming the absence of class I inhibition or degradation. Mechanistic rescue experiments with competitive ligands, a negative control analog, the NEDD8-activating enzyme inhibitor MLN4924, and the proteasome inhibitor MG132 demonstrated that degradation required CRBN engagement, target binding, neddylation, and proteasome function. Wash-out experiments showed sustained HDAC6/10 depletion for at least 8 h after compound removal. Quantitative proteomics confirmed that **AP1** has a narrow target profile, limited to HDAC6/10 and several known CRBN neosubstrates, including IKZF1, IKZF3, ZFP91, and RAB28. In contrast, phenylglutarimide-based analogs lack these effects on neosubstrates, as evidenced by immunoblot analysis. In functional assays, **AP1** induced G1-phase cell cycle arrest in MM.1S cells and significantly impaired the migration of MDA-MB-231 breast cancer cells. However, it caused minimal effects on proliferation in MM.1S and MCF-7 cells, despite sustained target degradation. Moreover, **AP1** had no measurable impact on the autophagy markers LC3-I/II or p62.

In conclusion, by varying warhead, linker, and E3 ligand combinations, this work identified **AP1** as the first-in-class, highly selective dual HDAC6/10 degrader. It combines nanomolar potency, durable and class IIb-selective target removal, and measurable phenotypic effects without intrinsic cytotoxicity. These attributes make **AP1** a valuable probe for studying class IIb HDAC biology and a promising starting point for the development of new therapeutic modalities.

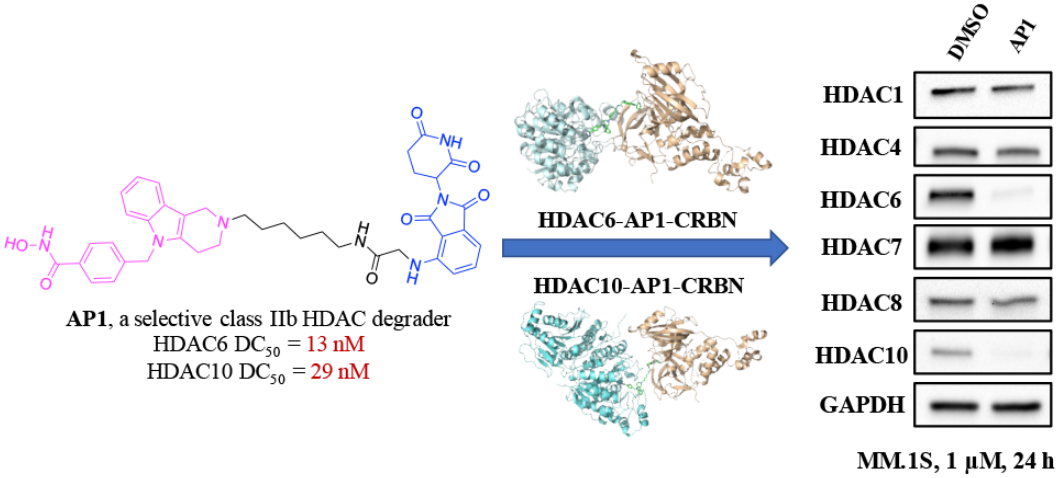

Figure 12. Design and characterization of the first dual HDAC6/10-selective degrader. Figure reprinted with the permission of American Chemical Society (License number: 6134121485864). Copyright © 2025, American Chemical Society.

The second project (chapter 3) aimed at the development of potent and selective HDAC8 degraders (Figure 13). HDAC8 is a member of class I and is localized in both the nucleus and the cytoplasm. It regulates non-histone substrates and functions as a scaffolding protein. Its overexpression in hematological and solid malignancies contributes to cancer progression, while current inhibitors offer limited selectivity and target only the catalytic activity of HDAC8. To overcome these limitations, two series of CRBN-recruiting PROTACs were designed using PCI-34051 as the HDAC8 ligand. Molecular modeling studies suggested that the *para*-position of the phenyl ring could serve as a suitable linker attachment point. This led to the design and synthesis of IMiD-based (**BP1–BP5**) and phenylglutarimide (PG)-based (**BP6–BP10**) PROTACs containing different alkyl and PEG linkers.

Most compounds showed strong HDAC8 inhibition, efficient CRBN binding, and good cell permeability. Western blot experiments using MM.1S cell lysates identified **BP1** and **BP6** as potent degraders with DC_{50} values of 20 nM and 81 nM, respectively. **BP1** induced the degradation of the CRBN neosubstrates IKZF1/3 and displayed cytotoxicity, whereas **BP6** did not affect neosubstrates and remained non-cytotoxic. Rescue and TR-FRET experiments confirmed that degradation relied on the target engagement of HDAC8 and CRBN, as well as on proteasomal activity. Quantitative proteomics and immunoblotting experiments confirmed the high selectivity for HDAC8 without affecting other HDAC isoforms, including HDAC3. Moreover, **BP6**-mediated HDAC8 degradation led to p53 stabilization, thereby increasing the sensitivity of leukemia cells to the MEK inhibitor cobimetinib and the MDM2 antagonist idasanutlin. In contrast, **BP1** exerted broader cytotoxic effects due to neosubstrate depletion.

Taken together, two potent but functionally distinct HDAC8 degraders were developed in this project: the IMiD-based **BP1** functions as a cytotoxic degrader, whereas the PG-based **BP6** acts as a selective, non-cytotoxic agent that stabilizes p53 and potentiates combination therapies in leukemia.

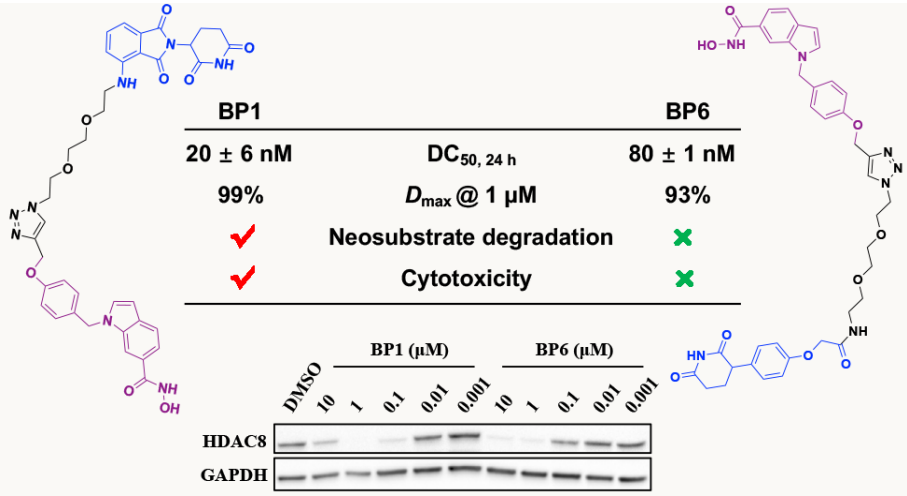

Figure 13. Discovery of selective HDAC8 degrader with anti-cancer activity. Figure reprinted with the permission of American Chemical Society (License number: 6181440411995). Copyright © 2026, American Chemical Society.

The third project (chapter 4) focused on the targeted HDACs degradation *via* direct recruitment of the CUL4 complex adaptor protein DDB1 using linker-less degraders (Figure 14).

Using a hybrid design approach, the HDAC inhibitor vorinostat was fused with either non-covalent or covalent DDB1 binders, yielding three candidates: **SZ-1** (non-covalent), **SZ-2** (covalent, chloroacetyl warhead), and **SZ-3** (covalent, bromoacetyl warhead). **SZ-1** displayed HDAC inhibition but lacked degradation activity. **SZ-2** emerged as the most effective HDAC degrader, while **SZ-3** showed weaker degradation potency. In MM.1S cells, **SZ-2** nearly completely eliminated HDAC1 ($D_{max,\ 24\ h}$ = 99%, $DC_{50,\ 24\ h}$ = 2.55 μM) and strongly reduced HDAC2 levels ($D_{max,\ 24\ h}$ = 90%) with insignificant effects on other isoforms. In MCF-7 cells, **SZ-2** partially degraded HDAC1 ($D_{max,\ 24\ h}$ = 38%). Additionally, **SZ-2** suppressed proliferation in both cell lines (IC_{50} (MM.1S) = 3.28 μM; IC_{50} (MCF-7) = 3.46 μM), increased the acetylation levels of histone H3 and α-tubulin, and induced apoptosis in MM.1S cells. Further mechanistic studies confirmed that the covalent chloroacetyl warhead is essential for the activity of **SZ-2**.

In conclusion, **SZ-2** was identified as the first HDAC degrader that directly recruits DDB1. Its capacity to selectively degrade HDAC1/2 and exert strong anti-myeloma effects highlights

direct DDB1 recruitment as a feasible and effective alternative to CRBN- and VHL-based PROTAC strategies, thus providing a promising basis for future optimization studies.

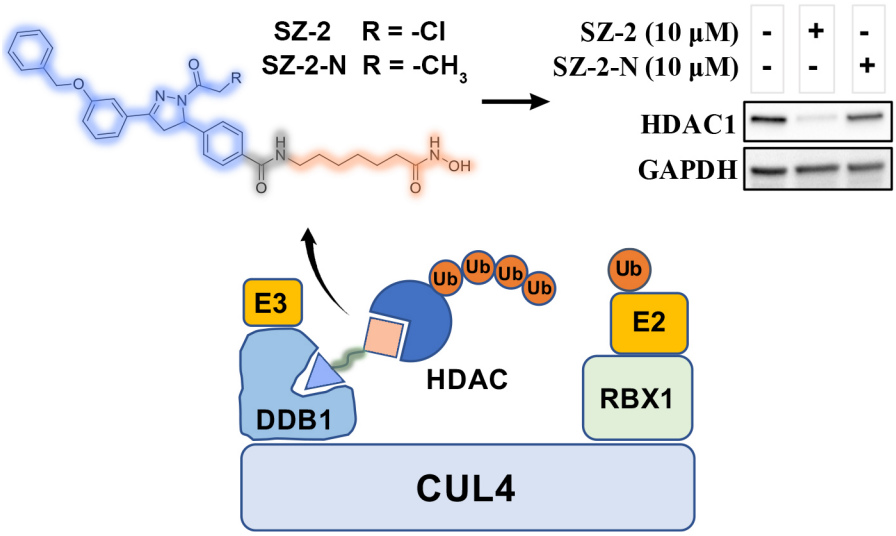

Figure 14. Covalent compound **SZ-2** induces HDAC1 degradation by directly recruiting DDB1. Figure reprinted with the permission of American Chemical Society (License number: 6134130293253). Copyright © 2025, American Chemical Society.

Collectively, these projects advanced the field of targeted epigenetic regulation by developing selective PROTAC degraders for class IIb isoforms and HDAC8, as well as by pioneering the use of the DDB1-CUL4 ubiquitin ligase complex for HDAC degradation. The findings will provide important insights and practical frameworks for developing highly selective and efficient HDAC degraders with clinical relevance.

6 References

(1) Waddington, C. H. The epigenotype. 1942. *Int. J. Epidemiol.* **2012**, *41* (1), 10-13.

(2) Tronick, E.; Hunter, R. G. Waddington, Dynamic Systems, and Epigenetics. *Front. Behav. Neurosci.* **2016**, *10*, 107.

(3) Bird, A. Perceptions of epigenetics. *Nature* **2007**, *447* (7143), 396-398.

(4) Li, E. Chromatin modification and epigenetic reprogramming in mammalian development. *Nat. Rev. Genet.* **2002**, *3* (9), 662-673.

(5) Webster, A. K.; Phillips, P. C. Epigenetics and individuality: from concepts to causality across timescales. *Nat. Rev. Genet.* **2025**, *26* (6), 406-423.

(6) Yang, X. J.; Seto, E. HATs and HDACs: from structure, function and regulation to novel strategies for therapy and prevention. *Oncogene* **2007**, *26* (37), 5310-5318.

(7) Glozak, M. A.; Sengupta, N.; Zhang, X.; Seto, E. Acetylation and deacetylation of non-histone proteins. *Gene* **2005**, *363*, 15-23.

(8) Calao, M.; Burny, A.; Quivy, V.; Dekoninck, A.; Van Lint, C. A pervasive role of histone acetyltransferases and deacetylases in an NF-kappaB-signaling code. *Trends Biochem. Sci.* **2008**, *33* (7), 339-349.

(9) Kotwal, A.; Amere Subbarao, S. Hsp90 regulates HDAC3-dependent gene transcription while HDAC3 regulates the functions of Hsp90. *Cell. Signal.* **2020**, *76*, 109801.

(10) Rao, R.; Fiskus, W.; Ganguly, S.; Kambhampati, S.; Bhalla, K. N. HDAC inhibitors and chaperone function. *Adv. Cancer Res.* **2012**, *116*, 239-262.

(11) Luo, L.; Martin, S. C.; Parkington, J.; Cadena, S. M.; Zhu, J.; Ibebunjo, C.; Summermatter, S.; Londraville, N.; Patora-Komisarska, K.; Widler, L.; Zhai, H.; Trendelenburg, A. U.; Glass, D. J.; Shi, J. HDAC4 Controls Muscle Homeostasis through Deacetylation of Myosin Heavy Chain, PGC-1alpha, and Hsc70. *Cell Rep.* **2019**, *29* (3), 749-763 e712.

(12) Canettieri, G.; Morantte, I.; Guzmán, E.; Asahara, H.; Herzig, S.; Anderson, S. D.; Yates, J. R., 3rd; Montminy, M. Attenuation of a phosphorylation-dependent activator by an HDAC-PP1 complex. *Nat. Struct. Biol.* **2003**, *10* (3), 175-181.

(13) Chen, C. S.; Weng, S. C.; Tseng, P. H.; Lin, H. P.; Chen, C. S. Histone acetylation-independent effect of histone deacetylase inhibitors on Akt through the reshuffling of protein phosphatase 1 complexes. *J. Biol. Chem.* **2005**, *280* (46), 38879-38887.

(14) Zhang, Y.; Li, N.; Caron, C.; Matthias, G.; Hess, D.; Khochbin, S.; Matthias, P. HDAC-6 interacts with and deacetylates tubulin and microtubules in vivo. *EMBO J.* **2003**, *22* (5), 1168-1179.

(15) Balmik, A. A.; Chinnathambi, S. Inter-relationship of Histone Deacetylase-6 with Tau-cytoskeletal organization and remodeling. *Eur. J. Cell Biol.* **2022**, *101* (2), 151202.

(16) Sun, S.; Xu, Z.; He, L.; Shen, Y.; Yan, Y.; Lv, X.; Zhu, X.; Li, W.; Tian, W. Y.; Zheng, Y.; Lin, S.; Sun, Y.; Li, L. Metabolic regulation of cytoskeleton functions by HDAC6-catalyzed alpha-tubulin lactylation. *Nat. Commun.* **2024**, *15* (1), 8377.

(17) Raouf, Y. S. Targeting histone deacetylases: Emerging applications beyond cancer. *Drug Discov. Today* **2024**, *29* (9), 104094.

(18) Park, S. Y.; Kim, J. S. A short guide to histone deacetylases including recent progress on class II enzymes. *Exp. Mol. Med.* **2020**, *52* (2), 204-212.

(19) Yang, F. F.; Hu, T.; Liu, J. Q.; Yu, X. Q.; Ma, L. Y. Histone deacetylases (HDACs) as the promising immunotherapeutic targets for hematologic cancer treatment. *Eur. J. Med. Chem.* **2023**, *245* (Pt 2), 114920.
(20) Li, Y.; Seto, E. HDACs and HDAC Inhibitors in Cancer Development and Therapy. *Cold Spring Harb. Perspect. Med.* **2016**, *6* (10).
(21) Gregoretti, I. V.; Lee, Y. M.; Goodson, H. V. Molecular evolution of the histone deacetylase family: functional implications of phylogenetic analysis. *J. Mol. Biol.* **2004**, *338* (1), 17-31.
(22) Porter, N. J.; Christianson, D. W. Structure, mechanism, and inhibition of the zinc-dependent histone deacetylases. *Curr. Opin. Struct. Biol.* **2019**, *59*, 9-18.
(23) Reichert, N.; Choukrallah, M. A.; Matthias, P. Multiple roles of class I HDACs in proliferation, differentiation, and development. *Cell Mol. Life Sci.* **2012**, *69* (13), 2173-2187.
(24) Millard, C. J.; Watson, P. J.; Fairall, L.; Schwabe, J. W. R. Targeting Class I Histone Deacetylases in a "Complex" Environment. *Trends Pharmacol. Sci.* **2017**, *38* (4), 363-377.
(25) Wang, X.; Wang, Y.; Liu, S.; Zhang, Y.; Xu, K.; Ji, L.; Kornberg, R. D.; Zhang, H. Class I histone deacetylase complex: Structure and functional correlates. *Proc. Natl. Acad. Sci. U. S. A.* **2023**, *120* (30), e2307598120.
(26) Christianson, D. W. Chemical Versatility in Catalysis and Inhibition of the Class IIb Histone Deacetylases. *Acc. Chem. Res.* **2024**, *57* (8), 1135-1148.
(27) Kaur, S.; Rajoria, P.; Chopra, M. HDAC6: A unique HDAC family member as a cancer target. *Cell. Oncol. (Dordr.)* **2022**, *45* (5), 779-829.
(28) Hai, Y.; Shinsky, S. A.; Porter, N. J.; Christianson, D. W. Histone deacetylase 10 structure and molecular function as a polyamine deacetylase. *Nat. Commun.* **2017**, *8*, 15368.
(29) Tong, J. J.; Liu, J.; Bertos, N. R.; Yang, X. J. Identification of HDAC10, a novel class II human histone deacetylase containing a leucine-rich domain. *Nucleic Acids Res.* **2002**, *30* (5), 1114-1123.
(30) Cheng, F.; Zheng, B.; Wang, J.; Zhao, G.; Yao, Z.; Niu, Z.; He, W. Histone deacetylase 10, a potential epigenetic target for therapy. *Biosci. Rep.* **2021**, *41* (6).
(31) Oehme, I.; Linke, J. P.; Böck, B. C.; Milde, T.; Lodrini, M.; Hartenstein, B.; Wiegand, I.; Eckert, C.; Roth, W.; Kool, M.; Kaden, S.; Gröne, H. J.; Schulte, J. H.; Lindner, S.; Hamacher-Brady, A.; Brady, N. R.; Deubzer, H. E.; Witt, O. Histone deacetylase 10 promotes autophagy-mediated cell survival. *Proc. Natl. Acad. Sci. U. S. A.* **2013**, *110* (28), E2592-2601.
(32) Yuan, H.; Marmorstein, R. Structural basis for sirtuin activity and inhibition. *J. Biol. Chem.* **2012**, *287* (51), 42428-42435.
(33) Chen, B.; Zang, W.; Wang, J.; Huang, Y.; He, Y.; Yan, L.; Liu, J.; Zheng, W. The chemical biology of sirtuins. *Chem. Soc. Rev.* **2015**, *44* (15), 5246-5264.
(34) Villagra, A.; Cheng, F.; Wang, H. W.; Suarez, I.; Glozak, M.; Maurin, M.; Nguyen, D.; Wright, K. L.; Atadja, P. W.; Bhalla, K.; Pinilla-Ibarz, J.; Seto, E.; Sotomayor, E. M. The histone deacetylase HDAC11 regulates the expression of interleukin 10 and immune tolerance. *Nat. Immunol.* **2009**, *10* (1), 92-100.
(35) Chen, H.; Xie, C.; Chen, Q.; Zhuang, S. HDAC11, an emerging therapeutic target for metabolic disorders. *Front. Endocrinol. (Lausanne)* **2022**, *13*, 989305.

(36) Núñez-Álvarez, Y.; Suelves, M. HDAC11: a multifaceted histone deacetylase with proficient fatty deacylase activity and its roles in physiological processes. *FEBS J.* **2022**, *289* (10), 2771-2792.
(37) Liu, Y.; Tong, X.; Hu, W.; Chen, D. HDAC11: A novel target for improved cancer therapy. *Biomed. Pharmacother.* **2023**, *166*, 115418.
(38) Olawade, D. B.; Rashad, I.; Egbon, E.; Teke, J.; Ovsepian, S. V.; Boussios, S. Reversing Epigenetic Dysregulation in Neurodegenerative Diseases: Mechanistic and Therapeutic Considerations. *Int. J. Mol. Sci.* **2025**, *26* (10).
(39) Bose, C.; Hindle, A.; Smith, S. C.; Strickland, J.; Zhang, C.; Guzman, I.; Baker, A.; Ponomarev, I.; Manczak, M.; Shin, A. C.; Pal, R.; Singh, S. P.; Lawrence, J. J. Low-dose dietary vorinostat increases brain histone acetylation levels and reduces oxidative stress in an Alzheimer's disease mouse model. *J. Alzheimers Dis.* **2025**, 13872877251352107.
(40) Schäker-Hübner, L.; Toledano-Pinedo, M.; Eimermacher, S.; Krasniqi, V.; Porro-Pérez, A.; Tan, K.; Horn, G.; Stegen, P.; Elsinghorst, P. W.; Wille, T.; Pietsch, M.; Gütschow, M.; Marco-Contelles, J.; Hansen, F. K. Contilisant-Belinostat Hybrids: Polyfunctionalized Indole Derivatives as Multineurotarget Drugs for the Potential Treatment of Alzheimer's Disease. *ACS Pharmacol. Transl. Sci.* **2025**, *8* (3), 831-840.
(41) O'Mahony, A. G.; Mazzocchi, M.; Morris, A.; Morales-Prieto, N.; Guinane, C.; Wyatt, S. L.; Collins, L. M.; Sullivan, A. M.; O'Keeffe, G. W. The class-IIa HDAC inhibitor TMP269 promotes BMP-Smad signalling and is neuroprotective in in vitro and in vivo 6-hydroxydopamine models of Parkinson's disease. *Neuropharmacology* **2025**, *268*, 110319.
(42) Pham, K. Y.; Khanal, S.; Bohara, G.; Rimal, N.; Song, S. H.; Nguyen, T. T. K.; Hong, I. S.; Cho, J.; Kang, J. S.; Lee, S.; Choi, D. Y.; Yook, S. HDAC6 inhibitor-loaded brain-targeted nanocarrier-mediated neuroprotection in methamphetamine-driven Parkinson's disease. *Redox Biol.* **2025**, *79*, 103457.
(43) Reisbitzer, A.; Hollitzer, C.; Geraci, A.; Schaefer, J.; Burghaus, M.; Bruns, J.; Urban, J.; Kurz, T.; Krauß, S. Inhibition of class IIa HDACs reduces mutant HTT aggregation by affecting RNA stability. *Front. Mol. Neurosci.* **2025**, *18*, 1579194.
(44) Macabuag, N.; Esmieu, W.; Breccia, P.; Jarvis, R.; Blackaby, W.; Lazari, O.; Urbonas, L.; Eznarriaga, M.; Williams, R.; Strijbosch, A.; Van de Bospoort, R.; Matthews, K.; Clissold, C.; Ladduwahetty, T.; Vater, H.; Heaphy, P.; Stafford, D. G.; Wang, H. J.; Mangette, J. E.; McAllister, G.; Beaumont, V.; Vogt, T. F.; Wilkinson, H. A.; Doherty, E. M.; Dominguez, C. Developing HDAC4-Selective Protein Degraders To Investigate the Role of HDAC4 in Huntington's Disease Pathology. *J. Med. Chem.* **2022**, *65* (18), 12445-12459.
(45) Pai, P.; D'Mello, R. S.; Brahme, O. M.; Gogineni, Y. V.; Shetty, M. G.; Sundara, B. K. Unlocking cardiac health: exploring the role of class I HDACs in cardiovascular diseases. *Mol. Cell Biochem.* **2025**.
(46) Zhang, L. Y.; Wang, Y. Y.; Wen, R.; Zhang, T. N.; Yang, N. Role of Histone Deacetylase and Inhibitors in Cardiovascular Diseases. *Cell Prolif.* **2025**, e70077.
(47) Theodoropoulou, M. A.; Mantzourani, C.; Kokotos, G. Histone Deacetylase (HDAC) Inhibitors as a Novel Therapeutic Option Against Fibrotic and Inflammatory Diseases. *Biomolecules* **2024**, *14* (12).

(48) Yue, K.; Sun, S.; Jia, G.; Qin, M.; Hou, X.; Chou, C. J.; Huang, C.; Li, X. First-in-Class Hydrazide-Based HDAC6 Selective Inhibitor with Potent Oral Anti-Inflammatory Activity by Attenuating NLRP3 Inflammasome Activation. *J. Med. Chem.* **2022**, *65* (18), 12140-12162.
(49) Duan, X.; Xing, Z.; Qiao, L.; Qin, S.; Zhao, X.; Gong, Y.; Li, X. The role of histone post-translational modifications in cancer and cancer immunity: functions, mechanisms and therapeutic implications. *Front. Immunol.* **2024**, *15*, 1495221.
(50) Liang, T.; Wang, F.; Elhassan, R. M.; Cheng, Y.; Tang, X.; Chen, W.; Fang, H.; Hou, X. Targeting histone deacetylases for cancer therapy: Trends and challenges. *Acta Pharm. Sin. B* **2023**, *13* (6), 2425-2463.
(51) Shen, C.; Li, M.; Duan, Y.; Jiang, X.; Hou, X.; Xue, F.; Zhang, Y.; Luo, Y. HDAC inhibitors enhance the anti-tumor effect of immunotherapies in hepatocellular carcinoma. *Front. Immunol.* **2023**, *14*, 1170207.
(52) Fan, Y.; Ji, X.; Yuan, K.; Wu, Q.; Lou, M. HDAC1 Mediates Immunosuppression of the Tumor Microenvironment in Non-Small Cell Lung Cancer. *J. Inflamm. Res.* **2025**, *18*, 3333-3347.
(53) Gao, J.; Zhang, H.; Liu, S.; Guo, L.; Zeng, X.; Yuan, W.; Li, T.; He, S. HDAC1 promotes basal autophagy and proliferation of colorectal cancer cells by mediating ATG16L1 deacetylation. *Biochem. Biophys. Res. Commun.* **2024**, *735*, 150667.
(54) Smalley, J. P.; Baker, I. M.; Pytel, W. A.; Lin, L. Y.; Bowman, K. J.; Schwabe, J. W. R.; Cowley, S. M.; Hodgkinson, J. T. Optimization of Class I Histone Deacetylase PROTACs Reveals that HDAC1/2 Degradation is Critical to Induce Apoptosis and Cell Arrest in Cancer Cells. *J. Med. Chem.* **2022**, *65* (7), 5642-5659.
(55) Eom, M.; Oh, S. S.; Lkhagvadorj, S.; Han, A.; Park, K. H. HDAC1 Expression in Invasive Ductal Carcinoma of the Breast and Its Value as a Good Prognostic Factor. *Korean J. Pathol.* **2012**, *46* (4), 311-317.
(56) Jin, J.; Iakova, P.; Jiang, Y.; Lewis, K.; Sullivan, E.; Jawanmardi, N.; Donehower, L.; Timchenko, L.; Timchenko, N. A. Transcriptional and translational regulation of C/EBPbeta-HDAC1 protein complexes controls different levels of p53, SIRT1, and PGC1alpha proteins at the early and late stages of liver cancer. *J. Biol. Chem.* **2013**, *288* (20), 14451-14462.
(57) Jo, H.; Shim, K.; Kim, H. U.; Jung, H. S.; Jeoung, D. HDAC2 as a target for developing anti-cancer drugs. *Comput. Struct. Biotechnol. J.* **2023**, *21*, 2048-2057.
(58) Chen, Z.; Hong, W.; Li, B.; He, D.; Ren, Z.; Cai, M.; Cheng, Y.; Liu, J.; Xu, E.; Du, Y.; Dong, Y.; Cai, S.; Shi, Q.; Qi, Z.; Zhong, Y. HDAC2 promotes colorectal tumorigenesis by triggering dysregulation of lipid metabolism through YAP1. *Cell. Signal.* **2025**, *128*, 111627.
(59) Ferrero, G.; Cardamone, M. D.; Luca, F.; Bourk, E.; Ricci, L.; Liu, W.; Gao, Y.; Burrone, G.; Muhammad, A.; Chan, S.; Smith, E.; Fan, T. C.; Cutrupi, S.; Garcia-Bassets, I.; De Bortoli, M.; Rosenfeld, M. G.; Perissi, V. Nonproteolytic ubiquitination regulates chromatin occupancy by the NCoR/SMRT/HDAC3 corepressor complex in MCF-7 breast cancer cells. *Proc. Natl. Acad. Sci. U. S. A.* **2025**, *122* (18), e2502805122.
(60) Long, J.; Fang, W. Y.; Chang, L.; Gao, W. H.; Shen, Y.; Jia, M. Y.; Zhang, Y. X.; Wang, Y.; Dou, H. B.; Zhang, W. J.; Zhu, J.; Liang, A. B.; Li, J. M.; Hu, J. Targeting HDAC3, a new partner protein of AKT in the reversal of chemoresistance in acute myeloid leukemia via DNA damage response. *Leukemia* **2017**, *31* (12), 2761-2770.

(61) Dasgupta, T.; Antony, J.; Braithwaite, A. W.; Horsfield, J. A. HDAC8 Inhibition Blocks SMC3 Deacetylation and Delays Cell Cycle Progression without Affecting Cohesin-dependent Transcription in MCF7 Cancer Cells. *J. Biol. Chem.* **2016**, *291* (24), 12761-12770.
(62) Sang, C.; Li, X.; Liu, J.; Chen, Z.; Xia, M.; Yu, M.; Yu, W. Reversible acetylation of HDAC8 regulates cell cycle. *EMBO Rep.* **2024**, *25* (9), 3925-3943.
(63) Oehme, I.; Deubzer, H. E.; Wegener, D.; Pickert, D.; Linke, J. P.; Hero, B.; Kopp-Schneider, A.; Westermann, F.; Ulrich, S. M.; von Deimling, A.; Fischer, M.; Witt, O. Histone deacetylase 8 in neuroblastoma tumorigenesis. *Clin. Cancer Res.* **2009**, *15* (1), 91-99.
(64) Mathias, R. A.; Guise, A. J.; Cristea, I. M. Post-translational modifications regulate class IIa histone deacetylase (HDAC) function in health and disease. *Mol. Cell Proteomics* **2015**, *14* (3), 456-470.
(65) Luo, Z.; Qing, X.; Benda, C.; Huang, Z.; Zhang, M.; Huang, Y.; Zhang, H.; Wang, L.; Lai, Y.; Ward, C.; Volpe, G.; Zhong, X.; Qin, B.; Zhuang, Q.; Esteban, M. A.; Li, W. Nuclear-cytoplasmic shuttling of class IIa histone deacetylases regulates somatic cell reprogramming. *Cell Regen.* **2019**, *8* (1), 21-29.
(66) Guttzeit, S.; Backs, J. Post-translational modifications talk and crosstalk to class IIa histone deacetylases. *J. Mol. Cell. Cardiol.* **2022**, *162*, 53-61.
(67) Cuttini, E.; Goi, C.; Pellarin, E.; Vida, R.; Brancolini, C. HDAC4 in cancer: A multitasking platform to drive not only epigenetic modifications. *Front. Mol. Biosci.* **2023**, *10*, 1116660.
(68) Wang, T.; Lu, Z.; Han, T.; Wang, Y.; Gan, M.; Wang, J. B. Deacetylation of Glutaminase by HDAC4 contributes to Lung Cancer Tumorigenesis. *Int. J. Biol. Sci.* **2022**, *18* (11), 4452-4465.
(69) Yang, J.; Gong, C.; Ke, Q.; Fang, Z.; Chen, X.; Ye, M.; Xu, X. Insights Into the Function and Clinical Application of HDAC5 in Cancer Management. *Front. Oncol.* **2021**, *11*, 661620.
(70) Cao, C.; Vasilatos, S. N.; Bhargava, R.; Fine, J. L.; Oesterreich, S.; Davidson, N. E.; Huang, Y. Functional interaction of histone deacetylase 5 (HDAC5) and lysine-specific demethylase 1 (LSD1) promotes breast cancer progression. *Oncogene* **2017**, *36* (1), 133-145.
(71) Dequiedt, F.; Kasler, H.; Fischle, W.; Kiermer, V.; Weinstein, M.; Herndier, B. G.; Verdin, E. HDAC7, a thymus-specific class II histone deacetylase, regulates Nur77 transcription and TCR-mediated apoptosis. *Immunity* **2003**, *18* (5), 687-698.
(72) de Barrios, O.; Galaras, A.; Trincado, J. L.; Azagra, A.; Collazo, O.; Meler, A.; Agraz-Doblas, A.; Bueno, C.; Ballerini, P.; Cazzaniga, G.; Stam, R. W.; Varela, I.; De Lorenzo, P.; Valsecchi, M. G.; Hatzis, P.; Menéndez, P.; Parra, M. HDAC7 is a major contributor in the pathogenesis of infant t(4;11) proB acute lymphoblastic leukemia. *Leukemia* **2021**, *35* (7), 2086-2091.
(73) Yang, C.; Croteau, S.; Hardy, P. Histone deacetylase (HDAC) 9: versatile biological functions and emerging roles in human cancer. *Cell. Oncol. (Dordr.)* **2021**, *44* (5), 997-1017.
(74) Ma, Z.; Liu, D.; Di, S.; Zhang, Z.; Li, W.; Zhang, J.; Xu, L.; Guo, K.; Zhu, Y.; Li, X.; Han, J.; Yan, X. Histone deacetylase 9 downregulation decreases tumor growth and promotes apoptosis in non-small cell lung cancer after melatonin treatment. *J. Pineal Res.* **2019**, *67* (2), e12587.
(75) Huang, Y.; Jian, W.; Zhao, J.; Wang, G. Overexpression of HDAC9 is associated with poor prognosis and tumor progression of breast cancer in Chinese females. *Onco Targets Ther.* **2018**, *11*, 2177-2184.

(76) Yao, Y. L.; Yang, W. M. Beyond histone and deacetylase: an overview of cytoplasmic histone deacetylases and their nonhistone substrates. *J. Biomed. Biotechnol.* **2011**, *2011*, 146493.
(77) Chang, P.; Li, H.; Hu, H.; Li, Y.; Wang, T. The Role of HDAC6 in Autophagy and NLRP3 Inflammasome. *Front. Immunol.* **2021**, *12*, 763831.
(78) Zhou, W.; Wang, J.; Wang, X.; Wang, B.; Zhao, Z.; Fu, J.; Wang, Y.; Zhang, X.; Zhu, P.; Jiang, M.; Cao, X. Degradation of HDAC10 by autophagy promotes IRF3-mediated antiviral innate immune responses. *Sci. Signal.* **2022**, *15* (765), eabo4356.
(79) Gracia-Hernandez, M.; Yende, A. S.; Gajendran, N.; Alahmadi, Z.; Li, X.; Munoz, Z.; Tan, K.; Noonepalle, S.; Shibata, M.; Villagra, A. Targeting HDAC6 improves anti-CD47 immunotherapy. *J. Exp. Clin. Cancer Res.* **2024**, *43* (1), 60.
(80) Tavares, M. O.; Milan, T. M.; Bighetti-Trevisan, R. L.; Leopoldino, A. M.; de Almeida, L. O. Pharmacological inhibition of HDAC6 overcomes cisplatin chemoresistance by targeting cancer stem cells in oral squamous cell carcinoma. *J. Oral Pathol. Med.* **2022**, *51* (6), 529-537.
(81) Ridinger, J.; Koeneke, E.; Kolbinger, F. R.; Koerholz, K.; Mahboobi, S.; Hellweg, L.; Gunkel, N.; Miller, A. K.; Peterziel, H.; Schmezer, P.; Hamacher-Brady, A.; Witt, O.; Oehme, I. Dual role of HDAC10 in lysosomal exocytosis and DNA repair promotes neuroblastoma chemoresistance. *Sci. Rep.* **2018**, *8* (1), 10039.
(82) Zhai, S.; Honin, I.; Schäker-Hübner, L.; Hanl, M.; Jacobi, L.; Dressler, F.; Pieńkowska, D. E.; König, P.; Gerhartz, J.; Voget, R.; Bendas, G.; Gutschow, M.; Meissner, F.; Burckhardt, B. B.; Nowak, R. P.; Steinebach, C.; Hansen, F. K. Development and Characterization of the First Selective Class IIb Histone Deacetylase Degraders. *J. Med. Chem.* **2025**, *68* (13), 13793-13821.
(83) Zheng, Y.; Zhu, G.; Tang, Y.; Yan, J.; Han, S.; Yin, J.; Peng, B.; He, X.; Liu, W. HDAC6, A Novel Cargo for Autophagic Clearance of Stress Granules, Mediates the Repression of the Type I Interferon Response During Coxsackievirus A16 Infection. *Front. Microbiol.* **2020**, *11*, 78.
(84) Zhu, Q.; Zhang, K.; Cao, Y.; Hu, Y. Adipose stem cell exosomes, stimulated by pro-inflammatory factors, enhance immune evasion in triple-negative breast cancer by modulating the HDAC6/STAT3/PD-L1 pathway through the transporter UCHL1. *Cancer Cell Int.* **2024**, *24* (1), 385.
(85) Mardones, C.; Navarrete-Munoz, C.; Armijo, M. E.; Salgado, K.; Rivas-Valdes, F.; Gonzalez-Pecchi, V.; Farkas, C.; Villagra, A.; Hepp, M. I. Role of HDAC6-STAT3 in immunomodulatory pathways in Colorectal cancer cells. *Mol. Immunol.* **2023**, *164*, 98-111.
(86) Liu, X.; Wang, Y.; Zhang, R.; Jin, T.; Qu, L.; Jin, Q.; Zheng, J.; Sun, J.; Wu, Z.; Wang, L.; Liu, T.; Zhang, Y.; Meng, X.; Wang, Y.; Wei, N. HDAC10 Is Positively Associated With PD-L1 Expression and Poor Prognosis in Patients With NSCLC. *Front. Oncol.* **2020**, *10*, 485.
(87) Zhang, H.; Yao, J.; Ajmal, I.; Farooq, M. A.; Jiang, W. shRNA-mediated gene silencing of HDAC11 empowers CAR-T cells against prostate cancer. *Front. Immunol.* **2024**, *15*, 1369406.
(88) Dokmanovic, M.; Clarke, C.; Marks, P. A. Histone deacetylase inhibitors: overview and perspectives. *Mol. Cancer Res.* **2007**, *5* (10), 981-989.
(89) Marks, P. A. The clinical development of histone deacetylase inhibitors as targeted anticancer drugs. *Expert Opin. Investig. Drugs* **2010**, *19* (9), 1049-1066.

(90) West, A. C.; Johnstone, R. W. New and emerging HDAC inhibitors for cancer treatment. *J. Clin. Invest.* **2014**, *124* (1), 30-39.
(91) Ho, T. C. S.; Chan, A. H. Y.; Ganesan, A. Thirty Years of HDAC Inhibitors: 2020 Insight and Hindsight. *J. Med. Chem.* **2020**, *63* (21), 12460-12484.
(92) Tsuji, N.; Kobayashi, M.; Nagashima, K.; Wakisaka, Y.; Koizumi, K. A new antifungal antibiotic, trichostatin. *J. Antibiot. (Tokyo)* **1976**, *29* (1), 1-6.
(93) Yoshida, M.; Horinouchi, S.; Beppu, T. Trichostatin A and trapoxin: novel chemical probes for the role of histone acetylation in chromatin structure and function. *Bioessays* **1995**, *17* (5), 423-430.
(94) Jung, M.; Hoffmann, K.; Brosch, G.; Loidl, P. Analogues of trichostatin a and trapoxin B as histone deacetylase inhibitors. *Bioorg. Med. Chem. Lett.* **1997**, *7* (13), 1655-1658.
(95) Stopper, D.; Biermann, L.; Watson, P. R.; Li, J.; König, B.; Gaynes, M. N.; Pessanha de Carvalho, L.; Klose, J.; Hanl, M.; Hamacher, A.; Schäker-Hübner, L.; Ramsbeck, D.; Held, J.; Christianson, D. W.; Kassack, M. U.; Hansen, F. K. Exploring Alternative Zinc-Binding Groups in Histone Deacetylase (HDAC) Inhibitors Uncovers DS-103 as a Potent Ethylhydrazide-Based HDAC Inhibitor with Chemosensitizing Properties. *J. Med. Chem.* **2025**, *68* (4), 4426-4452.
(96) Talom, A.; Barhoi, A.; Jirpu, T.; Dawn, B.; Ghosh, A. Clinical progress and functional modalities of HDAC inhibitor-based combination therapies in cancer treatment. *Clin. Transl. Oncol.* **2025**.
(97) Duvic, M.; Vu, J. Vorinostat in cutaneous T-cell lymphoma. *Drugs Today (Barc.)* **2007**, *43* (9), 585-599.
(98) Parveen, R.; Harihar, D.; Chatterji, B. P. Recent histone deacetylase inhibitors in cancer therapy. *Cancer* **2023**, *129* (21), 3372-3380.
(99) Iyer, S. P.; Foss, F. F. Romidepsin for the Treatment of Peripheral T-Cell Lymphoma. *Oncologist* **2015**, *20* (9), 1084-1091.
(100) Rashidi, A.; Cashen, A. F. Belinostat for the treatment of relapsed or refractory peripheral T-cell lymphoma. *Future Oncol.* **2015**, *11* (11), 1659-1664.
(101) Sun, Y.; Hong, J. H.; Ning, Z.; Pan, D.; Fu, X.; Lu, X.; Tan, J. Therapeutic potential of tucidinostat, a subtype-selective HDAC inhibitor, in cancer treatment. *Front. Pharmacol.* **2022**, *13*, 932914.
(102) Sivaraj, D.; Green, M. M.; Gasparetto, C. Panobinostat for the management of multiple myeloma. *Future Oncol.* **2017**, *13* (6), 477-488.
(103) Beninger, P. Givinostat Oral Suspension. *Clin. Ther.* **2024**, *46* (7), 601-602.
(104) Di Bello, E.; Noce, B.; Fioravanti, R.; Mai, A. Current HDAC Inhibitors in Clinical Trials. *Chimia (Aarau)* **2022**, *76* (5), 448-453.
(105) McClure, J. J.; Li, X.; Chou, C. J. Advances and Challenges of HDAC Inhibitors in Cancer Therapeutics. *Adv. Cancer Res.* **2018**, *138*, 183-211.
(106) Yang, F.; Zhao, N.; Ge, D.; Chen, Y. Next-generation of selective histone deacetylase inhibitors. *RSC Adv.* **2019**, *9* (34), 19571-19583.
(107) Chen, S.; Zheng, Y.; Liang, B.; Yin, Y.; Yao, J.; Wang, Q.; Liu, Y.; Neamati, N. The application of PROTAC in HDAC. *Eur. J. Med. Chem.* **2023**, *260*, 115746.

(108) Sakamoto, K. M.; Kim, K. B.; Kumagai, A.; Mercurio, F.; Crews, C. M.; Deshaies, R. J. Protacs: chimeric molecules that target proteins to the Skp1-Cullin-F box complex for ubiquitination and degradation. *Proc. Natl. Acad. Sci. U. S. A.* **2001**, *98* (15), 8554-8559.
(109) Lai, A. C.; Crews, C. M. Induced protein degradation: an emerging drug discovery paradigm. *Nat. Rev. Drug Discov.* **2017**, *16* (2), 101-114.
(110) Vassilev, L. T.; Vu, B. T.; Graves, B.; Carvajal, D.; Podlaski, F.; Filipovic, Z.; Kong, N.; Kammlott, U.; Lukacs, C.; Klein, C.; Fotouhi, N.; Liu, E. A. In vivo activation of the p53 pathway by small-molecule antagonists of MDM2. *Science* **2004**, *303* (5659), 844-848.
(111) Schneekloth, A. R.; Pucheault, M.; Tae, H. S.; Crews, C. M. Targeted intracellular protein degradation induced by a small molecule: En route to chemical proteomics. *Bioorg. Med. Chem. Lett.* **2008**, *18* (22), 5904-5908.
(112) Paiva, S. L.; Crews, C. M. Targeted protein degradation: elements of PROTAC design. *Curr. Opin. Chem. Biol.* **2019**, *50*, 111-119.
(113) Pettersson, M.; Crews, C. M. PROteolysis TArgeting Chimeras (PROTACs) - Past, present and future. *Drug Discov. Today: Technol.* **2019**, *31*, 15-27.
(114) Ge, J.; Li, S.; Weng, G.; Wang, H.; Fang, M.; Sun, H.; Deng, Y.; Hsieh, C. Y.; Li, D.; Hou, T. PROTAC-DB 3.0: an updated database of PROTACs with extended pharmacokinetic parameters. *Nucleic Acids Res.* **2025**, *53* (D1), D1510-D1515.
(115) Hu, Z.; Crews, C. M. Recent Developments in PROTAC-Mediated Protein Degradation: From Bench to Clinic. *ChemBioChem* **2022**, *23* (2), e202100270.
(116) Chirnomas, D.; Hornberger, K. R.; Crews, C. M. Protein degraders enter the clinic - a new approach to cancer therapy. *Nat. Rev. Clin. Oncol.* **2023**, *20* (4), 265-278.
(117) Ma, Z.; Zhou, J. NDA Submission of Vepdegestrant (ARV-471) to U.S. FDA: The Beginning of a New Era of PROTAC Degraders. *J. Med. Chem.* **2025**, *68* (14), 14129-14136.
(118) Kamaraj, R.; Ghosh, S.; Das, S.; Sen, S.; Kumar, P.; Majumdar, M.; Dasgupta, R.; Mukherjee, S.; Das, S.; Ghose, I.; Pavek, P.; Raja Karuppiah, M. P.; Chuturgoon, A. A.; Anand, K. Targeted Protein Degradation (TPD) for Immunotherapy: Understanding Proteolysis Targeting Chimera-Driven Ubiquitin-Proteasome Interactions. *Bioconjug. Chem.* **2024**, *35* (8), 1089-1115.
(119) Gregory, J. A.; Hickey, C. M.; Chavez, J.; Cacace, A. M. New therapies on the horizon: Targeted protein degradation in neuroscience. *Cell Chem. Biol.* **2024**, *31* (9), 1688-1698.
(120) Kong, D.; Meng, L.; Lin, P.; Wu, G. Advancements in PROTAC-based therapies for neurodegenerative diseases. *Future Med. Chem.* **2025**, *17* (5), 591-605.
(121) Espinoza-Chávez, R. M.; Salerno, A.; Liuzzi, A.; Ilari, A.; Milelli, A.; Uliassi, E.; Bolognesi, M. L. Targeted Protein Degradation for Infectious Diseases: from Basic Biology to Drug Discovery. *ACS Bio Med. Chem. Au* **2023**, *3* (1), 32-45.
(122) Liang, J.; Wu, Y.; Lan, K.; Dong, C.; Wu, S.; Li, S.; Zhou, H. B. Antiviral PROTACs: Opportunity borne with challenge. *Cell Insight* **2023**, *2* (3), 100092.
(123) Rodríguez-Gimeno, A.; Galdeano, C. Drug Discovery Approaches to Target E3 Ligases. *ChemBioChem* **2025**, *26* (1), e202400656.
(124) Liu, Y.; Yang, J.; Wang, T.; Luo, M.; Chen, Y.; Chen, C.; Ronai, Z.; Zhou, Y.; Ruppin, E.; Han, L. Expanding PROTACtable genome universe of E3 ligases. *Nat. Commun.* **2023**, *14* (1), 6509.

(125) Min, J.; Mayasundari, A.; Keramatnia, F.; Jonchere, B.; Yang, S. W.; Jarusiewicz, J.; Actis, M.; Das, S.; Young, B.; Slavish, J.; Yang, L.; Li, Y.; Fu, X.; Garrett, S. H.; Yun, M. K.; Li, Z.; Nithianantham, S.; Chai, S.; Chen, T.; Shelat, A.; Lee, R. E.; Nishiguchi, G.; White, S. W.; Roussel, M. F.; Potts, P. R.; Fischer, M.; Rankovic, Z. Phenyl-Glutarimides: Alternative Cereblon Binders for the Design of PROTACs. *Angew. Chem. Int. Ed.* **2021**, *60* (51), 26663-26670.
(126) Vicente, A. T. S.; Salvador, J. A. R. MDM2-Based Proteolysis-Targeting Chimeras (PROTACs): An Innovative Drug Strategy for Cancer Treatment. *Int. J. Mol. Sci.* **2022**, *23* (19).
(127) Wang, C.; Zhang, Y.; Shi, L.; Yang, S.; Chang, J.; Zhong, Y.; Li, Q.; Xing, D. Recent advances in IAP-based PROTACs (SNIPERs) as potential therapeutic agents. *J. Enzyme Inhib. Med. Chem.* **2022**, *37* (1), 1437-1453.
(128) Murray, I. A.; Patterson, A. D.; Perdew, G. H. Aryl hydrocarbon receptor ligands in cancer: friend and foe. *Nat. Rev. Cancer* **2014**, *14* (12), 801-814.
(129) Zhang, X.; Luukkonen, L. M.; Eissler, C. L.; Crowley, V. M.; Yamashita, Y.; Schafroth, M. A.; Kikuchi, S.; Weinstein, D. S.; Symons, K. T.; Nordin, B. E.; Rodriguez, J. L.; Wucherpfennig, T. G.; Bauer, L. G.; Dix, M. M.; Stamos, D.; Kinsella, T. M.; Simon, G. M.; Baltgalvis, K. A.; Cravatt, B. F. DCAF11 Supports Targeted Protein Degradation by Electrophilic Proteolysis-Targeting Chimeras. *J. Am. Chem. Soc.* **2021**, *143* (13), 5141-5149.
(130) Zhang, X.; Crowley, V. M.; Wucherpfennig, T. G.; Dix, M. M.; Cravatt, B. F. Electrophilic PROTACs that degrade nuclear proteins by engaging DCAF16. *Nat. Chem. Biol.* **2019**, *15* (7), 737-746.
(131) Henning, N. J.; Manford, A. G.; Spradlin, J. N.; Brittain, S. M.; Zhang, E.; McKenna, J. M.; Tallarico, J. A.; Schirle, M.; Rape, M.; Nomura, D. K. Discovery of a Covalent FEM1B Recruiter for Targeted Protein Degradation Applications. *J. Am. Chem. Soc.* **2022**, *144* (2), 701-708.
(132) Vyas, R.; Kumar, R.; Clermont, F.; Helfricht, A.; Kalev, P.; Sotiropoulou, P.; Hendriks, I. A.; Radaelli, E.; Hochepied, T.; Blanpain, C.; Sablina, A.; van Attikum, H.; Olsen, J. V.; Jochemsen, A. G.; Vertegaal, A. C.; Marine, J. C. RNF4 is required for DNA double-strand break repair in vivo. *Cell Death Differ.* **2013**, *20* (3), 490-502.
(133) Rodriguez, M. S.; Egaña, I.; Lopitz-Otsoa, F.; Aillet, F.; Lopez-Mato, M. P.; Dorronsoro, A.; Lobato-Gil, S.; Sutherland, J. D.; Barrio, R.; Trigueros, C.; Lang, V. The RING ubiquitin E3 RNF114 interacts with A20 and modulates NF-kappaB activity and T-cell activation. *Cell Death Dis.* **2014**, *5* (8), e1399.
(134) Chen, J.; Feng, D.; Zhu, R.; Li, H.; Chen, L. Advances in KEAP1-based PROTACs as emerging therapeutic modalities: Structural basis and progress. *Redox Biol.* **2025**, *85*, 103781.
(135) Doyle, J. M.; Gao, J.; Wang, J.; Yang, M.; Potts, P. R. MAGE-RING protein complexes comprise a family of E3 ubiquitin ligases. *Mol. Cell* **2010**, *39* (6), 963-974.
(136) Bond, M. J.; Crews, C. M. Proteolysis targeting chimeras (PROTACs) come of age: entering the third decade of targeted protein degradation. *RSC Chem. Biol.* **2021**, *2* (3), 725-742.
(137) Lipinski, C. A.; Lombardo, F.; Dominy, B. W.; Feeney, P. J. Experimental and computational approaches to estimate solubility and permeability in drug discovery and development settings. *Adv. Drug Deliv. Rev.* **1997**, *23* (1-3), 3-25.

(138) Cantrill, C.; Chaturvedi, P.; Rynn, C.; Petrig Schaffland, J.; Walter, I.; Wittwer, M. B. Fundamental aspects of DMPK optimization of targeted protein degraders. *Drug Discov. Today* **2020**, *25* (6), 969-982.
(139) Hughes, S. J.; Ciulli, A. Molecular recognition of ternary complexes: a new dimension in the structure-guided design of chemical degraders. *Essays Biochem.* **2017**, *61* (5), 505-516.
(140) Chan, K. H.; Zengerle, M.; Testa, A.; Ciulli, A. Impact of Target Warhead and Linkage Vector on Inducing Protein Degradation: Comparison of Bromodomain and Extra-Terminal (BET) Degraders Derived from Triazolodiazepine (JQ1) and Tetrahydroquinoline (I-BET726) BET Inhibitor Scaffolds. *J. Med. Chem.* **2018**, *61* (2), 504-513.
(141) Zhang, L.; Riley-Gillis, B.; Vijay, P.; Shen, Y. Acquired Resistance to BET-PROTACs (Proteolysis-Targeting Chimeras) Caused by Genomic Alterations in Core Components of E3 Ligase Complexes. *Mol. Cancer Ther.* **2019**, *18* (7), 1302-1311.
(142) Ottis, P.; Palladino, C.; Thienger, P.; Britschgi, A.; Heichinger, C.; Berrera, M.; Julien-Laferriere, A.; Roudnicky, F.; Kam-Thong, T.; Bischoff, J. R.; Martoglio, B.; Pettazzoni, P. Cellular Resistance Mechanisms to Targeted Protein Degradation Converge Toward Impairment of the Engaged Ubiquitin Transfer Pathway. *ACS Chem. Biol.* **2019**, *14* (10), 2215-2223.
(143) Jiang, B.; Gao, Y.; Che, J.; Lu, W.; Kaltheuner, I. H.; Dries, R.; Kalocsay, M.; Berberich, M. J.; Jiang, J.; You, I.; Kwiatkowski, N.; Riching, K. M.; Daniels, D. L.; Sorger, P. K.; Geyer, M.; Zhang, T.; Gray, N. S. Discovery and resistance mechanism of a selective CDK12 degrader. *Nat. Chem. Biol.* **2021**, *17* (6), 675-683.
(144) Kandel, R.; Jung, J.; Neal, S. Proteotoxic stress and the ubiquitin proteasome system. *Semin. Cell Dev. Biol.* **2024**, *156*, 107-120.
(145) Casan, J. M. L.; Seymour, J. F. Degraders upgraded: the rise of PROTACs in hematological malignancies. *Blood* **2024**, *143* (13), 1218-1230.
(146) Dong, G.; Ding, Y.; He, S.; Sheng, C. Molecular Glues for Targeted Protein Degradation: From Serendipity to Rational Discovery. *J. Med. Chem.* **2021**, *64* (15), 10606-10620.
(147) Imaide, S.; Riching, K. M.; Makukhin, N.; Vetma, V.; Whitworth, C.; Hughes, S. J.; Trainor, N.; Mahan, S. D.; Murphy, N.; Cowan, A. D.; Chan, K. H.; Craigon, C.; Testa, A.; Maniaci, C.; Urh, M.; Daniels, D. L.; Ciulli, A. Trivalent PROTACs enhance protein degradation via combined avidity and cooperativity. *Nat. Chem. Biol.* **2021**, *17* (11), 1157-1167.
(148) Cotton, A. D.; Nguyen, D. P.; Gramespacher, J. A.; Seiple, I. B.; Wells, J. A. Development of Antibody-Based PROTACs for the Degradation of the Cell-Surface Immune Checkpoint Protein PD-L1. *J. Am. Chem. Soc.* **2021**, *143* (2), 593-598.
(149) Shih, P. C.; Naganuma, M.; Demizu, Y.; Naito, M. Current Status of Oligonucleotide-Based Protein Degraders. *Pharmaceutics* **2023**, *15* (3).
(150) Lim, S.; Khoo, R.; Peh, K. M.; Teo, J.; Chang, S. C.; Ng, S.; Beilhartz, G. L.; Melnyk, R. A.; Johannes, C. W.; Brown, C. J.; Lane, D. P.; Henry, B.; Partridge, A. W. bioPROTACs as versatile modulators of intracellular therapeutic targets including proliferating cell nuclear antigen (PCNA). *Proc. Natl. Acad. Sci. U. S. A.* **2020**, *117* (11), 5791-5800.
(151) Hatakeyama, S.; Watanabe, M.; Fujii, Y.; Nakayama, K. I. Targeted destruction of c-Myc by an engineered ubiquitin ligase suppresses cell transformation and tumor formation. *Cancer Res.* **2005**, *65* (17), 7874-7879.

(152) Pan, T.; Zhang, Y.; Zhou, N.; He, X.; Chen, C.; Liang, L.; Duan, X.; Lin, Y.; Wu, K.; Zhang, H. A recombinant chimeric protein specifically induces mutant KRAS degradation and potently inhibits pancreatic tumor growth. *Oncotarget* **2016**, *7* (28), 44299-44309.
(153) Liu, H.; Ren, C.; Sun, R.; Wang, H.; Zhan, Y.; Yang, X.; Jiang, B.; Chen, H. Reactive oxygen species-responsive Pre-PROTAC for tumor-specific protein degradation. *Chem. Commun. (Camb.)* **2022**, *58* (72), 10072-10075.
(154) Jin, Y. H.; Lu, M. C.; Wang, Y.; Shan, W. X.; Wang, X. Y.; You, Q. D.; Jiang, Z. Y. Azo-PROTAC: Novel Light-Controlled Small-Molecule Tool for Protein Knockdown. *J. Med. Chem.* **2020**, *63* (9), 4644-4654.
(155) Yang, C.; Yang, Y.; Li, Y.; Ni, Q.; Li, J. Radiotherapy-Triggered Proteolysis Targeting Chimera Prodrug Activation in Tumors. *J. Am. Chem. Soc.* **2023**, *145* (1), 385-391.
(156) Dikic, I. Proteasomal and Autophagic Degradation Systems. *Annu. Rev. Biochem.* **2017**, *86*, 193-224.
(157) Słabicki, M.; Yoon, H.; Koeppel, J.; Nitsch, L.; Roy Burman, S. S.; Di Genua, C.; Donovan, K. A.; Sperling, A. S.; Hunkeler, M.; Tsai, J. M.; Sharma, R.; Guirguis, A.; Zou, C.; Chudasama, P.; Gasser, J. A.; Miller, P. G.; Scholl, C.; Fröhling, S.; Nowak, R. P.; Fischer, E. S.; Ebert, B. L. Small-molecule-induced polymerization triggers degradation of BCL6. *Nature* **2020**, *588* (7836), 164-168.
(158) Słabicki, M.; Kozicka, Z.; Petzold, G.; Li, Y. D.; Manojkumar, M.; Bunker, R. D.; Donovan, K. A.; Sievers, Q. L.; Koeppel, J.; Suchyta, D.; Sperling, A. S.; Fink, E. C.; Gasser, J. A.; Wang, L. R.; Corsello, S. M.; Sellar, R. S.; Jan, M.; Gillingham, D.; Scholl, C.; Fröhling, S.; Golub, T. R.; Fischer, E. S.; Thomä, N. H.; Ebert, B. L. The CDK inhibitor CR8 acts as a molecular glue degrader that depletes cyclin K. *Nature* **2020**, *585* (7824), 293-297.
(159) Hsia, O.; Hinterndorfer, M.; Cowan, A. D.; Iso, K.; Ishida, T.; Sundaramoorthy, R.; Nakasone, M. A.; Imrichova, H.; Schätz, C.; Rukavina, A.; Husnjak, K.; Wegner, M.; Correa-Sáez, A.; Craigon, C.; Casement, R.; Maniaci, C.; Testa, A.; Kaulich, M.; Dikic, I.; Winter, G. E.; Ciulli, A. Targeted protein degradation via intramolecular bivalent glues. *Nature* **2024**, *627* (8002), 204-211.
(160) Sasso, J. M.; Tenchov, R.; Wang, D.; Johnson, L. S.; Wang, X.; Zhou, Q. A. Molecular Glues: The Adhesive Connecting Targeted Protein Degradation to the Clinic. *Biochemistry* **2023**, *62* (3), 601-623.
(161) Fischer, F.; Alves Avelar, L. A.; Murray, L.; Kurz, T. Designing HDAC-PROTACs: lessons learned so far. *Future Med. Chem.* **2022**, *14* (3), 143-166.
(162) Patel, U.; Smalley, J. P.; Hodgkinson, J. T. PROTAC chemical probes for histone deacetylase enzymes. *RSC Chem. Biol.* **2023**, *4* (9), 623-634.
(163) Hussain, M. S.; Zhang, L.; Rana, A. J.; Maqbool, M.; Ashique, S.; Khan, Y.; Jakhmola, V.; Hanbashi, A.; Mawkili, W.; Khan, G. Epigenetic therapy meets targeted protein degradation: HDAC-PROTACs in cancer treatment. *Future Med. Chem.* **2025**, *17* (14), 1725-1737.
(164) Xiao, Y.; Wang, J.; Zhao, L. Y.; Chen, X.; Zheng, G.; Zhang, X.; Liao, D. Discovery of histone deacetylase 3 (HDAC3)-specific PROTACs. *Chem. Commun. (Camb.)* **2020**, *56* (68), 9866-9869.
(165) Cao, F.; de Weerd, S.; Chen, D.; Zwinderman, M. R. H.; van der Wouden, P. E.; Dekker, F. J. Induced protein degradation of histone deacetylases 3 (HDAC3) by proteolysis targeting chimera (PROTAC). *Eur. J. Med. Chem.* **2020**, *208*, 112800.

(166) Yang, K.; Song, Y.; Xie, H.; Wu, H.; Wu, Y. T.; Leisten, E. D.; Tang, W. Development of the first small molecule histone deacetylase 6 (HDAC6) degraders. *Bioorg. Med. Chem. Lett.* **2018**, *28* (14), 2493-2497.
(167) An, Z.; Lv, W.; Su, S.; Wu, W.; Rao, Y. Developing potent PROTACs tools for selective degradation of HDAC6 protein. *Protein Cell* **2019**, *10* (8), 606-609.
(168) Wu, H.; Yang, K.; Zhang, Z.; Leisten, E. D.; Li, Z.; Xie, H.; Liu, J.; Smith, K. A.; Novakova, Z.; Barinka, C.; Tang, W. Development of Multifunctional Histone Deacetylase 6 Degraders with Potent Antimyeloma Activity. *J. Med. Chem.* **2019**, *62* (15), 7042-7057.
(169) Yang, H.; Lv, W.; He, M.; Deng, H.; Li, H.; Wu, W.; Rao, Y. Plasticity in designing PROTACs for selective and potent degradation of HDAC6. *Chem. Commun. (Camb.)* **2019**, *55* (98), 14848-14851.
(170) Yang, K.; Zhao, Y.; Nie, X.; Wu, H.; Wang, B.; Almodovar-Rivera, C. M.; Xie, H.; Tang, W. A Cell-Based Target Engagement Assay for the Identification of Cereblon E3 Ubiquitin Ligase Ligands and Their Application in HDAC6 Degraders. *Cell Chem. Biol.* **2020**, *27* (7), 866-876 e868.
(171) Cao, Z.; Gu, Z.; Lin, S.; Chen, D.; Wang, J.; Zhao, Y.; Li, Y.; Liu, T.; Li, Y.; Wang, Y.; Lin, H.; He, B. Attenuation of NLRP3 Inflammasome Activation by Indirubin-Derived PROTAC Targeting HDAC6. *ACS Chem. Biol.* **2021**, *16* (12), 2746-2751.
(172) Sinatra, L.; Yang, J.; Schliehe-Diecks, J.; Dienstbier, N.; Vogt, M.; Gebing, P.; Bachmann, L. M.; Sönnichsen, M.; Lenz, T.; Stühler, K.; Schöler, A.; Borkhardt, A.; Bhatia, S.; Hansen, F. K. Solid-Phase Synthesis of Cereblon-Recruiting Selective Histone Deacetylase 6 Degraders (HDAC6 PROTACs) with Antileukemic Activity. *J. Med. Chem.* **2022**, *65* (24), 16860-16878.
(173) Garcha, H. K.; Olaoye, O. O.; Sedighi, A.; Pölöske, D.; Hariri, P.; Yu, W.; Abdallah, D. I.; Moriggl, R.; de Araujo, E. D.; Gunning, P. T. Monoselective Histone Deacetylase 6 PROTAC Degrader Shows In Vivo Tractability. *J. Med. Chem.* **2025**, *68* (6), 6165-6177.
(174) Yang, K.; Wu, H.; Zhang, Z.; Leisten, E. D.; Nie, X.; Liu, B.; Wen, Z.; Zhang, J.; Cunningham, M. D.; Tang, W. Development of Selective Histone Deacetylase 6 (HDAC6) Degraders Recruiting Von Hippel-Lindau (VHL) E3 Ubiquitin Ligase. *ACS Med. Chem. Lett.* **2020**, *11* (4), 575-581.
(175) Keuler, T.; König, B.; Buckreiss, N.; Kraft, F. B.; Konig, P.; Schäker-Hübner, L.; Steinebach, C.; Bendas, G.; Gütschow, M.; Hansen, F. K. Development of the first non-hydroxamate selective HDAC6 degraders. *Chem. Commun. (Camb.)* **2022**, *58* (79), 11087-11090.
(176) Stopper, D.; Honin, I.; Feller, F.; Hansen, F. K. Development of Ethyl-Hydrazide-Based Selective Histone Deacetylase 6 (HDAC6) PROTACs. *ACS Med. Chem. Lett.* **2025**, *16* (3), 487-495.
(177) Xia, K.; Qiu, T.; Jian, Y.; Liu, H.; Chen, H.; Liu, X.; Chen, Z.; Wang, L. Degradation of histone deacetylase 6 alleviates ROS-mediated apoptosis in renal ischemia-reperfusion injury. *Biomed. Pharmacother.* **2023**, *165*, 115128.
(178) Bockstiegel, J.; Wurnig, S. L.; Engelhardt, J.; Enns, J.; Hansen, F. K.; Weindl, G. Pharmacological inhibition of HDAC6 suppresses NLRP3 inflammasome-mediated IL-1beta release. *Biochem. Pharmacol.* **2023**, *215*, 115693.

(179) Lobera, M.; Madauss, K. P.; Pohlhaus, D. T.; Wright, Q. G.; Trocha, M.; Schmidt, D. R.; Baloglu, E.; Trump, R. P.; Head, M. S.; Hofmann, G. A.; Murray-Thompson, M.; Schwartz, B.; Chakravorty, S.; Wu, Z.; Mander, P. K.; Kruidenier, L.; Reid, R. A.; Burkhart, W.; Turunen, B. J.; Rong, J. X.; Wagner, C.; Moyer, M. B.; Wells, C.; Hong, X.; Moore, J. T.; Williams, J. D.; Soler, D.; Ghosh, S.; Nolan, M. A. Selective class IIa histone deacetylase inhibition via a nonchelating zinc-binding group. *Nat. Chem. Biol.* **2013**, *9* (5), 319-325.
(180) Kadier, K.; Niu, T.; Ding, B.; Chen, B.; Qi, X.; Chen, D.; Cheng, X.; Fang, Y.; Zhou, J.; Zhao, W.; Liu, Z.; Yuan, Y.; Zhou, Z.; Dong, X.; Yang, B.; He, Q.; Cao, J.; Jiang, L.; Zhu, C. L. PROTAC-Mediated HDAC7 Protein Degradation Unveils Its Deacetylase-Independent Proinflammatory Function in Macrophages. *Adv. Sci. (Weinh.)* **2024**, *11* (36), e2309459.
(181) Jin, Y.; Qi, X.; Yu, X.; Cheng, X.; Chen, B.; Wu, M.; Zhang, J.; Yin, H.; Lu, Y.; Zhou, Y.; Pang, A.; Lin, Y.; Jiang, L.; Shi, Q.; Geng, S.; Zhou, Y.; Yao, X.; Li, L.; Duan, H.; Che, J.; Cao, J.; He, Q.; Dong, X. Discovery of a potential hematologic malignancies therapy: Selective and potent HDAC7 PROTAC degrader targeting non-enzymatic function. *Acta Pharm. Sin. B* **2025**, *15* (3), 1659-1679.
(182) Chotitumnavee, J.; Yamashita, Y.; Takahashi, Y.; Takada, Y.; Iida, T.; Oba, M.; Itoh, Y.; Suzuki, T. Selective degradation of histone deacetylase 8 mediated by a proteolysis targeting chimera (PROTAC). *Chem. Commun. (Camb.)* **2022**, *58* (29), 4635-4638.
(183) Sun, Z.; Deng, B.; Yang, Z.; Mai, R.; Huang, J.; Ma, Z.; Chen, T.; Chen, J. Discovery of pomalidomide-based PROTACs for selective degradation of histone deacetylase 8. *Eur. J. Med. Chem.* **2022**, *239*, 114544.
(184) Huang, J.; Zhang, J.; Xu, W.; Wu, Q.; Zeng, R.; Liu, Z.; Tao, W.; Chen, Q.; Wang, Y.; Zhu, W. G. Structure-Based Discovery of Selective Histone Deacetylase 8 Degraders with Potent Anticancer Activity. *J. Med. Chem.* **2023**, *66* (2), 1186-1209.
(185) Darwish, S.; Ghazy, E.; Heimburg, T.; Herp, D.; Zeyen, P.; Salem-Altintas, R.; Ridinger, J.; Robaa, D.; Schmidtkunz, K.; Erdmann, F.; Schmidt, M.; Romier, C.; Jung, M.; Oehme, I.; Sippl, W. Design, Synthesis and Biological Characterization of Histone Deacetylase 8 (HDAC8) Proteolysis Targeting Chimeras (PROTACs) with Anti-Neuroblastoma Activity. *Int. J. Mol. Sci.* **2022**, *23* (14).
(186) Xiao, Y.; Awasthee, N.; Liu, Y.; Meng, C.; He, M. Y.; Hale, S.; Karki, R.; Lin, Z.; Mosterio, M.; Garcia, B. A.; Kridel, R.; Liao, D.; Zheng, G. Discovery of a Highly Potent and Selective HDAC8 Degrader: Advancing the Functional Understanding and Therapeutic Potential of HDAC8. *J. Med. Chem.* **2024**.
(187) Zhao, C.; Zhang, J.; Zhou, H.; Setroikromo, R.; Poelarends, G. J.; Dekker, F. J. Exploration of Hydrazide-Based HDAC8 PROTACs for the Treatment of Hematological Malignancies and Solid Tumors. *J. Med. Chem.* **2024**, *67* (16), 14016-14039.
(188) Milazzo, G.; Mercatelli, D.; Di Muzio, G.; Triboli, L.; De Rosa, P.; Perini, G.; Giorgi, F. M. Histone Deacetylases (HDACs): Evolution, Specificity, Role in Transcriptional Complexes, and Pharmacological Actionability. *Genes (Basel)* **2020**, *11* (5).
(189) Shinsky, S. A.; Christianson, D. W. Polyamine Deacetylase Structure and Catalysis: Prokaryotic Acetylpolyamine Amidohydrolase and Eukaryotic HDAC10. *Biochemistry* **2018**, *57* (22), 3105-3114.

(190) Lambona, C.; Zwergel, C.; Fioravanti, R.; Valente, S.; Mai, A. Histone deacetylase 10: A polyamine deacetylase from the crystal structure to the first inhibitors. *Curr. Opin. Struct. Biol.* **2023**, *82*, 102668.
(191) Hu, E.; Chen, Z.; Fredrickson, T.; Zhu, Y.; Kirkpatrick, R.; Zhang, G. F.; Johanson, K.; Sung, C. M.; Liu, R.; Winkler, J. Cloning and characterization of a novel human class I histone deacetylase that functions as a transcription repressor. *J. Biol. Chem.* **2000**, *275* (20), 15254-15264.
(192) Chakrabarti, A.; Oehme, I.; Witt, O.; Oliveira, G.; Sippl, W.; Romier, C.; Pierce, R. J.; Jung, M. HDAC8: a multifaceted target for therapeutic interventions. *Trends Pharmacol. Sci.* **2015**, *36* (7), 481-492.
(193) Kang, Y.; Nian, H.; Rajendran, P.; Kim, E.; Dashwood, W. M.; Pinto, J. T.; Boardman, L. A.; Thibodeau, S. N.; Limburg, P. J.; Löhr, C. V.; Bisson, W. H.; Williams, D. E.; Ho, E.; Dashwood, R. H. HDAC8 and STAT3 repress BMF gene activity in colon cancer cells. *Cell Death Dis.* **2014**, *5* (10), e1476.
(194) Chakrabarti, A.; Melesina, J.; Kolbinger, F. R.; Oehme, I.; Senger, J.; Witt, O.; Sippl, W.; Jung, M. Targeting histone deacetylase 8 as a therapeutic approach to cancer and neurodegenerative diseases. *Future Med. Chem.* **2016**, *8* (13), 1609-1634.
(195) Banerjee, S.; Adhikari, N.; Amin, S. A.; Jha, T. Histone deacetylase 8 (HDAC8) and its inhibitors with selectivity to other isoforms: An overview. *Eur. J. Med. Chem.* **2019**, *164*, 214-240.
(196) Biswas, S.; Rao, C. M. Epigenetic tools (The Writers, The Readers and The Erasers) and their implications in cancer therapy. *Eur. J. Pharmacol.* **2018**, *837*, 8-24.
(197) Pu, J.; Liu, T.; Wang, X.; Sharma, A.; Schmidt-Wolf, I. G. H.; Jiang, L.; Hou, J. Exploring the role of histone deacetylase and histone deacetylase inhibitors in the context of multiple myeloma: mechanisms, therapeutic implications, and future perspectives. *Exp. Hematol. Oncol.* **2024**, *13* (1), 45.
(198) LIU, J.; PLEWE, M. B.; LEE, M. R.; HAN, X.; CHEN, L.; ZHANG, C.; WANG, J. MODIFIED PROTEINS AND PROTEIN DEGRADERS. *WO 2021/239117* **2021**.
(199) Meyers, M.; Cismoski, S.; Panidapu, A.; Chie-Leon, B.; Nomura, D. K. Targeted Protein Degradation through Recruitment of the CUL4 Complex Adaptor Protein DDB1. *ACS Chem. Biol.* **2024**, *19* (1), 58-68.

7 Appendix

7.1 Appendix I. Python scripts used for data extraction and visualization of Figure 2

Data extraction of Figure 2:

```
from Bio import Entrez
import pandas as pd
import time
Entrez.email = "shizhai@uni-bonn.de"
hdac_list = ["HDAC1", "HDAC2", "HDAC3", "HDAC4", "HDAC5", "HDAC6", "HDAC7", "HDAC8", "HDAC9", "HDAC10", "HDAC11"]
cancer_list = ["Bladder cancer", "Breast cancer", "Cervical cancer", "Cholangiocarcinoma", "Chondrosarcoma", "Colorectal cancer", "Endometrial cancer", "Esophageal cancer","Gastric cancer", "Glioma cancer","Head and neck cancer","Leukemia", "Lip cancer", "Liver cancer", "Lung cancer", "Lymphoma", "Melanoma", "Myeloma", "Neuroblastoma", "Oral cancer", "Osteosarcoma", "Ovarian cancer", "Pancreatic cancer", "Prostate cancer", "Renal cancer", "Rhabdomyosarcoma", "Skin cancer", "Synovial Sarcoma", "Thyroid cancer", "Urothelial cancer"]
exclude_prefixes = ["Corrigendum", "Correction", "Erratum", "Retraction"]
results = []
for hdac in hdac_list:
    for cancer in cancer_list:
        query = f' {hdac} AND {cancer} NOT review[Publication Type]'
        handle = Entrez.esearch(db="pubmed", term=query, retmax=10000)
        record = Entrez.read(handle)
        id_list = record["IdList"]
        valid_count = 0
        batch_size = 200
        for start in range(0, len(id_list), batch_size):
            batch_ids = id_list[start:start + batch_size]
            summary_handle = Entrez.esummary(db="pubmed", id=",".join(batch_ids))
            summaries = Entrez.read(summary_handle)
            for item in summaries:
```

```
                    title = item.get("Title", "")
                    if not any(title.startswith(prefix) for prefix in exclude_prefixes):
                        valid_count += 1
                time.sleep(0.3)
            results.append((hdac, cancer, valid_count))
df = pd.DataFrame(results, columns=["HDAC", "Cancer", "Count"])
df.to_csv("hdac_cancer_counts_filtered_no_reviews.csv", index=False, encoding="utf-8-sig")
print("hdac_cancer_counts_filtered_no_reviews.csv")
```

Data visualization of Figure 2:

```
import pandas as pd
import matplotlib.pyplot as plt
import seaborn as sns
import matplotlib.ticker as ticker
def generate_hdac_cancer_heatmap(input_csv, output_png, title="HDAC Isoforms vs Cancer Types"):
    df = pd.read_csv(input_csv)
    df_pivot = df.pivot(index="Cancer", columns="HDAC", values="Count").fillna(0).astype(int)
    desired_order = [f"HDAC{i}" for I in range(1, 12) if f"HDAC{i}" in df_pivot.columns]
    df_pivot = df_pivot[desired_order]
    plt.figure(figsize=(12, 16))
    ax = sns.heatmap(
        df_pivot,
        cmap="YlGnBu",
        annot=True
        fmt="d",
        linewidths=0.5,
        annot_kws={"weight": "bold"},
        cbar_kws={"shrink": 1.0, 'label': 'Frequency'}
    )
```

```
    ax.set_xlabel("")
    ax.set_ylabel("")
    ax.set_xticklabels(
        ax.get_xticklabels(),
        rotation=45,
        ha="left",
        fontsize=10,
        weight='bold',
        rotation_mode="anchor"
    )
    ax.set_yticklabels(ax.get_yticklabels(), fontsize=10, weight='bold')
    ax.xaxis.set_label_position('top')
    ax.xaxis.tick_top()
    plt.title(title, fontsize=16, weight='bold', pad=20)
    cbar = ax.collections[0].colorbar
    cbar.ax.tick_params(labelsize=10, width=1.2)
    cbar.set_label("Frequency", weight='bold', fontsize=12)
    cbar.ax.yaxis.set_major_locator(ticker.MaxNLocator(integer=True))
    for label in cbar.ax.get_yticklabels():
        label.set_weight('bold')
    box = ax.get_position()
    ax.set_position([box.x0, box.y0, box.width * 0.93, box.height])
    plt.tight_layout()
    plt.savefig(output_png, dpi=300)
    plt.close()
    print(f"Heatmap saved to: {output_png}")
generate_hdac_cancer_heatmap(
    input_csv="/Users/zhaishiyang/Desktop/hdac_cancer_counts_filtered_no_reviews.csv",
    output_png="HDAC_Cancer_Type_Heatmap.png"
)
```

7.2 Appendix II. Publication I: Development and characterization of the first selective class IIb histone deacetylase degraders

The following pages include the article “Development and characterization of the first selective class IIb histone deacetylase degraders” as it was published in the Journal of Medicinal Chemistry by the American Chemical Society.

The article is reprinted with the permission from:

Shiyang Zhai, Irina Honin, Linda Schäker-Hübner, Maria Hanl, Lukas Jacobi, Finn Dressler, Dominika Ewa Pieńkowska, Philipp König, Jan Gerhartz, Rabea Voget, Gerd Bendas, Michael Gütschow, Felix Meissner, Bjoern B. Burckhardt, Radosław P. Nowak, Christian Steinebach, Finn K. Hansen.

J. Med. Chem. **2025**, 68, 13, 13793–13821.

https://doi.org/10.1021/acs.jmedchem.5c00674

Journal of Medicinal Chemistry

pubs.acs.org/jmc

Article

Development and Characterization of the First Selective Class IIb Histone Deacetylase Degraders

Shiyang Zhai, Irina Honin, Linda Schäker-Hübner, Maria Hanl, Lukas Jacobi, Finn Dressler, Dominika Ewa Pieńkowska, Philipp König, Jan Gerhartz, Rabea Voget, Gerd Bendas, Michael Gütschow, Felix Meissner, Bjoern B. Burckhardt, Radosław P. Nowak, Christian Steinebach, and Finn K. Hansen*

Cite This: *J. Med. Chem.* 2025, 68, 13793−13821

Read Online

ACCESS | Metrics & More | Article Recommendations | Supporting Information

ABSTRACT: Proteolysis-targeting chimeras (PROTACs) are emerging new therapeutic modalities that facilitate the targeted degradation of disease-relevant proteins via an event-driven mode of action. In this work, we report the design, synthesis, and biological evaluation of the first-in-class selective degraders of the class IIb histone deacetylases (HDACs) 6 and 10. To this end, the dual HDAC6/10 inhibitor tubastatin A and a ring-opened analog were connected via well-established PROTAC linkers to pomalidomide and phenylglutarimides as cereblon recruiters. This approach led to the discovery of **AP1** (HDAC6 DC_{50} = 13 nM; HDAC10 DC_{50} = 29 nM) as a potent degrader of class IIb HDACs. Importantly, **AP1** neither degraded HDAC1/8 (class I) and HDAC4/7 (class IIa), nor induced histone H3 hyperacetylation, thereby confirming its selectivity for class IIb HDACs. Due to its low cytotoxicity against hematological and solid cancer cell lines, **AP1** represents a valuable tool compound for the chemical knockdown of class IIb HDACs.

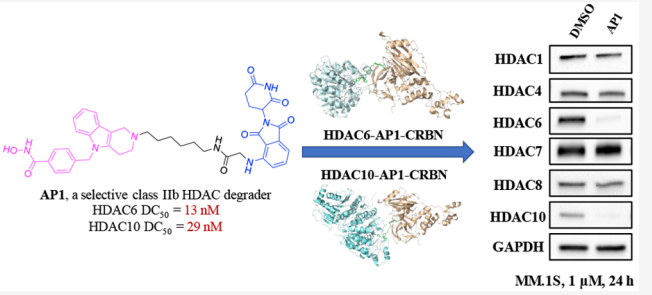

INTRODUCTION

Protein acetylation, a critical post-translational modification, regulates crucial cellular processes such as enzymatic activity, subcellular localization, and protein interactions. Moreover, it impacts cell signaling, turnover, differentiation, and survival.[1] In this process, histone acetyltransferases (HATs) transfer acetyl groups (acetylation), and histone deacetylases (HDACs) remove them (deacetylation), thereby influencing both histone and nonhistone proteins in various cellular functions.[2,3] As essential epigenetic regulators, HDACs have captured significant attention through extensive research spanning multiple stages of tumor development over the past decades, with their dysregulation contributing to tumorigenesis.[1−3]

Mammalian HDACs, 18 subtypes in total, were categorized into four classes based on their sequences, structural features, and cellular localization, among which, class I (HDAC1, 2, 3 and 8), class II (HDAC4, 5, 7, 9, 6 and 10), and class IV (HDAC11) are Zn^{2+}-dependent. In contrast, members of class III (Sirt1−7) depend on NAD^+. Class II HDACs can be further divided into class IIa (HDAC4, 5, 7, and 9) and class IIb (HDAC6 and 10). Notably, the key characteristics of class IIb HDACs are that they are primarily located in the cytoplasm and have acetylated nonhistone proteins as primary substrates.[4] Substantial progress has been made to develop efficacious HDAC inhibitors (HDACi) to combat various HDAC-related diseases, including cancer. To date, four HDACi have been approved by the FDA for diverse cancer treatments.[3,5] However, despite their promising impact on cancer growth, the widespread use of nonselective HDACi is associated with various side effects.[5] This underscores the need for exploring more targeted approaches to achieve subtype- or class-selective HDAC inactivation, aiming for both efficacy and enhanced safety in therapeutic interventions. To this end, class IIb HDACs gained much attention.

HDAC6, as one of the Zn^{2+}-dependent class IIb members, can regulate various biological processes via its deacetylation activity on acetylated lysines in nonhistone proteins, such as cellular proliferation, motility, apoptosis, DNA damage response, activation of heat shock response, transcriptional repression as well as metabolic response.[1] Beyond deacetylation, HDAC6 can also contribute to cellular processes like protecting against stress-induced protein aggregation and facilitating the transport of ubiquitinated proteins via the zinc-finger ubiquitin-binding domain (UBD) and a dynein-binding domain in its structure.[1] Since HDAC6 participates in several biological processes via different enzymological and nonenzymological functions, the continuous development of

Received: March 7, 2025
Revised: May 21, 2025
Accepted: June 4, 2025
Published: June 18, 2025

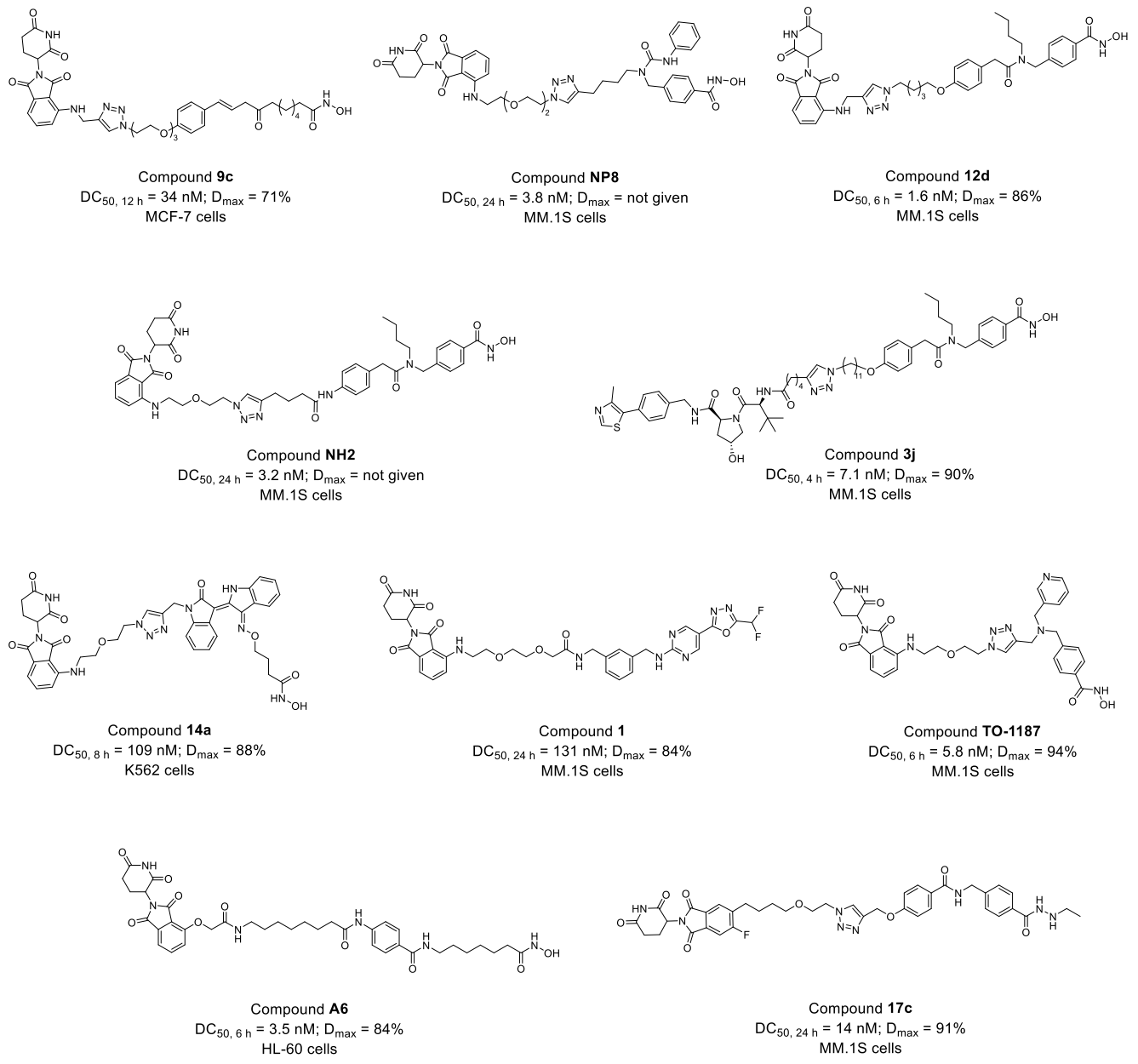

Figure 1. Reported selective HDAC6 PROTACs and their respective degradation efficiencies.

inhibitors and degraders for HDAC6 has emerged as a hot topic.[6−16]

HDAC10, the other member of class IIb, functions as a potent polyamine deacetylase with a notable preference for N^8-acetylspermidine hydrolysis over acetylated lysine.[17] Importantly, HDAC10 plays a significant role in various biological processes related to cancer, such as cellular proliferation, apoptosis, invasion, autophagy, and drug resistance.[18,19] Notably, its involvement in promoting cellular survival through autophagy has been reported in neuroblastoma.[20,21] In terms of drug resistance, elevated HDAC10 levels have been associated with protecting cancer cells from chemotherapy, and HDAC10 inhibition has been reported to increase cancer cell sensitivity to chemotherapy.[18,19] These findings underscore the potential of HDAC10 as a promising therapeutic target in cancer treatment.

Structurally distinctive within the Zn^{2+}-dependent HDAC family, HDAC6 and HDAC10 feature two deacetylase domains. In HDAC6, both domains are active with different functions: deacetylase domain 1 (DD1) focuses on deacetylating substrates with acetylated lysine at their C terminus,[1] while deacetylase domain 2 (DD2) exclusively targets peptides featuring an internal acetylated lysine residue. Conversely, HDAC10 possesses an active polyamine deacetylase (PDAC) domain and an inactive pseudodeacetylase (ΨDAC) domain.[17,22] Key residues in the active site of HDAC10, such as E274 (zebrafish numbering), contribute to its specificity for polyamine substrates.[17,22] The unique ηA2 helix and a specific loop induce steric constriction in the active site, thereby influencing its deacetylase activities.[17] Despite differences in substrate selectivity, crystal structures reveal a typical assembly pattern for HDAC6 and HDAC10,[17,22] opening avenues for developing molecular tools to achieve dual inactivation for both targets.

In contrast to the occupancy-driven pharmacology of classical inhibitors, proteolysis-targeting chimeras (PROTACs)

https://doi.org/10.1021/acs.jmedchem.5c00674
J. Med. Chem. 2025, 68, 13793−13821

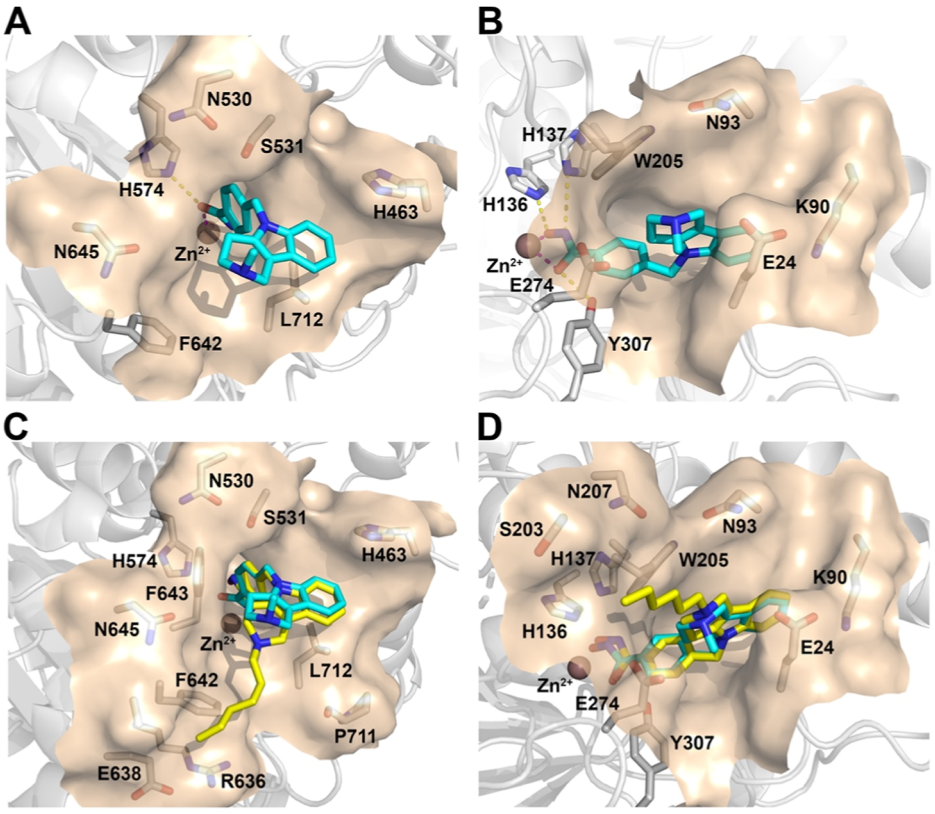

Figure 2. (A,B) Binding mode of tubastatin A (cyan) in *Danio rerio* HDAC6 (A; PDB: 6THV) and *Danio rerio* HDAC10 (B; PDB: 6WBQ). (C,D) Docking pose of the tubastatin A derivative in *Danio rerio* HDAC6 (C) and *Danio rerio* HDAC10 (D). Hydrogen bonds are indicated by yellow dashes, and the metal chelation interaction is indicated by purple dashes.

represent a small molecule-based heterobifunctional tool with an event-driven mode of action (MoA). This catalytic MoA relies on hijacking the endogenous ubiquitination process in cells, thereby tagging the protein of interest (POI) for degradation by the proteasome.[23] Consequently, PROTAC-induced degradation reduces cellular POI levels, offering potential therapeutic applications across various diseases.

To date, several PROTACs have been reported to be selective HDAC6 degraders (Figure 1). Most of these PROTACs utilize hydroxamic acid-based HDAC6 ligands as warheads and recruit either cereblon (CRBN)[8−11,13−15,24] or von Hippel−Lindau (VHL)[12] as E3 ligases. Notably, these PROTACs exhibit potent HDAC6 degradation, with some achieving DC_{50} values in the low nanomolar range. Previous studies include degraders based on HDAC6-selective inhibitors (e.g., nexturastat A, an indirubin-based HDAC6 inhibitor, and TO-317), nonselective HDAC inhibitors (e.g., crebinostat and vorinostat), and HDAC6/8-selective inhibitors.[8−12,14,15,24−26] In addition to the above-mentioned hydroxamic acid-based PROTACs, we reported the first nonhydroxamate selective HDAC6 degraders in 2022. These degraders employed a difluoromethyl-1,3,4-oxadiazole warhead as a zinc-binding group and engaged CRBN or VHL as E3 ligases.[16] In addition, an ethyl hydrazide-based selective HDAC6 degrader recruiting CRBN was also reported by our group in 2025.[27] Interestingly, HDAC6 PROTACs have also been explored as potential therapeutic agents beyond cancer, including applications of a nexturastat A-based degrader in renal ischemia-reperfusion injury (RIRI),[25] and both indirubin-derived and vorinostat-derived degraders in inflammation.[14,28] However, none of these above-mentioned studies have examined the effects of HDAC6 PROTACs on HDAC10 protein levels, the other member of the class IIb HDAC family.

In this study, we aimed to develop the first selective dual HDAC6/10 PROTAC degraders. To this end, we utilized tubastatin A derivatives as HDAC6/10 warheads, which were linked through suitable PROTAC spacers to pomalidomide or phenylglutarimides as CRBN recruiters.

RESULTS AND DISCUSSION

Design of Dual HDAC6/10 Degraders. Tubastatin A (HDAC6 pIC_{50} = 7.0; HDAC10 pIC_{50} = 7.9) was selected as the POI binder due to its dual inhibition of HDAC6 and HDAC10, as demonstrated in NanoBRET-based target engagement assays.[29] Additionally, the available cocrystal structures of tubastatin A in complex with *Danio rerio* HDAC6 and HDAC10 enabled structure-based PROTAC design. According to the elucidated crystal structures of *D. rerio* HDAC6 (PDB: 6THV)[30] and HDAC10 (PDB: 6WBQ)[31] in complex with tubastatin A, it is evident that tubastatin A exhibits a notable capacity for effective interaction with both targets within their respective catalytic pockets. In the case of HDAC6 (Figure 2A), the hydroxamic acid group of tubastatin A establishes a hydrogen bond with residue H574 and engages in chelation with the Zn^{2+} ion within the catalytic tunnel. Similarly, for HDAC10 (Figure 2B), interactions of the hydroxamic acid group with His136 and His137, alongside chelation with the Zn^{2+} ion, are also observed. The tricyclic tetrahydro-γ-carboline capping group of tubastatin A has been shown to interact with residues E24 and W205. In contrast, the

https://doi.org/10.1021/acs.jmedchem.5c00674
J. Med. Chem. 2025, 68, 13793−13821

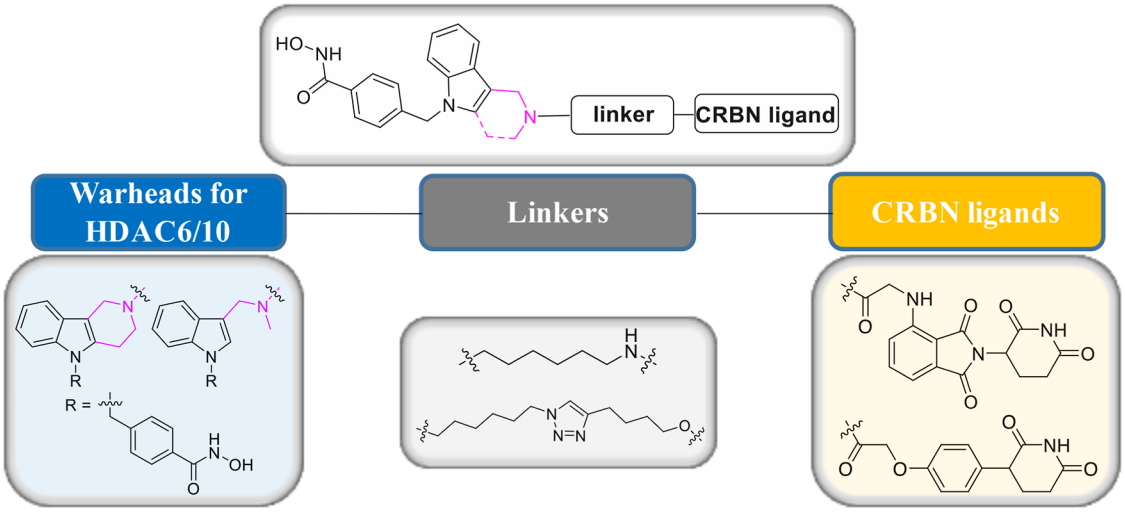

Figure 3. Design of potential class IIb HDAC degraders.

residue E274 can form electrostatic interactions with the tertiary amine in the capping group. Notably, E24 and E274 are critical for HDAC10 selectivity, facilitating the deep insertion of tubastatin A into the HDAC10 catalytic pocket. In light of these documented observations, tubastatin A emerges as a promising ligand candidate for developing dual degraders targeting both class IIb HDACs.

To determine the optimal anchor point on tubastatin A for the attachment of PROTAC linkers, as illustrated in Figure 2A, an analysis of tubastatin A's conformation within HDAC6 reveals multiple possibilities in the capping group for linker extension, specifically at positions C1, C6, as well as on the tertiary amine. In contrast, for HDAC10 (Figure 2B), both C1 and C6 are buried into the pocket, which may increase the probability of collisions between the linker-attached ligand and nearby residues, such as E24 and K90. Therefore, a tubastatin A derivative featuring a flexible hexyl chain attached to the tertiary amine, designed to mimic the PROTAC linker, was docked into the catalytic pockets of both HDAC6 and HDAC10 (Figure 2C,D). Notably, this derivative aligns well with the cocrystal structures of tubastatin A bound to both HDAC6 and HDAC10, with the hexyl chain extending beyond the pocket boundaries in both cases. Consequently, the tertiary amine in the capping group of tubastatin A was identified as an optimal anchor point.

A PROTAC molecule typically comprises a POI warhead, an E3 ligase recruiter, and a linker to connect both ligands. In contrast to tubastatin A, acknowledged for its enhanced selectivity toward HDAC10 relative to HDAC6 (8-fold), a bicyclic derivative featuring a dimethylamine moiety in the capping group demonstrated even greater selectivity, reaching up to 40-fold.[29] Consequently, as shown in Figure 3, tubastatin A and its bicyclic derivative were utilized as warheads in the present study. The flexible alkyl chain, as a commonly reported linker type, was employed in the design. Furthermore, since the variation of the E3 ligase ligand has been shown to impact degrader activity as well as stability,[32] two different CRBN ligands, specifically pomalidomide and a phenylglutarimide derivative, were chosen as E3 ligase recruiters.

Chemistry. Scheme 1 illustrates the synthesis of protected POI ligands with the attached linkers and the synthesis of CRBN ligands. Briefly, to synthesize compounds **4** and **5** (Scheme 1A), commercially available phenylhydrazine and *tert*-butyl 4-oxopiperidine-1-carboxylate were used as starting materials to generate tricyclic compound **1**. Subsequently, the alkylation of the indole with methyl 4-(bromomethyl)benzoate afforded compound **2**. Compound **2** was hydrolyzed with lithium hydroxide monohydrate and acidified with hydrochloric acid to release the carboxylic acid group. The resulting compound was subjected to a HATU-mediated amide coupling reaction with *O*-benzylhydroxylamine hydrochloride to yield compound **3**. Subsequently, the Boc-protecting group in compound **3** was removed with trifluoroacetic acid (TFA). The released secondary amine was then alkylated with *tert*-butyl (6-bromohexyl)carbamate to furnish compound **4** and 1-azido-6-bromohexane to generate compound **5**.

For the synthesis of the bicyclic warhead compound **9** (Scheme 1B), a previously reported method was employed.[29] Starting from the commercially available 1*H*-indole-3-carbaldehyde, a substitution reaction was performed to provide compound **6**. In the next step, the reductive amination of **6** with methylamine afforded **7**. Afterward, the secondary amine of compound **7** was substituted with *tert*-butyl (6-bromohexyl)carbamate to yield compound **8**. Following the hydrolysis of methyl ester in compound **8** and subsequent acidification to form the carboxylic acid moiety, the *O*-benzyl-protected compound **9** was generated through a HATU-mediated amide coupling reaction.

The synthesis of CRBN ligands is summarized in Scheme 1C. The pomalidomide-based intermediate **10**[33] and the phenylglutarimide building block **13**[32] were synthesized following previously reported methods. The carboxylic acid products of compounds **10** and **13** were obtained by the deprotection reactions using TFA. Subsequently, compounds **12** and **15** were synthesized via HATU-mediated esterification of **11** and **14** with hex-5-yn-1-ol.

Following the synthesis of linker-attached warhead ligands and E3 ligase recruiters, the final key intermediates for PROTACs were synthesized using either amide coupling reactions or Cu(I)-catalyzed azide-alkyne cycloadditions. Scheme 2 displays the synthesis of PROTACs **AP1**−**AP6**. Briefly, the *tert*-butyloxycarbonyl protecting group in compound **4** was removed with TFA. Afterward, amide coupling reactions with HATU and DIPEA in anhydrous DMF were carried out between deprotected compound **4** and compound **11** or **14**, forming compounds **16** and **17**, respectively. The

https://doi.org/10.1021/acs.jmedchem.5c00674
J. Med. Chem. 2025, 68, 13793−13821

Scheme 1. Synthesis of the Protected POI Ligands with Attached Linkers and CRBN ligands[a]

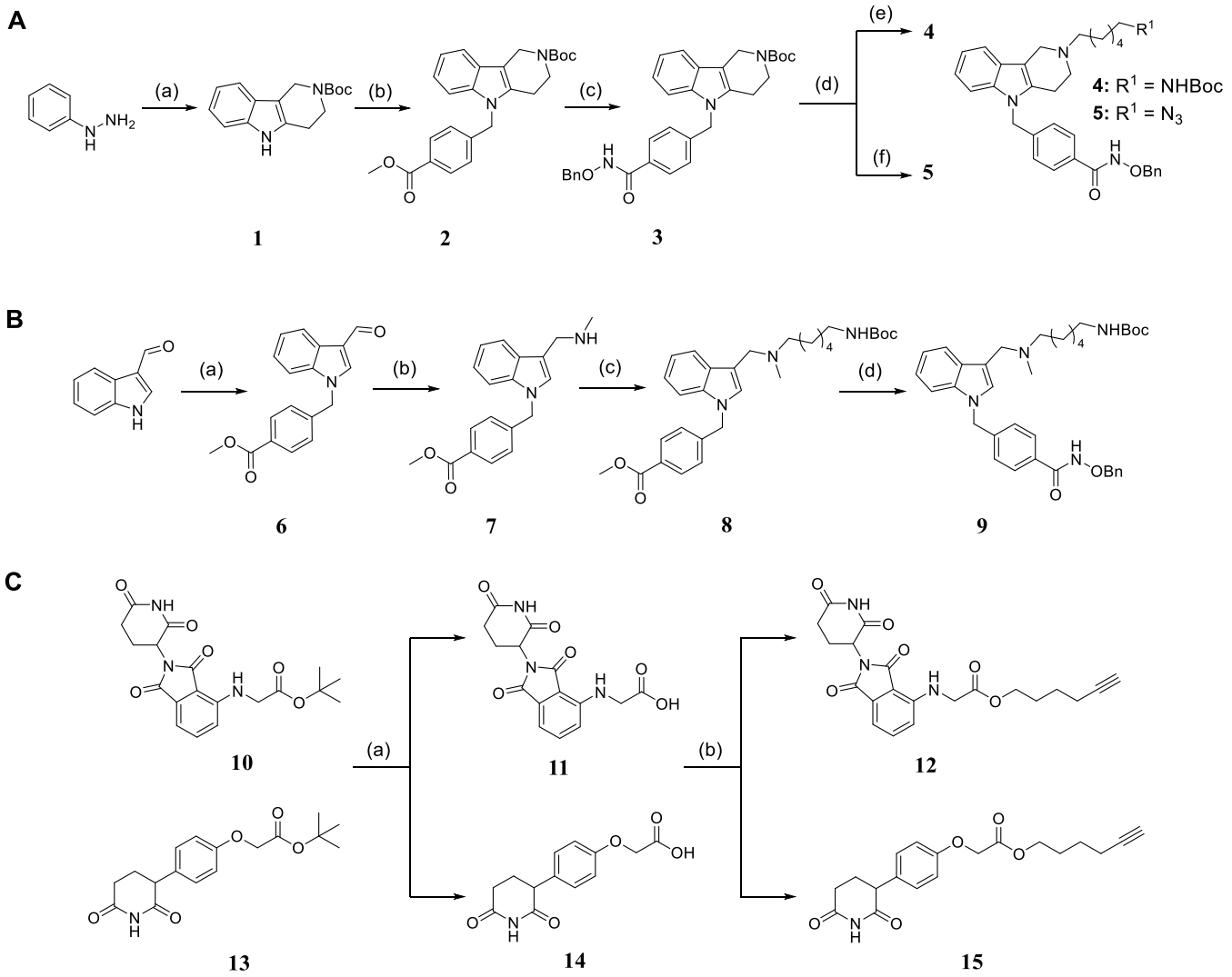

[a]A: (a) *tert*-butyl 4-oxopiperidine-1-carboxylate, 2,4,6-tripropyl-1,3,5,2,4,6-trioxatriphosphinane 2,4,6-trioxide (50% solution in EtOAc), toluene, 90 °C, 16 h, 60%;[34] (b) methyl 4-(bromomethyl)benzoate, Cs_2CO_3, ACN, reflux, 15 h, 57%;[35] (c) (i) LiOH × H_2O, THF/MeOH/H_2O, rt, 17 h; (ii) HCl (0.5 M in H_2O); (iii) *O*-benzylhydroxylamine hydrochloride, HATU, DIPEA, anhydrous DMF, rt, 16 h, 75% (three steps); (d) TFA, CH_2Cl_2, rt, 2 h; (e) *tert*-butyl (6-bromohexyl)carbamate, K_2CO_3, anhydrous DMF, rt, 18 h, 66% (two steps); (f) 1-azido-6-bromohexane, K_2CO_3, anhydrous DMF, rt, 20 h, 71% (two steps); B: (a) methyl 4-(bromomethyl)benzoate, Cs_2CO_3, ACN, reflux, 15 h, 99%;[35] (b) (i) $MeNH_2$, MeOH, rt, 19 h; (ii) $NaBH_4$, MeOH, 0 °C to rt, 3 h, 87% (two steps);[29,36] (c) *tert*-butyl (6-bromohexyl)carbamate, K_2CO_3, anhydrous DMF, rt, 15 h, 67%; (d) (i) LiOH × H_2O, THF/MeOH/H_2O, rt, 16.5 h; (ii) HCl (0.5 M in H_2O); (iii) *O*-benzylhydroxylamine hydrochloride, HATU, DIPEA, anhydrous DMF, rt, 17 h, 80% (three steps); C: (a) TFA, CH_2Cl_2, rt, 2 h; (b) hex-5-yn-1-ol, HATU, DIPEA, anhydrous DMF, rt, 15 h, two-step yield, 55% (compound **12**), 69% (compound **15**).

same procedure was used to generate compounds **20** and **21**. For compound **5**, featuring an azide group at the linker terminus, Cu(I)-catalyzed azide-alkyne cycloaddition reactions[37] were carried out to afford compounds **18** and **19**. Afterward, the benzyl protecting groups in compounds **16**−**21** were removed under a hydrogen atmosphere using Pd/C (5%) as a catalyst to release the zinc-binding groups and to furnish the desired PROTACs **AP1**−**AP6**.

Target Engagement Assays and Evaluation of Physicochemical Properties. All synthesized PROTACs were evaluated for their in vitro inhibitory activity against HDAC6 and HDAC10 using fluorogenic enzyme inhibition assays with Z-Lys(Ac)-AMC or Ac-spermidine-AMC as substrates. The results are summarized in Table 1. All compounds exhibited potent inhibitory activities with IC_{50} values in the double- or even single-digit nanomolar concentration range, indicating effective target engagement of both class IIb HDACs in vitro. Next, we performed cellular CRBN target engagement studies using a NanoBRET assay. As previously published, HEK293T cells stably expressing Nano-Luc-CRBN were used for competition experiments with a BODIPY-lenalidomide tracer.[38] All PROTACs demonstrated IC_{50} values in a single- or double-digit micromolar range, verifying CRBN target engagement and cell permeability. Consistent with previous reports,[39] we noticed that some pomalidomide-based PROTACs showed autofluorescence signals at high concentrations in the NanoBRET assay. The compounds affected with high background fluorescence are indicated with an asterisk in the Table 1, where the IC_{50} represents an upper estimate. Notably, the phenylglutarimides

https://doi.org/10.1021/acs.jmedchem.5c00674
J. Med. Chem. 2025, 68, 13793−13821

Scheme 2. Synthesis of PROTACs AP1−AP6[a]

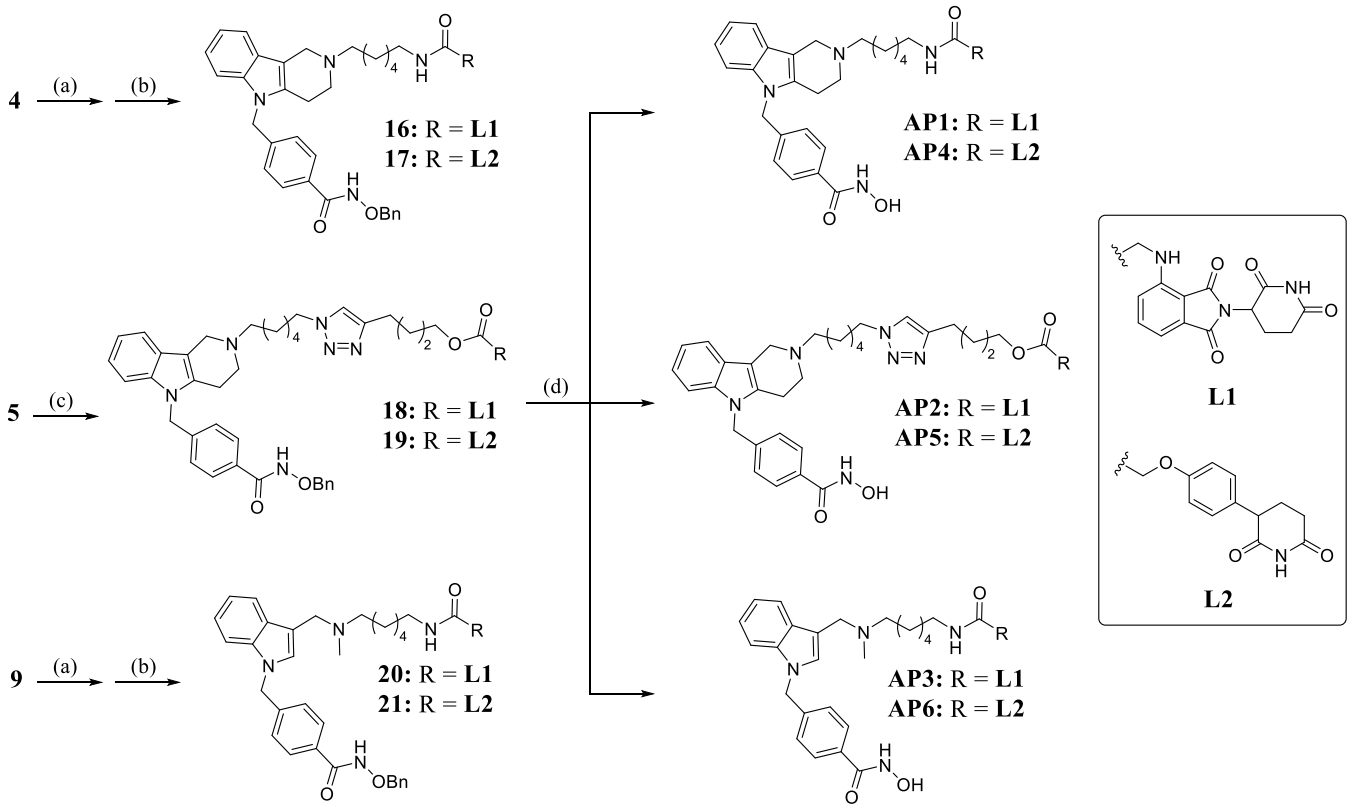

[a](a) TFA, CH_2Cl_2, rt, 2 h; (b) compound **11** or **14**, HATU, DIPEA, anhydrous DMF, rt, 17 h, 54−88% (two steps); (c) compound **12** or **15**, ascorbic acid, $CuSO_4$, DMF/H_2O (10:1), rt, 2−4 h, 54−59%; (d) H_2, Pd/C, EtOH/MeOH, rt, overnight, 9−33%.

Table 1. Evaluation of AP1−AP6 for Target Engagement and Physicochemical Properties

Cmpd.	IC_{50} (μM) HDAC6[a]	HDAC10[b]	CRBN	M_r (g/mol)	elog $D_{7.4}$[c]	TPSA (Å^2)[d]	PPB (%)[e]	NRotB[f]
AP1	0.040 ± 0.005	0.022 ± 0.003	*7.5	734	1.8	182.18	96.7	16
AP2	0.047 ± 0.003	0.017 ± 0.003	*4.4	858	2.3	210.09	96.7	21
AP3	0.026 ± 0.002	0.007 ± 0.001	*80.8	722	1.3	182.18	97	18
AP4	0.025 ± 0.0005	0.023 ± 0.003	2.2	666	1.6	142.00	96.3	16
AP5	0.049 ± 0.005	0.015 ± 0.002	2.5	790	2.2	169.91	96.7	21
AP6	0.031 ± 0.0005	0.012 ± 0.004	15.6	654	1.2	142.00	96.1	18
vorinostat	0.033 ± 0.003	n.d.	n.d.	n.d.	n.d.	n.d.	n.d.	n.d.
quisinostat	0.105 ± 0.009	0.005 ± 0.0004	n.d.	n.d.	n.d.	n.d.	n.d.	n.d.
lenalidomide	n.d.	n.d.	0.6	n.d.	n.d.	n.d.	n.d.	n.d.
tubastatin A[g]	0.016 ± 0.0003	0.22 ± 0.02	n.d.	n.d.	n.d.	n.d.	n.d.	n.d.

[a]Z-Lys(Ac)-AMC was used as substrate. [b]Ac-spermidine-AMC was used as substrate. [c]Distribution coefficients at pH = 7.4 were estimated by a HPLC-based method. [d]Topological polar surface area is given in Å^2. [e]Plasma protein binding, experimentally determined percentage of compound bound to human serum albumin. [f]NRotB, number of rotatable bonds; n.d.: not determined. [g]HDAC inhibition data taken from literature.[41,42] Asterisks (*) indicate compounds with high background fluorescence, IC_{50} values should be considered as an upper estimate.

AP4-**AP6** exhibited stronger CRBN target engagement than the pomalidomide-based degraders **AP1**-**AP3**, highlighting the phenylglutarimide scaffold as an effective and simplified CRBN ligand.

An overview of the physicochemical properties of the synthesized degraders is provided in Table 1 to assess their drug-likeness. In general, PROTACs **AP1** to **AP6** are characterized by a moderate molecular weight, lipophilicity (partition coefficients were experimentally determined by an HPLC method), and polar surface area. As expected, the cyclization of the HDAC warhead in **AP1**, **AP2**, **AP4**, and **AP5** led to a somewhat higher log *D* value. Representatives of the pomalidomide-based series (**L1**) are slightly more lipophilic and show higher topological polar surface areas than their phenylglutarimide counterparts. PROTACs **AP1** to **AP6** are tightly bound to plasma proteins as indicated by the experimentally determined binding to human serum albumin (fu < 0.05), which is, however, a common feature of degraders with linear rotatable linkers.[40]

Since some immunomodulatory drugs (IMiDs) such as pomalidomide and IMiD-based PROTACs showed limited stability under cell culture conditions and in body fluids,[32] we investigated the plasma stability of **AP1**−**AP6** and the parent HDAC6/10 inhibitor tubastatin A. All compounds were tested

https://doi.org/10.1021/acs.jmedchem.5c00674
J. Med. Chem. 2025, 68, 13793−13821

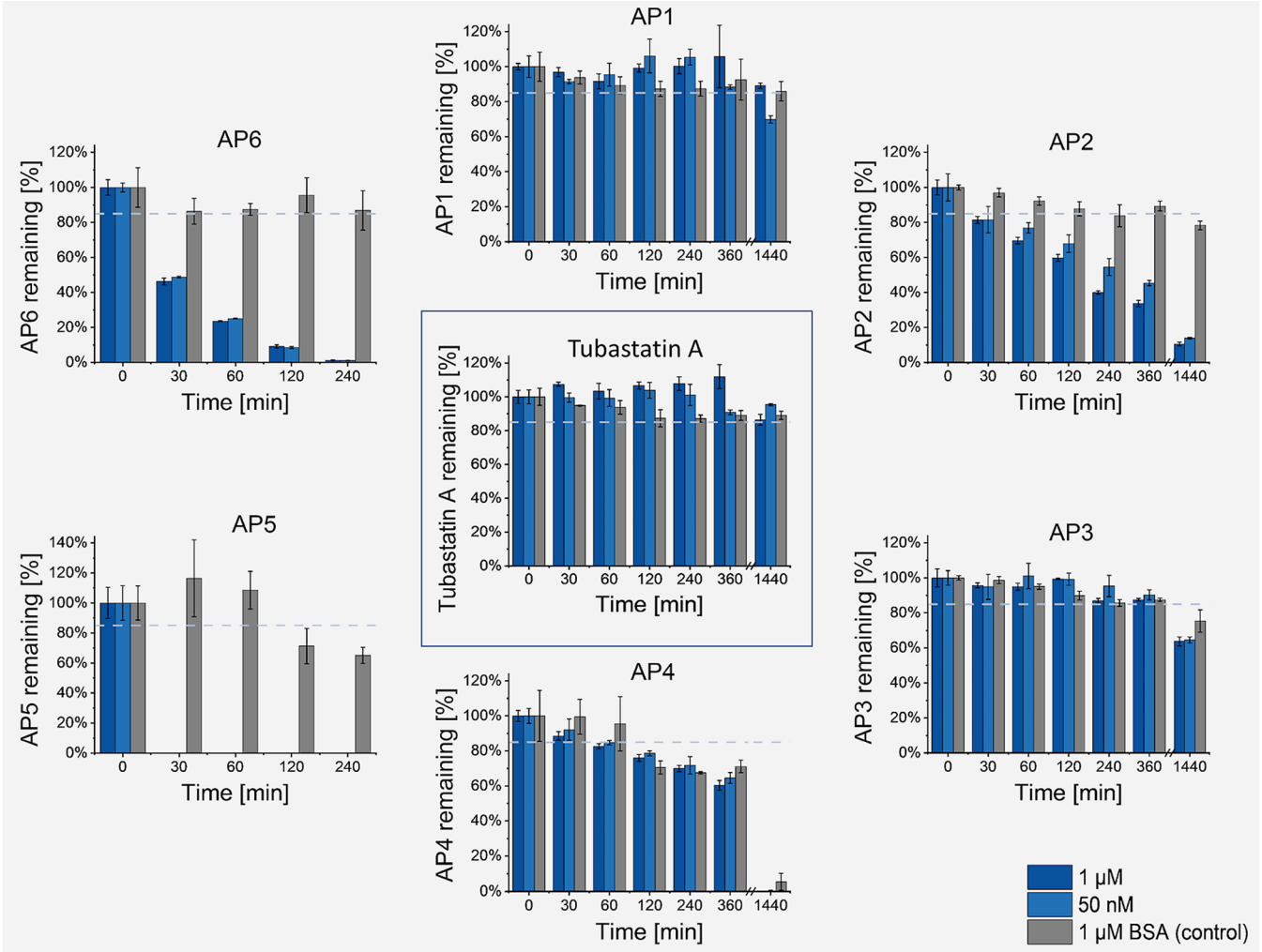

Figure 4. Human plasma stability of **AP1**−**AP6** and tubastatin A over 24 h at concentrations of 50 nM and 1 μM. 4% bovine serum albumin (BSA) containing 1 μM of the respective AP compound (absence of plasma enzymes) served as control. The dashed line indicates the acceptance limit of −15% according to international bioanalytical guidelines (ICH guideline M10 on bioanalytical method validation).

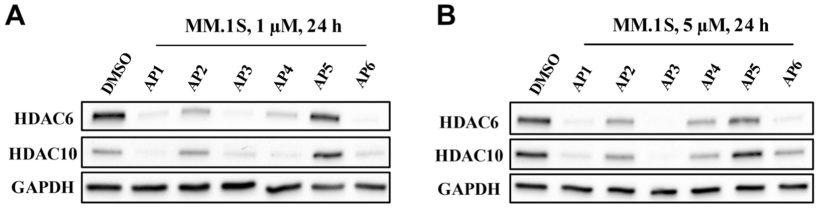

Figure 5. (A,B) Degradation of HDAC6 and HDAC10 mediated by degraders **AP1**−**AP6** at different concentrations. MM.1S cells were treated with **AP1**−**AP6** at concentrations of 1 μM (A) and 5 μM (B) for 24 h. HDAC6 and HDAC10 levels were detected by Western blot. GAPDH was used as the loading control. Representative images from a total of n = 3 replicates.

at concentrations of 50 nM and 1 μM in human plasma as well as control experiments in 4% bovine serum albumin (BSA, absence of plasma enzymes) were performed to investigate chemical stability. The results are summarized in Figure 4. While the parent inhibitor, tubastatin A, remained stable under all conditions, the degraders **AP1**−**AP6** were characterized by structure-related stabilities. Notably, the triazole-linked compounds **AP2** and **AP5** showed the lowest stability within their respective series (pomalidomide- or phenylglutarimide-based). A comparison of the tubastatin A derivatives (**AP1** and **AP4**) with their ring-opened analogs (**AP3** and **AP6**) confirmed the superior stability of tubastatin A-based degraders. Among them, **AP1** demonstrated stability comparable to tubastatin A at 1 μM, making it the most stable degrader in this set.

Class IIb HDAC Degradation by AP1−**AP6.** Following the target engagement and human plasma stability assays, we evaluated the degradation efficacy of compounds **AP1-AP6**. Western blot analyses of HDAC6 and HDAC10 protein levels were performed after treatment of MM.1S cells with 1 or 5 μM of each PROTAC for 24 h. As shown in Figure 5A,B, compounds **AP1**, **AP3**, **AP4**, and **AP6** exhibited robust degradation of both class IIb HDACs, with **AP2** displaying moderate efficacy. In contrast, minimal degradation of both targets was observed in the case of compound **AP5**. The low

https://doi.org/10.1021/acs.jmedchem.5c00674
J. Med. Chem. 2025, 68, 13793−13821

degradation efficacy of **AP2** and **AP5** is in very good agreement with their low stability (see Figure 4).

The quantified maximal degradation (D_{max}) data are presented in Table 2. Notably, compounds **AP1**, **AP3**, **AP4**, and **AP6** exhibited degradation levels of over 80% for both targets at certain concentrations, except for the HDAC10 degradation under the treatment of **AP6**. **AP1** turned out to be the most efficient dual degrader of this set at 1 μM with D_{max} values of 95% against HDAC6 and 93% against HDAC10, respectively. Conversely, compound **AP2** showed approximately 20% degradation of both targets at 5 μM, while achieving 68% degradation of HDAC6 at 1 μM. However, no degradation of HDAC10 was observed at this concentration. Compound **AP5** demonstrated only slight degradation of both targets at 5 μM, with negligible effects observed at 1 μM. The relatively diminished degradation potencies of compounds **AP2** and **AP5**, when compared with **AP1**, **AP3**, **AP4**, and **AP6**, may also be attributed to their longer linkers, potentially affecting the formation of a productive ternary complex.

Table 2. D_{max} and DC_{50} Data for HDAC6 and HDAC10 in MM.1S Cells after Treatment with AP1−AP6 for 24 h

	HDAC6 degradation (%)[a]		HDAC10 degradation (%)[a]		DC_{50} (nM, 24 h)[b]	
Cmpd.	1 μM	5 μM	1 μM	5 μM	HDAC6	HDAC10
AP1	95	96	93	88	13 ± 3.4	29 ± 1.1
AP2	68	24	n.e.	19	n.d.	n.d.
AP3	94	99	85	94	16 ± 3.9	50 ± 2.7
AP4	89	30	84	41	1.3 ± 0.5	1.7 ± 0.9
AP5	n.e.	9	n.e.	3	n.d.	n.d.
AP6	96	95	75	56	4.5 ± 0.4	7.9 ± 3.3

[a]Percentage of degraded HDAC6 or HDAC10 protein after 24 h treatment of MM.1S cells with 1 or 5 μM of each compound, mean of n = 3 replicates. [b]Mean ± SD of n = 2 biologically independent experiments, each performed in triplicates; n.d.: not determined; n.e.: no effect (no degradation).

DC_{50} Value Determination and "Hook Effect". To further elucidate the degradation efficiency of the synthesized class IIb HDAC degraders, **AP1**, **AP3**, **AP4**, and **AP6** were selected for the determination of their DC_{50} values for HDAC6 and HDAC10 in MM1.S cells (Figure 6). As depicted in Table 2, all four compounds demonstrated potent DC_{50} values toward HDAC6 and HDAC10. Notably, **AP4** emerged as the most potent degrader for both HDAC6 and HDAC10, with DC_{50} values of 1.3 nM and 1.7 nM, respectively. Furthermore, it is noteworthy that all four compounds exhibited stronger degradation potency toward HDAC6 compared to HDAC10. The most significant difference, reaching 3.1-fold ($DC_{50,\ HDAC10}/DC_{50,\ HDAC6}$), was observed for **AP3** featuring a bicyclic warhead and a pomalidomide-based CRBN ligand. In contrast, the lowest difference of 1.3-fold was observed with **AP4**, comprising tubastatin A as the POI ligand and a phenylglutarimide derivative-based CRBN ligand. Consistent with the experiments at 1 and 5 μM (Figure 5), the phenylglutarimides **AP4** and **AP6** showed a "hook effect". In contrast, the pomalidomide-based PROTACs **AP1** and **AP3** did degrade HDAC6 and HDAC10 in a concentration-dependent manner. Another notable structure−degradation relationship was observed for the tubastatin A-based degraders **AP1** and **AP4** which demonstrated stronger degradation potency toward class IIb HDACs than the corresponding bicyclic derivative-based degraders (see **AP1** vs **AP3** and **AP4** vs **AP6**; see Table 2 and Figure 6). When comparing the degradation efficacy of the pomalidomide-based degraders with the phenylglutarimides, it is evident that the phenylglutarimides have lower DC_{50} values (see **AP1** vs **AP4** and **AP3** vs **AP6**; see Table 2 and Figure 6). However, this improvement comes at the expense of a prominent "hook effect".

AP1, A Tubastatin A and Pomalidomide-Based Degrader, Induced Selective Degradation of Class IIb HDACs. Next, we continued our assessment of degradation in multiple myeloma MM1.S cells. To better understand these class IIb HDAC degraders, we further conducted degradation selectivity studies to investigate their abilities to degrade other subtypes of HDACs. Here, we chose the isoforms of HDAC1

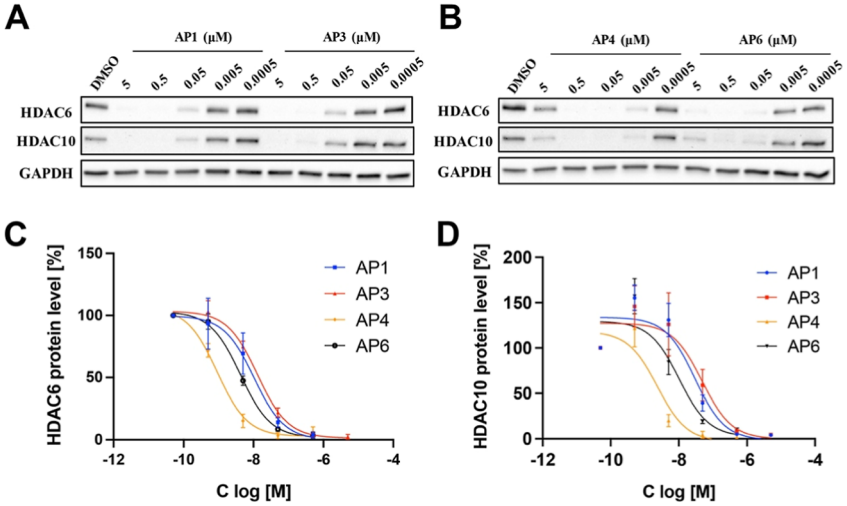

Figure 6. Determination of DC_{50} values of **AP1**, **AP3**, **AP4**, and **AP6** for HDAC6 and HDAC10. (A,B) Western blot analysis of HDAC6 and HDAC10 degradation in MM.1S cells treated for 24 h with **AP1**, **AP3**, **AP4**, and **AP6** at different concentrations. GAPDH was selected as loading control. Representative image of n = 2 biologically independent experiments, each performed in triplicates. (C,D) DC_{50} values were obtained by fitting D_{max} values to a variable slope response model (three parameters). Representative graph of n = 2 biologically independent experiments, each performed in triplicates. For mean ± SD see Table 2.

https://doi.org/10.1021/acs.jmedchem.5c00674
J. Med. Chem. 2025, 68, 13793−13821

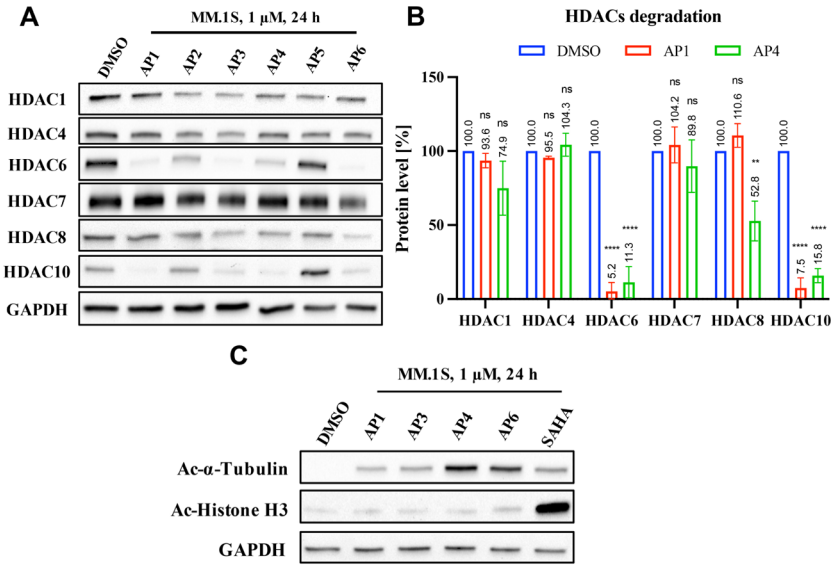

Figure 7. Degradation selectivity of the investigated class IIb HDAC degraders. (A) MM.1S cells were treated with 1 μM of the respective degrader for 24 h. HDAC1, 4, 6, 7, 8, and 10 levels were detected by Western blot. GAPDH was chosen as loading control. Representative image of $n = 3$ replicates. (B) Densitometric analysis of HDAC1, 4, 6, 7, 8, and 10 levels after treatment with **AP1** and **AP4.** Data from $n = 3$ replicates. Statistical analysis was performed by using one-way ANOVA in GraphPad Prism 8. Statistical significance was indicated with asterisks (ns = no significance; ** = $p < 0.01$; **** = $p < 0.0001$). (C) Representative immunoblot analysis of acetylated α-tubulin and histone H3. MM.1S cells were incubated for 24 h at a concentration of 1 μM. Afterward, cell lysates were immunoblotted with an antiacetyl-α-tubulin and antiacetyl-histone H3 antibody. Vorinostat (SAHA) was used as positive control, and GAPDH was chosen as loading control. Representative image of $n = 2$ biologically independent experiments, each performed in triplicates.

and HDAC8 from class I and HDAC4 and 7 from class IIa. For **AP3** and **AP6**, which contain the bicyclic derivative-based warhead, both PROTACs showed a trend toward degrading HDAC1, HDAC4, HDAC7 and HDAC8 compared to the vehicle control group (Figure 7A). In contrast, the tubastatin A-based degrader **AP4** caused no relevant HDAC1, HDAC4, or HDAC7 degradation but significant HDAC8 degradation, while **AP1** induced no off-target degradation at all (Figure 7B).

To investigate the cellular target engagement, the acetylation levels of HDAC substrate proteins like Ac-α-tubulin and Ac-histone H3 were investigated by immunoblot analysis for **AP1**, **AP3**, **AP4**, and **AP6** treated cells using vorinostat (SAHA) as a positive control (Figure 7C). All compounds caused an upregulation of Ac-α-tubulin, a known substrate of HDAC6, thereby indicating an inhibition of HDAC6 activity. The pomalidomide-based degraders **AP1** and **AP3** induced upregulation of Ac-α-tubulin comparable to vorinostat. This effect is even more pronounced in the case of the phenylglutarimides **AP4** and **AP6**. These results are consistent with the corresponding DC_{50} values of the HDAC6 degradation. In contrast, no degrader upregulated Ac-histone H3 levels, a substrate of HDAC1−3, while treatment with the positive control vorinostat resulted in strong hyperacetylation of histone H3.

Since PROTACs with rigid linkers often improve potency and selectivity in targeted protein degradation,[43−45] two PROTACs (**AP7** and **AP8**, Figure 8A) with rigid linkers were designed and synthesized to replace the flexible linker in **AP1**. Both chosen rigid linkers are similar in length to **AP1** (see Scheme S1A for synthetic details, Supporting Information). As a first step, the degradation ability of **AP7** and **AP8** on HDAC6 and HDAC10 was evaluated. Interestingly, both degraders exhibited comparable HDAC6 and 10 degradation potencies to **AP1** at 1 μM in MM.1S cells. Of note, a "hook effect" in HDAC6 degradation was observed for **AP8** at 5 μM (Figure 8A). Next, we evaluated the degradation selectivity of **AP7** and **AP8** using HDAC8, a common off-target of HDAC6 modulators,[46] as representative isoform. Noteworthy, both degraders with rigid linkers exhibited noticeable HDAC8 degradation, whereas the more flexible **AP1** had minimal impact on HDAC8 levels (Figure 8A).

As reported by Geraldy et al. and Herbst-Gervasoni et al., the basic nitrogen atom in tetrahydro-γ-carboline capping group of tubastatin A is critical for potent HDAC10 binding due to electrostatic interactions,[29,31] while the introduction of fluorine into the linker of HDAC6 inhibitors can enhance HDAC6 selectivity.[47,48] Therefore, to gain deeper insights into the structure−degradation relationships of this compound series, two PROTACs (**AP9** and **AP10**, Figure 8B) were designed and synthesized that utilize an amide group to connect to the linker (see Scheme S1B in the Supporting Information for synthetic details). In **AP10**, the benzyl linker was replaced by a fluorinated analog. The effects of **AP9** and **AP10** on HDAC6, HDAC10, and HDAC8 degradation were evaluated by immunoblot analysis and the results are summarized in Figure 8B. As expected, both newly designed PROTACs, along with **AP1**, demonstrated potent HDAC6 degradation at 1 and 5 μM in MM.1S cells. In contrast to **AP7** and **AP8**, which feature a rigid linker and induce noticeable HDAC8 degradation, **AP9** and **AP10**, bearing a flexible linker and an amide connecting unit, showed minimal impact on HDAC8 levels. Notably, replacing the basic nitrogen atom with an amide bond at the anchor point significantly affected HDAC10 degradation; both **AP9** and **AP10** induced reduced HDAC10 degradation compared to **AP1** at both concentrations tested. Based on the results summarized in Figure 8, several key structure−degradation relationships can be identified: (1) introduction of a rigid linker (as in **AP7** and **AP8**) led to off-target HDAC8 degradation; (2) amide-linked PROTACs (**AP9** and **AP10**) preferentially degraded HDAC6,

https://doi.org/10.1021/acs.jmedchem.5c00674
J. Med. Chem. 2025, 68, 13793−13821

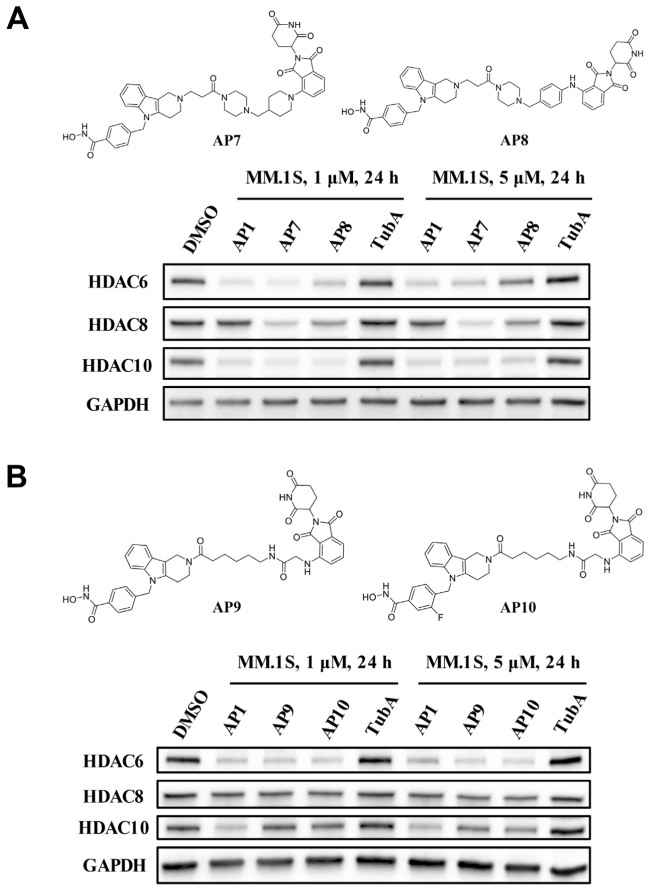

Figure 8. Degradation selectivity of **AP1**, and **AP7**−**AP10**. MM.1S cells were treated with 1 or 5 μM of the respective degraders, (A) **AP7** or **AP8** and (B) **AP9** or **AP10** for 24 h. In both cases, HDAC6, 8, and 10 levels were detected by Western blot. GAPDH was chosen as loading control and tubastatin A (TubA) as negative control. Representative image of n = 3 replicates.

with reduced activity against HDAC10 and no effect on HDAC8; and (3) fluorination of the linker (**AP10**) appears to be a promising strategy for developing effective HDAC6 degraders.

Taken together, **AP4**, despite its single-digit nanomolar DC_{50} values for HDAC6 and HDAC10, was not considered for detailed mode-of action studies as it showed a pronounced hook effect and significantly degraded HDAC8, indicating limited selectivity. The rigid-linker degraders **AP7** and **AP8** are unsuitable as tool compounds for the selective chemical knockdown of HDAC6 and HDAC10 due to their noticeable HDAC8 degradation. Similarly, the amide-linked degraders **AP9** and **AP10** were excluded due to their diminished HDAC10 degradation. Instead, **AP1** with its flexible linker and a basic nitrogen atom at the anchor point, emerged as a potent and highly selective class IIb HDAC degrader. **AP1** spares HDAC1, 4, 7 and 8 while avoiding histone H3 hyperacetylation, confirming the absence of class I HDAC inhibition or degradation. Furthermore, **AP1** showed no evidence of a "hook effect" and displayed high plasma stability. Consequently, **AP1** was chosen for subsequent mode-of-action studies.

AP1 Degrades Class IIb HDACs via the Ubiquitin-Proteasome System. To confirm the ubiquitin-proteasome system's (UPS) involvement in the degradation of HDAC6 and HDAC10, we conducted rescue experiments using binding competitors and UPS inhibitors. In addition, we synthesized a non-degrading control **AP1-N**, which contains a methylated glutarimide ring (Scheme S1C, Supporting Information), and thus cannot bind to CRBN. Since pretreatment with competitors can increase cytotoxicity, we reduced the treatment time to 6 h. Initial experiments without cotreatments confirmed that the reduced treatment time does not affect the degradation of class IIb HDACs by our PROTACs (Figure 9A). In the subsequent mode of action studies, we pretreated MM.1S cells for 0.5 h with 10 μM of the binding competitors

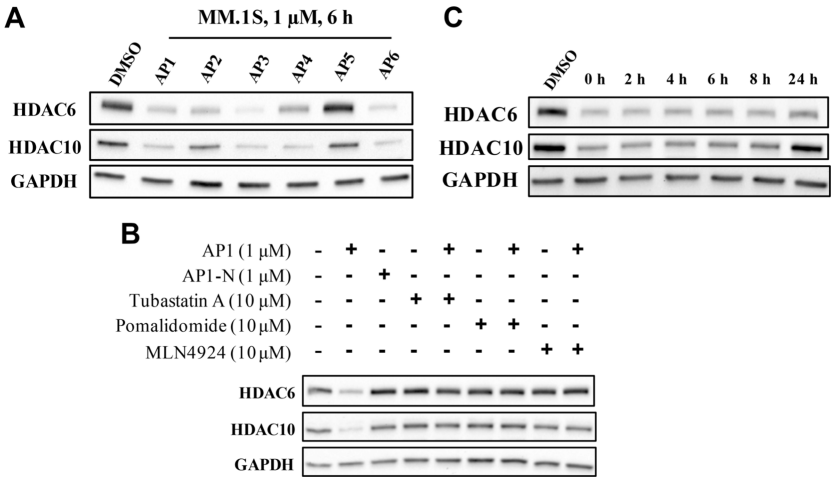

Figure 9. Rescue experiments with degrader **AP1**. (A) MM.1S cells were treated with 1 μM of the respective PROTACs for 6 h. HDAC6 and 10 levels were detected by Western blot. DMSO served as vehicle control and GAPDH was chosen as loading control. Representative image of n = 3 replicates. (B) Pretreatments of MM.1S cells for 30 min were carried out in the cotreatment groups containing the tubastatin A (10 μM), pomalidomide (10 μM), MLN4924 (10 μM), and then treated for 6 h with 1 μM of **AP1**. GAPDH was chosen as loading control. **AP1** served as positive and **AP1-N** as negative control. Representative image of n = 2 biologically independent experiments, each performed in triplicates. (C) Protein recovery at different time points after wash-out of **AP1**. MM.1S cells were treated with **AP1** (1 μM) for 24 h. Compound **AP1** was washed out at 0 h in the figure and drug-free medium was then supplemented to each group for protein recovery investigation. HDAC6 and HDAC10 protein levels were monitored at various time points post wash-out using Western blot, with GAPDH serving as a loading control. Representative image of n = 3 replicates.

https://doi.org/10.1021/acs.jmedchem.5c00674
J. Med. Chem. 2025, 68, 13793−13821

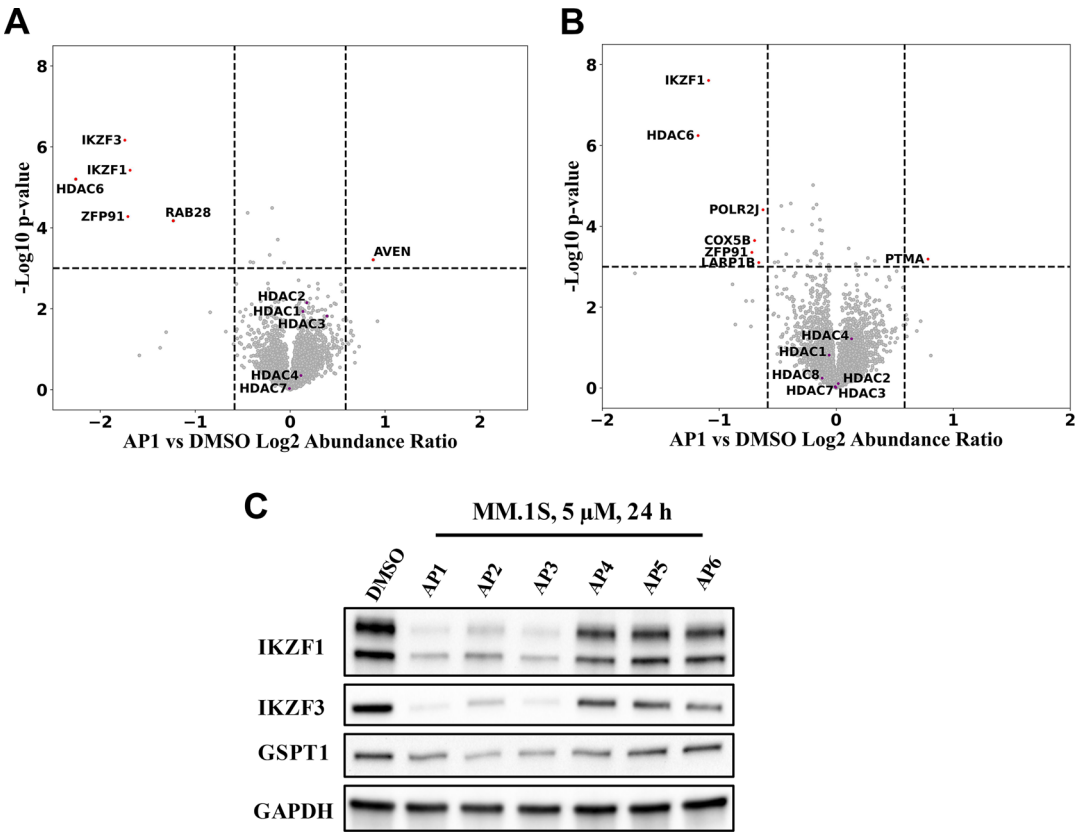

Figure 10. Quantitative proteomics data for **AP1** and evaluation of neosubstrate degradation by **AP1**−**AP6**. (A) Quantitative proteomics of MM.1S cell lysates after treatment with **AP1** (1 μM) for 5 h. Hits are labeled in red dots with the thresholds: Fold change >1.5 and P value <0.001. Other HDAC subtypes are labeled in purple dots. (B) Quantitative proteomics of MOLT-4 cell lysates after treatment with **AP1** (1 μM) for 5 h. Hits are labeled in red dots with the thresholds: Fold change > 1.5 and P value < 0.001. Other HDAC subtypes are labeled in purple dots. (C) Neosubstrate degradation caused by **AP1**−**AP6** in MM.1S cells. MM.1S cells were treated with DMSO or **AP1**−**AP6** (5 μM) for 24 h. IKZF1, IKZF3, and GSPT1 levels were detected by Western blot. GAPDH was used as the loading control. Representative image of n = 3 replicates.

tubastatin A and pomalidomide as well as the NEDD8-activating enzyme inhibitor MLN4924. Afterward, the cells were treated for 6 h with **AP1** (1 μM). The results are summarized in Figure 9B. Only the treatment with **AP1** alone induced significant degradation of HDAC6 and HDAC10, whereas **AP1-N** could not reduce the protein levels of either isoform. HDAC6 and HDAC10 levels were recovered for the groups with pretreatments, thereby confirming that **AP1** induces class IIb HDAC degradation via binding to CRBN and HDACs and leading to neddylation-dependent degradation. In addition, rescue experiments with the proteasome inhibitor MG132 demonstrated that the **AP1**-induced degradation of HDAC6 and HDAC10 is proteasome-dependent (Figure S1, Supporting Information). Furthermore, wash-out experiments with **AP1** confirmed that both HDAC6 and HDAC10 degradation is retained 8 h after the wash-out step, thereby indicating that the degradation effect of **AP1** is long-lasting (Figure 9C).

Quantitative Proteomics Analyses and Neosubstrate Degradation. In order to analyze the selectivity profile of **AP1** by an orthogonal method, we performed quantitative proteomics analysis. To this end, MM.1S cells were treated for 6 h with 1 μM of **AP1**, tubastatin A, and vehicle control (DMSO) and subsequently subjected to MS-based whole proteome analysis. Despite the unreliable detection of HDAC6 and HDAC10, likely due to low protein expression levels, we successfully monitored the protein levels of HDAC1−3 and HDAC7. None of the detected HDACs were significantly downregulated, confirming **AP1**'s excellent selectivity toward HDAC6 and HDAC10 (Figure S2, Supporting Information). In the next step, we repeated the proteomics study in MM.1S cells using diaPASEF-based mass spectrometry. In this case, we were able to detect HDAC6 but not HDAC10. However, the results clearly indicate that HDAC6 but none of the other detected HDAC isoforms was downregulated (Figure 10A). Furthermore, we observed degradation of the CRBN neosubstrates IKZF1, IKFZ3, ZFP91, and RAB28. To further investigate the effects on neosubstrates, the protein levels of IKZF1, IKZF3, and GSPT1 were assessed after treating MM.1S cells with **AP1**−**AP6** (5 μM) for 24 h. The results revealed strong degradation of IKZF1 and IKZF3, along with a moderate reduction in GSPT1 levels, by the IMiD-based degraders **AP1**−**AP3**. In contrast, the phenylglutarimide-based degraders **AP4**−**AP6** had no substantial impact on neosubstrate levels (Figure 10C). Rescue experiments by pretreatment with MLN4924 and tubastatin A demonstrated that MLN4924 but not tubastatin A could prevent the degradation of IKZF1 (Figure S3, Supporting Information). These results indicate that **AP1**-induced neosubstrate degradation occurs via CRBN and not HDAC engagement.

To further investigate the proteome-wide degradation specificity of **AP1**, we performed quantitative proteomics analysis in MOLT-4 cells. In this experiment, HDAC6, but not HDAC10, could be quantified. Among the identified HDACs

https://doi.org/10.1021/acs.jmedchem.5c00674
J. Med. Chem. 2025, 68, 13793−13821

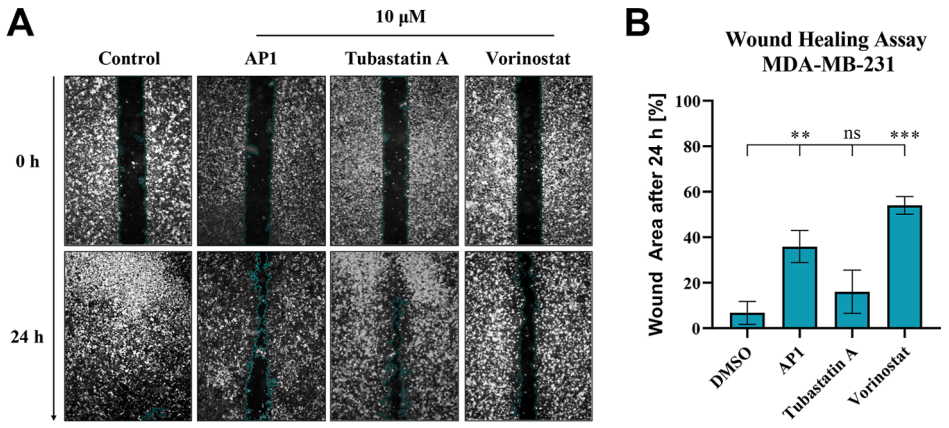

Figure 11. Wound healing assay. MDA-MB-231 cells were treated with 10 μM of the respective compounds or the vehicle control (DMSO) for 24 h. (A) Representative images taken immediately after removal of the cell culture inserts (0 h) and after 24 h. (B) Quantification of the remaining wound area compared to the initial wound area. Mean ± SD, at least $n = 2$ biologically independent replicates. Significances were determined by one-way ANOVA followed by Dunnett's multiple comparisons test (ns = $p \geq 0.05$; ** = $p \leq 0.01$ and *** = $p \leq 0.001$).

(HDAC1−4 and HDAC6−8), **AP1** selectively degraded HDAC6 after 5 h of incubation with 1 μM of **AP1** (Figure 10B). In addition, degradation of the CRBN neosubstrates IKZF1 and ZFP1 was observed. In conclusion, MS-based whole proteome analysis, in combination with our Western blot results verified that **AP1** is a selective degrader of HDAC6/10.

Cell Viability Assays. Since both HDAC6 and HDAC10 are involved in the pathogenesis of cancer, single treatments with either selective HDAC6 or HDAC10 inhibitors have demonstrated only low to moderate effects on cell viability,[48−50] we aimed to investigate the potential antiproliferative effects of dual HDAC6/10 degraders. Consequently, we tested **AP1**−**AP6** in viability assays against the multiple myeloma cell line MM.1S as well as the breast cancer cell line MCF-7. Both cell lines were selected because they are widely used to characterize HDAC6 degraders,[8,10,12] and serve as representative models of hematological and solid cancers. Interestingly, all compounds showed low or no inhibition of cell viability (Table S1 and Figure S4, Supporting Information). Long-term Western blot experiments after 48 and 72 h of treatment with **AP1**, **AP3**, **AP4**, and **AP6** confirmed that HDAC6 and HDAC10 degradation is sustained after 72 h in MM.1S cells (Figure S5, Supporting Information). Thus, these results indicate that the absence of antiproliferative activity after 72 h is not a result of instability of the degraders. To rule out that the limited antiproliferative effects in MCF-7 cells comes from absence of degradation, we treated MCF-7 cells for 24 h with 1 or 5 μM of **AP1**-**AP6** and analyzed the HDAC6 and HDAC10 levels by immunoblot analysis (Figure S6, Supporting Information). Consistent with the results obtained in MM.1S cells, **AP1**, **AP3**, **AP4** and **AP6** were identified as potent degraders of HDAC6 and HDAC10, while **AP2** and **AP5** were less effective. Again, the phenylglutarimides **AP4** and **AP6** showed a pronounced "hook effect" at 5 μM.

AP1's Effects on Cell Cycle Arrest, Autophagy, and Cell Migration. Noticing that HDAC6/10 degraders **AP1**−**AP6** showed no antiproliferative effects on MM.1S and MCF-7 cells (Table S1 and Figure S4, Supporting Information), we further tested **AP1** for its effects on other cell pathways, such as cell cycle arrest, autophagy induction, and its impact on cell migration. Treatment of MM.1S cells with 10 μM of **AP1** for 48 h induced a significant prolongation of the G1-phase, while treatment with the parent inhibitor tubastatin A did not lead to significant changes in the cell cycle (Figure S7, Supporting Information). **AP1** at 1 and 5 μM did not affect the LC3 I and LC3 II levels when compared with vehicle (DMSO) and positive control (chloroquine), indicating that **AP1** did not affect autophagy of MM.1S cells (Figure S8, Supporting Information). Next, we used the MDA-MB-231 cell line to investigate the antimigratory properties of tubastatin A and **AP1**. The parent inhibitor tubastatin A had no significant effects on cell migration, while **AP1** attenuated cell migration significantly (Figure 11).

DISCUSSION AND CONCLUSIONS

The first HDAC6 PROTACs were reported by Tang and co-workers in 2018.[8] Interestingly, despite employing a non-selective inhibitor as the HDAC warhead, the authors achieved selective HDAC6 degradation. Since then, various selective HDAC6 degraders have been developed using derivatives of nonselective inhibitors (e.g., crebinostat and vorinostat),[8,15] HDAC6-selective inhibitors (e.g., nexturastat A),[9−12] and HDAC6/8-selective inhibitors[26] as HDAC recruiters. However, none of these studies have investigated the effects of HDAC6 PROTACs on HDAC10 protein levels. Very recently, Gunning and co-workers reported the monoselective HDAC6 PROTAC degrader TO-1187.[24] This compound marks a significant advancement in the HDAC degrader field, demonstrating effective in vivo HDAC6 degradation without observable toxicity, thereby providing encouraging evidence for the safety of pharmacological HDAC6 degradation. However, the study did not assess HDAC10 degradation. Consequently, the tubastatin A-derived PROTACs disclosed in this study represent the first selective degraders of class IIb HDACs. Selective HDAC10 degradation has not yet been achieved, but it remains a key goal for expanding the toolbox of HDAC degraders. This goal may be achievable in the future by using acetylpolyamine mimetics as HDAC10-specific warheads.[17]

Taken together, our work demonstrates the successful design, synthesis, and biological evaluation of first-in-class selective degraders for the class IIb HDACs 6 and 10. Utilizing the dual HDAC6/10 inhibitor tubastatin A and a ring-opened analog, we connected these molecules to pomalidomide and a phenylglutarimide derivative via established PROTAC linkers to act as cereblon recruiters. This approach led to the discovery

https://doi.org/10.1021/acs.jmedchem.5c00674
J. Med. Chem. 2025, 68, 13793−13821

of **AP1**, a potent degrader of class IIb HDACs (HDAC6 DC_{50} = 13 nM; HDAC10 DC_{50} = 29 nM). Importantly, **AP1** showed no significant degradation of HDAC1/8 (class I) and HDAC4/7 (class IIa), nor did it induce histone H3 hyperacetylation, confirming its selectivity for class IIb HDACs. Furthermore, **AP1** exhibited low cytotoxicity against hematological and solid cancer cell lines, making it a valuable tool compound for the chemical knockdown of class IIb HDACs.

EXPERIMENTAL SECTION

Chemistry. *General Information.* Chemicals were obtained from abcr GmbH, Acros Organics, Carbolution Chemicals, Fluorochem, Sigma-Aldrich, TCI Chemicals, BLDpharm or VWR and used without further purification. Technical grade solvents were distilled prior to use. For all HPLC purposes, acetonitrile in HPLC-grade quality (HiPerSolv CHROMANORM, *VWR*) was used. Water was purified with a PURELAB flex (*ELGA VEOLIA*). Air-sensitive reactions were carried out under argon atmosphere utilizing standard Schlenk techniques. If no solvent is stated an aqueous solution was prepared with demineralized water. Mixtures of two or more solvents are specified as "solvent A"/"solvent B", 3/1, *v*/*v*; meaning that 100 mL of the respective mixture consists of 75 mL of "solvent A" and 25 mL of "solvent B". Thin-layer chromatography (TLC) was carried out on prefabricated plates (silica gel 60, F_{254}, Merck). Components were visualized either by irradiation with ultraviolet light (254 or 366 nm) or by staining appropriately. Column Chromatography: If not stated otherwise, column chromatography was carried out on silica gel (60 Å, 40−60 μm, Acros Organics). In addition, a flash column system (puriFlash XS 520 Plus, Advion Interchim Scientific) was utilized for the purification of the synthesized compounds. Nuclear Magnetic Resonance Spectroscopy (NMR): Proton (^{1}H) and carbon (^{13}C) NMR spectra were recorded either on a Bruker AVANCE 500 MHz at a frequency of 500 MHz (^{1}H) and 126 MHz (^{13}C) or on a Bruker AVANCE III HD 600 MHz at a frequency of 600 MHz (^{1}H) and 151 MHz (^{13}C). The chemical shifts are given in parts per million (ppm). As solvents deuterated chloroform ($CDCl_3$) and deuterated dimethyl sulfoxide (DMSO-d_6) were used. The residual solvent signal ($CDCl_3$: ^{1}H NMR: 7.26 ppm, ^{13}C NMR: 77.1 ppm; DMSO-d_6: ^{1}H NMR: 2.50 ppm, ^{13}C NMR: 39.52 ppm) was used for calibration. The multiplicity of each signal is reported as singulet (s), doublet (d), triplet (t), quartet (q), pentet (p), sextet (sext), multiplet (m) or combinations thereof. Multiplicities and coupling constants are reported as measured and might disagree with the expected values. Mass Spectrometry: High resolution electrospray ionization mass spectra (HRMS-ESI) were acquired with Bruker Daltonik GmbH micrOTOF coupled to a an LC Packings Ultimate HPLC system and controlled by micrOTOFControl3.4 and HyStar 3.2-LC/MS, with a Bruker Daltonik GmbH ESI-qTOF Impact II coupled to a Dionex UltiMateTM 3000 UHPLC system and controlled by micrOTOFControl 4.0 and HyStar 3.2-LC/MS or with a micrOTOF-Q mass spectrometer (Bruker) with ESI-source coupled with an HPLC Dionex UltiMate 3000 (Thermo Scientific). Low resolution electrospray ionization mass spectra (LRMS-ESI) were acquired with an Advion expression compact mass spectrometer (CMS) coupled with an automated TLC plate reader Plate Express (Advion). High Performance Liquid Chromatography (HPLC): A Thermo Fisher Scientific UltiMate 3000 UHPLC system with a Nucleodur 100−5 C18 (250 × 4.6 mm, Macherey Nagel) with a flow rate of 1 mL/min and a temperature of 25 °C or a 100−5 C18 (100 × 3 mm, Macherey Nagel) with a flow rate of 0.5 mL/min and a temperature of 25 °C with an appropriate gradient were used. For preparative purposes a AZURA Prep. 500/1000 gradient system (Knauer) with a Nucleodur 110−5 C18 HTec (150 × 32 mm, Macherey Nagel) column with 20 mL/min was used. Detection was implemented by UV absorption measurement at a wavelength of λ = 220 nm and λ = 250 nm. Bidest. H_2O (A) and ACN (B) were used as eluents with an addition of 0.1% TFA for eluent A. **Purity:** The purity of all final compounds was 95% or higher. Purity was determined via HPLC with the Nucleodur 100−5 C18 (250 × 4.6 mm, Macherey Nagel) at 250 nm. After column equilibration for 5 min, a linear gradient from 5% A to 95% B in 5 min followed by an isocratic regime of 95% B for 12 min was used.

GENERAL PROCEDURES

General Procedure A for the Synthesis of Compound 16−17 and 20−21. To a solution of compound **11** or **14** (1.0−1.1 equiv) in anhydrous DMF (3 mL), HATU (2 equiv) and DIPEA (3 equiv) were added. The mixture was stirred at room temperature for 0.5 h. Afterward, a solution of Boc-deprotected compound **4** or **9** (1 eq) in anhydrous DMF (2 mL) was added and the reaction mixture was then stirred for 17 h at room temperature. The mixture was poured into water (100 mL) and extracted with ethyl acetate (3 × 30 mL). The combined organic layer was then washed with water (3 × 50 mL) and followed by brine (50 mL), dried over anhydrous Na_2SO_4, filtered, and concentrated in vacuo to yield the crude products, which were subsequently purified by silica column chromatography.

General Procedure B for the Synthesis of Compound 18−19. To a solution of compound **12** or **15** (1 equiv) in DMF/H_2O (5 mL/0.5 mL), compound **5** (1.05 equiv), ascorbic acid (3 equiv), and $CuSO_4$ (1 equiv) were added. The mixture was stirred at room temperature for 2−4 h. Next, the mixture was poured into water (100 mL) and extracted with ethyl acetate (3 × 30 mL). The combined organic layer was then washed with water (3 × 50 mL)and followed by brine (50 mL), dried over anhydrous Na_2SO_4, filtered, and concentrated in vacuo to provide the crude products, which were then purified by flash column chromatography (0→10% MeOH in EtOAc, 0−10 min; 10% MeOH in EtOAc, 10−30 min).

General Procedure C for the Synthesis of Compounds AP1−AP10, and AP1-N. To a solution of compound **16−21**, **S4**, **S5**, **S8**, **S9**, **S11** (1 equiv) in methanol/ethanol (10 mL), Pd/C (5% palladium on carbon, 0.05 equiv) was added. The flask was evacuated and flushed with H_2 and the mixture was stirred at room temperature under H_2 atmosphere overnight. The completion of the reaction was monitored by HPLC and additional $Pd(OH)_2$/C (0.05 equiv) was added into the system if the conversion was not complete.[51] The resulting reaction solution was filtered over Celite and the solvents removed under reduced pressure. The subsequent purification was carried out utilizing reverse phase flash column chromatography (0→100% ACN in water, 0−30 min) or preparative HPLC.

Compound Characterization. *tert-Butyl 1,3,4,5-Tetrahydro-2H-pyrido[4,3-b] Indole-2-carboxylate (1).* To a solution of phenylhydrazine hydrochloride (10.0 g, 69.2 mmol, 1 equiv) and *tert*-butyl 4-oxopiperidine-1-carboxylate (15.2 g, 76.1 mmol, 1.1 equiv) in toluene (150 mL), 2,4,6-tripropyl-1,3,5,2,4,6-trioxatriphosphinane 2,4,6-trioxide (11.0 mL, 17.3 mmol, 0.25 equiv, 50% solution in EtOAc) was added as the catalyst. The mixture was stirred at 90 °C for 16 h. The completion of the reaction was monitored by TLC. The solvent was removed in vacuo. The crude product was then dissolved in a mixture of ethyl acetate (100 mL) and water (100 mL). The extraction was performed with the ethyl acetate (3 × 100 mL) and the combined organic layer was washed with brine and dried over anhydrous Na_2SO_4. The filtrate was concentrated in vacuo to afford the crude product, which was then purified by silica column (CyH/EtOAc 2:1, *v*/*v*) to yield compound **1** (11.3 g, 60%). **^{1}H NMR** (500 MHz, $CDCl_3$): δ

https://doi.org/10.1021/acs.jmedchem.5c00674
J. Med. Chem. 2025, 68, 13793−13821

7.92 (s, 1H), 7.45 (dd, J = 7.7, 1.3 Hz, 1H), 7.34−7.29 (m, 1H), 7.16 (ddd, J = 8.1, 7.1, 1.3 Hz, 1H), 7.10 (td, J = 7.4, 1.1 Hz, 1H), 4.65 (s, 2H), 3.82 (t, J = 5.7 Hz, 2H), 2.88−2.79 (m, 2H), 1.51 (s, 9H). **^{13}C NMR** (126 MHz, $CDCl_3$): δ 155.4, 136.0, 132.1, 125.8, 121.8, 119.7, 117.8, 110.8, 107.8, 80.0, 41.3, 28.6, 28.5, 23.7. **LC−MS (ESI)**, $[M - H]^-$ m/z: 271.1.

*tert-Butyl 5-(4-(Methoxycarbonyl)benzyl)-1,3,4,5-tetrahydro-2H-pyrido[4,3-b]indole-2-carboxylate (**2**).* To a solution of compound **1** (4.00 g, 14.7 mmol, 1 equiv) in acetonitrile (100 mL), methyl 4-(bromomethyl)benzoate (3.53 g, 15.4 mmol, 1.05 equiv) and Cs_2CO_3 (9.57 g, 29.4 mmol, 2 equiv) were added. The mixture was stirred and refluxed for 15 h. The completion of the reaction was monitored by TLC. The solvent was removed in vacuo. The crude product was then dissolved in a mixture of ethyl acetate (75 mL) and water (75 mL). The extraction was performed with the ethyl acetate (3 × 50 mL) and the combined organic layer was washed with brine (50 mL) and dried over anhydrous Na_2SO_4. The filtrate was concentrated in vacuo to afford the crude product, which was then purified by silica column (CyH/EtOAc 4:1, v/v) to afford compound **2** (3.51 g, 57%). **^{1}H NMR** (500 MHz, $CDCl_3$): δ 7.97−7.91 (m, 2H), 7.54−7.48 (m, 1H), 7.19 (dt, J = 8.1, 1.0 Hz, 1H), 7.14 (dtd, J = 14.0, 6.9, 1.4 Hz, 2H), 7.08−7.03 (m, 2H), 5.30 (s, 2H), 4.69 (s, 2H), 3.89 (s, 3H), 3.81 (t, J = 5.7 Hz, 2H), 2.70 (t, J = 5.5 Hz, 2H), 1.50 (s, 9H). **^{13}C NMR** (126 MHz, $CDCl_3$): δ 166.8, 155.3, 143.0, 136.9, 133.6, 130.3, 129.6, 126.2, 125.6, 121.8, 119.8, 118.0, 109.3, 108.0, 80.1, 52.3, 46.4, 41.3, 28.6, 27.1, 22.7. **LC−MS (ESI)**, $[M + H]^+$ m/z: 421.3.

*tert-Butyl 5-(4-((benzyloxy)carbamoyl)benzyl)-1,3,4,5-tetrahydro-2H-pyrido[4,3-b]indole-2-carboxylate (**3**).* To a solution of compound **2** (3.00 g, 7.14 mmol, 1 equiv) in THF/MeOH/H_2O (60 mL/12 mL/12 mL), LiOH·H_2O (0.784 g, 17.8 mmol, 2.5 equiv) was added. The mixture was stirred at room temperature for about 17 h. Heating at 50 °C for extra 1−2 h was performed when the reaction was not complete. Upon the completion of the hydrolysis, the solvents were removed in vacuo. The crude product was dissolved with water (50 mL) and acidified with HCl (0.5 M in water) until no more precipitate was formed. The resulting precipitate was collected via filtration, washed with water and dried in vacuo for the next step without further purification. To a solution of the dried precipitate (2.81 g, 6.91 mmol, 1 equiv) in anhydrous DMF (60 mL), HATU (5.26 g, 13.8 mmol, 2 equiv) and DIPEA (2.68 g, 20.7 mmol, 3 equiv) were added. The mixture was stirred for 30 min at room temperature. Afterward, *O*-benzylhydroxylamine hydrochloride (2.21 g, 13.8 mmol, 2 equiv) was added and the reaction mixture was stirred for 16 h. The completion of the reaction was monitored by TLC. The mixture was poured into water (150 mL) and extracted with ethyl acetate (3 × 50 mL). The combined organic layer was then washed with water (3 × 50 mL) and followed by brine (50 mL), dried over anhydrous Na_2SO_4, filtered, and concentrated in vacuo to afford the crude product, which was then purified by flash column chromatography (0 → 50% EtOAc in CyH, 0−10 min; 50% EtOAc in CyH, 10−35 min) to generate compound **3** (2.67 g, 75%). **^{1}H NMR** (600 MHz, $CDCl_3$): δ 8.59 (s, 1H), 7.56 (d, J = 7.9 Hz, 2H), 7.49 (d, J = 7.3 Hz, 1H), 7.41 (dd, J = 7.3, 2.2 Hz, 2H), 7.38−7.33 (m, 3H), 7.19−7.09 (m, 3H), 7.00 (d, J = 8.0 Hz, 2H), 5.26 (s, 2H), 5.00 (s, 2H), 4.67 (s, 2H), 3.79 (t, J = 5.8 Hz, 2H), 2.67 (t, J = 5.7 Hz, 2H), 1.49 (s, 9H). **^{13}C NMR** (151 MHz, $CDCl_3$): δ 166.0, 155.3, 142.1, 136.8, 135.4, 134.1, 131.2, 129.4, 129.0, 128.8, 127.7, 126.5, 125.5, 121.8, 119.8, 118.0, 109.3, 107.9, 80.1, 78.5, 46.2, 41.6, 40.8, 28.6, 22.6. **LC−MS (ESI)**, $[M - H]^-$ m/z: 510.4.

*tert-Butyl (6-(5-(4-((benzyloxy)carbamoyl)benzyl)-1,3,4,5-tetrahydro-2H-pyrido[4,3-b]indol-2-yl)hexyl)carbamate (**4**).* To a solution of compound **3** (1.46 g, 2.86 mmol, 1 equiv) in DCM (20 mL), TFA (4 mL) was added. The mixture was stirred at room temperature for 2 h and the complete removal of *tert*-butyl group was monitored by HPLC. Afterward, the mixture was dried in vacuo to offer the crude product for the next step. To a solution of the resulting crude product in anhydrous DMF (50 mL), *tert*-butyl (6-bromohexyl)carbamate (1.20 g, 4.29 mmol, 1.5 equiv) and K_2CO_3 (0.790 g, 5.72 mmol, 2 equiv) were added. The mixture was stirred at room temperature for 18 h. The completion of the reaction was monitored by HPLC. The mixture was poured into water (150 mL) and extracted with ethyl acetate (3 × 50 mL). The combined organic layer was then washed with water (3 × 50 mL) and followed by brine (50 mL), dried over anhydrous Na_2SO_4, filtered, and concentrated in vacuo to yield the crude product, which was then purified by silica column chromatography (EtOAc: MeOH 10:1, v/v) to yield compound **4** (1.16 g, 66%). **^{1}H NMR** (600 MHz, $CDCl_3$): δ 7.54 (d, J = 8.0 Hz, 2H), 7.41 (ddd, J = 14.4, 7.2, 1.9 Hz, 3H), 7.37−7.31 (m, 3H), 7.16−7.06 (m, 3H), 6.96 (d, J = 8.1 Hz, 2H), 5.23 (s, 2H), 4.98 (s, 2H), 3.85 (s, 2H), 3.09 (q, J = 6.8 Hz, 2H), 2.99−2.91 (m, 2H), 2.76 (d, J = 5.8 Hz, 2H), 2.68 (t, J = 7.9 Hz, 2H), 1.69−1.64 (m, 2H), 1.50−1.48−1.46 (m, 2H), 1.43 (s, 9H), 1.36−1.33 (m, 4H). **^{13}C NMR** (151 MHz, $CDCl_3$): δ 165. 8, 156.2, 141. 9, 136.9, 135.5, 133.1, 131.2, 129.4, 128.9, 128.9, 128.7, 128.6, 127.8, 126.5, 125.9, 121.6, 119.7, 117.9, 109.3, 107.5, 79.2, 78.3, 57.5, 50.5, 49.5, 46.3, 40.6, 30.1, 28.6, 27.2, 26.8, 26.7, 22.2. **LC−MS (ESI)**, $[M + H]^+$ m/z: 611.4.

*4-((2-(6-Azidohexyl)-1,2,3,4-tetrahydro-5H-pyrido[4,3-b]-indol-5-yl)methyl)-N-(benzyloxy)benzamide (**5**).* To a solution of compound **3** (0.850 g, 1.66 mmol, 1 equiv) in DCM (20 mL), TFA (4 mL) was added. The mixture was stirred at room temperature for 2 h and the complete removal of *tert*-butyl group was monitored by HPLC. Afterward, the mixture was dried in vacuo to provide the crude product for the next step. To a solution of the resulting crude product in anhydrous DMF (30 mL), 1-azido-6-bromohexane (0.514 g, 2.49 mmol, 1.5 equiv) and K_2CO_3 (0.459 g, 3.32 mmol, 2 equiv) were added. The mixture was stirred at room temperature for 20 h. The completion of the reaction was monitored by HPLC. The mixture was poured into water (150 mL) and extracted with ethyl acetate (3 × 50 mL). The combined organic layer was then washed with water (3 × 50 mL) and followed by brine (50 mL), dried over anhydrous Na_2SO_4, filtered, and concentrated in vacuo to afford the crude product, which was then purified by flash column chromatography (0−10% MeOH in DCM, 0−10 min; 10% MeOH in DCM, 10−35 min) to provide compound **5** (0.634 g, 71%). Synthesis of 1-azido-6-bromohexane followed previously reported methods.[52] **^{1}H NMR** (600 MHz, $CDCl_3$): δ 8.99 (s, 1H), 7.54 (d, J = 8.0 Hz, 2H), 7.41 (ddd, J = 18.9, 7.0, 2.0 Hz, 3H), 7.38−7.32 (m, 3H), 7.15−7.06 (m, 3H), 6.98 (d, J = 8.0 Hz, 2H), 5.23 (s, 2H), 4.98 (s, 2H), 3.79 (s, 2H), 3.27 (t, J = 6.9 Hz, 2H), 2.89 (d, J = 5.8 Hz, 2H), 2.74 (d, J = 5.7 Hz, 2H), 2.65 (t, J = 7.8 Hz, 2H), 1.67 (q, J = 7.6 Hz, 2H), 1.62 (p, J = 7.1 Hz, 2H), 1.46−1.37 (m, 4H). **^{13}C NMR** (151 MHz, $CDCl_3$): δ 165.6, 142.0, 136.9, 135.5, 133.4, 131.2, 129.4, 129.4, 128.9, 128.8, 128.7, 128.6, 127.7, 126.6, 126.0, 121.4, 119.6, 117. 9, 109.2,

https://doi.org/10.1021/acs.jmedchem.5c00674
J. Med. Chem. 2025, 68, 13793−13821

108.2, 78.3, 57.9, 51.5, 50.7, 49.7, 46.3, 28.9, 27.2, 27.2, 26.8, 22.6. **LC−MS (ESI)**, $[M + H]^+$ *m/z*: 537.5.

*Methyl 4-((3-Formyl-1H-indol-1-yl)methyl)benzoate (**6**).* To a solution of 1*H*-indole-3-carbaldehyde (3.00 g, 20.7 mmol, 1 equiv) in acetonitrile (50 mL), methyl 4-(bromomethyl)benzoate (4.97 g, 21.7 mmol, 1.05 equiv) was added. The mixture was stirred and refluxed for 15 h. The solvent was removed in vacuo. The crude product was then dissolved by a mixture of ethyl acetate (75 mL) and water (75 mL). The subsequent extraction was performed with the ethyl acetate (3 × 50 mL) and the combined organic layer was washed with brine (50 mL) and dried over Na_2SO_4. The filtrate was concentrated in vacuo to provide the crude, which was then purified by silica column chromatography (DCM: MeOH 50:1, *v*/*v*) to yield compound **6** (5.98 g, 99%). **^{1}H NMR** (600 MHz, $CDCl_3$): δ 10.02 (s, 1H), 8.34 (dt, *J* = 7.8, 1.2 Hz, 1H), 8.04−7.98 (m, 2H), 7.75 (s, 1H), 7.34−7.28 (m, 2H), 7.27−7.25 (m, 1H), 7.22 (d, *J* = 8.1 Hz, 2H), 5.43 (s, 2H), 3.90 (s, 3H). **^{13}C NMR** (151 MHz, $CDCl_3$): δ 184.8, 166. 6, 140.5, 138.6, 137.5, 130.5, 130.4, 127.0, 125.6, 124.5, 123.4, 122.4, 118.9, 110.4, 52.4, 50.8. **LC−MS (ESI)**, $[M + H]^+$ *m/z*: 294.1.

*Methyl 4-((3-((Methylamino)methyl)-1H-indol-1-yl)-methyl)benzoate (**7**).* To a solution of compound **6** (4.00 g, 13.6 mmol, 1 equiv) in MeOH and DCM (100 mL: 10 mL), methylamine (2.09 mL, 20.5 mmol, 1.5 equiv, 9.8 M in MeOH) was added. The mixture was stirred at room temperature for 19 h. The complete consumption of the starting material was monitored by HPLC. Afterward, the mixture was cooled in ice bath and $NaBH_4$ (1.03 g, 27.3 mmol, 2 equiv) was added slowly. The reaction mixture was then stirred for another 3 h. The completion of the reaction was monitored by HPLC. The resulting mixture was filtered and the filtrate was then concentrated in vacuo to provide the crude product (3.66 g, 87%) which was used without further purification. **^{1}H NMR** (600 MHz, $CDCl_3$): δ 7.97−7.92 (m, 2H), 7.68 (dd, *J* = 7.1, 1.6 Hz, 1H), 7.22 (s, 1H), 7.20−7.20−7.17 (m, 2H), 7.15−7.13 (m, 3H), 5.32 (s, 2H), 4.03 (s, 2H), 3.88 (s, 3H), 2.50 (s, 3H). **^{13}C NMR** (151 MHz, $CDCl_3$): δ 166.8, 142.6, 136.6, 130.2, 129.7, 128.0, 127.9, 126.8, 122.4, 120.0, 119.1, 111.7, 109.9, 52.3, 50.0, 45.6, 34.8. **LC−MS (ESI)**, $[M - H]^-$ *m/z*: 307.3.

*Methyl 4-((3-(((6-((tert-Butoxycarbonyl)amino)hexyl)-(methyl)amino)methyl)-1H-indol-1-yl)methyl)benzoate (**8**).* To a solution of compound 7 (2.79 g, 9.05 mmol, 1 equiv) in anhydrous DMF (60 mL), *tert*-butyl (6-bromohexyl)-carbamate (3.80 g, 13.6 mmol, 1.5 equiv) and K_2CO_3 (2.50 g, 18.1 mmol, 2 equiv) were added. The mixture was stirred at room temperature for 15 h. The completion of the reaction was monitored by HPLC. The mixture was poured into water (150 mL) and extracted with ethyl acetate (3 × 50 mL). The combined organic layer was then washed with water (3 × 50 mL)and followed by brine (50 mL), dried over anhydrous Na_2SO_4, filtered, and concentrated in vacuo to provide the crude product, which was then purified by silica column (DCM: MeOH 50:1, *v*/*v*, 1% Et_3N) to afford compound **8** (3.08 g, 67%). **^{1}H NMR** (600 MHz, DMSO-d_6): δ 7.91−7.86 (m, 2H), 7.63 (d, *J* = 7.8 Hz, 1H), 7.39−7.32 (m, 2H), 7.29−7.23 (m, 2H), 7.07 (ddd, *J* = 8.2, 7.0, 1.2 Hz, 1H), 7.03−6.98 (m, 1H), 6.75−6.67 (m, 1H), 5.48 (s, 2H), 3.81 (s, 3H), 3.61 (s, 2H), 2.87 (q, *J* = 7.2, 6.7 Hz, 2H), 2.34 (t, *J* = 7.3 Hz, 2H), 2.12 (s, 3H), 1.46 (dq, *J* = 14.6, 7.4, 6.9 Hz, 2H), 1.36 (s, 9H), 1.34 (t, *J* = 6.7 Hz, 2H), 1.28−1.19 (m, 4H). **^{13}C NMR** (151 MHz, DMSO-d_6): δ 165.9, 155.5, 143.9, 136.2, 129.4, 128.6, 128.2, 127.0, 121.3, 119.5, 118.8, 111.8, 109.9, 77.2, 56.5, 54.9, 52.4, 52.0, 48.5, 41.7, 29.5, 28.2, 26.8, 26.6, 26.2. **LC−MS (ESI)**, $[M + H]^+$ *m/z*: 508.5.

*tert-Butyl (6-(((1-(4-((benzyloxy)carbamoyl)benzyl)-1H-indol-3-yl)methyl)(methyl)amino)hexyl)carbamate (**9**).* To a solution of compound **8** (3.08 g, 6.07 mmol, 1 equiv) in THF/MeOH/H2O (60 mL/12 mL/12 mL) was added LiOH·H_2O (0.509 g, 12.1 mmol, 2 equiv), the mixture was stirred at room temperature for 16.5 h. Heating at 50 °C for extra 1−2 h was operated when the reaction was not complete. Upon the completion of the hydrolysis, the solvent was removed in vacuo. The crude was dissolved with water and acidified with HCl (0.5 M in water) until no more precipitate is formed, the resulting precipitate was collected via filtration, washed with water and dried in vacuo for the next step without further purification. To a solution of the dried precipitate (2.64 g, 5.35 mmol, 1 equiv) prepared in the last step in anhydrous DMF (60 mL) were added HATU (4.07 g, 10.7 mmol, 2 equiv) and DIPEA (2.07 g, 16.0 mmol, 3 equiv), the mixture was stirred for 30 min at room temperature, after which, *O*-benzylhydroxylamine hydrochloride (1.71 g, 10.7 mmol, 2 equiv) was added into the system and stirred for 17 h. Completion of the reaction was monitored by TLC. The mixture was poured into water (150 mL) and extracted with ethyl acetate (3 × 50 mL). The combined organic layer was then washed with water (3 × 50 mL) and followed by brine(50 mL), dried over anhydrous Na_2SO_4, filtered and concentrated in vacuo to offer the crude, which was then purified by silica column (DCM: MeOH 50:1, *v*/*v*, 1% Et_3N) to offer the compound **9** (2.55 g, 80%). **^{1}H NMR** (600 MHz, $CDCl_3$): δ 7.68 (d, *J* = 7.7 Hz, 1H), 7.61 (d, *J* = 7.9 Hz, 2H), 7.42 (dd, *J* = 7.4, 2.0 Hz, 2H), 7.38−7.31 (m, 3H), 7.19−7.14 (m, 2H), 7.14−7.10 (m, 2H), 7.09 (d, *J* = 8.1 Hz, 2H), 5.30 (s, 2H), 5.01 (s, 2H), 3.74 (s, 2H), 2.96 (q, *J* = 6.9 Hz, 2H), 2.42 (t, *J* = 7.6 Hz, 2H), 2.28 (s, 3H), 1.53 (p, *J* = 7.3 Hz, 2H), 1.42 (s, 9H), 1.36 (p, *J* = 7.3 Hz, 2H), 1.26 (q, *J* = 7.3 Hz, 2H), 1.24−1.17 (m, 2H). **^{13}C NMR** (151 MHz, $CDCl_3$): δ 165.5, 156.2, 141.6, 136.5, 135.6, 131.5, 129.4, 129.4, 128.8, 128.7, 128.6, 128.1, 127.8, 127.0, 122.1, 119.7, 119.7, 109.7, 79.3, 78.3, 63.9, 56.6, 52.5, 49.8, 42.2, 40.6, 30.0, 28.6, 27.0, 26.5. **LC−MS (ESI)**, $[M + H]^+$ *m/z*: 599.6.

*Hex-5-yn-1-yl (2-(2,6-Dioxopiperidin-3-yl)-1,3-dioxoisoindolin-4-yl)glycinate (**12**).* The *tert*-butyl (2-(2,6-dioxopiperidin-3-yl)-1,3-dioxoisoindolin-4-yl)glycinate (compound **10**, 1.36 g) was synthesized following the previously reported method.[33] To a solution of compound **10** (0.590 g, 1.52 mmol, 1 equiv) in DCM (15 mL) was added TFA (3 mL), the mixture was stirred at room temperature for 2 h, the complete removal of *tert*-butyl group was monitored by TLC, after which, the mixture was dried in vacuo to offer the crude, compound **11**, for the next step. To a solution of the resulting crude in anhydrous DMF (15 mL) were added HATU (1.16 g, 3.05 mmol, 2 equiv) and DIPEA (0.591 g, 4.57 mmol, 3 equiv), the mixture was stirred for 30 min at room temperature, after which, hex-5-yn-1-ol (0.299 g, 3.05 mmol, 2 equiv) was added into the system and stirred for 15 h. Completion of the reaction was monitored by HPLC. The mixture was poured into water (100 mL) and extracted with ethyl acetate (3 × 30 mL). The combined organic layer was then washed with water (3 × 50 mL) and followed by brine (50 mL), dried over anhydrous Na_2SO_4, filtered and concentrated in vacuo to offer the crude, which was then

https://doi.org/10.1021/acs.jmedchem.5c00674
J. Med. Chem. 2025, 68, 13793−13821

purified by silica column (CyH/EtOAc, 1:1, *v*/*v*) to offer the compound **12** (0.343 g, 55%).

^{1}H NMR (600 MHz, $CDCl_3$): δ 8.09 (s, 1H), 7.52 (dd, *J* = 8.5, 7.2 Hz, 1H), 7.17 (d, *J* = 7.2 Hz, 1H), 6.78 (d, *J* = 8.5 Hz, 1H), 6.70 (s, 1H), 4.93 (dd, *J* = 12.4, 5.4 Hz, 1H), 4.23 (t, *J* = 6.5 Hz, 2H), 4.07 (s, 2H), 2.93−2.86 (m, 1H), 2.86−2.70 (m, 2H), 2.23 (td, *J* = 7.0, 2.6 Hz, 2H), 2.17−2.10 (m, 1H), 1.97 (t, *J* = 2.6 Hz, 1H), 1.85−1.75 (m, 2H), 1.60−1.56 (m, 2H). **^{13}C NMR** (151 MHz, $CDCl_3$): δ 171.1, 169.7, 169.3, 168.3, 167.6, 145.8, 136.4, 132.7, 116.7, 112.7, 111.4, 83.8, 69.1, 65.3, 49.1, 44.6, 31.5, 27.7, 24.9, 22.9, 18.2. **LC−MS (ESI)**, $[M + H]^+$ *m*/*z*: 412.2.

*Hex-5-yn-1-yl 2-(4-(2,6-dioxopiperidin-3-yl)phenoxy)-acetate (**15**).* The *tert*-butyl 2-(4-(2,6-dioxopiperidin-3-yl)-phenoxy)acetate (compound **13**, 2.00 g) was synthesized following a previously reported method.[32] To a solution of compound **13** (0.490 g, 1.53 mmol, 1 equiv) in DCM (15 mL) TFA (3 mL) was added, the mixture was stirred at room temperature for 2 h. The complete removal of *tert*-butyl group was monitored by TLC. Afterward, the mixture was dried in vacuo to provide the crude product, compound **14**, for the next step. To a solution of the resulting crude in anhydrous DMF (15 mL) HATU (1.17 g, 3.07 mmol, 2 equiv) and DIPEA (0.595 g, 4.60 mmol, 3 equiv) were added. The mixture was stirred for 30 min at room temperature. Next, hex-5-yn-1-ol (0.301 g, 3.07 mmol, 2 equiv) was added to the reaction mixture and stirred for 15 h. The completion of the reaction was monitored by HPLC. The mixture was poured into water (100 mL) and extracted with ethyl acetate (3 × 30 mL). The combined organic layer was then washed with water (3 × 50 mL) and followed by brine (50 mL), dried over anhydrous Na_2SO_4, filtered, and concentrated in vacuo to offer the crude product, which was then purified by silica column (CyH/EtOAc, 1:1, *v*/*v*) to afford compound **15** (0.364 g, 69%). **^{1}H NMR** (600 MHz, $CDCl_3$): δ 7.99 (s, 1H), 7.17−7.10 (m, 2H), 6.95−6.87 (m, 2H), 4.62 (s, 2H), 4.24 (t, *J* = 6.5 Hz, 2H), 3.74 (dd, *J* = 9.9, 5.1 Hz, 1H), 2.73 (dt, *J* = 17.7, 5.3 Hz, 1H), 2.64 (ddd, *J* = 17.7, 10.1, 5.2 Hz, 1H), 2.30−2.17 (m, 4H), 1.96 (t, *J* = 2.6 Hz, 1H), 1.83−1.76 (m, 2H), 1.60−1.54 (m, 2H). **^{13}C NMR** (151 MHz, $CDCl_3$): δ 173.3, 172.3, 169.0, 157.5, 130.3, 129.4, 115.3, 83.8, 69.0, 65.5, 65.0, 47.3, 31.1, 27.7, 26.5, 24.9, 18.1. **LC−MS (ESI)**, $[M - H]^-$ *m*/*z*: 342.1.

*N-(Benzyloxy)-4-((2-(6-(2-((2-(2,6-dioxopiperidin-3-yl)-1,3-dioxoisoindolin-4-yl)amino)acetamido)hexyl)-1,2,3,4-tetrahydro-5H-pyrido[4,3-b]indol-5-yl)methyl)benzamide (**16**).* Prepared by following the **General procedure A**. Starting from deprotected compound **4** (0.197 g, 0.385 mmol, 1 equiv), compound **11** (0.140 g, 0.424 mmol, 1.1 equiv), HATU (0.293 g, 0.770 mmol, 2 equiv) and DIPEA (202 μL, 1.16 mmol, 3 equiv). The crude product was purified by silica column (DCM/MeOH, 20:1, *v*/*v*, 1% Et_3N) to afford compound **16** (0.279 g, 88%). **^{1}H NMR** (600 MHz, DMSO-d_6): δ 11.66 (s, 1H), 11.08 (s, 1H), 8.06 (t, *J* = 5.7 Hz, 1H), 7.68−7.62 (m, 2H), 7.59 (dd, *J* = 8.5, 7.1 Hz, 1H), 7.46−7.32 (m, 6H), 7.09 (d, *J* = 8.1 Hz, 2H), 7.06 (d, *J* = 7.1 Hz, 1H), 7.05−7.02 (m, 1H), 6.99 (t, *J* = 7.4 Hz, 1H), 6.94 (t, *J* = 5.6 Hz, 1H), 6.86 (d, *J* = 8.5 Hz, 1H), 5.38 (s, 2H), 5.07 (dd, *J* = 12.7, 5.5 Hz, 1H), 4.89 (s, 2H), 3.92 (d, *J* = 5.6 Hz, 2H), 3.65 (s, 2H), 3.10 (q, *J* = 6.6 Hz, 2H), 2.88 (dd, *J* = 5.5, 3.3 Hz, 1H), 2.87−2.78 (m, 2H), 2.74 (s, 2H), 2.60 (dd, *J* = 4.6, 2.6 Hz, 1H), 2.59−2.55 (m, 2H), 2.53 (dd, *J* = 13.4, 4.5 Hz, 1H), 2.05−1.99 (m, 1H), 1.54 (h, *J* = 7.0 Hz, 2H), 1.43 (p, *J* = 7.0 Hz, 2H), 1.35−1.21 (m, 4H). **^{13}C NMR** (151 MHz, DMSO-d_6): δ 172.7, 170.0, 168.7, 168.2, 167.3, 163.9, 145.8, 142.1, 136.3, 136.1, 135.9, 133.9, 132.0, 131.2, 128.9, 128.3, 128.2, 127.4, 126.4, 125.3, 120.6, 118.8, 117.4, 110.9, 109.9, 109.5, 76.9, 57.2, 50.2, 49.1, 48.6, 45.4, 45.2, 38.5, 30.9, 29.0, 26.6, 26.3, 22.6, 22.3, 22.1. **LC−MS (ESI)**, $[M + H]^+$ *m*/*z*: 824.7.

*N-(Benzyloxy)-4-((2-(6-(2-(4-(2,6-dioxopiperidin-3-yl)-phenoxy)acetamido)hexyl)-1,2,3,4-tetrahydro-5H-pyrido-[4,3-b]indol-5-yl)methyl)benzamide (**17**).* Prepared by following the **General procedure A**. Starting from deprotected compound **4** (0.295 g, 0.578 mmol, 1 equiv), compound **14** (0.152 g, 0.578 mmol, 1 equiv), HATU (0.440 g, 1.16 mmol, 2 equiv) and DIPEA (303 μL, 1.73 mmol, 3 equiv). The crude product was purified by silica column (EtOAc/MeOH, 20:1, *v*/*v*, 1% Et_3N) to yield compound **17** (0.342 g, 78%). **^{1}H NMR** (600 MHz, $CDCl_3$): δ 8.31 (s, 1H), 7.57 (d, *J* = 8.1 Hz, 2H), 7.46−7.37 (m, 3H), 7.36−7.32 (m, 2H), 7.17−7.07 (m, 4H), 6.97 (d, *J* = 8.1 Hz, 2H), 6.93−6.85 (m, 2H), 6.59 (t, *J* = 6.0 Hz, 1H), 5.24 (s, 2H), 4.99 (s, 2H), 4.44 (s, 2H), 3.93 (s, 2H), 3.72−3.66 (m, 1H), 3.31 (q, *J* = 6.8 Hz, 2H), 3.10−2.97 (m, 2H), 2.80 (s, 2H), 2.73 (d, *J* = 7.8 Hz, 2H), 2.68 (dt, *J* = 17.7, 5.1 Hz, 1H), 2.59 (ddd, *J* = 17.7, 10.2, 5.3 Hz, 1H), 2.25−2.19 (m, 1H), 2.19−2.13 (m, 1H), 1.70 (d, *J* = 9.5 Hz, 2H), 1.53 (p, *J* = 7.1 Hz, 2H), 1.39−1.30 (m, 4H). **^{13}C NMR** (151 MHz, $CDCl_3$): δ 173.4, 172.4, 170.1, 168.2, 156.8, 141.8, 137.0, 135.5, 132.8, 131.3, 130.8, 129.7, 129.4, 128.9, 128.7, 128.6, 127.8, 126.5, 125.7, 121.8, 119.8, 117.9, 115.2, 115.2, 109.4, 78.4, 67.6, 57.0, 50.3, 49.4, 47.2, 46.3, 39.0, 34.6, 31.1, 29.5, 27.0, 26.6, 26.3, 23.5. **LC−MS (ESI)**, $[M + H]^+$ *m*/*z*: 756.6.

*4-(1-(6-(5-(4-((Benzyloxy)carbamoyl)benzyl)-1,3,4,5-tetrahydro-2H-pyrido[4,3-b]indol-2-yl)hexyl)-1H-1,2,3-triazol-4-yl)butyl (2-(2,6-dioxopiperidin-3-yl)-1,3-dioxoisoindolin-4-yl)glycinate (**18**).* Prepared by following the **General procedure B**. Starting from compound **5** (0.241 g, 0.449 mmol, 1.05 equiv), compound **12** (0.176 g, 0.428 mmol, 1 equiv), ascorbic acid (0.226 g, 1.28 mmol, 3 equiv) and $CuSO_4$ (0.0683 g, 0.428 mmol, 1 equiv). The crude product was purified by flash column chromatography to afford compound **18** (0.239 mg, 59%). **^{1}H NMR** (600 MHz, $CDCl_3$): δ 9.68 (s, 1H), 8.73 (s, 1H), 7.62 (d, *J* = 7.8 Hz, 2H), 7.48 (t, *J* = 7.7 Hz, 1H), 7.44−7.35 (m, 3H), 7.35−7.28 (m, 3H), 7.17 (q, *J* = 8.5 Hz, 2H), 7.11 (dd, *J* = 10.1, 7.1 Hz, 2H), 6.95 (d, *J* = 7.8 Hz, 2H), 6.75 (d, *J* = 8.4 Hz, 1H), 6.67 (t, *J* = 5.8 Hz, 1H), 5.24 (s, 2H), 4.99 (s, 2H), 4.86 (dd, *J* = 12.4, 5.4 Hz, 1H), 4.30 (d, *J* = 7.9 Hz, 2H), 4.18 (s, 2H), 4.02 (d, *J* = 5.7 Hz, 2H), 3.33 (s, 2H), 2.97 (s, 2H), 2.83−2.55 (m, 6H), 2.10−2.01 (m, 2H), 1.88 (s, 4H), 1.70 (s, 4H), 1.45−1.19 (m, 6H). **^{13}C NMR** (151 MHz, $CDCl_3$): δ 171.4, 169.8, 169.3, 168.7, 167.6, 165.6, 145.8, 141.0, 137.2, 136.4, 135.6, 132.6, 131.6, 129.4, 128.8, 128.7, 128.6, 128.1, 126.4, 125.1, 122.7, 120.5, 118.0, 116.9, 112.6, 111.2, 109.8, 78.4, 65.5, 60.6, 55.2, 50.0, 49.7, 49.1, 48.8, 46.5, 44.6, 32.0, 31.5, 29.8, 28.2, 26.2, 25.8, 25.3, 24.5, 22.8. **LC−MS (ESI)**, $[M + H]^+$ *m*/*z*: 948.7.

*4-(1-(6-(5-(4-((Benzyloxy)carbamoyl)benzyl)-1,3,4,5-tetrahydro-2H-pyrido[4,3-b]indol-2-yl)hexyl)-1H-1,2,3-triazol-4-yl)butyl 2-(4-(2,6-dioxopiperidin-3-yl)phenoxy)acetate (**19**).* Prepared by following the **General procedure B**. Starting from compound **15** (0.163 g, 0.475 mmol, 1 equiv), **5** (0.268 g, 0.498 mmol, 1.05 equiv), ascorbic acid (0.251 g, 1.42 mmol, 3 equiv) and $CuSO_4$ (0.0758 g, 0.475 mmol, 1 equiv). The crude product was purified by flash column chromatography to furnish compound **19** (0.228 g, 54%). **^{1}H NMR** (600 MHz, $CDCl_3$): δ 9.27 (s, 1H), 8.25 (s, 1H), 7.59 (d, *J* = 7.5 Hz, 2H), 7.50−7.37 (m, 3H), 7.36−7.28 (m, 3H), 7.24−7.11 (m, 3H),

https://doi.org/10.1021/acs.jmedchem.5c00674
J. Med. Chem. 2025, 68, 13793−13821

7.11−7.07 (m, 2H), 6.98 (d, J = 7.7 Hz, 2H), 6.87 (d, J = 8.2 Hz, 2H), 5.25 (s, 2H), 4.99 (s, 2H), 4.59 (s, 2H), 4.30 (d, J = 7.1 Hz, 2H), 4.21 (d, J = 5.3 Hz, 2H), 4.00 (s, 2H), 3.68 (dd, J = 9.9, 5.0 Hz, 1H), 3.08 (d, J = 24.2 Hz, 2H), 2.91−2.63 (m, 6H), 2.63−2.56 (m, 1H), 2.26−2.09 (m, 3H), 1.90 (m, 2H), 1.71 (m, 6H), 1.50−1.29 (m, 4H). **^{13}C NMR** (151 MHz, $CDCl_3$): δ 173.4, 172.4, 170.5, 169.1, 157.4, 157.2, 141.6, 137.0, 135.5, 131.4, 130.4, 129.7, 129.4, 129.0, 128.9, 128.7, 128.6, 127.9, 126.5, 125.6, 122.0, 120.9, 120.0, 117.9, 115.2, 109.5, 78.4, 65.6, 65.2, 56.4, 50.2, 49.5, 47.3, 46.5, 46.4, 32.1, 31,6, 31.1, 30.1, 28.2, 26.6, 26.5, 26.2, 25.8, 25.3. **LC−MS (ESI)**, $[M + H]^+$ m/z: 880.7.

*N-(Benzyloxy)-4-((3-(((6-(2-((2-(2,6-dioxopiperidin-3-yl)-1,3-dioxoisoindolin-4-yl)amino)acetamido)hexyl)(methyl)-amino)methyl)-1H-indol-1-yl)methyl)benzamide (**20**).* Prepared by following the **General procedure A**. Starting from deprotected compound **9** (0.300 g, 0.601 mmol, 1 equiv), compound **11** (0.199 g, 0.601 mmol, 1 equiv), HATU (0.457 g, 1.20 mmol, 2 equiv) and DIPEA (315 μL, 1.80 mmol, 3 equiv). The crude product was purified by silica column (DCM/MeOH, 10:1, v/v, 1% Et_3N) to provide compound **20** (0.381 g, 80%). **^{1}H NMR** (600 MHz, DMSO-d_6): δ 11.74 (s, 1H), 11.09 (s, 1H), 9.67 (s, 1H), 8.13 (t, J = 5.7 Hz, 1H), 7.82−7.74 (m, 2H), 7.68 (d, J = 8.0 Hz, 2H), 7.58 (dd, J = 8.5, 7.1 Hz, 1H), 7.50−7.46 (m, 1H), 7.44−7.32 (m, 4H), 7.28 (d, J = 8.0 Hz, 2H), 7.20−7.11 (m, 2H), 7.06 (d, J = 7.1 Hz, 1H), 6.94 (t, J = 5.6 Hz, 1H), 6.86 (d, J = 8.5 Hz, 1H), 5.53 (s, 2H), 5.06 (dd, J = 12.8, 5.5 Hz, 1H), 4.89 (s, 2H), 3.92 (d, J = 5.5 Hz, 2H), 3.17 (s, 2H), 3.00−2.90 (m, 2H), 2.90−2.84 (m, 1H), 2.69 (s, 3H), 2.62−2.51 (m, 2H), 2.02 (dtd, J = 12.8, 5.2, 2.2 Hz, 1H), 1.68 (s, 2H), 1.41 (t, J = 6.8 Hz, 2H), 1.28−1.24 (m, 6H). **^{13}C NMR** (151 MHz, DMSO-d_6): δ 172.8, 170.0, 168.7, 168.2, 167.3, 164.0, 145.8, 141.3, 136.2, 135.8, 132.2, 132.0, 131.5, 128.9, 128.3, 128.0, 127.4, 127.0, 122.1, 120.1, 119.0, 118.26, 117.4, 116.3, 114.3, 110.9, 110.7, 109.9, 76.9, 54.1, 49.7, 48.9, 48.6, 45.1, 38.6, 38.3, 31.0, 28.8, 25.8, 25.7, 23.5, 22.1. **LC−MS (ESI)**, $[M + H]^+$ m/z: 812.6.

*N-(Benzyloxy)-4-((3-(((6-(2-(4-(2,6-dioxopiperidin-3-yl)-phenoxy)acetamido)hexyl)(methyl)amino)methyl)-1H-indol-1-yl)methyl)benzamide (**21**).* Prepared by following the **General procedure A**. Starting from deprotected compound **9** (0.722 g, 1.45 mmol, 1 equiv), compound **14** (0.381, 1.45 mmol, 1 equiv), HATU (1.10 g, 2.90 mmol, 2 equiv) and DIPEA (757 μL, 4.34 mmol, 3 equiv). The crude product was purified by silica column (EtOAc/MeOH, 10:1, v/v, 1% Et_3N) to provide compound **21** (0.582 g, 54%). **^{1}H NMR** (600 MHz, $CDCl_3$): δ 7.63 (td, J = 6.8, 1.7 Hz, 3H), 7.43−7.39 (m, 2H), 7.36−7.27 (m, 4H), 7.20−7.13 (m, 3H), 7.13−7.11 (m, 2H), 7.06 (d, J = 8.1 Hz, 2H), 6.90−6.85 (m, 2H), 6.68 (t, J = 6.0 Hz, 1H), 5.27 (s, 2H), 5.00 (s, 2H), 4.34 (s, 2H), 3.94 (s, 2H), 3.71−3.68 (m, 1H), 3.20 (q, J = 6.8 Hz, 2H), 2.69 (dt, J = 17.7, 5.1 Hz, 1H), 2.64−2.60 (m, 1H), 2.57 (q, J = 8.0, 6.7 Hz, 2H), 2.42 (s, 3H), 2.22 (ddd, J = 14.0, 8.6, 5.1 Hz, 1H), 2.16 (ddd, J = 13.8, 10.3, 4.7 Hz, 1H), 1.59 (p, J = 7.5 Hz, 2H), 1.43 (p, J = 7.2 Hz, 2H), 1.28 (ddd, J = 8.5, 5.6, 1.8 Hz, 2H), 1.19 (td, J = 8.2, 3.9 Hz, 2H). **^{13}C NMR** (151 MHz, $CDCl_3$): δ 173.4, 172.4, 170.1, 168.4, 156.8, 141.3, 136.4, 135.7, 131.7, 130.8, 129.6, 129.4, 128.8, 128.7, 128.7, 128.6, 127.9, 127.2, 126.9, 122.38, 120.2, 119.1, 115.2, 110.0, 78.3, 67.4, 55.6, 52.0, 49.8, 47.3, 41.3, 38.9, 31.2, 29.3, 26.6, 26.4, 26.2, 26.0. **LC−MS (ESI)**, $[M + H]^+$ m/z: 744.5.

*4-((2-(6-(2-((2-(2,6-Dioxopiperidin-3-yl)-1,3-dioxoisoindolin-4-yl)amino)acetamido)hexyl)-1,2,3,4-tetrahydro-5H-pyrido[4,3-b]indol-5-yl)methyl)-N-hydroxybenzamide (**AP1**).* Prepared by following the **General procedure C**. Starting from compound **16** (0.273 g, 0.332 mmol, 1 equiv), the crude product was purified by reverse phase flash column chromatography to yield compound **AP1** (21.5 mg, 9%). **^{1}H NMR** (600 MHz, DMSO-d_6): δ 11.15 (s, 1H), 11.09 (s, 1H), 9.67 (s, 1H), 9.00 (s, 1H), 8.09 (t, J = 5.7 Hz, 1H), 7.72−7.64 (m, 2H), 7.60 (dd, J = 8.5, 7.1 Hz, 1H), 7.53 (d, J = 7.8 Hz, 1H), 7.49 (d, J = 8.2 Hz, 1H), 7.19−7.11 (m, 3H), 7.09 (t, J = 7.1 Hz, 2H), 6.95 (t, J = 5.6 Hz, 1H), 6.87 (d, J = 8.5 Hz, 1H), 5.52 (d, J = 16.9 Hz, 1H), 5.41 (d, J = 16.9 Hz, 1H), 5.07 (dd, J = 12.8, 5.5 Hz, 1H), 4.74−4.66 (m, 1H), 4.32 (dd, J = 14.4, 8.0 Hz, 1H), 3.93 (d, J = 5.1 Hz, 2H), 3.83 (dd, J = 13.1, 5.5 Hz, 1H), 3.49 (dtd, J = 13.2, 9.4, 8.9, 5.9 Hz, 1H), 3.28−3.23 (m, 2H), 3.15−3.10 (m, 3H), 3.03 (dt, J = 17.2, 7.0 Hz, 1H), 2.89 (dddd, J = 17.1, 13.8, 5.5, 1.6 Hz, 1H), 2.62−2.55 (m, 2H), 2.03 (dtd, J = 13.0, 5.4, 2.3 Hz, 1H), 1.76 (dh, J = 22.0, 6.6 Hz, 2H), 1.45 (p, J = 7.0 Hz, 2H), 1.33 (dq, J = 9.5, 5.8 Hz, 4H). **^{13}C NMR** (151 MHz, DMSO-d_6): δ 172.8, 170.0, 168.7, 168.3, 167.3, 163.7, 145.8, 141.0, 136.5, 136.2, 132.1, 131.9, 131.4, 127.2, 126.6, 124.4, 121.9, 119.7, 117.8, 117.4, 111.0, 110.1, 109.9, 102.1, 55.1, 49.3, 48.3, 45.8, 45.6, 45.2, 38.4, 34.4, 31.0, 28.8, 25.8, 25.7, 23.6, 22.1. **HRMS (ESI)** m/z: $[M + H]^+$ calcd for $C_{40}H_{43}N_7O_7$, 734.3297; found, 734.3304.

*4-(1-(6-(5-(4-(Hydroxycarbamoyl)benzyl)-1,3,4,5-tetrahydro-2H-pyrido[4,3-b]indol-2-yl)hexyl)-1H-1,2,3-triazol-4-yl)-butyl (2-(2,6-dioxopiperidin-3-yl)-1,3-dioxoisoindolin-4-yl)-glycinate (**AP2**).* Prepared by following the **General procedure C**. Starting from compound **18** (0.146 g, 0.154 mmol, 1 equiv), the crude product was purified by reverse phase flash column chromatography to yield compound **AP2** (16.6 mg, 13%). **^{1}H NMR** (600 MHz, DMSO-d_6): δ 11.09 (s, 1H), 8.98 (s, 1H), 7.82 (d, J = 4.5 Hz, 1H), 7.68−7.62 (m, 2H), 7.54 (ddd, J = 19.6, 8.5, 7.1 Hz, 1H), 7.41−7.37 (m, 1H), 7.35 (d, J = 8.1 Hz, 1H), 7.16−7.05 (m, 3H), 7.05−7.01 (m, 1H), 7.01−6.92 (m, 2H), 6.92−6.85 (m, 1H), 5.37 (s, 2H), 5.07 (dd, J = 12.8, 5.5 Hz, 1H), 4.28 (t, J = 7.1 Hz, 2H), 4.20 (dd, J = 10.0, 6.1 Hz, 2H), 4.12 (h, J = 3.2 Hz, 2H), 3.58 (s, 2H), 3.47 (s, 1H), 2.88 (ddd, J = 16.9, 13.8, 5.5 Hz, 1H), 2.75 (t, J = 5.7 Hz, 2H), 2.71 (d, J = 5.5 Hz, 2H), 2.63−2.56 (m, 3H), 2.53 (dd, J = 14.9, 4.3 Hz, 1H), 2.31−2.23 (m, 1H), 2.04 (dtd, J = 13.1, 5.4, 2.3 Hz, 1H), 1.80 (p, J = 7.2 Hz, 2H), 1.62 (dq, J = 6.9, 3.6, 2.8 Hz, 4H), 1.53 (p, J = 7.3 Hz, 2H), 1.32 (q, J = 7.5 Hz, 2H), 1.26 (ddd, J = 14.1, 7.8, 5.2 Hz, 2H). **^{13}C NMR** (151 MHz, DMSO-d_6): δ 172.5, 170.2, 168.7, 167.7, 167.2, 163.9, 146.4, 141.6, 136.2, 136.0, 134.1, 132.0, 131.7, 129.5, 127.2, 126.3, 125.3, 121.6, 120.5, 118.7, 117.7, 117.3, 114.3, 111.2, 109.5, 107.9, 64.4, 57.2, 51.2, 50.3, 49.2, 49.1, 45.3, 43.8, 30.9, 29.7, 27.6, 26.7, 26.3, 25.8, 25.3, 24.5, 22.5, 22.1. **HRMS (ESI)** m/z: $[M + H]^+$ calcd for $C_{46}H_{51}N_9O_8$, 858.3933; found, 858.3920.

*4-((3-(((6-(2-((2-(2,6-Dioxopiperidin-3-yl)-1,3-dioxoisoindolin-4-yl)amino)acetamido)hexyl)(methyl)amino)methyl)-1H-indol-1-yl)methyl)-N-hydroxybenzamide Trifluoroacetate (**AP3**).* Prepared by following the **General procedure C**. Starting from compound **20** (0.386 g, 0.475 mmol, 1 equiv), the crude product was purified by reverse phase flash column chromatography to yield compound **AP3** (70.0 mg, 20%). **^{1}H NMR** (600 MHz, DMSO-d_6): δ 11.15 (s, 1H), 11.09 (s, 1H), 9.33 (s, 1H), 9.00 (s, 1H), 8.09 (t, J = 5.7 Hz, 1H), 7.81−7.74 (m, 2H), 7.71−7.66 (m, 2H), 7.59 (dd, J = 8.5, 7.1 Hz, 1H), 7.50 (d, J = 8.1 Hz, 1H), 7.26 (d, J = 8.3 Hz, 2H), 7.21−7.13 (m, 2H), 7.07 (d, J = 7.1 Hz, 1H), 6.94 (t, J = 5.6 Hz, 1H),

https://doi.org/10.1021/acs.jmedchem.5c00674
J. Med. Chem. 2025, 68, 13793−13821

6.86 (d, J = 8.6 Hz, 1H), 5.53 (s, 2H), 5.06 (dd, J = 12.8, 5.4 Hz, 1H), 4.53 (d, J = 13.8 Hz, 1H), 4.41 (d, J = 13.1 Hz, 1H), 3.92 (d, J = 5.6 Hz, 2H), 3.18−3.12 (m, 1H), 3.10 (q, J = 6.7 Hz, 2H), 2.96 (s, 1H), 2.89 (ddd, J = 17.0, 13.9, 5.5 Hz, 1H), 2.70 (s, 3H), 2.62−2.51 (m, 2H), 2.02 (dtd, J = 12.8, 5.3, 2.3 Hz, 1H), 1.67 (s, 2H), 1.41 (q, J = 6.6 Hz, 2H), 1.31−1.22 (m, 4H). **^{13}C NMR** (151 MHz, DMSO-d_6): δ 172.8, 170.0, 168.7, 168.3, 167.3, 163.8, 158.1 (q, J = 30.5 Hz), 145.8, 140.8, 136.2, 135.9, 132.2, 132.0, 132.0, 127.9, 127.2, 127.0, 122.1, 120.1, 119.0, 118.4, 117.4, 116.4, 110.9, 110.7, 109.8, 54.2, 49.8, 48.9, 48.6, 45.2, 38.6, 38.3, 31.0, 28.8, 25.8, 25.7, 23.5, 22.1. **HRMS (ESI)** m/z: $[M + H]^+$ calcd for $C_{39}H_{43}N_7O_7$, 722.3297; found, 722.3302.

*4-((2-(6-(2-(4-(2,6-Dioxopiperidin-3-yl)phenoxy)-acetamido)hexyl)-1,2,3,4-tetrahydro-5H-pyrido[4,3-b]indol-5-yl)methyl)-N-hydroxybenzamide (**AP4**).* Prepared by following the **General procedure C**. Starting from compound **17** (0.289 g, 0.382 mmol, 1 equiv), the crude product was purified by reverse phase flash column chromatography to yield compound **AP4** (23.4 mg, 9%). **^{1}H NMR** (600 MHz, DMSO-d_6): δ 11.15 (s, 1H), 10.78 (s, 1H), 9.64 (s, 1H), 9.05−8.95 (m, 1H), 8.06 (t, J = 5.9 Hz, 1H), 7.72−7.65 (m, 2H), 7.51 (dd, J = 25.2, 8.0 Hz, 2H), 7.17−7.12 (m, 4H), 7.09 (t, J = 7.5 Hz, 1H), 6.95−6.88 (m, 2H), 5.57−5.37 (m, 2H), 4.69 (s, 1H), 4.45 (s, 2H), 4.32 (s, 1H), 3.82 (s, 1H), 3.79 (dd, J = 11.5, 4.9 Hz, 1H), 3.52−3.41 (m, 1H), 3.25 (s, 2H), 3.15 (q, J = 6.7 Hz, 3H), 3.03 (s, 1H), 2.65 (ddd, J = 17.2, 11.8, 5.3 Hz, 1H), 2.49−2.45 (m, 1H), 2.15 (dtd, J = 13.1, 11.7, 4.5 Hz, 1H), 2.00 (dq, J = 13.2, 4.8 Hz, 1H), 1.75 (s, 2H), 1.48 (p, J = 7.2 Hz, 2H), 1.33 (ddt, J = 15.1, 8.8, 5.5 Hz, 4H). **^{13}C NMR** (151 MHz, DMSO-d_6): δ 174.4, 173.4, 167.5, 163.7, 156.6, 141.0, 136.5, 131.9, 131.8, 131.5, 129.5, 127.2, 126.6, 124.4, 121.9, 119.6, 117.8, 114.5, 110.1, 102.2, 67.1, 55.1, 49.4, 48.3, 46.5, 45.6, 38.1, 31.3, 28.8, 26.0, 25.8, 25.7, 23.6, 19.7. **HRMS (ESI)** m/z: $[M + H]^+$ calcd for $C_{38}H_{43}N_5O_6$, 666.3286; found, 666.3292.

*4-(1-(6-(5-(4-(Hydroxycarbamoyl)benzyl)-1,3,4,5-tetrahydro-2H-pyrido[4,3-b]indol-2-yl)hexyl)-1H-1,2,3-triazol-4-yl)-butyl 2-(4-(2,6-Dioxopiperidin-3-yl)phenoxy)acetate (**AP5**).* Prepared by following the **General procedure C**. Starting from compound **19** (0.125 g, 0.142 mmol, 1 equiv), the crude product was purified by reverse phase flash column chromatography to yield compound **AP5** (23.9 mg, 21%). **^{1}H NMR** (600 MHz, DMSO-d_6): δ 11.12 (s, 1H), 10.80 (s, 1H), 9.00 (s, 1H), 7.84 (s, 1H), 7.71−7.64 (m, 2H), 7.41 (dd, J = 7.7, 1.2 Hz, 1H), 7.37 (d, J = 8.1 Hz, 1H), 7.16−7.11 (m, 2H), 7.09 (d, J = 8.3 Hz, 2H), 7.05 (ddd, J = 8.2, 7.0, 1.3 Hz, 1H), 7.00 (td, J = 7.4, 7.0, 1.0 Hz, 1H), 6.91−6.86 (m, 2H), 5.39 (s, 2H), 4.78 (s, 2H), 4.30 (t, J = 7.1 Hz, 2H), 4.16 (q, J = 4.4, 2.9 Hz, 2H), 3.80 (dd, J = 11.6, 4.9 Hz, 1H), 3.60 (s, 2H), 2.77 (t, J = 5.7 Hz, 2H), 2.73 (d, J = 5.5 Hz, 2H), 2.69−2.61 (m, 3H), 2.56−2.53 (m, 1H), 2.51−2.39 (m, 2H), 2.20−2.12 (m, 1H), 2.04−1.98 (m, 1H), 1.82 (p, J = 7.2 Hz, 2H), 1.64 (p, J = 4.0, 3.6 Hz, 4H), 1.55 (p, J = 7.3 Hz, 2H), 1.35 (p, J = 7.1 Hz, 2H), 1.28 (ddd, J = 14.2, 8.1, 5.5 Hz, 2H). **^{13}C NMR** (151 MHz, DMSO-d_6): δ 174.3, 174.3, 173.4, 173.3, 168.8, 156.5, 146.4, 141.6, 136.2, 134.1, 131.8, 131.7, 129.5, 127.2, 126.3, 125.4, 121.6, 120.5, 118.7, 117.4, 114.3, 109.5, 107.9, 64.6, 64.2, 57.2, 50.3, 49.2, 49.1, 46.5, 45.3, 31.3, 29.7, 27.6, 26.7, 26.3, 25.9, 25.8, 25.3, 24.5, 22.5. **HRMS (ESI)** m/z: $[M + H]^+$ calcd for $C_{44}H_{51}N_7O_7$, 790.3923; found, 790.3909.

*4-((3-(((6-(2-(4-(2,6-Dioxopiperidin-3-yl)phenoxy)-acetamido)hexyl)(methyl)amino)methyl)-1H-indol-1-yl)-methyl)-N-hydroxybenzamide Trifluoroacetate (**AP6**).* Prepared by following the **General procedure C**. Starting from compound **21** (0.512 g, 0.688 mmol, 1 equiv), the crude was purified by reverse phase flash column chromatography to yield compound **AP6** (0.147 g, 33%). **^{1}H NMR** (600 MHz, DMSO-d_6): δ 11.15 (s, 1H), 10.78 (s, 1H), 9.41 (s, 1H), 9.00 (s, 1H), 8.06 (t, J = 5.9 Hz, 1H), 7.82−7.73 (m, 2H), 7.72−7.65 (m, 2H), 7.50 (d, J = 8.3 Hz, 1H), 7.30−7.23 (m, 2H), 7.21−7.16 (m, 1H), 7.16−7.13 (m, 2H), 6.95−6.88 (m, 2H), 5.53 (s, 2H), 4.53 (d, J = 13.9 Hz, 1H), 4.45 (s, 2H), 4.43−4.31 (m, 1H), 3.79 (dd, J = 11.5, 4.9 Hz, 1H), 3.20−3.08 (m, 3H), 2.97 (s, 1H), 2.70 (s, 3H), 2.65 (ddd, J = 17.1, 11.8, 5.3 Hz, 1H), 2.49−2.45 (m, 1H), 2.15 (dtd, J = 13.1, 11.7, 4.4 Hz, 1H), 2.00 (dq, J = 13.2, 4.8 Hz, 1H), 1.68 (q, J = 7.9 Hz, 2H), 1.44 (t, J = 6.9 Hz, 2H), 1.34−1.21 (m, 4H). **^{13}C NMR** (151 MHz, DMSO-d_6): δ 174.4, 173.4, 167.5, 163.8, 158.1 (q, J = 30.5 Hz), 156.7, 140.8, 135.9, 132.2, 132.0, 131.8, 129.5, 127.9, 127.2, 127.0, 122.1, 120.1, 119.0, 114.5, 110.7, 102.8, 67.1, 56.0, 54.2, 49.8, 48.9, 46.5, 38.6, 38.0, 31.3, 28.8, 26.0, 25.8, 25.7. **HRMS (ESI)** m/z: $[M + H]^+$ calcd for $C_{37}H_{43}N_5O_6$, 654.3286; found, 654.3290.

*4-((2-(3-(4-((1-(2-(2,6-Dioxopiperidin-3-yl)-1,3-dioxoisoindolin-4-yl)piperidin-4-yl)methyl)piperazin-1-yl)-3-oxopropyl)-1,2,3,4-tetrahydro-5H-pyrido[4,3-b]indol-5-yl)methyl)-N-hydroxybenzamide Trifluoroacetate (**AP7**).* Preparation followed the **General procedure C** starting from compound **S4** (0.039 g, 0.043 mmol, 1 equiv). The crude product was purified with preparative HPLC to provide compound **AP7** (8.8 mg, 25%). **^{1}H NMR** (600 MHz, DMSO-d_6): δ 11.15 (s, 1H), 11.07 (s, 1H), 9.92 (s, 1H), 9.00 (s, 1H), 7.73−7.65 (m, 3H), 7.50 (t, J = 6.9 Hz, 2H), 7.35 (d, J = 7.8 Hz, 2H), 7.13 (tt, J = 15.0, 7.6 Hz, 4H), 5.59−5.36 (m, 2H), 5.08 (dd, J = 13.0, 5.5 Hz, 1H), 4.74 (d, J = 14.3 Hz, 1H), 4.56−4.28 (m, 2H), 4.05 (s, 1H), 3.88 (s, 1H), 3.73 (d, J = 11.0 Hz, 2H), 3.54 (m, 6H), 3.23−2.98 (m, 8H), 2.89 (dt, J = 23.1, 8.6 Hz, 4H), 2.65−2.52 (m, 2H), 2.10−1.97 (m, 2H), 1.88 (d, J = 12.3 Hz, 2H), 1.46 (s, 2H). **^{13}C NMR** (151 MHz, DMSO-d_6): δ 172.8, 170.0, 167.9, 167.0, 166.3, 163.7, 158.2 (q, J = 31.1 Hz), 149.9, 141.0, 136.6, 135.8, 133.6, 131.9, 131.4, 127.2, 126.5, 124.4, 123.9, 121.9, 119.7, 118.1, 117.7, 116.5, 116.2, 114.6, 110.2, 102.0, 61.0, 55.0, 51.2, 50.3, 49.4, 48.8, 48.6, 45.6, 30.9, 29.6, 27.3, 26.4, 22.1, 19.6. **HRMS (ESI)** m/z: $[M + H]^+$ calcd for $C_{45}H_{51}N_8O_7$, 815.3875; found, 815.3894.

*4-((2-(3-(4-(4-((2-(2,6-Dioxopiperidin-3-yl)-1,3-dioxoisoindolin-4-yl)amino)benzyl)piperazin-1-yl)-3-oxopropyl)-1,2,3,4-tetrahydro-5H-pyrido[4,3-b]indol-5-yl)methyl)-N-hydroxybenzamide (**AP8**).* Preparation followed the **General procedure C** starting from compound **S5** (0.051 g, 0.056 mmol, 1 equiv). The crude product was purified by reverse phase flash chromatography to afford compound **AP8** (7.2 mg, 16%). **^{1}H NMR** (600 MHz, DMSO-d_6): δ 11.10 (s, 1H), 8.38 (s, 1H), 7.63 (d, J = 8.0 Hz, 2H), 7.60 (t, J = 7.9 Hz, 1H), 7.39 (dd, J = 13.8, 8.1 Hz, 2H), 7.35 (d, J = 8.1 Hz, 1H), 7.28 (m, 4H), 7.23 (d, J = 7.0 Hz, 1H), 7.03 (dd, J = 13.7, 7.7 Hz, 3H), 6.98 (t, J = 7.4 Hz, 1H), 5.37 (s, 2H), 5.11 (dd, J = 12.7, 5.4 Hz, 1H), 3.63 (s, 2H), 3.48 (t, J = 5.4 Hz, 2H), 3.45 (d, J = 9.6 Hz, 4H), 2.89 (ddd, J = 16.9, 13.6, 5.4 Hz, 1H), 2.80 (q, J = 7.5, 6.5 Hz, 4H), 2.70 (t, J = 5.6 Hz, 2H), 2.61−2.51 (m, 4H), 2.33 (dt, J = 30.4, 5.0 Hz, 4H), 2.06 (m, 1H). **^{13}C NMR** (151 MHz, DMSO-d_6): δ 172.8, 170.0, 169.6, 168.3, 167.0, 163.8, 142.9, 141.5, 138.2, 136.3, 136.2, 134.0, 133.6, 132.4, 131.9, 129.9, 127.1, 126.2, 125.3, 121.8, 120.5, 119.3, 118.7, 117.4, 113.3, 111.8, 109.5, 107.9, 61.3, 53.4, 52.8, 52.3, 50.2, 49.1,

https://doi.org/10.1021/acs.jmedchem.5c00674
J. Med. Chem. 2025, 68, 13793−13821

48.7, 45.3, 45.0, 41.0, 31.0, 30.8, 22.5, 22.1. **HRMS (ESI)** m/z: $[M + H]^+$ calcd for $C_{46}H_{47}N_8O_7$: 823.3562, found: 823.3550.

*4-((2-(6-(2-((2-(2,6-Dioxopiperidin-3-yl)-1,3-dioxoisoindolin-4-yl)amino)acetamido)hexanoyl)-1,2,3,4-tetrahydro-5H-pyrido[4,3-b]indol-5-yl)methyl)-N-hydroxybenzamide (**AP9**).* Preparation followed the **General procedure C** starting from compound **S8** (0.2 g, 0.239 mmol, 1 equiv). The crude product was purified with preparative HPLC to afford compound **AP9** (72 mg, 40%). ^{1}H NMR (600 MHz, DMSO-d_6): δ 11.11 (s, 1H), 11.08 (s, 1H), 8.97 (s, 2H), 8.05 (q, J = 5.8 Hz, 1H), 7.65 (dd, J = 7.9, 3.2 Hz, 2H), 7.61−7.55 (m, 1H), 7.49 (dd, J = 19.7, 7.7 Hz, 1H), 7.39 (t, J = 9.3 Hz, 1H), 7.11−7.05 (m, 3H), 7.02 (m, 1H), 6.94 (t, J = 5.8 Hz, 1H), 6.86 (d, J = 8.5 Hz, 1H), 5.40 (s, 2H), 5.07 (dd, J = 12.8, 5.4 Hz, 1H), 4.68 (d, J = 12.0 Hz, 2H), 3.91 (s, 2H), 3.86 (t, J = 5.4 Hz, 1H), 3.80 (t, J = 5.3 Hz, 1H), 3.09 (p, J = 6.4 Hz, 2H), 2.93−2.85 (m, 1H), 2.81 (t, J = 6.1 Hz, 1H), 2.72 (t, J = 6.9 Hz, 1H), 2.62−2.51 (m, 2H), 2.41 (q, J = 7.6 Hz, 2H), 2.06−1.99 (m, 1H), 1.52 (h, J = 7.6 Hz, 2H), 1.47−1.37 (m, 2H), 1.28 (p, J = 7.6, 7.1 Hz, 2H). ^{13}C NMR (151 MHz, DMSO-d_6): δ 172.7, 171.1, 170.0, 168.7, 168.2, 167.3, 163.9, 145.8, 141.4, 136.3, 136.2, 133.6, 132.0, 131.8, 127.2, 126.3, 125.0, 121.0, 119.1, 117.6, 117.4, 110.9, 109.9, 109.7, 106.7, 45.4, 45.2, 42.4, 42.0, 38.4, 32.9, 32.5, 31.0, 28.9, 26.1, 24.5, 24.4, 22.1. **HRMS (ESI)** m/z: $[M + H]^+$ calcd for $C_{40}H_{41}N_7O_8$: 748.3089, found: 748.3081.

*4-((2-(6-(2-((2-(2,6-Dioxopiperidin-3-yl)-1,3-dioxoisoindolin-4-yl)amino)acetamido)hexanoyl)-1,2,3,4-tetrahydro-5H-pyrido[4,3-b]indol-5-yl)methyl)-3-fluoro-N-hydroxybenzamide Trifluoroacetate (**AP10**).* Preparation followed the **General procedure C** starting from compound **S9** (0.102 g, 0.119 mmol, 1 equiv). The crude product was purified with preparative HPLC to afford compound **AP10** (40 mg, 44%). ^{1}H NMR (600 MHz, DMSO-d_6): δ 11.23 (s, 1H), 11.08 (s, 1H), 9.10 (s, 1H), 8.09−8.02 (m, 1H), 7.63−7.47 (m, 3H), 7.45 (d, J = 7.7 Hz, 1H), 7.39 (dd, J = 8.0, 4.3 Hz, 1H), 7.06 (m, 2H), 6.93 (t, J = 5.5 Hz, 1H), 6.85 (d, J = 8.6 Hz, 1H), 6.77 (q, J = 7.3 Hz, 1H), 5.44 (s, 2H), 5.06 (dd, J = 12.8, 5.5 Hz, 1H), 4.68 (d, J = 13.3 Hz, 2H), 3.91 (d, J = 5.3 Hz, 2H), 3.88−3.83 (m, 1H), 3.83−3.77 (m, 1H), 3.13−3.05 (m, 2H), 2.92−2.85 (m, 1H), 2.82 (s, 1H), 2.72 (s, 1H), 2.62−2.54 (m, 2H), 2.44−2.37 (m, 2H), 2.06−1.99 (m, 1H), 1.56−1.48 (m, 2H), 1.42 (s, 2H), 1.27 (dq, J = 16.6, 9.6, 8.9 Hz, 2H). ^{13}C NMR (151 MHz, DMSO-d_6): δ 172.8, 171.1, 170.0, 168.7, 168.2, 167.3, 162.5, 145.8, 140.1, 136.2, 136.2, 134.3, 133.70 (d, J = 3.7 Hz), 132.0, 128.5 (d, J = 3.1 Hz), 125.1, 123.2, 121.1, 119.2, 117.6, 117.4, 113.9 (d, J = 20.2 Hz), 110.9, 109.9, 109.6, 106.9, 45.8 (d, J = 7.5 Hz), 45.2, 42.4, 42.0, 38.5, 32.9, 32.5, 31.0, 28.9, 26.1, 24.6, 24.4, 22.1. ^{19}F NMR (471 MHz, DMSO): δ −74.5, −118.0. **HRMS (ESI)** m/z: $[M + Na]^+$ calcd for $C_{40}H_{40}FN_7O_8$: 788.2815, found: 788.2817.

*N-Hydroxy-4-((2-(6-(2-((2-(1-methyl-2,6-dioxopiperidin-3-yl)-1,3-dioxoisoindolin-4-yl)amino)acetamido)hexyl)-1,2,3,4-tetrahydro-5H-pyrido[4,3-b]indol-5-yl)methyl)-benzamide (**AP-N**).* Prepared by following the **General procedure C** starting from compound **S11** (0.168 g, 0.200 mmol, 1 equiv). The crude product was purified by reverse phase flash chromatography to provide compound **AP-N** (37.3 mg, 25%). **^{1}H NMR** (600 MHz, DMSO-d_6): δ 11.14 (s, 1H), 9.65 (s, 1H), 9.00 (s, 1H), 8.09 (t, J = 5.8 Hz, 1H), 7.68 (d, J = 8.3 Hz, 2H), 7.61 (dd, J = 8.5, 7.1 Hz, 1H), 7.52 (d, J = 7.9 Hz, 1H), 7.48 (d, J = 8.2 Hz, 1H), 7.14 (dd, J = 8.3, 3.3 Hz, 3H), 7.09 (dd, J = 7.2, 2.3 Hz, 2H), 6.95 (t, J = 5.6 Hz, 1H), 6.87 (d, J = 8.5 Hz, 1H), 5.46 (d, J = 45.4 Hz, 2H), 5.14 (dd, J = 13.0, 5.4 Hz, 1H), 4.69 (s, 1H), 4.31 (s, 1H), 3.93 (d, J = 5.5 Hz, 2H), 3.82 (s, 1H), 3.47 (s, 1H), 3.27−3.04 (m, 6H), 3.02 (s, 3H), 2.95 (ddd, J = 17.2, 13.9, 5.4 Hz, 1H), 2.76 (ddd, J = 17.2, 4.5, 2.6 Hz, 1H), 2.63−2.52 (m, 1H), 2.05 (dtd, J = 12.9, 5.4, 2.6 Hz, 1H), 1.74 (s, 2H), 1.45 (p, J = 7.1 Hz, 2H), 1.32 (tt, J = 11.0, 6.8 Hz, 4H). **^{13}C NMR** (151 MHz, DMSO-d_6): δ 171.8, 169.8, 168.7, 168.2, 167.2, 163.7, 145.8, 141.0, 136.5, 136.2, 132.0, 131.9, 131.7, 127.2, 126.6, 124.5, 121.8, 119.6, 117.8, 117.4, 111.0, 110.1, 109.8, 102.2, 55.2, 49.4, 49.1, 48.3, 45.6, 45.2, 38.4, 31.1, 28.8, 26.6, 25.8, 25.7, 23.7, 21.4, 19.8. **HRMS (ESI)** m/z: $[M + H]^+$ calcd for $C_{41}H_{45}N_7O_7$, 748.3453; found, 748.3438.

*tert-Butyl 4-((1-(2-(2,6-Dioxopiperidin-3-yl)-1,3-dioxoisoindolin-4-yl)piperidin-4-yl)methyl)piperazine-1-carboxylate (**S1**).* To a solution of 2-(2,6-dioxopiperidin-3-yl)-4-fluoroisoindoline-1,3-dione (0.2 g, 0.724 mmol) in anhydrous DMSO (15 mL) was added *tert*-butyl 4-(piperidin-4-ylmethyl)piperazine-1-carboxylate (0.226 g, 0.796 mmol, 1.1 eq) and *N*,*N*-diisopropylethylamine (0.187 g, 1.45 mmol, 2 eq). The mixture was stirred at 100 °C for 17.5 h. The completion of the reaction was monitored by TLC. After cooling to room temperature, the mixture was poured into water (100 mL) and extracted with ethyl acetate (3 × 30 mL). The combined organic layer was then washed with water (3 × 30 mL) and followed by brine (30 mL), dried over anhydrous Na_2SO_4, filtered, and concentrated in vacuo to afford the crude product, which was then purified by silica column chromatography (DCM: MeOH 15:1, v/v) to generate the compound **S1** (0.339g, 87%). **^{1}H NMR** (600 MHz, DMSO-d_6): δ 11.06 (s, 1H), 7.67 (dd, J = 8.5, 7.1 Hz, 1H), 7.32 (dd, J = 9.1, 7.9 Hz, 2H), 5.08 (dd, J = 12.8, 5.5 Hz, 1H), 3.68 (d, J = 11.8 Hz, 2H), 3.34−3.31 (m, 4H), 2.93−2.82 (m, 3H), 2.62−2.51 (m, 2H), 2.30 (t, J = 5.0 Hz, 4H), 2.19 (d, J = 7.2 Hz, 2H), 2.02 (dtd, J = 12.8, 5.3, 2.2 Hz, 1H), 1.81 (d, J = 12.8 Hz, 2H), 1.71 (ddq, J = 10.9, 7.3, 3.7 Hz, 1H), 1.40 (s, 9H), 1.31 (qd, J = 12.0, 3.8 Hz, 2H). **^{13}C NMR** (151 MHz, DMSO-d_6): δ 172.7, 170.0, 167.1, 166.2, 153.8, 150.1, 135.7, 133.7, 123.9, 116.2, 114.3, 78.7, 63.8, 53.0, 50.9, 50.9, 48.7, 32.1, 30.9, 30.4, 28.0, 22.0. **LC−MS (ESI)**, $[M + H]^+$ m/z: 540.5.

*tert-Butyl 3-(5-(4-((Benzyloxy)carbamoyl)benzyl)-1,3,4,5-tetrahydro-2H-pyrido[4,3-b]indol-2-yl)propanoate (**S2**).* To a solution of compound **3** (0.4 g, 0.782 mmol, 1 equiv) in DCM (20 mL), TFA (4 mL) was added. The mixture was stirred at room temperature for 2 h and the complete removal of *tert*-butyl group was monitored by HPLC. Afterward, the mixture was dried in vacuo to provide the crude product for the next step. To a solution of the resulting crude product in anhydrous DMF (20 mL), *tert*-butyl 3-bromopropanoate (0.327 g, 1.56 mmol, 2 equiv) and K_2CO_3 (0.324 g, 2.35 mmol, 3 equiv) were added. The mixture was stirred at 60 °C for 24 h. The completion of the reaction was monitored by HPLC. After cooling to room temperature, the mixture was poured into water (150 mL) and extracted with ethyl acetate (3 × 50 mL). The combined organic layer was then washed with water (3 × 50 mL) and followed by brine (50 mL), dried over anhydrous Na_2SO_4, filtered, and concentrated in vacuo to yield the crude product, which was then purified by silica column chromatography (DCM: MeOH 15:1, v/v) to yield compound **S2** (0.204 g, 48%). **^{1}H NMR** (600 MHz, DMSO-d_6): δ 11.67 (s, 1H), 7.64 (d, J = 8.1 Hz, 2H), 7.43 (d, J = 7.4 Hz, 2H), 7.38 (dd, J = 8.0, 6.4 Hz, 3H), 7.36−7.32 (m, 2H), 7.08−7.04 (m, 2H), 7.04−6.96 (m, 2H), 5.38 (s, 2H), 4.89 (s,

https://doi.org/10.1021/acs.jmedchem.5c00674
J. Med. Chem. 2025, 68, 13793−13821

2H), 3.63 (s, 2H), 2.83−2.77 (m, 4H), 2.70 (d, J = 5.5 Hz, 2H), 2.47 (t, J = 7.1 Hz, 2H), 1.38 (s, 9H). **^{13}C NMR** (151 MHz, DMSO-d_6): δ 171.4, 164.1, 142.2, 136.3, 135.9, 134.0, 131.2, 128.9, 128.3, 127.4, 126.4, 126.3, 125.3, 120.6, 118.8, 117.3, 109.5, 107.8, 79.5, 76.9, 52.9, 49.9, 48.9, 45.3, 33.7, 27.7, 22.5. **LC−MS (ESI)**, $[M - H]^-$ m/z: 538.5.

*tert-Butyl 4-(4-((2-(2,6-dioxopiperidin-3-yl)-1,3-dioxoisoindolin-4-yl)amino)benzyl)piperazine-1-carboxylate (**S3**).* Compound **S3** was synthesized following a reported method.[53] To a solution of commercially available 2-(2,6-dioxopiperidin-3-yl)-4-iodoisoindoline-1,3-dione (0.2 g, 0.521 mmol, 1 equiv) and *tert*-butyl 4-(4-aminobenzyl)piperazine-1-carboxylate (0.228 g, 0.781 mmol, 1.5 equiv) in dioxane and water (10 mL: 1 mL), X-Phos (0.05 g, 0.104 mmol, 0.2 equiv), K_2CO_3 (0.144 g, 1.04 mmol, 2 equiv) and $Pd_2(dba)_3$ (24 mg, 0.03 mmol, 0.05 equiv) were added. The air in the system was pumped out and replaced with argon, the mixture was stirred at 90 °C for 18 h under argon atmospheres. After cooling to room temperature, the resulting mixture was filtered over Celite and the filter cake was washed with ethyl acetate (ca. 50 mL). The collected solution was dried under reduced pressure to afford the crude product, which was then purified by silica column chromatography (ethyl acetate) to yield compound **S3** (0.138 g, 49%). **^{1}H NMR** (500 MHz, DMSO-d_6): δ 10.92 (s, 1H), 8.37 (s, 1H), 7.63 (t, J = 7.8 Hz, 1H), 7.46 (d, J = 8.4 Hz, 1H), 7.39 (d, J = 7.4 Hz, 2H), 7.33 (d, J = 7.9 Hz, 2H), 7.26 (d, J = 7.1 Hz, 1H), 5.09 (dd, J = 12.7, 5.4 Hz, 1H), 3.14 (s, 8H), 2.91 (ddd, J = 19.0, 13.8, 5.4 Hz, 1H), 2.69−2.61 (m, 2H), 2.58 (td, J = 13.1, 4.5 Hz, 2H), 2.09 (ddd, J = 13.1, 5.5, 2.5 Hz, 1H), 1.42 (s, 9H). **^{13}C NMR** (126 MHz, DMSO-d_6): δ 172.1, 169.3, 168.0, 166.6, 153.4, 142.5, 140.5, 135.8, 132.2, 130.5, 121.1, 119.3, 118.1, 113.2, 78.8, 60.3, 51.4, 48.6, 42.2, 30.7, 27.8, 21.9. **LC−MS (ESI)**, $[M + H]^+$ m/z: 548.2.

*N-(Benzyloxy)-4-((2-(3-(4-((1-(2-(2,6-dioxopiperidin-3-yl)-1,3-dioxoisoindolin-4-yl)piperidin-4-yl)methyl)piperazin-1-yl)-3-oxopropyl)-1,2,3,4-tetrahydro-5H-pyrido[4,3-b]indol-5-yl)methyl)benzamide (**S4**).* After the removal of the *tert*-butyloxycarbonyl protecting group in both compound **S1** and compound **S2** with TFA, both resulting products were used to synthesize the compound **S4**. Briefly, to a solution of the Boc-deprotected product (0.094 g, 0.194 mmol, 1 equiv) from compound **S2** in anhydrous DMF (10 mL), HATU (0.147 g, 0.387 mmol, 2 equiv) and DIPEA (0.075 g, 0.581 mmol, 3 equiv) were added, the mixture was stirred for 30 min at room temperature, after which, the Boc-deprotected product (0.094 g, 0.213 mmol, 1.1 equiv) from compound **S1** was added into the system and stirred for 16 h. The mixture was concentrated and the solvent was removed in vacuo to yield the crude product, which was then purified by silica column chromatography (DCM: MeOH 15:1, v/v, 1% Et_2NH) to afford compound **S4** (43 mg, 25%). **^{1}H NMR** (600 MHz, DMSO-d_6): δ 11.71 (s, 1H), 11.06 (s, 1H), 7.71−7.61 (m, 3H), 7.46−7.39 (m, 3H), 7.39−7.29 (m, 6H), 7.08 (d, J = 8.0 Hz, 2H), 7.06−7.03 (m, 1H), 7.02−6.97 (m, 1H), 5.40 (s, 2H), 5.08 (dd, J = 12.8, 5.5 Hz, 1H), 4.88 (s, 2H), 3.68 (d, J = 11.9 Hz, 4H), 3.48 (d, J = 16.3 Hz, 4H), 2.94−2.79 (m, 6H), 2.78−2.69 (m, 2H), 2.61 (dq, J = 6.6, 3.6, 2.7 Hz, 1H), 2.59−2.51 (m, 2H), 2.41−2.25 (m, 4H), 2.18 (d, J = 7.0 Hz, 2H), 2.06−1.97 (m, 1H), 1.81 (d, J = 12.6 Hz, 2H), 1.71 (s, 1H), 1.34−1.23 (m, 4H). **^{13}C NMR** (151 MHz, DMSO-d_6): δ 173.2, 170.4, 167.5, 166.7, 164.5, 150.6, 142.6, 136.8, 136.3, 136.2, 134.1, 131.7, 129.3, 128.7, 127.9, 126.8, 125.7, 124.3, 119.3, 117.9, 116.7, 114.8, 110.0, 77.4, 64.1, 55.3, 54.0, 53.3, 51.4, 51.4, 49.2, 45.9, 45.5, 36.2, 32.6, 31.4, 30.9, 29.4, 22.5. **LC−MS (ESI)**, $[M + H]^+$ m/z: 905.7.

*N-(Benzyloxy)-4-((2-(3-(4-(4-((2-(2,6-dioxopiperidin-3-yl)-1,3-dioxoisoindolin-4-yl)amino)benzyl)piperazin-1-yl)-3-oxopropyl)-1,2,3,4-tetrahydro-5H-pyrido[4,3-b]indol-5-yl)methyl)benzamide (**S5**).* After the removal of the *tert*-butyloxycarbonyl protecting group in both compound **S2** and compound **S3** with TFA, both resulting products were used to synthesize the compound **S5**. Briefly, to a solution of the Boc-deprotected product (0.084 g, 0.173 mmol, 1 equiv) from compound **S2** in anhydrous DMF (10 mL) were added HATU (0.132 g, 0.346 mmol, 2 equiv) and DIPEA (0.067 g, 0.519 mmol, 3 equiv), the mixture was stirred for 30 min at room temperature, after which, the Boc-deprotected product (0.093 g, 0.208 mmol, 1.2 equiv) from compound **S3** was added into the system and stirred for 16 h. The mixture was concentrated and the solvent was removed in vacuo to yield the crude product, which was then purified by silica column chromatography (DCM: MeOH 15:1, v/v, 1% Et_2NH) to afford compound **S5** (56 mg, 35%). **^{1}H NMR** (600 MHz, DMSO-d_6): δ 8.39 (s, 1H), 7.64 (d, J = 7.9 Hz, 2H), 7.62−7.58 (m, 1H), 7.41 (d, J = 8.2 Hz, 3H), 7.39−7.32 (m, 4H), 7.29 (s, 4H), 7.24 (d, J = 7.0 Hz, 1H), 7.07 (d, J = 7.9 Hz, 2H), 7.03 (d, J = 7.9 Hz, 1H), 7.00 (d, J = 7.7 Hz, 1H), 5.39 (s, 2H), 5.12 (dt, J = 12.9, 3.7 Hz, 1H), 4.88 (s, 2H), 3.64 (s, 2H), 3.49 (s, 2H), 3.46 (d, J = 11.0 Hz, 4H), 2.90 (td, J = 15.8, 13.8, 4.8 Hz, 1H), 2.84−2.78 (m, 4H), 2.71 (d, J = 6.2 Hz, 2H), 2.60 (d, J = 6.5 Hz, 2H), 2.58−2.52 (m, 2H), 2.34 (d, J = 30.4 Hz, 4H), 2.07 (dt, J = 12.6, 5.3 Hz, 1H). **^{13}C NMR** (151 MHz, DMSO-d_6): δ 172.7, 169.9, 169.6, 168.3, 167.0, 163.9, 142.9, 142.1, 138.2, 136.3, 136.2, 135.9, 134.0, 133.6, 132.4, 131.2, 129.9, 128.8, 128.3, 128.2, 127.4, 126.3, 125.3, 121.8, 120.5, 119.3, 118.8, 117.4, 113.3, 111.8, 109.5, 107.9, 76.9, 61.3, 53.4, 52.8, 52.3, 50.2, 49.1, 48.7, 45.3, 45.0, 41.0, 30.9, 30.8, 22.5, 22.1. **LC−MS (ESI)**, $[M + H]^+$ m/z: 913.4.

*tert-Butyl 6-(2-((2-(2,6-Dioxopiperidin-3-yl)-1,3-dioxoisoindolin-4-yl)amino)acetamido)hexanoate (**S6**).* To a solution of compound **10** (0.514 g, 1.33 mmol) in DCM (15 mL) was added TFA (3 mL) and the mixture was stirred for 2 h. The complete removal of *tert*-butyl group was monitored by TLC. The solvent was then removed and the crude was subjected to a PyCloP-mediated amide coupling reaction. To a solution of the obtained crude carboxylic acid (0.440 g, 1.33 mmol, 1 equiv) in anhydrous DMF were added *tert*-butyl 6-aminohexanoate (0.261 g, 1.39 mmol, 1.05 equiv), PyCloP (0.671 g, 1.59 mmol, 1.2 equiv), and DIPEA (0.429 g, 3.32 mmol, 2.5 equiv). The mixture was stirred at room temperature for 17 h. The mixture was poured into water (150 mL) and extracted with ethyl acetate (3 × 50 mL). The combined organic layers were then washed with water (3 × 30 mL), followed by brine (30 mL), dried over anhydrous Na_2SO_4, filtered, and concentrated in vacuo to afford the crude product, which was then purified by silica column chromatography (DCM: MeOH 20:1, v/v) to generate the compound **S6** (0.567g, 85%). **^{1}H NMR** (600 MHz, DMSO-d_6): δ 11.08 (s, 1H), 8.06 (t, J = 5.4 Hz, 1H), 7.59 (t, J = 7.8 Hz, 1H), 7.07 (d, J = 7.1 Hz, 1H), 6.93 (t, J = 5.5 Hz, 1H), 6.86 (d, J = 8.5 Hz, 1H), 5.07 (dd, J = 12.8, 5.4 Hz, 1H), 3.91 (d, J = 5.6 Hz, 2H), 3.08 (q, J = 6.6 Hz, 2H), 2.94−2.84 (m, 1H), 2.63−2.51 (m, 2H), 2.15 (t, J = 7.3 Hz, 2H), 2.07−1.99 (m, 1H), 1.47 (p, J = 7.4 Hz, 2H), 1.38 (m, 11H), 1.23 (p, J = 7.5, 7.1 Hz, 2H). **^{13}C NMR** (151 MHz, DMSO-d_6): δ 172.8, 172.2, 170.0, 168.7, 168.2, 167.3, 145.8, 136.2, 132.0, 117.4, 110.9, 109.9, 79.4,

https://doi.org/10.1021/acs.jmedchem.5c00674
J. Med. Chem. 2025, 68, 13793−13821

48.6, 45.2, 38.4 34.7, 31.0, 28.7, 27.7, 25.7, 24.3, 22.1. **LC−MS (ESI)**, $[M - H]^-$ m/z: 499.7.

*tert-Butyl 5-(4-((Benzyloxy)carbamoyl)-2-fluorobenzyl)-1,3,4,5-tetrahydro-2H-pyrido[4,3-b]indole-2-carboxylate (**S7**).* For the synthesis of compound **S7**, the intermediate *tert*-butyl 5-(2-fluoro-4-(methoxycarbonyl)benzyl)-1,3,4,5-tetrahydro-2*H*-pyrido[4,3-*b*]indole-2-carboxylate (3.92 g) was first synthesized following the procedure to obtain compound **2**, by using methyl 4-(bromomethyl)-3-fluorobenzoate as a reactant. This intermediate was then hydrolyzed to afford the carboxylic acid compound 4-((2-(*tert*-butoxycarbonyl)-1,2,3,4-tetrahydro-5*H*-pyrido[4,3-*b*]indol-5-yl)methyl)-3-fluorobenzoic acid (3.33 g, 88%), which was subjected to an HATU-mediated aimde coupling reaction following the preparation steps of compound **3** to generate compound **S7** (2.42 g, 58%). **^{1}H NMR** (600 MHz, $CDCl_3$): δ 7.51−7.45 (m, 2H), 7.42−7.38 (m, 2H), 7.38−7.32 (m, 3H), 7.22−7.09 (m, 4H), 6.53 (t, J = 7.6 Hz, 1H), 5.30 (s, 2H), 5.00 (s, 2H), 4.67 (d, J = 1.7 Hz, 2H), 3.80 (t, J = 5.7 Hz, 2H), 2.69 (t, J = 5.7 Hz, 2H), 1.49 (s, 9H). **^{13}C NMR** (151 MHz, $CDCl_3$): δ 160.6, 158.9, 155.2, 136.6, 135.1, 133.2 (d, J = 57.4 Hz), 133.0, 129.3, 128.9, 128.7, 128.2 (d, J = 4.4 Hz), 128.2, 125.5, 122.8, 121.8, 119.8, 118.0, 114.6 (d, J = 22.2 Hz), 114.5, 109.1, 108.1, 80.0, 78.3, 41.2, 40.1(d, J = 5.5 Hz), 28.5, 26.9, 22.4. ^{19}F NMR (565 MHz, $CDCl_3$): δ −117.6. **LC−MS (ESI)**, $[M - H]^-$ m/z: 528.4.

*N-(Benzyloxy)-4-((2-(6-(2-((2-(2,6-dioxopiperidin-3-yl)-1,3-dioxoisoindolin-4-yl)amino)acetamido)hexanoyl)-1,2,3,4-tetrahydro-5H-pyrido[4,3-b]indol-5-yl)methyl)benzamide (**S8**).* For the synthesis of compound **S8**, the protecting groups in compound **S6** (0.15 g, 0.3 mmol, 1 equiv) and compound **3** (0.161 g, 0.315 mmol, 1.05 equiv) were removed with TFA (2 mL) in DCM (5 mL), respectively. To a solution of the deprotected compound **S6** (0.133 g, 0.3 mmol, 1equiv) in anhydrous DMF were added HATU (0.228 g, 0.599 mmol, 2 equiv) and DIPEA (0.116 g, 0.899 mmol, 3 equiv), the mixture was stirred at 0 °C for 30 min. Subsequently, a solution of deprotected compound **3** (0.129 g, 0.315 mmol, 1.05 equiv) in anhydrous DMF was added into the system, which was stirred for 18 h from 0 °C to room temperature. The solvent was removed in vacuo to afford the crude product, which was purified by silica column chromatography (DCM: MeOH 15:1, v/v) to yield compound **S8** (0.205 g, 82%). **^{1}H NMR** (600 MHz, DMSO-d_6): δ 11.68 (s, 1H), 11.08 (s, 1H), 8.06 (t, J = 5.3 Hz, 1H), 7.65 (m, 2H), 7.61−7.56 (m, 1H), 7.49 (dd, J = 19.7, 7.7 Hz, 1H), 7.38 (m, 5H), 7.14−6.99 (m, 4H), 6.94 (t, J = 5.3 Hz, 1H), 6.88−6.82 (m, 1H), 5.41 (s, 2H), 5.11−5.03 (m, 1H), 4.88 (s, 2H), 4.68 (d, J = 11.9 Hz, 2H), 3.95−3.88 (m, 2H), 3.83 (dt, J = 34.0, 5.5 Hz, 2H), 3.09 (p, J = 6.9 Hz, 2H), 2.93−2.84 (m, 1H), 2.81 (t, J = 5.9 Hz, 1H), 2.71 (t, J = 5.9 Hz, 1H), 2.62−2.52 (m, 2H), 2.41 (dt, J = 12.5, 6.2 Hz, 2H), 2.07−1.99 (m, 1H), 1.51 (dt, J = 19.0, 9.4 Hz, 2H), 1.46−1.38 (m, 2H), 1.31−1.24 (m, 2H). **^{13}C NMR** (151 MHz, DMSO-d_6): δ 172.7, 171.1, 170.0, 168.7, 168.2, 167.3, 164.1, 145.8, 142.0, 136.3, 136.1, 135.8, 133.6, 132.0, 131.3, 128.9, 128.3, 127.5, 126.4, 125.0, 121.0, 119.1, 117.6, 117.4, 110.9, 109.9, 109.7, 106.7, 76.9, 45.4, 45.2, 42.5, 42.1, 38.4, 32.7, 32.5, 30.9, 28.9, 26.1, 24.5, 24.4, 22.1. **LC−MS (ESI)**, $[M + H]^+$ m/z: 838.6.

*N-(Benzyloxy)-4-((2-(6-(2-((2-(2,6-dioxopiperidin-3-yl)-1,3-dioxoisoindolin-4-yl)amino)acetamido)hexanoyl)-1,2,3,4-tetrahydro-5H-pyrido[4,3-b]indol-5-yl)methyl)-3-fluorobenzamide (**S9**).* Compound **S9** was prepared following the same procedure for the synthesis of compound **S8** by using compound **S7** (0.167 g, 0.315 mmol, 1.05 equiv) and its deprotected form (0.135 g, 0.315 mmol, 1.05 equiv). The crude product was purified by silica column chromatography (DCM: MeOH 15:1, v/v) to afford compound **S9** (0.108 g, 42%). **^{1}H NMR** (600 MHz, DMSO-d_6): δ 11.79 (s, 1H), 11.08 (s, 1H), 8.05 (q, J = 5.7 Hz, 1H), 7.61−7.47 (m, 3H), 7.46−7.41 (m, 2H), 7.37 (m, 4H), 7.08 (t, J = 7.5 Hz, 1H), 7.07−7.01 (m, 2H), 6.94 (t, J = 5.3 Hz, 1H), 6.85 (dd, J = 8.5, 2.4 Hz, 1H), 6.79 (q, J = 7.8 Hz, 1H), 5.45 (s, 2H), 5.06 (dd, J = 12.8, 5.5 Hz, 1H), 4.89 (s, 2H), 4.68 (d, J = 12.6 Hz, 2H), 3.95−3.88 (m, 2H), 3.85 (t, J = 5.6 Hz, 1H), 3.80 (t, J = 5.5 Hz, 1H), 3.09 (p, J = 6.3 Hz, 2H), 2.88 (ddd, J = 17.0, 13.9, 5.4 Hz, 1H), 2.81 (t, J = 5.9 Hz, 1H), 2.71 (p, J = 7.6, 6.4 Hz, 1H), 2.62−2.51 (m, 2H), 2.45−2.36 (m, 2H), 2.02 (m, 1H), 1.52 (dq, J = 14.9, 7.4 Hz, 2H), 1.47−1.37 (m, 2H), 1.28 (p, J = 7.6, 7.1 Hz, 2H). **^{13}C NMR** (151 MHz, DMSO-d_6): δ 172.7, 171.1, 170.0, 168.7, 168.2, 167.3, 162.7, 145.8, 136.2, 136.1, 135.7, 134.3, 133.7, 133.5 (d, J = 7.5 Hz), 132.0, 128.9, 128.6, 128.6 (d, J = 4.1 Hz), 128.3, 125.1, 124.8, 123.4, 121.1, 119.2, 117.6, 117.4, 114.1 (d, J = 22.0 Hz), 110.9, 109.9, 109.6, 106.9, 77.0, 45.8 (d, J = 4.2 Hz), 45.2, 42.4, 42.0, 38.4, 32.9, 32.5, 31.0, 28.9, 26.1, 24.5, 24.4, 22.1. **^{19}F NMR** (471 MHz, DMSO): δ −117.8. **LC−MS (ESI)**, $[M - H]^-$ m/z: 854.6.

*N-(Benzyloxy)-4-((2-(6-(2-((2-(1-methyl-2,6-dioxopiperidin-3-yl)-1,3-dioxoisoindolin-4-yl)amino)acetamido)hexyl)-1,2,3,4-tetrahydro-5H-pyrido[4,3-b]indol-5-yl)methyl)-benzamide (**S11**).* Compound **S10** was synthesized following the reported method.[33] After the removal of the protecting group in both compound **4** and compound **S10** with TFA, both resulting products were used afterward for the synthesis of compound **S11**. Briefly, to a solution of the resulting product (0.139 g, 0.402 mmol, 1 equiv) from compound **S10** in anhydrous DMF (10 mL) were added HATU (0.306 g, 0.804 mmol, 2 equiv) and DIPEA (0.156 g, 1.21 mmol, 3 equiv). The mixture was stirred for 30 min at room temperature. Afterward the resulting product (0.205 g, 0.402 mmol, 1 equiv) from compound **4** was added into the system and stirred overnight. After extraction with DCM, the combined organic layer was then washed with water for three times and followed by brine once, dried over anhydrous Na_2SO_4, filtered and concentrated in vacuo to yield the crude, which was then purified by flash column chromatography (0→6.2% MeOH in DCM, 0−10 min; 6.2% MeOH in DCM, 10−30 min) to afford the compound **S11** (0.176 g, 52%). **^{1}H NMR** (600 MHz, DMSO-d_6): δ 11.70 (s, 1H), 8.74−8.48 (m, 1H), 8.09 (t, J = 5.7 Hz, 1H), 7.67 (d, J = 8.0 Hz, 2H), 7.60 (dd, J = 8.5, 7.1 Hz, 1H), 7.53−7.45 (m, 2H), 7.43 (d, J = 7.5 Hz, 2H), 7.40−7.33 (m, 3H), 7.14 (t, J = 8.0 Hz, 2H), 7.11−7.03 (m, 2H), 6.95 (t, J = 5.6 Hz, 1H), 6.87 (d, J = 8.5 Hz, 1H), 5.46 (s, 2H), 5.14 (dd, J = 13.0, 5.4 Hz, 1H), 4.89 (s, 2H), 4.40 (s, 2H), 3.93 (d, J = 5.5 Hz, 2H), 3.54 (s, 2H), 3.21−3.14 (m, 2H), 3.12 (q, J = 6.7 Hz, 2H), 3.09−3.02 (m, 2H), 3.02 (s, 3H), 3.00−2.88 (m, 1H), 2.76 (ddd, J = 17.2, 4.5, 2.6 Hz, 1H), 2.59−2.51 (m, 1H), 2.04 (dtd, J = 12.9, 5.4, 2.6 Hz, 1H), 1.72 (q, J = 7.6, 7.2 Hz, 2H), 1.44 (p, J = 7.1 Hz, 2H), 1.37−1.29 (m, 4H). **^{13}C NMR** (151 MHz, DMSO-d_6): δ 171.7, 169.8, 168.7, 168.2, 167.2, 164.0, 145.8, 139.6, 136.5, 136.2, 135.8, 132.0, 131.8, 131.4, 128.9, 128.7, 128.3, 127.4, 126.6, 124.5, 121.7, 120.5, 119.6, 117.8, 117.4, 111.0, 110.0, 109.8, 76.9, 55.3, 49.4, 49.1, 48.4, 45.6, 45.2, 38.4, 31.1, 28.8, 26.6, 25.8, 25.8, 24.0, 21.4, 20.0. **LC−MS (ESI)**, $[M + H]^+$ m/z: 838.6.

https://doi.org/10.1021/acs.jmedchem.5c00674
J. Med. Chem. 2025, 68, 13793−13821

BIOLOGICAL AND PHYSICOCHEMICAL EVALUATION

HDAC Inhibition Assays. *In Vitro HDAC6 Assay.* The in vitro inhibitory activity against HDAC6 was measured using our previously published assay protocol.[48,54,55] In short, 3-fold serial dilutions of test compounds and controls were prepared in assay buffer (50 mM Tris-HCl (pH 8.0), 137 mM NaCl, 2.7 mM KCl, 1.0 mM $MgCl_2 \cdot 6\ H_2O$, and 0.1 mg/mL BSA). These serial dilutions (5.0 μL) were transferred into 96-well microplates (OptiPlate-96 F, black, PerkinElmer). 35 μL of the fluorogenic substrate ZMAL (Z-Lys(Ac)-AMC; 21.43 μM in assay buffer) and 10 μL of human recombinant HDAC enzyme solution (HDAC6 - BPS Bioscience, Catalog# 50006) in assay buffer were added.[56] The total assay volume of 50 μL (max. 1% DMSO) was incubated at 37 °C for 90 min. Subsequently, 50 μL trypsin solution (0.4 mg/mL trypsin in buffer: 50 mM Tris-HCl (pH 8.0), 100 mM NaCl) was added, followed by 30 min of incubation at 37 °C. Fluorescence (excitation, 355 nm; emission, 460 nm) was measured using a FLUOstar OPTIMA microplate reader (BMG LABTECH). All compounds were tested in duplicate. Reported mean IC_{50}-values, including standard deviation, were calculated from at least two independent experiments.

In Vitro HDAC10 Assay. HDAC10 inhibition assays were performed by Reaction Biology Corp. (Malvern PA, USA; CAT# HDAC10). In short, either 10 μL of reaction buffer (20 mM Na_2HPO_4 (pH 8.0), 100 mM NaCl, 0.25 mM EDTA, 10 mM Mesna, 0.01% Brij35, 1% DMSO) or 10 μL of human full-length HDAC10 (aa2-669end, Accession #NM_032019.5, N-terminal GST-TEV-tag, expressed in Sf9 insect cells) enzyme solution in reaction buffer was transferred into 384-well microplates (flat bottom, black, Corning—#3573). Next, 3-fold serial dilutions of test compounds and controls in DMSO were added using acoustic technology (Echo550 Liquid Handler, BeckmanCoulter; nanoliters) and the mixture was preincubated for 20 min. Subsequently, 10 μL of substrate solution (Ac-spermidine-AMC; final assay concentration: 12.5 μM) in reaction buffer was added and the final assay volume of 20 μL was incubated at 30 °C. After 1 h of incubation time, "stop"-solution (borate buffer (pH 9.5), NDA; final assay concentration: 167 μM) was added. Fluorescence (excitation, 355 nm; emission, 460 nm) was measured using an EnVision microplate reader (PerkinElmer). All compounds were tested in duplicate. Reported mean IC_{50}-values, including standard deviation, were calculated from at least two independent experiments.

CRBN Target Engagement Assay. The assay was performed as previously described by Zerfas et al.[38] HEK293T cells stably expressing NanoLuc-CRBN were cultured in DMEM (Gibco, Life Technologies) supplemented with 10% FBS. Cells were resuspended at 2×10^5 cells/mL in 21 mL Opti-MEM I (Gibco, Life Technologies) and mixed with 600 μL BODIPY-lenalidomide fluorescent tracer (stock at 10 μM diluted in tracer dilution buffer 31.25% PEG-400, 12.5 mM HEPES, pH 7.5, filtered using a 0.22 μm nitrocellulose membrane) to reach final concentration of the tracer at 278 nM. The cell-tracer mixture was then plated in a white polystyrene 384-well plate (Corning, 3570) at 50 μL/well. After plating, the assay plate was centrifuged (400*g*, 5 min) and protected from light. Compounds for testing were added to the plate using a D300e Digital Dispenser (Tecan) in duplicate 12 pt titrations from a 10 mM stock in DMSO, with DMSO normalized to 1% total volume. The plate was then placed in an incubator at 37 °C, 5% CO_2 for 2 h. After incubation, the plate was removed and set on the bench to cool to room temperature (~10 min). The NanoLuc substrate (500X solution, Promega Catalog number N2160 for 1000 assay kit) and extracellular inhibitor (1500× solution, Promega Catalog number N2160 for 1000 assay kit) were diluted in Opti-MEM I (Gibco, Life Technologies) to prepare a 3× solution, which was added to each well (25 μL/well). The plate was read on a Pherastar FSX (BMG Labtech) microplate reader with simultaneous dual emission capabilities at 450 and 520 nm for 10 cycles. The NanoBRET ratio was calculated by dividing the signal at 520 nm by the signal at 450 nm and multiplying by 1000 for each sample and averaged across 10 read cycles to create each data point. The data was plotted in GraphPad Prism 10 and the curves were fitted using Variable Slope equation to obtain the EC_{50} values.

DETERMINATION OF PHYSICOCHEMICAL PROPERTIES

Log$D_{7.4}$ Measurements. The determination of the log $D_{7.4}$ values was performed by a chromatographic method as described previously.[57] Briefly, the system was calibrated by plotting the retention times of six different drugs (atenolol, metoprolol, labetalol, diltiazem, triphenylene, permethrin) versus their literature known log$D_{7.4}$ values to obtain a calibration line ($R^2 \geq 0.95$). Subsequently, the mean retention times of the analytes were taken to calculate their log $D_{7.4}$ values with aid of the calibration line.

Plasma Protein Binding Studies. PPB was estimated by correlating the logarithmic retention times of the analytes on a CHIRALPAK HSA 50 × 3 mm, 5 μm column with the literature known %PPB values (converted into log *K* values) of the following drugs: warfarin, ketoprofen, budesonide, nizatidine, indomethacin, acetylsalicylic acid, carbamazepine, piroxicam, nicardipine, and cimetidine. Samples were dissolved in MeCN/DMSO 9:1 to achieve a final concentration of 0.5 mg/mL. The mobile phase A was 50 mM NH_4Ac adjusted to pH 7.4 with ammonia, while mobile phase B was *i*PrOH. The flow rate was set to 1.0 mL/min, the UV detector was set to 254 nm, and the column temperature was kept at 30 °C. After injecting 3 μL of the sample, a linear gradient from 100% A to 30% *i*PrOH in 5.4 min was applied. From 5.4 to 18 min, 30% *i*PrOH was kept, followed by switching back to 100% A in 1.0 min and a re-equilibration time of 6 min. With the aid of the calibration line ($R^2 \geq 0.92$), the log *K* values of new substances were calculated and converted to their % PPB values.

Molecular Descriptor Calculations. Calculated values for the topological polar surface area (TPSA) and number of rotatable bonds (NRotB) were determined using the free web tool SwissADME.[58]

Plasma Stability. To determine the ex vivo stability of AP1−6 in human plasma, fresh whole blood was collected in 3K-EDTA collection tubes (SARSTEDT AG & Co. KG, Nümbrecht, Germany) and plasma was obtained by centrifugation at 2000 rpm for 10 min. The plasma was warmed to 37 °C, and the compound solution was added to achieve final concentrations of 50 nM and 1 μM, respectively. A control was prepared in 4% BSA (w/V) in water containing 1 μM of the respective compound. Each approach was applied in triplicate. All samples were incubated at 37 °C and shaken at 400 rpm over 24 h. Sample collection was conducted 0, 30, 60, 120, 240, 360, and 1440 min. The samples were immediately

https://doi.org/10.1021/acs.jmedchem.5c00674
J. Med. Chem. 2025, 68, 13793−13821

precipitated with ice-cold acetonitrile, which contained the internal standard. Following vortexing and shaking for 30 min at 1000 rpm, the samples were centrifuge dated for 10 min at a speed of 14,000 rpm. The supernatant was evaporated under a gentle stream of nitrogen at a temperature of 37 °C and the residues were covered and stored in a refrigerator at 4 °C. Following the final sampling period, all residues were reconstituted in 70/20/10 water/dimethyl sulfoxide/formic acid (v/v, containing 10% formic acid) and analyzed.

For separation and quantification, a LC−MS/MS system consisting of an Agilent 1200 series HPLC (Agilent, Waldbronn, Germany) coupled to a Sciex 4000 triple quadrupole mass spectrometer (Sciex, Darmstadt, Germany) with an ESI interface was used. Sample handling was performed by a CTC HTS Pal system (CTC Analytics AG, Zwingen, Switzerland). Chromatographic separation was achieved using a XBridge BEH C18 3.0 × 150 HPLC column under gradient conditions (mobile phases: 0.1% formic acid in water and 0.1% formic acid in methanol). The flow rate was set to 300 μL/min. The following settings per compound were applied: AP1), $[M + H]^+$ 734.3 → 442.4 *m/z*; DP 113 V, EP 10 V, CE 38 V, CXP 13 V; AP2), $[M + H]^+$ 858.4 → 566.4 *m/z*; DP 115 V, EP 11 V, CE 37 V, CXP 17 V; AP3), $[M + H]^+$ 722.7 → 279.3 *m/z*; DP 95 V, EP 10 V, CE 34 V, CXP 15 V; AP4), $[M + H]^+$ 666.6→374.1 *m/z*; DP 96 V, EP 9 V, CE 34 V, CXP 11 V; AP5), $[M + H]^+$ 790.4 → 293.2 *m/z*; DP 95 V, EP 9 V, CE 36 V, CXP 15 V; AP6), $[M + H]^+$ 654.7→279.4 *m/z*; DP 90 V, EP 10 V, CE 29 V, CXP 15 V; Tubastatin A), $[M + H]^+$ 336.2→293.2 *m/z*; DP 85 V, EP 10 V, CE 19 V, CXP 15 V; Compounds were monitored by multiple reaction monitoring with a dwell time of 75 ms and positive ionization mode.

Western Blotting. Western blots on HDAC 1, 4, 6, 7, 8, 10, IKZF1, IKZF3, GSPT1, LC3 I/II, acetylated histone H3, acetylated α-tubulin and GAPDH in MM.1S cells, as well as the HDAC6, 10 and GAPDH in MCF-7 cells were performed according to a previously published protocol.[59−61] In brief, the treated MM.1S or MCF-7 cells were collected and lyzed with cell extraction buffer (ThermoFisher Scientific Inc.; Waltham, MA, USA), supplemented with 0.1 mM PMSF, Halt Protease Inhibitor (Thermo Fisher), and sodium orthovanadate (ThermoFisher Scientific Inc.; Waltham, MA, USA). Protein concentration was determined using a BCA kit (ThermoFisher Scientific Inc.; Waltham, MA, USA). Equal amounts of protein (25 μg) from the lysates was denatured by Laemmli 2× Concentrate (Catalog# S3401-10VL, Sigma-Aldrich, St. Louis, MO, USA), and Precision Plus Protein Unstained Standard was used as molecular weight marker (Catalog# 1610363, Bio-Rad, Hercules, CA, USA). SDS-PAGE was performed with precast gels with a polymerization degree of 4−15% (for ac-histone H3) and 10% or 12% for other proteins (Mini-PROTEAN TGX Stain-Free; Bio-Rad Laboratories GmbH, Germany). Afterward, proteins were transferred to Trans-Blot Turbo-PVDF membranes (Merck). The membrane was blocked with skimmed milk powder in Tris-buffered saline-Tween 20 (with 0.2% Tween 20) for 60 min, followed by three washing cycles of 10 min using Tris-buffered saline-Tween 20. Next, membranes were incubated with primary antibodies for a total of 60 min at room temperature under slight agitation and then incubated at 4 °C overnight. Membranes were rinsed again three times before applying the secondary antirabbit IgG HRP-conjugated mAbs (R&D Systems, Inc., Minneapolis, USA) or antimouse IgG HRP-conjugated mAbs (Santa Cruz Biotechnology, Texas, USA) for 90 min. After rinsing of the secondary antibody, membranes were detected using the ClarityECL Western Blotting Substrate (Bio-Rad). For quantitative determination, the StainFree technique was employed (Bio-Rad), which allows the imaging of whole protein in SDS-PAGE before blotting and normalization on the transferred membrane against the total protein. Pixel density analysis was performed with the IMAGE LAB software (Bio-Rad). Primary antibodies were used as antibody solutions in 1:1000−1:20,000 dilutions. Anti-HDAC1 (Catalog#5356S, Cell Signaling Technology, Denver, MA, USA), anti-HDAC4 (Catalog#7628S, Cell Signaling Technology, Denver, MA, USA), anti-HDAC6 (Catalog#7558S, Cell Signaling Technology, Denver, MA, USA), antiacetyl-histone H3 (Catalog#9677S, Cell Signaling Technology, Denver, MA, USA), antiacetyl-α-tubulin (Catalog#5335S, Cell Signaling Technology, Denver, MA, USA), anti-HDAC8 (Catalog#66042S, Cell Signaling Technology, Denver, MA, USA), anti-HDAC10 (Catalog#H3413, Sigma-Aldrich, St. Louis, MO, USA), anti-GAPDH (Catalog# T0004, Affinity Biosciences, Cincinnati, OH, USA), anti-HDAC7 (Catalog#33418S, Cell Signaling Technology, Denver, MA, USA), anti-IKZF1 (Catalog#14859S, Cell Signaling Technology, Denver, MA, USA), anti-IKZF3 (Catalog#15103S, Cell Signaling Technology, Denver, MA, USA), anti-GSPT1 (Catalog#sc-66000, Santa Cruz Biotechnology, Texas, USA), anti-LC3A/B (Catalog#12741T, Cell Signaling Technology, Denver, MA, USA).

Cell Assays. *Cell Culture.* MM.1S cells were obtained by the American Type Culture Collection (ATCC, Manassas, VA, USA). Cells were cultured in RPMI 1640 (Life Technologies, Darmstadt, Germany) supplemented with 10% fetal bovine serum (PAN Biotech GmbH, Aidenbach, Germany), 100 IU/mL penicillin and 0.1 mg/mL streptomycin (PAN Biotech GmbH, Aidenbach, Germany) and 1 mM sodium pyruvate (ThermoFisher Scientific Inc.; Waltham, MA, USA) and were incubated at 37 °C under humidified air with 5% CO_2. MCF-7 cells were obtained by the American Type Culture Collection (ATCC, Manassas, VA, USA). Cells were cultured in Dulbecco's modified Eagle's medium (DMEM, Gibco) already containing L-glutamine and pyruvate, and supplemented with 10% fetal bovine serum (PAN Biotech GmbH, Aidenbach, Germany), 100 IU/mL penicillin and 0.1 mg/mL streptomycin (PAN Biotech GmbH, Aidenbach, Germany), and were incubated at 37 °C under humidified air with 5% CO_2. The human breast cancer cell line MDA-MB-231 (HTB-26) was cultivated in DMEM medium (Catalog#41966-029, Gibco, ThermoFisher Scientific Inc.) supplemented with 10% FBS (PAN Biotech GmbH), 100 IU/mL penicillin and 0.1 mg/mL streptomycin (PAN Biotech GmbH). Cells were incubated at a humidified atmosphere at 37 °C containing 5% CO_2. Cells were detached with trypsin/EDTA (0.05%/0.02% in DPBS, PAN Biotech GmbH). Mycoplasma contamination was routinely excluded by PCR.

CellTiterGlo 2.0 Assay in MM.1S Cells. 2500 MM.1S cells/well were seeded in white 384-well plates (Greiner Bio-One, Kremsmuenster, Austria). The final assay volume was 25 μL. A 200-fold dilution series was prepared in DMSO and further diluted to 10-fold in medium and added to the cells. The final DMSO concentration was 0.5%. The toxicity of compounds was determined after 72 h using the CellTiter-Glo 2.0 Cell Viability Assay (Promega, Madison, WI, USA, #G9242) according to the manufacturer's protocol. Subsequently, the luminescence was measured using a Tecan

https://doi.org/10.1021/acs.jmedchem.5c00674
J. Med. Chem. 2025, 68, 13793−13821

Spark (Tecan Group AG, Maennedorf, Swiss). Data was analyzed with the four-parameter logistic equation (GraphPad Prism 9.0, San Diego, CA, USA).

MTT Assay in MCF-7 Cells. Assays were conducted following previously reported methods.[54] MTT (3-(4,5-dimethylthiazol-2-yl)-2,5-diphenyltetrazolium bromide; Catalog# A2231; BioChemica, Applichem GmbH, Darmstadt, Germany) was used to measure cell viability. A total of 2500 MCF-7 cells were seeded in triplicates in 96-well plates (Starlab GmbH, Hamburg, Germany) with each well containing 200 μL of volume. These cells were subsequently treated with dilution series of different compounds. Following an incubation period of 72 h, 20 μL of freshly prepared MTT solution (5 mg/mL) was added and the mixture was incubated for 1 h at 37 °C and 5% CO_2. After removing the supernatant, the formazan dye was solubilized in 200 μL DMSO (Sigma-Aldrich, Steinheim, Germany). The absorbance was determined at 570 nm with background subtraction at 690 nm by a microplate photometer (Thermo Scientific Multiskan EX, Thermo Fisher Scientific). The acquired data was normalized to DPBS, considering 100% viability, and the half-maximal inhibitory concentration (IC_{50}) was determined by plotting dose response curves and nonlinear regression with GraphPad Prism (GraphPad Software, San Diego, CA, USA).

Cell Cycle Analysis. For cell cycle analysis, MM.1S cells were seeded at a density of 3×10^5 cells/well in a 12-well plate (Sarstedt AG & Co, Nümbrecht, Germany) and cultivated overnight at 37 °C and 5% CO_2. The next day, cells were treated with either vorinostat at 10 μM, tubastatin A at 10 μM, AP1 at 10 μM and 20 μM, AP1N at 10 μM and 20 μM or DMSO as negative control. After an incubation for 48 h under cell culture conditions, cells were washed using DPBS and centrifuged at. Afterward, ice cold 70% ethanol was added dropwise to the cell pellet and incubated for 30 min at 4 °C. In the next step, cells were rehydrated using DPBS and treated with 50 μg/mL RNase (Thermo Fisher Scientific Inc., Waltham, USA). Finally, Propidium Iodide was added to the cells at 3 μM, incubated for 15 min in the dark and cell cycle distribution was analyzed using Guava easyCyte HT 11 Flow Cytometer (Luminex Corporation, Austin, USA) and FlowJo v10.5.3 Software (BD Life Sciences, Franklin Lakes, USA).

Wound Healing Assay. For the wound healing assay, 2-well silicone inserts (Catalog#80209, ibidi, Gräfelfing, Germany) were positioned in 24-well plates (Starlab GmbH, Hamburg, Germany). A total of 21×10^3 MDA-MB-231 cells were seeded into each reservoir. After 24 h the cell culture inserts were removed and cells were treated with 10 μM of the respective compound. Images were acquired immediately after the removal of the culture inserts and again after 24 h using an Axiovert 200 microscope (Carl Zeiss Microscopy, Jena, Germany) at 10-fold magnification. In the meantime, cells were incubated at 37 °C and 5% CO_2. The acquired images were analyzed with ImageJ (Tiago Ferreira, Wayne Rasband), ZEN 3.0 blue edition (Carl Zeiss Microscopy, Oberkochen, Germany) and evaluated with GraphPad Prism 8 (San Diego, CA, USA). Wound closure was quantified as relative area (%) compared to initial gap area. The results were derived from at least two independent experiments.

■ QUANTITATIVE PROTEOMICS (MM.1S CELLS)

Sample Preparation for Whole-Proteome Analysis. Two million MM.1S cells were seeded in a T25 flask in 7 mL media the day before giving the treatments. After incubating for 24 h, 7 μL of DMSO or compounds in 10 mM stock solutions were given to the cells and the incubated for 6 h. The cells were collected and washed with DPBS twice, aspirate off DPBS and the cell pellets were frozen with liquid nitrogen and stored in −80 °C.

Frozen MM1.S cell pellets were lysed in 200 μL of urea lysis buffer (6 M urea, 2 M thiourea in 50 mM TRIS-HCl pH = 8.5). To degrade chromatin 7.5 U/mL of Benzonase (ThermoFisher Scientific Inc.; Waltham, MA, USA) was added to the samples before incubation for 10 min on ice. Samples were centrifuged for 10 min at 15,000g. Supernatants were transferred to new tubes and the concentration was determined using Pierce 660 nm Protein Assay Reagent (ThermoFisher Scientific Inc.; Waltham, MA, USA). Subsequently, urea concentration was reduced to 2 M and 100 μg of protein per sample was used for further processing. To reduce and alkylate cysteine bonds, 10 mM TCEP bond-breaker solution (ThermoFisher Scientific Inc.; Waltham, MA, USA) and 40 mM chloroacetamide were added simultaneously and incubated for 30 min at room temperature in the dark. Overnight digestion was carried out at room temperature by adding of 1 μg Trypsin/LysC per 100 μg of protein. Digestion was stopped by adding stop buffer (20% acetonitrile in ddH_2O and 6% TFA), followed by desalting of 40 μg of peptides on poly(styrene−divinylbenzene) reverse-phase sulfonated (SDB-RPS) plugs stacked in 200 μL pipet tips. Peptides were eluted with 50 μL of elution buffer (80% acetonitrile, 15% ddH_2O, 5% ammonia) per sample. Eluents were evaporated at 30 °C for 2 h. Dried peptides were resuspended in 12 μL of loading buffer (2% acetonitrile in 0.1% FA ddH_2O). Before application to the mass spectrometer, the concentration of each sample was adjusted to 300 ng/μL.

LC−MS/MS. Peptides in buffer A (0.1% FA in ddH_2O) were separated using a NeoVanquish HPLC system (ThermoFisher Scientific Inc.; Waltham, MA, USA) with a 25 cm Aurora Ultimate column (C18, 75 μm inner diameter) coupled to an Exploris 480 mass spectrometer (ThermoFisher Scientific Inc.; Waltham, MA, USA) via a nanoelectrospray source. Peptides were separated with a 90 min gradient, starting with 6% buffer B (80% acetonitrile, 0.1% FA in ddH_2O) increasing linearly to 25% after 70 min, followed by stepwise increase to 55% buffer B (78 min) and 95% buffer B (90 min) at a flowrate of 300 nL/min and a column temperature of 55 °C. A staggered, data-independent mass spectrometry method was used with a full MS scan ranging from 380 to 1020 m/z (resolution = 60,000, injection time = 55 ms, AGC target = 100). Each full MS scan was followed by 50 DIA scans spanning 400−1000 m/z (window size 12 m/z, resolution = 30,000, ion fill time = 55 ms, AGC target = 1000).

Gas-phase Fractionation Library. To create a sample-specific gas-phase-fractionation library 1 μL of each sample was pooled and six MS measurements form this pool were recorded. Each individual measurement covered a different m/z-window of 100, spanning in total a range between 400 and 1000 m/z. The library was created with DIA-NN software (version 1.8.1) using a *Homo sapiens* FASTA file (UniProt file form the 18.11.2021).

Identification, Quantification and Statistical Analysis. The raw files obtained from the mass spectrometer were destaggered using MSconvert (64 bit). Prior to processing of raw files, the run-specific mass accuracies for MS1 and MS2 and the scan windows were determined using DIAN-NN (version 1.8.1) with precursor FDR set to 1% and log-level set

https://doi.org/10.1021/acs.jmedchem.5c00674
J. Med. Chem. 2025, 68, 13793−13821

to 1. The MS raw files were processed by DIA-NN software (version 1.8.1) using the generated gas-phase fractionation library as reference (FDR = 1%, Scan window radius = 12, MS1 accuracy = 4.0 × 10^{-6}, MS2 accuracy 1.7 × 10^{-5}) and processed files were MaxLFQ normalized. Data was log-transformed and contaminants were removed. Protein groups were filtered based on 100% data completeness in at least one group. Missing values were replaced samples wise based on a random selection of values from a normal distribution (mean = downshifted 1.8 standard deviations, SD = 0.3). Determination of significant up- or downregulations was carried out by using a two-sample Welch's *t*-test (FDR = 0.05). Fold changes (*x*-axis) and *p*-values (*y*-axis) were plotted against each other for each condition vs DMSO and depicted as volcano plots.

DIAPASEF-BASED QUANTITATIVE PROTEOMICS (MM.1S AND MOLT4 CELLS)

Sample Preparation LFQ Quantitative Mass Spectrometry. Cells were lyzed by addition of lysis buffer (8 M Urea, 50 mM NaCl, 50 mM 4-(2-hydroxyethyl)-1-piperazineethanesulfonic acid (EPPS) pH 8.5, Protease and Phosphatase inhibitors) and homogenization by bead beating (BioSpec) for three repeats of 30 at 2400 strokes/min. Bradford assay was used to determine the final protein concentration in the clarified cell lysate. Fifty micrograms of protein for each sample was reduced, alkylated and precipitated using methanol/chloroform as previously described[62] and the resulting washed precipitated protein was allowed to air-dry. Precipitated protein was resuspended in 4 M urea, 50 mM HEPES pH 7.4, followed by dilution to 1 M urea with the addition of 200 mM EPPS, pH 8. Proteins were digested with the addition of LysC (1:50; enzyme/protein) and trypsin (1:50; enzyme/protein) for 12 h at 37 °C. Sample digests were acidified with formic acid to a pH of 2−3 before desalting using C18 solid phase extraction plates (SOLA, Thermo Fisher Scientific). Desalted peptides were dried in a vacuum-centrifuged and reconstituted in 0.1% formic acid for liquid chromatography−mass spectrometry analysis. Data were collected using a TimsTOF HT (Bruker Daltonics, Bremen, Germany) coupled to a nanoElute LC pump (Bruker Daltonics, Bremen, Germany) via a CaptiveSpray nanoelectrospray source. Peptides were separated on a reversed-phase C18 column (25 cm × 75 μm ID, 1.6 μM, IonOpticks, Australia) containing an integrated captive spray emitter. Peptides were separated using a 50 min gradient of 2−30% buffer B (acetonitrile in 0.1% formic acid) with a flow rate of 250 nL/min and column temperature maintained at 50 °C. The TIMS elution voltages were calibrated linearly with three points (Agilent ESI-L Tuning Mix Ions; 622, 922, 1222 *m*/*z*) to determine the reduced ion mobility coefficients ($1/K_0$). To perform diaPASEF, we used py_diAID,[63] a python package, to assess the precursor distribution in the *m*/*z*-ion mobility plane to generate a diaPASEF acquisition scheme with variable window isolation widths that are aligned to the precursor density in *m*/*z*. Data was acquired using twenty cycles with three mobility window scans each (creating 60 windows) covering the diagonal scan line for doubly and triply charged precursors, with singly charged precursors able to be excluded by their position in the *m*/*z*-ion mobility plane. These precursor isolation windows were defined between 350 to 1250 *m*/*z* and $1/k_0$ of 0.6−1.45 V·s/cm^2.

LC−MS Data Analysis. The diaPASEF raw file processing and controlling peptide and protein level false discovery rates, assembling proteins from peptides, and protein quantification from peptides were performed using library free analysis in DIA-NN 1.8.[64] Library free mode performs an in silico digestion of a given protein sequence database alongside deep learning-based predictions to extract the DIA precursor data into a collection of MS2 spectra. The search results are then used to generate a spectral library which is then employed for the targeted analysis of the DIA data searched against a Swissprot human database (January 2021). Database search criteria largely followed the default settings for directDIA including: tryptic with two missed cleavages, carbamidomethylation of cysteine, and oxidation of methionine and precursor Q-value (FDR) cutoff of 0.01. Precursor quantification strategy was set to Robust LC (high accuracy) with RT-dependent cross run normalization. Proteins with low sum of abundance (<2000 × no. of treatments) were excluded from further analysis and resulting data was filtered to only include proteins that had a minimum of 3 counts in at least 4 replicates of each independent comparison of treatment sample to the DMSO control. Protein abundances were scaled using in-house scripts in the R framework (R Development Core Team, 2014) and proteins with missing values were imputed by random selection from a Gaussian distribution either with a mean of the nonmissing values for that treatment group or with a mean equal to the median of the background (in cases when all values for a treatment group are missing). Significant changes comparing the relative protein abundance of these treatment to DMSO control comparisons were assessed by moderated *t*-test as implemented in the limma package within the R framework.[65]

Molecular Docking. Molecular docking was performed in MOE software (version 2022). The crystal structures of HDAC6 (PDB ID: 6THV) and HDAC10 (PDB ID: 6WBQ) were obtained from the Protein Data Bank. Briefly, the chemical structures of docked and modeled molecules were prepared and optimized based on the MMFF94X force field. The proteins (HDAC6 and HDAC10 crystal complexes) were processed as follows: removal of water molecules, addition of hydrogen atoms and partial charges, protonation based on the Amber10:EHT force field. For docking analysis, the binding site of the native ligand in each receptor was used to define the docking sites. Other MOE-docking parameters were set to default values and 30 predicted poses were retained during the docking process. The best poses of tubastatin A and its hexyl chain attached-derivative were kept based upon the docking score and the results from ligand interactions, followed by visually inspection. The Figures were generated using the PyMOL software (https://pymol.org/2/).

PAINS Analysis. PAINS Analysis We filtered all compounds for pan-assay interference compounds (PAINS) using the online filter http://zinc15.docking.org/patterns/home/. No compound was flagged as PAINS.

ASSOCIATED CONTENT

Data Availability Statement

Data Deposition Global proteomics data will be publicly available at the Fischer Lab's Proteomics database: https://proteomics.fischerlab.org.

Supporting Information

The Supporting Information is available free of charge at https://pubs.acs.org/doi/10.1021/acs.jmedchem.5c00674.

https://doi.org/10.1021/acs.jmedchem.5c00674
J. Med. Chem. 2025, 68, 13793−13821

Figures for rescue experiments in MCF-7 cells with MG-132; quantitative proteomics of MM.1S cell lysates after treatment with 1 μM of **AP1** or tubastatin A for 6 h; rescue experiment for IKZF1 in MM.1S cells; viability assay on MM.1S and MCF-7 cells; long-term degradation of HDAC6 and HDAC10 in MM.1S cells; degradation of HDAC6 and HDAC10 in MCF-7 cells; cell cycle regulation of MM.1S cells; autophagy effect of **AP1** in MM.1S cells; synthesis scheme of **AP7-AP10** and nondegrading control **AP1-N**; ^{1}H, ^{13}C, and ^{19}F NMR spectra of **AP1-AP10**, **AP1-N**; HR-MS spectra and HPLC chromatograms of **AP1-AP10**, **AP1-N**; immunoblot replicates for Figure 5A, Figure 5B, Figure 8A, Figure 8B, Figure 9A, Figure 9B (PDF)

Molecular strings formula (CSV)

AUTHOR INFORMATION

Corresponding Author

Finn K. Hansen − *Department of Pharmaceutical and Cell Biological Chemistry, Pharmaceutical Institute, University of Bonn, 53121 Bonn, Germany;* orcid.org/0000-0001-9765-5975; Email: finn.hansen@uni-bonn.de

Authors

Shiyang Zhai − *Department of Pharmaceutical and Cell Biological Chemistry, Pharmaceutical Institute, University of Bonn, 53121 Bonn, Germany;* orcid.org/0009-0005-6840-3177

Irina Honin − *Department of Pharmaceutical and Cell Biological Chemistry, Pharmaceutical Institute, University of Bonn, 53121 Bonn, Germany;* orcid.org/0009-0009-7091-8419

Linda Schäker-Hübner − *Department of Pharmaceutical and Cell Biological Chemistry, Pharmaceutical Institute, University of Bonn, 53121 Bonn, Germany*

Maria Hanl − *Department of Pharmaceutical and Cell Biological Chemistry, Pharmaceutical Institute, University of Bonn, 53121 Bonn, Germany*

Lukas Jacobi − *Institute of Innate Immunity, Department of Systems Immunology and Proteomics, Medical Faculty, University of Bonn, 53127 Bonn, Germany*

Finn Dressler − *Individualized Pharmacotherapy, Institute of Pharmaceutical and Medicinal Chemistry, University of Münster, 48149 Münster, Germany*

Dominika Ewa Pieńkowska − *Institute of Structural Biology, Medical Faculty, University of Bonn, 53127 Bonn, Germany*

Philipp König − *Department of Pharmaceutical and Cell Biological Chemistry, Pharmaceutical Institute, University of Bonn, 53121 Bonn, Germany*

Jan Gerhartz − *Institute of Structural Biology, Medical Faculty, University of Bonn, 53127 Bonn, Germany;* orcid.org/0009-0002-9457-4656

Rabea Voget − *Department of Pharmaceutical and Medicinal Chemistry, Pharmaceutical Institute, University of Bonn, 53121 Bonn, Germany*

Gerd Bendas − *Department of Pharmaceutical and Cell Biological Chemistry, Pharmaceutical Institute, University of Bonn, 53121 Bonn, Germany;* orcid.org/0000-0002-8667-7201

Michael Gütschow − *Department of Pharmaceutical and Medicinal Chemistry, Pharmaceutical Institute, University of Bonn, 53121 Bonn, Germany;* orcid.org/0000-0002-9376-7897

Felix Meissner − *Institute of Innate Immunity, Department of Systems Immunology and Proteomics, Medical Faculty, University of Bonn, 53127 Bonn, Germany*

Bjoern B. Burckhardt − *Individualized Pharmacotherapy, Institute of Pharmaceutical and Medicinal Chemistry, University of Münster, 48149 Münster, Germany;* orcid.org/0000-0002-1782-9937

Radosław P. Nowak − *Institute of Structural Biology, Medical Faculty, University of Bonn, 53127 Bonn, Germany;* orcid.org/0000-0002-0605-0071

Christian Steinebach − *Department of Pharmaceutical and Medicinal Chemistry, Pharmaceutical Institute, University of Bonn, 53121 Bonn, Germany;* orcid.org/0000-0001-5638-1955

Complete contact information is available at: https://pubs.acs.org/10.1021/acs.jmedchem.5c00674

Author Contributions

The manuscript was written through contributions of all authors. All authors have given approval to the final version of the manuscript.

Notes

The authors declare no competing financial interest.

ACKNOWLEDGMENTS

S.Z. is funded by China Scholarship Council (grant no. 202106150022). The work of I.H., L.S.-H., M.H., R.V., G.B., M.G., C.S., and F.K.H. was funded by the Deutsche Forschungsgemeinschaft (DFG, German Research Foundation)—GRK2873 (494832089). We thank Katherine A. Donovan, Eric S. Fischer and the Fischer Lab Degradation Proteomics Initiative for collection of the global proteomics data supported by NIH CA214608 and CA218278 (diaPASEF-based quantitative proteomics (MM.1S and MOLT4 cells)). The new NMR console for the 500 MHz NMR spectrometer used in this research was funded by the Deutsche Forschungsgemeinschaft (DFG, German Research Foundation) under project number 507275896. Peng Chen and Prof. Dr. Ingo Schmidt-Wolf are acknowledged for providing the LC3 A/B antibodies. We thank Martina Miranda and Mikhail Tsymliakov for their contribution to a synthetic building block. R.P.N. is a member of the excellence cluster ImmunoSensation2 funded by the Deutsche Forschungsgemeinschaft (DFG) under Germany's Excellence Strategy − EXC2151−390873048.

ABBREVIATIONS

BODIPY, 5,5-difluoro-5*H*-4λ5-dipyrrolo[1,2-*c*:2′,1′-*f*][1,3,2]-diazaborinin-4-ylium-5-uide; BSA, bovine serum albumin; DCM, dichloromethane; DIPEA, *N*,*N*-diisopropylethylamine; DMF, *N*,*N*-dimethylformamide; EtOAc, ethyl acetate; HATU, 1-[Bis(dimethylamino)methylene]-1*H*-1,2,3-triazolo[4,5-*b*]-pyridinium 3-oxide hexafluorophosphate; HDAC(s), histone deacetylase(s); HCl, hydrogen chloride; IMiD(s), immunomodulatory drug(s); LC3 A/B, microtubule-associated proteins 1A/1B light chain 3A/B; LiOH, lithium hydroxide; NAD+, nicotinamide adenine dinucleotide; PDB, protein data bank; PyCloP, Chlorotripyrrolidinophosphonium hexafluorophosphate; NanoBRET, nano bioluminescence resonance energy transfer; NanoLuc-CRBN, nanoluciferase cereblon; THF, tetrahydrofuran.

https://doi.org/10.1021/acs.jmedchem.5c00674
J. Med. Chem. 2025, 68, 13793−13821

REFERENCES

(1) Kaur, S.; Rajoria, P.; Chopra, M. HDAC6: A unique HDAC family member as a cancer target. *Cell. Oncol* **2022**, *45* (5), 779−829.
(2) Arrar, M.; Turnham, R.; Pierce, L.; de Oliveira, C. A.; McCammon, J. A. Structural insight into the separate roles of inositol tetraphosphate and deacetylase-activating domain in activation of histone deacetylase 3. *Protein Sci.* **2013**, *22* (1), 83−92.
(3) Ho, T. C. S.; Chan, A. H. Y.; Ganesan, A. Thirty Years of HDAC Inhibitors: 2020 Insight and Hindsight. *J. Med. Chem.* **2020**, *63* (21), 12460−12484.
(4) Chen, X.; He, Y.; Fu, W.; Sahebkar, A.; Tan, Y.; Xu, S.; Li, H. Histone Deacetylases (HDACs) and Atherosclerosis: A Mechanistic and Pharmacological Review. *Front. Cell Dev. Biol.* **2020**, *8*, 581015.
(5) Yang, F.; Zhao, N.; Ge, D.; Chen, Y. Next-generation of selective histone deacetylase inhibitors. *RSC Adv.* **2019**, *9* (34), 19571−19583.
(6) Wang, X. X.; Wan, R. Z.; Liu, Z. P. Recent advances in the discovery of potent and selective HDAC6 inhibitors. *Eur. J. Med. Chem.* **2018**, *143*, 1406−1418.
(7) Li, Y.; Sang, S.; Ren, W.; Pei, Y.; Bian, Y.; Chen, Y.; Sun, H. Inhibition of Histone Deacetylase 6 (HDAC6) as a therapeutic strategy for Alzheimer's disease: A review (2010−2020). *Eur. J. Med. Chem.* **2021**, *226*, 113874.
(8) Yang, K.; Song, Y.; Xie, H.; Wu, H.; Wu, Y. T.; Leisten, E. D.; Tang, W. Development of the first small molecule histone deacetylase 6 (HDAC6) degraders. *Bioorg. Med. Chem. Lett.* **2018**, *28* (14), 2493−2497.
(9) An, Z.; Lv, W.; Su, S.; Wu, W.; Rao, Y. Developing potent PROTACs tools for selective degradation of HDAC6 protein. *Protein Cell* **2019**, *10* (8), 606−609.
(10) Wu, H.; Yang, K.; Zhang, Z.; Leisten, E. D.; Li, Z.; Xie, H.; Liu, J.; Smith, K. A.; Novakova, Z.; Barinka, C.; Tang, W. Development of Multifunctional Histone Deacetylase 6 Degraders with Potent Antimyeloma Activity. *J. Med. Chem.* **2019**, *62* (15), 7042−7057.
(11) Yang, H.; Lv, W.; He, M.; Deng, H.; Li, H.; Wu, W.; Rao, Y. Plasticity in designing PROTACs for selective and potent degradation of HDAC6. *Chem. Commun.* **2019**, *55* (98), 14848−14851.
(12) Yang, K.; Wu, H.; Zhang, Z.; Leisten, E. D.; Nie, X.; Liu, B.; Wen, Z.; Zhang, J.; Cunningham, M. D.; Tang, W. Development of Selective Histone Deacetylase 6 (HDAC6) Degraders Recruiting Von Hippel-Lindau (VHL) E3 Ubiquitin Ligase. *ACS Med. Chem. Lett.* **2020**, *11* (4), 575−581.
(13) Yang, K.; Zhao, Y.; Nie, X.; Wu, H.; Wang, B.; Almodovar-Rivera, C. M.; Xie, H.; Tang, W. A Cell-Based Target Engagement Assay for the Identification of Cereblon E3 Ubiquitin Ligase Ligands and Their Application in HDAC6 Degraders. *Cell Chem. Biol.* **2020**, *27* (7), 866−876.e8.
(14) Cao, Z.; Gu, Z.; Lin, S.; Chen, D.; Wang, J.; Zhao, Y.; Li, Y.; Liu, T.; Li, Y.; Wang, Y.; Lin, H.; He, B. Attenuation of NLRP3 Inflammasome Activation by Indirubin-Derived PROTAC Targeting HDAC6. *ACS Chem. Biol.* **2021**, *16* (12), 2746−2751.
(15) Sinatra, L.; Yang, J.; Schliehe-Diecks, J.; Dienstbier, N.; Vogt, M.; Gebing, P.; Bachmann, L. M.; Sönnichsen, M.; Lenz, T.; Stühler, K.; Schöler, A.; Borkhardt, A.; Bhatia, S.; Hansen, F. K. Solid-Phase Synthesis of Cereblon-Recruiting Selective Histone Deacetylase 6 Degraders (HDAC6 PROTACs) with Antileukemic Activity. *J. Med. Chem.* **2022**, *65* (24), 16860−16878.
(16) Keuler, T.; König, B.; Buckreiss, N.; Kraft, F. B.; König, P.; Schäker-Hübner, L.; Steinebach, C.; Bendas, G.; Gütschow, M.; Hansen, F. K. Development of the first non-hydroxamate selective HDAC6 degraders. *Chem. Commun.* **2022**, *58* (79), 11087−11090.
(17) Hai, Y.; Shinsky, S. A.; Porter, N. J.; Christianson, D. W. Histone deacetylase 10 structure and molecular function as a polyamine deacetylase. *Nat. Commun.* **2017**, *8*, 15368.
(18) Cheng, F.; Zheng, B.; Wang, J.; Zhao, G.; Yao, Z.; Niu, Z.; He, W. Histone deacetylase 10, a potential epigenetic target for therapy. *Biosci. Rep.* **2021**, *41* (6), BSR20210462.
(19) Lambona, C.; Zwergel, C.; Fioravanti, R.; Valente, S.; Mai, A. Histone deacetylase 10: A polyamine deacetylase from the crystal structure to the first inhibitors. *Curr. Opin. Struct. Biol.* **2023**, *82*, 102668.
(20) Oehme, I.; Linke, J. P.; Böck, B. C.; Milde, T.; Lodrini, M.; Hartenstein, B.; Wiegand, I.; Eckert, C.; Roth, W.; Kool, M.; Kaden, S.; Gröne, H. J.; Schulte, J. H.; Lindner, S.; Hamacher-Brady, A.; Brady, N. R.; Deubzer, H. E.; Witt, O. Histone deacetylase 10 promotes autophagy-mediated cell survival. *Proc. Natl. Acad. Sci. U.S.A.* **2013**, *110* (28), E2592−E2601.
(21) Oehme, I.; Lodrini, M.; Brady, N. R.; Witt, O. Histone deacetylase 10-promoted autophagy as a druggable point of interference to improve the treatment response of advanced neuroblastomas. *Autophagy* **2013**, *9* (12), 2163−2165.
(22) Shinsky, S. A.; Christianson, D. W. Polyamine Deacetylase Structure and Catalysis: Prokaryotic Acetylpolyamine Amidohydrolase and Eukaryotic HDAC10. *Biochemistry* **2018**, *57* (22), 3105−3114.
(23) Pettersson, M.; Crews, C. M. Proteolysis TArgeting Chimeras (PROTACs) - Past, present and future. *Drug Discov. Today Technol.* **2019**, *31*, 15−27.
(24) Garcha, H. K.; Olaoye, O. O.; Sedighi, A.; Poloske, D.; Hariri, P.; Yu, W.; Abdallah, D. I.; Moriggl, R.; de Araujo, E. D.; Gunning, P. T. Monoselective Histone Deacetylase 6 PROTAC Degrader Shows In Vivo Tractability. *J. Med. Chem.* **2025**, *68* (6), 6165−6177.
(25) Xia, K.; Qiu, T.; Jian, Y.; Liu, H.; Chen, H.; Liu, X.; Chen, Z.; Wang, L. Degradation of histone deacetylase 6 alleviates ROS-mediated apoptosis in renal ischemia-reperfusion injury. *Biomed. Pharmacother.* **2023**, *165*, 115128.
(26) Darwish, S.; Heimburg, T.; Ridinger, J.; Herp, D.; Schmidt, M.; Romier, C.; Jung, M.; Oehme, I.; Sippl, W. Synthesis, Biochemical, and Cellular Evaluation of HDAC6 Targeting Proteolysis Targeting Chimeras. *Methods Mol. Biol.* **2023**, *2589*, 179−193.
(27) Stopper, D.; Honin, I.; Feller, F.; Hansen, F. K. Development of Ethyl-Hydrazide-Based Selective Histone Deacetylase 6 (HDAC6) PROTACs. *ACS Med. Chem. Lett.* **2025**, *16* (3), 487−495.
(28) Bockstiegel, J.; Wurnig, S. L.; Engelhardt, J.; Enns, J.; Hansen, F. K.; Weindl, G. Pharmacological inhibition of HDAC6 suppresses NLRP3 inflammasome-mediated IL-1beta release. *Biochem. Pharmacol.* **2023**, *215*, 115693.
(29) Géraldy, M.; Morgen, M.; Sehr, P.; Steimbach, R. R.; Moi, D.; Ridinger, J.; Oehme, I.; Witt, O.; Malz, M.; Nogueira, M. S.; Koch, O.; Gunkel, N.; Miller, A. K. Selective Inhibition of Histone Deacetylase 10: Hydrogen Bonding to the Gatekeeper Residue is Implicated. *J. Med. Chem.* **2019**, *62* (9), 4426−4443.
(30) Shen, S.; Svoboda, M.; Zhang, G.; Cavasin, M. A.; Motlova, L.; McKinsey, T. A.; Eubanks, J. H.; Ba řinka, C.; Kozikowski, A. P. Structural and in Vivo Characterization of Tubastatin A, a Widely Used Histone Deacetylase 6 Inhibitor. *ACS Med. Chem. Lett.* **2020**, *11* (5), 706−712.
(31) Herbst-Gervasoni, C. J.; Steimbach, R. R.; Morgen, M.; Miller, A. K.; Christianson, D. W. Structural Basis for the Selective Inhibition of HDAC10, the Cytosolic Polyamine Deacetylase. *ACS Chem. Biol.* **2020**, *15* (8), 2154−2163.
(32) Min, J.; Mayasundari, A.; Keramatnia, F.; Jonchere, B.; Yang, S. W.; Jarusiewicz, J.; Actis, M.; Das, S.; Young, B.; Slavish, J.; Yang, L.; Li, Y.; Fu, X.; Garrett, S. H.; Yun, M. K.; Li, Z.; Nithianantham, S.; Chai, S.; Chen, T.; Shelat, A.; Lee, R. E.; Nishiguchi, G.; White, S. W.; Roussel, M. F.; Potts, P. R.; Fischer, M.; Rankovic, Z. Phenyl-Glutarimides: Alternative Cereblon Binders for the Design of PROTACs. *Angew. Chem., Int. Ed.* **2021**, *60* (51), 26663−26670.
(33) Xie, S.; Sun, Y.; Liu, Y.; Li, X.; Li, X.; Zhong, W.; Zhan, F.; Zhu, J.; Yao, H.; Yang, D. H.; Chen, Z. S.; Xu, J.; Xu, S. Development of Alectinib-Based PROTACs as Novel Potent Degraders of Anaplastic Lymphoma Kinase (ALK). *J. Med. Chem.* **2021**, *64* (13), 9120−9140.
(34) Siddalingamurthy, E.; Mahadevan, K. M.; Jagadeesh, N. M.; Kumara, M. N. Synthesis Of Novel Γ-Carboline Derivatives And Their In Silico Studies On 5ht1, H1 And Ccr2 Antagonist Receptors. *Int. J. Pharm. Pharm. Sci.* **2014**, *6* (10), 548−554.
(35) Whitehouse, A. J.; Thomas, S. E.; Brown, K. P.; Fanourakis, A.; Chan, D. S.; Libardo, M. D. J.; Mendes, V.; Boshoff, H. I. M.; Floto,

https://doi.org/10.1021/acs.jmedchem.5c00674
J. Med. Chem. 2025, 68, 13793−13821

R. A.; Abell, C.; Blundell, T. L.; Coyne, A. G. Development of Inhibitors against Mycobacterium abscessus tRNA (m(1)G37) Methyltransferase (TrmD) Using Fragment-Based Approaches. *J. Med. Chem.* **2019**, *62* (15), 7210−7232.
(36) Ma, J.; Luo, J.; Jiang, K.; Zhang, G.; Liu, S.; Yin, B. Access to Polycyclic Thienoindolines via Formal [2 + 2+1] Cyclization of Alkynyl Indoles with S(8) and K(2)S. *Org. Lett.* **2021**, *23* (20), 8033−8038.
(37) Spiteri, C.; Moses, J. E. Copper-catalyzed azide-alkyne cycloaddition: regioselective synthesis of 1,4,5-trisubstituted 1,2,3-triazoles. *Angew. Chem., Int. Ed.* **2010**, *49* (1), 31−33.
(38) Zerfas, B. L.; Huerta, F.; Liu, H.; Du, G.; Gray, N. S.; Jones, L. H.; Nowak, R. P. Advancing targeted protein degrader discovery by measuring cereblon engagement in cells. *Methods Enzymol.* **2023**, *681*, 169−188.
(39) Nowak, R. P.; Ragosta, L.; Huerta, F.; Liu, H.; Ficarro, S. B.; Cruite, J. T.; Metivier, R. J.; Donovan, K. A.; Marto, J. A.; Fischer, E. S.; Zerfas, B. L.; Jones, L. H. Development of a covalent cereblon-based PROTAC employing a fluorosulfate warhead. *RSC Chem. Biol.* **2023**, *4* (11), 906−912.
(40) Steinebach, C.; Bricelj, A.; Murgai, A.; Sosič, I.; Bischof, L.; Ng, Y. L. D.; Heim, C.; Maiwald, S.; Proj, M.; Voget, R.; Feller, F.; Košmrlj, J.; Sapozhnikova, V.; Schmidt, A.; Zuleeg, M. R.; Lemnitzer, P.; Mertins, P.; Hansen, F. K.; Gütschow, M.; Krönke, J.; Hartmann, M. D. Leveraging Ligand Affinity and Properties: Discovery of Novel Benzamide-Type Cereblon Binders for the Design of PROTACs. *J. Med. Chem.* **2023**, *66* (21), 14513−14543.
(41) Mackwitz, M. K. W.; Hamacher, A.; Osko, J. D.; Held, J.; Scholer, A.; Christianson, D. W.; Kassack, M. U.; Hansen, F. K. Multicomponent Synthesis and Binding Mode of Imidazo[1,2-a]pyridine-Capped Selective HDAC6 Inhibitors. *Org. Lett.* **2018**, *20* (11), 3255−3258.
(42) Zeyen, P.; Zeyn, Y.; Herp, D.; Mahmoudi, F.; Yesiloglu, T. Z.; Erdmann, F.; Schmidt, M.; Robaa, D.; Romier, C.; Ridinger, J.; Herbst-Gervasoni, C. J.; Christianson, D. W.; Oehme, I.; Jung, M.; Kramer, O. H.; Sippl, W. Identification of histone deacetylase 10 (HDAC10) inhibitors that modulate autophagy in transformed cells. *Eur. J. Med. Chem.* **2022**, *234*, 114272.
(43) Han, X.; Wang, C.; Qin, C.; Xiang, W.; Fernandez-Salas, E.; Yang, C. Y.; Wang, M.; Zhao, L.; Xu, T.; Chinnaswamy, K.; Delproposto, J.; Stuckey, J.; Wang, S. Discovery of ARD-69 as a Highly Potent Proteolysis Targeting Chimera (PROTAC) Degrader of Androgen Receptor (AR) for the Treatment of Prostate Cancer. *J. Med. Chem.* **2019**, *62* (2), 941−964.
(44) Farnaby, W.; Koegl, M.; Roy, M. J.; Whitworth, C.; Diers, E.; Trainor, N.; Zollman, D.; Steurer, S.; Karolyi-Oezguer, J.; Riedmueller, C.; Gmaschitz, T.; Wachter, J.; Dank, C.; Galant, M.; Sharps, B.; Rumpel, K.; Traxler, E.; Gerstberger, T.; Schnitzer, R.; Petermann, O.; Greb, P.; Weinstabl, H.; Bader, G.; Zoephel, A.; Weiss-Puxbaum, A.; Ehrenhöfer-Wölfer, K.; Wöhrle, S.; Boehmelt, G.; Rinnenthal, J.; Arnhof, H.; Wiechens, N.; Wu, M. Y.; Owen-Hughes, T.; Ettmayer, P.; Pearson, M.; McConnell, D. B.; Ciulli, A. BAF complex vulnerabilities in cancer demonstrated via structure-based PROTAC design. *Nat. Chem. Biol.* **2019**, *15* (7), 672−680.
(45) Dong, Y.; Ma, T.; Xu, T.; Feng, Z.; Li, Y.; Song, L.; Yao, X.; Ashby, C. R., Jr.; Hao, G. F. Characteristic roadmap of linker governs the rational design of PROTACs. *Acta Pharm. Sin. B* **2024**, *14* (10), 4266−4295.
(46) Melesina, J.; Simoben, C. V.; Praetorius, L.; Bulbul, E. F.; Robaa, D.; Sippl, W. Strategies To Design Selective Histone Deacetylase Inhibitors. *ChemMedChem* **2021**, *16* (9), 1336−1359.
(47) Sandrone, G.; Cukier, C. D.; Zrubek, K.; Marchini, M.; Vergani, B.; Caprini, G.; Fossati, G.; Steinkühler, C.; Stevenazzi, A. Role of Fluorination in the Histone Deacetylase 6 (HDAC6) Selectivity of Benzohydroxamate-Based Inhibitors. *ACS Med. Chem. Lett.* **2021**, *12* (11), 1810−1817.
(48) Reßing, N.; Schliehe-Diecks, J.; Watson, P. R.; Sönnichsen, M.; Cragin, A. D.; Schöler, A.; Yang, J.; Schäker-Hübner, L.; Borkhardt, A.; Christianson, D. W.; Bhatia, S.; Hansen, F. K. Development of Fluorinated Peptoid-Based Histone Deacetylase (HDAC) Inhibitors for Therapy-Resistant Acute Leukemia. *J. Med. Chem.* **2022**, *65* (22), 15457−15472.
(49) Steimbach, R. R.; Herbst-Gervasoni, C. J.; Lechner, S.; Stewart, T. M.; Klinke, G.; Ridinger, J.; Géraldy, M. N. E.; Tihanyi, G.; Foley, J. R.; Uhrig, U.; Kuster, B.; Poschet, G.; Casero, R. A., Jr.; Medard, G.; Oehme, I.; Christianson, D. W.; Gunkel, N.; Miller, A. K. Aza-SAHA Derivatives Are Selective Histone Deacetylase 10 Chemical Probes That Inhibit Polyamine Deacetylation and Phenocopy HDAC10 Knockout. *J. Am. Chem. Soc.* **2022**, *144* (41), 18861−18875.
(50) Depetter, Y.; Geurs, S.; De Vreese, R.; Goethals, S.; Vandoorn, E.; Laevens, A.; Steenbrugge, J.; Meyer, E.; de Tullio, P.; Bracke, M.; D'Hooghe, M.; De Wever, O. Selective pharmacological inhibitors of HDAC6 reveal biochemical activity but functional tolerance in cancer models. *Int. J. Cancer* **2019**, *145* (3), 735−747.
(51) Li, Y.; Manickam, G.; Ghoshal, A.; Subramaniam, P. More Efficient Palladium Catalyst for Hydrogenolysis of Benzyl Groups. *Synth. Commun.* **2006**, *36* (7), 925−928.
(52) Wang, Y.; Gong, N.; Ma, C.; Zhang, Y.; Tan, H.; Qing, G.; Zhang, J.; Wang, Y.; Wang, J.; Chen, S.; Li, X.; Ni, Q.; Yuan, Y.; Gan, Y.; Chen, J.; Li, F.; Zhang, J.; Ou, C.; Zhao, Y.; Liu, X.; Liang, X. J. An amphiphilic dendrimer as a light-activable immunological adjuvant for in situ cancer vaccination. *Nat. Commun.* **2021**, *12* (1), 4964.
(53) Nutt, M. J.; Yee, Y. S.; Buyan, A.; Andrewartha, N.; Corry, B.; Yeoh, G. C. T.; Stewart, S. G. In pursuit of a selective hepatocellular carcinoma therapeutic agent: Novel thalidomide derivatives with antiproliferative, antimigratory and STAT3 inhibitory properties. *Eur. J. Med. Chem.* **2021**, *217*, 113353.
(54) Kraft, F. B.; Enns, J.; Honin, I.; Engelhardt, J.; Schöler, A.; Smith, S. T.; Meiler, J.; Schäker-Hübner, L.; Weindl, G.; Hansen, F. K. Groebke Blackburn Bienayme-mediated multi-component synthesis of selective HDAC6 inhibitors with anti-inflammatory properties. *Bioorg. Chem.* **2024**, *143*, 107072.
(55) Schäker-Hübner, L.; Warstat, R.; Ahlert, H.; Mishra, P.; Kraft, F. B.; Schliehe-Diecks, J.; Schöler, A.; Borkhardt, A.; Breit, B.; Bhatia, S.; Hügle, M.; Günther, S.; Hansen, F. K. 4-Acyl Pyrrole Capped HDAC Inhibitors: A New Scaffold for Hybrid Inhibitors of BET Proteins and Histone Deacetylases as Antileukemia Drug Leads. *J. Med. Chem.* **2021**, *64* (19), 14620−14646.
(56) Kraft, F. B.; Hanl, M.; Feller, F.; Schäker-Hübner, L.; Hansen, F. K. Photocaged Histone Deacetylase Inhibitors as Prodrugs in Targeted Cancer Therapy. *Pharmaceuticals* **2023**, *16* (3), 356.
(57) Steinebach, C.; Ng, Y. L. D.; Sosič, I.; Lee, C. S.; Chen, S.; Lindner, S.; Vu, L. P.; Bricelj, A.; Haschemi, R.; Monschke, M.; Steinwarz, E.; Wagner, K. G.; Bendas, G.; Luo, J.; Gütschow, M.; Krönke, J. Systematic exploration of different E3 ubiquitin ligases: an approach towards potent and selective CDK6 degraders. *Chem. Sci.* **2020**, *11* (13), 3474−3486.
(58) Daina, A.; Michielin, O.; Zoete, V. SwissADME: a free web tool to evaluate pharmacokinetics, drug-likeness and medicinal chemistry friendliness of small molecules. *Sci. Rep.* **2017**, *7*, 42717.
(59) Schäker-Hübner, L.; Haschemi, R.; Büch, T.; Kraft, F. B.; Brumme, B.; Schöler, A.; Jenke, R.; Meiler, J.; Aigner, A.; Bendas, G.; Hansen, F. K. Balancing Histone Deacetylase (HDAC) Inhibition and Drug-likeness: Biological and Physicochemical Evaluation of Class I Selective HDAC Inhibitors. *ChemMedChem* **2022**, *17* (9), No. e202100755.
(60) Sinatra, L.; Vogelmann, A.; Friedrich, F.; Tararina, M. A.; Neuwirt, E.; Colcerasa, A.; König, P.; Toy, L.; Yesiloglu, T. Z.; Hilscher, S.; Gaitzsch, L.; Papenkordt, N.; Zhai, S.; Zhang, L.; Romier, C.; Einsle, O.; Sippl, W.; Schutkowski, M.; Gross, O.; Bendas, G.; Christianson, D. W.; Hansen, F. K.; Jung, M.; Schiedel, M. Development of First-in-Class Dual Sirt2/HDAC6 Inhibitors as Molecular Tools for Dual Inhibition of Tubulin Deacetylation. *J. Med. Chem.* **2023**, *66* (21), 14787−14814.
(61) Feller, F.; Hansen, F. K. Targeted Protein Degradation of Histone Deacetylases by Hydrophobically Tagged Inhibitors. *ACS Med. Chem. Lett.* **2023**, *14* (12), 1863−1868.

(62) Donovan, K. A.; An, J.; Nowak, R. P.; Yuan, J. C.; Fink, E. C.; Berry, B. C.; Ebert, B. L.; Fischer, E. S. Thalidomide promotes degradation of SALL4, a transcription factor implicated in Duane Radial Ray syndrome. *Elife* **2018**, *7*, No. e38430.
(63) Skowronek, P.; Thielert, M.; Voytik, E.; Tanzer, M. C.; Hansen, F. M.; Willems, S.; Karayel, O.; Brunner, A.-D.; Meier, F.; Mann, M. Rapid and in-depth coverage of the (phospho-) proteome with deep libraries and optimal window design for dia-PASEF. *bioRxiv* **2022**, 2022.05.31.494163.
(64) Demichev, V.; Messner, C. B.; Vernardis, S. I.; Lilley, K. S.; Ralser, M. DIA-NN: neural networks and interference correction enable deep proteome coverage in high throughput. *Nat. Methods* **2020**, *17* (1), 41−44.
(65) Ritchie, M. E.; Phipson, B.; Wu, D.; Hu, Y.; Law, C. W.; Shi, W.; Smyth, G. K. limma powers differential expression analyses for RNA-sequencing and microarray studies. *Nucleic Acids Res.* **2015**, *43* (7), No. e47.

https://doi.org/10.1021/acs.jmedchem.5c00674
J. Med. Chem. 2025, 68, 13793−13821

Supplementary Information

Development and characterization of the first selective class IIb histone deacetylase degraders

Shiyang Zhai,[a] Irina Honin,[a] Linda Schäker-Hübner,[a] Maria Hanl,[a] Lukas Jacobi,[b] Finn Dressler[c] Dominika Ewa Pieńkowska,[d] Philipp König,[a] Jan Gerhartz,[d] Rabea Voget,[e] Gerd Bendas,[a] Michael Gütschow,[e] Felix Meissner,[b] Bjoern B. Burckhardt,[c] Radosław P. Nowak,[d] Christian Steinebach,[e] Finn K. Hansen[a]*

[a]Department of Pharmaceutical and Cell Biological Chemistry, Pharmaceutical Institute, University of Bonn, 53121 Bonn, Germany.

[b]Institute of Innate Immunity, Department of Systems Immunology and Proteomics, Medical Faculty, University of Bonn, 53127 Bonn, Germany.

[c]Individualized Pharmacotherapy, Institute of Pharmaceutical and Medicinal Chemistry, University of Münster, 48149 Münster, Germany

[d]Institute of Structural Biology, Medical Faculty, University of Bonn, 53127 Bonn, Germany.

[e]Department of Pharmaceutical and Medicinal Chemistry, Pharmaceutical Institute, University of Bonn, 53121 Bonn, Germany.

Table of contents

1. Supplementary Figures and Table S3

2. Synthesis of **AP7-AP10** and the non-degrading control **AP1-N** S8

3. ^{1}H, ^{13}C NMR, HR-MS and HPLC data of **AP1-AP10**, **AP1-N** S10

4. Immunoblot replicates S33

5. Reference S35

1. Supplementary Figures and Table

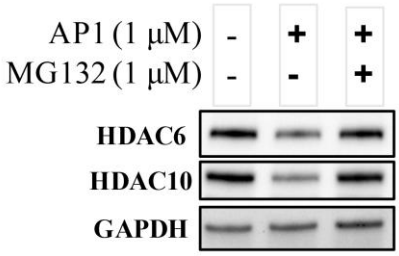

Figure S1. Rescue experiments with the proteasome inhibitor MG132. MCF-7 cells were treated with DMSO or **AP1** (1 μM) for 12 h. Pretreatments of MCF-7 cells for 1 h with MG132 (1 μM) were carried out in the co-treatment group, followed by **AP1** (1 μM) treatment for 12 h. HDAC6 and HDAC10 levels were detected by western blot. GAPDH was chosen as loading control. Representative image of n = 3 replicates.

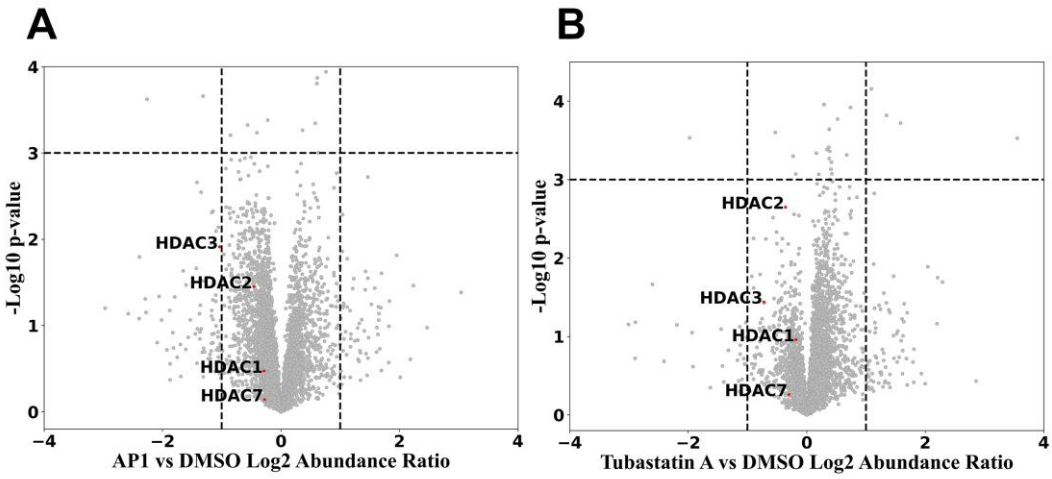

Figure S2. Quantitative proteomics of MM.1S cell lysates after treatment with 1 μM of **AP1** (A) or tubastatin A (B) for 6 hours. Hits are identified with the thresholds: Fold change > 2 and P value < 0.001. Detected HDAC subtypes are labelled in red dots.

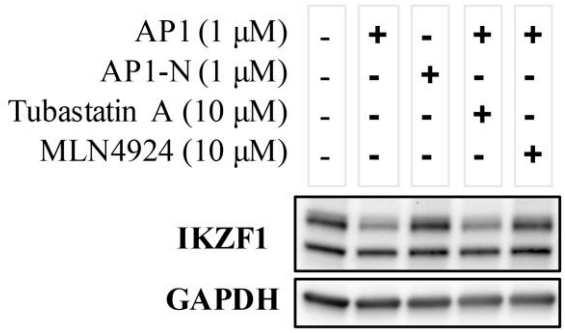

Figure S3. Rescue experiment for IKZF1 in MM.1S cells. MM.1S cells were treated with DMSO or **AP1** (1 μM) for 6 h. Pretreatments of MM.1S cells for 0.5 h with MLN4924 or tubastatin A (10 μM) were carried out in the co-treatment groups, followed by **AP1** (1 μM) treatment for 6 h. IKZF1 levels were detected by western blot. GAPDH was chosen as loading control. Representative image of n = 2 biologically independent experiments.

Table S1. Antiproliferative activity of **AP1-AP6** against MM.1S and MCF-7 cells.[a]

Cmpd.	IC_{50} (μM)	
	MM.1S	MCF-7
AP1	n.e.	n.e.
AP2	n.e.	n.e.
AP3	n.e.	n.e.
AP4	n.e.	n.e.
AP5	n.e.	n.e.
AP6	n.e.	n.e.
Tubastatin A	n.e.	n.e.
Vorinostat	0.64 ± 0.09	2.50 ± 0.33[b]

[a]mean ± SD of n = 3 independent experiments; n.e.: no effect (< 50% viability reduction at 25 μM); n.d.: not determined; [b]data taken from ref.[2] .

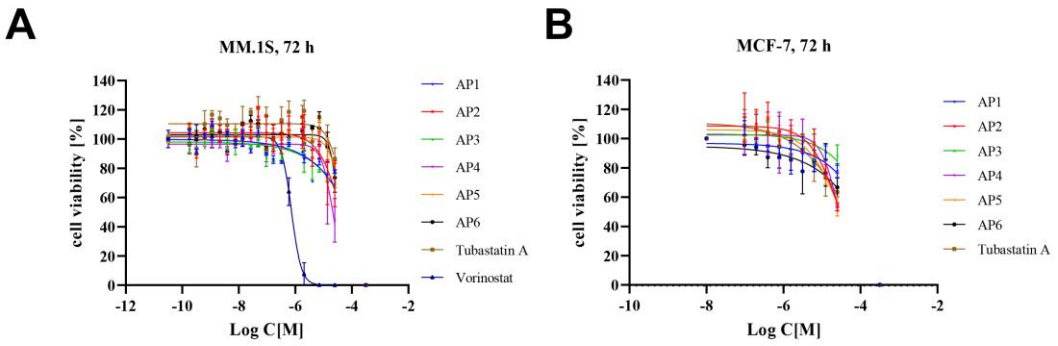

Figure S4. (A, B) Viability assay on MM.1S and MCF-7 cells. (A) CellTiterGlo® 2.0 assay on MM.1S cells. Tubastatin A and vorinostat were taken as positive control; (B) MTT assay on MCF-7 cells. Tubastatin A was taken as positive control. Data are represented from n = 3 independent experiments.

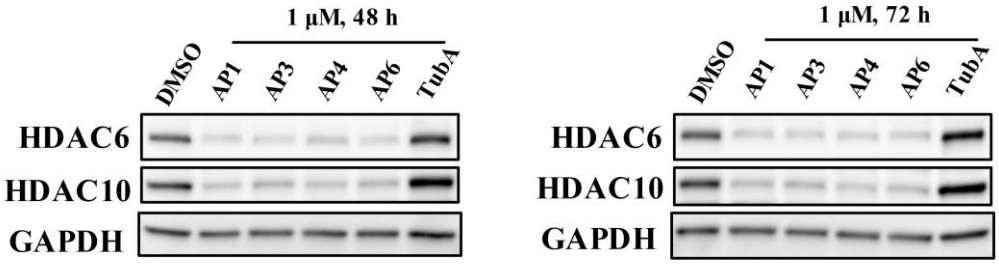

Figure S5. Long-term degradation of HDAC6 and HDAC10 caused by degraders **AP1**, **AP3**, **AP4**, and **AP6**. MM.1S cells were treated with DMSO, **AP1**, **AP3**, **AP4**, **AP6**, and tubastatin A at concentrations of 1 µM for 48 h and 72 h, respectively. HDAC6 and HDAC10 levels were detected by western blot. GAPDH was used as the loading control. Representative images from n = 2 replicates.

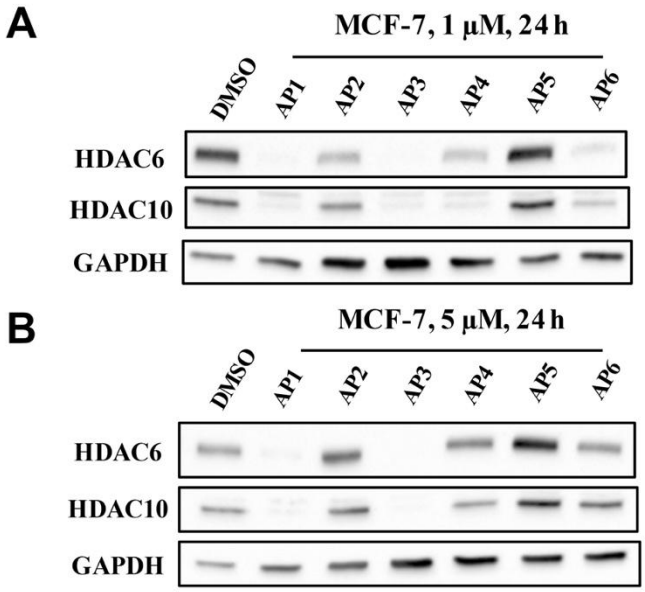

Figure S6. (A, B) Degradation of HDAC6 and HDAC10 mediated by degraders **AP1-AP6** at different concentrations in MCF-7 cells. MCF-7 cells were treated with **AP1-AP6** at concentrations of 1 µM (A) and 5 µM (B) for 24 h. HDAC6 and HDAC10 levels were detected by western blot. GAPDH was used as loading control. Representative images from a total of n = 3 replicates.

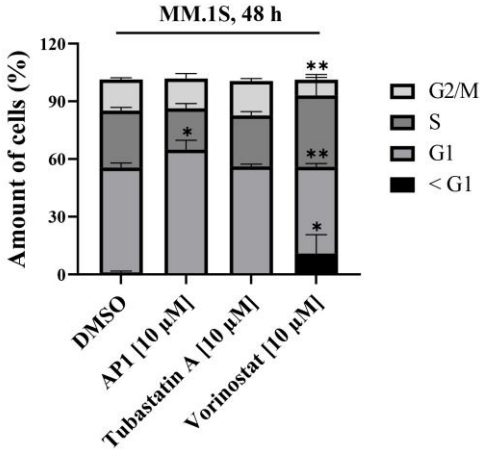

Figure S7. Cell cycle regulation of MM.1S cells treated for 48 h with either vehicle (DMSO), **AP1**, tubastatin A, or vorinostat at the indicated concentrations. The histogram shows the means ± SD of the percentages of cells in the respective phase of the cell cycle. The data were collected in n = 3 biologically

independent replicates, each measured as technical triplicate. Statistics were performed by One-way ANOVA following Dunnett's test with DMSO treated cells as control. *$p < 0.05$; **$p < 0.01$.

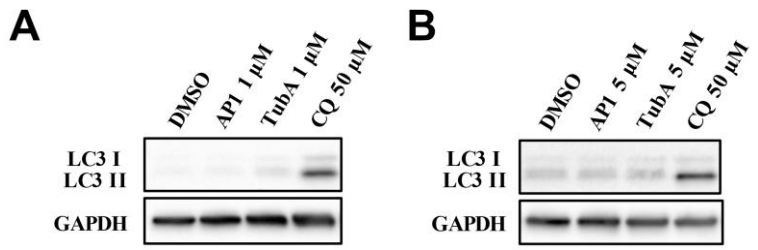

Figure S8. Autophagy effect of **AP1** and tubastatin A at indicated concentrations. MM.1S cells were treated with **AP1** and tubastatin A at 1 µM (A) or 5 µM (B) for 24 h. Chloroquine was used a positive control at 50 µM. LC3 I/II levels were detected by western blot. DMSO served as vehicle control and GAPDH was chosen as loading control. Representative image of n = 2 replicates.

2. Synthesis of AP7-AP10 and the non-degrading control AP1-N

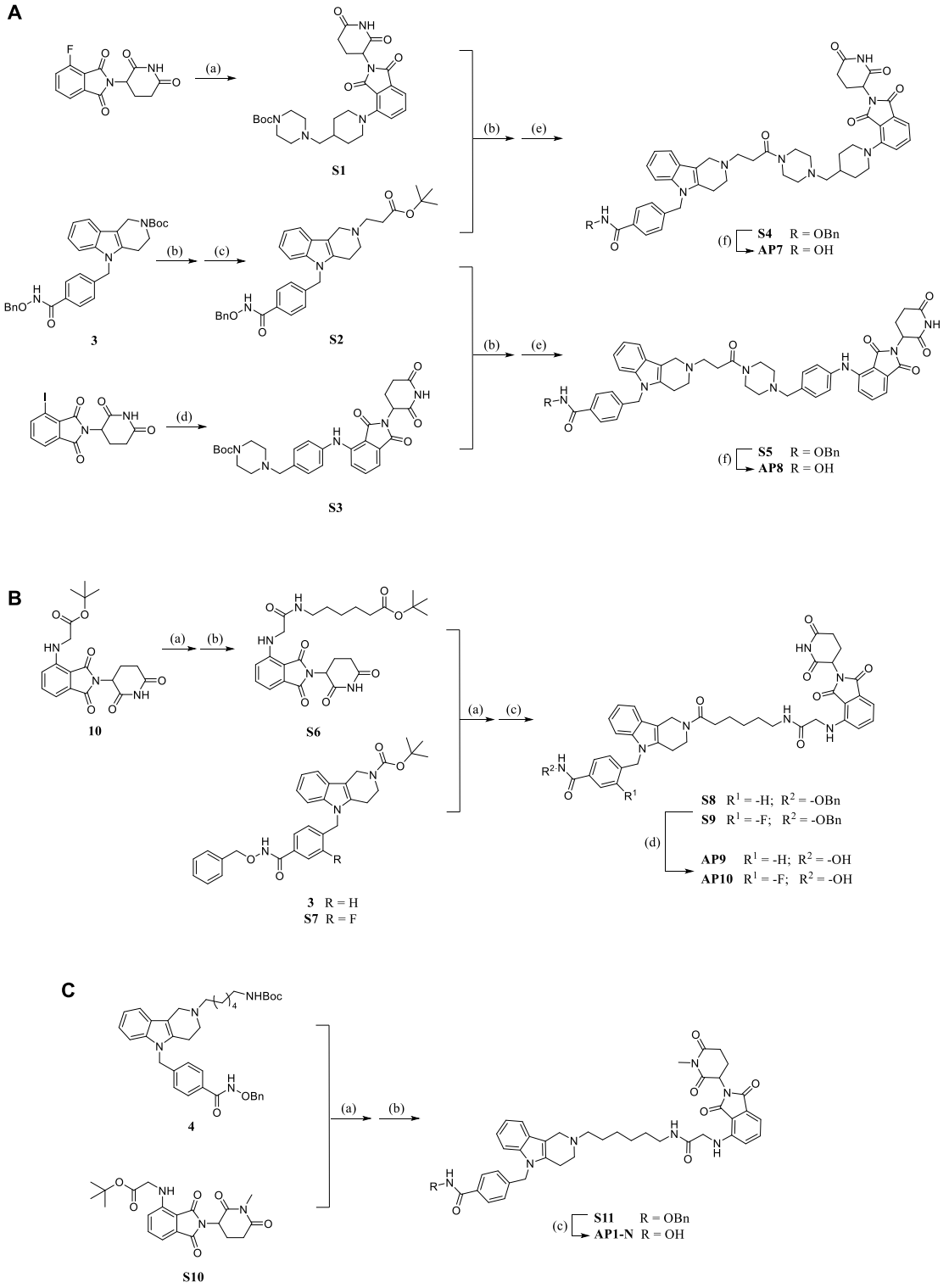

Scheme S1. Synthesis of **AP7-AP10**, as well as non-degrading control **AP1-N**. **A**: (a) *tert*-butyl 4-(piperidin-4-ylmethyl)piperazine-1-carboxylate, DIPEA, anhydrous DMSO, 100 °C, 17.5 h, 87%; (b)

TFA, DCM, rt, 2 h; (c) *tert*-butyl 3-bromopropanoate, K_2CO_3, anhydrous DMF, 60 °C, 24 h, two-step yield, 48%; (d) *tert*-butyl 4-(4-aminobenzyl)piperazine-1-carboxylate, dioxane:water (10:1), X-Phos, K_2CO_3, $Pd_2(dba)_3$, argon, 90 °C, 18 h, 48%; (e) HATU, DIPEA, anhydrous DMF, rt, 16 h, 25% (**S4**), 35% (**S5**); (f) H_2, Pd/C, DCM/MeOH, rt, 16 h, 25% (**AP7**), 16% (**AP8**). **B**: (a) TFA, DCM, rt, 2 h; (b) *tert*-butyl 6-aminohexanoate, PyCloP, DIPEA, anhydrous DMF, rt, 17 h, 85%; (c) HATU, DIPEA, anhydrous DMF, 0 °C to rt, 18 h, two-step yield, 82% (**S8**), 42% (**S9**); (d) H_2, Pd/C, DCM/MeOH, rt, 16 h, 40% (**AP9**), 44% (**AP10**). **C**: (a) TFA, DCM, rt, 2 h; (b) HATU, DIPEA, anhydrous DMF, rt, overnight, two step yield, 52%; (c) H_2, Pd/C, EtOH/MeOH, rt, 25%.

3. ^{1}H, ^{13}C NMR, HR-MS and HPLC data of AP1-AP10, AP1-N

^{1}H NMR spectrum of **AP1** (600 MHz, DMSO-d_6)

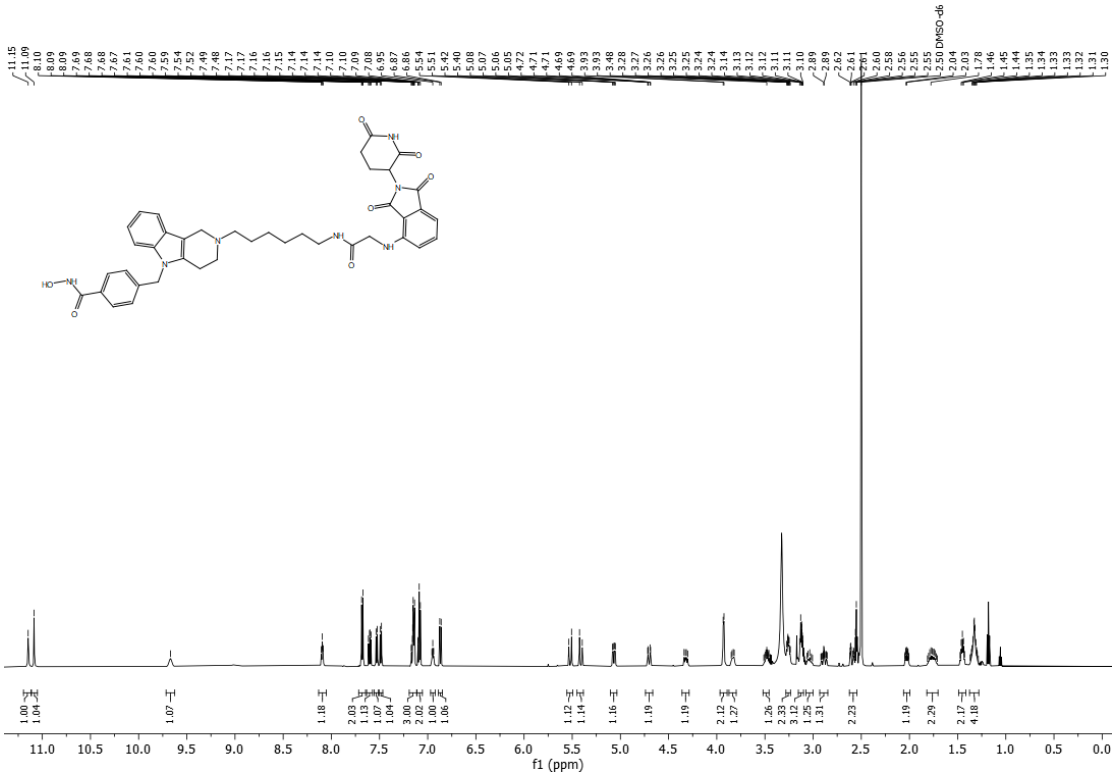

^{13}C NMR spectrum of **AP1** (151 MHz, DMSO-d_6)

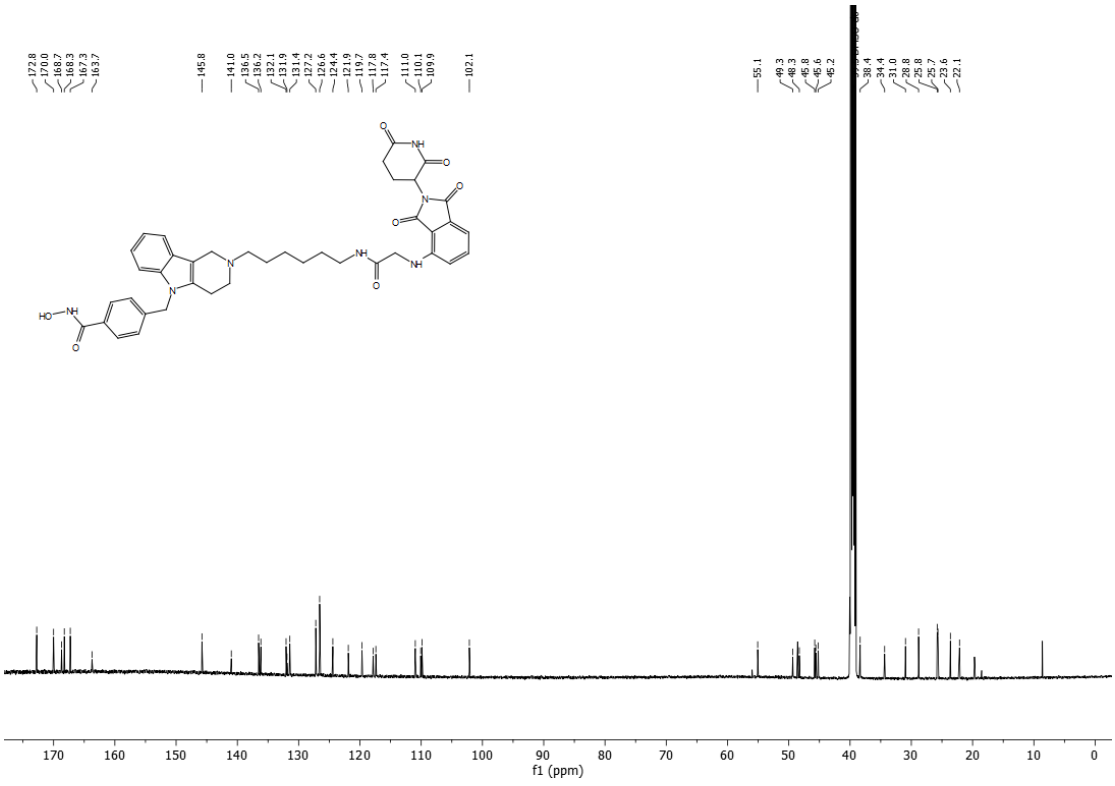

HR-MS spectrum of **AP1**

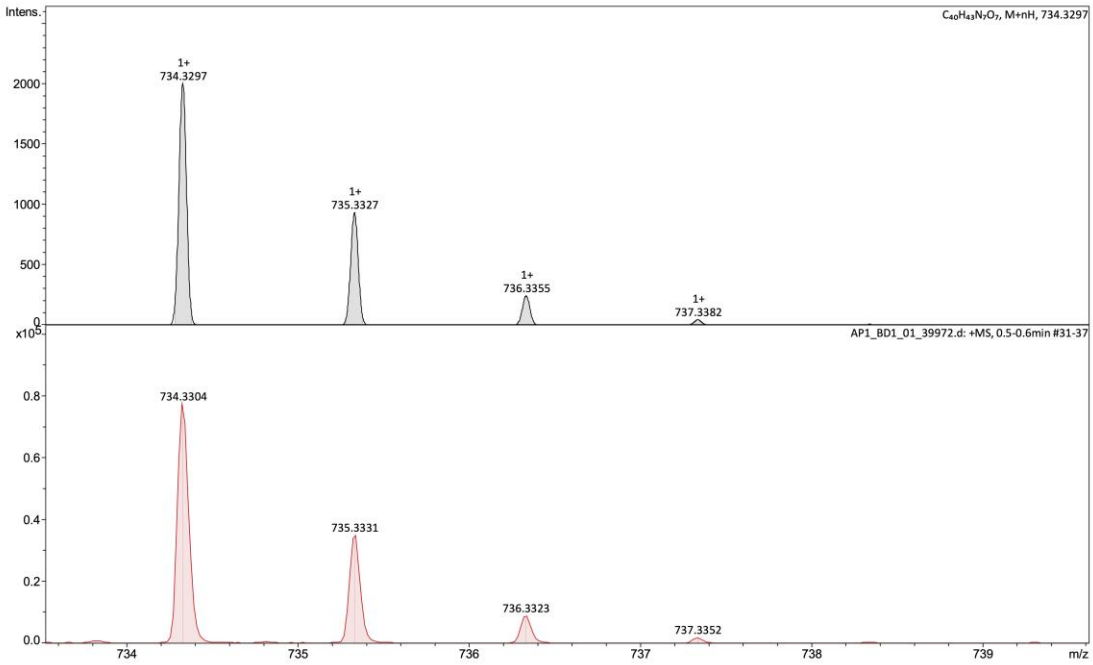

HPLC chromatogram of **AP1** (Purity: 98.1%)

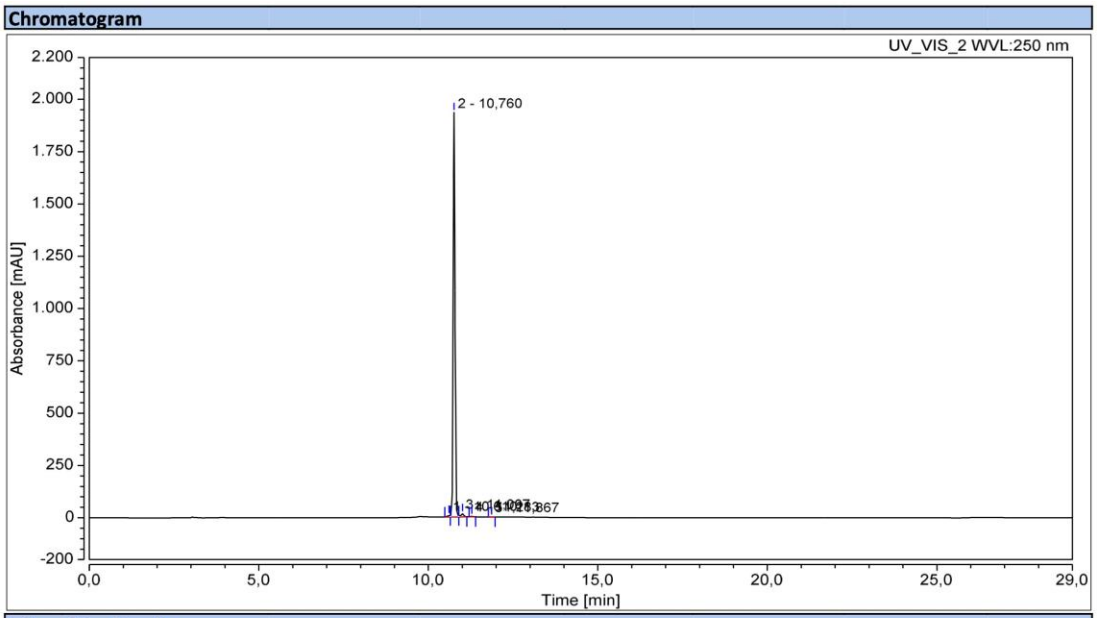

Integration Results

No.	Peak Name	Retention Time min	Area mAU*min	Height mAU	Relative Area %	Relative Height %	Amount n.a.
1		10,610	0,623	6,495	0,51	0,33	n.a.
2		10,760	118,778	1932,348	98,07	98,74	n.a.
3		11,007	1,500	14,838	1,24	0,76	n.a.
4		11,283	0,153	2,698	0,13	0,14	n.a.
5		11,867	0,061	0,643	0,05	0,03	n.a.
Total:			**121,114**	**1957,022**	**100,00**	**100,00**	

^{1}H NMR spectrum of **AP2** (600 MHz, DMSO-d_6)

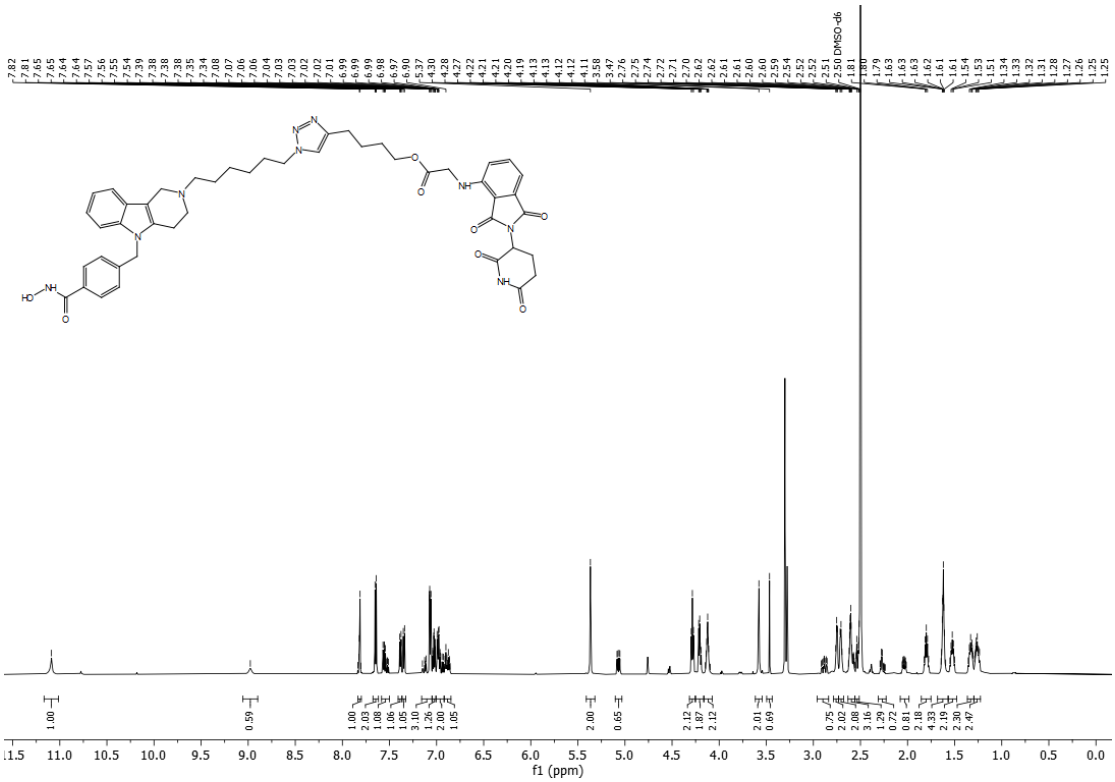

^{13}C NMR spectrum of **AP2** (151 MHz, DMSO-d_6)

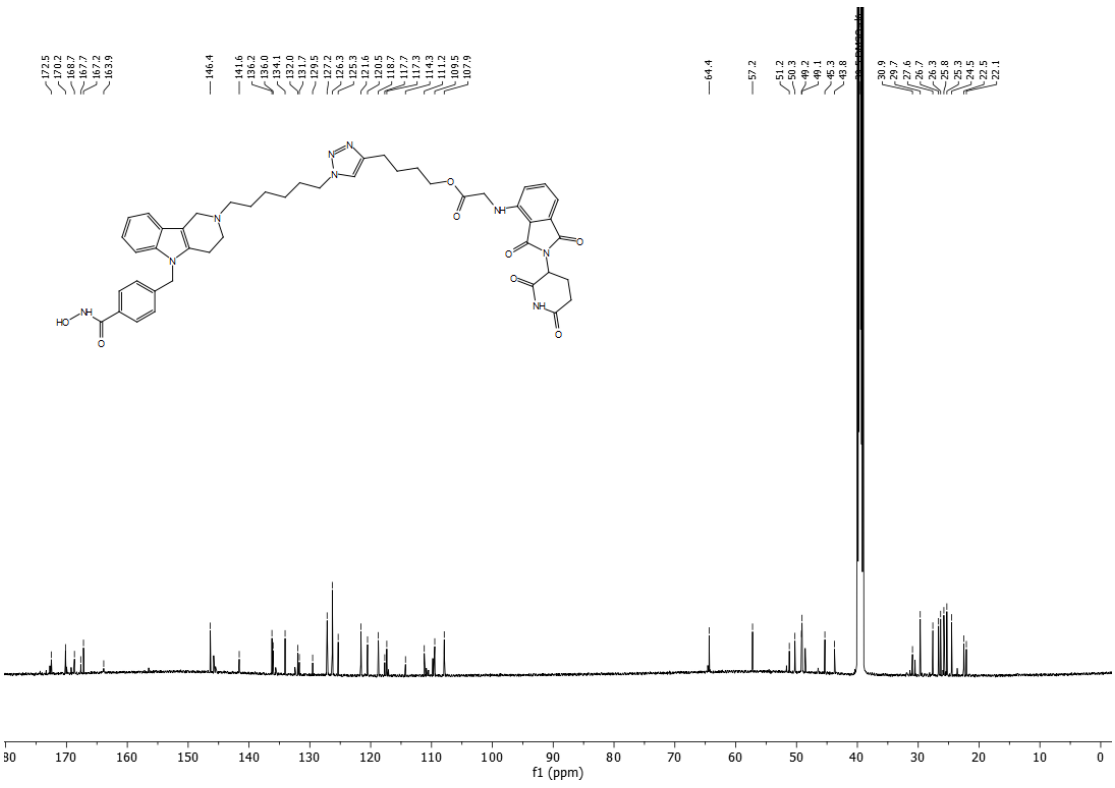

HR-MS spectrum of **AP2**

240523_P-575-FH_P031 #4-16 RT: 0.05-0.22 AV: 13 NL: 6.97E6
T: FTMS + p ESI Full ms [250.00-1000.00]

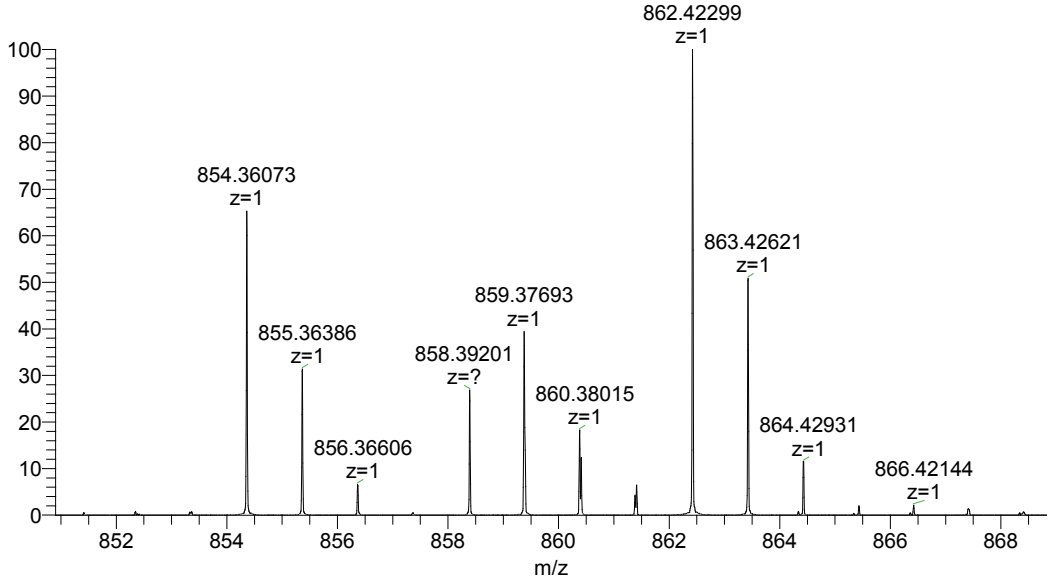

HPLC chromatogram of **AP2** (Purity: 95.4%)

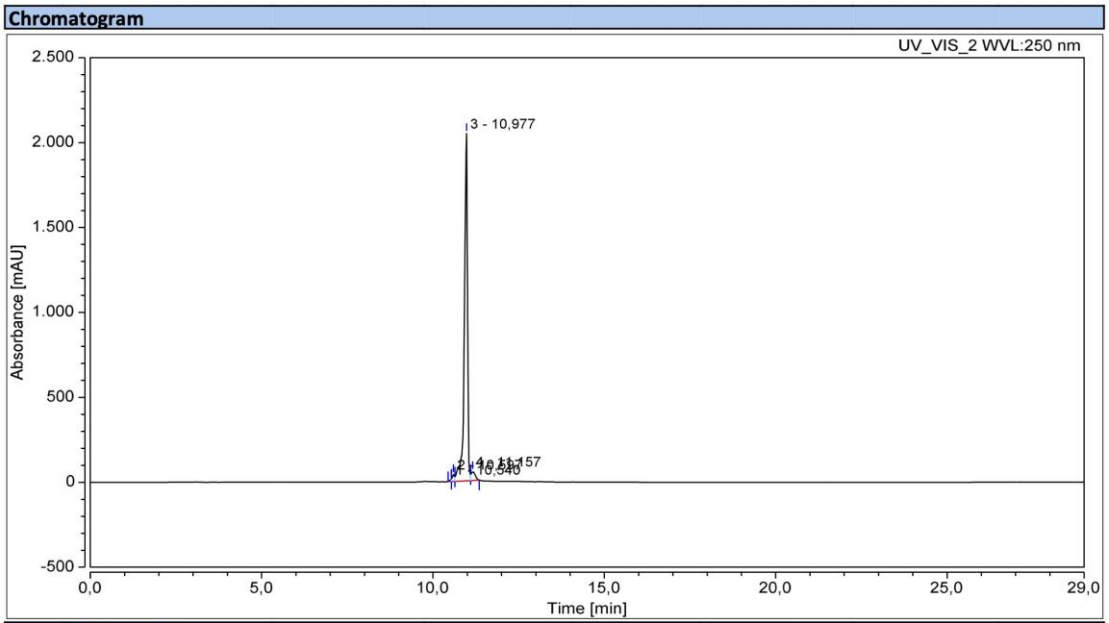

Integration Results

No.	Peak Name	Retention Time min	Area mAU*min	Height mAU	Relative Area %	Relative Height %	Amount n.a.
1		10,540	0,674	11,712	0,30	0,55	n.a.
2		10,597	2,825	39,832	1,25	1,85	n.a.
3		10,977	215,612	2043,851	95,40	95,14	n.a.
4		11,157	6,905	52,855	3,06	2,46	n.a.
Total:			**226,016**	**2148,250**	**100,00**	**100,00**	

^{1}H NMR spectrum of **AP3** (600 MHz, DMSO-d_6)

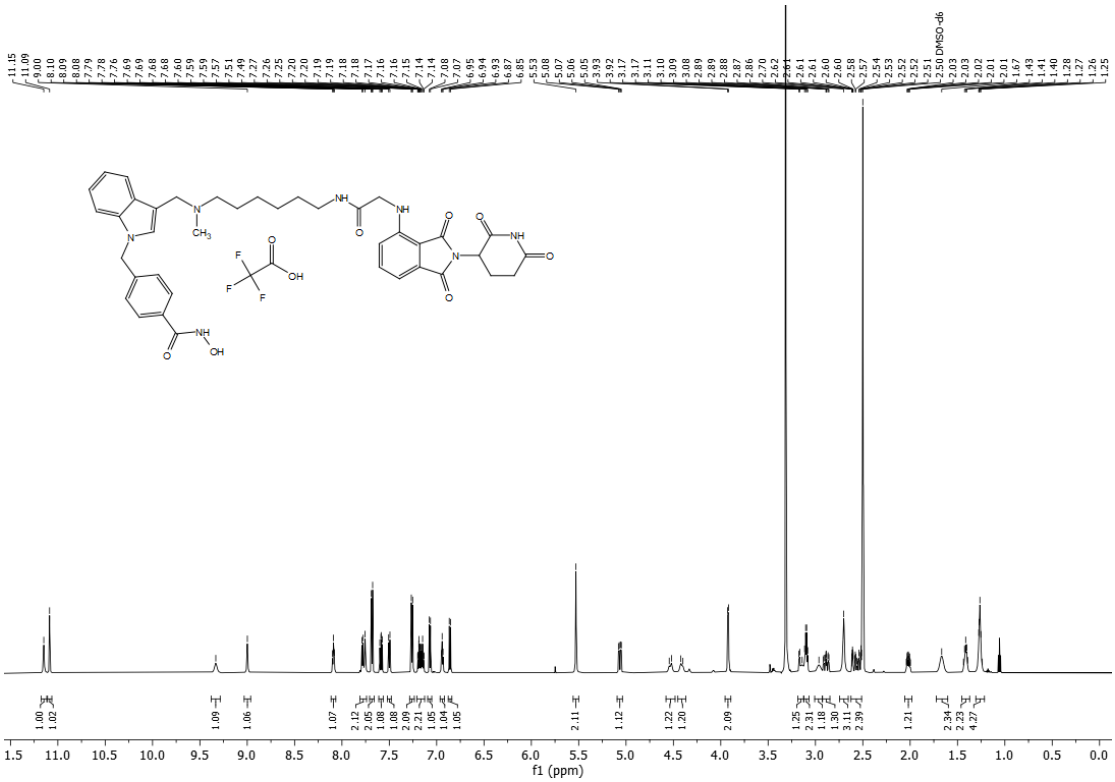

^{13}C NMR spectrum of **AP3** (151 MHz, DMSO-d_6)

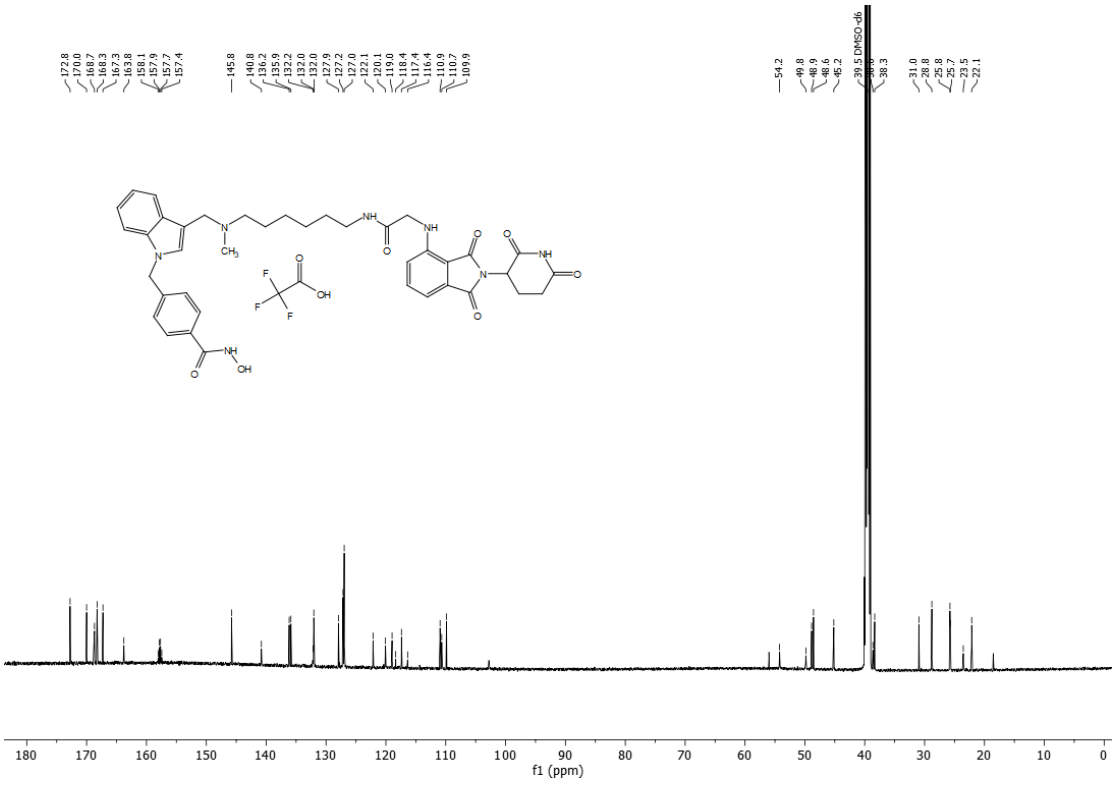

HR-MS spectrum of **AP3**

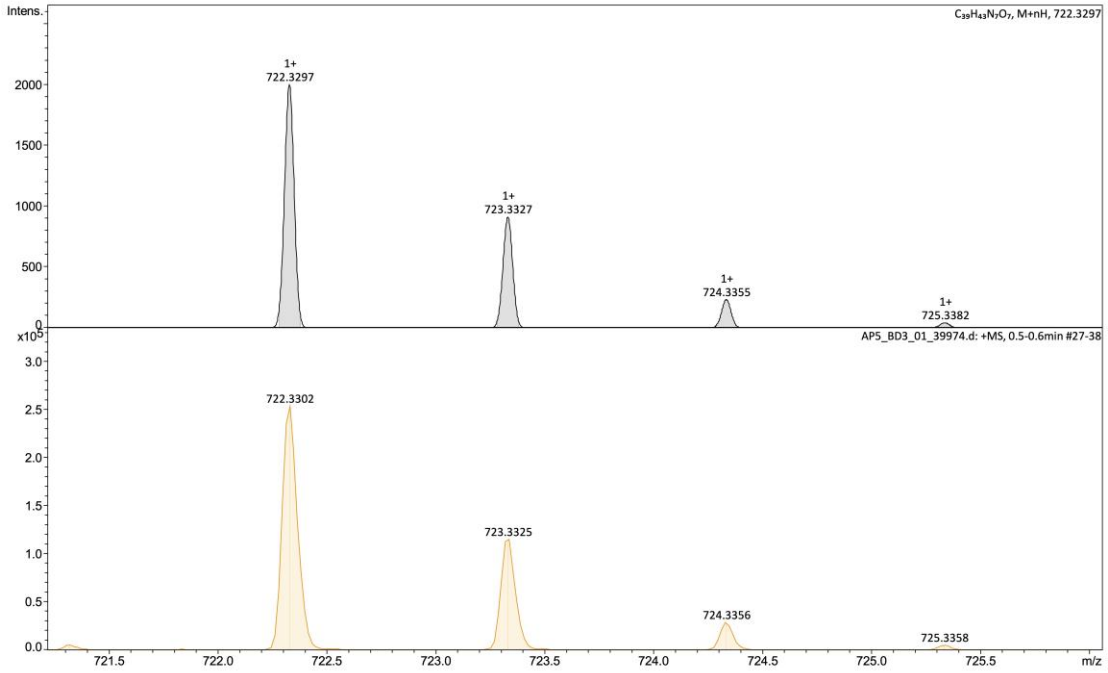

HPLC chromatograms of **AP3** (Purity: 98.1%)

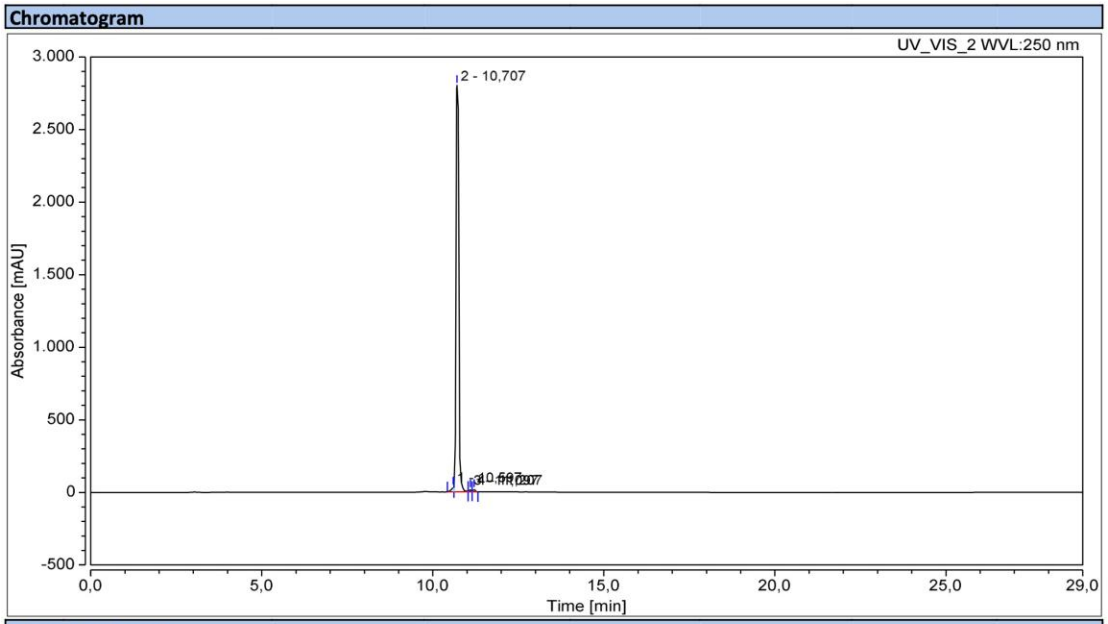

Integration Results

No.	Peak Name	Retention Time min	Area mAU*min	Height mAU	Relative Area %	Relative Height %	Amount n.a.
1		10,597	2,737	33,722	1,05	1,18	n.a.
2		10,707	256,219	2801,090	98,13	97,78	n.a.
3		11,097	0,991	13,746	0,38	0,48	n.a.
4		11,207	1,150	16,110	0,44	0,56	n.a.
Total:			**261,097**	**2864,668**	**100,00**	**100,00**	

^{1}H NMR spectrum of **AP4** (600 MHz, DMSO-d_6)

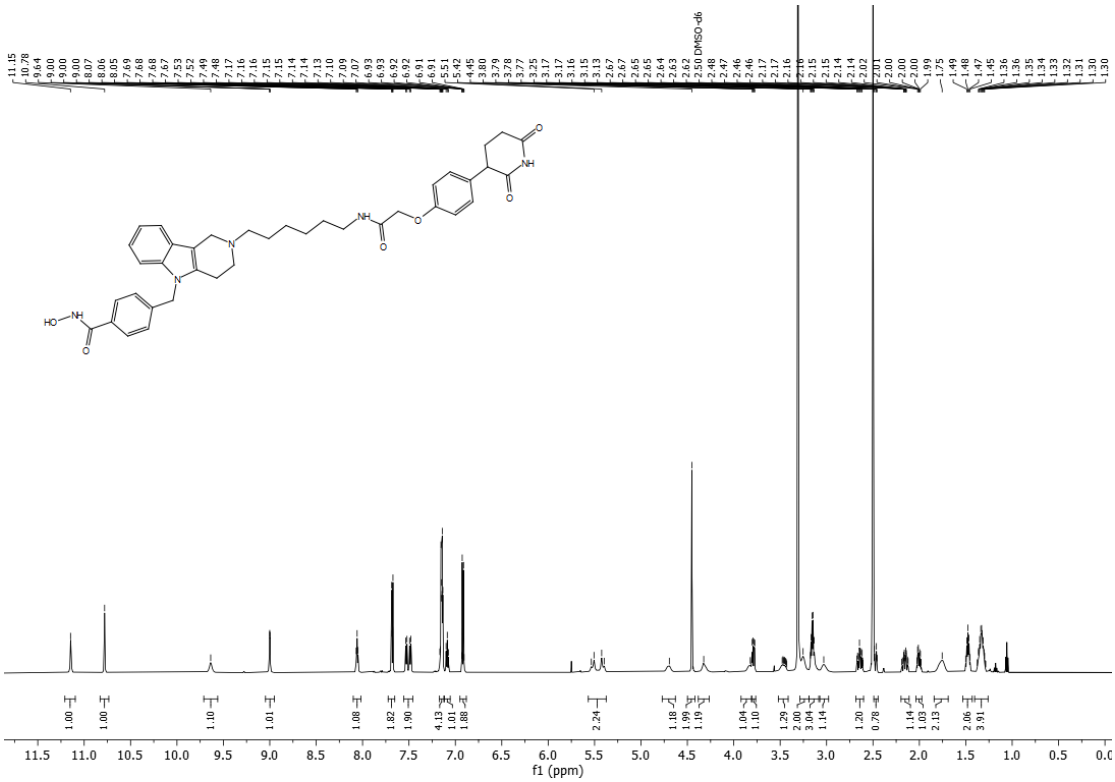

^{13}C NMR spectrum of **AP4** (151 MHz, DMSO-d_6)

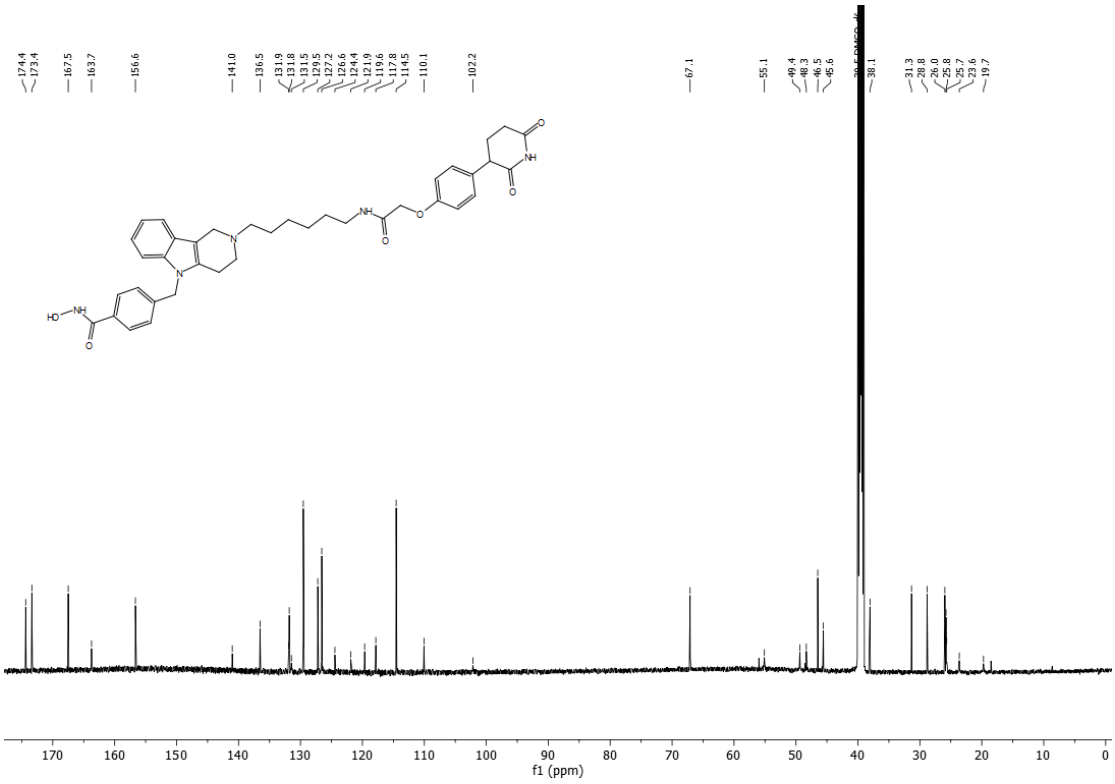

HR-MS spectrum of **AP4**

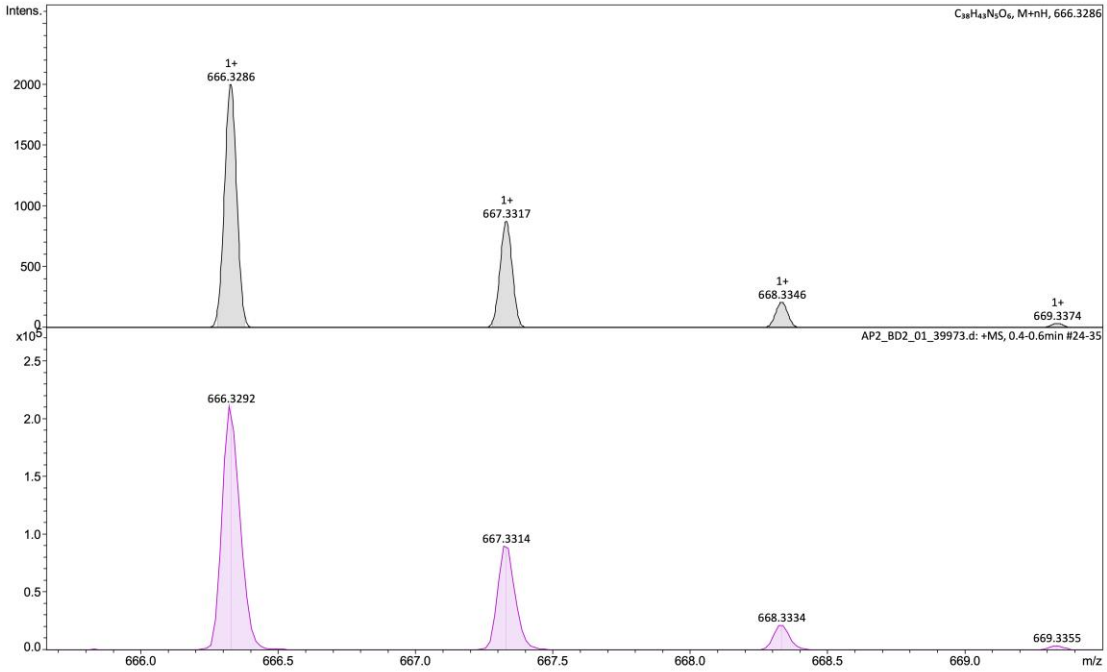

HPLC chromatograms of **AP4** (Purity: 98.9%)

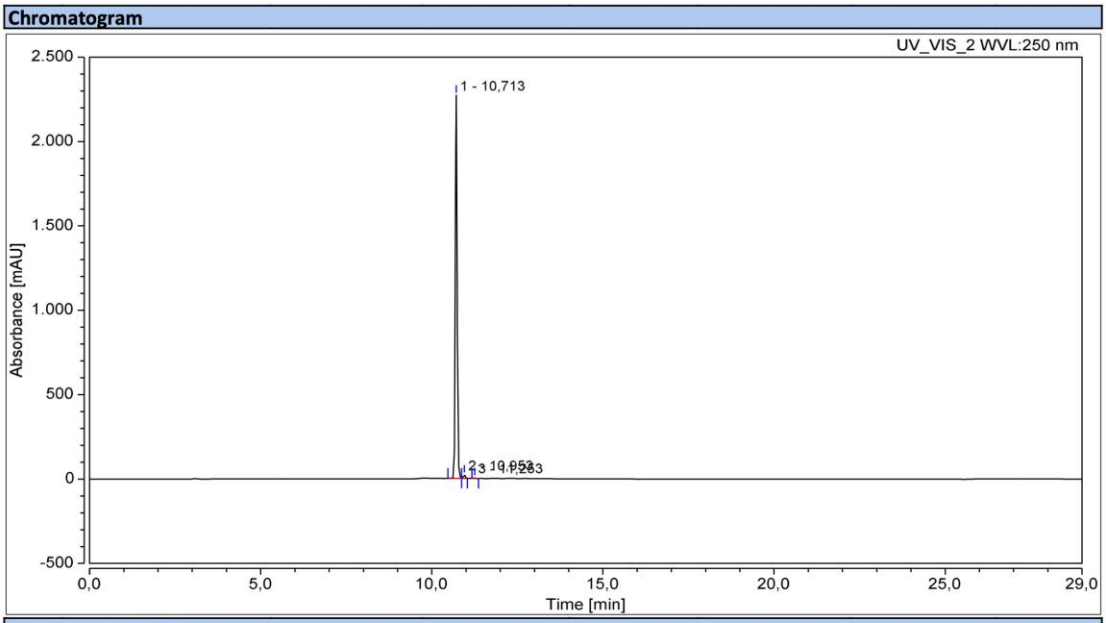

Integration Results

No.	Peak Name	Retention Time min	Area mAU*min	Height mAU	Relative Area %	Relative Height %	Amount n.a.
1		10,713	143,563	2270,069	98,89	98,98	n.a.
2		10,953	1,373	20,275	0,95	0,88	n.a.
3		11,253	0,232	3,045	0,16	0,13	n.a.
Total:			**145,168**	**2293,389**	**100,00**	**100,00**	

^{1}H NMR spectrum of **AP5** (600 MHz, DMSO-d_6)

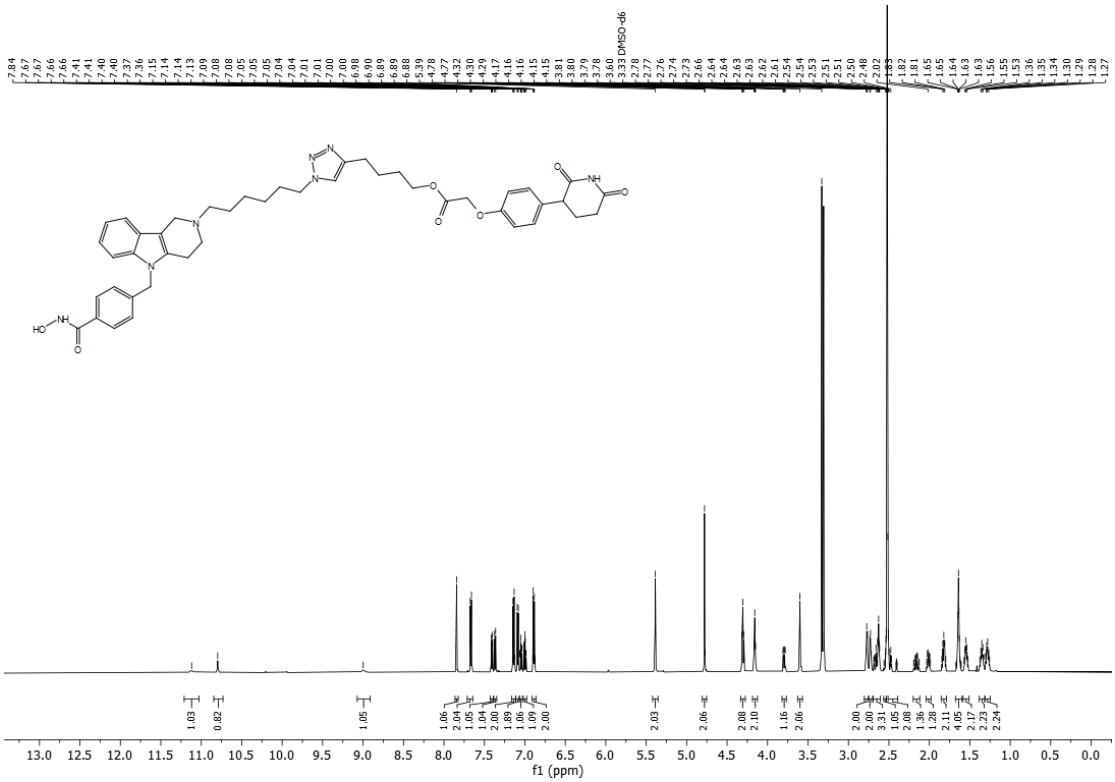

^{13}C NMR spectrum of **AP5** (151 MHz, DMSO-d_6)

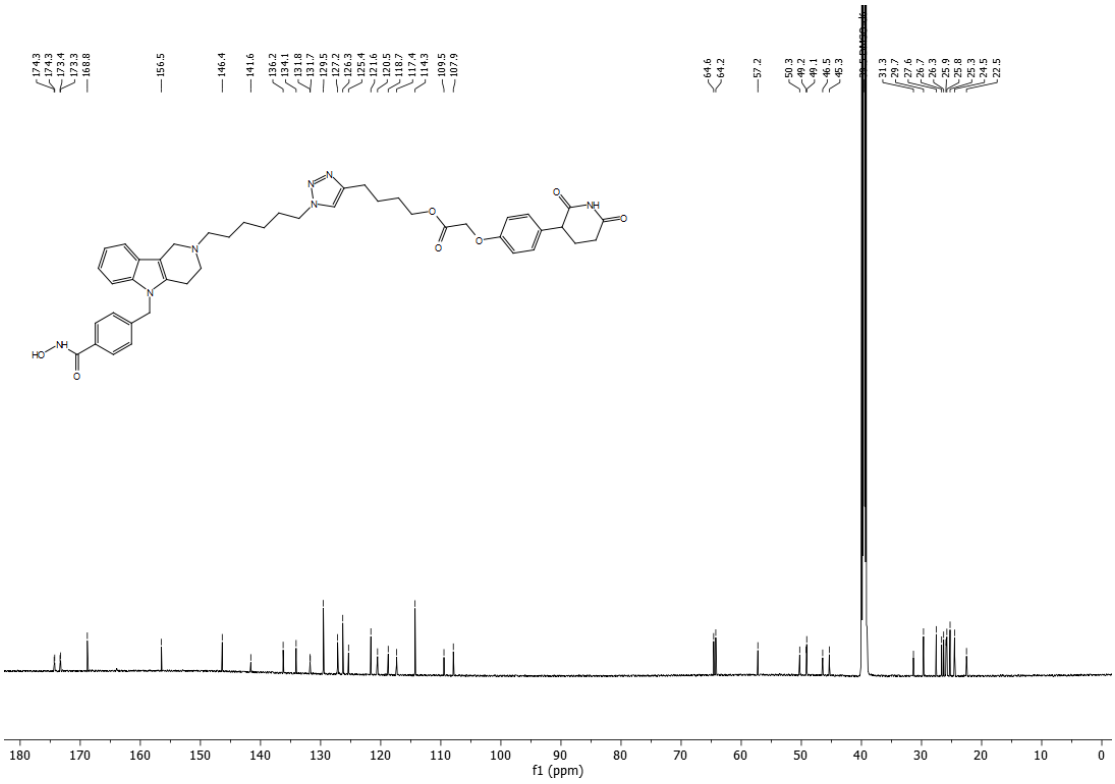

HR-MS spectrum of **AP5**

240523_P-575-FH_P032 #3-16 RT: 0.04-0.22 AV: 14 NL: 2.51E7
T: FTMS + p ESI Full ms [250.00-1000.00]

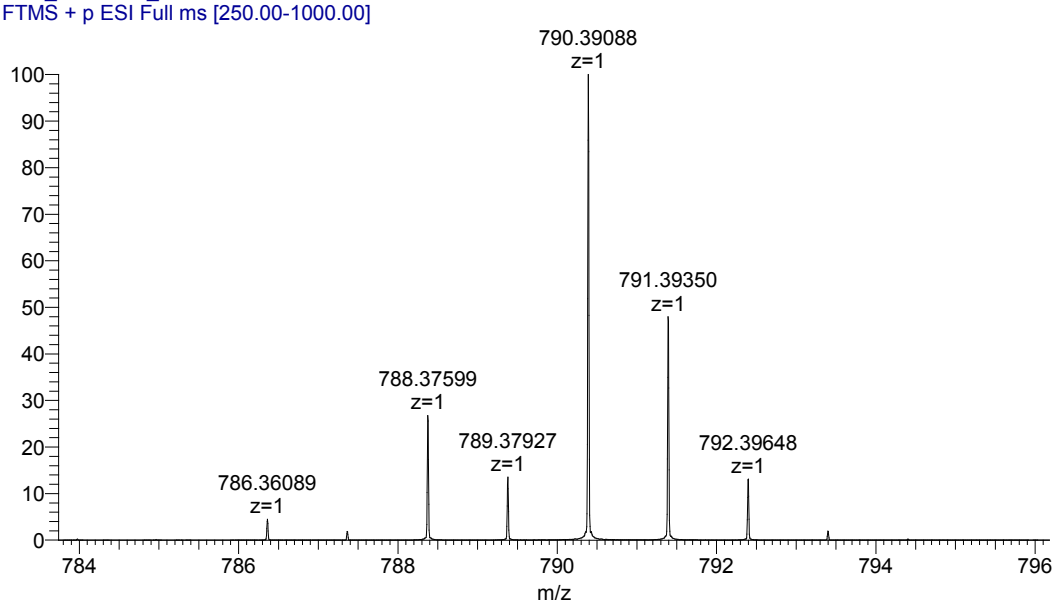

HPLC chromatograms of **AP5** (Purity: 98.0%)

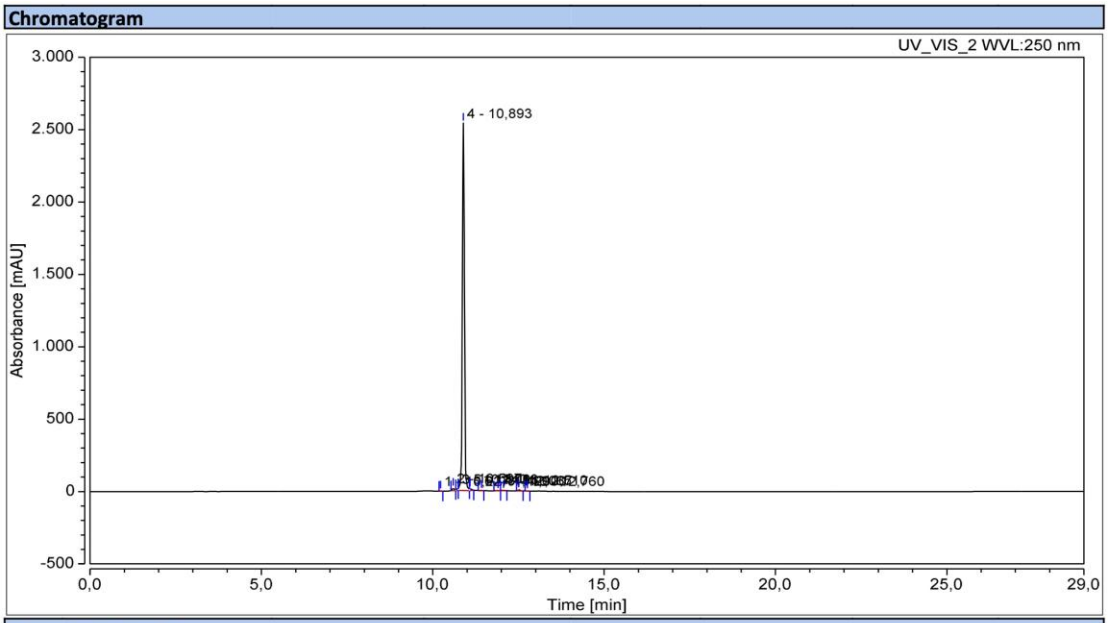

Integration Results

No.	Peak Name	Retention Time min	Area mAU*min	Height mAU	Relative Area %	Relative Height %	Amount n.a.
1		10,227	0,077	1,457	0,04	0,06	n.a.
2		10,597	1,182	17,087	0,64	0,66	n.a.
3		10,740	0,627	10,899	0,34	0,42	n.a.
4		10,893	181,834	2538,158	97,95	97,89	n.a.
5		11,083	0,840	11,344	0,45	0,44	n.a.
6		11,420	0,085	1,271	0,05	0,05	n.a.
7		11,900	0,109	1,070	0,06	0,04	n.a.
8		12,067	0,229	2,376	0,12	0,09	n.a.
9		12,510	0,536	7,382	0,29	0,28	n.a.
10		12,760	0,118	1,941	0,06	0,07	n.a.
Total:			**185,637**	**2592,986**	**100,00**	**100,00**	

^{1}H NMR spectrum of **AP6** (600 MHz, DMSO-d_6)

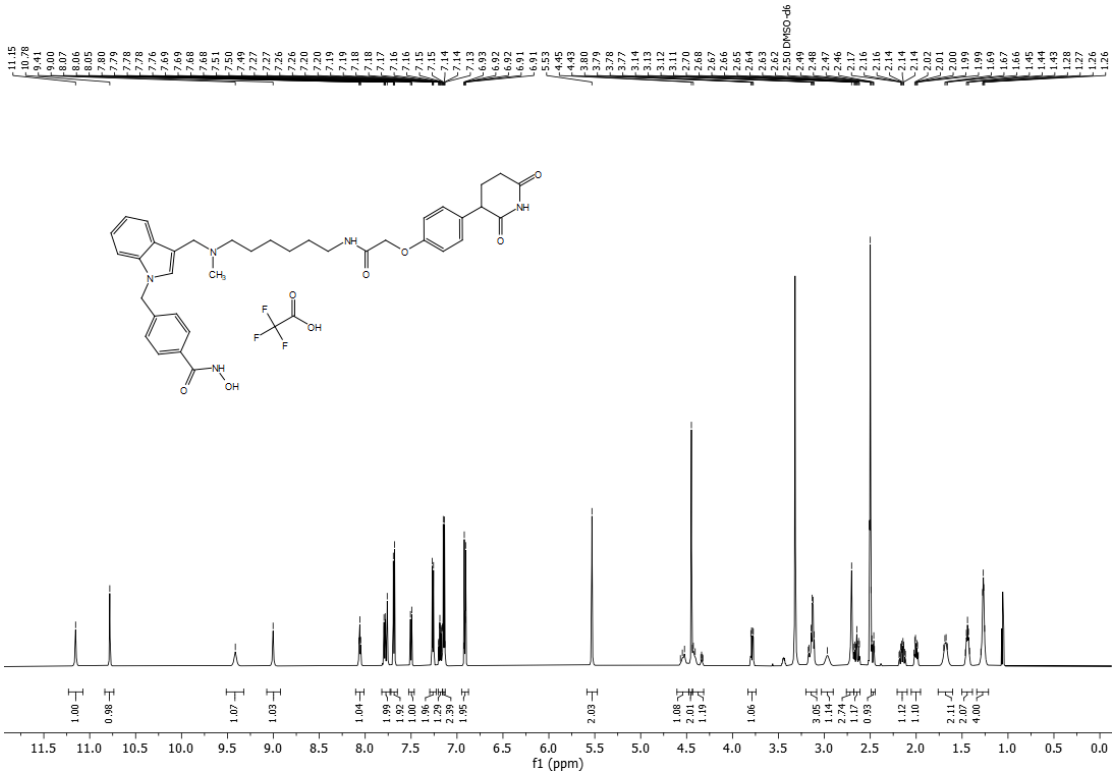

^{13}C NMR spectrum of **AP6** (151 MHz, DMSO-d_6)

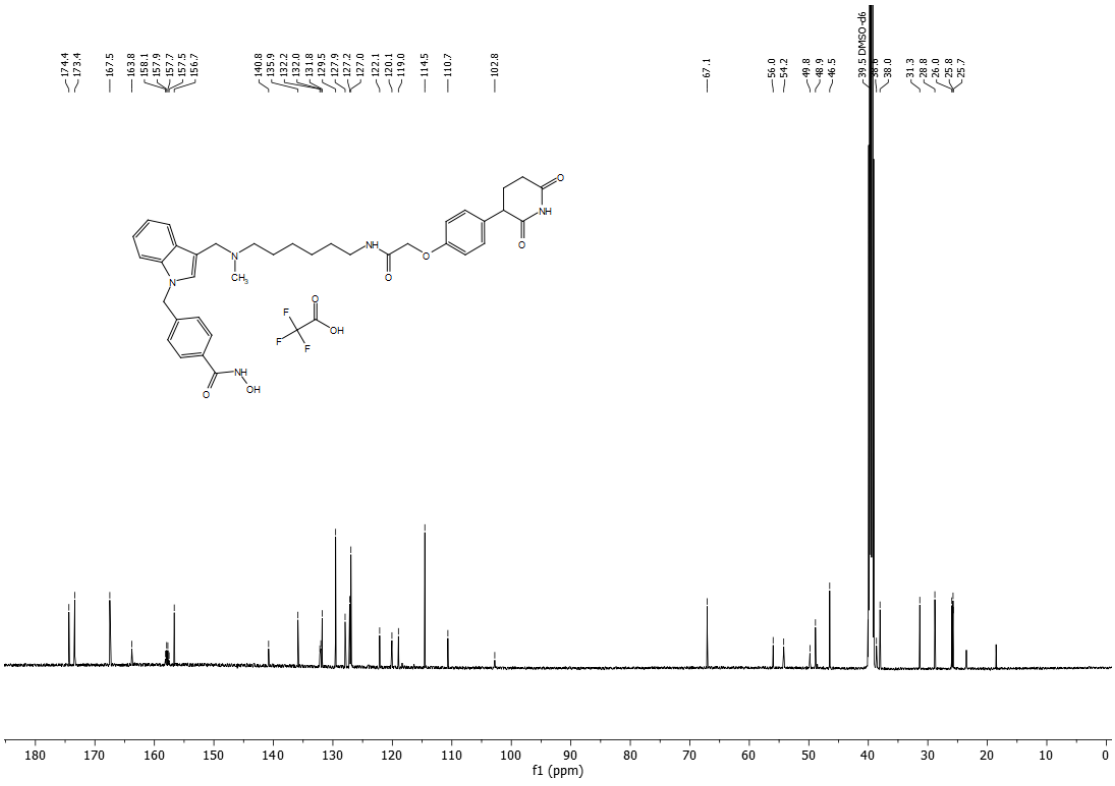

HR-MS spectrum of **AP6**

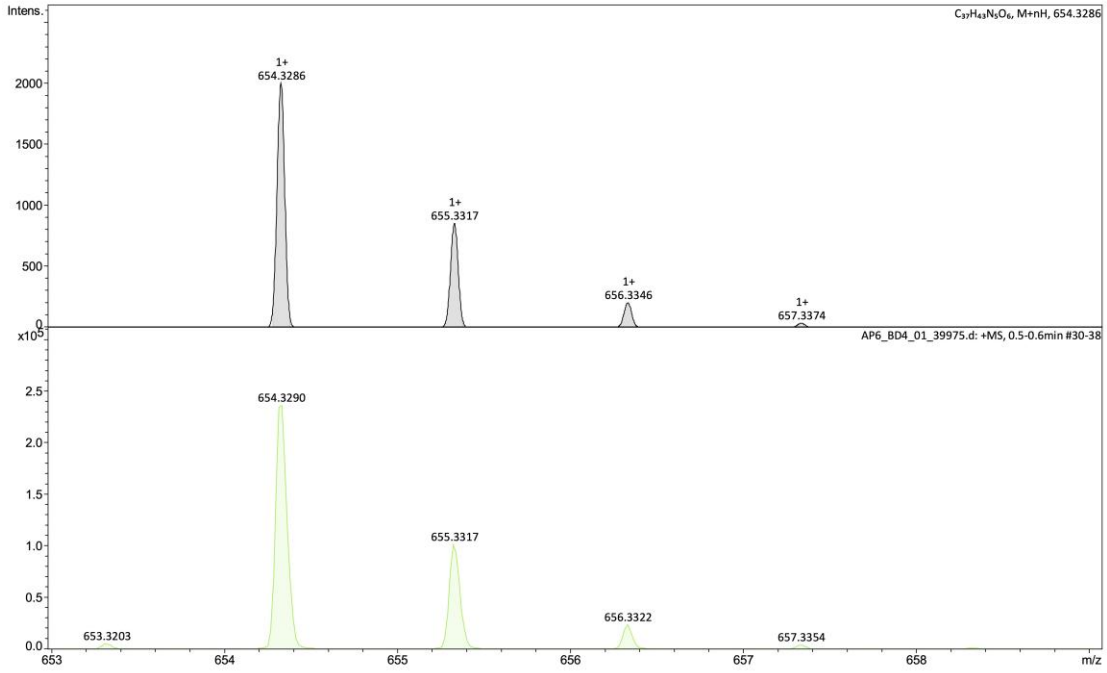

HPLC chromatograms of **AP6** (Purity: 99.2%)

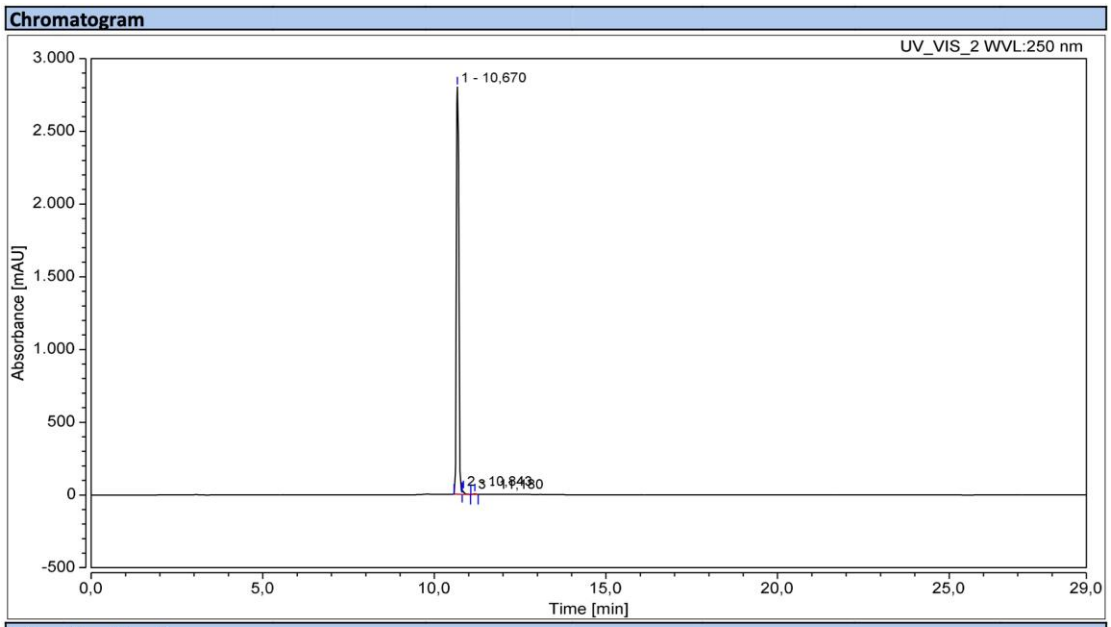

Integration Results

No.	Peak Name	Retention Time min	Area mAU*min	Height mAU	Relative Area %	Relative Height %	Amount n.a.
1		10,670	224,818	2798,499	99,22	99,04	n.a.
2		10,843	1,450	23,594	0,64	0,83	n.a.
3		11,180	0,308	3,592	0,14	0,13	n.a.
Total:			**226,576**	**2825,685**	**100,00**	**100,00**	

^{1}H NMR spectrum of **AP7** (600 MHz, DMSO-d_6)

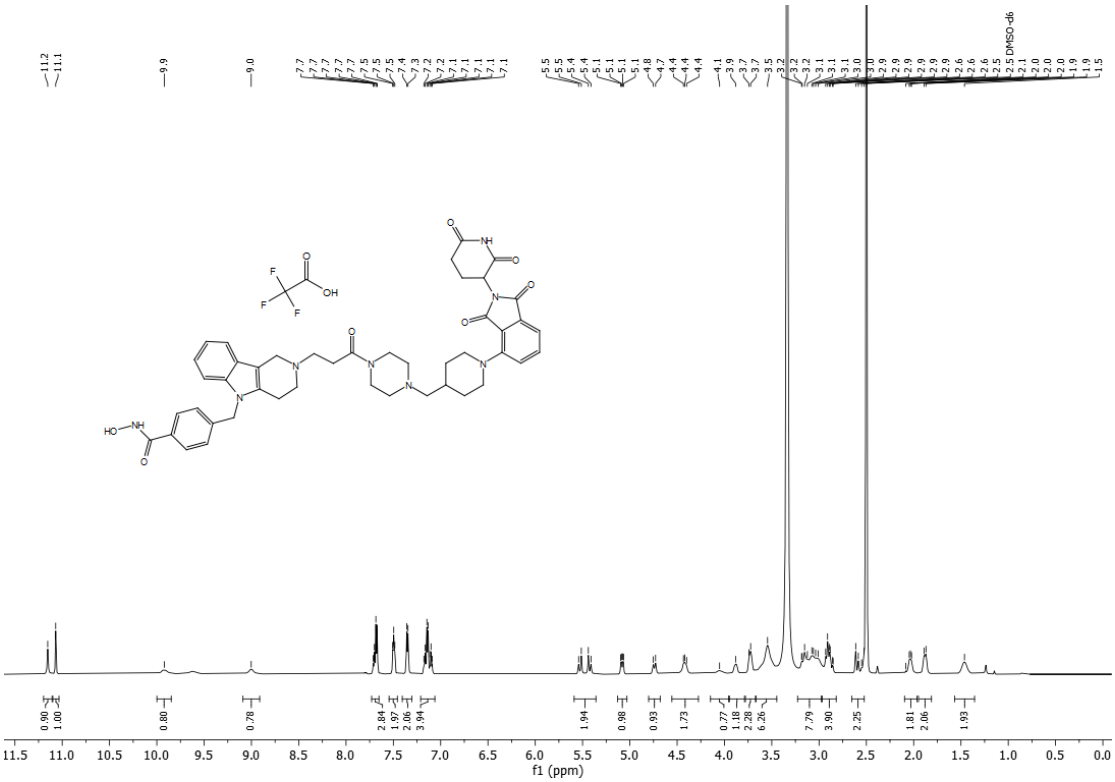

^{13}C NMR spectrum of **AP7** (151 MHz, DMSO-d_6)

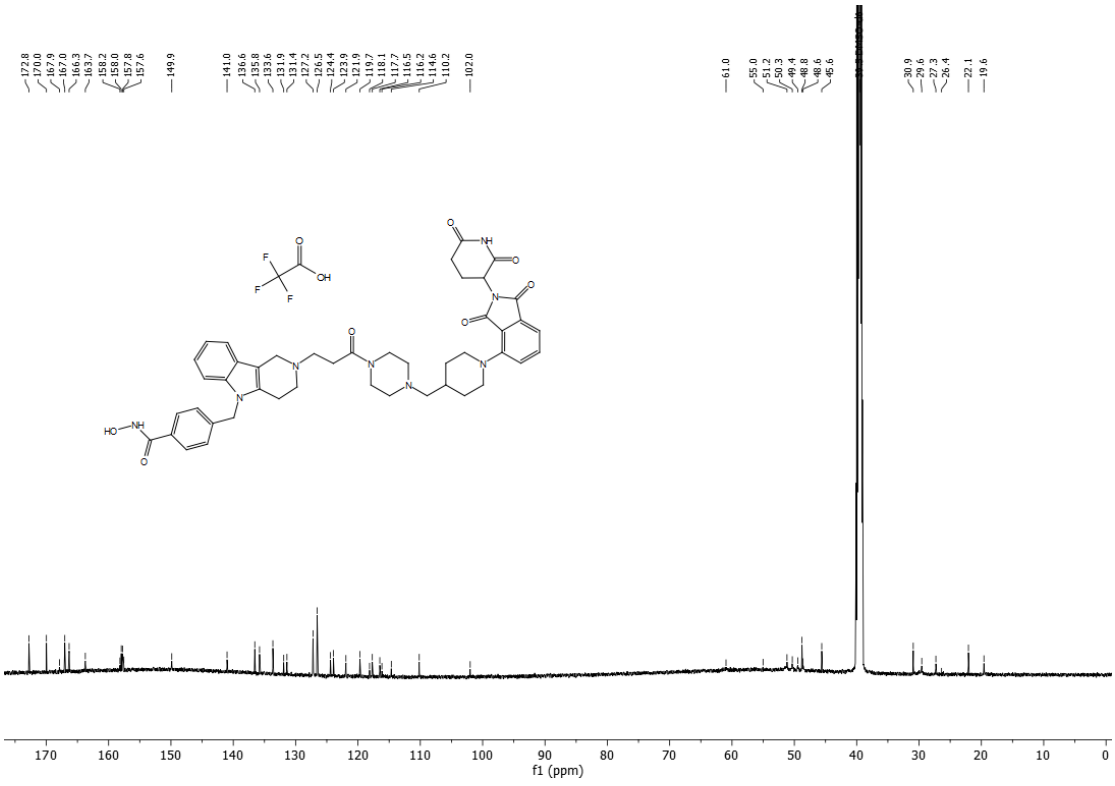

HR-MS spectrum of **AP7**

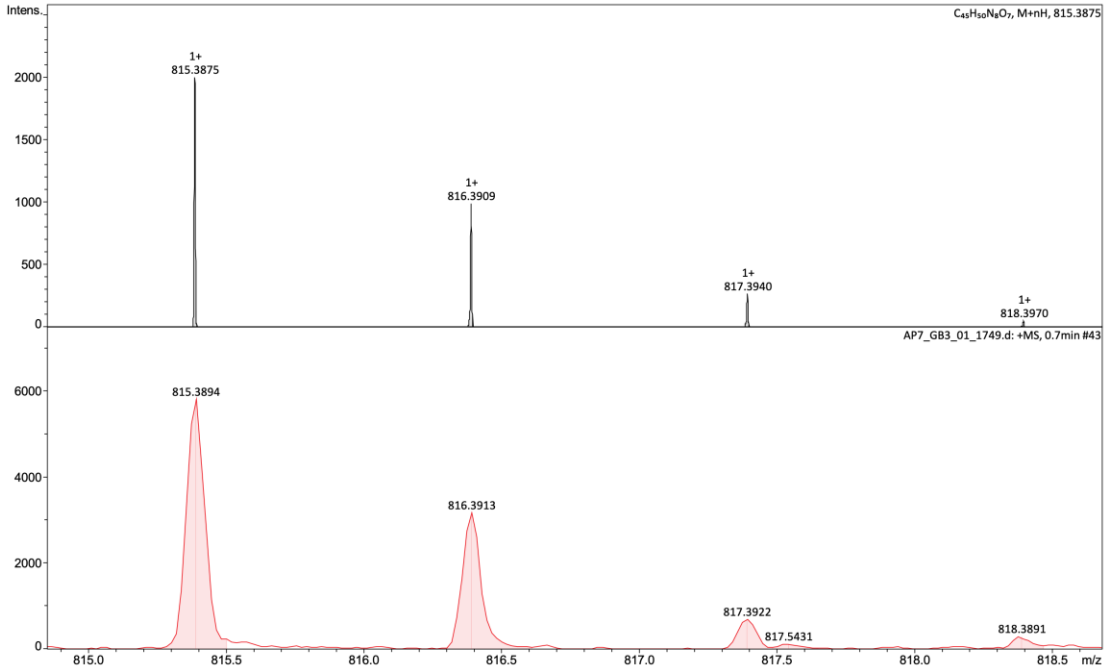

HPLC chromatograms of **AP7** (Purity: 99.8%)

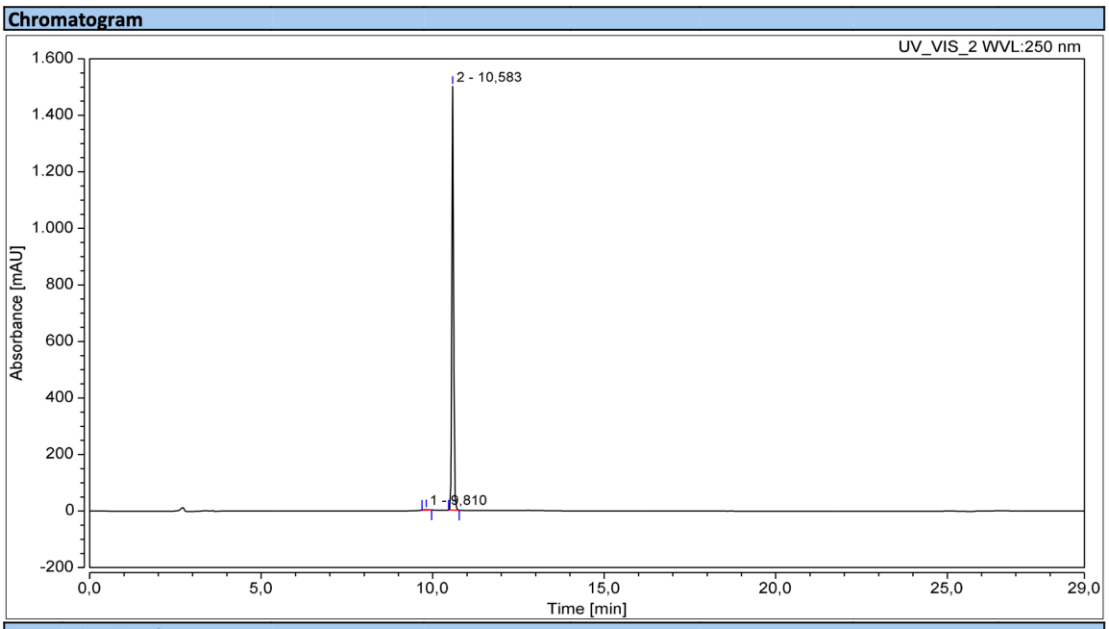

Integration Results

No.	Peak Name	Retention Time min	Area mAU*min	Height mAU	Relative Area %	Relative Height %	Amount n.a.
1		9,810	0,231	1,399	0,24	0,09	n.a.
2		10,583	95,867	1498,566	99,76	99,91	n.a.
Total:			**96,098**	**1499,965**	**100,00**	**100,00**	

^{1}H NMR spectrum of **AP8** (600 MHz, DMSO-d_6)

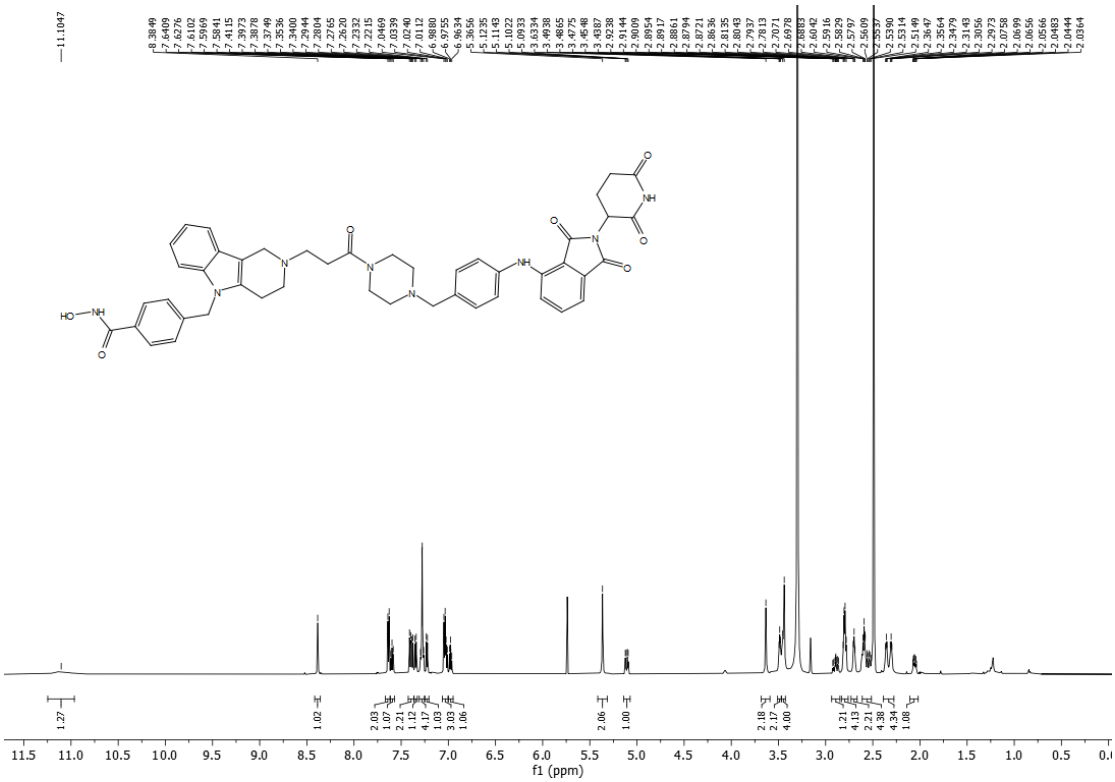

^{13}C NMR spectrum of **AP8** (151 MHz, DMSO-d_6)

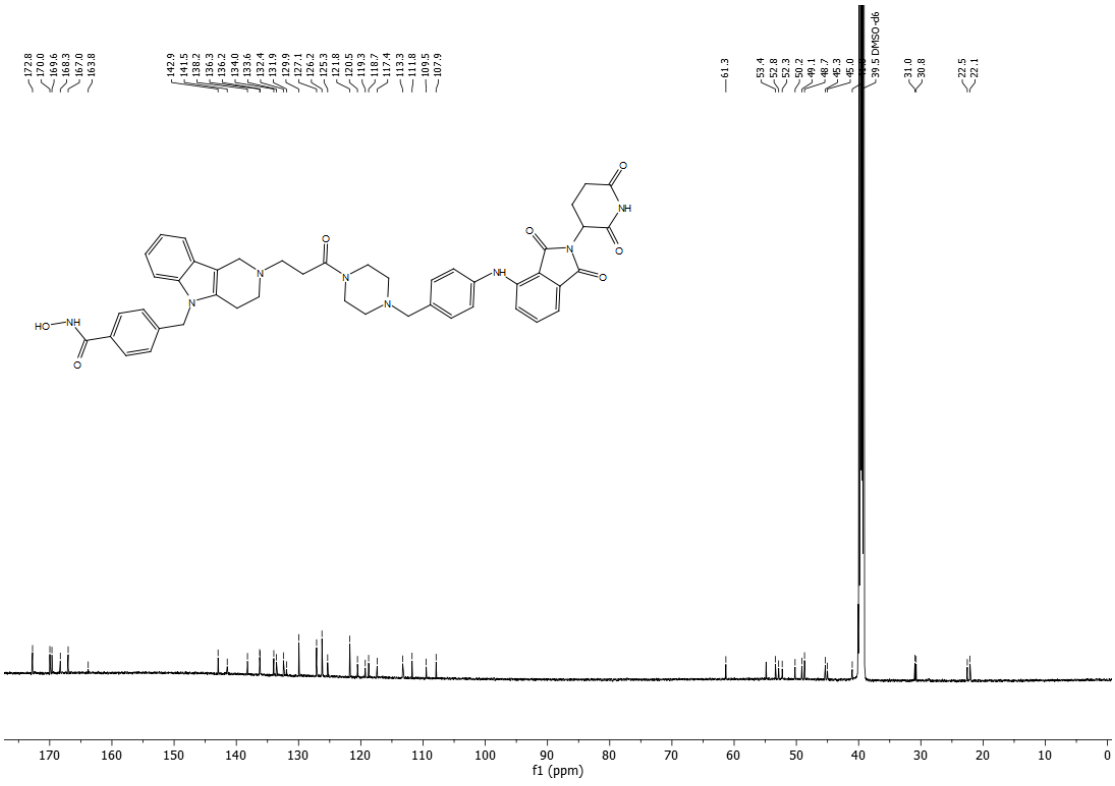

HR-MS spectrum of **AP8**

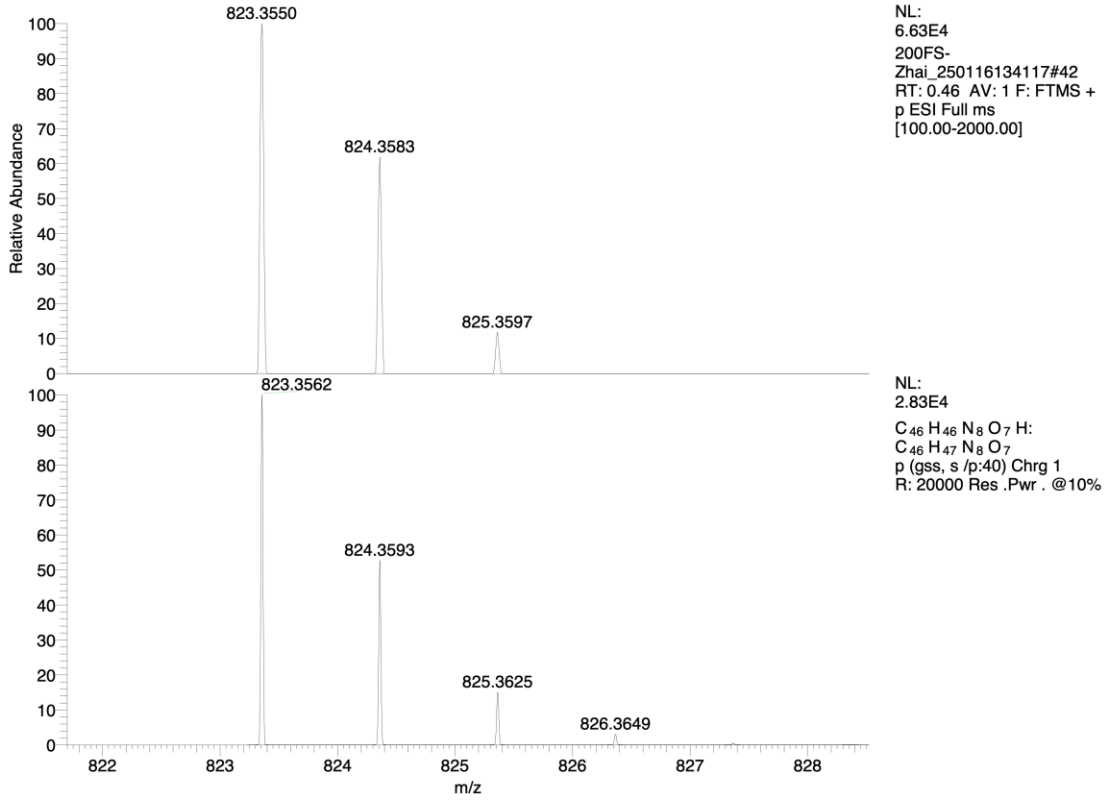

HPLC chromatograms of **AP8** (Purity: 98.0%)

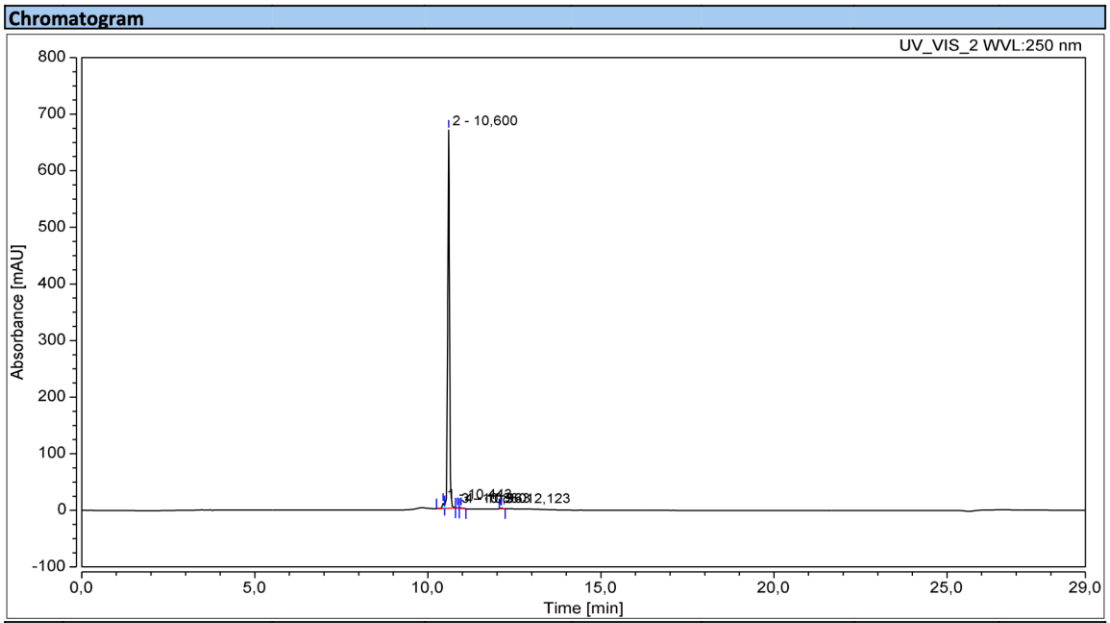

Integration Results

No.	Peak Name	Retention Time min	Area mAU*min	Height mAU	Relative Area %	Relative Height %	Amount n.a.
1		10,443	0,589	8,761	1,41	1,29	n.a.
2		10,600	40,847	668,249	97,98	98,21	n.a.
3		10,860	0,047	0,797	0,11	0,12	n.a.
4		10,963	0,102	1,195	0,24	0,18	n.a.
5		12,123	0,105	1,441	0,25	0,21	n.a.
Total:			**41,691**	**680,443**	**100,00**	**100,00**	

^{1}H NMR spectrum of **AP9** (600 MHz, DMSO-d_6)

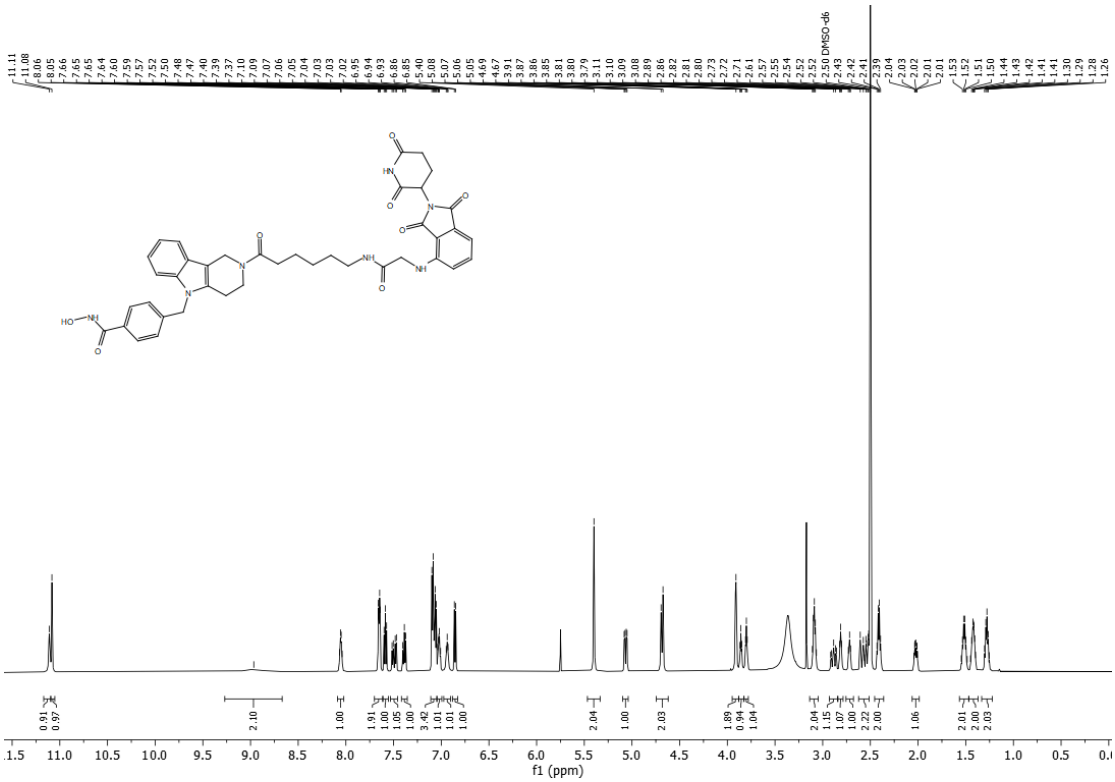

^{13}C NMR spectrum of **AP9** (151 MHz, DMSO-d_6)

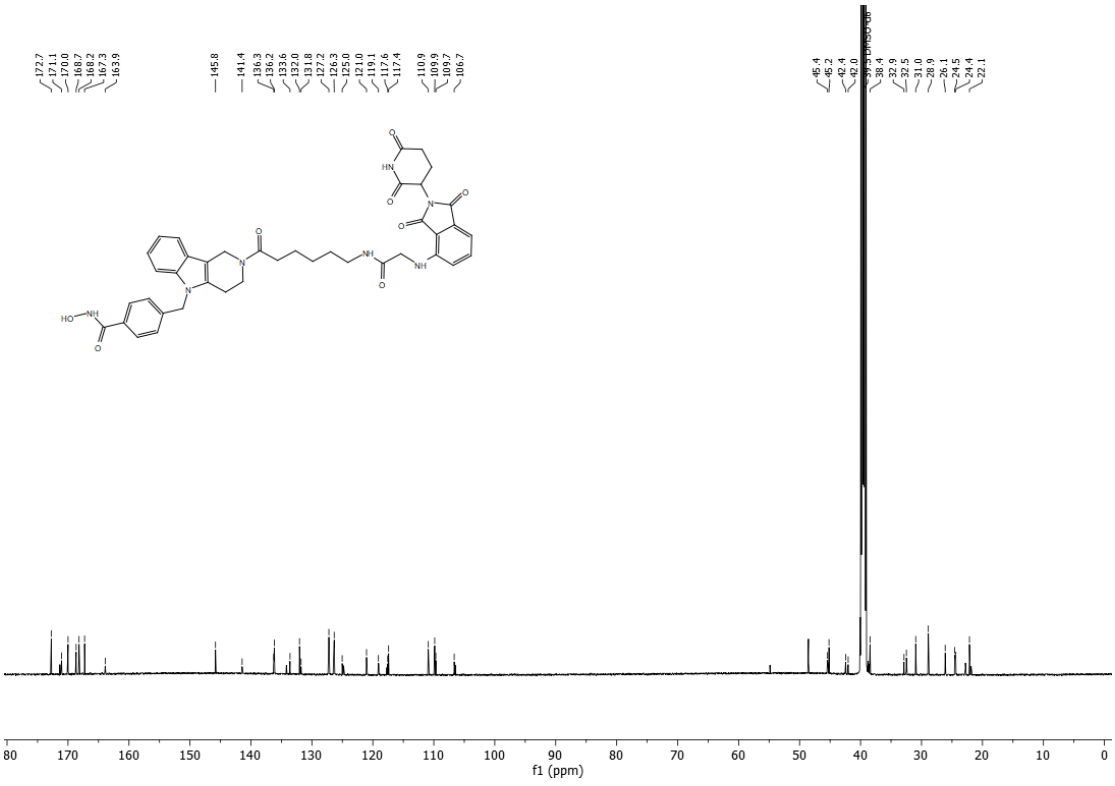

HR-MS spectrum of **AP9**

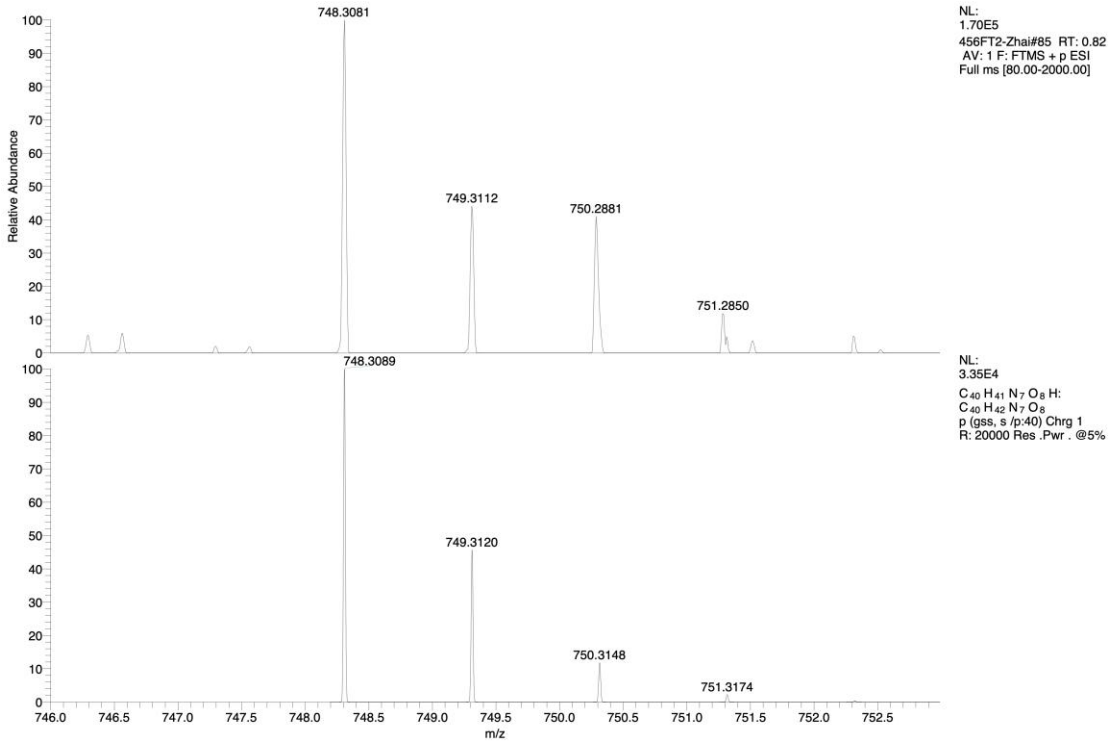

HPLC chromatograms of **AP9** (Purity: 99.4%)

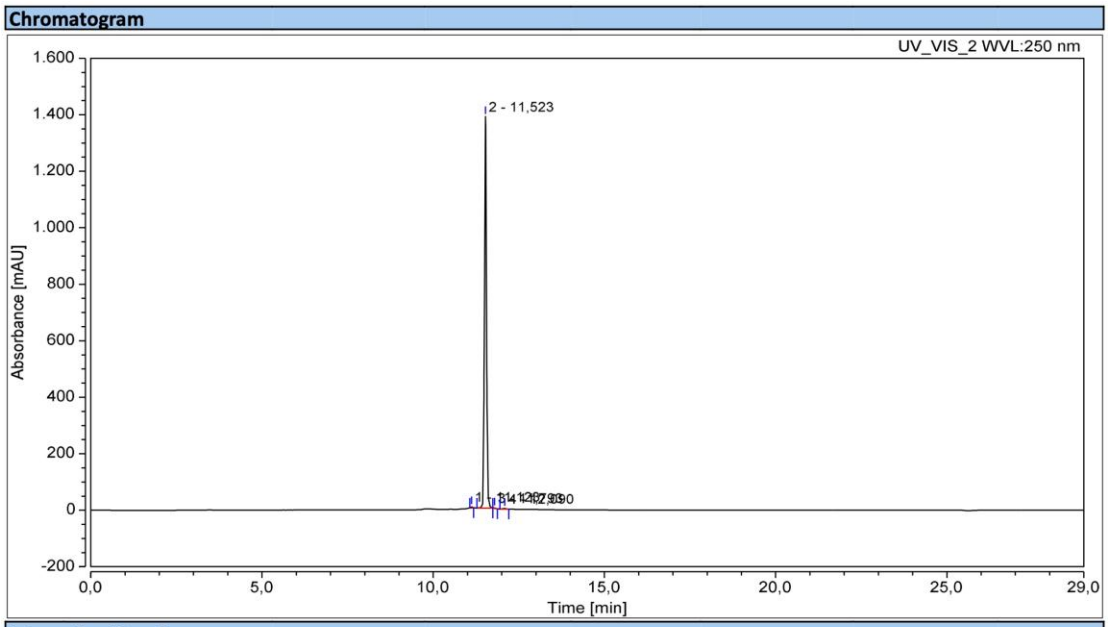

Integration Results

No.	Peak Name	Retention Time min	Area mAU*min	Height mAU	Relative Area %	Relative Height %	Amount n.a.
1		11,123	0,255	4,891	0,25	0,35	n.a.
2		11,523	101,450	1386,376	99,35	99,31	n.a.
3		11,793	0,144	2,263	0,14	0,16	n.a.
4		12,090	0,262	2,497	0,26	0,18	n.a.
Total:			**102,110**	**1396,026**	**100,00**	**100,00**	

^{1}H NMR spectrum of **AP10** (600 MHz, DMSO-d_6)

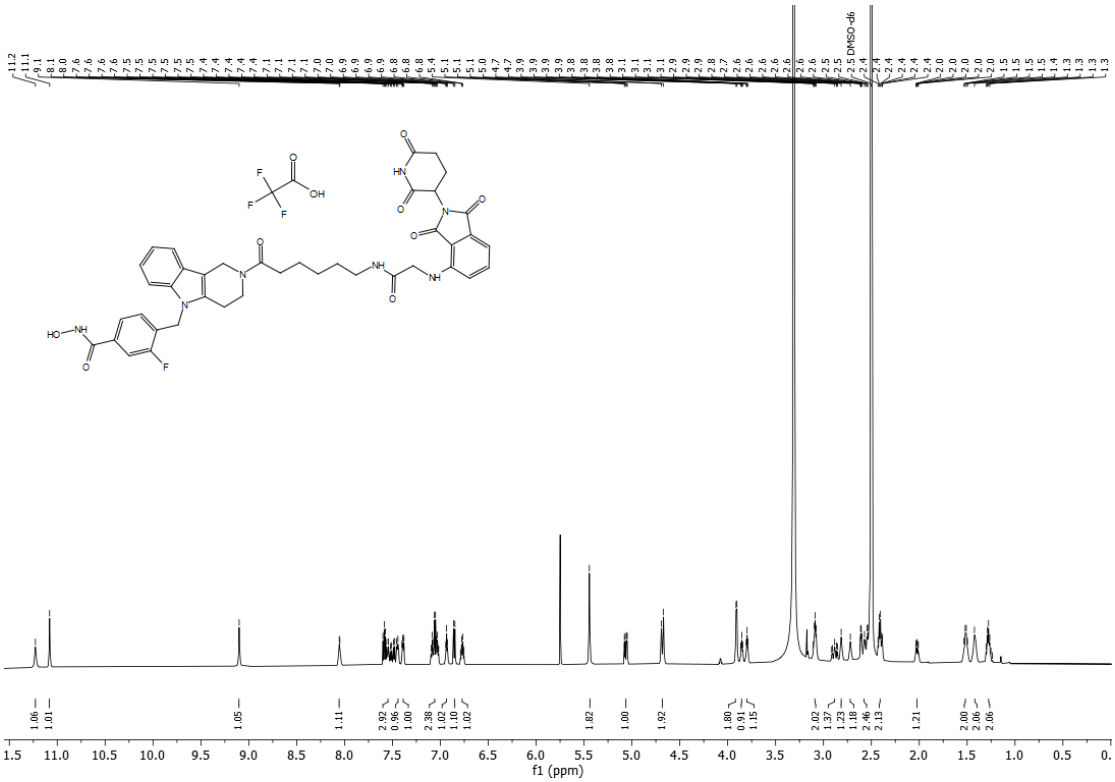

^{13}C NMR spectrum of **AP10** (151 MHz, DMSO-d_6)

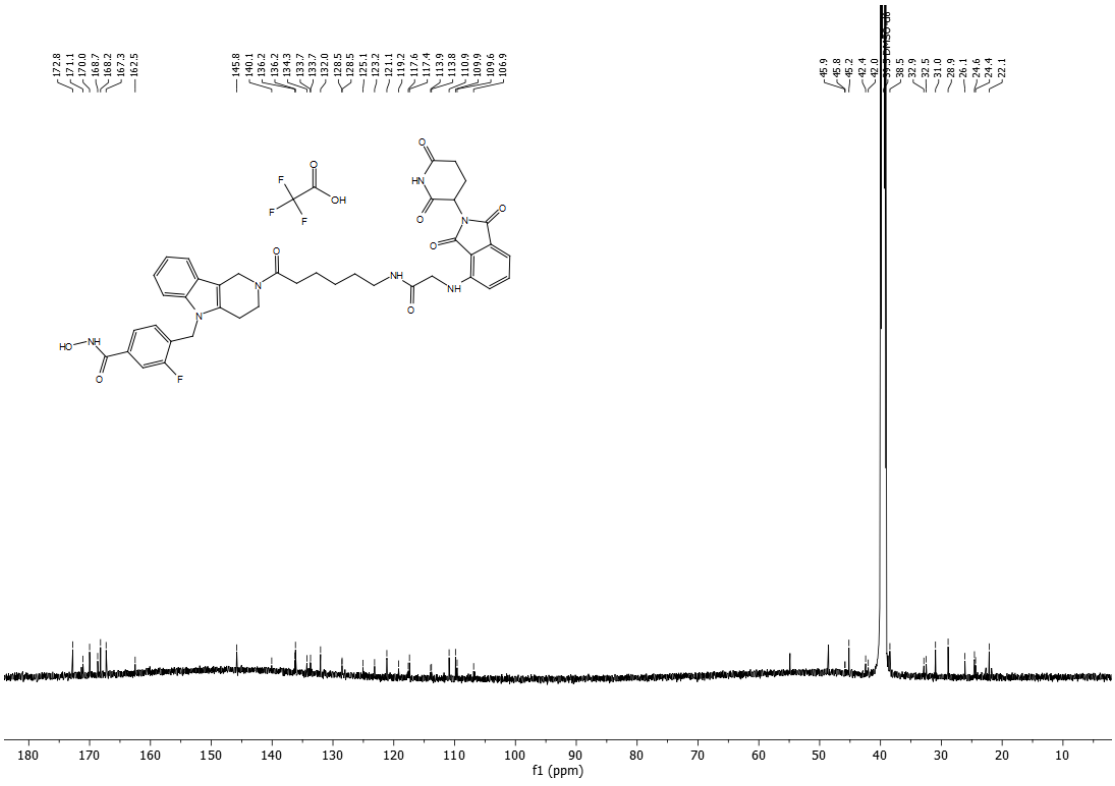

^{19}F NMR spectrum of **AP10** (151 MHz, DMSO-d_6)

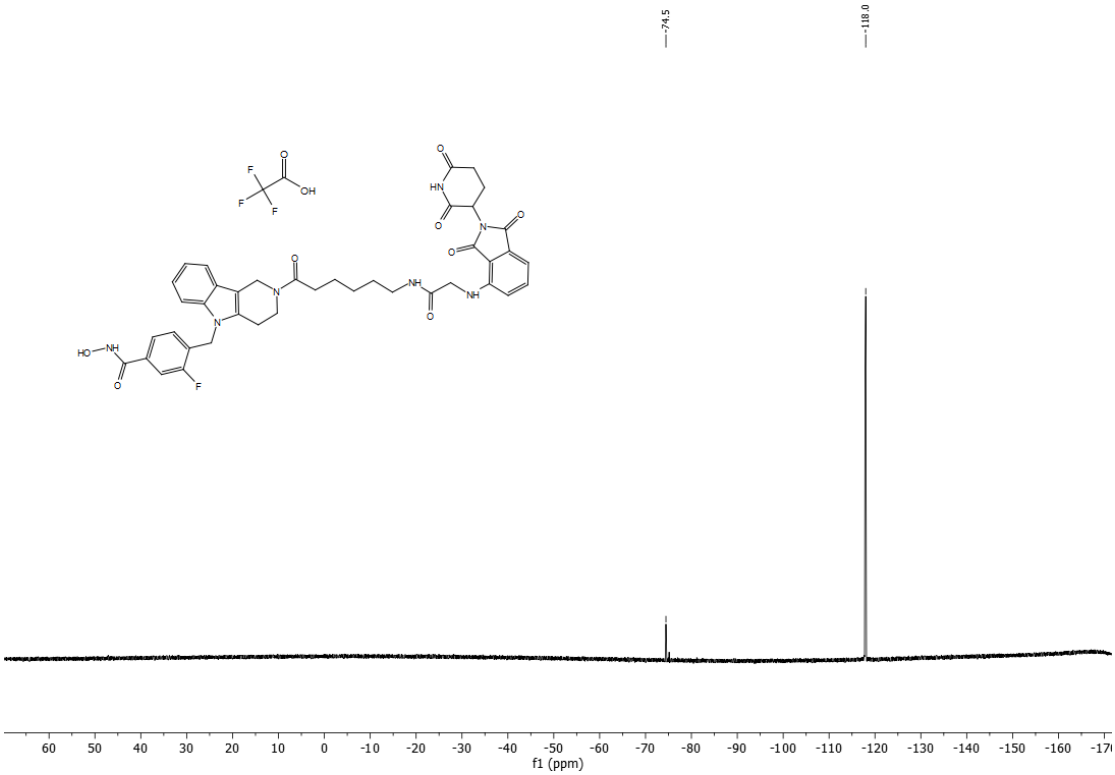

HR-MS spectrum of **AP10**

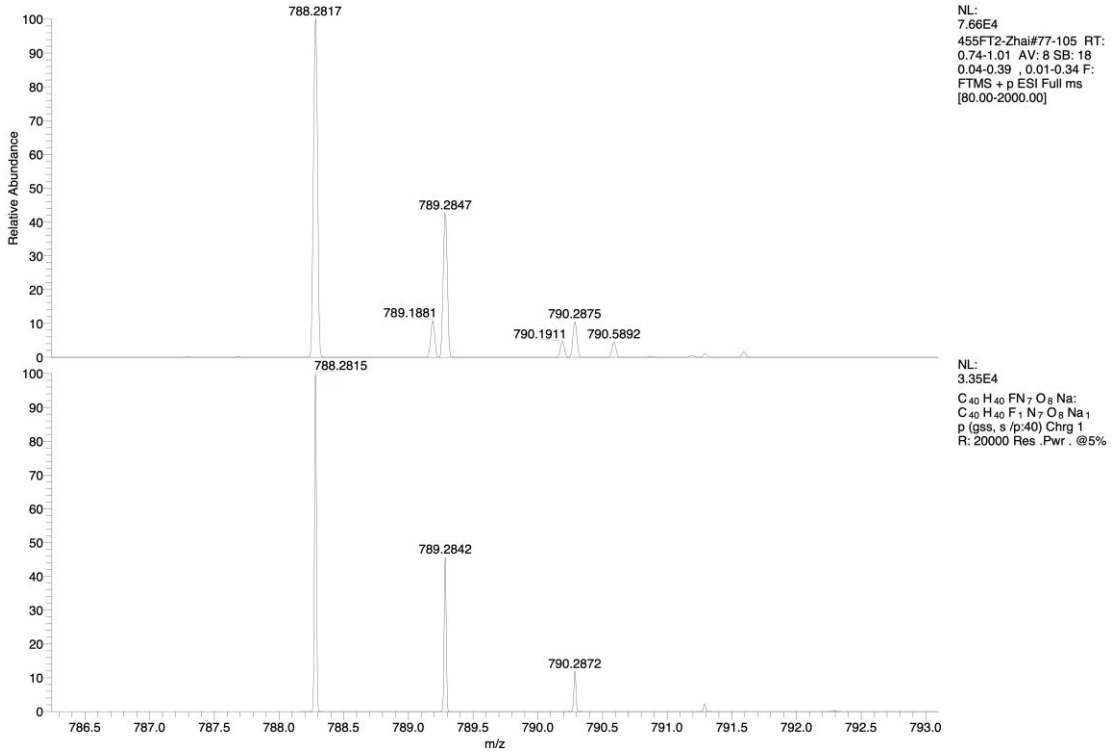

HPLC chromatograms of **AP10** (Purity: 99.9%)

Chromatogram

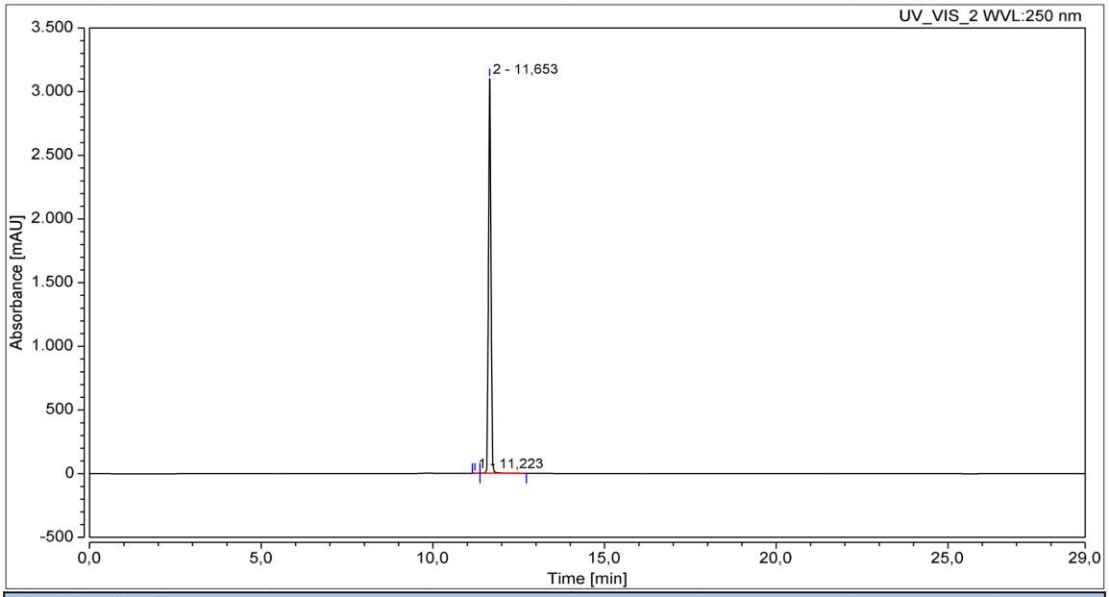

Integration Results

No.	Peak Name	Retention Time min	Area mAU*min	Height mAU	Relative Area %	Relative Height %	Amount n.a.
1		11,223	0,143	1,750	0,06	0,06	n.a.
2		11,653	259,587	3098,235	99,94	99,94	n.a.
Total:			**259,730**	**3099,985**	**100,00**	**100,00**	

^{1}H NMR spectrum of **AP1-N** (600 MHz, DMSO-d_6)

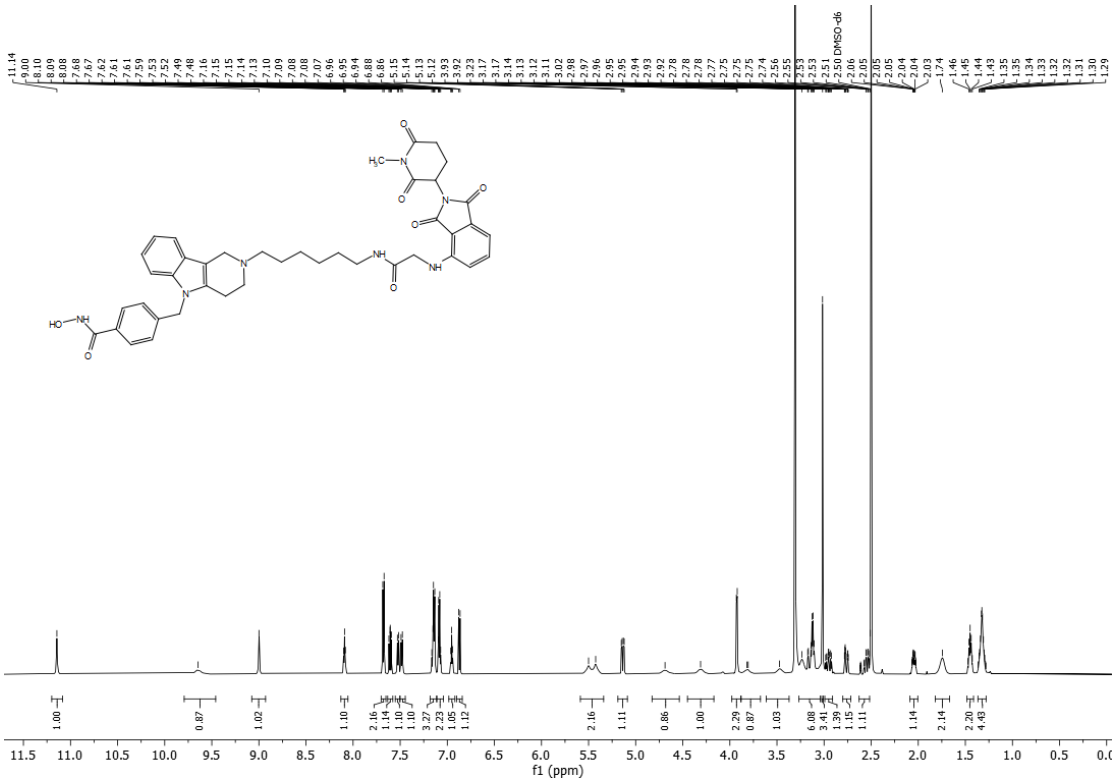

^{13}C NMR spectrum of **AP1-N** (151 MHz, DMSO-d_6)

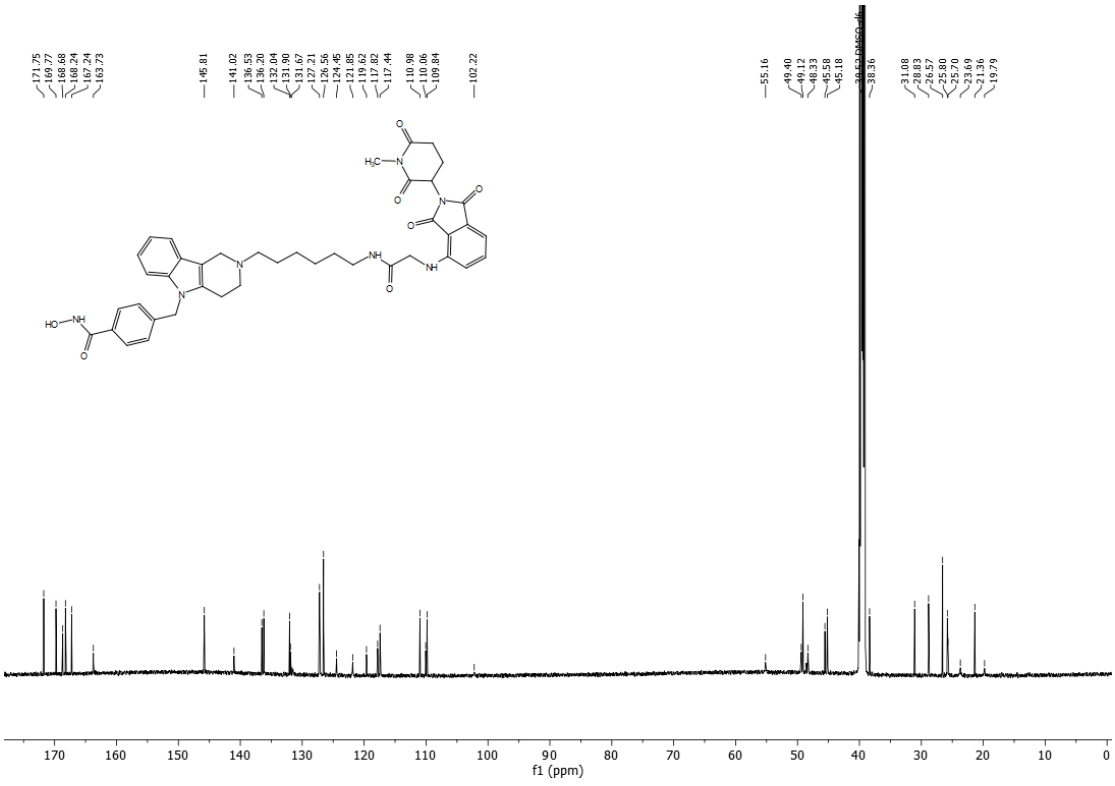

HR-MS spectrum of **AP1-N**

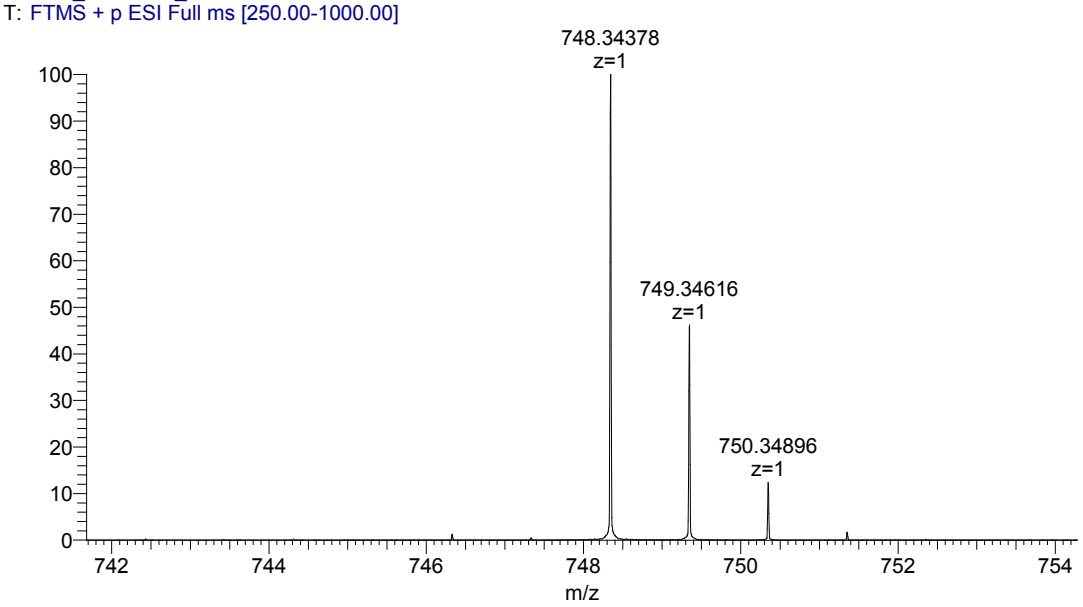

HPLC chromatograms of **AP1-N** (Purity: 97.2%)

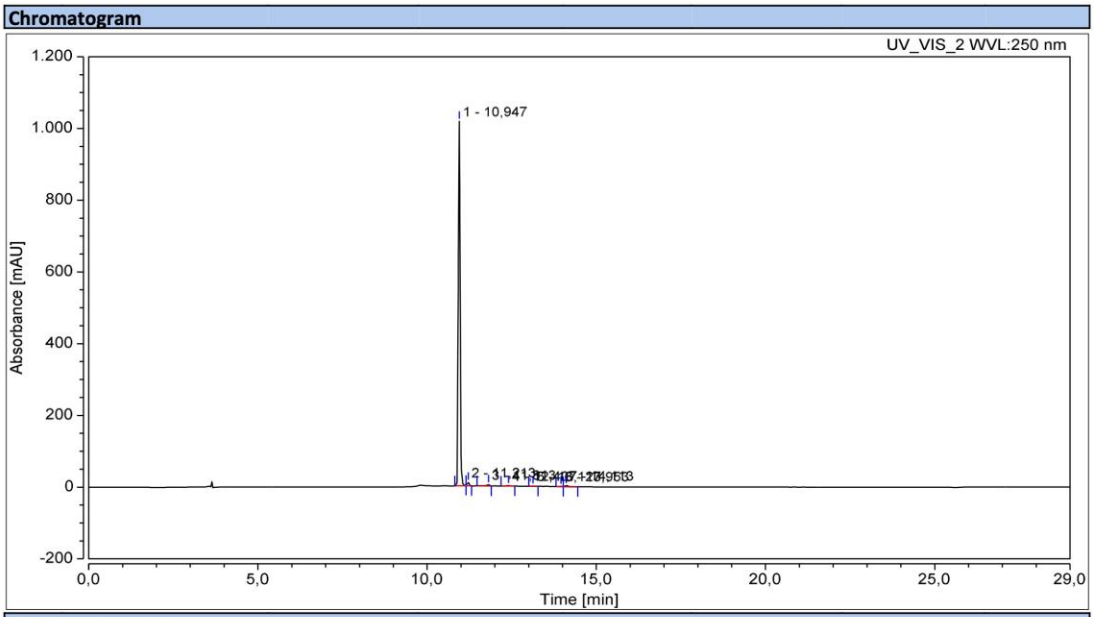

Integration Results

No.	Peak Name	Retention Time min	Area mAU*min	Height mAU	Relative Area %	Relative Height %	Amount n.a.
1		10,947	62,704	1016,594	97,24	98,09	n.a.
2		11,213	0,665	9,823	1,03	0,95	n.a.
3		11,813	0,389	3,512	0,60	0,34	n.a.
4		12,407	0,213	1,379	0,33	0,13	n.a.
5		13,127	0,075	0,624	0,12	0,06	n.a.
6		13,953	0,110	1,108	0,17	0,11	n.a.
7		14,113	0,326	3,376	0,51	0,33	n.a.
Total:			**64,481**	**1036,415**	**100,00**	**100,00**	

4. Immunoblot replicates

Replicates for Figure 5A

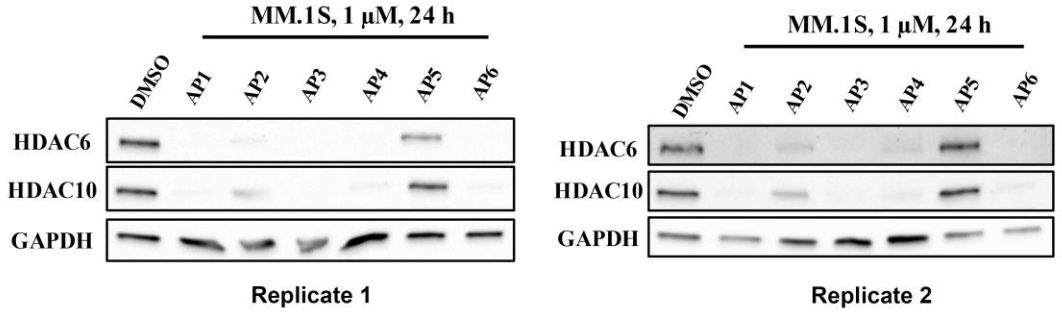

Replicates for Figure 5B

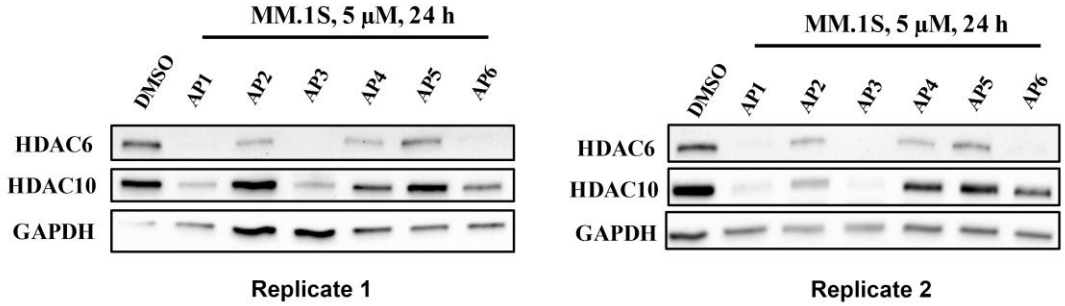

Replicates for Figure 8A

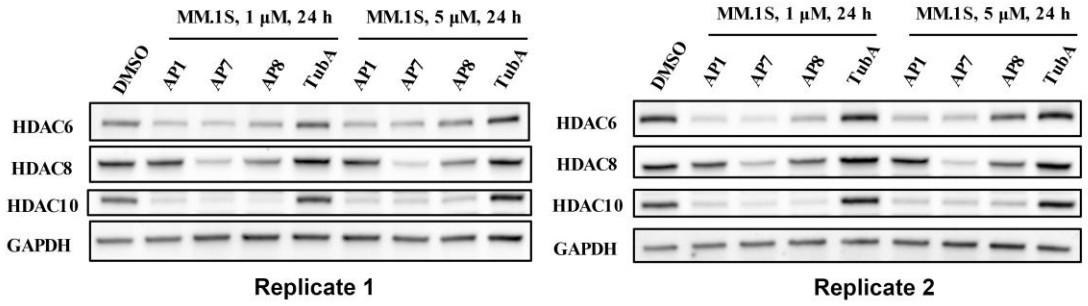

Replicates for Figure 8B

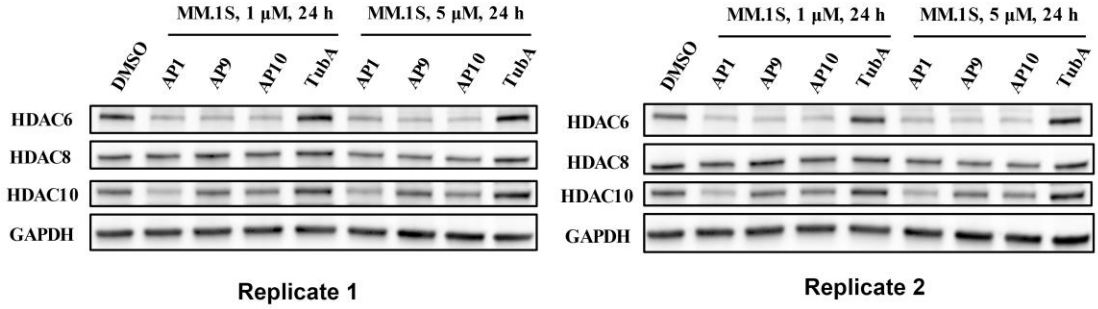

Replicates for Figure 9A

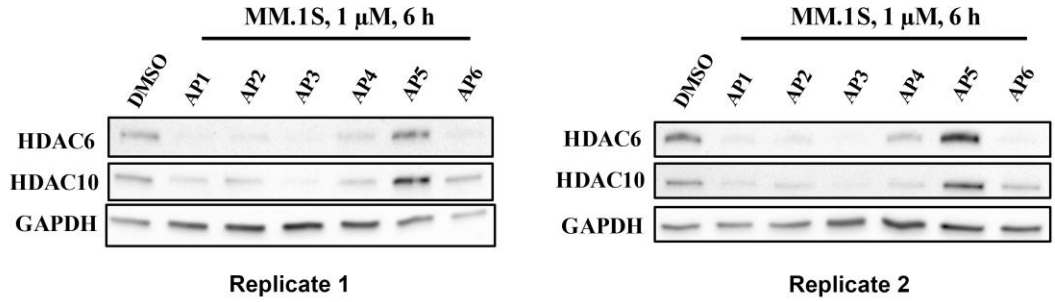

Replicates for Figure 9B

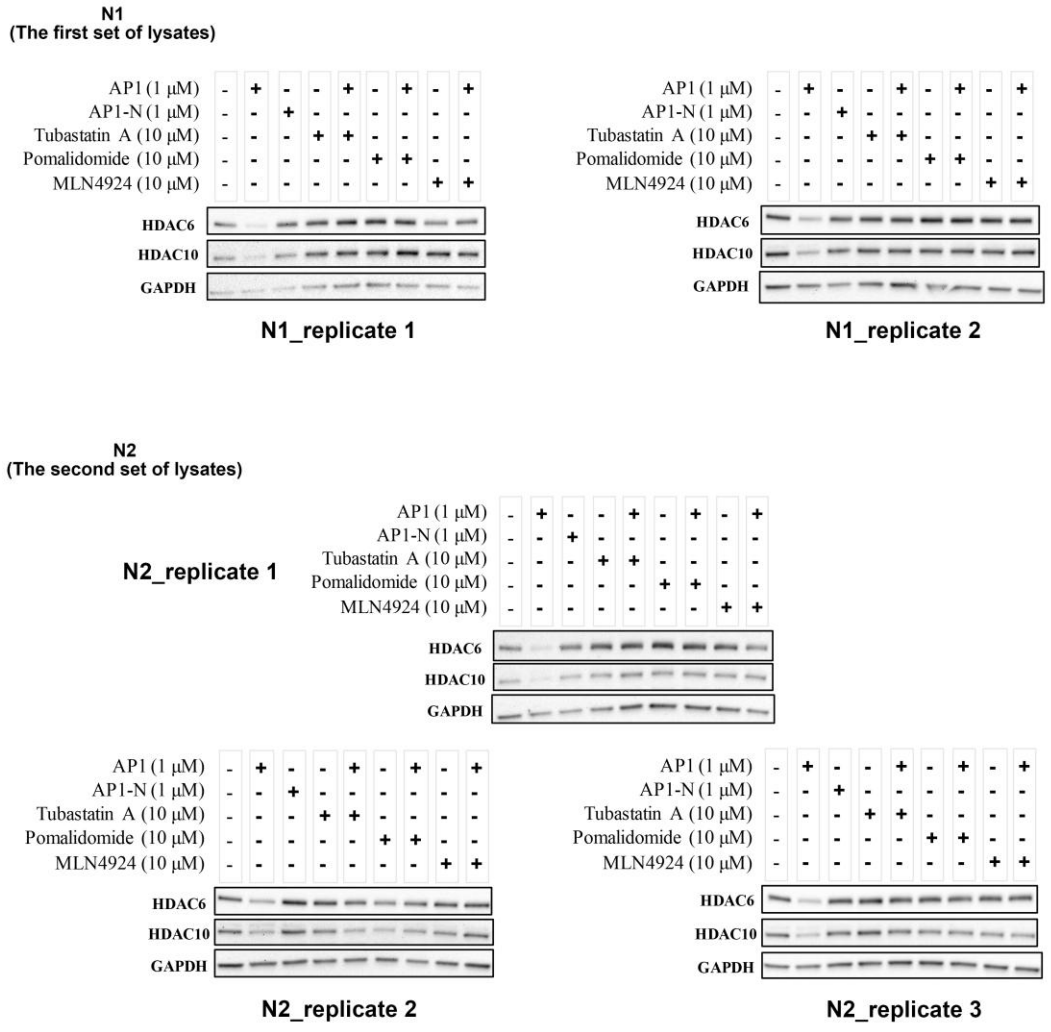

5. Reference

(1) Herbst-Gervasoni, C. J.; Steimbach, R. R.; Morgen, M.; Miller, A. K.; Christianson, D. W. Structural Basis for the Selective Inhibition of HDAC10, the Cytosolic Polyamine Deacetylase. *ACS Chem. Biol.* **2020**, *15* (8), 2154-2163.

(2) Zhao, C.; Tang, C.; Li, C.; Ning, W.; Hu, Z.; Xin, L.; Zhou, H. B.; Huang, J. Novel hybrid conjugates with dual estrogen receptor alpha degradation and histone deacetylase inhibitory activities for breast cancer therapy. *Bioorg. Med. Chem.* **2021**, *40*, 116185.

7.3 Appendix III. Publication II: Discovery of histone deacetylase 8 (HDAC8)-specific proteolysis-targeting chimeras with anti-cancer activity against hematological malignancies

The following pages include the article "Discovery of histone deacetylase 8 (HDAC8)-specific proteolysis-targeting chimeras with anti-cancer activity against hematological malignancies" as it was published in the Journal of Medicinal Chemistry by the American Chemical Society.

The article is reprinted with the permission from:

Shiyang Zhai, Marie Kemkes, Cindy-Esther Kponomaizoun, Jan Gerhartz, Felix Feller, Jia-Wey Tu, Dominika Ewa Pieńkowska, Julian-Schliehe Diecks, Ina Dressel, Michael Gütschow, Radosław P. Nowak, Christian Steinebach, Sanil Bhatia, Finn K. Hansen.

J. Med. Chem. **2026**, 69, 2, 918-943

https://doi.org/10.1021/acs.jmedchem.5c00939

Sanil Bhatia and Finn K. Hansen share the senior authorship.

Journal of Medicinal Chemistry

pubs.acs.org/jmc

Article

Discovery of Histone Deacetylase 8-Specific Proteolysis-Targeting Chimeras with Anticancer Activity against Hematological Malignancies

Shiyang Zhai, Marie Kemkes, Cindy-Esther Kponomaizoun, Jan Gerhartz, Felix Feller, Jia-Wey Tu, Dominika Ewa Pieńkowska, Julian Schliehe-Diecks, Ina Dressel, Michael Gütschow, Radosław P. Nowak, Christian Steinebach, Sanil Bhatia,* and Finn K. Hansen*

Cite This: *J. Med. Chem.* 2026, 69, 918−943

Read Online

ACCESS | Metrics & More | Article Recommendations | Supporting Information

ABSTRACT: Histone deacetylase 8 (HDAC8) has emerged as promising therapeutic target for several malignancies. In this study, we developed two series of cereblon (CRBN)-recruiting proteolysis-targeting chimeras (PROTACs) for targeted HDAC8 degradation, utilizing the selective HDAC8 inhibitor PCI-34051 as warhead. The pomalidomide/thalidomide-based series (**BP1**−**BP5**) exhibited strong antiproliferative activity against leukemia and multiple myeloma cells, accompanied by degradation of CRBN neosubstrates. In contrast, the phenyl glutarimide-based series (**BP6**−**BP10**) displayed low cytotoxicity, no neosubstrate degradation, and enhanced chemical stability. The hit compounds from both series, **BP1** ($DC_{50,\ 24\ h}$ = 20 nM, $D_{max,\ 24\ h}$ = 99%) and **BP6** ($DC_{50,\ 24\ h}$ = 81 nM, $D_{max,\ 24\ h}$ = 93%), demonstrated highly efficient and selective HDAC8 degradation. Pretreatment with **BP6** enhanced the tumor suppressor p53 stability, thereby significantly increasing the sensitivity of leukemia cells to the MDM2 antagonist idasanutlin than PCI-34051, highlighting its unique potential for combinatorial therapy without impacting neosubstrates.

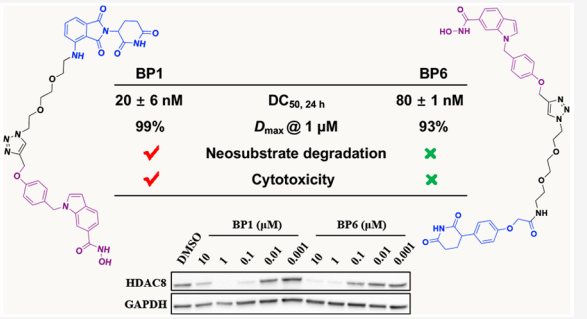

INTRODUCTION

Histone deacetylase 8 (HDAC8) is a unique member of the class I zinc-dependent HDAC family, localized in both the nucleus and cytoplasm.[1,2] It is known to play a crucial role in a wide range of biological processes, particularly in oncology.[3] While it is controversial whether HDAC8 has histones as substrates, its function extends to the regulation of nonhistone proteins such as SMC3, p53, ERRα, and cortactin, thereby affecting various cellular processes.[4,5] In addition to its frequently mentioned catalytic function, HDAC8 also has scaffolding functions that allow it to interact with transcription factors such as STAT3,[6] CREB,[7] and DEC1.[8] Its critical involvement in cancer biology is well-established, with implications in myeloid leukemia, T-cell lymphoma, hepatocellular carcinoma, breast, colon, and lung cancer.[3−5] For instance, increased HDAC8 expression was observed in myeloid leukemia,[9] and its specific inhibition has been shown to abrogate leukemic stem cells and delay the progression of acute myeloid leukemia.[10] Moreover, HDAC8 is essential for other biological functions, such as mammalian development,[11] oogenesis, and female fertility,[12] further demonstrating its multifaceted biological significance. Thus, HDAC8 emerges as a compelling target for the treatment of cancer and other diseases.

Although numerous HDAC8 inhibitors have been developed over the years, most of them have focused on targeting the catalytic function of HDAC8, showing limited selectivity and efficacy.[3,5,13−15] This underscores the need for novel therapeutic strategies that target both its deacetylase activity and nonenzymatic scaffolding functions.[16] Among the newer promising therapeutic strategies, the proteolysis-targeting chimera (PROTAC) technology for targeted protein degradation has initiated a new era in drug discovery.[17−20] A PROTAC molecule is assembled by combining a protein of interest (POI) ligand, an E3 ligase ligand, and a linker connecting the two warheads. These new therapeutic modalities induce polyubiquitination of the target protein, leveraging the endogenous ubiquitination process to facilitate its degradation via the 26S proteasome. Rather than simply inhibiting, a PROTAC molecule degrades the target protein, thereby eliminating both the catalytic and scaffolding functions of the

Received: April 4, 2025
Revised: December 9, 2025
Accepted: December 11, 2025
Published: January 2, 2026

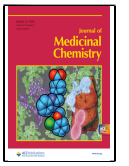

https://doi.org/10.1021/acs.jmedchem.5c00939
J. Med. Chem. 2026, 69, 918−943

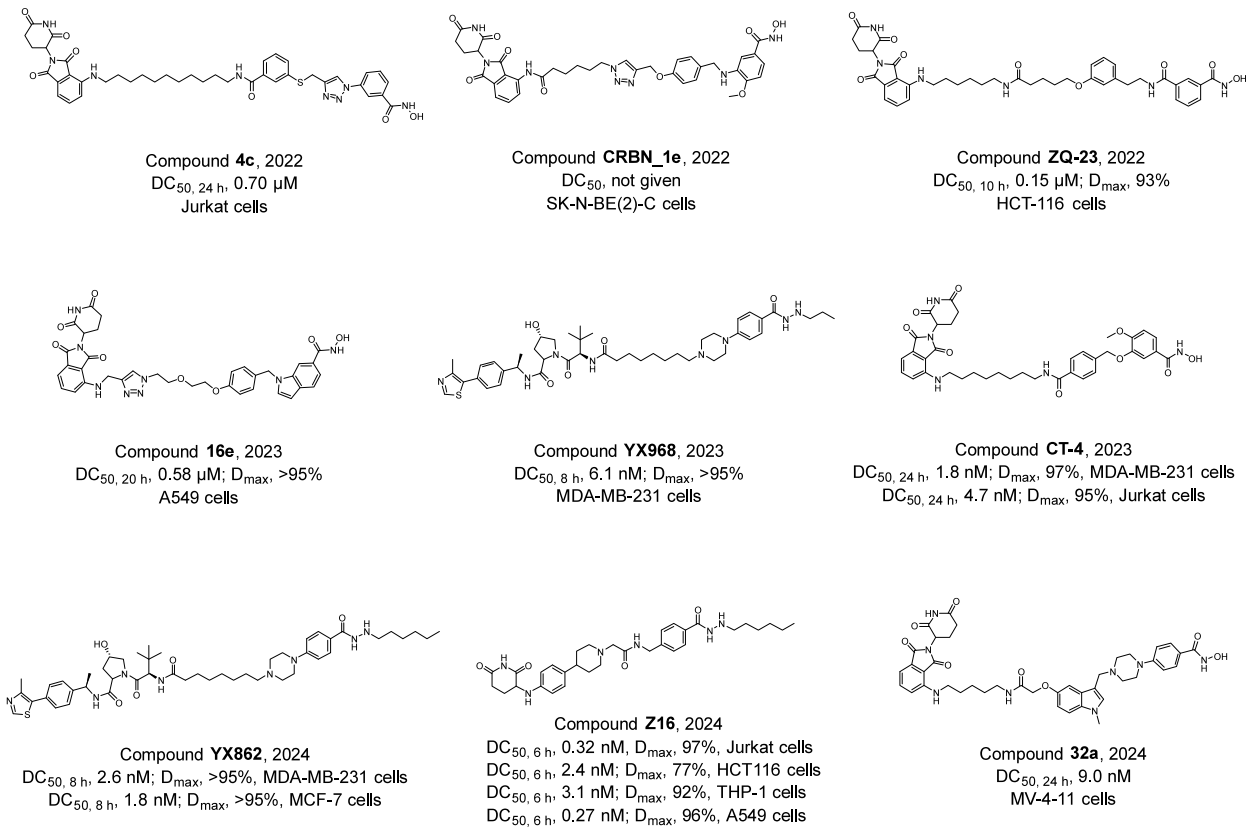

Figure 1. Reported HDAC8 PROTACs and their respective degradation efficiencies.

POI.[17−20] In particular, this method can achieve enhanced selectivity, providing a new way to achieve selective inactivation of a specific protein subtype.[17]

In the epigenetic field, especially the HDAC-related area, the PROTAC technology has enabled the degradation of 11 HDAC subtypes over the years, including HDAC1−8, HDAC10, Sirt2,[21] as well as Sirt6.[22] More recently, targeting HDAC8 for degradation with the PROTAC approach has received considerable attention, with the first HDAC8 PROTAC published by Chotitumnavee et al.[16] in 2022. In this report, the authors used a selective HDAC8 inhibitor as the POI warhead and pomalidomide as the E3 ligase ligand to recruit cereblon (CRBN), resulting in substantial HDAC8 degradation in Jurkat cells with a half maximal degradation concentration ($DC_{50,\ 24\ h}$) value of 0.70 μM.[16] The subsequent development of various HDAC8 PROTACs using different HDAC8 ligands and E3 ligase warheads, along with their respective potencies, is summarized in Figure 1.

The recruitment of CRBN or von Hippel-Lindau (VHL) as E3 ligases for HDAC8 degradation has been widely reported in various studies. As HDAC8 warheads, both hydroxamic acid−based and hydrazide-based HDAC8 ligands were employed. Among the representative molecules, the hydroxamic acid−based PROTAC **CT-4** demonstrated exceptional potency, achieving $DC_{50,\ 24\ h}$ values of 1.8 nM in MDA-MB-231 cells and 4.7 nM in Jurkat cells.[23] In addition, PROTAC **32a** was recently reported to induce HDAC8 degradation with a single-digit nanomolar $DC_{50,\ 24\ h}$ value.[24] Other hydroxamic acid−based PROTACs, such as compound **4c**,[16] **ZQ-23**,[25] and **16e**,[26] showed submicromolar DC_{50} values across different cell lines, with compound **CRBN_1e**[27] reported as a potent HDAC8 degrader. For the three hydrazide-based HDAC8 PROTACs, all exhibited DC_{50} values in the nanomolar concentration range. Compounds **YX968**[28] and **YX862**,[29] which recruit VHL as the E3 ligase, demonstrated potent HDAC8 degradation in MDA-MB-231 cells, achieving high D_{max} values (>95%) and low $DC_{50,\ 8\ h}$ values of 6.1 nM and 2.6 nM, respectively. Another hydrazide-based compound, **Z16**, recruits CRBN with a phenyl glutarimide-based ligand and demonstrated overall potent HDAC8 degradation in four different cancer cell lines, achieving a minimum $DC_{50,\ 6\ h}$ value of 0.27 nM in A549 cells.[30] Among reported HDAC8 PROTACs, two hydrazide-based examples, **YX862** (VHL-recruiting) and **Z16** (CRBN-based), have shown both high potency and selectivity. In contrast, hydroxamic acid−based PROTACs employing CRBN ligands generally display poor to moderate degradation potency or limited selectivity.

In the present study, two sets of selective HDAC8 PROTACs were designed utilizing the selective HDAC8 inhibitor PCI-34051 as well as immunomodulatory drug (IMiD)- and phenyl glutarimide (PG)-based CRBN ligands. Compared to previously reported PCI-34051-based HDAC8 PROTACs,[26] our compounds from both sets achieved prominent and selective HDAC8 degradation, with the IMiD-based degraders additionally exhibiting potent antiproliferative activity against MM.1S multiple myeloma and HL60 leukemia cells.

RESULTS AND DISCUSSION

Molecular Design and Synthesis

The selective HDAC8 ligand PCI-34051 was employed to develop HDAC8 PROTACs. Molecular modeling analysis was performed to determine the optimal linker attachment point

https://doi.org/10.1021/acs.jmedchem.5c00939
J. Med. Chem. 2026, 69, 918−943

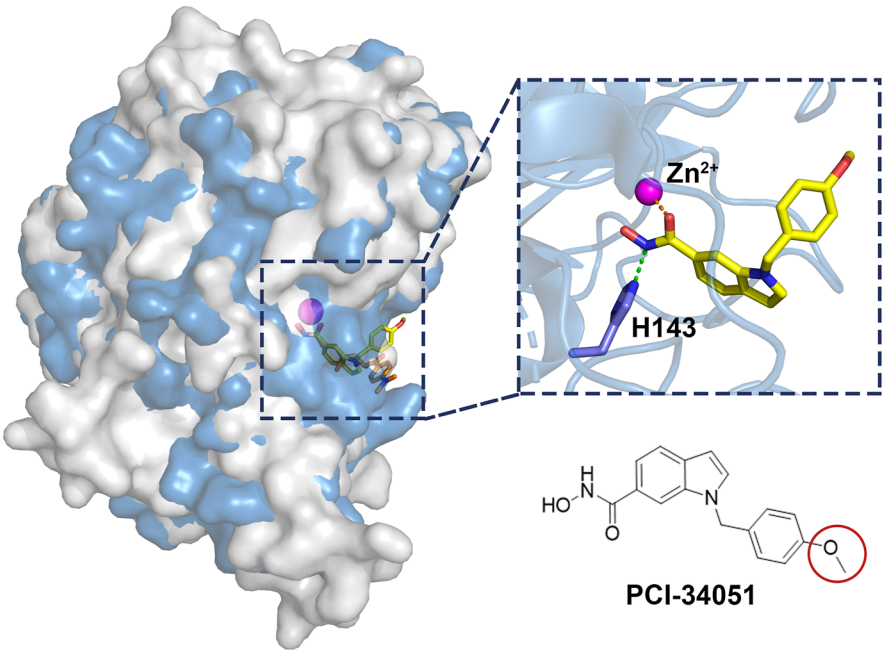

Figure 2. Superimposed structures of smHDAC8 (PDB: 6HQY, in gray) and human HDAC8 (PDB: 1T64, in blue). PCI-34051 is depicted in yellow and trichostatin A in orange. A hydrogen bond is shown in a green dashed line, while the metal chelation interaction is represented in an orange dashed line.

on the molecule. Based on the solved crystal structure of *Schistosoma mansoni* HDAC8 (smHDAC8) complexed with PCI-34051 (PDB: 6HQY), this ligand effectively interacts with residues within the catalytic pocket and exhibits selectivity for HDAC8.[31] Superimposing smHDAC8 (in gray) with the human HDAC8-trichostatin A complex (PDB: 1T64, in blue)[32] revealed strong alignments in their catalytic pockets and the zinc-binding groups of the ligands (Figure 2). In the human HDAC8 structure, the hydroxamic acid group of PCI-34051 complexes the zinc ion and forms a hydrogen bond with H143 within the binding pocket, while the 4-methoxybenzyl moiety in the molecule extends to the outside of the pocket. Similarly, docking of PCI-34051 into the human HDAC8 crystal structure (Figure S1, Supporting Information) confirmed that the 4-methoxybenzyl group protrudes from the binding pocket. These findings identified the 4-methoxybenzyl group of PCI-34051 as solvent-exposed and a suitable exit vector, with the *para*-position on the phenyl ring selected as the anchor point for designing HDAC8 PROTACs. Typically, a PROTAC molecule consists of a POI warhead, an E3 ligase recruiter, and a linker to connect both ligands.[17] Using PCI-34051 as the HDAC8 warhead, we incorporated commonly used flexible alkyl and PEG linkers into the PROTAC design. Additionally, IMiD- and PG-based ligands were employed as CRBN recruiters, as variations in the E3 ligase ligands have been shown to impact degrader activity and stability.[33]

As illustrated in Scheme 1A, the synthetic route begins with the commercially available methyl 1*H*-indole-6-carboxylate. The substitution reaction between this starting material and 1-(bromomethyl)-4-(prop-2-yn-1-yloxy)benzene resulted in the formation of compound **1**. Similarly, the reaction between methyl 1*H*-indole-6-carboxylate and *tert*-butyl 4-(bromomethyl)benzoate led to the generation of **2**. Subsequently, both compound **1** and compound **2** were subjected to hydrolysis using lithium hydroxide monohydrate, followed by acidification with hydrochloric acid to yield the carboxylic acids **3** and **4**. Compound **3** was then subjected to a HATU-mediated amide coupling reaction with *O*-tritylhydroxylamine, resulting in the synthesis of the key intermediate **5**. Subsequently, compound **6** was synthesized via another amide coupling reaction using **4** and *O*-benzylhydroxylamine hydrochloride as the reactants. Finally, the key intermediate **7** was obtained by removing the *tert*-butyl protecting group in **6** using trifluoroacetic acid (TFA).

Scheme 1B displays the synthesis of IMiD-based CRBN ligands. Starting from commercially available 2-(2,6-dioxopiperidin-3-yl)-4-fluoroisoindoline-1,3-dione, substitution reactions between this starting material and either 2-(2-(2-azidoethoxy)ethoxy)ethan-1-amine (**linker 1**) or 2-(2-(2-(2-azidoethoxy)ethoxy)ethoxy)ethan-1-amine (**linker 2**) yielded compound **8** and compound **9**, respectively. Similarly, reactions involving *tert*-butyl (6-aminohexyl)carbamate (**linker 3**) or *tert*-butyl (7-aminoheptyl)carbamate (**linker 4**) produced compounds **10** and **11**, respectively. For the synthesis of intermediate **12**, the phenol hydroxyl group in the commercially available 2-(2,6-dioxopiperidin-3-yl)-4-hydroxyisoindoline-1,3-dione was substituted with 1-chloro-6-iodohexane, affording the target compound with a chlorine atom at the terminus of the attached linker. Subsequently, the chlorine atom in compound **12** was replaced with an azido group, leading to the formation of compound **13**.

Scheme 1C shows the synthesis of PG-based CRBN ligands. The process begins with the deprotection of the readily available compound **14** using TFA to release the free carboxylic acid group. This deprotected product was then subjected to the HATU-mediated amide coupling reactions with **linker 1**−**4**, resulting in the formations of compound **15**−**18**. In an analogous fashion, intermediate **19** was obtained via esterification with 6-chlorohexan-1-ol. Afterward, the chlorine atom in compound **19** was subsequently replaced with an azido group to yield compound **20**.

https://doi.org/10.1021/acs.jmedchem.5c00939
J. Med. Chem. 2026, 69, 918−943

Scheme 1. Synthesis of HDAC8 Ligands and Linker-Attached CRBN Ligands[a]

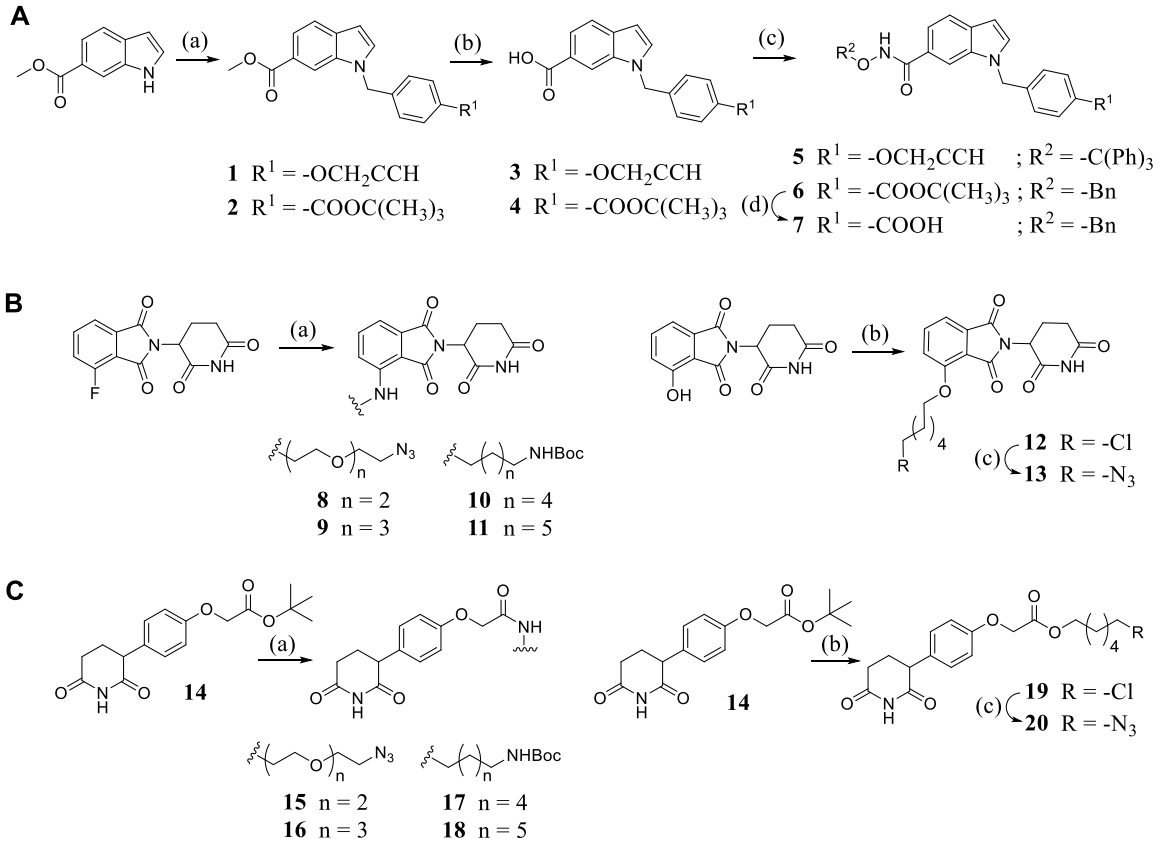

[a]Reagents and conditions: (**A**): (a) 1-(Bromomethyl)-4-(prop-2-yn-1-yloxy)benzene or *tert*-butyl 4-(bromomethyl)benzoate, Cs_2CO_3, ACN, Reflux, 2.5−6 h, 88−92%; (b) (i) LiOH × H_2O, THF/MeOH/H_2O, 50 °C, 21 h, (ii) HCl (0.5 M in H_2O), 49−82% (Two-step Yield); (c) *O*-Tritylhydroxylamine or *O*-benzylhydroxylamine Hydrochloride, HATU, DIPEA, Anhydrous DMF, rt, 15−16 h, 54−82%; (d) TFA, CH_2Cl_2, rt, 2 h. (**B**): (a) 2-(2-(2-Azidoethoxy)ethoxy)ethan-1-amine, 2-(2-(2-(2-azidoethoxy)ethoxy)ethoxy)ethan-1-amine, *tert*-butyl (6-aminohexyl)carbamate, or *tert*-butyl (7-aminoheptyl)carbamate, DIPEA, Anhydrous DMF, 90 °C, 15−17 h, 28−41%; (b) 1-Chloro-6-iodohexane, KI, $NaHCO_3$, Anhydrous DMF, Dark, 50 °C, 16 h, 71%; (c) NaN_3, DMF, 90 °C, 17 h, 72%. (**C**): (a) (i) TFA, CH_2Cl_2, rt, 2 h, (ii) 2-(2-(2-azidoethoxy)ethoxy)ethan-1-amine, 2-(2-(2-(2-azidoethoxy)ethoxy)ethoxy)ethan-1-amine, *tert*-butyl (6-aminohexyl)carbamate, or *tert*-butyl (7-aminoheptyl)carbamate, HATU, DIPEA, Anhydrous DMF, rt, 16−23 h, 40−76%; (b) (i) TFA, CH_2Cl_2, rt, 2 h, (ii) 6-Chlorohexan-1-ol, HATU, DIPEA, Anhydrous DMF, rt, 16 h, 67%; (c) NaN_3, DMF, 90 °C, 17 h, 86%.

Following the synthesis of HDAC8 ligands and linker-attached E3 ligase recruiters, the key intermediates for the desired HDAC8 PROTACs were synthesized using either Cu(I)-catalyzed azide−alkyne cycloadditions or amide coupling reactions. Scheme 2 summarizes the synthesis of the key intermediates **21**−**30**, the IMiD-based HDAC8 PROTACs **BP1**−**BP5**, as well as the PG-based degraders **BP6**−**BP10**. Briefly, compounds **8**, **9**, **13**, **15**, **16**, and **20**, each bearing an azido group at the linker terminus, were subjected to Cu(I)-catalyzed azide−alkyne cycloaddition reactions with compound **5**, leading to the formation of compounds **21**−**23** and **26**−**28**. These key intermediates contain a trityl-protected hydroxamic acid moiety. Subsequently, the trityl protecting group in **21**−**23** were removed by treatment with TFA in the presence of triisopropylsilane to generate the IMiD-based HDAC8 PROTACs **BP1**−**BP3**. Similarly, the deprotection of **26**−**28** afforded the PG-based HDAC8 PROTACs **BP6**-**BP8**. For the synthesis of the precursors **24**, **25** and **29**, **30** with a benzyl protecting group, compounds **10**, **11** and compounds **17**, **18** were first treated with TFA to remove the Boc-protecting group. The resulting deprotected products were then subjected to amide coupling reactions to yield the key intermediates **24**, **25** and **29**, **30**. Finally, the benzyl protecting groups in compounds **24**, **25** were removed under a hydrogen atmosphere using Pd/C (5%) as a catalyst to release the zinc-binding groups and to afford the desired IMiD-based HDAC8 PROTACs **BP4**−**BP5**. Similarly, the PG-based HDAC8 PROTACs **BP9**−**BP10** were derived from compounds **29**, **30** using the same approach. The structures of the synthesized HDAC8 PROTACs are summarized in Figure 3.

Target Engagement Assays and Physicochemical Properties

All synthesized PROTACs were first evaluated for their in vitro inhibitory activity against HDAC8 in fluorogenic enzyme inhibition assays using Leu(Ac)-Gly-Lys(TFA)-AMC as substrate.[34,35] The results are summarized in Table 1. Overall, all HDAC8 PROTACs, except **BP5**, exhibited inhibitory activities with IC_{50} values in the submicromolar concentration range, suggesting effective target engagement of HDAC8 in vitro. To further investigate cellular CRBN target engagement, NanoBRET assays were conducted as described in previously reported protocols.[36,37] All tested compounds exhibited IC_{50} values within the single- or double-digit micromolar range, confirming CRBN target engagement and cell permeability. Consistent with previous studies,[38] most IMiD-based HDAC8

https://doi.org/10.1021/acs.jmedchem.5c00939
J. Med. Chem. 2026, 69, 918−943

Scheme 2. Synthesis of IMiD- and PG-Based HDAC8 PROTACs[a]

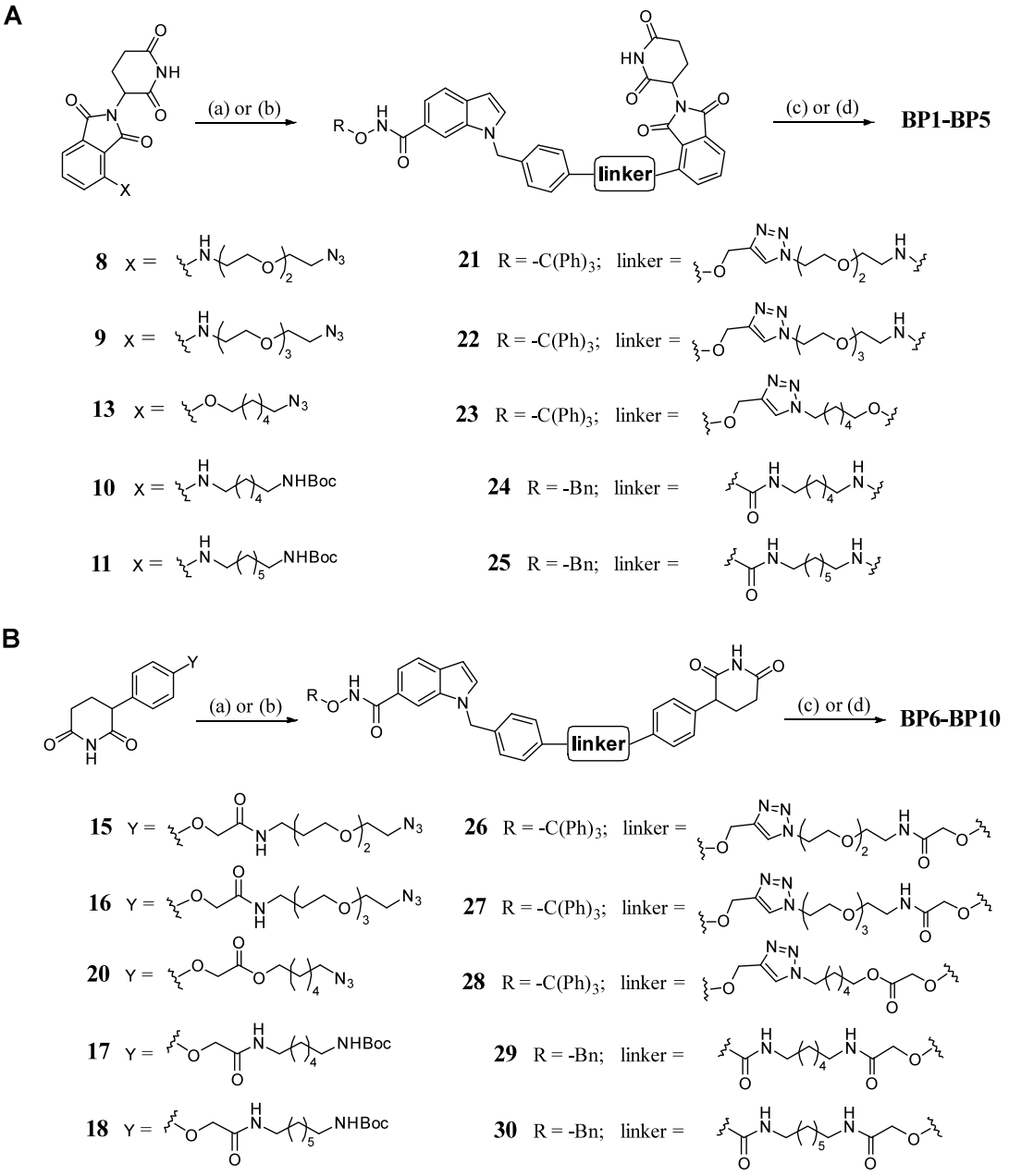

[a]Reagents and conditions: (**A** and **B**): (a) applied for **8**, **9**, **13**, **15**, **16**, and **20**: **5**, L-ascorbic Acid, $CuSO_4$, DMF/H_2O (10:1), rt, 2−4.5 h, 70−94%; (b) applied for **10**, **11**, **17**, and **18**: (i) TFA, DCM, rt, 2 h, (ii) **7**, HATU, DIPEA, Anhydrous DMF, rt, 16 h, 38−60% (Two-step Yields); (c) applied for **21**−**23** and **26**−**28**: Triisopropylsilane, TFA, DCM, rt, 2.5 h, 21−73%. (d) applied for **24**, **25** and **29**, **30**: H_2, Pd/C, EtOH/MeOH, rt, Overnight, 39−45%.

PROTACs showed autofluorescence signals at high concentrations in the NanoBRET assay. Compounds affected with high background fluorescence are marked with an asterisk in Table 1 and the reported IC_{50} values represent upper estimates. Interestingly, most PG-based HDAC8 degraders (except for **BP8** vs **BP3**), displayed stronger inhibition of HDAC8 but a weaker CRBN engagement compared to their IMiD-based counterparts. Next, we compared the physicochemical property profiles of PROTACs **BP1**−**BP10** along with the inhibitors PCI-34051 and CC-220. The phthalimide-based degraders displayed significantly higher lipophilicity ranging between elog D = 2.2 and 2.8 compared to PG-derived PROTACs, except for **BP8**. Notably, the lipophilicity of **BP1** to **BP5** is higher than those of the parent inhibitors, which might positively influence the permeability of the PROTACs. Degraders assembled via click chemistry (**BP1**−**BP3**, **BP6**−**BP8**) display a higher topological polar surface area due to the introduction of polar nitrogen atoms in the linker. Furthermore, we have determined the binding to human serum albumin, the most abundant protein in human blood plasma. Due to the presence of the hydroxamic acid group, a generally high plasma protein binding (PPB) value was expected. Indeed, the percentage of bound compound was estimated to be higher than 95% for PCI-34051 and most of the PROTACs. **BP1** and **BP6** constitute exceptions from this trend, presumably due to the PEGylated linker type.

https://doi.org/10.1021/acs.jmedchem.5c00939
J. Med. Chem. 2026, 69, 918−943

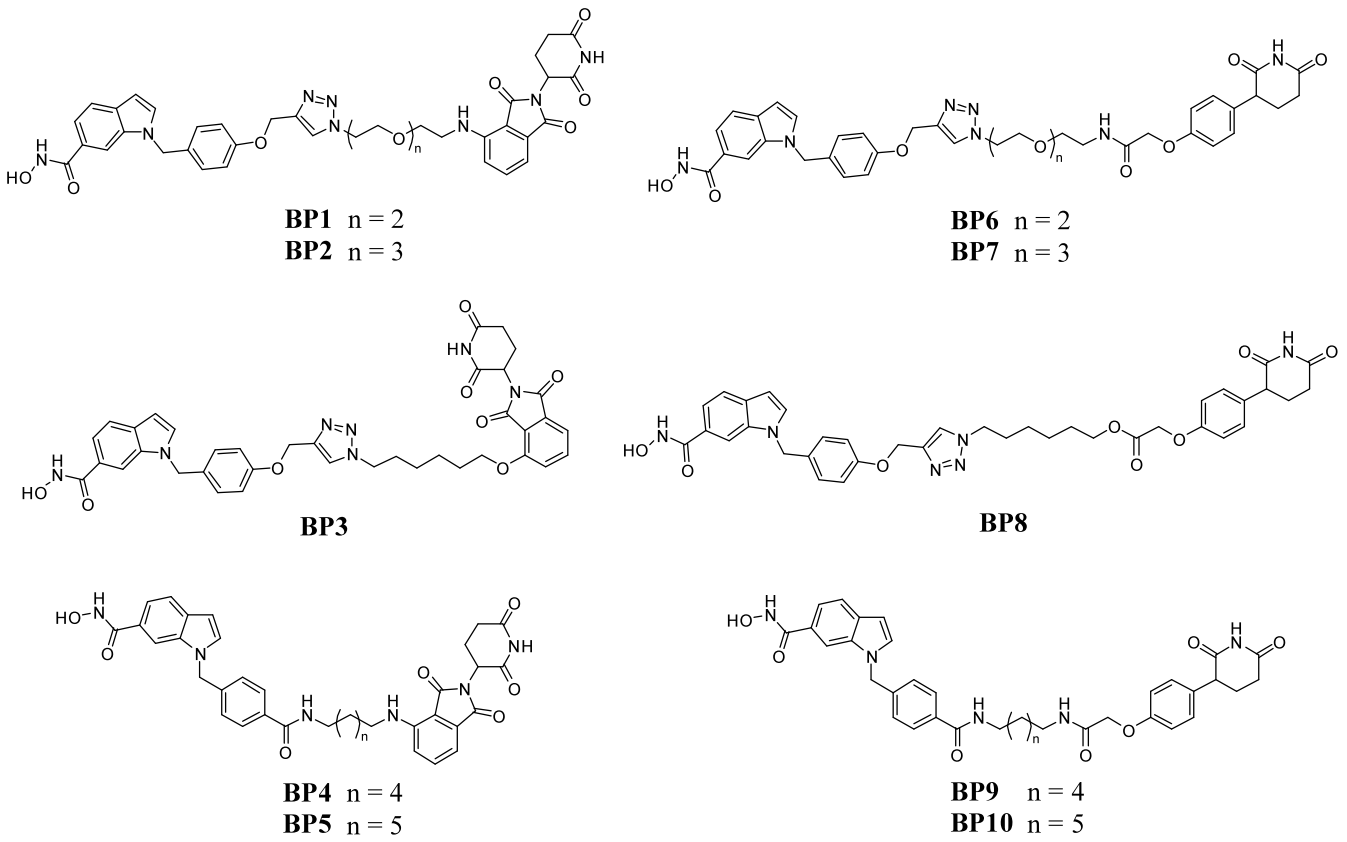

Figure 3. Structures of the IMiD- and PG-based HDAC8 PROTACs **BP1**−**BP10**.

Table 1. Evaluation of BP1−**BP10 for Target Engagement, Physicochemical Properties, and Maximal Degradation of HDAC8**

	IC_{50} (μM)							
compd	HDAC8[a]	CRBN[b]	M_r (g/mol)	elog $D_{7.4}$[c]	TPSA (Å^2)[d]	PPB (%)[e]	NRotB[f]	$D_{24\ h}$ (%)[g]
BP1	0.46 ± 0.05	7.5*	750.8	2.3	208	95	11	83
BP2	0.41 ± 0.02	0.13*	794.8	2.2	217	97	21	94
BP3	0.50 ± 0.05	1.6	719.8	2.5	187	97	16	92
BP4	0.62 ± 0.06	10*	664.7	2.5	179	97	15	53
BP5	1.07 ± 0.03	1.3*	678.8	2.8	179	97	16	93
BP6	0.26 ± 0.00	30	739.8	1.6	196	93	21	93
BP7	0.25 ± 0.00	36	783.8	1.6	206	96	24	90
BP8	0.68 ± 0.06	1.0	708.8	2.5	176	97	19	0
BP9	0.25 ± 0.03	19	653.7	1.7	167	96	18	94
BP10	0.36 ± 0.01	11	667.8	1.9	167	96	19	91
PCI-34051	0.16 ± 0.01	n.d.	296.3	1.8	63	96	5	n.d.
CC-220	n.d.	0.0015	449.5	1.6	88	85	6	n.d.

[a]Biochemical HDAC8 inhibition assay, Leu(Ac)-Gly-Lys(TFA)-AMC was used as substrate. [b]NanoBRET CRBN target engagement assay. Asterisks (*) indicate compounds with high background fluorescence; IC_{50} values should be considered as an upper estimate. n.d.: not determined. [c]Distribution coefficients at pH = 7.4 were estimated by a HPLC-based method. [d]Topological polar surface area is given in Å^2. [e]Plasma protein binding, experimentally determined percentage of compound bound to human serum albumin. [f]NRotB, number of rotatable bonds. [g]$D_{24\ h}$, maximal degradation of HDAC8 after treatment of MM.1S cells for 24 h with 5 μM of the respective degrader.

HDAC8 Degradation, Effects on CRBN Neosubstrates, and Antiproliferative Activity

In the next step, compounds **BP1**−**BP10** were evaluated for their HDAC8 degradation efficacy in MM.1S cells. As shown in Figure 4A, most degraders achieved substantial HDAC8 degradation at 5 μM after 24 h of incubation, except for **BP8** from the PG-based series (see Table 1 for $D_{24\ h}$ values). Under the same conditions, the protein levels of GSPT1 and IKZF3, known neosubstrates of CRBN ligands, were also assessed. As expected, strong degradation of IKZF3 was observed for IMiD-based degraders but not for the PG-based analogs. Significant GSPT1 degradation was induced by IMiD-based **BP1**−**BP2** and **BP4**−**BP5**, as well as the PG-based **BP10**.

To investigate the relationship between protein degradation and antiproliferative activity, we next evaluated the antiproliferative activity of the degraders in MM.1S and HL60 cells (Figure 4B). Interestingly, the IMiD-based PROTACs **BP1**−**BP5** displayed potent cytotoxicity in both cell lines, whereas the PG-based degraders **BP6**−**BP10** showed minimal or no antiproliferative effects. Specifically, the IMiD-based **BP1**−

https://doi.org/10.1021/acs.jmedchem.5c00939
J. Med. Chem. 2026, 69, 918−943

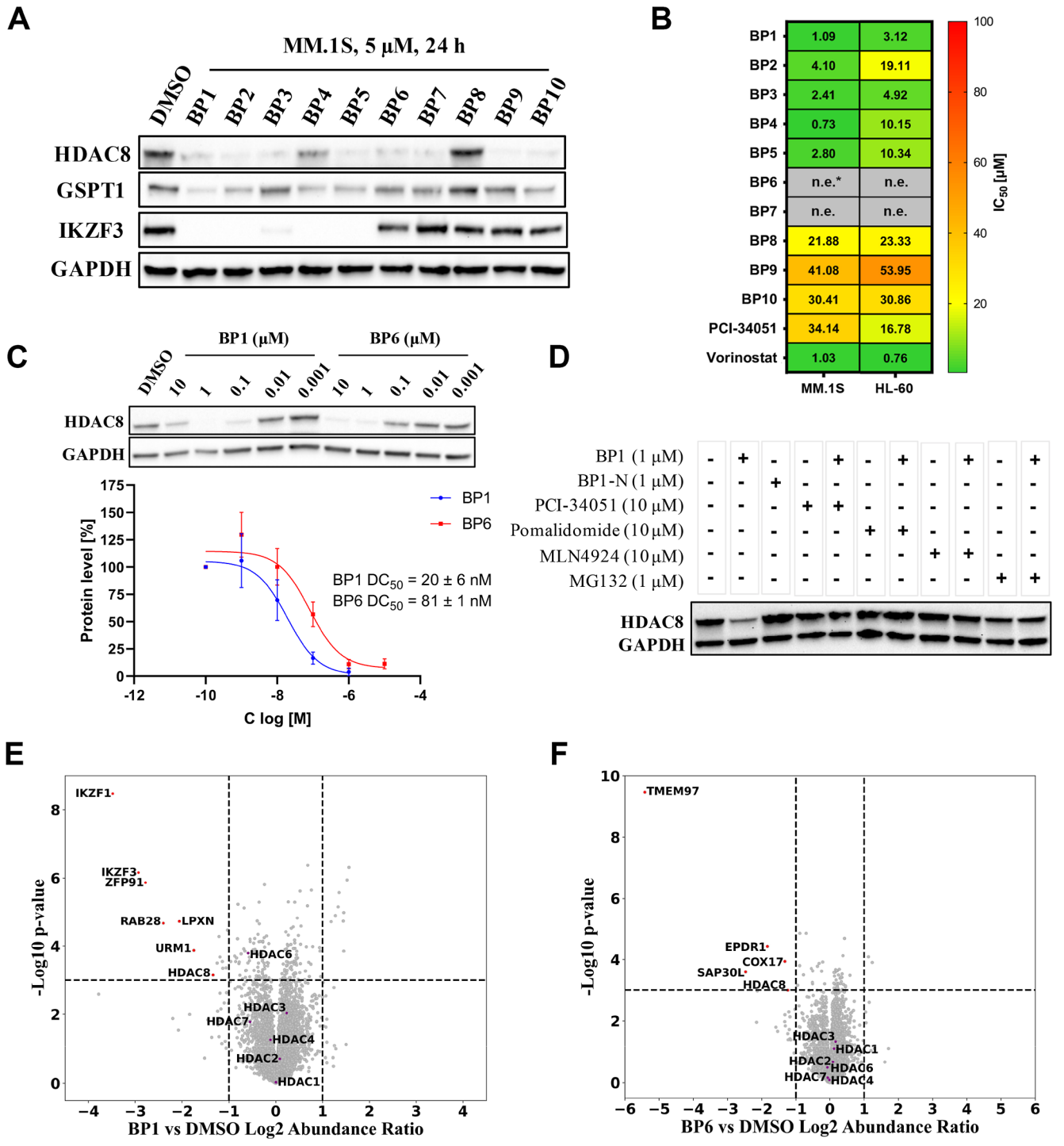

Figure 4. (A) Degradation of HDAC8, GSPT1, and IKZF3 mediated by HDAC8 PROTACs **BP1**−**BP10** in MM.1S cells. MM.1S cells were treated with **BP1**−**BP10** at a concentration of 5 μM for 24 h. HDAC8, GSPT1 and IKZF3 levels were detected by immunoblot analysis. DMSO was used as vehicle control and GAPDH as loading control. Representative images from a total of n = 3 replicates. (B) Antiproliferative activity of **BP1**−**BP10** against MM.1S and HL-60 cells. (C) Determination of HDAC8 DC_{50} values for IMiD-based **BP1** and PG-based **BP6**. MM.1S cells treated for 24 h with **BP1** and **BP6** at different concentrations. HDAC8 levels were detected by immunoblot analysis. DMSO was used as vehicle control and GAPDH as loading control. Pooled data from n = 2 biologically independent experiments, each performed in triplicates. One representative image is shown. (D) Rescue experiment for HDAC8. Pretreatments of MM.1S cells for 30 min were carried out in the cotreatment groups containing the PCI-34051 (10 μM), pomalidomide (10 μM), MLN4924 (10 μM), as well as MG132 (1 μM). Afterward, **BP1** (1 μM) was added, and the cells were incubated for an additional 6 h. DMSO was used as vehicle control and GAPDH as loading control. **BP1** served as positive control and **BP1**−**N** as negative control. Representative image of n = 2 biologically independent experiments, each performed in duplicates. (E,F) Quantitative proteomics of MOLT-4 cell lysates after treatment with 1 μM of **BP1** (E) or **BP6** (F) for 24 h. Important hits are labeled in red dots with the thresholds: Fold change ≥ 2 and P value ≤ 0.001. Other HDAC subtypes are labeled in purple dots.

https://doi.org/10.1021/acs.jmedchem.5c00939
J. Med. Chem. 2026, 69, 918−943

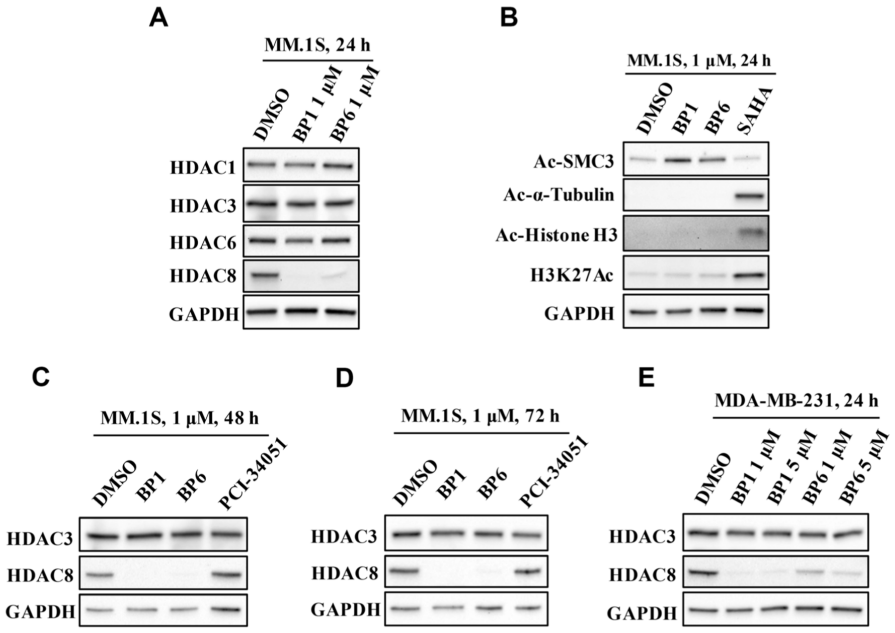

Figure 5. (A) Analysis of the HDAC8 selectivity of **BP1** and **BP6**. MM.1S cells were treated with **BP1** and **BP6** at a concentration of 1 μM for 24 h. HDAC1, HDAC3, HDAC6, and HDAC8 levels were detected by immunoblot analysis. DMSO was used as vehicle control and GAPDH as loading control. Representative images from a total of $n = 3$ replicates. (B) Analysis of protein levels of H3K27Ac, acetylated SMC3, α-tubulin, and histone H3. MM.1S cells were treated with **BP1** and **BP6** at a concentration of 1 μM for 24 h. Acetylated SMC3, acetylated α-tubulin, acetylated histone H3, and H3K27Ac levels were detected by immunoblot analysis. DMSO was used as vehicle control, vorinostat (SAHA) as positive control and GAPDH as loading control. Representative images of $n = 2$ biologically independent experiments, each performed in duplicates; H3K27Ac band from $n = 2$ biologically independent experiments. (C, D) Long-term degradation of HDAC3 and HDAC8 caused by **BP1** and **BP6**. MM.1S cells were treated with **BP1** and **BP6** at a concentration of 1 μM for 48 h (C) and 72 h (D). HDAC3 and HDAC8 levels were detected by immunoblot analysis. PCI-34051 was included as negative control. DMSO was used as vehicle control and GAPDH as loading control. Representative image from a total of $n = 3$ replicates (E) HDAC3 and HDAC8 degradation caused by **BP1** and **BP6** in MDA-MB-231 cells. MDA-MB-231 cells were treated with **BP1** and **BP6** at concentrations of 1 and 5 μM for 24 h. HDAC3 and HDAC8 levels were detected by immunoblot analysis. DMSO was used as vehicle control and GAPDH as loading control. Representative images from $n = 2$ replicates.

BP5 exhibited IC_{50} values ranging from 0.73 to 4.10 μM in MM.1S cells, with similar results observed in HL60 cells for **BP1** and **BP3**. These differences in antiproliferative activity between IMiD- and PG-based HDAC8 degraders may arise from their varying abilities to degrade neosubstrates. We further validated these findings in MM.1S and MV4−11 leukemia cells treated with pomalidomide alone, **BP6** alone, or their combination. While pomalidomide alone significantly reduced cell viability, **BP6** alone had no detectable effect. Importantly, the combination of **BP6** with pomalidomide did not produce any additional cytotoxicity compared to pomalidomide alone (Figure S2, Supporting Information). Based on the protein degradation and antiproliferative activity data, we selected the IMiD-based degrader **BP1** and the PG-based counterpart **BP6** for a detailed investigation.

DC_{50} Value Determination and Mode of Action Studies

Subsequently, to quantify the HDAC8 degradation efficiency of **BP1** and **BP6**, we determined their DC_{50} values. As shown in Figure 4C, both compounds displayed prominent HDAC8 degradation at low concentrations (e.g., 1 μM). A slight "hook effect" was observed at 10 μM for **BP1** but not for **BP6**. The quantification of the data revealed a DC_{50} value of 20 nM for **BP1** ($D_{max,\ 24\ h}$ = 99%), which was four times lower than that of **BP6** (DC_{50} = 81 nM, $D_{max,\ 24\ h}$ = 93%). Although the use of different cell lines complicates direct comparison, these results indicate that **BP1** and **BP6** exhibit enhanced degradation efficacy relative to the previously reported PCI-34051-based HDAC8 PROTAC 16e (DC_{50} = 580 nM in A549 cells).[26]

Since HDAC3 shares high structural similarity with HDAC8 and a previous study showed the dual degradation of these two subtypes,[28] we also investigated the HDAC3 degradation with both **BP1** and **BP6**. As a result, HDAC3 levels were not affected significantly at the tested concentrations (Figure S3, Supporting Information), confirming the selectivity for both compounds for HDAC8 over HDAC3. Additionally, time-course experiments were performed to examine the dynamics of HDAC8 degradation at 3, 6, 14, and 24 h. As shown in Figure S4 (Supporting Information), both compounds significantly degraded HDAC8 starting at 6 h, confirming their rapid activity in promoting HDAC8 degradation.

To confirm the involvement of ubiquitin-proteasome system (UPS) in the degradation of HDAC8 by **BP1**, rescue experiments were conducted using binding competitors as well as neddylation and proteasome inhibitors. Furthermore, the nondegrading control **BP1−N** (see Scheme S1, Supporting Information) containing a methylated glutarimide ring to prevent CRBN binding was synthesized and used for comparison. Due to the increased cytotoxicity from cotreatments and the confirmed HDAC8 degradation at 6 h, the treatment duration was reduced to 6 h. In the subsequent mode of action studies, MM.1S cells were pretreated for 0.5 h with competitors (PCI-34051 or pomalidomide), MLN4924 (neddylation inhibitor), or MG132 (proteasome inhibitor), followed by 6 h of treatment with **BP1** (1 μM); the results are summarized in Figure 4D. Only **BP1** alone induced significant HDAC8 degradation, whereas **BP1−N** had no effect. Furthermore, the HDAC8 level recovered for the groups

https://doi.org/10.1021/acs.jmedchem.5c00939
J. Med. Chem. 2026, 69, 918−943

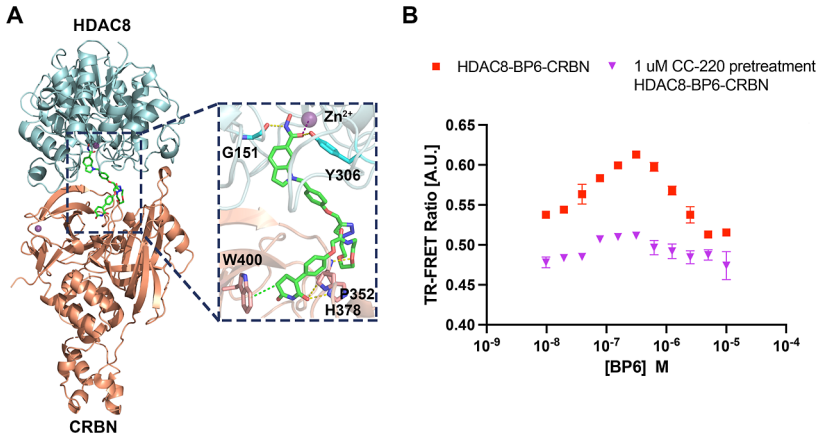

Figure 6. (A) Ternary complex modeling of HDAC8-**BP6**-CRBN using an established protocol.[40,41] HDAC8 is shown in light cyan and CRBN in light orange. Hydrogen bonds are shown as yellow dashes, H−π interactions are shown as green dashes and metal chelation is indicated as purple dashes. (B) TR-FRET ternary complex formation between HDAC8 and CRBN in the presence of **BP6**. CC-200 pretreatment (1 μM) diminished the formation of HDAC8-**BP6**-CRBN ternary complex. Data is shown as mean ± SD of n = 4 replicates.

with pretreatments, confirming that **BP1** induced HDAC8 degradation via HDAC8 and CRBN binding as well as neddylation-dependent proteasomal degradation.

Quantitative Proteomics, and Selectivity Studies

Next, we assessed the selectivity of **BP1** and **BP6** for HDAC subtype degradation using quantitative proteomics analysis. To this end, MOLT-4 cells were treated with 1 μM of **BP1** and **BP6** for 24 h. As shown in Figure 4E and Figure 4F, we successfully monitored the protein levels of HDAC1−4 and HDAC6−8. Significant HDAC8 degradation was observed for both **BP1** and **BP6**. Notably, none of other detected HDAC isoforms were significantly downregulated in both cases. Analysis of CRBN neosubstrate degradation revealed notable differences between **BP1** and **BP6**. PG-based **BP6** showed no reduction of protein levels of typical neosubstrates, whereas IMiD-based **BP1** induced significant degradation of well-characterized neosubstrates, including IKZF1, IKZF3, ZFP91, and RAB28. Overall, treatment with **BP1** resulted in a substantial alteration in the expression of approximately 250 and 200 upregulated and downregulated proteins, respectively, whereas **BP6** influenced the expression of only ∼60 and ∼40 proteins (Figure S5, Supporting Information). A considerable proportion of these differentially expressed proteins overlapped between **BP1** and **BP6**. This finding suggests that **BP6** exhibits greater specificity toward HDAC8 with reduced off-target effects, as indicated by the markedly lower number of proteins uniquely affected by **BP6** compared to **BP1**. These findings align closely with the immunoblot analysis results (Figure 4A) and provide a potential explanation for the distinct activity profiles observed in the viability assays (Figure 4B).

Based on these proteomics results, we further confirmed the selectivity of **BP1** and **BP6** through immunoblot analysis. In this experiment, HDAC1, HDAC3 and HDAC8 from class I HDACs as well as HDAC6 from class IIb were chosen as representative isoforms. Additionally, the levels of their substrate proteins Ac-histone H3 (known as a substrate for HDAC1−3), Ac-α-tubulin (known as HDAC6 substrate), and Ac-SMC3 (known as HDAC8 substrate) were also investigated. The results are summarized in Figure 5. As shown in Figure 5A, no significant degradation of HDAC1, HDAC3 and HDAC6 was observed for both compounds, consistent with the proteomics results, whereas HDAC8 was almost completely degraded. Figure 5B displays the levels of the monitored substrates; vorinostat (SAHA) was taken as a positive control. Notably, both **BP1** and **BP6** significantly upregulated Ac-SMC3 compared to the DMSO and vorinostat groups, indicating their potent HDAC8 inactivation. Again, the IMiD-based degrader **BP1** demonstrated stronger effects than the PG-based **BP6**, consistent with their DC_{50} values. Ac-α-tubulin, a marker of HDAC6 inhibition or degradation, showed no upregulation following **BP1** or **BP6** treatment, whereas a strong increase was observed with vorinostat. Similarly, neither degrader affected Ac-histone H3 levels, while vorinostat treatment induced histone H3 hyperacetylation. A previous study showed that H3K27 acetylation levels were inversely correlated with global HDAC8 protein levels.[26] Therefore, the Ac-histone H3 level was also investigated with a site-specific (Ac-Lys27) antibody. As shown in Figure 5B, H3K27Ac levels remained unchanged for both HDAC8 degraders. These results suggest that **BP1** and **BP6** reduce HDAC8 activity without affecting the activity of HDAC1 and HDAC6.

In summary, these findings confirm that both the IMiD-based **BP1** and PG-based degrader **BP6** selectively degrade HDAC8 without impacting other subtypes, identifying them as potent and selective HDAC8 degraders.

Compound Stability and Degradation in MDA-MB-231 Breast Cancer Cells

Compound stability is a critical factor in degrader development. Therefore, we assessed **BP1** and **BP6** for HDAC8 degradation in MM.1S cells following 48- and 72 h incubation periods. HDAC3 degradation was also investigated at these two time points. As shown in Figure 5C,D, no degradation for HDAC3 was observed, but both compounds effectively induced HDAC8 degradation even after 48 or 72 h of incubation, while the parent inhibitor PCI-34051 showed no reduction of HDAC8 level, as expected. However, HPLC experiments[39] indicated that a prolonged incubation of either PROTAC in PBS buffer at pH 7.4 led to a more pronounced decomposition of **BP1** compared to **BP6** (29% and 85% starting material left after 48 h, Figure S6, Supporting Information). Furthermore, **BP1** (Cl_{int} = 201 μL/min/mg) and **BP6** (Cl_{int} = 320 μL/min/mg) showed limited microsomal stability against human liver microsomes. Nevertheless, based on the data shown in Figure 5C,D, both compounds

https://doi.org/10.1021/acs.jmedchem.5c00939
J. Med. Chem. 2026, 69, 918−943

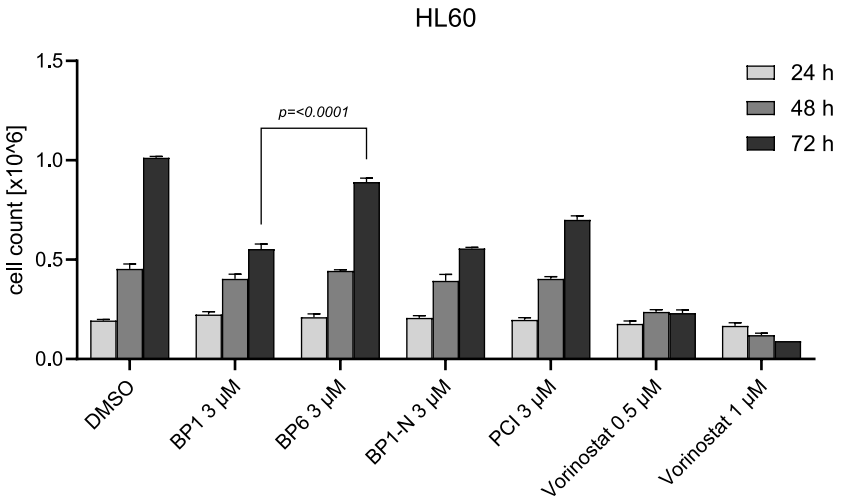

Figure 7. Cell proliferation assay was performed on HL60 leukemia cells treated with either DMSO, **BP1**, **BP6**, the nondegrading control **BP1−N** or PCI-34051 (PCI) at 3 μM. Vorinostat (0.5 μM or 1 μM) was included as a reference control. Cell counts were measured after 24, 48, and 72 h of treatment. The *y*-axis shows cell number, while the *x*-axis indicates the treatment conditions. Data represent mean ± standard deviation of three replicates per treatment group. Statistical analysis was performed using one-way ANOVA, followed by Tukey's multiple comparisons test to assess pairwise differences between groups. All data sets met the assumption of normality. Adjusted *P* values for all pairwise comparisons are provided in Supporting Information Table S1.

appear to be sufficiently stable to achieve potent and durable HDAC8 depletion.

To confirm that the degradation efficiency of **BP1** and **BP6** is not restricted to hematological cancers, we selected the triple-negative breast cancer cell line MDA-MB-231 as a representative solid cancer cell line. To this end, MDA-MB-231 cells were incubated with **BP1** or **BP6** in concentrations of 1 and 5 μM for 24 h; the results are depicted in Figure 5E. Under the tested conditions, significant HDAC8 degradation was observed in this cell line. The IMiD-based degrader **BP1** almost completely degraded HDAC8 and exhibited stronger HDAC8 degradation compared to PG-based **BP6**, aligning with the results from MM.1S cells. These findings highlight **BP1**'s superior HDAC8 degradation potency over **BP6** in hematological and solid cancer cells. Consistently, HDAC3 levels were unchanged in this cell line under the tested conditions.

Ternary Complex Modeling and TR-FRET Ternary Complex Assays

To elucidate the underlying molecular mechanism of **BP1**- and **BP6**-induced HDAC8 degradation, the formation of HDAC8-**BP1**/**BP6**-CRBN ternary complexes was investigated using both in silico modeling and in vitro assays. As a result, the modeling revealed convincing ternary complex formation for both **BP1** (Figure S7A, Supporting Information) and **BP6** (Figure 6A). In both models, the hydroxamic acid ZBG chelated the Zn^{2+} ion in the HDAC8 active site and engaged in hydrogen bonds with G151 and Y306. In turn, the glutarimide group of the CRBN ligand formed a key hydrogen bond with H378, along with additional hydrogen bonds and arene-H interactions with the residues within the thalidomide-binding pocket. Collectively, these interactions stabilize the ternary complex formation for **BP1** and **BP6**. Consistently, TR-FRET assays confirmed robust ternary complex formation for **BP6**, which was reduced by pretreatment with the CRBN ligand iberdomide (CC-200) by blocking the CRBN binding site (Figure 6B). In contrast, autofluorescence interference precluded reliable assessment of **BP1** (Figure S7B, Supporting Information), consistent with the observations in the Nano-BRET CRBN engagement assay.

BP1 Treatment Inhibits Cellular Proliferation of HL60 Leukemia Cells

To evaluate the antileukemic activity of HDAC8-targeting PROTACs, HL60 leukemia cells were treated with **BP1**, **BP6**, the nondegrading control **BP1−N**, or PCI-34051 (3 μM). Vorinostat was used as a control for the proliferation assay (Figure 7). Treatment with **BP1** resulted in a significant reduction in cell proliferation at 72 h compared to **BP6** and **BP1−N**. These findings are consistent with proteomics data, which showed that the PG-based **BP6** did not reduce the protein levels of typical neosubstrates. In contrast, the IMiD-based **BP1** induced significant degradation of well-characterized neosubstrates, such as IKZF1 and IKZF3, potentially contributing to the inhibition of HL60 cell proliferation.

BP6 Synergizes with the MEK Inhibitor Cobimentinib

Since **BP6** treatment alone did not induce degradation of neosubstrates or exhibited antileukemic effects in HL60 cells, it may serve as a useful tool for studying the specific consequences of HDAC8 loss. Thus, to identify potential therapeutic vulnerabilities associated with HDAC8 degradation, we utilized an ex vivo high-throughput drug screening platform.[42,43] This platform included a library of 48 clinically relevant chemotherapeutics and targeted inhibitors commonly used in leukemia treatment (Table S2, Supporting Information). HL60 cells were pretreated with **BP6** (1 μM) for 6 h to induce HDAC8 degradation before being seeded onto drug library plates for an additional 72 h (Figure 8A). Notably, **BP6**-treated cells exhibited significantly increased sensitivity to the MEK inhibitor cobimetinib compared to vehicle-treated control (Figure 8B). To validate these findings, we performed combination experiments using **BP6** with cobimetinib at 500 nM, 1 μM, and 2 μM in HL-60 and MV4−11 leukemia cells. Across all conditions, particularly at the lower concentrations, **BP6** consistently enhanced the cytotoxic effects of cobimetinib (Figure 8C,D). As controls, we included HDAC8 inhibitor PCI-34051 as well as **BP8**, a less efficient HDAC8 degrader

https://doi.org/10.1021/acs.jmedchem.5c00939
J. Med. Chem. 2026, 69, 918−943

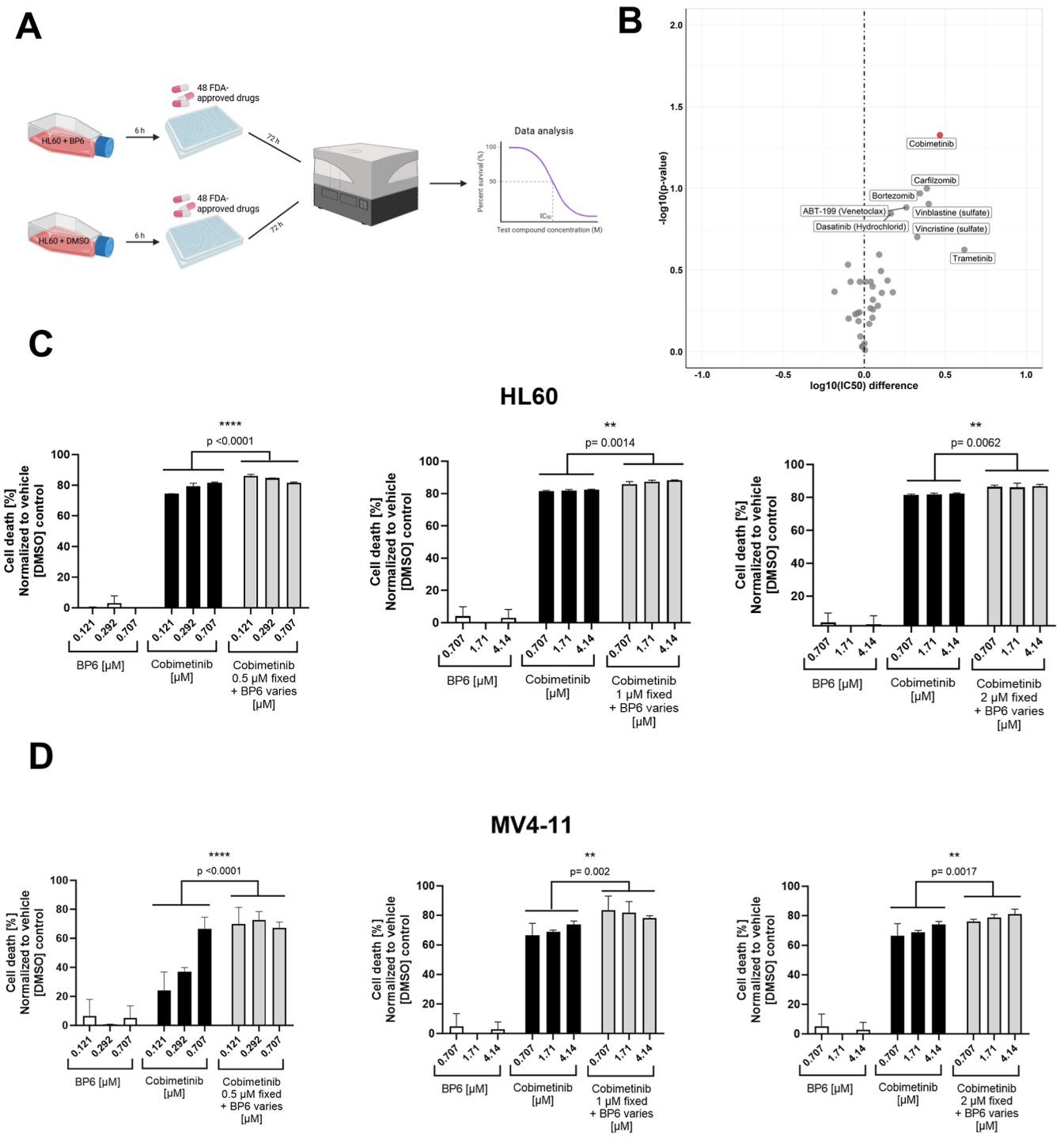

Figure 8. High-throughput drug combination screening. (A) HL60 cells were pretreated with either **BP6** (1 μM) or DMSO as a control for 6 h. Preprinted library plates containing of 48 FDA-approved agents used to treat leukemia were seeded with pretreated HL60 cells at a density of 0.04 $\times$ 10^6 per mL and incubated for 72 h. Cell viability was assessed via CellTiter-Glo luminescent assay and the IC_{50} values for the inhibitors were determined by plotting raw data (normalized to DMSO) with nonlinear regression [log(inhibitor) vs normalized response] variable slope function in GraphPadPrism. (B) Volcano Plot highlighting differential drug sensitivity after 6 h of **BP6** pretreatment vs DMSO. Threshold for significance was set to $p < 0.05$. Log10(IC_{50}) differences were calculated by subtracting the log10(IC_{50}) of the **BP6**-pretreated sample from that of the respective (DMSO) control. (C,D) Cell viability was assessed via CellTiter-Glo luminescent assay after 72 h. The *y*-axis shows cell death [%] normalized to each DMSO control, while the *x*-axis indicates the treatment conditions of cobimetinib (left) or **BP6** (middle and right). Error bars represent mean $\pm$ SD (n = 3). Statistical analysis was performed using two-way ANOVA, followed by Tukey's multiple comparisons test to assess pairwise differences between groups. All data sets met the assumption of normality.

from the same series as **BP6**. However, both PCI-34051 and **BP8** also increased sensitivity to cobimetinib to a similar extent as **BP6** (Figure S8, Supporting Information). These findings suggest that the observed enhancement of cobimetinib sensitivity is not solely dependent on HDAC8 degradation but is likely mediated by HDAC8 enzymatic inhibition. These

https://doi.org/10.1021/acs.jmedchem.5c00939
J. Med. Chem. 2026, 69, 918−943

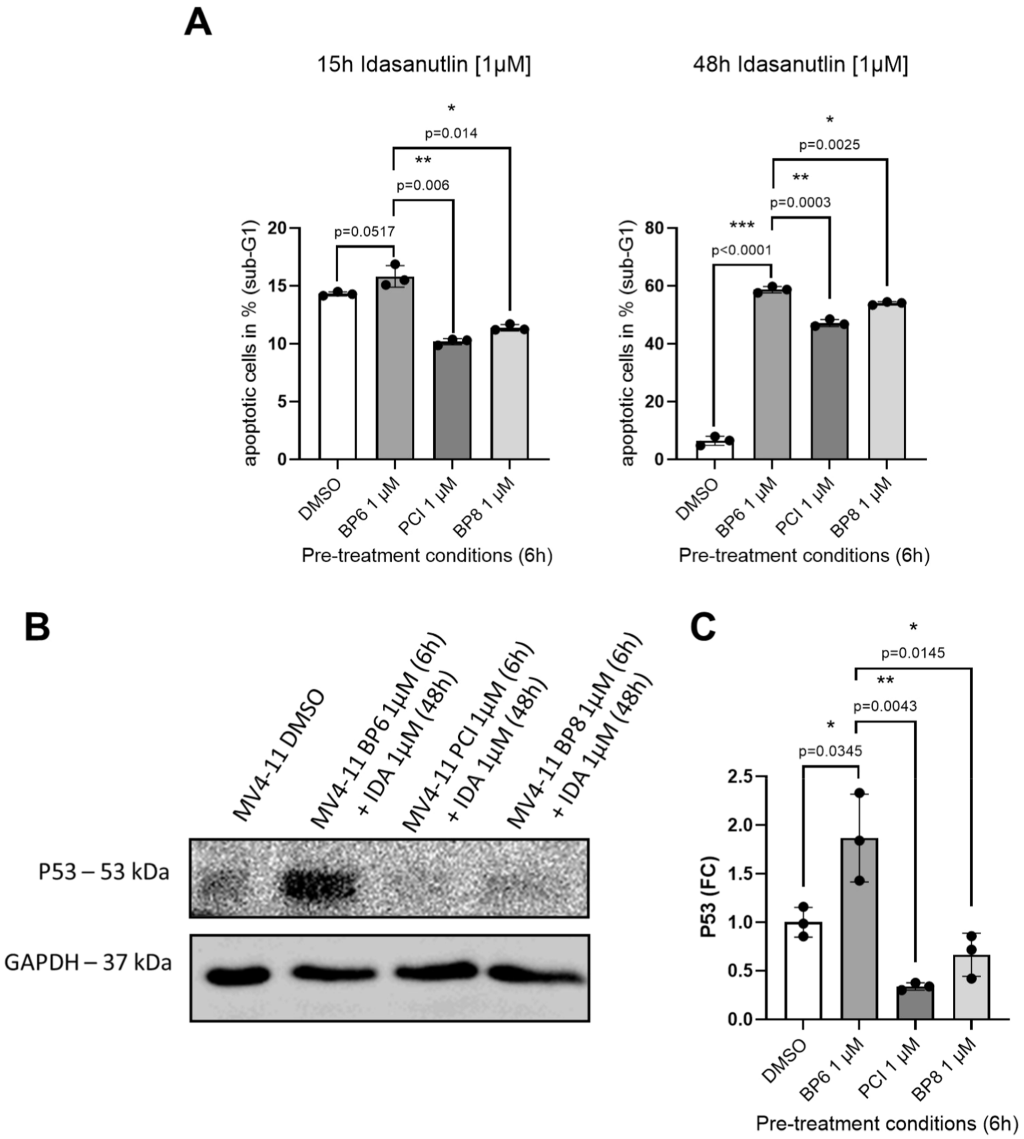

Figure 9. Effect of HDAC8 modulation on drug-induced cell death. (A) Cells were pretreated with either HDAC8 PROTAC (**BP6**), negative control PROTAC (**BP8**), or HDAC8 inhibitor (PCI) for 6 h prior to treatment with idasanutlin. Idasanutlin was treated at 1 μM. Apoptotic cells [%] were measured after 15 or 48 h. Error bars represent mean ± SD (n = 3). Statistical analysis was performed using a student's t-test (unpaired, two-tailed). (B) MV4−11 cells were pretreated with **BP6** for 6 h and followed by 48 h treatment of idasanutlin (IDA). Cell lysates were analyzed by Western blotting with antibodies against p53 and GAPDH. (C) Densitometric analysis of Western blot bands corresponding to p53 protein levels. Protein expression was normalized to the respective loading control (GAPDH) and presented relative to control conditions. Error bars represent mean ± SD (n = 3). Statistical analysis was performed using a student's t-test (unpaired, two-tailed).

results align with previous studies demonstrating that HDAC inhibition can potentiate sensitivity to MEK inhibitors,[44] suggesting that targeting HDAC8 may enhance the therapeutic efficacy of MEK inhibition in leukemia.

BP6-Mediated HDAC8 Degradation Stabilizes the Tumor Suppressor p53 and Sensitizes Leukemia Cells to MDM2 Inhibition

Previous studies have shown that HDAC8 interacts with and deacetylates p53, reducing its stability and pro-apoptotic activity, whereas HDAC8-deficient cells display p53 hyperactivation and increased apoptosis under genotoxic stress.[10,45] We therefore hypothesized that HDAC8 degradation would enhance p53 activation compared to HDAC8 inhibition. To investigate the impact of HDAC8 modulation on p53 activity and drug response, we compared selective HDAC8 degradation (**BP6**) with HDAC8 inhibition (PCI-34051) in TP53 wild-type MV4−11 cells. We also included **BP8**, a less efficient HDAC8 degrader from the same series as **BP6**, as a control. Pretreatment with **BP6** for 6 h sensitized MV4−11 cells to the MDM2 antagonist idasanutlin, leading to significantly higher apoptosis after 15 and 48 h of treatment, in contrast to PCI-34051 and **BP8** (Figure 9A). In line with the previous studies,[10,45] **BP6** pretreatment markedly increased p53 stability compared to PCI-34051 and **BP8** (Figure 9B). These findings highlight that **BP6**, despite its modest intrinsic cytotoxicity in leukemia cells, effectively primes p53-mediated apoptosis and represents a promising candidate for combinatorial therapeutic strategies targeting p53-dependent pathways in leukemia.

■ CONCLUSIONS

This study reports on the design, synthesis, and biological evaluation of two sets of HDAC8 PROTACs. Both series

https://doi.org/10.1021/acs.jmedchem.5c00939
J. Med. Chem. 2026, 69, 918−943

utilize PCI-34051 as a selective HDAC8 warhead in combination with established linkers and either IMiD- or PG-based CRBN recruiters. This strategy led to the discovery of IMiD-based **BP1** and its PG-based counterpart **BP6** as potent and highly selective HDAC8 degraders with a $DC_{50,\ 24\ h}$ of 20 nM and 81 nM in MM.1S cells, respectively. Interestingly, **BP1** and **BP6** exhibited notable differences in several aspects, particularly in cytotoxicity, neosubstrates degradation, and chemical stability. Specifically, the IMiD-based **BP1** induced potent degradation of GSPT1 and IKZF3, accompanied by promising cytotoxicity in MM.1S and HL60 cells, whereas the PG-based **BP6** showed neither neosubstrate degradation nor cellular toxicity. Notably, the PG-based **BP6** demonstrated significantly greater chemical stability than the IMiD-based **BP1** in PBS buffer (pH 7.4) after 48 h of incubation. **BP6** pretreatment promoted p53 stabilization, leading to a significantly stronger sensitization of leukemia cells to the MDM2 inhibitor (idasanutlin) than observed with PCI-34051. These findings highlight **BP6** as a promising candidate for combinatorial approaches that potentiate p53 signaling while sparing neosubstrate degradation.

EXPERIMENTAL SECTION

Chemistry

General Information. Chemicals and solvents are commercially available and used without further purification, if not stated otherwise. For all HPLC purposes, acetonitrile in HPLC-grade quality (HiPerSolv CHROMANORM, VWR) was used. Water was purified with a PURELAB flex (ELGA VEOLIA). Air-sensitive reactions were carried out under nitrogen or argon atmosphere. Mixtures of two or more solvents are specified as "solvent A"/"solvent B", 3/1, *v*/*v*; meaning that 100 mL of the respective mixture consists of 75 mL of "solvent A" and 25 mL of "solvent B". Thin-layer chromatography (TLC) was carried out on prefabricated plates (silica gel 60, F_{254}, Merck). Components were visualized either by irradiation with ultraviolet light (254 or 366 nm) or by staining appropriately. Column Chromatography: If not stated otherwise, column chromatography was carried out on silica gel (60 Å, 40−60 μm, Acros Organics). In addition, a flash column system (puriFlash XS 520 Plus, Advion Interchim Scientific) was utilized for the purification of the synthesized compounds. Nuclear Magnetic Resonance Spectroscopy (NMR): Proton (^{1}H) and carbon (^{13}C) NMR spectra were recorded either on a Bruker AVANCE 500 MHz at a frequency of 500 MHz (^{1}H) and 126 MHz (^{13}C) or on a Bruker AVANCE III HD 600 MHz at a frequency of 600 MHz (^{1}H) and 151 MHz (^{13}C). The chemical shifts are given in parts per million (ppm). As solvents deuterated chloroform ($CDCl_3$) and deuterated dimethyl sulfoxide (DMSO-d_6) were used. The residual solvent signal ($CDCl_3$: ^{1}H NMR: 7.26 ppm, ^{13}C NMR: 77.1 ppm; DMSO-d_6: ^{1}H NMR: 2.50 ppm, ^{13}C NMR: 39.52 ppm) was used for calibration. The multiplicity of each signal is reported as singulet (s), doublet (d), triplet (t), quartet (q), pentet (p), sextet (sext), multiplet (m) or combinations thereof. Multiplicities and coupling constants are reported as measured and might disagree with the expected values. Mass Spectrometry: High resolution electrospray ionization mass spectra (HRMS-ESI) were acquired with Bruker Daltonik GmbH micrOTOF coupled to a an LC Packings Ultimate HPLC system and controlled by micrOTOFControl3.4 and HyStar 3.2-LC/MS, with a BrukerDaltonik GmbH ESI-qTOF Impact II coupled to a Dionex UltiMateTM 3000 UHPLC system and controlled by micrOTOFControl 4.0 and HyStar 3.2-LC/MS or with a micrOTOF-Q mass spectrometer (Bruker) with ESI-source coupled with an HPLC Dionex UltiMate 3000 (Thermo Scientific). Low resolution electrospray ionization mass spectra (LRMS-ESI) were acquired with an Advion expression compact mass spectrometer (CMS) coupled with an automated TLC plate reader Plate Express (Advion). High Performance Liquid Chromatography (HPLC): A Thermo Fisher Scientific UltiMate 3000 UHPLC system with a Nucleodur 100−5C18 (250 × 4.6 mm, Macherey Nagel) with a flow rate of 1 mL/min and a temperature of 25 °C or a 100−5 C18 (100 × 3 mm, Macherey Nagel) with a flow rate of 0.5 mL/min and a temperature of 25 °C with an appropriate gradient were used. For preparative purposes a AZURA Prep. 500/1000 gradient system (Knauer) with a Nucleodur 110−5 C18 HTec (150 × 32 mm, Macherey Nagel) column with 20 mL/min was used. Detection was implemented by UV absorption measurement at a wavelength of λ = 220 nm and λ = 250 nm. Bidest. H_2O (A) and ACN (B) were used as eluents with an addition of 0.1% TFA for eluent A. **Purity:** The purity of all final compounds was 95% or higher. Purity was determined via HPLC with the Nucleodur 100−5 C18 (250 × 4.6 mm, Macherey Nagel) at 250 nm. After column equilibration for 5 min, a linear gradient from 5% A to 95% B in 5 min followed by an isocratic regime of 95% B for 12 min was used.

General Procedures

General Procedure a for the Synthesis of Compound 21−23 and 26−28. To the solution of cereblon ligands with an azido group at the linker terminus (1 equiv) in DMF/H_2O (5 mL/0.5 mL), compound **5** (1.05 equiv), ascorbic acid (3 equiv), and $CuSO_4$ (1 equiv) were added. The mixture was stirred at room temperature for 2−4.5 h. Next, the mixture was poured into water (100 mL) and extracted with ethyl acetate (3 × 30 mL). The combined organic layer was then washed with water (3 × 50 mL) and followed by brine (50 mL), dried over anhydrous Na_2SO_4, filtered, and concentrated in vacuo to provide the crude products, which were then purified by silica column chromatography.

General Procedure B for the Synthesis of Compound 24−25 and 29−30. To a solution of cereblon ligands with an Boc-protected amino group at the linker terminus (1 equiv) in DCM (5 mL), TFA (2 mL) was added and the mixture was stirred at room temperature for 2 h. The complete removal of *tert*-butyl group was monitored by TLC. Afterward, the mixture was dried in vacuo to provide the crude product for the next step. To a solution of compound **7** (1.05 equiv) in anhydrous DMF (3 mL), HATU (2 equiv) and DIPEA (3 equiv) were added. The mixture was stirred at room temperature for 0.5 h. Afterward, a solution of the respective Boc-deprotected compound (1 equiv) in anhydrous DMF (2 mL) was added and the reaction mixture was then stirred for 16 h at room temperature. The mixture was poured into water (100 mL) and extracted with ethyl acetate (3 × 30 mL). The combined organic layer was then washed with water (3 × 50 mL) and brine (50 mL), dried over anhydrous Na_2SO_4, filtered, and concentrated in vacuo to yield the crude products, which were subsequently purified by silica column chromatography.

General Procedure C for the Synthesis of Compounds BP1−BP3 and BP6−BP8. To a solution of compound **21−23** and **26−28** in DCM (5 mL), triisopropylsilane (0.5 mL) was added. The mixture was stirred for 30 min, followed by the addition of TFA (2 mL). The reaction was then stirred at room temperature for 2.5 h. Subsequently, the solvents were evaporated under reduced pressure and the crude product was purified by reverse-phase flash column chromatography (0→100% ACN in water, 0−30 min).

General Procedure D for the Synthesis of Compounds BP4−BP5 and BP9−BP10. To a solution of compound **24−25** and **29−30** (1 equiv) in methanol/ethanol (10 mL), Pd/C (5% palladium on carbon, 0.05 equiv) was added. The flask was evacuated and flushed with H_2 and the mixture was stirred at room temperature under H_2 atmosphere overnight. The completion of the reaction was monitored by HPLC and additional $Pd(OH)_2/C$ (0.05 equiv) was added to the system if the conversion was not complete.[46] The resulting reaction solution was filtered over Celite and the solvents were removed under reduced pressure. The subsequent purification was carried out utilizing reverse-phase flash column chromatography (0→100% ACN in water, 0−30 min).

*Methyl 1-(4-(prop-2-yn-1-yloxy)benzyl)-1H-indole-6-carboxylate (**1**).* To a solution of 1-(bromomethyl)-4-(prop-2-yn-1-yloxy)benzene (2.40 g, 10.7 mmol, 1 equiv) and Cs_2CO_3 (6.95 g, 21.3 mmol, 2 equiv) in acetonitrile (150 mL), methyl 1*H*-indole-6-carboxylate

https://doi.org/10.1021/acs.jmedchem.5c00939
J. Med. Chem. 2026, 69, 918−943

(2.05 g, 11.7 mmol, 1.1 equiv) was added. The mixture was refluxed for 2.5 h. The completion of the reaction was monitored by TLC. The solvent was removed in vacuo. The crude product was then dissolved in a mixture of ethyl acetate (100 mL) and water (100 mL). The extraction was performed with the ethyl acetate (3 × 100 mL) and the combined organic layers were washed with brine and dried over anhydrous Na_2SO_4. The filtrate was concentrated in vacuo to afford the crude product, which was then purified by silica column (CyH/EtOAc 3:1, *v*/*v*) to yield compound **1** (3.01 g, 88%). **^{1}H NMR** (600 MHz, $CDCl_3$) δ: 8.11 (d, J = 1.3 Hz, 1H), 7.80 (dd, J = 8.3, 1.4 Hz, 1H), 7.65 (d, J = 8.3 Hz, 1H), 7.25 (d, J = 3.1 Hz, 1H), 7.10 − 7.06 (m, 2H), 6.94 − 6.90 (m, 2H), 6.57 (dd, J = 3.1, 0.9 Hz, 1H), 5.32 (s, 2H), 4.66 (d, J = 2.4 Hz, 2H), 3.92 (s, 3H), 2.51 (t, J = 2.4 Hz, 1H). **^{13}C NMR** (151 MHz, $CDCl_3$) δ: 168.3, 157.3, 135.8, 132.4, 131.4, 130.1, 128.4, 123.5, 120.7, 120.7, 115.4, 112.1, 102.2, 78.5, 75.8, 56.0, 52.1, 49.7. **LC−MS (ESI)** $[M + H]^+$ m/z: 320.2.

*Methyl 1-(4-(tert-butoxycarbonyl)benzyl)-1H-indole-6-carboxylate (**2**).* To a solution of *tert*-butyl 4-(bromomethyl)benzoate (2.00 g, 7.38 mmol, 1 equiv) and Cs_2CO_3 (4.81 g, 14.8 mmol, 2 equiv) in acetonitrile (150 mL), methyl 1*H*-indole-6-carboxylate (1.42 g, 8.11 mmol, 1.1 equiv) was added. The mixture was refluxed for 6 h. The completion of the reaction was monitored by TLC. The crude product was obtained following the procedures for preparing compound **1**, which was then purified by silica column (CyH/EtOAc 4:1, *v*/*v*) to yield compound **2** (2.47 g, 92%). **^{1}H NMR** (600 MHz, $CDCl_3$) δ: 8.01 (d, J = 1.4 Hz, 1H), 7.92 − 7.89 (m, 2H), 7.80 (dd, J = 8.4, 1.4 Hz, 1H), 7.65 (dd, J = 8.4, 0.7 Hz, 1H), 7.26 − 7.23 (m, 1H), 7.10 (d, J = 8.1 Hz, 2H), 6.59 (dd, J = 3.1, 0.9 Hz, 1H), 5.41 (s, 2H), 3.88 (s, 3H), 1.55 (s, 9H). **^{13}C NMR** (151 MHz, CDCl3) δ: 168.2, 165.4, 141.7, 135.8, 132.5, 131.7, 131.5, 130.2, 126.5, 123.8, 120.9, 120.8, 112.0, 102.6, 81.3, 52.1, 50.0, 28.3. **LC−MS (ESI)** $[M - H]^-$ m/z: 364.1.

*1-(4-(Prop-2-yn-1-yloxy)benzyl)-1H-indole-6-carboxylic Acid (**3**).* To a solution of compound **1** (3.01 g, 9.43 mmol, 1 equiv) in THF/MeOH/H_2O (60 mL/12 mL/12 mL), LiOH·H_2O (0.593 g, 14.1 mmol, 1.5 equiv) was added. The mixture was stirred at room temperature for about 18 h. Heating at 50 °C for additional 1−2 h was performed when the reaction was not complete. Upon the completion of the hydrolysis, the solvents were removed in vacuo. The crude product was dissolved with water (50 mL) and acidified with HCl (0.5 M in water) until no more precipitate was formed. The resulting precipitate was collected via filtration, washed with water and dried in vacuo, followed by the purification with silica column (CyH/EtOAc 4:1, *v*/*v*) to yield compound **3** (2.55 g, 89%). **^{1}H NMR** (500 MHz, DMSO-d_6) δ: 12.53 (s, 1H), 8.08 (q, J = 1.0 Hz, 1H), 7.70 (d, J = 3.1 Hz, 1H), 7.65 − 7.60 (m, 2H), 7.18 − 7.12 (m, 2H), 6.95 − 6.90 (m, 2H), 6.57 (dd, J = 3.2, 0.9 Hz, 1H), 5.44 (s, 2H), 4.74 (d, J = 2.4 Hz, 2H), 3.50 (t, J = 2.4 Hz, 1H). **^{13}C NMR** (126 MHz, DMSO-d_6) δ: 168.2, 156.5, 134.9, 132.5, 131.8, 130.7, 128.1, 123.5, 120.1, 120.0, 114.9, 112.1, 101.3, 79.1, 78.1, 55.4, 48.6. **LC−MS (ESI)** $[M - H]^-$ m/z: 306.1.

*1-(4-(tert-Butoxycarbonyl)benzyl)-1H-indole-6-carboxylic Acid (**4**).* To a solution of compound **2** (2.00 g, 5.47 mmol, 1 equiv) in THF/MeOH/H_2O (60 mL/12 mL/12 mL), LiOH·H_2O (0.574 g, 13.7 mmol, 2.5 equiv) was added. The mixture was stirred at room temperature for about 20.5 h. The crude product was obtained following the procedures for preparing compound **3**, which was then purified by silica column (DCM: MeOH 15:1, *v*/*v*) to yield compound **4** (0.94 g, 49%). **^{1}H NMR** (600 MHz, $CDCl_3$) δ: 8.11 (dd, J = 1.6, 0.9 Hz, 1H), 7.93 (d, J = 8.3 Hz, 2H), 7.88 (dd, J = 8.4, 1.4 Hz, 1H), 7.69 (dd, J = 8.3, 0.6 Hz, 1H), 7.30 (d, J = 3.1 Hz, 1H), 7.14 (d, J = 8.3 Hz, 2H), 6.63 (dd, J = 3.1, 0.9 Hz, 1H), 5.44 (s, 2H), 1.56 (s, 9H). **^{13}C NMR** (151 MHz, $CDCl_3$) δ: 172.9, 165.4, 141.5, 135.8, 133.2, 132.0, 131.8, 130.2, 126.6, 122.7, 121.4, 120.9, 112.8, 102.8, 81.3, 50.1, 28.3. **LC−MS (ESI)** $[M - H]^-$ m/z: 350.2.

*1-(4-(Prop-2-yn-1-yloxy)benzyl)-N-(trityloxy)-1H-indole-6-carboxamide (**5**).* To a solution of compound **3** (2.50 g, 8.19 mmol, 1 equiv) in anhydrous DMF (50 mL) were added HATU (6.23 g, 16.4 mmol, 2 equiv) and DIPEA (3.17 g, 24.6 mmol, 3 equiv). The mixture was stirred for 30 min at room temperature, after which *O*-tritylhydroxylamine (3.38 g, 12.3 mmol, 1.5 equiv) was added into the system and the mixture was stirred for additional 15 h. Completion of the reaction was monitored by TLC. The mixture was poured into water (150 mL) and extracted with ethyl acetate (3 × 50 mL). The combined organic layers were then washed with water (3 × 50 mL), followed by brine (50 mL), dried over anhydrous Na_2SO_4, filtered, and concentrated in vacuo to yield the crude product, which was then purified by silica column (CyH/EtOAc 4:1, *v*/*v*) to afford compound **5** (2.49 g, 54%). **^{1}H NMR** (600 MHz, $CDCl_3$) δ: 7.87 (s, 1H), 7.63 (s, 1H), 7.56 (d, J = 7.6 Hz, 5H), 7.50 (d, J = 8.2 Hz, 1H), 7.37 − 7.26 (m, 10H), 7.19 (d, J = 3.1 Hz, 1H), 7.06 (d, J = 8.3 Hz, 1H), 7.04 − 7.00 (m, 2H), 6.91 − 6.87 (m, 2H), 6.50 (d, J = 3.1 Hz, 1H), 5.22 (s, 2H), 4.66 (d, J = 2.4 Hz, 2H), 2.51 (t, J = 2.4 Hz, 1H). **^{13}C NMR** (151 MHz, $CDCl_3$) δ: 167.4, 157.3, 142.1, 135.7, 131.6, 130.9, 130.0, 129.8, 129.1, 128.4, 128.1, 128.1, 127.9, 127.8, 127.4, 125.5, 120.8, 115.4, 110.1, 102.0, 93.3, 78.5, 75.8, 56.0, 49.7. **LC−MS (ESI)** $[M - H]^-$ m/z: 561.4.

*tert-Butyl 4-((6-((benzyloxy)carbamoyl)-1H-indol-1-yl)methyl)benzoate (**6**).* To a solution of compound **4** (0.94 g, 2.67 mmol, 1 equiv) in anhydrous DMF (30 mL) were added HATU (2.03 g, 5.35 mmol, 2 equiv) and DIPEA (1.04 g, 8.02 mmol, 3 equiv). The mixture was stirred for 30 min at room temperature, after which *O*-benzylhydroxylamine hydrochloride (0.85 g, 5.35 mmol, 2 equiv) was added into the system and the mixture was stirred for 16 h. The crude product was obtained following the procedures for preparing compound **5**, which was then purified by silica column (CyH/EtOAc 2:1, *v*/*v*) to yield compound **6** (1.00 g, 82%). **^{1}H NMR** (600 MHz, $CDCl_3$) δ: 7.92 − 7.87 (m, 2H), 7.79 − 7.76 (m, 1H), 7.61 (d, J = 8.3 Hz, 1H), 7.47 − 7.41 (m, 2H), 7.40 − 7.33 (m, 3H), 7.29 (dd, J = 8.2, 1.4 Hz, 1H), 7.24 (d, J = 3.1 Hz, 1H), 7.09 (d, J = 8.1 Hz, 2H), 6.59 (dd, J = 3.1, 0.8 Hz, 1H), 5.39 (s, 2H), 5.03 (s, 2H), 1.57 (s, 9H). **^{13}C NMR** (151 MHz, $CDCl_3$) δ: 167.3, 165.4, 141.5, 136.0, 135.6, 131.8, 131.8, 131.1, 130.2, 129.5, 128.9, 128.8, 126.6, 125.3, 121.2, 117.7, 110.0, 102.6, 81.3, 78.4, 50.1, 28.3. **LC−MS (ESI)** $[M + H]^+$ m/z: 457.4. Compound **7** was obtained by removing the *tert*-butyl protecting group in compound **6** using TFA.

*4-((2-(2-(2-Azidoethoxy)ethoxy)ethyl)amino)-2-(2,6-dioxopiperidin-3-yl)isoindoline-1,3-dione (**8**).* As reported,[47] to a solution of 2-(2,6-dioxopiperidin-3-yl)-4-fluoroisoindoline-1,3-dione (0.20 g, 0.72 mmol, 1 equiv) in anhydrous DMF (10 mL) were added **linker 1** (0.14 g, 0.80 mmol, 1.1 equiv) and DIPEA (0.19 g, 1.5 mmol, 2 equiv). The mixture was stirred at 90 °C for 17 h. The completion of the reaction was monitored by HPLC. The mixture was cooled and poured into water (100 mL) and extracted with ethyl acetate (3 × 30 mL). The combined organic layer was then washed with water (3 × 50 mL), followed by brine (50 mL), dried over anhydrous Na_2SO_4, filtered, and concentrated in vacuo to yield the crude product, which was then purified by silica column (CyH/EtOAc, 1:1, *v*/*v*) to afford compound **8** (0.17 g, 34%). **^{1}H NMR** (600 MHz, $CDCl_3$) δ: 8.37 (s, 1H), 7.48 (dd, J = 8.5, 7.1 Hz, 1H), 7.09 (d, J = 7.1 Hz, 1H), 6.92 (d, J = 8.5 Hz, 1H), 6.49 (t, J = 5.7 Hz, 1H), 4.91 (dd, J = 12.4, 5.3 Hz, 1H), 3.73 (t, J = 5.4 Hz, 2H), 3.67 (s, 6H), 3.47 (q, J = 5.5 Hz, 2H), 3.37 (t, J = 5.0 Hz, 2H), 2.90 − 2.68 (m, 3H), 2.11 (ddt, J = 10.5, 5.4, 2.5 Hz, 1H). **^{13}C NMR** (151 MHz, $CDCl_3$) δ: 171.3, 169.4, 168.6, 167.7, 147.0, 136.2, 132.6, 116.9, 111.8, 110.4, 70.8, 70.8, 70.2, 69.7, 50.8, 49.0, 42.5, 31.5, 22.9. **LC−MS (ESI)** $[M + H]^+$ m/z: 431.3.

*4-((2-(2-(2-(2-Azidoethoxy)ethoxy)ethoxy)ethyl)amino)-2-(2,6-dioxopiperidin-3-yl)isoindoline-1,3-dione (**9**).* To a solution of 2-(2,6-dioxopiperidin-3-yl)-4-fluoroisoindoline-1,3-dione (0.20 g, 0.72 mmol, 1 equiv) in anhydrous DMF (10 mL) were added **linker 2** (0.17 g, 0.80 mmol, 1.1 equiv) and DIPEA (0.19 g, 1.45 mmol, 2 equiv). The mixture was stirred at 90 °C for 17 h. The crude product was obtained following the procedures for preparing compound **8**, which was then purified by silica column (CyH/EtOAc 1:2, *v*/*v*) to yield compound **9** (0.14 g, 41%). **^{1}H NMR** (600 MHz, $CDCl_3$) δ: 8.12 (s, 1H), 7.49 (dd, J = 8.5, 7.1 Hz, 1H), 7.10 (d, J = 7.1 Hz, 1H), 6.93 (d, J = 8.5 Hz, 1H), 4.91 (dd, J = 12.3, 5.4 Hz, 1H), 3.72 (t, J = 5.4 Hz, 2H), 3.70 − 3.63 (m, 10H), 3.47 (t, J = 5.4 Hz, 2H), 3.38 (t, J = 5.0 Hz, 2H), 2.92 − 2.85 (m, 1H), 2.84 − 2.69 (m, 2H), 2.12 (dtd, J = 11.7, 4.6, 4.1, 2.2 Hz, 1H). **^{13}C NMR** (151 MHz, $CDCl_3$) δ: 171.1,

https://doi.org/10.1021/acs.jmedchem.5c00939
J. Med. Chem. 2026, 69, 918−943

169.4, 168.4, 167.7, 147.0, 136.2, 132.6, 117.0, 111.8, 110.4, 70.9, 70.8, 70.2, 69.6, 50.8, 49.0, 42.6, 31.6, 22.9. **LC−MS (ESI)** $[M + H]^+$ m/z: 475.3.

*tert-Butyl (6-((2-(2,6-dioxopiperidin-3-yl)-1,3-dioxoisoindolin-4-yl)amino)hexyl)carbamate (**10**).* To a solution of 2-(2,6-dioxopiperidin-3-yl)-4-fluoroisoindoline-1,3-dione (0.225 g, 0.81 mmol, 1 equiv) in anhydrous DMF (10 mL) were added **linker 3** (0.18 g, 0.81 mmol, 1 equiv) and DIPEA (0.21 g, 1.63 mmol, 2 equiv). The mixture was stirred at 90 °C for 15.5 h. The crude product was obtained following the procedures for preparing compound **8**, which was then purified by silica column (DCM/EtOAc 5:1, *v*/*v*) to yield compound **10** (0.11 g, 28%). **^{1}H NMR** (600 MHz, $CDCl_3$) δ: 8.22 (s, 1H), 7.48 (dd, J = 8.5, 7.1 Hz, 1H), 7.08 (d, J = 7.0 Hz, 1H), 6.87 (d, J = 8.5 Hz, 1H), 4.91 (dd, J = 12.3, 5.3 Hz, 1H), 3.25 (t, J = 7.1 Hz, 2H), 3.10 (t, J = 7.1 Hz, 2H), 2.88 (dt, J = 16.7, 2.8 Hz, 1H), 2.84 − 2.69 (m, 2H), 2.15 − 2.09 (m, 1H), 1.66 (p, J = 7.2 Hz, 2H), 1.49 (p, J = 7.3 Hz, 2H), 1.43 (s, 9H), 1.41 (d, J = 7.1 Hz, 2H), 1.39 − 1.32 (m, 2H). **^{13}C NMR** (151 MHz, $CDCl_3$) δ: 171.2, 169.6, 168.5, 167.8, 156.2, 147.1, 136.3, 132.6, 116.8, 111.6, 110.0, 79.3, 49.0, 42.7, 40.6, 31.5, 30.1, 29.3, 28.6, 26.7, 26.6, 22.9. **LC−MS (ESI)** $[M - H]^-$ m/z: 471.3.

*tert-Butyl (7-((2-(2,6-dioxopiperidin-3-yl)-1,3-dioxoisoindolin-4-yl)amino)heptyl)carbamate (**11**).* To a solution of 2-(2,6-dioxopiperidin-3-yl)-4-fluoroisoindoline-1,3-dione (0.22 g, 0.80 mmol, 1 equiv) in anhydrous DMF (10 mL) were added **linker 4** (0.18 g, 0.80 mmol, 1 equiv) and DIPEA (0.21 g, 1.59 mmol, 2 equiv). The mixture was stirred at 90 °C for 15 h. The crude product was obtained following the procedures for preparing compound **8**, which was then purified by silica column (DCM/EtOAc 5:1, *v*/*v*) to yield compound **11** (0.14 g, 37%). **^{1}H NMR** (600 MHz, $CDCl_3$) δ: 8.18 (s, 1H), 7.49 (dd, J = 8.5, 7.1 Hz, 1H), 7.08 (d, J = 7.0 Hz, 1H), 6.87 (d, J = 8.5 Hz, 1H), 6.22 (s, 1H), 4.91 (dd, J = 12.3, 5.3 Hz, 1H), 4.56 (s, 1H), 3.25 (t, J = 7.0 Hz, 2H), 3.09 (d, J = 7.2 Hz, 2H), 2.88 (dd, J = 16.4, 4.0 Hz, 1H), 2.84 − 2.69 (m, 2H), 2.17 − 2.09 (m, 1H), 1.65 (p, J = 7.1 Hz, 2H), 1.47 (dd, J = 14.6, 7.5 Hz, 2H), 1.44 (s, 9H), 1.42 − 1.38 (m, 2H), 1.37 − 1.30 (m, 4H). **^{13}C NMR** (151 MHz, $CDCl_3$) δ: 171.1, 169.7, 168.6, 167.8, 156.2, 147.1, 136.3, 132.6, 116.8, 111.6, 110.0, 79.3, 49.0, 42.7, 40.7, 31.6, 30.1, 29.2, 29.0, 28.6, 26.9, 26.8, 23.0. **LC−MS (ESI)** $[M - H]^-$ m/z: 485.3.

*4-((6-Chlorohexyl)oxy)-2-(2,6-dioxopiperidin-3-yl)isoindoline-1,3-dione (**12**).* Following a reported method,[48] to a solution of 2-(2,6-dioxopiperidin-3-yl)-4-hydroxyisoindoline-1,3-dione (0.20 g, 0.73 mmol, 1 equiv) and 1-chloro-6-iodohexane (0.27 g, 1.09 mmol, 1.5 equiv) in DMF (10 mL) were added potassium iodide (72.6 mg, 0.44 mmol, 0.6 equiv) and $NaHCO_3$ (0.37 g, 4.38 mmol, 6 equiv). The mixture was stirred at 60 °C in the dark for 20 h. The completion of the reaction was monitored by TLC. After cooling to room temperature, the solution was filtered through Celite to remove the insoluble material, washed with ethyl acetate, and the filtrate was concentrated under reduced pressure to afford the crude product, which was then purified by silica column (CyH/EtOAc, 1:1, *v*/*v*) to yield compound **12** (0.20 g, 71%). **^{1}H NMR** (600 MHz, $CDCl_3$) δ: 8.11 (s, 1H), 7.67 (dd, J = 8.5, 7.3 Hz, 1H), 7.45 (d, J = 7.2 Hz, 1H), 7.21 (d, J = 8.4 Hz, 1H), 4.95 (dd, J = 12.5, 5.4 Hz, 1H), 4.18 (t, J = 6.4 Hz, 2H), 3.55 (t, J = 6.6 Hz, 2H), 2.93 − 2.85 (m, 1H), 2.85 − 2.69 (m, 2H), 2.12 (dtd, J = 12.4, 4.8, 2.2 Hz, 1H), 1.94 − 1.86 (m, 2H), 1.85 − 1.77 (m, 2H), 1.54 (tdd, J = 13.6, 6.2, 3.1 Hz, 4H). **^{13}C NMR** (151 MHz, $CDCl_3$) δ: 171.0, 168.2, 167.2, 165.8, 156.8, 136.7, 134.0, 119.0, 117.3, 115.9, 69.3, 49.2, 45.1, 32.5, 31.5, 28.9, 26.6, 25.3, 22.8. **LC−MS (ESI)** $[M + H]^+$ m/z: 393.2.

*4-((6-Azidohexyl)oxy)-2-(2,6-dioxopiperidin-3-yl)isoindoline-1,3-dione (**13**).* To a solution of compound **12** (0.20 g, 0.52 mmol, 1 equiv) in DMF (10 mL) was added sodium azide (0.17 g, 2.60 mmol, 5 equiv). The mixture was stirred at 90 °C for 16 h. The mixture was cooled, poured into water (100 mL), and extracted with ethyl acetate (3 × 30 mL). The combined organic layers were then washed with water (3 × 50 mL) and followed by brine (50 mL), dried over anhydrous Na_2SO_4, filtered, and concentrated in vacuo to yield the crude product, which was then purified by silica column (CyH/EtOAc, 1:1, *v*/*v*) to afford compound **13** (0.15 g, 72%). **^{1}H NMR** (600 MHz, $CDCl_3$) δ: 8.12 (s, 1H), 7.67 (dd, J = 8.5, 7.3 Hz, 1H), 7.45 (d, J = 7.3 Hz, 1H), 7.21 (d, J = 8.5 Hz, 1H), 4.95 (dd, J = 12.5, 5.4 Hz, 1H), 4.18 (t, J = 6.4 Hz, 2H), 3.29 (t, J = 6.9 Hz, 2H), 2.93 − 2.85 (m, 1H), 2.85 − 2.69 (m, 2H), 2.12 (dtd, J = 12.6, 4.9, 2.3 Hz, 1H), 1.94 − 1.85 (m, 2H), 1.64 (dt, J = 14.5, 7.0 Hz, 2H), 1.56 (dtd, J = 9.2, 7.2, 5.7 Hz, 2H), 1.51 − 1.43 (m, 2H). **^{13}C NMR** (151 MHz, $CDCl_3$) δ: 171.0, 168.2, 167.2, 165.8, 156.8, 136.6, 134.0, 119.0, 117.3, 115.9, 69.3, 51.5, 49.2, 31.5, 28.9, 28.9, 26.5, 25.6, 22.8. **LC−MS (ESI)** $[M - H]^-$ m/z: 398.2.

*N-(2-(2-(2-Azidoethoxy)ethoxy)ethyl)-2-(4-(2,6-dioxopiperidin-3-yl)phenoxy)acetamide (**15**).* The *tert*-butyl 2-(4-(2,6-dioxopiperidin-3-yl)phenoxy)acetate (compound **14**, 2.00 g) was synthesized following a previously reported method.[33] To a solution of compound **14** (0.125 g, 0.39 mmol, 1 equiv) in DCM (5 mL), TFA (2 mL) was added and the mixture was stirred at room temperature for 2 h. The complete removal of *tert*-butyl group was monitored by TLC. Afterward, the mixture was dried in vacuo to provide the crude product for the next step. To a solution of the resulting crude product in anhydrous DMF (5 mL), HATU (0.29 g, 0.76 mmol, 2 equiv) and DIPEA (0.15 g, 1.14 mmol, 3 equiv) were added. The mixture was stirred for 30 min at room temperature. Next, 2-(2-(2-azidoethoxy)-ethoxy)ethan-1-amine (0.10 g, 0.57 mmol, 1.5 equiv) was added to the reaction mixture and stirred for 23 h. The completion of the reaction was monitored by HPLC. The mixture was poured into water (100 mL) and extracted with ethyl acetate (3 × 30 mL). The combined organic layers were then washed with water (3 × 50 mL), followed by brine (50 mL), dried over anhydrous Na_2SO_4, filtered, and concentrated in vacuo to yield the crude product, which was then purified by silica column (EtOAc) to afford compound **15** (0.11 g, 70%). **^{1}H NMR** (600 MHz, $CDCl_3$) δ: 8.10 (s, 1H), 7.20 − 7.12 (m, 2H), 6.99 (t, J = 5.8 Hz, 1H), 6.96 − 6.90 (m, 2H), 4.49 (s, 2H), 3.73 (dd, J = 10.1, 5.1 Hz, 1H), 3.66 (t, J = 5.0 Hz, 2H), 3.65 − 3.58 (m, 6H), 3.56 (dd, J = 6.2, 4.6 Hz, 2H), 3.36 (t, J = 5.1 Hz, 2H), 2.74 (dt, J = 17.7, 5.1 Hz, 1H), 2.65 (ddd, J = 17.8, 10.3, 5.3 Hz, 1H), 2.33 − 2.17 (m, 2H). **^{13}C NMR** (151 MHz, $CDCl_3$) δ: 173.2, 172.3, 168.2, 156.9, 130.7, 129.6, 115.3, 70.7, 70.5, 70.2, 69.9, 67.6, 50.8, 47.4, 38.9, 31.2, 26.5. **LC−MS (ESI)** $[M + H]^+$ m/z: 420.3.

*N-(2-(2-(2-(2-Azidoethoxy)ethoxy)ethoxy)ethyl)-2-(4-(2,6-dioxopiperidin-3-yl)phenoxy)acetamide (**16**).* Compound **16** was synthesized following the procedure for compound **15**. After the reaction of deprotected compound **14** (65 mg, 0.25 mmol, 1 equiv), 2-(2-(2-(2-azidoethoxy)ethoxy)ethoxy)ethan-1-amine (81 mg, 0.37 mmol, 1.5 equiv), HATU (0.19 g, 0.49 mmol, 2 equiv) and DIPEA (96 mg, 0.74 mmol, 3 equiv) in anhydrous DMF (5 mL) for 23 h, compound **16** (45.5 mg, 40%) was obtained after the workup and purification (silica column, EtOAc) steps. **^{1}H NMR** (600 MHz, $CDCl_3$) δ: 8.14 (s, 1H), 7.19 − 7.13 (m, 2H), 7.02 (t, J = 5.8 Hz, 1H), 6.95 − 6.90 (m, 2H), 4.49 (s, 2H), 3.73 (dd, J = 10.2, 5.1 Hz, 1H), 3.68 − 3.62 (m, 8H), 3.62 − 3.57 (m, 4H), 3.55 (q, J = 5.3 Hz, 2H), 3.36 (t, J = 5.0 Hz, 2H), 2.74 (dt, J = 17.7, 5.1 Hz, 1H), 2.65 (ddd, J = 17.8, 10.3, 5.3 Hz, 1H), 2.31 − 2.17 (m, 2H). **^{13}C NMR** (151 MHz, $CDCl_3$) δ: 173.3, 172.3, 168.2, 156.9, 130.7, 129.6, 115.3, 70.8, 70.7, 70.7, 70.5, 70.2, 69.8, 67.6, 50.8, 47.4, 38.9, 31.2, 26.5. **LC−MS (ESI)** $[M - H]^-$ m/z: 462.3.

*tert-Butyl (6-(2-(4-(2,6-dioxopiperidin-3-yl)phenoxy)acetamido)-hexyl)carbamate (**17**).* Compound **17** was synthesized following the procedure for compound **15**. After the reaction of deprotected compound **14** (0.16 g, 0.63 mmol, 1 equiv), *tert*-butyl (6-aminohexyl)carbamate (0.14g, 0.66 mmol, 1.05 equiv), HATU (0.48 g, 1.25 mmol, 2 equiv) and DIPEA (0.24 g, 1.88 mmol, 3 equiv) in anhydrous DMF (10 mL) for 16 h, compound **17** (0.22 g, 76%) was obtained after the workup and purification (silica column, CyH/EtOAc, 2:1, *v*/*v*) steps. **^{1}H NMR** (600 MHz, $CDCl_3$) δ: 8.11 (s, 1H), 7.17 (d, J = 8.5 Hz, 2H), 6.96 − 6.89 (m, 2H), 6.56 (t, J = 5.6 Hz, 1H), 4.49 (s, 2H), 3.74 (dd, J = 10.2, 5.2 Hz, 1H), 3.33 (qd, J = 6.9, 3.6 Hz, 2H), 3.08 (t, J = 7.1 Hz, 2H), 2.74 (dt, J = 17.7, 5.0 Hz, 1H), 2.66 (ddd, J = 17.7, 10.3, 5.3 Hz, 1H), 2.33 − 2.18 (m, 2H), 1.72 (s, 2H), 1.53 (h, J = 7.0, 5.9 Hz, 2H), 1.44 (s, 9H), 1.31 (p, J = 3.8 Hz, 4H). **^{13}C NMR** (151 MHz, $CDCl_3$) δ: 173.3, 172.2, 168.1, 156.9, 156.2, 130.8, 129.7, 115.3, 79.4, 67.6, 47.4, 40.7, 39.0, 31.2,

https://doi.org/10.1021/acs.jmedchem.5c00939
J. Med. Chem. 2026, 69, 918−943

30.1, 29.6, 28.6, 26.5, 26.5, 26.4. **LC−MS (ESI)** $[M - H]^-$ *m/z*: 460.3.

*tert-Butyl (7-(2-(4-(2,6-dioxopiperidin-3-yl)phenoxy)acetamido)-heptyl)carbamate (**18**).* Compound **18** was synthesized following the procedure for compound **15**. After the reaction of deprotected compound **14** (0.14 g, 0.52 mmol, 1 equiv), *tert*-butyl (7-aminoheptyl)carbamate (0.13g, 0.54 mmol, 1.05 equiv), HATU (0.39 g, 1.03 mmol, 2 equiv) and DIPEA (0.20 g, 1.55 mmol, 3 equiv) in anhydrous DMF (10 mL) for 16 h, compound **18** (0.18 g, 73%) was obtained after the workup and purification (silica column, CyH/EtOAc, 2:1, *v/v*) steps. **^{1}H NMR** (600 MHz, $CDCl_3$) *δ*: 8.10 (s, 1H), 7.20 − 7.13 (m, 2H), 6.96 − 6.89 (m, 2H), 6.52 (d, *J* = 6.3 Hz, 1H), 4.49 (s, 2H), 3.74 (dd, *J* = 10.2, 5.1 Hz, 1H), 3.33 (dh, *J* = 13.1, 6.6 Hz, 2H), 3.09 (t, *J* = 7.1 Hz, 2H), 2.74 (dt, *J* = 17.7, 5.1 Hz, 1H), 2.66 (ddd, *J* = 17.7, 10.3, 5.3 Hz, 1H), 2.32 − 2.17 (m, 2H), 1.91 (s, 2H), 1.52 (p, *J* = 6.7 Hz, 2H), 1.44 (s, 9H), 1.34 − 1.24 (m, 6H). **^{13}C NMR** (151 MHz, $CDCl_3$) *δ*: 173.3, 172.2, 168.1, 156.9, 156.2, 130.8, 129.7, 115.3, 79.3, 67.6, 47.4, 40.7, 39.2, 31.3, 30.1, 29.6, 29.1, 28.6, 26.9, 26.8, 26.5. **LC−MS (ESI)** $[M - H]^-$ *m/z*: 474.3.

*6-Chlorohexyl 2-(4-(2,6-dioxopiperidin-3-yl)phenoxy)acetate (**19**).* Compound **19** was synthesized following the procedure for compound **15**. After the reaction of deprotected compound **14** (0.10 g, 0.38 mmol, 1 equiv), 6-chlorohexan-1-ol (62 mg, 0.46 mmol, 1.2 equiv), HATU (0.29 g, 0.76 mmol, 2 equiv) and DIPEA (0.15 g, 1.14 mmol, 3 equiv) in anhydrous DMF (5 mL) for 16 h, compound **19** (97 mg, 67%) was obtained after the workup and purification (silica column, CyH/EtOAc/Et_3N, 1:1:0.1, *v/v/v*) steps. **^{1}H NMR** (600 MHz, $CDCl_3$) *δ*: 7.98 (s, 1H), 7.14 (d, *J* = 8.6 Hz, 2H), 6.91 (d, *J* = 8.8 Hz, 2H), 4.62 (s, 2H), 4.21 (t, *J* = 6.6 Hz, 2H), 3.74 (dd, *J* = 9.9, 5.0 Hz, 1H), 3.52 (td, *J* = 6.7, 1.7 Hz, 2H), 2.73 (dt, *J* = 17.7, 5.2 Hz, 1H), 2.64 (ddd, *J* = 17.8, 10.1, 5.2 Hz, 1H), 2.32 − 2.16 (m, 2H), 1.76 (p, *J* = 6.9 Hz, 2H), 1.67 (p, *J* = 6.9 Hz, 2H), 1.50 − 1.42 (m, 2H), 1.40 − 1.31 (m, 2H). **^{13}C NMR** (151 MHz, $CDCl_3$) *δ*: 173.3, 172.3, 169.0, 157.5, 130.3, 129.4, 115.2, 65.6, 65.4, 47.3, 45.0, 32.5, 31.1, 28.5, 26.5, 26.5, 25.3. **LC−MS (ESI)** $[M - H]^-$ *m/z*: 380.1.

*6-Azidohexyl 2-(4-(2,6-dioxopiperidin-3-yl)phenoxy)acetate (**20**).* Compound **20** was synthesized following the procedure for compound **13**. After the reaction of compound **19** (91 mg, 0.24 mmol, 1 equiv), sodium azide (77 mg, 1.19 mmol, 5 equiv) in anhydrous DMF (5 mL) for 16 h at 90 °C, compound **20** (79 mg, 86%) was obtained after the workup and purification (silica column, CyH/EtOAc/Et_3N, 1:1:0.1, *v/v/v*) steps. **^{1}H NMR** (600 MHz, $CDCl_3$) *δ*: 7.98 (s, 1H), 7.14 (d, *J* = 8.7 Hz, 2H), 6.91 (d, *J* = 8.7 Hz, 2H), 4.62 (s, 2H), 4.21 (t, *J* = 6.6 Hz, 2H), 3.74 (dd, *J* = 9.9, 5.1 Hz, 1H), 3.26 (t, *J* = 6.9 Hz, 2H), 2.73 (dt, *J* = 17.7, 5.2 Hz, 1H), 2.64 (ddd, *J* = 17.7, 10.1, 5.2 Hz, 1H), 2.32 − 2.16 (m, 2H), 1.71 − 1.63 (m, 2H), 1.58 (d, *J* = 8.0 Hz, 2H), 1.44 − 1.31 (m, 4H). **^{13}C NMR** (151 MHz, $CDCl_3$) *δ*: 173.3, 172.3, 169.0, 157.5, 130.3, 129.4, 115.2, 65.6, 65.4, 51.4, 47.3, 31.1, 28.8, 28.5, 26.5, 26.4, 25.5. **LC−MS (ESI)** $[M - H]^-$ *m/z*: 387.2.

*1-(4-((1-(2-(2-(2-((2-(2,6-Dioxopiperidin-3-yl)-1,3-dioxoisoindolin-4-yl)amino)ethoxy)ethoxy)-ethyl)-1H-1,2,3-triazol-4-yl)methoxy)benzyl)-N-(trityloxy)-1H-indole-6-carboxamide (**21**).* Compound **21** was prepared following the **General procedure A** starting from compound **8** (0.10 g, 0.23 mmol, 1 equiv), compound **5** (0.14 g, 0.25 mmol, 1.05 equiv), ascorbic acid (0.12 g, 0.70 mmol, 3 equiv), and $CuSO_4$ (37 mg, 0.23 mmol, 1 equiv). The crude product was purified by silica column (DCM/MeOH, 50:1, *v/v*) to provide compound **21** (0.20 g, 85%). **^{1}H NMR** (600 MHz, $CDCl_3$) *δ*: 8.23 (s, 1H), 7.95 (s, 1H), 7.81 (s, 1H), 7.64 (s, 1H), 7.55 (d, *J* = 7.7 Hz, 5H), 7.49 (d, *J* = 8.3 Hz, 1H), 7.40 (dd, *J* = 8.5, 7.1 Hz, 1H), 7.31 (q, *J* = 6.5, 5.5 Hz, 6H), 7.29 − 7.27 (m, 2H), 7.26 − 7.22 (m, 1H), 7.18 (d, *J* = 3.1 Hz, 1H), 7.04 (d, *J* = 7.1 Hz, 2H), 6.98 (d, *J* = 8.4 Hz, 2H), 6.88 − 6.79 (m, 3H), 6.49 (d, *J* = 3.1 Hz, 1H), 5.19 (s, 2H), 5.10 (s, 2H), 4.85 (dd, *J* = 12.3, 5.3 Hz, 1H), 4.54 (t, *J* = 5.1 Hz, 2H), 3.87 (t, *J* = 5.0 Hz, 2H), 3.63 (t, *J* = 5.2 Hz, 2H), 3.62 − 3.54 (m, 4H), 3.38 (t, *J* = 5.2 Hz, 2H), 2.83 − 2.77 (m, 1H), 2.75 − 2.63 (m, 2H), 2.08 − 2.03 (m, 1H). **^{13}C NMR** (151 MHz, $CDCl_3$) *δ*: 171.6, 171.2, 169.5, 168.6, 167.7, 158.0, 147.0, 145.4, 142.2, 136.2, 132.6, 131.3, 130.9, 129.8, 129.1, 128.5, 128.1, 128.1, 127.9, 127.9, 127.4, 125.4, 124.2, 123.7, 121.2, 120.8, 116.8, 115.2, 111.9, 102.0, 82.2, 70.7, 70.6, 69.6, 69.4, 62.2, 50.5, 49.8, 49.0, 42.4, 31.5, 22.8. **LC−MS (ESI)** $[M - H]^-$ *m/z*: 991.6.

*1-(4-((1-(2-(2-(2-(2-((2-(2,6-Dioxopiperidin-3-yl)-1,3-dioxoisoindolin-4-yl)amino)ethoxy)ethoxy)-ethoxy)ethyl)-1H-1,2,3-triazol-4-yl)methoxy)benzyl)-N-(trityloxy)-1H-indole-6-carboxamide (**22**).* Compound **22** was prepared following the **General procedure A** starting from compound **9** (0.13 g, 0.27 mmol, 1 equiv), compound **5** (0.16 g, 0.29 mmol, 1.05 equiv), ascorbic acid (0.14 g, 0.82 mmol, 3 equiv), and $CuSO_4$ (43 mg, 0.27 mmol, 1 equiv). The crude product was purified by silica column (DCM/MeOH, 50:1, *v/v*) to provide compound **22** (0.21 g, 75%). **^{1}H NMR** (600 MHz, $CDCl_3$) *δ*: 8.22 (s, 1H), 7.93 (s, 1H), 7.81 (s, 1H), 7.64 (s, 1H), 7.55 (d, *J* = 7.6 Hz, 5H), 7.48 (d, *J* = 8.2 Hz, 1H), 7.43 (dd, *J* = 8.5, 7.1 Hz, 1H), 7.31 (q, *J* = 6.8, 6.3 Hz, 6H), 7.28 (d, *J* = 7.1 Hz, 2H), 7.24 (dd, *J* = 4.4, 1.6 Hz, 1H), 7.18 (d, *J* = 3.1 Hz, 1H), 7.06 (d, *J* = 7.1 Hz, 1H), 7.03 (d, *J* = 7.7 Hz, 1H), 7.00 (d, *J* = 8.4 Hz, 2H), 6.88 (d, *J* = 8.5 Hz, 2H), 6.84 (d, *J* = 8.5 Hz, 1H), 6.48 (d, *J* = 3.1 Hz, 1H), 5.20 (s, 2H), 5.14 (s, 2H), 4.87 (dd, *J* = 12.3, 5.4 Hz, 1H), 4.51 (t, *J* = 5.0 Hz, 2H), 3.85 (t, *J* = 5.0 Hz, 2H), 3.63 (t, *J* = 5.4 Hz, 2H), 3.62 − 3.58 (m, 4H), 3.57 (s, 4H), 3.38 (t, *J* = 5.4 Hz, 2H), 2.87 − 2.79 (m, 1H), 2.78 − 2.65 (m, 2H), 2.07 (ddd, *J* = 12.2, 6.2, 3.2 Hz, 1H). **^{13}C NMR** (151 MHz, $CDCl_3$) *δ*: 171.6, 171.2, 169.4, 168.5, 167.7, 158.0, 146.9, 145.4, 142.2, 136.2, 132.6, 131.4, 130.9, 129.8, 129.1, 128.5, 128.1, 128.1, 127.9, 127.9, 127.4, 125.4, 124.3, 123.7, 121.2, 120.8, 116.9, 115.2, 111.8, 102.0, 82.2, 70.8, 70.7, 70.6, 69.6, 69.5, 69.5, 62.2, 50.5, 49.8, 49.0, 42.4, 31.5, 22.9. **LC−MS (ESI)** $[M - H]^-$ *m/z*: 1035.7.

*1-(4-((1-(6-((2-(2,6-Dioxopiperidin-3-yl)-1,3-dioxoisoindolin-4-yl)oxy)hexyl)-1H-1,2,3-triazol-4-yl)methoxy)benzyl)-N-(trityloxy)-1H-indole-6-carboxamide (**23**).* Compound **23** was prepared following the **General procedure A** starting from compound **13** (0.10 g, 0.24 mmol, 1 equiv), compound **5** (0.14 g, 0.25 mmol, 1.05 equiv), ascorbic acid (0.13 g, 0.72 mmol, 3 equiv), and $CuSO_4$ (38 mg, 0.24 mmol, 1 equiv). The crude product was purified by silica column (DCM/MeOH, 30:1, *v/v*) to provide compound **23** (0.18 g, 78%). **^{1}H NMR** (600 MHz, $CDCl_3$) *δ*: 8.24 (s, 1H), 7.95 (s, 1H), 7.64 (t, *J* = 7.9 Hz, 3H), 7.54 (d, *J* = 7.7 Hz, 5H), 7.48 (d, *J* = 8.3 Hz, 1H), 7.42 (d, *J* = 7.2 Hz, 1H), 7.32 (t, *J* = 7.5 Hz, 6H), 7.28 (d, *J* = 7.2 Hz, 2H), 7.24 (dd, *J* = 4.0, 1.8 Hz, 1H), 7.20 − 7.14 (m, 2H), 7.04 (d, *J* = 8.4 Hz, 1H), 7.00 (d, *J* = 8.4 Hz, 2H), 6.91 − 6.86 (m, 2H), 6.48 (d, *J* = 3.1 Hz, 1H), 5.20 (s, 2H), 5.16 (s, 2H), 4.90 (dd, *J* = 12.4, 5.4 Hz, 1H), 4.36 (t, *J* = 7.1 Hz, 2H), 4.12 (tt, *J* = 9.3, 4.6 Hz, 2H), 2.78 (dtd, *J* = 30.0, 13.1, 12.7, 3.7 Hz, 2H), 2.66 (ddd, *J* = 16.3, 13.1, 4.8 Hz, 1H), 2.07 (dtd, *J* = 12.4, 7.0, 6.5, 3.9 Hz, 1H), 1.95 (p, *J* = 7.3 Hz, 2H), 1.83 (dt, *J* = 12.6, 6.1 Hz, 2H), 1.57 (p, *J* = 7.6 Hz, 2H), 1.40 (ddd, *J* = 15.2, 8.5, 6.2 Hz, 2H). **^{13}C NMR** (151 MHz, $CDCl_3$) *δ*: 171.1, 168.3, 167.1, 165.9, 158.0, 156.7, 147.0, 145.4, 142.1, 136.7, 133.9, 131.3, 130.9, 129.8, 129.1, 128.4, 128.1, 128.0, 127.9, 127.8, 127.4, 125.4, 123.0, 121.2, 120.8, 119.0, 116.0, 115.3, 110.2, 102.0, 82.1, 69.2, 62.3, 53.6, 50.2, 49.7, 49.2, 30.0, 28.6, 26.0, 25.3, 22.7. **LC−MS (ESI)** $[M - H]^-$ *m/z*: 960.6.

*N-(Benzyloxy)-1-(4-((6-((2-(2,6-dioxopiperidin-3-yl)-1,3-dioxoisoindolin-4-yl)amino)hexyl)-carbamoyl)benzyl)-1H-indole-6-carboxamide (**24**).* Compound **24** was prepared following the **General procedure B** starting from deprotected compound **10** (42 mg, 0.11 mmol, 1 equiv), compound **7** (47 mg, 0.12 mmol, 1.05 equiv), HATU (85 mg, 0.22 mmol, 2 equiv), and DIPEA (43 mg, 0.34 mmol, 3 equiv). The crude product was purified by silica column (CyH/EtOAc, 1:5, *v/v*) to provide compound **24** (51 mg, 60%). **^{1}H NMR** (600 MHz, DMSO-d_6) *δ*: 11.61 (s, 1H), 11.07 (s, 1H), 8.35 (t, *J* = 5.7 Hz, 1H), 7.91 (dt, *J* = 1.6, 0.8 Hz, 1H), 7.78 − 7.73 (m, 2H), 7.68 (d, *J* = 3.1 Hz, 1H), 7.61 (dd, *J* = 8.4, 0.7 Hz, 1H), 7.55 (dd, *J* = 8.6, 7.1 Hz, 1H), 7.44 (ddd, *J* = 8.2, 4.2, 1.6 Hz, 3H), 7.41 − 7.33 (m, 3H), 7.25 − 7.21 (m, 2H), 7.06 (d, *J* = 8.6 Hz, 1H), 7.00 (d, *J* = 7.0 Hz, 1H), 6.57 (dd, *J* = 3.1, 0.9 Hz, 1H), 6.51 (t, *J* = 5.9 Hz, 1H), 5.53 (s, 2H), 5.04 (dd, *J* = 12.8, 5.5 Hz, 1H), 4.92 (s, 2H), 3.27 (q, *J* = 6.7 Hz, 2H), 3.22 (q, *J* = 6.7 Hz, 2H), 2.87 (ddd, *J* = 17.1, 13.9, 5.5 Hz, 1H), 2.63 − 2.51 (m, 2H), 2.02 (dtd, *J* = 10.3, 5.2, 2.5 Hz, 1H), 1.56 (h, *J* = 7.0 Hz, 2H), 1.50 (p, *J* = 7.2 Hz, 2H), 1.34 (tdd, *J* = 15.2, 8.5, 4.8 Hz, 4H). **^{13}C NMR** (151 MHz, DMSO-d_6) *δ*: 172.8, 170.0, 168.9, 167.3,

https://doi.org/10.1021/acs.jmedchem.5c00939
J. Med. Chem. 2026, 69, 918−943

165.8, 165.3, 146.4, 140.9, 136.2, 136.0, 135.1, 134.0, 132.2, 131.9, 130.8, 128.9, 128.3, 128.2, 127.4, 126.6, 125.2, 120.2, 118.0, 117.1, 110.3, 109.7, 109.0, 101.4, 77.0, 48.8, 48.5, 41.8, 40.1, 30.9, 29.0, 28.6, 26.1, 26.0, 22.1. **LC−MS (ESI)** $[M + H]^+$ m/z: 755.5.

*N-(Benzyloxy)-1-(4-((7-((2-(2,6-dioxopiperidin-3-yl)-1,3-dioxoisoindolin-4-yl)amino)heptyl)-carbamoyl)benzyl)-1H-indole-6-carboxamide (**25**).* Compound **25** was prepared following the **General procedure B** starting from deprotected compound **11** (67 mg, 0.17 mmol, 1 equiv), compound **7** (73 mg, 0.18 mmol, 1.05 equiv), HATU (0.13 g, 0.35 mmol, 2 equiv), and DIPEA (68 mg, 0.52 mmol, 3 equiv). The crude product was purified by silica column (CyH/EtOAc, 1:5, *v/v*) to provide compound **25** (78 mg, 59%). **^{1}H NMR** (600 MHz, DMSO-d_6) δ: 11.61 (s, 1H), 11.07 (s, 1H), 8.34 (t, J = 5.7 Hz, 1H), 7.93 − 7.88 (m, 1H), 7.79 − 7.72 (m, 2H), 7.68 (d, J = 3.1 Hz, 1H), 7.63 − 7.59 (m, 1H), 7.55 (dd, J = 8.6, 7.0 Hz, 1H), 7.44 (ddd, J = 8.2, 4.4, 1.6 Hz, 3H), 7.40 − 7.33 (m, 3H), 7.23 (d, J = 8.2 Hz, 2H), 7.07 (d, J = 8.6 Hz, 1H), 7.00 (d, J = 7.0 Hz, 1H), 6.57 (dd, J = 3.1, 0.9 Hz, 1H), 6.50 (t, J = 5.9 Hz, 1H), 5.53 (s, 2H), 5.04 (dd, J = 12.9, 5.5 Hz, 1H), 4.92 (s, 2H), 3.27 (q, J = 6.6 Hz, 2H), 3.21 (q, J = 6.7 Hz, 2H), 2.87 (ddd, J = 17.0, 13.9, 5.4 Hz, 1H), 2.62 − 2.51 (m, 2H), 2.05 − 1.99 (m, 1H), 1.56 (p, J = 6.9 Hz, 2H), 1.49 (p, J = 7.2 Hz, 2H), 1.37 − 1.26 (m, 6H). **^{13}C NMR** (151 MHz, DMSO-d_6) δ: 172.8, 170.0, 168.9, 167.3, 165.7, 165.3, 146.4, 140.9, 136.2, 136.0, 135.1, 134.0, 132.2, 131.9, 130.7, 128.8, 128.3, 128.2, 127.4, 126.6, 125.2, 120.2, 118.0, 117.1, 110.3, 109.7, 109.0, 101.4, 76.9, 48.8, 48.5, 41.8, 40.1, 30.9, 29.0, 28.6, 28.4, 26.4, 26.3, 22.1. **LC−MS (ESI)** $[M + H]^+$ m/z: 769.5.

*1-(4-((1-(2-(2-(2-(2-(4-(2,6-Dioxopiperidin-3-yl)phenoxy)-acetamido)ethoxy)ethoxy)ethyl)-1H-1,2,3-triazol-4-yl)methoxy)-benzyl)-N-(trityloxy)-1H-indole-6-carboxamide (**26**).* Compound **26** was prepared following the **General procedure A** starting from compound **15** (60 mg, 0.14 mmol, 1 equiv), compound **5** (85 mg, 0.15 mmol, 1.05 equiv), ascorbic acid (76 mg, 0.43 mmol, 3 equiv), and $CuSO_4$ (23 mg, 0.14 mmol, 1 equiv). The crude product was purified by silica column (DCM/MeOH, 15:1, *v/v*) to provide compound **26** (0.10 g, 72%). **^{1}H NMR** (600 MHz, $CDCl_3$) δ: 8.00 (d, J = 5.6 Hz, 2H), 7.75 (s, 1H), 7.63 (s, 1H), 7.55 (d, J = 7.7 Hz, 5H), 7.49 (d, J = 8.3 Hz, 1H), 7.31 (q, J = 7.1 Hz, 6H), 7.29 − 7.27 (m, 2H), 7.24 (dd, J = 4.6, 1.6 Hz, 1H), 7.19 (d, J = 3.1 Hz, 1H), 7.12 − 7.08 (m, 2H), 7.04 (d, J = 8.2 Hz, 1H), 7.00 (d, J = 8.5 Hz, 2H), 6.94 (d, J = 9.2 Hz, 1H), 6.89 − 6.83 (m, 4H), 6.49 (d, J = 3.1 Hz, 1H), 5.20 (s, 2H), 5.15 (s, 2H), 4.49 (t, J = 5.1 Hz, 2H), 4.41 (s, 2H), 3.84 (t, J = 5.1 Hz, 2H), 3.67 (dd, J = 10.3, 5.1 Hz, 1H), 3.53 (dd, J = 6.0, 3.2 Hz, 2H), 2.70 (dt, J = 17.7, 4.9 Hz, 1H), 2.61 (ddd, J = 17.8, 10.5, 5.3 Hz, 1H), 2.19 (dtd, J = 22.3, 10.4, 9.5, 4.9 Hz, 2H), 1.69 (s, 6H). **^{13}C NMR** (151 MHz, $CDCl_3$) δ: 173.5, 172.5, 168.5, 168.2, 158.0, 156.8, 147.0, 145.4, 143.9, 135.7, 132.0, 131.5, 130.9, 129.8, 129.7, 129.1, 128.5, 128.3, 128.1, 128.1, 127.9, 127.4, 124.2, 124.1, 121.2, 118.0, 115.3, 115.2, 109.8, 102.1, 82.2, 70.6, 70.3, 69.8, 69.4, 67.5, 62.2, 49.8, 47.3, 45.9, 38.9, 31.2, 26.5. **LC−MS (ESI)** $[M - H]^-$ m/z: 980.7.

*1-(4-((1-(1-(4-(2,6-Dioxopiperidin-3-yl)phenoxy)-2-oxo-6,9,12-trioxa-3-azatetradecan-14 yl)-1H-1,2,3-triazol-4-yl)methoxy)benzyl)-N-(trityloxy)-1H-indole-6-carboxamide (**27**).* Compound **27** was prepared following the **General procedure A** starting from compound **16** (46 mg, 0.098 mmol, 1 equiv), compound **5** (58 mg, 0.10 mmol, 1.05 equiv), ascorbic acid (52 mg, 0.29 mmol, 3 equiv), and $CuSO_4$ (16 mg, 0.098 mmol, 1 equiv). The crude product was purified by silica column (DCM/MeOH, 15:1, *v/v*) to provide compound **27** (70 mg, 70%). **^{1}H NMR** (600 MHz, $CDCl_3$) δ: 8.37 (s, 1H), 7.86 (s, 1H), 7.79 (d, J = 3.3 Hz, 1H), 7.63 (d, J = 8.3 Hz, 1H), 7.46 (dd, J = 8.3, 1.5 Hz, 1H), 7.33 − 7.28 (m, 15H), 7.25 − 7.23 (m, 1H), 7.08 − 7.04 (m, 3H), 7.00 (d, J = 8.2 Hz, 2H), 6.90 − 6.86 (m, 1H), 6.83 (dd, J = 17.1, 8.5 Hz, 4H), 6.56 (d, J = 3.2 Hz, 1H), 5.26 (s, 2H), 5.12 (s, 2H), 4.49 (dt, J = 9.9, 5.1 Hz, 2H), 4.39 (s, 2H), 3.81 (dt, J = 20.7, 5.2 Hz, 2H), 3.66 (dd, J = 10.3, 5.1 Hz, 1H), 3.56 − 3.53 (m, 2H), 3.46 (t, J = 4.9 Hz, 2H), 3.42 (q, J = 5.3 Hz, 2H), 2.78 − 2.06 (m, 10H). **^{13}C NMR** (151 MHz, $CDCl_3$) δ: 173.6, 172.6, 168.5, 167.7, 157.9, 156.8, 147.0, 145.4, 143.7, 135.7, 131.9, 131.4, 130.8, 129.8, 129.6, 129.1, 128.4, 128.3, 128.1, 127.9, 127.4, 124.5, 123.7, 121.2, 118.0, 115.3, 115.3, 109.8, 102.2, 82.2, 70.6, 70.5, 70.5, 70.4, 69.7, 69.4, 67.5, 62.0, 49.8, 47.3, 45.9, 38.9, 31.2, 26.4. **LC−MS (ESI)** $[M - H]^-$ m/z: 1024.6.

*6-(4-((4-((6-((Trityloxy)carbamoyl)-1H-indol-1-yl)methyl)-phenoxy)methyl)-1H-1,2,3-triazol-1-yl)hexyl 2-(4-(2,6-dioxopiperidin-3-yl)phenoxy)acetate (**28**).* Compound **28** was prepared following the **General procedure A** starting from compound **20** (73 mg, 0.19 mmol, 1 equiv), compound **5** (0.11 g, 0.20 mmol, 1.05 equiv), ascorbic acid (99 mg, 0.56 mmol, 3 equiv) and $CuSO_4$ (30 mg, 0.19 mmol, 1 equiv). The crude product was purified by silica column (DCM/MeOH, 20:1, *v/v*) to provide compound **28** (0.17 g, 94%). **^{1}H NMR** (600 MHz, $CDCl_3$) δ: 8.00 (d, J = 16.3 Hz, 1H), 7.90 (s, 1H), 7.63 (s, 1H), 7.59 − 7.52 (m, 6H), 7.49 (d, J = 8.3 Hz, 1H), 7.35 − 7.27 (m, 9H), 7.26 − 7.23 (m, 1H), 7.19 (d, J = 3.1 Hz, 1H), 7.12 (dd, J = 9.6, 3.1 Hz, 2H), 7.02 (dd, J = 15.8, 8.6 Hz, 3H), 6.93 − 6.85 (m, 4H), 6.49 (d, J = 3.1 Hz, 1H), 5.21 (s, 2H), 5.17 (s, 2H), 4.61 (s, 2H), 4.32 (t, J = 7.1 Hz, 2H), 4.17 (t, J = 6.5 Hz, 2H), 3.70 (dd, J = 9.9, 5.0 Hz, 1H), 2.69 (dt, J = 17.7, 5.2 Hz, 1H), 2.61 (ddd, J = 17.7, 10.1, 5.3 Hz, 1H), 2.26 − 2.14 (m, 2H), 1.87 (p, J = 7.3 Hz, 2H), 1.62 (q, J = 6.9 Hz, 2H), 1.32 (dq, J = 12.7, 8.5, 6.1 Hz, 4H). **^{13}C NMR** (151 MHz, $CDCl_3$) δ: 173.4, 172.5, 169.1, 168.1, 158.0, 157.4, 147.0, 145.4, 144.0, 135.8, 132.3, 132.0, 131.4, 130.3, 129.8, 129.4, 129.1, 128.5, 128.4, 128.1, 127.9, 127.4, 122.8, 122.7, 121.3, 117.5, 115.4, 115.2, 110.0, 102.1, 82.2, 65.6, 65.2, 62.3, 50.4, 49.8, 47.3, 31.1, 30.2, 28.4, 26.5, 26.1, 25.3. **LC−MS (ESI)** $[M - H]^-$ m/z: 949.7.

*N-(Benzyloxy)-1-(4-((6-(2-(4-(2,6-dioxopiperidin-3-yl)phenoxy)-acetamido)hexyl)carbamoyl)-benzyl)-1H-indole-6-carboxamide (**29**).* Compound **29** was prepared following the **General procedure B** starting from deprotected compound **17** (70 mg, 0.20 mmol, 1 equiv), compound **7** (82 mg, 0.20 mmol, 1.05 equiv), HATU (0.15 g, 0.39 mmol, 2 equiv), and DIPEA (76 mg, 0.58 mmol, 3 equiv). The crude product was purified by silica column (EtOAc/MeOH, 30:1, *v/v*) to provide compound **29** (67 mg, 46%). **^{1}H NMR** (600 MHz, DMSO-d_6) δ: 11.61 (s, 1H), 10.77 (s, 1H), 8.34 (t, J = 5.7 Hz, 1H), 8.01 (t, J = 5.8 Hz, 1H), 7.91 (s, 1H), 7.78 − 7.72 (m, 2H), 7.68 (d, J = 3.1 Hz, 1H), 7.61 (d, J = 8.3 Hz, 1H), 7.45 (ddd, J = 8.2, 4.9, 1.6 Hz, 3H), 7.41 − 7.32 (m, 3H), 7.23 (d, J = 8.1 Hz, 2H), 7.16 − 7.10 (m, 2H), 6.93 − 6.86 (m, 2H), 6.57 (dd, J = 3.1, 0.8 Hz, 1H), 5.53 (s, 2H), 4.92 (s, 2H), 4.43 (s, 2H), 3.78 (dd, J = 11.5, 4.9 Hz, 1H), 3.20 (q, J = 6.7 Hz, 2H), 3.10 (q, J = 6.8 Hz, 2H), 2.63 (ddd, J = 17.0, 11.7, 5.2 Hz, 1H), 2.49 − 2.43 (m, 1H), 2.14 (dtd, J = 13.2, 11.7, 4.4 Hz, 1H), 2.04 − 1.95 (m, 1H), 1.47 (p, J = 7.2 Hz, 2H), 1.41 (dd, J = 8.6, 5.5 Hz, 2H), 1.28 − 1.23 (m, 4H). **^{13}C NMR** (151 MHz, DMSO-d_6) δ: 174.3, 173.4, 167.4, 165.7, 165.3, 156.7, 140.9, 136.0, 135.1, 134.0, 131.9, 131.7, 130.7, 129.5, 128.8, 128.3, 128.2, 127.4, 126.6, 125.2, 120.2, 118.0, 114.5, 109.7, 101.4, 77.0, 67.1, 48.8, 46.5, 45.8, 38.2, 31.3, 29.0, 29.0, 26.1, 26.0, 26.0. **LC−MS (ESI)** $[M + H]^+$ m/z: 744.6.

*N-(Benzyloxy)-1-(4-((7-(2-(4-(2,6-dioxopiperidin-3-yl)phenoxy)-acetamido)heptyl)carbamoyl)-benzyl)-1H-indole-6-carboxamide (**30**).* Compound **30** was prepared following the **General procedure B** starting from deprotected compound **18** (71 mg, 0.19 mmol, 1 equiv), compound **7** (80 mg, 0.20 mmol, 1.05 equiv), HATU (0.14 g, 0.38 mmol, 2 equiv), and DIPEA (73 mg, 0.57 mmol, 3 equiv). The crude product was purified by silica column (EtOAc/MeOH, 30:1, *v/v*) to provide compound **30** (55 mg, 38%). **^{1}H NMR** (600 MHz, DMSO-d_6) δ: 11.61 (s, 1H), 10.77 (s, 1H), 8.34 (t, J = 5.7 Hz, 1H), 8.01 (t, J = 5.9 Hz, 1H), 7.93 − 7.90 (m, 1H), 7.78 − 7.73 (m, 2H), 7.68 (d, J = 3.1 Hz, 1H), 7.61 (d, J = 8.3 Hz, 1H), 7.45 (ddd, J = 8.2, 5.1, 1.6 Hz, 3H), 7.41 − 7.33 (m, 3H), 7.25 − 7.20 (m, 2H), 7.15 − 7.10 (m, 2H), 6.92 − 6.87 (m, 2H), 6.57 (dd, J = 3.1, 0.9 Hz, 1H), 5.52 (s, 2H), 4.92 (s, 2H), 4.43 (s, 2H), 3.78 (dd, J = 11.5, 4.9 Hz, 1H), 3.20 (q, J = 6.7 Hz, 2H), 3.10 (q, J = 6.7 Hz, 2H), 2.64 (ddd, J = 17.3, 11.9, 5.4 Hz, 1H), 2.49 − 2.44 (m, 1H), 2.15 (dtd, J = 13.2, 11.7, 4.4 Hz, 1H), 1.99 (dq, J = 13.2, 4.9 Hz, 1H), 1.47 (t, J = 7.0 Hz, 2H), 1.41 (p, J = 7.2 Hz, 2H), 1.25 (qd, J = 11.0, 9.1, 4.7 Hz, 6H). **^{13}C NMR** (151 MHz, DMSO-d_6) δ: 174.8, 173.9, 167.9, 166.2, 165.8, 157.2, 141.4, 136.5, 135.6, 134.5, 132.4, 132.2, 131.2, 130.0, 129.3, 128.8, 128.7, 127.9, 127.1, 125.7, 120.7, 118.5, 115.0, 110.2, 101.9, 77.5, 67.6, 49.3,

https://doi.org/10.1021/acs.jmedchem.5c00939
J. Med. Chem. 2026, 69, 918−943

47.0, 40.6, 38.7, 31.8, 29.5, 29.5, 28.9, 26.9, 26.8, 26.5. **LC−MS (ESI)** $[M + H]^+$ m/z: 758.6.

*1-(4-((1-(2-(2-(2-((2-(2,6-Dioxopiperidin-3-yl)-1,3-dioxoisoindolin-4-yl)amino)ethoxy)ethoxy)ethyl)-1H-1,2,3-triazol-4-yl)methoxy)benzyl)-N-hydroxy-1H-indole-6-carboxamide (**BP1**).* Compound **BP1** was prepared following **General procedure C**. Starting from compound **21** (0.15 g, 0.15 mmol, 1 equiv), the crude product was purified by reverse-phase flash column chromatography to yield compound **BP1** (29 mg, 26%). **^{1}H NMR** (600 MHz, DMSO-d_6) δ: 11.10 (d, J = 5.8 Hz, 2H), 8.90 (s, 1H), 8.15 (s, 1H), 7.98 (s, 1H), 7.64 (d, J = 3.1 Hz, 1H), 7.60 (d, J = 8.3 Hz, 1H), 7.55 (dd, J = 8.6, 7.1 Hz, 1H), 7.47 (dd, J = 8.3, 1.5 Hz, 1H), 7.22 − 7.16 (m, 2H), 7.11 (d, J = 8.6 Hz, 1H), 7.04 (d, J = 7.0 Hz, 1H), 7.00 − 6.94 (m, 2H), 6.59 (t, J = 5.8 Hz, 1H), 6.54 (dd, J = 3.1, 0.8 Hz, 1H), 5.39 (s, 2H), 5.12 − 5.01 (m, 3H), 4.52 (t, J = 5.2 Hz, 2H), 3.83 (t, J = 5.2 Hz, 2H), 3.57 (t, J = 5.4 Hz, 2H), 3.53 (hept, J = 2.7 Hz, 4H), 3.43 (q, J = 5.5 Hz, 2H), 2.89 (ddd, J = 17.1, 13.9, 5.4 Hz, 1H), 2.65 − 2.53 (m, 2H), 2.03 (ddt, J = 13.0, 5.5, 2.4 Hz, 1H). **^{13}C NMR** (151 MHz, DMSO-d_6) δ: 172.7, 170.0, 168.9, 167.2, 165.2, 157.4, 146.3, 142.4, 136.2, 135.0, 132.0, 131.4, 130.4, 130.2, 128.4, 125.6, 124.8, 120.0, 117.8, 117.4, 114.7, 110.7, 109.3, 109.2, 101.1, 69.5, 69.5, 68.8, 68.7, 61.1, 49.4, 48.6, 48.5, 41.6, 30.9, 22.1. **HRMS (ESI)**: m/z $[M + H]^+$ calcd for $C_{38}H_{38}N_8O_9$, 751.2835; found, 751.2845.

*1-(4-((1-(2-(2-(2-(2-((2-(2,6-Dioxopiperidin-3-yl)-1,3-dioxoisoindolin-4-yl)amino)ethoxy)ethoxy)ethoxy)ethyl)-1H-1,2,3-triazol-4-yl)methoxy)benzyl)-N-hydroxy-1H-indole-6-carboxamide (**BP2**).* Compound **BP2** was prepared following **General procedure C**. Starting from compound **22** (0.19 g, 0.18 mmol, 1 equiv), the crude product was purified by reverse-phase flash column chromatography to yield compound **BP2** (40 mg, 28%). **^{1}H NMR** (600 MHz, DMSO-d_6) δ: 11.07 (s, 2H), 8.87 (s, 1H), 8.13 (s, 1H), 7.95 (s, 1H), 7.61 (d, J = 3.1 Hz, 1H), 7.59 − 7.53 (m, 2H), 7.44 (dd, J = 8.3, 1.5 Hz, 1H), 7.19 − 7.15 (m, 2H), 7.10 (d, J = 8.6 Hz, 1H), 7.03 (d, J = 7.0 Hz, 1H), 6.98 − 6.94 (m, 2H), 6.57 (t, J = 5.8 Hz, 1H), 6.51 (dd, J = 3.1, 0.9 Hz, 1H), 5.37 (s, 2H), 5.07 (s, 2H), 5.04 (dd, J = 13.0, 5.6 Hz, 1H), 4.49 (t, J = 5.2 Hz, 2H), 3.78 (t, J = 5.2 Hz, 2H), 3.56 (t, J = 5.4 Hz, 2H), 3.51 (dd, J = 5.8, 3.3 Hz, 2H), 3.50 − 3.43 (m, 6H), 3.42 (q, J = 5.6 Hz, 2H), 2.87 (ddd, J = 17.1, 13.9, 5.4 Hz, 1H), 2.62 − 2.51 (m, 2H), 2.01 (dtd, J = 13.0, 5.4, 2.4 Hz, 1H). **^{13}C NMR** (126 MHz, DMSO-d_6) δ: 172.7, 170.0, 168.9, 167.2, 165.2, 157.4, 146.4, 142.4, 136.2, 135.0, 132.0, 131.3, 130.4, 130.2, 128.4, 125.6, 124.7, 120.0, 117.8, 117.4, 114.7, 110.6, 109.3, 109.2, 101.1, 69.7, 69.6, 69.5, 68.8, 68.6, 61.1, 49.3, 48.5, 41.6, 30.9, 22.1. **HRMS (ESI)**: m/z $[M + H]^+$ calcd for $C_{40}H_{42}N_8O_{10}$, 795.3097; found, 795.3107.

*1-(4-((1-(6-((2-(2,6-Dioxopiperidin-3-yl)-1,3-dioxoisoindolin-4-yl)oxy)hexyl)-1H-1,2,3-triazol-4-yl)methoxy)benzyl)-N-hydroxy-1H-indole-6-carboxamide (**BP3**).* Compound **BP3** was prepared following **General procedure C**. Starting from compound **23** (0.15 g, 0.16 mmol, 1 equiv), the crude product was purified by reverse-phase flash column chromatography to yield compound **BP3** (24 mg, 21%). **^{1}H NMR** (600 MHz, DMSO-d_6) δ: 11.08 (s, 2H), 8.87 (s, 1H), 8.18 (s, 1H), 7.95 (s, 1H), 7.79 (dd, J = 8.5, 7.3 Hz, 1H), 7.62 (d, J = 3.1 Hz, 1H), 7.57 (d, J = 8.3 Hz, 1H), 7.49 (d, J = 8.5 Hz, 1H), 7.46 − 7.40 (m, 2H), 7.21 − 7.15 (m, 2H), 6.99 − 6.93 (m, 2H), 6.51 (dd, J = 3.1, 0.9 Hz, 1H), 5.37 (s, 2H), 5.12 − 5.02 (m, 3H), 4.34 (t, J = 7.1 Hz, 2H), 4.17 (t, J = 6.3 Hz, 2H), 2.87 (ddd, J = 17.1, 13.9, 5.5 Hz, 1H), 2.63 − 2.51 (m, 2H), 2.02 (dtd, J = 12.4, 5.1, 2.2 Hz, 1H), 1.83 (p, J = 7.3 Hz, 2H), 1.77 − 1.69 (m, 2H), 1.47 (p, J = 7.6 Hz, 2H), 1.30 (qd, J = 9.6, 8.8, 6.3 Hz, 2H). **^{13}C NMR** (151 MHz, DMSO-d_6) δ: 172.7, 169.9, 166.8, 165.3, 165.2, 157.4, 156.0, 142.5, 137.0, 135.0, 133.2, 131.4, 130.4, 130.3, 128.4, 125.6, 124.3, 120.0, 119.8, 117.8, 116.2, 115.1, 114.7, 109.3, 101.1, 68.6, 61.1, 49.3, 48.7, 48.5, 30.9, 29.5, 28.1, 25.4, 24.6, 22.0. **HRMS (ESI)**: m/z $[M + H]^+$ calcd for $C_{38}H_{37}N_7O_8$, 720.2776; found, 720.2781.

*1-(4-((6-((2-(2,6-Dioxopiperidin-3-yl)-1,3-dioxoisoindolin-4-yl)amino)hexyl)carbamoyl)benzyl)-N-hydroxy-1H-indole-6-carboxamide (**BP4**).* Compound **BP4** was prepared following **General procedure D**. Starting from compound **24** (41 mg, 0.055 mmol, 1 equiv), the crude product was purified by reverse-phase flash column chromatography to yield compound **BP4** (16 mg, 45%). **^{1}H NMR** (600 MHz, DMSO-d_6) δ: 11.06 (s, 2H), 8.86 (s, 1H), 8.34 (t, J = 5.7 Hz, 1H), 7.89 (s, 1H), 7.78 − 7.70 (m, 2H), 7.66 (d, J = 3.1 Hz, 1H), 7.59 (d, J = 8.3 Hz, 1H), 7.55 (dd, J = 8.6, 7.1 Hz, 1H), 7.45 (dd, J = 8.3, 1.4 Hz, 1H), 7.24 (d, J = 8.1 Hz, 2H), 7.07 (d, J = 8.6 Hz, 1H), 7.01 (d, J = 7.0 Hz, 1H), 6.56 (d, J = 3.1 Hz, 1H), 6.51 (t, J = 5.9 Hz, 1H), 5.52 (s, 2H), 5.04 (dd, J = 12.8, 5.5 Hz, 1H), 3.27 (t, J = 6.7 Hz, 2H), 3.21 (q, J = 6.6 Hz, 2H), 2.87 (ddd, J = 17.0, 13.9, 5.4 Hz, 1H), 2.63 − 2.51 (m, 2H), 2.02 (dtd, J = 12.8, 5.3, 2.3 Hz, 1H), 1.56 (p, J = 7.1 Hz, 2H), 1.50 (p, J = 7.1 Hz, 2H), 1.41 − 1.28 (m, 4H). **^{13}C NMR** (151 MHz, DMSO-d_6) δ: 172.8, 170.0, 168.9, 167.3, 165.8, 165.2, 146.4, 140.9, 136.2, 135.1, 134.0, 132.2, 131.6, 130.4, 127.4, 126.6, 125.7, 120.1, 117.9, 117.1, 110.3, 109.3, 109.0, 101.3, 48.8, 48.5, 41.8, 40.1, 30.9, 29.0, 28.6, 26.1, 26.0, 22.1. **HRMS (ESI)**: m/z $[M + H]^+$ calcd for $C_{36}H_{36}N_6O_8$, 665.2718; found, 665.2722.

*1-(4-((7-((2-(2,6-Dioxopiperidin-3-yl)-1,3-dioxoisoindolin-4-yl)amino)heptyl)carbamoyl)benzyl)-N-hydroxy-1H-indole-6-carboxamide (**BP5**).* Compound **BP5** was prepared following **General procedure D**. Starting from compound **25** (61 mg, 0.079 mmol, 1 equiv), the crude product was purified by reverse-phase flash column chromatography to yield compound **BP5** (21 mg, 39%). **^{1}H NMR** (600 MHz, DMSO-d_6) δ: 11.07 (s, 2H), 8.88 (s, 1H), 8.34 (t, J = 5.6 Hz, 1H), 7.89 (s, 1H), 7.77 − 7.71 (m, 2H), 7.66 (d, J = 3.1 Hz, 1H), 7.61 − 7.52 (m, 2H), 7.45 (dd, J = 8.3, 1.4 Hz, 1H), 7.23 (d, J = 8.2 Hz, 2H), 7.07 (d, J = 8.6 Hz, 1H), 7.01 (d, J = 7.0 Hz, 1H), 6.56 (dd, J = 3.1, 0.8 Hz, 1H), 6.51 (t, J = 5.9 Hz, 1H), 5.52 (s, 2H), 5.04 (dd, J = 12.8, 5.5 Hz, 1H), 3.29 − 3.25 (m, 2H), 3.20 (q, J = 6.7 Hz, 2H), 2.88 (ddd, J = 17.1, 13.9, 5.5 Hz, 1H), 2.62 − 2.51 (m, 2H), 2.02 (dtd, J = 13.0, 5.4, 2.4 Hz, 1H), 1.56 (p, J = 7.0 Hz, 2H), 1.48 (p, J = 7.2 Hz, 2H), 1.34 − 1.27 (m, 6H). **^{13}C NMR** (151 MHz, DMSO-d_6) δ: 172.8, 170.0, 168.9, 167.3, 165.7, 165.1, 146.4, 140.9, 136.2, 135.1, 134.0, 132.2, 131.6, 130.4, 127.4, 126.6, 125.8, 120.1, 117.9, 117.1, 110.3, 109.3, 109.0, 101.3, 48.8, 48.5, 41.8, 40.1, 30.9, 29.0, 28.6, 28.4, 26.4, 26.3, 22.1. **HRMS (ESI)**: m/z $[M + H]^+$ calcd for $C_{37}H_{38}N_6O_7$, 679.2875; found, 679.2877.

*1-(4-((1-(2-(2-(2-(2-(4-(2,6-Dioxopiperidin-3-yl)phenoxy)-acetamido)ethoxy)ethoxy)ethyl)-1H-1,2,3-triazol-4-yl)methoxy)-benzyl)-N-hydroxy-1H-indole-6-carboxamide (**BP6**).* Compound **BP6** was prepared following **General procedure C**. Starting from compound **26** (96 mg, 0.097 mmol, 1 equiv), the crude product was purified by reverse-phase flash column chromatography to yield compound **BP6** (52 mg, 73%). **^{1}H NMR** (600 MHz, DMSO-d_6) δ: 11.08 (s, 1H), 10.77 (s, 1H), 8.87 (s, 1H), 8.14 (s, 1H), 8.01 (t, J = 5.8 Hz, 1H), 7.95 (s, 1H), 7.61 (d, J = 3.1 Hz, 1H), 7.59 − 7.55 (m, 1H), 7.44 (dd, J = 8.2, 1.5 Hz, 1H), 7.21 − 7.15 (m, 2H), 7.15 − 7.09 (m, 2H), 7.00 − 6.93 (m, 2H), 6.93 − 6.86 (m, 2H), 6.51 (dd, J = 3.1, 0.9 Hz, 1H), 5.37 (s, 2H), 5.08 (s, 2H), 4.50 (t, J = 5.2 Hz, 2H), 4.45 (s, 2H), 3.86 − 3.71 (m, 3H), 3.48 (dd, J = 5.8, 3.4 Hz, 2H), 3.46 − 3.42 (m, 2H), 3.39 (t, J = 5.9 Hz, 2H), 3.26 (q, J = 5.9 Hz, 2H), 2.64 (ddd, J = 17.2, 11.8, 5.3 Hz, 1H), 2.49 − 2.44 (m, 1H), 2.14 (dtd, J = 13.1, 11.7, 4.4 Hz, 1H), 2.02 − 1.96 (m, 1H). **^{13}C NMR** (151 MHz, DMSO-d_6) δ: 174.4, 173.4, 167.7, 165.3, 157.4, 156.6, 142.5, 135.0, 131.8, 131.4, 130.4, 130.3, 129.5, 128.4, 125.6, 124.8, 120.0, 117.8, 114.7, 114.5, 109.3, 101.1, 69.5, 69.3, 68.7, 68.6, 67.0, 61.1, 49.4, 48.5, 46.5, 38.2, 31.4, 25.9. **HRMS (ESI)**: m/z $[M + H]^+$ calcd for $C_{38}H_{41}N_7O_9$, 740.3039; found, 740.3044.

*1-(4-((1-(1-(4-(2,6-Dioxopiperidin-3-yl)phenoxy)-2-oxo-6,9,12-trioxa-3-azatetradecan-14 yl)-1H-1,2,3-triazol-4-yl)methoxy)benzyl)-N-hydroxy-1H-indole-6-carboxamide (**BP7**).* Compound **BP7** was prepared following **General procedure C**. Starting from compound **27** (64 mg, 0.063 mmol, 1 equiv), the crude product was purified by reverse-phase flash column chromatography to yield compound **BP7** (29 mg, 59%). **^{1}H NMR** (600 MHz, DMSO-d_6) δ: 11.08 (s, 1H), 10.77 (s, 1H), 8.87 (s, 1H), 8.14 (s, 1H), 8.02 (t, J = 5.8 Hz, 1H), 7.95 (s, 1H), 7.61 (d, J = 3.1 Hz, 1H), 7.57 (d, J = 8.2 Hz, 1H), 7.44 (dd, J = 8.2, 1.5 Hz, 1H), 7.21 − 7.16 (m, 2H), 7.16 − 7.10 (m, 2H), 7.00 − 6.94 (m, 2H), 6.93 − 6.87 (m, 2H), 6.51 (dd, J = 3.1, 0.9 Hz, 1H), 5.37 (s, 2H), 5.08 (s, 2H), 4.50 (t, J = 5.2 Hz, 2H), 4.45 (s, 2H), 3.82 − 3.74 (m, 3H), 3.52 − 3.48 (m, 2H), 3.45 (dq, J = 4.3, 2.9, 2.3 Hz, 6H), 3.41 (t, J = 6.0 Hz, 2H), 3.27 (q, J = 6.0 Hz, 2H), 2.64 (ddd, J = 17.2, 11.8, 5.3 Hz, 1H), 2.49 − 2.44 (m, 1H), 2.14 (dtd, J = 13.1, 11.7, 4.4 Hz, 1H), 2.03 − 1.96 (m, 1H). **^{13}C NMR** (151 MHz,

https://doi.org/10.1021/acs.jmedchem.5c00939
J. Med. Chem. 2026, 69, 918−943

DMSO-d_6) δ: 174.4, 173.4, 167.7, 165.2, 157.4, 156.6, 142.4, 135.0, 131.8, 131.4, 130.4, 130.3, 129.5, 128.4, 125.6, 124.8, 120.0, 117.8, 114.7, 114.5, 109.3, 101.1, 69.6, 69.6, 69.5, 68.7, 68.6, 67.0, 61.1, 49.4, 48.6, 48.5, 46.5, 38.2, 31.4, 25.9. **HRMS (ESI)**: m/z $[M + H]^+$ calcd for $C_{40}H_{45}N_7O_{10}$, 784.3301; found, 784.3307.

*6-(4-((4-((6-(Hydroxycarbamoyl)-1H-indol-1-yl)methyl)-phenoxy)methyl)-1H-1,2,3-triazol-1-yl)hexyl 2-(4-(2,6-dioxopiperidin-3-yl)phenoxy)acetate (**BP8**).* Compound **BP8** was prepared following **General procedure C**. Starting from compound **28** (0.16 mg, 0.17 mmol, 1 equiv), the crude product was purified by reverse-phase flash column chromatography to yield compound **BP8** (79 mg, 66%). **^{1}H NMR** (600 MHz, DMSO-d_6) δ: 11.08 (s, 1H), 10.77 (s, 1H), 8.87 (s, 1H), 8.17 (s, 1H), 7.97 − 7.93 (m, 1H), 7.62 (d, J = 3.1 Hz, 1H), 7.57 (dd, J = 8.3, 0.6 Hz, 1H), 7.44 (dd, J = 8.3, 1.5 Hz, 1H), 7.21 − 7.16 (m, 2H), 7.14 − 7.10 (m, 2H), 6.99 − 6.95 (m, 2H), 6.89 − 6.84 (m, 2H), 6.52 (dd, J = 3.1, 0.9 Hz, 1H), 5.38 (s, 2H), 5.07 (s, 2H), 4.76 (s, 2H), 4.32 (t, J = 7.1 Hz, 2H), 4.09 (t, J = 6.5 Hz, 2H), 3.77 (dd, J = 11.6, 4.9 Hz, 1H), 2.64 (ddd, J = 17.2, 11.8, 5.3 Hz, 1H), 2.49 − 2.43 (m, 1H), 2.14 (dtd, J = 13.2, 11.7, 4.4 Hz, 1H), 2.02 − 1.95 (m, 1H), 1.78 (p, J = 7.2 Hz, 2H), 1.55 (p, J = 6.7 Hz, 2H), 1.32 − 1.25 (m, 2H), 1.25 − 1.17 (m, 2H). **^{13}C NMR** (151 MHz, DMSO-d_6) δ: 174.3, 173.4, 168.8, 165.2, 157.4, 156.5, 142.5, 135.0, 131.8, 131.4, 130.4, 130.3, 129.5, 128.4, 125.6, 124.3, 120.0, 117.8, 114.7, 114.3, 109.3, 101.1, 64.6, 64.3, 61.1, 49.2, 48.5, 46.5, 31.4, 29.5, 27.8, 25.9, 25.3, 24.6. **HRMS (ESI)**: m/z $[M + H]^+$ calcd for $C_{38}H_{40}N_6O_8$, 709.2980; found, 709.2981.

*1-(4-((6-(2-(4-(2,6-Dioxopiperidin-3-yl)phenoxy)acetamido)-hexyl)carbamoyl)benzyl)-N-hydroxy-1H-indole-6-carboxamide (**BP9**).* Compound **BP9** was prepared following **General procedure D**. Starting from compound **29** (61 mg, 0.083 mmol, 1 equiv), the crude product was purified by reverse-phase flash column chromatography to yield compound **BP9** (21 mg, 39%). **^{1}H NMR** (600 MHz, DMSO-d_6) δ: 11.06 (s, 1H), 10.77 (s, 1H), 8.86 (s, 1H), 8.33 (t, J = 5.7 Hz, 1H), 8.02 (t, J = 5.9 Hz, 1H), 7.89 (s, 1H), 7.78 − 7.71 (m, 2H), 7.66 (d, J = 3.2 Hz, 1H), 7.62 − 7.56 (m, 1H), 7.45 (dd, J = 8.3, 1.4 Hz, 1H), 7.27 − 7.20 (m, 2H), 7.17 − 7.09 (m, 2H), 6.94 − 6.86 (m, 2H), 6.56 (dd, J = 3.1, 0.8 Hz, 1H), 5.52 (s, 2H), 4.43 (s, 2H), 3.78 (dd, J = 11.5, 4.9 Hz, 1H), 3.20 (q, J = 6.8 Hz, 2H), 3.10 (q, J = 6.7 Hz, 2H), 2.64 (ddd, J = 17.1, 11.7, 5.2 Hz, 1H), 2.49 − 2.43 (m, 1H), 2.15 (dtd, J = 13.1, 11.7, 4.4 Hz, 1H), 2.00 (dq, J = 13.2, 4.9 Hz, 1H), 1.44 (dp, J = 30.3, 7.1 Hz, 4H), 1.25 (dq, J = 10.5, 5.5, 4.8 Hz, 4H). **^{13}C NMR** (151 MHz, DMSO-d_6) δ: 174.4, 173.4, 167.4, 165.8, 165.2, 156.7, 140.9, 135.1, 134.0, 131.7, 131.6, 130.4, 129.5, 127.4, 126.6, 125.7, 120.1, 117.9, 114.5, 109.3, 101.4, 67.1, 48.8, 46.5, 40.1, 38.2, 31.3, 29.0, 29.0, 26.1, 26.0, 26.0. **HRMS (ESI)**: m/z $[M + H]^+$ calcd for $C_{36}H_{39}N_5O_7$, 654.2922; found, 654.2927.

*1-(4-((7-(2-(4-(2,6-Dioxopiperidin-3-yl)phenoxy)acetamido)-heptyl)carbamoyl)benzyl)-N-hydroxy-1H-indole-6-carboxamide (**BP10**).* Compound **BP10** was prepared following **General procedure D**. Starting from compound **30** (49 mg, 0.065 mmol, 1 equiv), the crude product was purified by reverse-phase flash column chromatography to yield compound **BP10** (18 mg, 41%). **^{1}H NMR** (600 MHz, DMSO-d_6) δ: 11.06 (s, 1H), 10.77 (s, 1H), 8.86 (s, 1H), 8.33 (t, J = 5.7 Hz, 1H), 8.01 (t, J = 5.9 Hz, 1H), 7.89 (s, 1H), 7.78 − 7.71 (m, 2H), 7.66 (d, J = 3.1 Hz, 1H), 7.59 (d, J = 8.2 Hz, 1H), 7.45 (dd, J = 8.3, 1.4 Hz, 1H), 7.24 (d, J = 8.3 Hz, 2H), 7.16 − 7.10 (m, 2H), 6.93 − 6.87 (m, 2H), 6.56 (dd, J = 3.1, 0.8 Hz, 1H), 5.52 (s, 2H), 4.43 (s, 2H), 3.78 (dd, J = 11.5, 4.9 Hz, 1H), 3.20 (q, J = 6.6 Hz, 2H), 3.10 (q, J = 6.7 Hz, 2H), 2.64 (ddd, J = 17.4, 11.9, 5.4 Hz, 1H), 2.49 − 2.44 (m, 1H), 2.15 (dtd, J = 13.2, 11.7, 4.5 Hz, 1H), 2.00 (dq, J = 13.2, 4.8 Hz, 1H), 1.47 (p, J = 7.1 Hz, 2H), 1.41 (p, J = 7.2 Hz, 2H), 1.29 − 1.19 (m, 6H). **^{13}C NMR** (151 MHz, DMSO-d_6) δ: 174.3, 173.4, 167.4, 165.7, 165.1, 156.7, 140.9, 135.1, 134.0, 131.7, 131.6, 130.4, 129.5, 127.4, 126.6, 125.8, 120.1, 117.9, 114.5, 109.3, 101.3, 67.1, 48.8, 46.5, 40.1, 38.2, 31.3, 29.0, 29.0, 28.4, 26.4, 26.3, 26.0. **HRMS (ESI)**: m/z $[M + H]^+$ calcd for $C_{37}H_{41}N_5O_7$, 668.3079; found, 668.3080.

*N-Hydroxy-1-(4-((1-(2-(2-(2-((2-(1-methyl-2,6-dioxopiperidin-3-yl)-1,3-dioxoisoindolin-4-yl)amino)ethoxy)ethoxy)ethyl)-1H-1,2,3-triazol-4-yl)methoxy)benzyl)-1H-indole-6-carboxamide (**BP1−N**).* Compound **BP1−N** was prepared following **General procedure C**. Starting from compound **S3** (0.10 g, 0.10 mmol, 1 equiv), the crude product was purified by reverse-phase flash column chromatography to yield compound **BP1−N** (31 mg, 40%). **^{1}H NMR** (600 MHz, DMSO-d_6) δ: 11.08 (s, 1H), 8.87 (s, 1H), 8.12 (s, 1H), 7.96 (s, 1H), 7.61 (d, J = 3.1 Hz, 1H), 7.57 (d, J = 8.3 Hz, 1H), 7.54 (dd, J = 8.5, 7.1 Hz, 1H), 7.44 (dd, J = 8.2, 1.4 Hz, 1H), 7.21 − 7.12 (m, 2H), 7.09 (d, J = 8.6 Hz, 1H), 7.02 (d, J = 7.0 Hz, 1H), 6.98 − 6.90 (m, 2H), 6.57 (t, J = 5.8 Hz, 1H), 6.51 (d, J = 3.1 Hz, 1H), 5.37 (s, 2H), 5.11 (dd, J = 13.0, 5.4 Hz, 1H), 5.05 (s, 2H), 4.49 (t, J = 5.2 Hz, 2H), 3.80 (t, J = 5.2 Hz, 2H), 3.55 (t, J = 5.4 Hz, 2H), 3.50 (hept, J = 2.7 Hz, 4H), 3.41 (q, J = 5.5 Hz, 2H), 2.99 (s, 3H), 2.93 (ddd, J = 17.2, 13.9, 5.4 Hz, 1H), 2.74 (ddd, J = 17.2, 4.5, 2.6 Hz, 1H), 2.56 − 2.51 (m, 1H), 2.02 (dtd, J = 13.0, 5.4, 2.5 Hz, 1H). **^{13}C NMR** (151 MHz, DMSO-d_6) δ: 171.7, 169.8, 168.9, 167.2, 165.2, 157.4, 146.4, 142.4, 136.2, 135.0, 132.0, 131.3, 130.4, 130.2, 128.4, 125.6, 124.7, 120.0, 117.8, 117.4, 114.7, 110.7, 109.3, 109.2, 101.1, 69.5, 69.5, 68.7, 68.7, 61.1, 49.4, 49.1, 48.5, 41.6, 31.1, 26.5, 21.3. **HRMS (ESI)**: m/z $[M + H]^+$ calcd for $C_{39}H_{40}N_8O_9$, 765.2991; found, 765.2997.

*4-((2-(2-(2-Azidoethoxy)ethoxy)ethyl)amino)-2-(1-methyl-2,6-dioxopiperidin-3-yl)isoindoline-1,3-dione (**S2**).* Compound **S1** was synthesized following a reported method.[49] To a solution of compound **S1** (0.10 g, 0.34 mmol, 1 equiv) in anhydrous DMSO (5 mL) were added **linker 1** (63 mg, 0.36 mmol, 1.05 equiv) and DIPEA (0.09 g, 0.69 mmol, 2 equiv). The mixture was stirred at 90 °C for 17 h. The crude product was obtained following the procedures for preparing compound **8**, which was then purified by silica column (CyH/EtOAc 1:1, v/v) to yield compound **S2** (74 mg, 48%). ^{1}H NMR (600 MHz, $CDCl_3$) δ: 7.49 (dd, J = 8.5, 7.2 Hz, 1H), 7.10 (d, J = 7.1 Hz, 1H), 6.92 (d, J = 8.5 Hz, 1H), 4.95 − 4.87 (m, 1H), 3.73 (t, J = 5.4 Hz, 2H), 3.68 (t, J = 5.4 Hz, 6H), 3.48 (t, J = 5.4 Hz, 2H), 3.38 (t, J = 5.0 Hz, 2H), 3.21 (s, 3H), 2.98 − 2.89 (m, 1H), 2.81 − 2.70 (m, 2H), 2.12 − 2.06 (m, 1H). ^{13}C NMR (151 MHz, $CDCl_3$) δ: 171.4, 169.6, 169.1, 167.9, 146.9, 136.1, 132.7, 116.9, 111.8, 110.6, 70.9, 70.9, 70.3, 69.8, 50.8, 49.8, 42.5, 32.1, 27.4, 22.3. **LC−MS (ESI)** $[M + H]^+$ m/z: 445.2.

*1-(4-((1-(2-(2-(2-((2-(1-Methyl-2,6-dioxopiperidin-3-yl)-1,3-dioxoisoindolin-4-yl)amino)ethoxy)ethoxy)ethyl)-1H-1,2,3-triazol-4-yl)-methoxy)benzyl)-N-(trityloxy)-1H-indole-6-carboxamide (**S3**).* Compound **S3** was prepared following the **General procedure A** starting from compound **S2** (67 mg, 0.15 mmol, 1 equiv), compound **5** (89 mg, 0.16 mmol, 1.05 equiv), ascorbic acid (80 mg, 0.45 mmol, 3 equiv) and $CuSO_4$ (24 mg, 0.15 mmol, 1 equiv). The crude product was purified by silica column (EtOAc/MeOH, 100:1, v/v) to provide compound **S3** (0.11 g, 75%). ^{1}H NMR (600 MHz, $CDCl_3$) δ: 7.85 (s, 1H), 7.80 (d, J = 2.9 Hz, 1H), 7.65 − 7.58 (m, 1H), 7.58 − 7.47 (m, 2H), 7.41 (td, J = 8.5, 1.9 Hz, 1H), 7.39 − 7.34 (m, 1H), 7.34 − 7.26 (m, 12H), 7.26 − 7.22 (m, 2H), 7.06 − 6.96 (m, 3H), 6.87 − 6.77 (m, 3H), 6.56 − 6.47 (m, 1H), 5.23 (s, 2H), 5.07 (s, 2H), 4.86 (dt, J = 12.5, 4.9 Hz, 1H), 4.52 (dt, J = 9.9, 4.9 Hz, 2H), 3.86 (dt, J = 15.1, 5.0 Hz, 2H), 3.66 − 3.51 (m, 6H), 3.37 (dt, J = 15.1, 5.4 Hz, 2H), 3.13 (s, 3H), 2.93 − 2.84 (m, 1H), 2.74 − 2.62 (m, 2H), 2.00 (m, 1H). ^{13}C NMR (151 MHz, $CDCl_3$) δ: 171.5, 171.3, 169.6, 169.3, 167.9, 157.9, 147.0, 145.4, 143.7, 136.2, 132.6, 132.0, 131.4, 129.8, 129.1, 128.3, 128.1, 128.1, 127.9, 127.9, 127.4, 124.4, 124.2, 123.5, 121.2, 117.7, 116.8, 115.3, 111.8, 102.2, 82.2, 70.6, 70.6, 69.5, 69.5, 62.0, 50.6, 50.0, 49.8, 42.4, 32.0, 27.3, 22.1. **LC−MS (ESI)** $[M - H]^-$ m/z: 1005.6.

Biological and Physicochemical Evaluation

HDAC8 Inhibition Assays. Dilutions of test compounds and reference inhibitor PCI-34051 were prepared in clear 96-well microplates (SpectraPlate, 96-well, PerkinElmer Inc.). To this end, the respective DMSO stock solutions were prediluted appropriately in DMSO followed by a 3-fold serial dilution in assay buffer (50 mM Tris−HCl, 137 mM NaCl, 2.7 mM KCl, 1 mM $MgCl_2$; pH 8.0; 1.0 mg/mL BSA). A total of 11 different concentrations, starting from 100 μM, for each compound were produced. Next, 5.0 μL of these serial dilutions in assay buffer were transferred into black 96-well microplates (OptiPlate, 96-well, black, PerkinElmer Inc.). 35 μL (100 μM) of the fluorogenic substrate Leu(Ac)-Gly-Lys(TFA)-AMC ((*S*)-

https://doi.org/10.1021/acs.jmedchem.5c00939
J. Med. Chem. 2026, 69, 918−943

2-[2-((*S*)-2-acetamido-4-methylpentanamido)acetamido]-*N*-(4-methyl-2-oxo-2H-chromen-7-yl)-6-(2,2,2-trifluoroacetamido)-hexanamide)[34,35] and 10 μL of human recombinant HDAC8 (BPS Bioscence, Catalog#50008) enzyme solution in assay buffer were added, and the assay was incubated for 90 min at 37 °C (total volume: 50 μL, max. 1% DMSO). Afterward, 50 μL of trypsin (1 mg/mL) in trypsin buffer (50 mM Tris HCl, 100 mM NaCl; pH 8.0) were added, followed by incubation at 37 °C for 30 min. Fluorescence (excitation: 355 nm, emission: 460 nm) was measured using a FLUOstar OPTIMA microplate reader (BMG LABTECH). Compounds were tested at least twice in duplicates; the 50% inhibitory concentration (IC_{50}) was determined by plotting normalized dose response curves using nonlinear regression (GraphPad Prism 9.5).

CRBN Target Engagement Assay. The assay was performed as previously described by Zerfas et al.[36] HEK293T cells stably expressing NanoLuc-CRBN were cultured in DMEM (Gibco, Life Technologies) supplemented with 10% FBS. Cells were resuspended at 2 × 10^5 cells/mL in 21 mL Opti-MEM I (Gibco, Life Technologies) and mixed with 600 μL BODIPY-lenalidomide fluorescent tracer (stock at 10 μM diluted in tracer dilution buffer 31.25% PEG-400, 12.5 mM HEPES, pH 7.5, filtered using a 0.22 μm nitrocellulose membrane) to reach final concentration of the tracer at 278 nM. The cell-tracer mixture was then plated in a white polystyrene 384-well plate (Corning, 3570) at 50 μL/well. After plating, the assay plate was centrifuged (400*g*, 5 min) and protected from light. Compounds for testing were added to the plate using a D300e Digital Dispenser (Tecan) in duplicate 12 pt titrations from a 10 mM stock in DMSO, with DMSO normalized to 1% total volume. The plate was then placed in an incubator at 37 °C, 5% CO_2 for 2 h. After incubation, the plate was removed and set on the bench to cool to room temperature (∼10 min). The NanoLuc substrate (500X solution, Promega Catalog number N2160 for 1000 assay kit) and extracellular inhibitor (1500X solution, Promega Catalog number N2160 for 1000 assay kit) were diluted in Opti-MEM I (Gibco, Life Technologies) to prepare a 3X solution, which was added to each well (25 μL/well). The plate was read on a Pherastar FSX (BMG Labtech) microplate reader with simultaneous dual emission capabilities at 450 and 520 nm for 10 cycles. The NanoBRET ratio was calculated by dividing the signal at 520 nm by the signal at 450 nm and multiplying by 1000 for each sample and averaged across 10 read cycles to create each data point. The data was plotted in GraphPad Prism 10 and the curves were fitted using Variable Slope equation to obtain the EC_{50} values.

Determination of Physicochemical Properties. *Log $D_{7.4}$ Measurements.* The determination of the log $D_{7.4}$ values was performed by a chromatographic method as described previously.[50] Briefly, the system was calibrated by plotting the retention times of six different drugs (atenolol, metoprolol, labetalol, diltiazem, triphenylene, permethrin) versus their literature known log $D_{7.4}$ values to obtain a calibration line ($R^2 \geq 0.95$). Subsequently, the mean retention times of the analytes were taken to calculate their log $D_{7.4}$ values with aid of the calibration line.

Plasma Protein Binding Studies. HSA binding was estimated by correlating the logarithmic retention times of the analytes on a CHIRALPAK HSA 50 × 3 mm, 5 μm column with the literature known %PPB values (converted into log *K* values) of the following drugs: warfarin, ketoprofen, budesonide, nizatidine, indomethacin, acetylsalicylic acid, carbamazepine, piroxicam, nicardipine, and cimetidine according to previously published methods.[51] Samples were dissolved in MeCN/DMSO 9:1 to achieve a final concentration of 0.5 mg/mL. The mobile phase A was 50 mM NH_4Ac adjusted to pH 7.4 with ammonia, while mobile phase B was *i*PrOH. The flow rate was set to 1.0 mL/min, the UV detector was set to 254 nm, and the column temperature was kept at 30 °C. After injecting 2 μL of the sample, a linear gradient from 100% A to 30% *i*PrOH in 5.4 min was applied. From 5.4 to 18 min, 30% *i*PrOH was kept, followed by switching back to 100% A in 1.0 min and a re-equilibration time of 6 min. With the aid of the calibration line ($R^2 \geq 0.95$), the log *K* values of new substances were calculated and converted to their %HSA values.

Metabolic Stability in Microsomes

Assays were performed in 96-deepwell-plates ("incubation plate"). Experiments were conducted on a horizontal shaker with a fitted heating block ("Thermomixer", Eppendorf). Test and reference items stock solutions were prepared in DMSO or ACN, respectively. The test item stock solutions were further diluted in DMSO/H_2O (1:1, v/v) and the verapamil stock solution was diluted in ACN to obtain working solutions of 100-fold higher strength than the intended final test concentration in experimental incubations (1 μM in the presence of 0.5% DMSO for test items, 1% ACN for verapamil). The assay was performed using human liver microsomes at 0.5 mg/mL.

The incubation solutions (final volume: 700 μL) consisted of 350 μL of a microsomal suspension (1 mg/mL protein; i.e. final 0.5 mg/mL in incubation) in reaction buffer (potassium phosphate buffer 50 mM, pH 7.4, supplemented with 3 mM $MgCl_2$ and 1 mM EDTA), 273 μL reaction buffer, and 7 μL of test item or positive control working solution, respectively. Components were pipetted into the respective wells of the "incubation plate" in the order given above and prewarmed on a horizontal shaker equipped with a fitted heating block. For the test item, two wells were prepared as reaction wells, and two wells were prepared as negative control wells.

The experiment was initiated by the addition of 70 μL of a 10 mM NADPH solution in reaction buffer to the prewarmed (37 °C) microsomes/buffer/test item mix to facilitate Phase I metabolism. 70 μL samples were removed from the incubations after 0, 10, 30, and 60 min and transferred to the "quenching plate" for sample preparation containing ACN supplemented with the internal standards (ISTD, 1 μM diazepam, 1 μM griseofulvin and 10 μM diclofenac). Verapamil was used as high clearance positive control in order to demonstrate the microsomal CYP enzyme activity. Incubations containing verapamil were run in parallel with test item incubations. Samples were drawn after 0 and 30 min. Microsomal metabolic activity was assessed in terms of verapamil turnover, i.e. loss of verapamil.

Negative controls using microsome without NADPH were run in parallel to experimental incubations to verify that any apparent loss of test item in the assay incubation was due to metabolism. For negative controls, 70 μL assay buffer instead of 70 μL NADPH solution was added to the negative control incubations. All incubations were run in duplicates ($n = 2$).

All incubations were stopped and precipitated by addition of 2 volumes of ACN containing the internal standards. After vigorously shaking (10 s) the samples were centrifuged (2200*g*) for 5 min at room temperature. Aliquots of the particle-free supernatants were diluted with an equal volume of H_2O and subsequently subjected to LC−MS analysis.

Western Blotting

Western blots on HDAC1, 3, 6, 8, acetylated histone H3 (Lys9/Lys14), H3K27Ac, acetylated SMC-3, GSPT1, IKZF3 and GAPDH in MM.1S cells, HDAC8 and GAPDH in MDA-MB-231 cells, as well as p53 in MV4-11 cells were performed according to a previously published protocol.[52−54] In brief, MM.1S or MDA-MB-231 were collected and lysed with cell extraction buffer (ThermoFisher Scientific Inc.; Waltham, MA, USA), supplemented with 0.1 mM PMSF, Halt Protease Inhibitor (Thermo Fisher), and sodium orthovanadate (ThermoFisher Scientific Inc.; Waltham, MA, USA). Protein concentration was determined using a BCA kit (ThermoFisher Scientific Inc.; Waltham, MA, USA). Equal amounts of protein (25 μg) from the lysates was denatured by Laemmli 2× Concentrate (Catalog#S3401-10VL, Sigma-Aldrich, St. Louis, MO, USA), and Precision Plus Protein Unstained Standard was used as molecular weight marker (Catalog#1610363, Bio-Rad, Hercules, CA, USA). SDS-PAGE was performed with precast gels with a polymerization degree of 4−15% (for ac-histone H3) and 10% or 12% for other proteins (Mini-PROTEAN TGX Stain-Free; Bio-Rad Laboratories GmbH, Germany). Afterward, proteins were transferred to Trans-Blot Turbo-PVDF membranes (Bio-Rad). The membrane was blocked with skimmed milk powder in Tris-buffered saline-Tween 20 (with 0.2% Tween 20) for 60 min, followed by three washing cycles of 10 min using Tris-buffered saline-Tween 20. Next, membranes were

https://doi.org/10.1021/acs.jmedchem.5c00939
J. Med. Chem. 2026, 69, 918−943

incubated with primary antibodies for a total of 60 min at room temperature under slight agitation and then incubated at 4 °C overnight. Membranes were rinsed again three times before applying the secondary antirabbit IgG HRP-conjugated mAbs (R&D Systems, Inc., Minneapolis, USA) or antimouse IgG HRP-conjugated mAbs (Santa Cruz Biotechnology, Texas, USA) for 90 min. After rinsing of the secondary antibody, membranes were detected using the ClarityECL Western Blotting Substrate (Bio-Rad). For quantitative determination, the StainFree technique was employed (Bio-Rad), which allows the imaging of whole lysates in SDS-PAGE before blotting and normalization against the total protein. Normalization for Figure 9B,C was conducted against the housekeeping protein GAPDH. Pixel density analysis was performed with the IMAGE LAB software (Bio-Rad). Primary antibodies were used as antibody solutions in 1:1000−1:20000 dilutions. Anti-HDAC1 (Catalog#5356S, Cell Signaling Technology, Denver, MA, USA), anti-HDAC3 (Catalog#85057S, Cell Signaling Technology, Denver, MA, USA), anti-HDAC6 (Catalog#7558S, Cell Signaling Technology, Denver, MA, USA), anti-HDAC8 (Catalog#66042S, Cell Signaling Technology, Denver, MA, USA), antiacetyl-histone H3 (Lys9/Lys14) (Catalog#9677S, Cell Signaling Technology, Denver, MA, USA), H3K27Ac (Catalog#4353S, Cell Signaling Technology, Denver, MA, USA), antiacetyl-α-tubulin (Catalog#5335, Cell Signaling Technology, Denver, MA, USA), antiacetyl-SMC3 (MABE1925-100UG, EMD Millipore Corp, USA), anti-IKZF3 (Catalog#14859S, Cell Signaling Technology, Denver, MA, USA), anti-GSPT1 (Catalog#sc-66000, Santa Cruz Biotechnology, Texas, USA), anti-p53 (Catalog#9282, Cell Signaling Technology, Denver, MA, USA) anti-GAPDH (Catalog#T0004, Affinity Biosciences, Cincinnati, OH, USA), anti-GAPDH (Catalog#2118S and #5174, Cell Signaling Technology, Denver, MA, USA).

Cell Culture

MM.1S cells were obtained by the American Type Culture Collection (ATCC, Manassas, VA, USA). Cells were cultured in RPMI 1640 (Life Technologies, Darmstadt, Germany) supplemented with 10% fetal bovine serum (PAN Biotech GmbH, Aidenbach, Germany), 100 IU/mL penicillin and 0.1 mg/mL streptomycin (PAN Biotech GmbH, Aidenbach, Germany) and 1 mM sodium pyruvate (ThermoFisher Scientific Inc.; Waltham, MA, USA) and were incubated at 37 °C under humidified air with 5% CO_2. MDA-MB-231 cells were obtained by the American Type Culture Collection (ATCC, Manassas, VA, USA). Cells were cultured in Dulbecco's Modified Eagle's Medium (DMEM, Gibco) already containing L-glutamine and pyruvate, and supplemented with 10% fetal bovine serum (PAN Biotech GmbH, Aidenbach, Germany), 100 IU/mL penicillin and 0.1 mg/mL streptomycin (PAN Biotech GmbH, Aidenbach, Germany), and were incubated at 37 °C under humidified air with 5% CO_2. HL-60 (acute myeloid leukemia or AML) and MV4−11 (AML) cells were obtained from DSMZ, Braunschweig, Germany. HL-60 and MV4−11 cells were cultured in RPMI1640 GlutaMAX (Gibco) supplemented with 10−20% FBS (Sigma-Aldrich) and penicillin streptomycin (Gibco) and maintained at 37 °C with 5% CO_2.

Proliferation Assessment by Trypan Blue

To evaluate cell viability and proliferation under different compound treatments trypan blue based exclusion test was performed on HL60 cells that were treated for time intervals 24, 48, and 72 h with either DMSO or novel HDAC8 PROTACs at 3 μM or positive controls PCI-34051 and vorinostat at 0.5 μM and 1 μM by using Vi-CELL BLU cell counter (Beckman Coulter).

IC_{50} Determination

HL-60 and MM.1S cells were seeded at a density of 0.04×10^6 per mL in a white 384-well plate (Corning), in which increasing concentrations (0.05−50 μM) of novel PROTACs, alongside the positive controls PCI-34051 and vorinostat were preprinted (D300e Digital Dispenser, Tecan). After 72 h of incubation, cell viability was assessed using the ATP-based CellTiter-Glo luminescent assay (Promega), following the manufacturer's instructions. To determine the IC_{50} values for each tested PROTAC, raw data (acquired in triplicates) were normalized to the DMSO control and analyzed using nonlinear regression curve in GraphPad Prism.

High Throughput Drug Screening of Pretreated Cells

HL-60 cells (0.25×10^6 per mL) were treated with the HDAC8 PROTAC **BP6** (1 μM) or DMSO as a control for 6 h. After 6 h of pretreatment, ex vivo high throughput drug screening was performed (list of the drugs, Table S2, Supporting Information). To this end, treated cells were seeded at a density of 0.04×10^6 per mL in a white 384-well plate (Corning), in which increasing concentrations (0.005−25 μM) of 48 FDA-approved agents routinely used to treat leukemia, were preprinted (D300e Digital Dispenser, Tecan). After 72 h of incubation, cell viability was assessed using the ATP-based CellTiter-Glo luminescent assay (Promega), following the manufacturer's instructions. To determine the IC_{50} values for each tested drug, raw data (acquired in triplicates) were normalized to the DMSO control and analyzed using nonlinear regression curve in GraphPad Prism.

Cell Viability Determination of Cobimetinib Treated Cells

MV4−11 and HL-60 cells were seeded at a density of 0.1×10^6 per mL on a white 384-well plate (Corning), in which increasing concentrations (0.005−25 μM) of **BP6**, cobimetinib and the combination of a fix cobimetinib concentration (0.5, 1, 2 μM) and increasing concentration of **BP6**, were preprinted (D300e Digital Dispenser, Tecan). After 72 h of incubation, cell viability was assessed using the ATP-based CellTiter-Glo luminescent assay (Promega), following the manufacturer's instructions. Raw data were normalized to each DMSO control and analyzed in GraphPad Prism.

FACS-Based Analysis of Apoptotic Cell Death

MV4−11 cells (0.25×10^6 per mL) were pretreated with either HDAC8 PROTAC (**BP6**), negative control PROTAC (**BP8**) or HDAC8 inhibitor (PCI) for 6 h prior to treatment with 1 μM idasanutlin. Apoptotic cells were quantified 15 or 48 h after treatment by flow cytometry based on DNA content. Nuclei displaying hypodiploid DNA, observed as a sub-G1 population to the left of the diploid (2N) peak in the DNA histogram, were classified as apoptotic. Nuclei were prepared by lysing cells in a hypotonic lysis buffer (1% sodium citrate, 0.1% Triton X-100, 50 μg/mL propidium iodide) and subsequently analyzed by flow cytometry.

Quantitative Proteomics. *Sample Preparation LFQ Quantitative mass Spectrometry.* MOLT-4 Cells were lysed by addition of lysis buffer (8 M Urea, 50 mM NaCl, 50 mM 4-(2-hydroxyethyl)-1-piperazineethanesulfonic acid (EPPS) pH 8.5, Protease and Phosphatase inhibitors) and homogenization by bead beating (BioSpec) for three repeats of 30 at 2400 strokes/min. Bradford assay was used to determine the final protein concentration in the clarified cell lysate. Fifty micrograms of protein for each sample was reduced, alkylated and precipitated using methanol/chloroform as previously described[55] and the resulting washed precipitated protein was allowed to air-dry. Precipitated protein was resuspended in 4 M urea, 50 mM HEPES pH 7.4, followed by dilution to 1 M urea with the addition of 200 mM EPPS, pH 8. Proteins were digested with the addition of LysC (1:50; enzyme/protein) and trypsin (1:50; enzyme/protein) for 12 h at 37 °C. Sample digests were acidified with formic acid to a pH of 2−3 before desalting using C18 solid phase extraction plates (SOLA, Thermo Fisher Scientific). Desalted peptides were dried in a vacuum-centrifuged and reconstituted in 0.1% formic acid for liquid chromatography−mass spectrometry analysis. Data were collected using a TimsTOF HT (Bruker Daltonics, Bremen, Germany) coupled to a nanoElute LC pump (Bruker Daltonics, Bremen, Germany) via a CaptiveSpray nanoelectrospray source. Peptides were separated on a reversed-phase C18 column (25 cm × 75 μm ID, 1.6 μM, IonOpticks, Australia) containing an integrated captive spray emitter. Peptides were separated using a 50 min gradient of 2−30% buffer B (acetonitrile in 0.1% formic acid) with a flow rate of 250 nL/min and column temperature maintained at 50 °C. The TIMS elution voltages were calibrated linearly with three points (Agilent ESI-L Tuning Mix Ions; 622, 922, 1222 m/z) to determine the reduced ion mobility coefficients ($1/K_0$). To perform diaPASEF, we used py_diAID,[56] a python package, to assess the precursor

https://doi.org/10.1021/acs.jmedchem.5c00939
J. Med. Chem. 2026, 69, 918−943

distribution in the m/z-ion mobility plane to generate a diaPASEF acquisition scheme with variable window isolation widths that are aligned to the precursor density in m/z. Data was acquired using 20 cycles with three mobility window scans each (creating 60 windows) covering the diagonal scan line for doubly and triply charged precursors, with singly charged precursors able to be excluded by their position in the m/z-ion mobility plane. These precursor isolation windows were defined between 350−1250 m/z and $1/k_0$ of 0.6−1.45 V·s/cm^2.

LC−MS Data Analysis. The diaPASEF raw file processing and controlling peptide and protein level false discovery rates, assembling proteins from peptides, and protein quantification from peptides were performed using library free analysis in DIA-NN 1.8.[57] Library free mode performs an in silico digestion of a given protein sequence database alongside deep learning-based predictions to extract the DIA precursor data into a collection of MS2 spectra. The search results are then used to generate a spectral library which is then employed for the targeted analysis of the DIA data searched against a Swissprot human database (January 2021). Database search criteria largely followed the default settings for directDIA including: tryptic with two missed cleavages, carbamidomethylation of cysteine, and oxidation of methionine and precursor Q-value (FDR) cutoff of 0.01. Precursor quantification strategy was set to Robust LC (high accuracy) with RT-dependent cross run normalization. Proteins with low sum of abundance (<2000 × no. of treatments) were excluded from further analysis and resulting data was filtered to only include proteins that had a minimum of 3 counts in at least 4 replicates of each independent comparison of treatment sample to the DMSO control. Protein abundances were scaled using in-house scripts in the R framework (R Development Core Team, 2014) and proteins with missing values were imputed by random selection from a Gaussian distribution either with a mean of the nonmissing values for that treatment group or with a mean equal to the median of the background (in cases when all values for a treatment group are missing). Significant changes comparing the relative protein abundance of these treatment to DMSO control comparisons were assessed by moderated t-test as implemented in the limma package within the R framework.[58] Graphs in the paper were generated with Python 3.10. Venn diagrams were generated by comparing the significant protein entries with FDR < 0.1 of both **BP1** and **BP6**. Gene set enrichment was performed by adding all significant proteins to the string framework and comparing the enriched terms (FDR < 0.05).

Time-Resolved Fluorescence Resonance Energy Transfer Assays. *Expression and Purification of SpyCatcher S50C.* SpyCatcher S50C was expressed in *Escherichia coli* Rosetta (DE3). Cultures were grown in LB medium supplemented with kanamycin (100 μg/mL) and chloramphenicol (100 μg/mL) at 37 °C, 130 rpm, to an OD600 of 0.87. Protein expression was induced with 1 mM IPTG at 18 °C overnight. Cells were harvested by centrifugation (4000g, 20 min, 4 °C) and lysed via sonification in lysis buffer (50 mM Tris−HCl, pH 8.0, 200 mM NaCl, 10 mM imidazole, 1 mM TCEP, 1 mM PMSF). After ultracentrifugation, the supernatant was batch-bound to Ni−NTA agarose beads, washed with wash buffer (50 mM Tris−HCl, pH 8.0, 200 mM NaCl, 20 mM imidazole, 1 mM TCEP), and eluted with buffer containing 50 mM Tris−HCl pH 8.0, 200 mM NaCl, 400 mM imidazole, and 1 mM TCEP. Eluted protein was further purified by size-exclusion chromatography on a Superdex 75 16/600 GL column (Cytiva) equilibrated in SEC buffer (50 mM HEPES, pH 7.5, 200 mM NaCl, 0.1 mM TCEP). Fractions containing SpyCatcher S50C were concentrated and flash-frozen in liquid nitrogen.

Labeling of SpyCatcher S50C with BODIPY-FL-maleimide. Purified SpyCatcher S50C was incubated with 8 mM DTT at 4 °C for 1 h. DTT was removed by size-exclusion chromatography (Superdex 75 16/600 GL, Cytiva) in 50 mM Tris pH 7.5, 150 mM NaCl, 0.1 mM TCEP). BODIPY-FL-maleimide (Thermo Fisher), dissolved in DMSO, was added at a 1.1-fold molar excess over SpyCatcher S50C, and labeling was carried out overnight at 4 °C. Labeled protein was purified by size-exclusion chromatography (Superdex 75 16/600 GL, Cytiva) in 50 mM Tris pH 7.5, 150 mM NaCl, 1 mM TCEP, concentrated, flash-frozen in liquid nitrogen, and stored at − 80 °C.

CRBN-DDB1 Expression and Labeling. Human Flag-Spy-TEV-CRBN and His6-TEV-DDB1ΔB[59] in pAV-derived vectors[60] were expressed in *Trichoplusia ni* High-Five insect cells using the baculovirus expression system (Invitrogen). Cells were lysed via sonification in 50 mM Tris−HCl pH 8.0, 200 mM NaCl, 1 mM TCEP, 1 mM PMSF and 1x cOmplete Tablet (Roche, Cat. No. 11836170001). Following ultracentrifugation, Benzonase Nuclease (Millipore, Cat. No. 70664-3) was added at 0.001% and the soluble fraction was incubated with Flag-M2 sepharose beads, washed with 50 mM Tris−HCl pH 8.0, 200 mM NaCl, 1 mM TCEP and eluted by wash buffer supplemented with 0.15 mg/mL Flag peptide (GeneScript, Cat. No. RP10586-1). The elution was further purified via ion exchange chromatography (Poros 50HQ). The resulting fractions were pooled and covalently labeled with BODIPY-FL-SpyCatcherS50C by overnight incubation at 4 °C in a stoichiometric ratio. The labeled protein was purified via size exclusion chromatography in 25 mM HEPES pH 7.5, 200 mM NaCl and 1 mM TCEP. The protein-containing fractions were concentrated using ultrafiltration (Millipore), flash frozen in liquid nitrogen and stored at −80 °C.

Time-Resolved Fluorescence Resonance Energy Transfer. The compounds were dispensed into 384-well microplates (Corning, Cat. No. 4514) using a D300e Digital Dispenser (Tecan) at a final concentration of 1% DMSO. Assay mixtures contained 100 nM GST-HDAC8 (SinoBiological, cat. No. 10864-H09B), 500 nM BODIPY-FL-SpyCatcher-CRBN-DDB1, and 1:80 HTRF Anti-GST mAb Tb-Conjugate (Revvity, Cat. No. 61GSTTLF) in buffer (50 mM HEPES, pH 7.5, 200 mM NaCl, 1 mM TCEP, 0.1% Poloxamer 188). Reactions were incubated for 10 min at room temperature prior to TR-FRET measurements. Plates were read on a PHERAstar FSX microplate reader (BMG Labtech). Following excitation of terbium at 337 nm, emissions at 490 nm (terbium) and 520 nm (BODIPY-FL) were recorded, and TR-FRET signals were calculated as the 520/490 nm ratio. Data represents experiments with n = 4, each consisting of ten technical replicates per well, and were analyzed in GraphPad Prism v10.2.2.

Molecular Modeling. For the preparation of small molecules and protein, the chemical structures of docked and modeled molecules were prepared and optimized based on the MMFF94X force field; The receptors (crystal complexes) were processed as follows: removal of water molecules, addition of hydrogen atoms and partial charges, protonation based on the Amber10:EHT force field. For figure generation, the obtained modeling results were saved as PDB format and the figures were generated using the PyMOL software (https://pymol.org/2/).

Molecular Docking. Molecular docking was performed in the MOE software (version 2022). The crystal structures of *S. mansoni* HDAC8 (PDB: 6HQY) and human HDAC8 (PDB: 1T64) were obtained from the Protein Data Bank. Superimposing was conducted with the "superpose" function in the software. For docking analysis, the binding site of the native ligand in each receptor was used to define the docking sites. Other MOE-docking parameters were set to default values and 30 predicted poses were retained during the docking process. The best poses were kept based upon the docking score and the results from ligand interactions, followed by visually inspection.

Ternary Complex Modeling. The crystal structure human CRBN (PDB ID: 8OIZ) were obtained from the Protein Data Bank. The complex of human HDAC8 with PCI-34051 docked inside was obtained from molecular docking section. The isolated CRBN was obtained by deleting the DDB1 part in the CRBN-DDB1 complex. Ternary complex modeling was performed in MOE software (version 2022). The method 4B[40,41] was conducted in the software by submitting the prepared HDAC8 complex, CRBN as well as the degraders. The best pose was kept based on the modeling score and the result from ligand interactions, followed by visual inspection.

PAINS Analysis. We filtered all compounds for pan-assay interference compounds (PAINS) using the online filter http://

https://doi.org/10.1021/acs.jmedchem.5c00939
J. Med. Chem. 2026, 69, 918−943

zinc15.docking.org/patterns/home/. No compound was flagged as PAINS.

■ ASSOCIATED CONTENT

Data Availability Statement

Global proteomics data will be publicly available at the Fischer Lab's Proteomics database: https://proteomics.fischerlab.org.

Supporting Information

The Supporting Information is available free of charge at https://pubs.acs.org/doi/10.1021/acs.jmedchem.5c00939.

Electronic Supporting Information (ESI) available: Figures for docking pose of PCI-34051 in human HDAC8; Figures for comparisons of proteomics result of **BP1** and **BP6**; Table for the list of 48 FDA-approved drugs along with their target used for high-throughput drug screening; MM.1S and MV4−11 leukemia cells treated with pomalidomide alone, **BP6** alone, or their combination; cobimetinib combination experiments with either PCI-34051 or **BP8**; Synthetic scheme for preparation of the nondegrading control **BP1−N**; ^{1}H and ^{13}C NMR spectra of BP1-BP10, BP1−N; HR-MS spectra and HPLC chromatograms of **BP1−BP10, BP1−N** (PDF)

Molecular strings formula (CSV)

Coordinate information on docked complexes (PDB)

Superimposed structures of smHDAC8 and human HDAC8_Figure 2 (PDB)

Ternary complex modeling of Human HDAC8-BP1-CRBN_Figure S7 (PDB)

Ternary complex modeling of Human HDAC8-BP6-CRBN_Figure 6 (PDB)

■ AUTHOR INFORMATION

Corresponding Authors

Sanil Bhatia − *Department of Paediatric Oncology, Haematology and Clinical Immunology, Medical Faculty, Heinrich-Heine University Dusseldorf, 40225 Düsseldorf, Germany*; orcid.org/0000-0001-6494-7744; Email: sanil.bhatia@med.uni-duesseldorf.de

Finn K. Hansen − *Department of Pharmaceutical and Cell Biological Chemistry, Pharmaceutical Institute, University of Bonn, 53121 Bonn, Germany*; orcid.org/0000-0001-9765-5975; Email: finn.hansen@uni-bonn.de

Authors

Shiyang Zhai − *Department of Pharmaceutical and Cell Biological Chemistry, Pharmaceutical Institute, University of Bonn, 53121 Bonn, Germany*; orcid.org/0009-0005-6840-3177

Marie Kemkes − *Department of Paediatric Oncology, Haematology and Clinical Immunology, Medical Faculty, Heinrich-Heine University Dusseldorf, 40225 Düsseldorf, Germany*

Cindy-Esther Kponomaizoun − *Department of Pharmaceutical and Cell Biological Chemistry, Pharmaceutical Institute, University of Bonn, 53121 Bonn, Germany*

Jan Gerhartz − *Institute of Structural Biology, Medical Faculty, University of Bonn, 53127 Bonn, Germany*; orcid.org/0009-0002-9457-4656

Felix Feller − *Department of Pharmaceutical and Cell Biological Chemistry, Pharmaceutical Institute, University of Bonn, 53121 Bonn, Germany*; orcid.org/0009-0007-1820-772X

Jia-Wey Tu − *Department of Paediatric Oncology, Haematology and Clinical Immunology, Medical Faculty, Heinrich-Heine University Dusseldorf, 40225 Düsseldorf, Germany*

Dominika Ewa Pieńkowska − *Institute of Structural Biology, Medical Faculty, University of Bonn, 53127 Bonn, Germany*

Julian Schliehe-Diecks − *Department of Paediatric Oncology, Haematology and Clinical Immunology, Medical Faculty, Heinrich-Heine University Dusseldorf, 40225 Düsseldorf, Germany*

Ina Dressel − *Institute of Structural Biology, Medical Faculty, University of Bonn, 53127 Bonn, Germany*

Michael Gütschow − *Department of Pharmaceutical and Medicinal Chemistry, Pharmaceutical Institute, University of Bonn, 53121 Bonn, Germany*; orcid.org/0000-0002-9376-7897

Radosław P. Nowak − *Institute of Structural Biology, Medical Faculty, University of Bonn, 53127 Bonn, Germany*; orcid.org/0000-0002-0605-0071

Christian Steinebach − *Department of Pharmaceutical and Medicinal Chemistry, Pharmaceutical Institute, University of Bonn, 53121 Bonn, Germany*; orcid.org/0000-0001-5638-1955

Complete contact information is available at: https://pubs.acs.org/10.1021/acs.jmedchem.5c00939

Author Contributions

S.B. and F.K.H. contributed equally to this work as senior authors. The manuscript was written through contributions of all authors. All authors have given approval to the final version of the manuscript.

Notes

The authors declare no competing financial interest.

■ ACKNOWLEDGMENTS

S.Z. is funded by China Scholarship Council (grant no. 202106150022). The work of M.G., C.S., and F.K.H. was funded by the Deutsche Forschungsgemeinschaft (DFG, German Research Foundation)−GRK2873 (494832089). C.S. received financial support from the "Fonds der Chemischen Industrie (FCI)". R.P.N. is a member of the excellence cluster ImmunoSensation2 funded by the Deutsche Forschungsgemeinschaft (DFG) under Germany's Excellence Strategy (EXC2151-390873048). This work was funded by the Deutsche Forschungsgemeinschaft (DFG, German Research Foundation) 270650915 (Research Training Group GRK 2158). S.B. additionally acknowledges the financial support from Elterninitiative Kinderkrebsklinik e.V and DFG BH 162/4-1 (528968169). The new NMR console for the 500 MHz NMR spectrometer used in this research was funded by the Deutsche Forschungsgemeinschaft (DFG, German Research Foundation) under project number 507275896. We thank Katherine A. Donovan, Eric S. Fischer and the Fischer Lab Degradation Proteomics Initiative for collection of the global proteomics data supported by NIH CA214608 and CA218278.

■ ABBREVIATIONS

ACN, acetonitrile; AMC, 7-amino-4-methylcoumarin; BODIPY, 5,5-difluoro-5H-4λ5-dipyrrolo[1,2-*c*:2′,1′-*f*][1,3,2]-diazaborinin-4-ylium-5-uide; CREB, cAMP response element-binding protein; DC_{50}, half maximal degradation; DCM, dichloromethane; DEC1, deleted in esophageal cancer 1; DIPEA, *N*,*N*-diisopropylethylamine; D_{max}, maximal degradation, DMF, *N*,*N*-dimethylformamide; DMSO, dimethyl sulfoxide; EDTA, ethylenediaminetetraacetic acid; ERRα, estrogen-related receptor alpha; FBS, fetal bovine serum; FDA, Food and Drug Administration; FDR, false discovery rate; GAPDH, glyceraldehyde 3-phosphate dehydrogenase; GSPT1, eukaryotic peptide chain release factor GTP-binding subunit ERF3A; HATU, 1-[bis(dimethylamino)methylene]-1*H*-1,2,3-triazolo[4,5-*b*]pyridinium 3-oxide hexafluorophosphate; HCl, hydrogen chloride; HDAC(s), histone deacetylase(s); HEPES, 4-(2-hydroxyethyl)-1-piperazineethanesulfonic acid; IKZF1, Ikaros family zinc finger protein 1; IKZF3, Ikaros family zinc finger protein 3; IPTG, isopropyl β-D-1-thiogalactopyranoside; LiOH, lithium hydroxide; MEK, mitogen-activated protein kinase kinase; NADPH, nicotinamide adenine dinucleotide phosphate; NanoBRET, nano bioluminescence resonance energy transfer; NanoLuc-CRBN, nanoluciferase cereblon; PBS, phosphate-buffered saline; RAB28, Ras-related protein Rab-28; PMSF, phenylmethylsulfonyl fluoride; PROTAC(s), proteolysis-targeting chimera(s); SMC3, structural maintenance of chromosomes protein 3; STAT3, signal transducer and activator of transcription 3; Sirt2, sirtuin 2; Sirt6, sirtuin 6; TCEP, tris(2-carboxyethyl)phosphine; THF, tetrahydrofuran; TR-FRET, time-resolved fluorescence resonance energy transfer; ZFP91, zinc finger protein 91.

■ REFERENCES

(1) Hu, E.; Chen, Z.; Fredrickson, T.; Zhu, Y.; Kirkpatrick, R.; Zhang, G. F.; Johanson, K.; Sung, C. M.; Liu, R.; Winkler, J. Cloning and characterization of a novel human class I histone deacetylase that functions as a transcription repressor. *J. Biol. Chem.* **2000**, *275* (20), 15254−15264.

(2) Li, J.; Chen, S.; Cleary, R. A.; Wang, R.; Gannon, O. J.; Seto, E.; Tang, D. D. Histone deacetylase 8 regulates cortactin deacetylation and contraction in smooth muscle tissues. *Am. J. Physiol. Cell Physiol.* **2014**, *307* (3), C288−C295.

(3) Banerjee, S.; Adhikari, N.; Amin, S. A.; Jha, T. Histone deacetylase 8 (HDAC8) and its inhibitors with selectivity to other isoforms: An overview. *Eur. J. Med. Chem.* **2019**, *164*, 214−240.

(4) Chakrabarti, A.; Oehme, I.; Witt, O.; Oliveira, G.; Sippl, W.; Romier, C.; Pierce, R. J.; Jung, M. HDAC8: a multifaceted target for therapeutic interventions. *Trends Pharmacol. Sci.* **2015**, *36* (7), 481−492.

(5) Chakrabarti, A.; Melesina, J.; Kolbinger, F. R.; Oehme, I.; Senger, J.; Witt, O.; Sippl, W.; Jung, M. Targeting histone deacetylase 8 as a therapeutic approach to cancer and neurodegenerative diseases. *Future Med. Chem.* **2016**, *8* (13), 1609−1634.

(6) Kang, Y.; Nian, H.; Rajendran, P.; Kim, E.; Dashwood, W. M.; Pinto, J. T.; Boardman, L. A.; Thibodeau, S. N.; Limburg, P. J.; Lohr, C. V.; Bisson, W. H.; Williams, D. E.; Ho, E.; Dashwood, R. H. HDAC8 and STAT3 repress BMF gene activity in colon cancer cells. *Cell Death Dis.* **2014**, *5* (10), No. e1476.

(7) Gao, J.; Siddoway, B.; Huang, Q.; Xia, H. Inactivation of CREB mediated gene transcription by HDAC8 bound protein phosphatase. *Biochem. Biophys. Res. Commun.* **2009**, *379* (1), 1−5.

(8) Qian, Y.; Zhang, J.; Jung, Y. S.; Chen, X. DEC1 coordinates with HDAC8 to differentially regulate TAp73 and DeltaNp73 expression. *PLoS One* **2014**, *9* (1), No. e84015.

(9) Bradbury, C. A.; Khanim, F. L.; Hayden, R.; Bunce, C. M.; White, D. A.; Drayson, M. T.; Craddock, C.; Turner, B. M. Histone deacetylases in acute myeloid leukaemia show a distinctive pattern of expression that changes selectively in response to deacetylase inhibitors. *Leukemia* **2005**, *19* (10), 1751−1759.

(10) Qi, J.; Singh, S.; Hua, W. K.; Cai, Q.; Chao, S. W.; Li, L.; Liu, H.; Ho, Y.; McDonald, T.; Lin, A.; Marcucci, G.; Bhatia, R.; Huang, W. J.; Chang, C. I.; Kuo, Y. H. HDAC8 Inhibition Specifically Targets Inv(16) Acute Myeloid Leukemic Stem Cells by Restoring p53 Acetylation. *Cell Stem Cell* **2015**, *17* (5), 597−610.

(11) Haberland, M.; Mokalled, M. H.; Montgomery, R. L.; Olson, E. N. Epigenetic control of skull morphogenesis by histone deacetylase 8. *Genes Dev.* **2009**, *23* (14), 1625−1630.

(12) Singh, V. P.; Yueh, W. T.; Gerton, J. L.; Duncan, F. E. Oocyte-specific deletion of Hdac8 in mice reveals stage-specific effects on fertility. *Reproduction* **2019**, *157* (3), 305−316.

(13) Amin, S. A.; Adhikari, N.; Jha, T. Structure-activity relationships of hydroxamate-based histone deacetylase-8 inhibitors: reality behind anticancer drug discovery. *Future Med. Chem.* **2017**, *9* (18), 2211−2237.

(14) Adhikari, N.; Amin, S. A.; Jha, T. Selective and nonselective HDAC8 inhibitors: a therapeutic patent review. *Pharm. Pat. Anal.* **2018**, *7* (6), 259−276.

(15) Amin, S. A.; Adhikari, N.; Jha, T. Structure-activity relationships of HDAC8 inhibitors: Non-hydroxamates as anticancer agents. *Pharmacol. Res.* **2018**, *131*, 128−142.

(16) Chotitumnavee, J.; Yamashita, Y.; Takahashi, Y.; Takada, Y.; Iida, T.; Oba, M.; Itoh, Y.; Suzuki, T. Selective degradation of histone deacetylase 8 mediated by a proteolysis targeting chimera (PROTAC). *Chem. Commun. (Camb.)* **2022**, *58* (29), 4635−4638.

(17) Pettersson, M.; Crews, C. M. Proteolysis TArgeting Chimeras (PROTACs) - Past, present and future. *Drug Discovery Today Technol.* **2019**, *31*, 15−27.

(18) Paiva, S. L.; Crews, C. M. Targeted protein degradation: elements of PROTAC design. *Curr. Opin. Chem. Biol.* **2019**, *50*, 111−119.

(19) Bekes, M.; Langley, D. R.; Crews, C. M. PROTAC targeted protein degraders: the past is prologue. *Nat. Rev. Drug Discovery* **2022**, *21* (3), 181−200.

(20) Hu, Z.; Crews, C. M. Recent Developments in PROTAC-Mediated Protein Degradation: From Bench to Clinic. *ChemBioChem* **2022**, *23* (2), No. e202100270.

(21) Chen, S.; Zheng, Y.; Liang, B.; Yin, Y.; Yao, J.; Wang, Q.; Liu, Y.; Neamati, N. The application of PROTAC in HDAC. *Eur. J. Med. Chem.* **2023**, *260*, 115746.

(22) Huang, J.; Su, J.; Wang, H.; Chen, J.; Tian, Y.; Zhang, J.; Feng, T.; Di, L.; Lu, X.; Sheng, H.; Zhu, Q.; Chen, X.; Wang, J.; He, X.; Yerkinkazhina, Y.; Xie, Z.; Shu, Y.; Kang, T.; Tang, H.; Qian, J.; Zhu, W. G. Discovery of Novel PROTAC SIRT6 Degraders with Potent Efficacy against Hepatocellular Carcinoma. *J. Med. Chem.* **2024**, *67* (19), 17319−17349.

(23) Zhao, C.; Chen, D.; Suo, F.; Setroikromo, R.; Quax, W. J.; Dekker, F. J. Discovery of highly potent HDAC8 PROTACs with anti-tumor activity. *Bioorg. Chem.* **2023**, *136*, 106546.

(24) Ibrahim, H. S.; Guo, M.; Hilscher, S.; Erdmann, F.; Schmidt, M.; Schutkowski, M.; Sheng, C.; Sippl, W. Probing class I histone deacetylases (HDAC) with proteolysis targeting chimera (PROTAC) for the development of highly potent and selective degraders. *Bioorg. Chem.* **2024**, *153*, 107887.

(25) Sun, Z.; Deng, B.; Yang, Z.; Mai, R.; Huang, J.; Ma, Z.; Chen, T.; Chen, J. Discovery of pomalidomide-based PROTACs for selective degradation of histone deacetylase 8. *Eur. J. Med. Chem.* **2022**, *239*, 114544.

(26) Huang, J.; Zhang, J.; Xu, W.; Wu, Q.; Zeng, R.; Liu, Z.; Tao, W.; Chen, Q.; Wang, Y.; Zhu, W. G. Structure-Based Discovery of Selective Histone Deacetylase 8 Degraders with Potent Anticancer Activity. *J. Med. Chem.* **2023**, *66* (2), 1186−1209.

(27) Darwish, S.; Ghazy, E.; Heimburg, T.; Herp, D.; Zeyen, P.; Salem-Altintas, R.; Ridinger, J.; Robaa, D.; Schmidtkunz, K.;

https://doi.org/10.1021/acs.jmedchem.5c00939
J. Med. Chem. 2026, 69, 918−943

Erdmann, F.; Schmidt, M.; Romier, C.; Jung, M.; Oehme, I.; Sippl, W. Design, Synthesis and Biological Characterization of Histone Deacetylase 8 (HDAC8) Proteolysis Targeting Chimeras (PROTACs) with Anti-Neuroblastoma Activity. *Int. J. Mol. Sci.* **2022**, *23* (14), 7535.
(28) Xiao, Y.; Hale, S.; Awasthee, N.; Meng, C.; Zhang, X.; Liu, Y.; Ding, H.; Huo, Z.; Lv, D.; Zhang, W.; He, M.; Zheng, G.; Liao, D. HDAC3 and HDAC8 PROTAC dual degrader reveals roles of histone acetylation in gene regulation. *Cell Chem. Biol.* **2023**, *30* (11), 1421−1435.e12.
(29) Xiao, Y.; Awasthee, N.; Liu, Y.; Meng, C.; He, M. Y.; Hale, S.; Karki, R.; Lin, Z.; Mosterio, M.; Garcia, B. A.; Kridel, R.; Liao, D.; Zheng, G. Discovery of a Highly Potent and Selective HDAC8 Degrader: Advancing the Functional Understanding and Therapeutic Potential of HDAC8. *J. Med. Chem.* **2024**, *67* (15), 12784−12806.
(30) Zhao, C.; Zhang, J.; Zhou, H.; Setroikromo, R.; Poelarends, G. J.; Dekker, F. J. Exploration of Hydrazide-Based HDAC8 PROTACs for the Treatment of Hematological Malignancies and Solid Tumors. *J. Med. Chem.* **2024**, *67* (16), 14016−14039.
(31) Marek, M.; Shaik, T. B.; Heimburg, T.; Chakrabarti, A.; Lancelot, J.; Ramos-Morales, E.; Da Veiga, C.; Kalinin, D.; Melesina, J.; Robaa, D.; Schmidtkunz, K.; Suzuki, T.; Holl, R.; Ennifar, E.; Pierce, R. J.; Jung, M.; Sippl, W.; Romier, C. Characterization of Histone Deacetylase 8 (HDAC8) Selective Inhibition Reveals Specific Active Site Structural and Functional Determinants. *J. Med. Chem.* **2018**, *61* (22), 10000−10016.
(32) Somoza, J. R.; Skene, R. J.; Katz, B. A.; Mol, C.; Ho, J. D.; Jennings, A. J.; Luong, C.; Arvai, A.; Buggy, J. J.; Chi, E.; Tang, J.; Sang, B. C.; Verner, E.; Wynands, R.; Leahy, E. M.; Dougan, D. R.; Snell, G.; Navre, M.; Knuth, M. W.; Swanson, R. V.; McRee, D. E.; Tari, L. W. Structural snapshots of human HDAC8 provide insights into the class I histone deacetylases. *Structure* **2004**, *12* (7), 1325−1334.
(33) Min, J.; Mayasundari, A.; Keramatnia, F.; Jonchere, B.; Yang, S. W.; Jarusiewicz, J.; Actis, M.; Das, S.; Young, B.; Slavish, J.; Yang, L.; Li, Y.; Fu, X.; Garrett, S. H.; Yun, M. K.; Li, Z.; Nithianantham, S.; Chai, S.; Chen, T.; Shelat, A.; Lee, R. E.; Nishiguchi, G.; White, S. W.; Roussel, M. F.; Potts, P. R.; Fischer, M.; Rankovic, Z. Phenyl-Glutarimides: Alternative Cereblon Binders for the Design of PROTACs. *Angew. Chem., Int. Ed. Engl.* **2021**, *60* (51), 26663−26670.
(34) Bradner, J. E.; West, N.; Grachan, M. L.; Greenberg, E. F.; Haggarty, S. J.; Warnow, T.; Mazitschek, R. Chemical phylogenetics of histone deacetylases. *Nat. Chem. Biol.* **2010**, *6* (3), 238−243.
(35) Madsen, A. S.; Olsen, C. A. Substrates for efficient fluorometric screening employing the NAD-dependent sirtuin 5 lysine deacylase (KDAC) enzyme. *J. Med. Chem.* **2012**, *55* (11), 5582−5590.
(36) Zerfas, B. L.; Huerta, F.; Liu, H.; Du, G.; Gray, N. S.; Jones, L. H.; Nowak, R. P. Advancing targeted protein degrader discovery by measuring cereblon engagement in cells. *Methods Enzymol.* **2023**, *681*, 169−188.
(37) Zhai, S.; Honin, I.; Schäker-Hübner, L.; Hanl, M.; Jacobi, L.; Dressler, F.; Pieńkowska, D. E.; König, P.; Gerhartz, J.; Voget, R.; Bendas, G.; Gütschow, M.; Meissner, F.; Burckhardt, B. B.; Nowak, R. P.; Steinebach, C.; Hansen, F. K. Development and characterization of the first selective class IIb histone deacetylase degraders. *J. Med. Chem.* **2025**, *68*, 13793−13821.
(38) Nowak, R. P.; Ragosta, L.; Huerta, F.; Liu, H.; Ficarro, S. B.; Cruite, J. T.; Metivier, R. J.; Donovan, K. A.; Marto, J. A.; Fischer, E. S.; Zerfas, B. L.; Jones, L. H. Development of a covalent cereblon-based PROTAC employing a fluorosulfate warhead. *RSC Chem. Biol.* **2023**, *4* (11), 906−912.
(39) Bricelj, A.; Dora Ng, Y. L.; Ferber, D.; Kuchta, R.; Müller, S.; Monschke, M.; Wagner, K. G.; Krönke, J.; Sosič, I.; Gütschow, M.; Steinebach, C. Influence of Linker Attachment Points on the Stability and Neosubstrate Degradation of Cereblon Ligands. *ACS Med. Chem. Lett.* **2021**, *12* (11), 1733−1738.
(40) Drummond, M. L.; Williams, C. I. In Silico Modeling of PROTAC-Mediated Ternary Complexes: Validation and Application. *J. Chem. Inf. Model.* **2019**, *59* (4), 1634−1644.
(41) Drummond, M. L.; Henry, A.; Li, H.; Williams, C. I. Improved Accuracy for Modeling PROTAC-Mediated Ternary Complex Formation and Targeted Protein Degradation via New In Silico Methodologies. *J. Chem. Inf. Model.* **2020**, *60* (10), 5234−5254.
(42) Oikonomou, A.; Watrin, T.; Valsecchi, L.; Scharov, K.; Savino, A. M.; Schliehe-Diecks, J.; Bardini, M.; Fazio, G.; Bresolin, S.; Biondi, A.; Borkhardt, A.; Bhatia, S.; Cazzaniga, G.; Palmi, C. Synergistic drug interactions of the histone deacetylase inhibitor givinostat (ITF2357) in CRLF2-rearranged pediatric B-cell precursor acute lymphoblastic leukemia identified by high-throughput drug screening. *Heliyon* **2024**, *10* (13), No. e34033.
(43) Oikonomou, A.; Valsecchi, L.; Quadri, M.; Watrin, T.; Scharov, K.; Procopio, S.; Tu, J. W.; Vogt, M.; Savino, A. M.; Silvestri, D.; Valsecchi, M. G.; Biondi, A.; Borkhardt, A.; Bhatia, S.; Cazzaniga, G.; Fazio, G.; Bardini, M.; Palmi, C. High-throughput screening as a drug repurposing strategy for poor outcome subgroups of pediatric B-cell precursor Acute Lymphoblastic Leukemia. *Biochem. Pharmacol.* **2023**, *217*, 115809.
(44) Faião-Flores, F.; Emmons, M. F.; Durante, M. A.; Kinose, F.; Saha, B.; Fang, B.; Koomen, J. M.; Chellappan, S. P.; Maria-Engler, S. S.; Rix, U.; Licht, J. D.; Harbour, J. W.; Smalley, K. S. M. HDAC Inhibition Enhances the In Vivo Efficacy of MEK Inhibitor Therapy in Uveal Melanoma. *Clin. Cancer Res.* **2019**, *25* (18), 5686−5701.
(45) Hua, W. K.; Qi, J.; Cai, Q.; Carnahan, E.; Ayala Ramirez, M.; Li, L.; Marcucci, G.; Kuo, Y. H. HDAC8 regulates long-term hematopoietic stem-cell maintenance under stress by modulating p53 activity. *Blood* **2017**, *130* (24), 2619−2630.
(46) Li, Y.; Manickam, G.; Ghoshal, A.; Subramaniam, P. More Efficient Palladium Catalyst for Hydrogenolysis of Benzyl Groups. *Synth. Commun.* **2006**, *36* (7), 925−928.
(47) Zhang, X.; Thummuri, D.; He, Y.; Liu, X.; Zhang, P.; Zhou, D.; Zheng, G. Utilizing PROTAC technology to address the on-target platelet toxicity associated with inhibition of BCL-X(L). *Chem. Commun. (Camb.)* **2019**, *55* (98), 14765−14768.
(48) Zhou, L.; Chen, W.; Cao, C.; Shi, Y.; Ye, W.; Hu, J.; Wang, L.; Zhou, W. Design and synthesis of alpha-naphthoflavone chimera derivatives able to eliminate cytochrome P450 (CYP)1B1-mediated drug resistance via targeted CYP1B1 degradation. *Eur. J. Med. Chem.* **2020**, *189*, 112028.
(49) Liu, Q.; Tu, G.; Hu, Y.; Jiang, Q.; Liu, J.; Lin, S.; Yu, Z.; Li, G.; Wu, X.; Tang, Y.; Huang, X.; Xu, J.; Liu, Y.; Wu, L. Discovery of BP3 as an efficacious proteolysis targeting chimera (PROTAC) degrader of HSP90 for treating breast cancer. *Eur. J. Med. Chem.* **2022**, *228*, 114013.
(50) Steinebach, C.; Ng, Y. L. D.; Sosič, I.; Lee, C. S.; Chen, S.; Lindner, S.; Vu, L. P.; Bricelj, A.; Haschemi, R.; Monschke, M.; Steinwarz, E.; Wagner, K. G.; Bendas, G.; Luo, J.; Gutschow, M.; Kronke, J. Systematic exploration of different E3 ubiquitin ligases: an approach towards potent and selective CDK6 degraders. *Chem. Sci.* **2020**, *11* (13), 3474−3486.
(51) Valko, K.; Nunhuck, S.; Bevan, C.; Abraham, M. H.; Reynolds, D. P. Fast gradient HPLC method to determine compounds binding to human serum albumin. Relationships with octanol/water and immobilized artificial membrane lipophilicity. *J. Pharm. Sci.* **2003**, *92* (11), 2236−2248.
(52) Schäker-Hübner, L.; Haschemi, R.; Buch, T.; Kraft, F. B.; Brumme, B.; Schöler, A.; Jenke, R.; Meiler, J.; Aigner, A.; Bendas, G.; Hansen, F. K. Balancing Histone Deacetylase (HDAC) Inhibition and Drug-likeness: Biological and Physicochemical Evaluation of Class I Selective HDAC Inhibitors. *ChemMedChem* **2022**, *17* (9), No. e202100755.
(53) Sinatra, L.; Vogelmann, A.; Friedrich, F.; Tararina, M. A.; Neuwirt, E.; Colcerasa, A.; König, P.; Toy, L.; Yesiloglu, T. Z.; Hilscher, S.; Gaitzsch, L.; Papenkordt, N.; Zhai, S.; Zhang, L.; Romier, C.; Einsle, O.; Sippl, W.; Schutkowski, M.; Gross, O.; Bendas, G.; Christianson, D. W.; Hansen, F. K.; Jung, M.; Schiedel, M. Development of First-in-Class Dual Sirt2/HDAC6 Inhibitors as Molecular Tools for Dual Inhibition of Tubulin Deacetylation. *J. Med. Chem.* **2023**, *66* (21), 14787−14814.

https://doi.org/10.1021/acs.jmedchem.5c00939
J. Med. Chem. 2026, 69, 918−943

(54) Feller, F.; Hansen, F. K. Targeted Protein Degradation of Histone Deacetylases by Hydrophobically Tagged Inhibitors. *ACS Med. Chem. Lett.* **2023**, *14* (12), 1863−1868.
(55) Donovan, K. A.; An, J.; Nowak, R. P.; Yuan, J. C.; Fink, E. C.; Berry, B. C.; Ebert, B. L.; Fischer, E. S. Thalidomide promotes degradation of SALL4, a transcription factor implicated in Duane Radial Ray syndrome. *eLife* **2018**, *7*, No. e38430.
(56) Skowronek, P.; Thielert, M.; Voytik, E.; Tanzer, M. C.; Hansen, F. M.; Willems, S.; Karayel, O.; Brunner, A.-D.; Meier, F.; Mann, M. Rapid and in-depth coverage of the (phospho-) proteome with deep libraries and optimal window design for dia-PASEF. *Mol. Cell. Proteomics* **2022**, *21* (9), 100279.
(57) Demichev, V.; Messner, C. B.; Vernardis, S. I.; Lilley, K. S.; Ralser, M. DIA-NN: neural networks and interference correction enable deep proteome coverage in high throughput. *Nat. Methods* **2020**, *17* (1), 41−44.
(58) Ritchie, M. E.; Phipson, B.; Wu, D.; Hu, Y.; Law, C. W.; Shi, W.; Smyth, G. K. limma powers differential expression analyses for RNA-sequencing and microarray studies. *Nucleic Acids Res.* **2015**, *43* (7), No. e47.
(59) Wang, E. S.; Verano, A. L.; Nowak, R. P.; Yuan, J. C.; Donovan, K. A.; Eleuteri, N. A.; Yue, H.; Ngo, K. H.; Lizotte, P. H.; Gokhale, P. C.; Gray, N. S.; Fischer, E. S. Acute pharmacological degradation of Helios destabilizes regulatory T cells. *Nat. Chem. Biol.* **2021**, *17* (6), 711−717.
(60) Abdulrahman, W.; Uhring, M.; Kolb-Cheynel, I.; Garnier, J. M.; Moras, D.; Rochel, N.; Busso, D.; Poterszman, A. A set of baculovirus transfer vectors for screening of affinity tags and parallel expression strategies. *Anal. Biochem.* **2009**, *385* (2), 383−385.

https://doi.org/10.1021/acs.jmedchem.5c00939
J. Med. Chem. 2026, 69, 918−943

Supporting Information

Discovery of histone deacetylase 8 (HDAC8)-specific proteolysis-targeting chimeras with anti-cancer activity against hematological malignancies

Shiyang Zhai,[a] Marie Kemkes,[b] Cindy-Esther Kponomaizoun,[a] Jan Gerhartz,[c] Felix Feller,[a] Jia-Wey Tu,[b] Dominika Ewa Pieńkowska,[c] Julian Schliehe-Diecks,[b] Ina Dressel,[c] Michael Gütschow,[d] Radosław P. Nowak,[c] Christian Steinebach,[d] Sanil Bhatia,[b],* Finn K. Hansen[a],*

[a] Department of Pharmaceutical and Cell Biological Chemistry, Pharmaceutical Institute, University of Bonn, Bonn 53121, Germany.

[b] Department of Paediatric Oncology, Haematology and Clinical Immunology, Medical Faculty, Heinrich-Heine University Dusseldorf, Düsseldorf 40225, Germany

[c] Institute of Structural Biology, Medical Faculty, University of Bonn, Bonn 53127, Germany.

[d] Department of Pharmaceutical and Medicinal Chemistry, Pharmaceutical Institute, University of Bonn, Bonn 53121, Germany.

Corresponding Authors:

*sanil.bhatia@med.uni-duesseldorf.de

*finn.hansen@uni-bonn.de

Table of contents

1. Synthesis of non-degrading control **BP1-N** S3

2. Supplementary Figures and Table S3

3. ^{1}H, ^{13}C NMR, HR-MS spectra and HPLC chromatograms of **BP1-BP10**, **BP1-N** S11

4. References S33

1. Synthesis of non-degrading control BP1-N

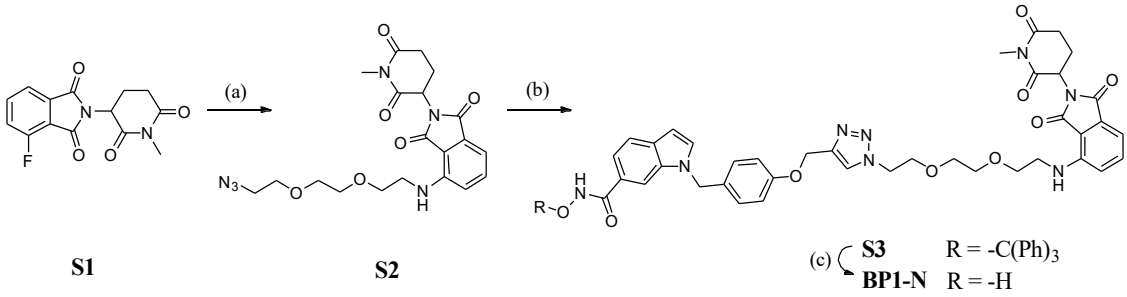

Scheme S1. (a) 2-(2-(2-Azidoethoxy)ethoxy)ethan-1-amine, DIPEA, anhydrous DMSO, 90 °C, 17 h, 48%; (b) **5**, L-ascorbic acid, $CuSO_4$, DMF/H_2O (10:1), rt, 22 h, 75%; (c) triisopropylsilane, TFA, DCM, rt, 2.5 h, 40%.

2. Supplementary Figures and Table

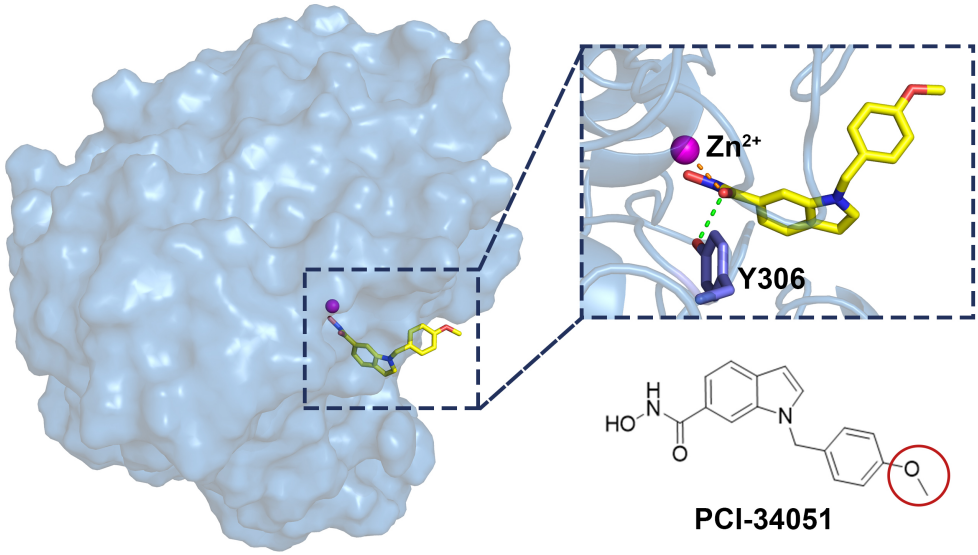

Figure S1. Docking pose of PCI-34051 in the human HDAC8 (PDB: 1T64). PCI-34051 is depicted in yellow. A hydrogen bond is shown in a green dashed line, while the metal chelation interaction is represented in an orange dashed line.

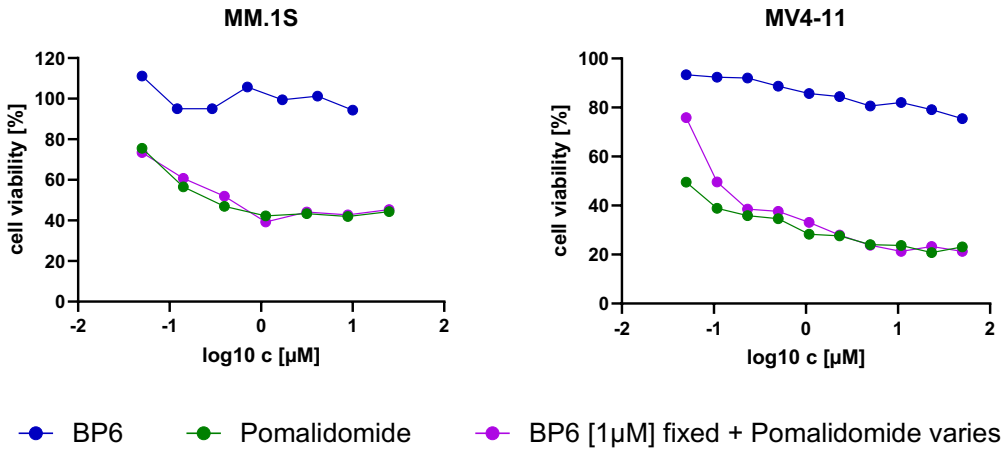

Figure S2. Cell viability was assessed via CellTiter-Glo luminescent assay after 72h. The y-axis shows cell viability [%] normalized to each DMSO control, while the x-axis indicates the treatment conditions [µM].

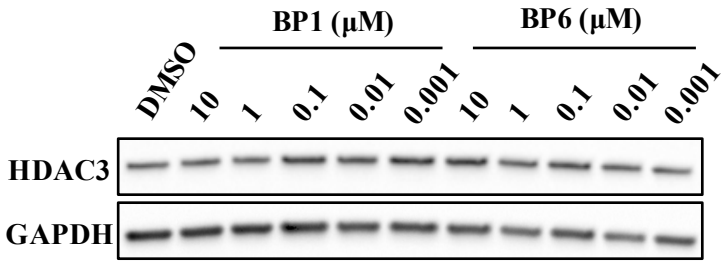

Figure S3. HDAC3 degradation induced by IMiD-based **BP1** and PG-based **BP6** at different concentrations. MM.1S cells treated for 24 h with **BP1** and **BP6** at different concentrations. HDAC3 levels were detected by immunoblot analysis. DMSO was used as vehicle control and GAPDH as loading control. Representative image from n = 2 biologically independent experiments, each performed in duplicates.

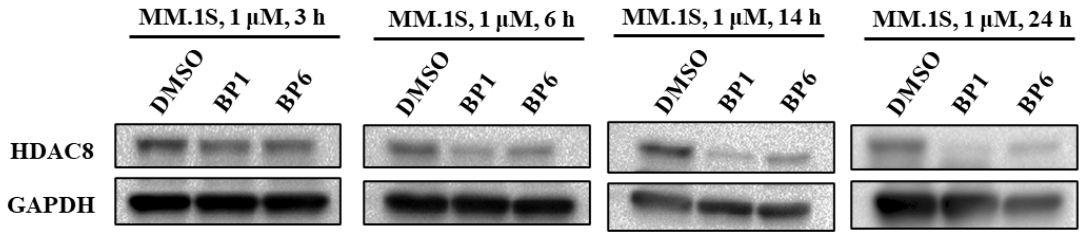

Figure S4. HDAC8 degradation by IMiD-based **BP1** and PG-based **BP6** at different time points. MM.1S cells treated for 3, 6, 14, and 24 h, respectively, with **BP1** and **BP6** at 1 µM. HDAC8

levels were detected by immunoblot analysis. DMSO samples from different incubation time points were used as vehicle control and GAPDH as loading control. Representative image from n = 2 replicates.

A

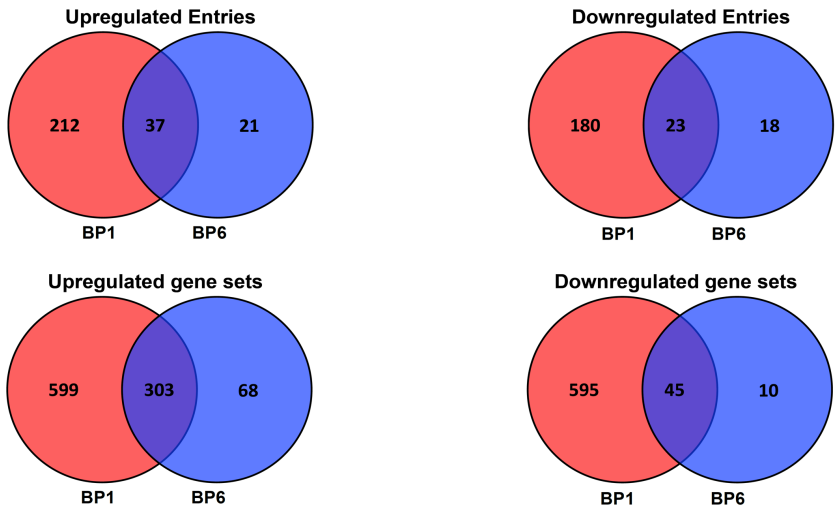

B

Top 10 upregulated proteins between shared BP1 and BP6				
	BP1		BP6	
Gene Symbol	log2(FC)	-log10(FDR)	log2(FC)	-log10(FDR)
HMGB1	1.45	2.21	1.24	2.10
IER3IP1	1.07	1.40	1.15	1.25
CEP85L	0.79	1.22	1.04	1.07
EIF1AX	0.93	1.40	0.60	1.04
RAC1	0.80	1.32	0.69	1.10
HNRNPA1	0.72	1.72	0.59	1.83
RER1	0.76	1.31	0.44	1.48
HNRNPA3	0.63	1.84	0.46	1.59
DOK1	0.52	1.14	0.55	1.11
HINT1	0.65	2.29	0.40	1.63

Top 10 upregulated proteins in BP1		
Gene Symbol	log2(FC)	-log10(FDR)
ACTN1	1.56	3.94
CORO1B	1.52	3.70
GIPC1	1.45	3.01
PNMA2	1.44	2.87
VCL	1.35	3.45
SERPINH1	1.33	3.13
MYL4	1.27	2.94
GALNT6	1.24	1.55
OAS3	1.18	2.86
PSRC1	1.09	1.02

Top 10 upregulated proteins in BP6		
Gene Symbol	log2(FC)	-log10(FDR)
MT-ND1	1.13	2.25
RBIS	0.71	1.26
NT5C3B	0.64	1.06
INO80E	0.54	1.12
POTEJ	0.46	1.31
WRAP73	0.39	1.22
HEXIM2	0.38	1.16
DDX19A	0.37	1.24
ADI1	0.36	1.30
CFAP298	0.35	1.85

Top 10 downregulated proteins between shared BP1 and BP6				
	BP1		BP6	
Gene Symbol	log2(FC)	-log10(FDR)	log2(FC)	-log10(FDR)
RIC1	-3.78	1.43	-0.78	1.83
SAP30L	-1.24	1.15	-2.47	1.89
EPDR1	-0.98	1.65	-1.83	2.54
HDAC8	-1.34	1.75	-1.24	1.49
FBLL1	-1.25	2.00	-0.89	2.87
BANF1	-1.14	2.02	-0.95	1.61
COX17	-0.68	1.01	-1.33	2.11
TOMM5	-0.72	1.10	-0.80	1.03
GSKIP	-0.69	1.10	-0.83	1.05
MAGOH	-0.81	3.20	-0.55	1.95

Top 10 downregulated proteins in BP1		
Gene Symbol	log2(FC)	-log10(FDR)
IKZF1	-3.48	5.66
IKZF3	-2.93	3.83
ZFP91	-2.78	3.65
RAB28	-2.40	2.82
TUBAL3	-2.20	1.03
LPXN	-2.06	2.86
SLC20A1	-1.84	1.09
URM1	-1.75	2.23
EVI2B	-1.45	1.01
CENPM	-1.21	2.51

Top 10 downregulated proteins in BP6		
Gene Symbol	log2(FC)	-log10(FDR)
TMEM97	-5.42	6.42
MED21	-2.13	1.48
FAM193B	-1.33	1.01
RBFA	-1.21	1.07
UVRAG	-1.03	1.12
NA	-0.91	1.18
LAMP2	-0.89	2.03
METAP2	-0.71	2.87
CD1C	-0.68	1.36
RNASEH1	-0.55	1.08

Figure S5. Comparisons of proteomics result of **BP1** and **BP6**. (A) Venn diagrams comparing the deregulated protein entries (upper row) or differential enriched gene sets (lower row) that were found either in **BP1**, **BP6** or shared between both. The inclusion cut-off for the protein entries was set to FDR<0.1. Gene set enrichment analysis was performed via String and included genes had to pass FDR<0.05. (B) Tables comparing the log2(FC) and –log10(FDR) of the 10 most positively/negatively enriched proteins that are either shared (left column) or exclusive found in **BP1** or **BP6**.

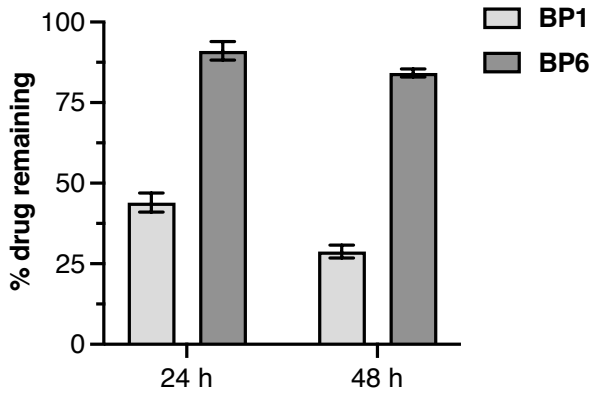

Figure S6. Compound stability in PBS buffer at pH 7.4. Percentage remaining compound left after incubation of ACN/buffer mixtures for the indicated times. The content was determined by an HPLC method.[1] All of the data were the average of at least three independent experiments.

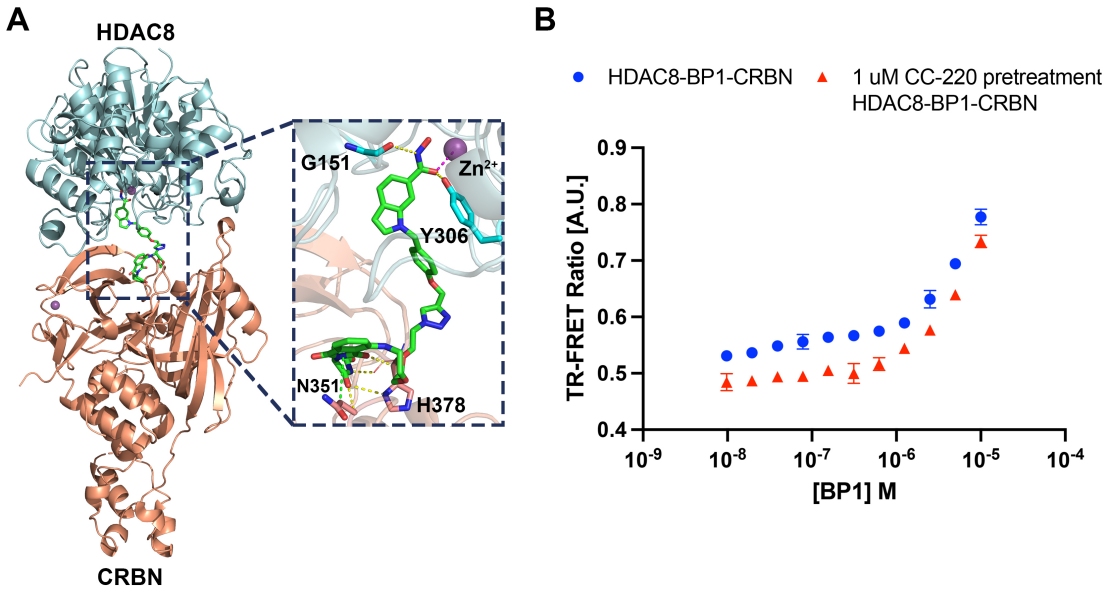

Figure S7. (A) Ternary complex modeling of HDAC8-**BP1**-CRBN. Hydrogen bonds are shown as yellow dashes, H–π interactions are shown as green dashes and metal chelation is indicated as purple dashes. (B) TR-FRET ternary complex formation between HDAC8 and CRBN in presence of **BP1** and in presence of CC-200 pretreatment (1 μM). Data is shown as mean ± SD of n = 4 replicates. Note that autofluorescence interference was observed.

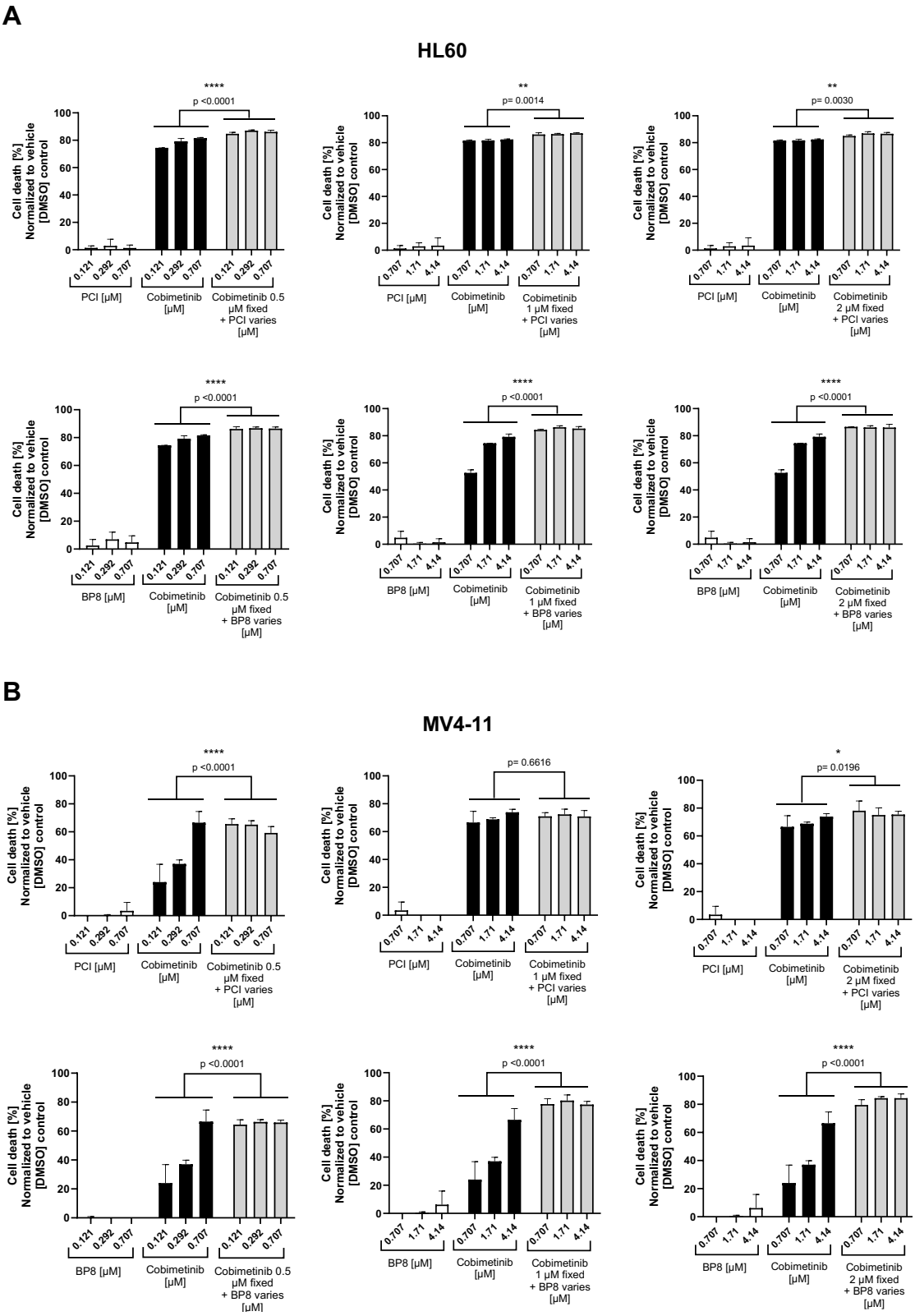

Figure S8. (A, B) Cell viability of HL60 (A) and MV4-11 (B) cells was assessed via CellTiter-Glo luminescent assay after 72h. The y-axis shows cell death [%] normalized to each DMSO control, while the x-axis indicates the treatment conditions of Cobimetinib (left), BP8 (middle) or PCI-34051or PCI (right). Error bars represent mean ± SD (n = 3). Statistical analysis was performed using two-way

ANOVA, followed by Tukey's multiple comparisons test to assess pairwise differences between groups. All datasets met the assumption of normality.

Table S1. Adjusted P values for all pairwise comparisons among the treatment conditions shown in **Figure 7**.

Condition	24 h	48 h	72 h
DMSO – BP1 3 µM	ns p=0.1700	ns P=0.0759	**** P<0.0001
DMSO – BP6 3 µM	ns p=0.7419	ns P=0.9942	**** P<0.0001
DMSO – BP1-N 3 µM	ns p=0.8836	* p=0.0244	**** p<0.0001
DMSO – PCI 3 µM	ns p>0.9999	ns p=0.0759	**** p<0.0001
DMSO – Vorinostat 0.5 µM	ns p=0.7419	**** p<0.0001	**** p<0.0001
DMSO – Vorinostat 1 µM	ns p=0.2687	**** p<0.0001	**** p<0.0001
BP1 3 µM – BP6 3 µM	ns p=0.8836	ns p=0.2163	**** p<0.0001
BP1 3 µM – BP1-N 3 µM	ns p=0.7419	ns p=0.9942	ns p>0.9999
BP1 3 µM – PCI 3 µM	ns p=0.2687	ns p>0.9999	**** p<0.0001

BP1 3 µM – Vorinostat 0.5 µM	* p=0.0122	**** p<0.0001	**** p<0.0001
BP1 3 µM – Vorinostat 1 µM	** p=0.0024	**** p<0.0001	**** p<0.0001
BP6 3 µM – BP1-N 3 µM	ns p>0.9999	ns p=0.0759	**** p<0.0001
BP6 3 µM – PCI 3 µM	ns p=0.8836	ns p=0.2163	**** p<0.0001
BP6 3 µM – Vorinostat 0.5 µM	ns p=0.1037	**** p<0.0001	**** p<0.0001
BP6 3 µM – Vorinostat 1 µM	* p=0.0210	**** p<0.0001	**** p<0.0001
BP1-N 3 µM – PCI 3 µM	ns p=0.9668	ns p=0.9942	**** p<0.0001
BP1-N 3 µM – Vorinostat 0.5 µM	ns p=0.1700	**** p<0.0001	**** p<0.0001
BP1-N 3 µM – Vorinostat 1 µM	* p=0.0362	**** p<0.0001	**** p<0.0001
PCI 3 µM – Vorinostat 0.5 µM	ns p=0.5698	**** p<0.0001	**** p<0.0001
PCI 3 µM – Vorinostat 1 µM	ns p=0.1700	**** p<0.0001	**** p<0.0001

Table S2. List of 48 FDA-approved drugs along with their target used for high-throughput drug screening.

Compounds	Target	Compounds	Target
5-Azacytidine	Antimetabolite	Panobinostat	HDAC inhibitor
5-Fluorouracil	Antimetabolite	Romidepsin	HDAC inhibitor
6-Mercaptopurine	Antimetabolite	Bortezomib	Proteasome inhibitor
6-Thioguanine	Antimetabolite	Carfilzomib	Proteasome inhibitor
Clofarabine	Antimetabolite	Ibrutinib	BTK inhibitor
Cytarabine	Antimetabolite	Dinaciclib	CDK inhibitor
Cyclocytidine	Antimetabolite	Imatinib	Bcr-Abl inhibitor
Nelarabine	Antimetabolite	Nilotinib	Bcr-Abl inhibitor
Gemcitabine	Antimetabolite	Ponatinib	Bcr-Abl; FGFR; FLT3; VEGFR
Methotrexate	Antimetabolite	Bosutinib	Bcr-Abl; Src
Cladribine	Antimetabolite	Dasatinib	Bcr-Abl; Src
Decitabine	Antimetabolite	Olaparib	PARP inhibitor
Vinblastine	Antimitotic	Midostaurin	PKC; VEGFR2; PDGFR; FLT3
Vincristine	Antimitotic	Quizartinib	FLT3 inhibitor
Cyclophosphamide	Alkylating agent	Baricitinib	JAK inhibitor
Idarubicin	Topoisomerase inhibitor	Momelotinib	JAK inhibitor
Epirubicin	Topoisomerase inhibitor	Ruxolitinib	JAK inhibitor
Etoposide	Topoisomerase inhibitor	Everolimus	mTOR inhibitor
Mitoxantrone	Topoisomerase inhibitor	Rapamycin	mTOR inhibitor
Daunorubicin	Topoisomerase inhibitor	Trametinib	MEK inhibitor
Doxorubicin	Topoisomerase inhibitor	Cobimetinib	MEK inhibitor
Amsacrine	Topoisomerase inhibitor	Venetoclax	BCL-2 inhibitor
Dexamethasone	GC/GCR complex	Enasidenib	IDH2 inhibitor
Prednisone	GC/GCR complex	Ivosidenib	IDH1 inhibitor

3. ^{1}H, ^{13}C NMR, HR-MS spectra and HPLC chromatograms of BP1-BP10, BP1-N

^{1}H NMR spectrum of **BP1** (600 MHz, DMSO-d_6)

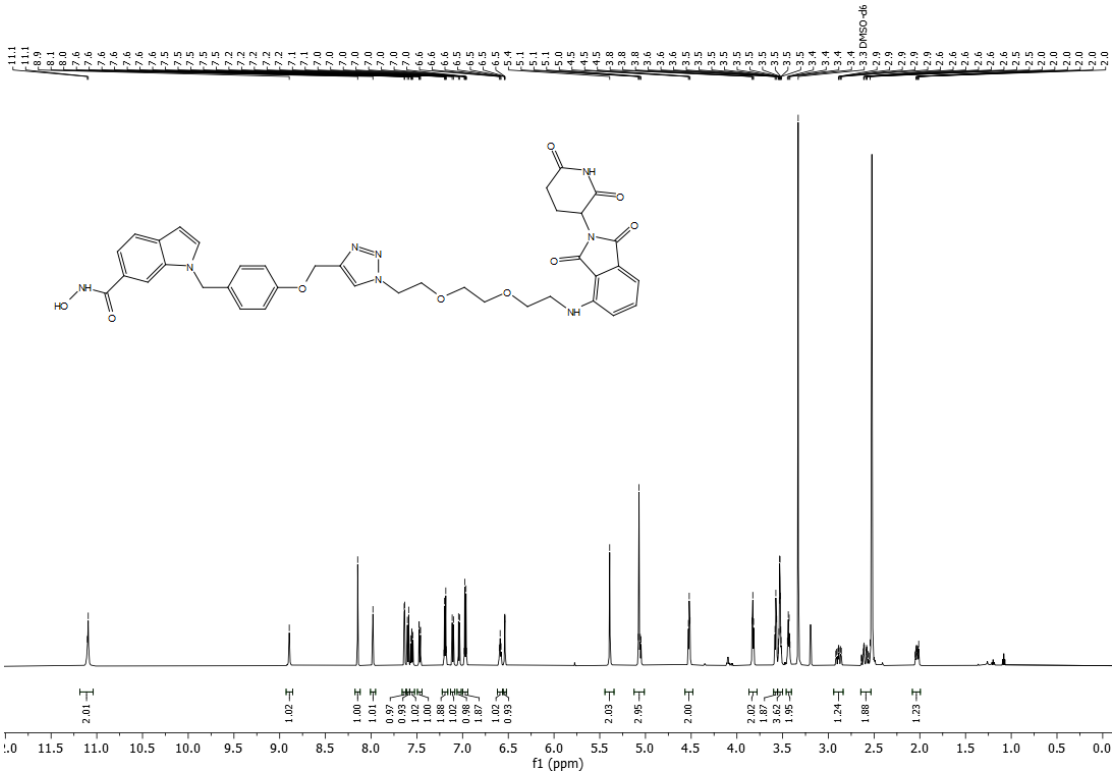

^{13}C NMR spectrum of **BP1** (600 MHz, DMSO-d_6)

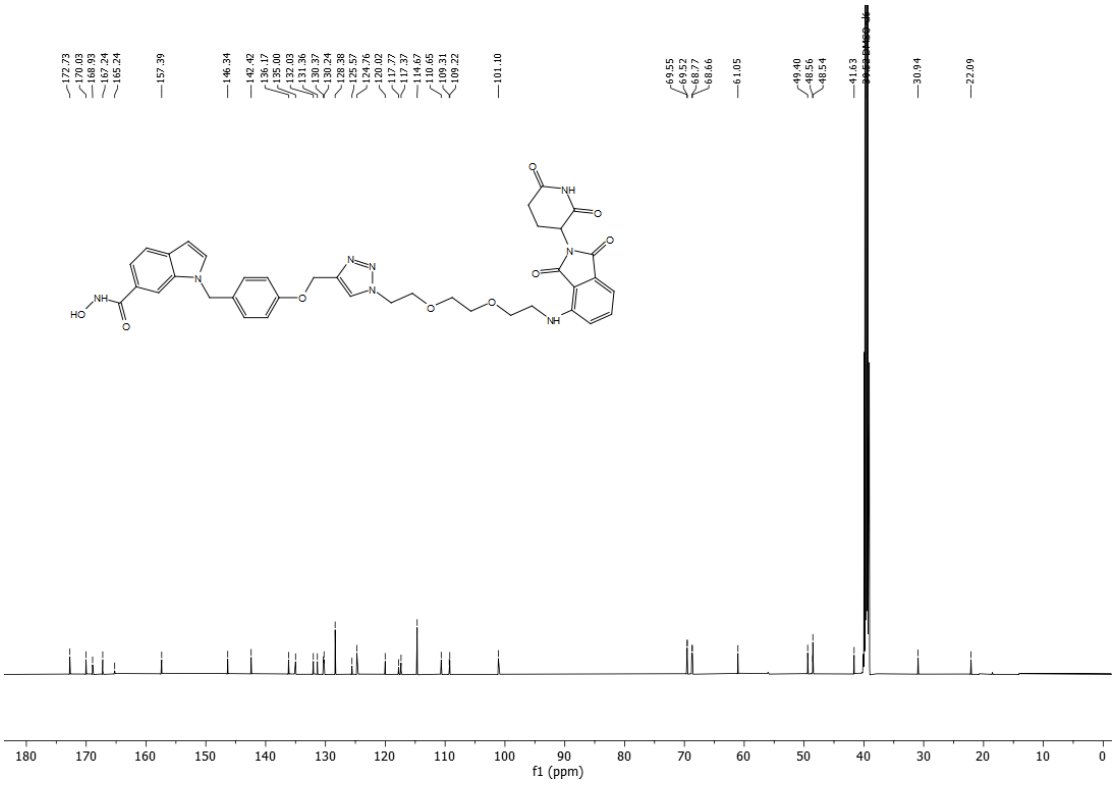

HR-MS spectrum of **BP1**

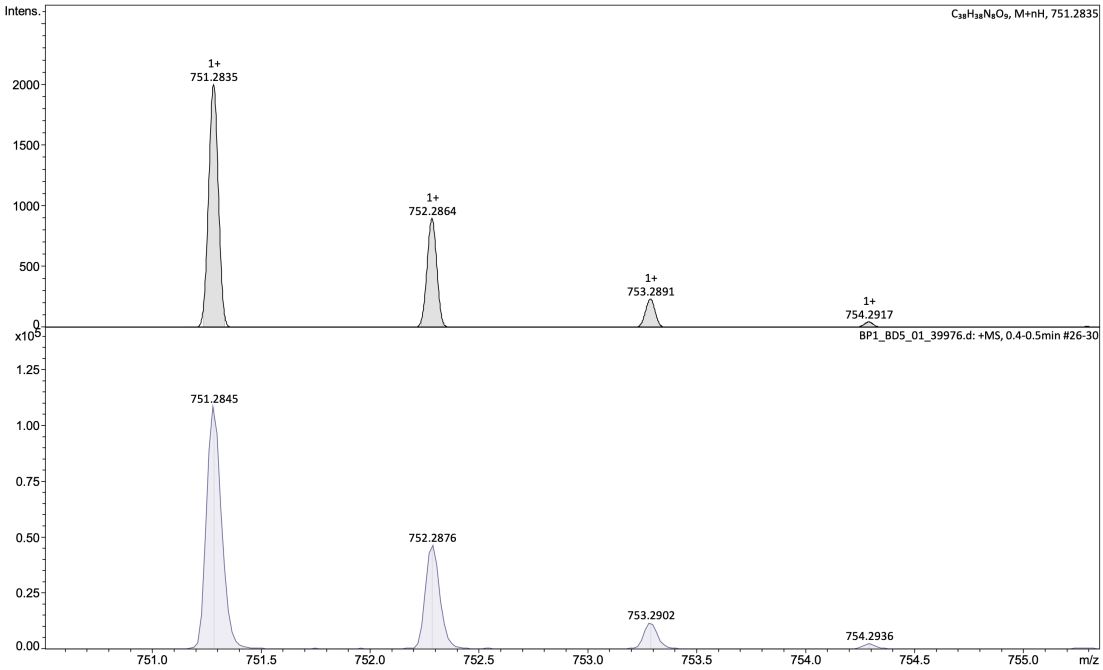

HPLC chromatogram of **BP1** (Purity: 99.3%)

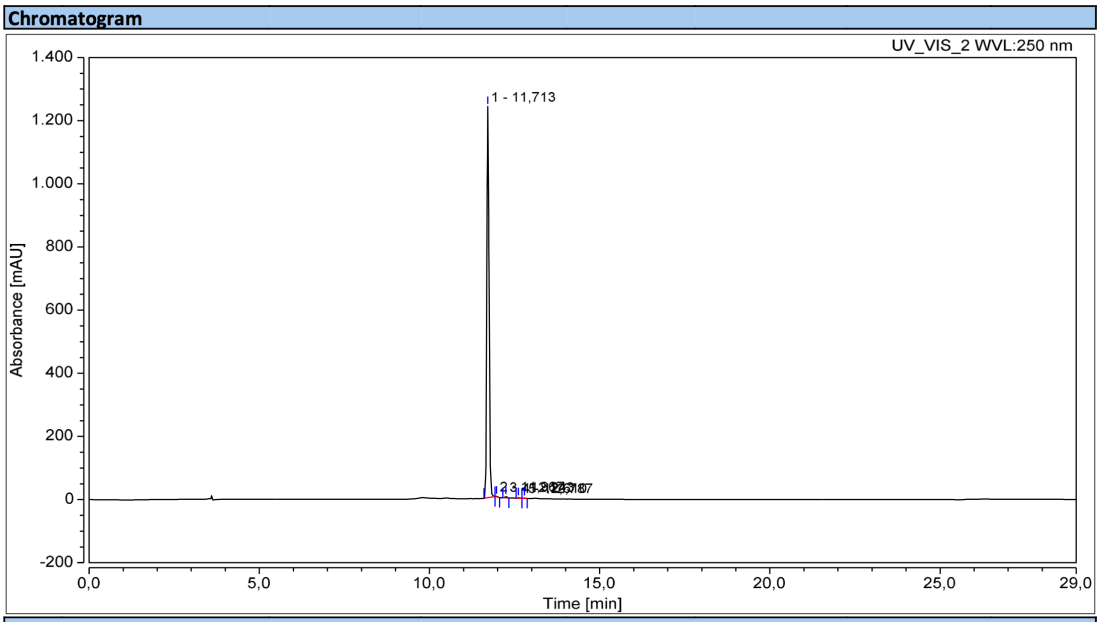

Integration Results

No.	Peak Name	Retention Time min	Area mAU*min	Height mAU	Relative Area %	Relative Height %	Amount n.a.
1		11,713	91,201	1238,556	99,34	99,30	n.a.
2		11,967	0,139	1,989	0,15	0,16	n.a.
3		12,243	0,282	4,014	0,31	0,32	n.a.
4		12,610	0,101	1,483	0,11	0,12	n.a.
5		12,787	0,088	1,195	0,10	0,10	n.a.
Total:			**91,811**	**1247,237**	**100,00**	**100,00**	

^{1}H NMR spectrum of **BP2** (600 MHz, DMSO-d_6)

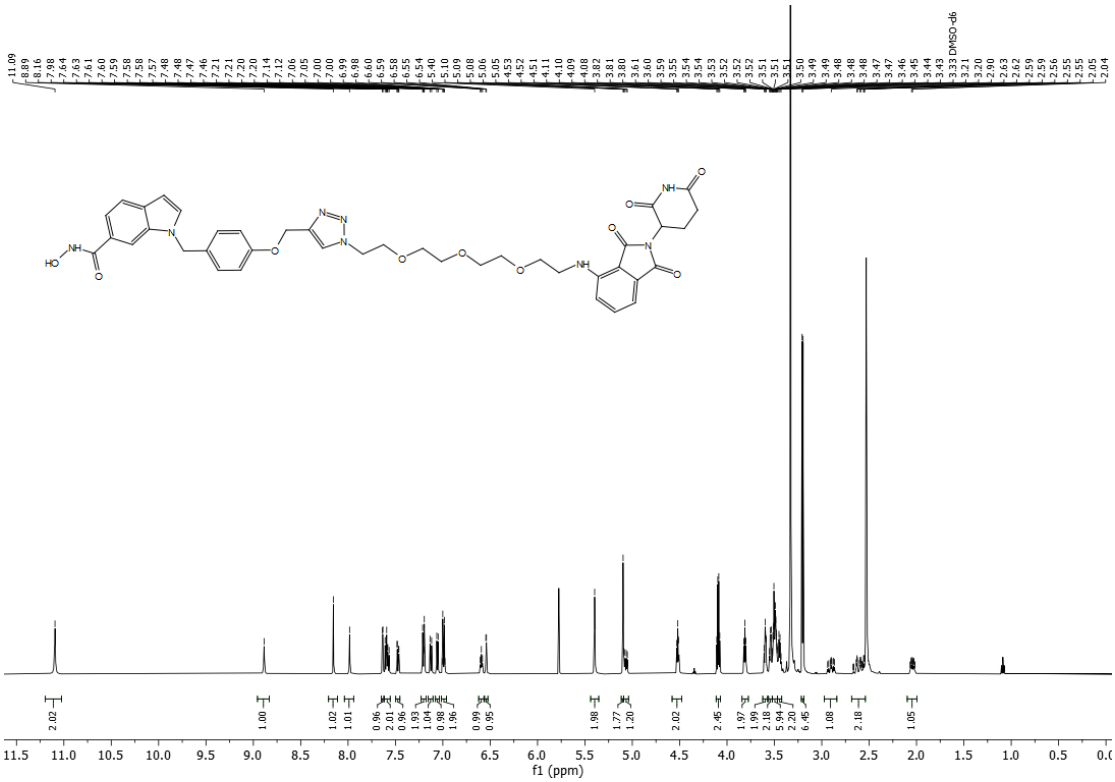

^{13}C NMR spectrum of **BP2** (600 MHz, DMSO-d_6)

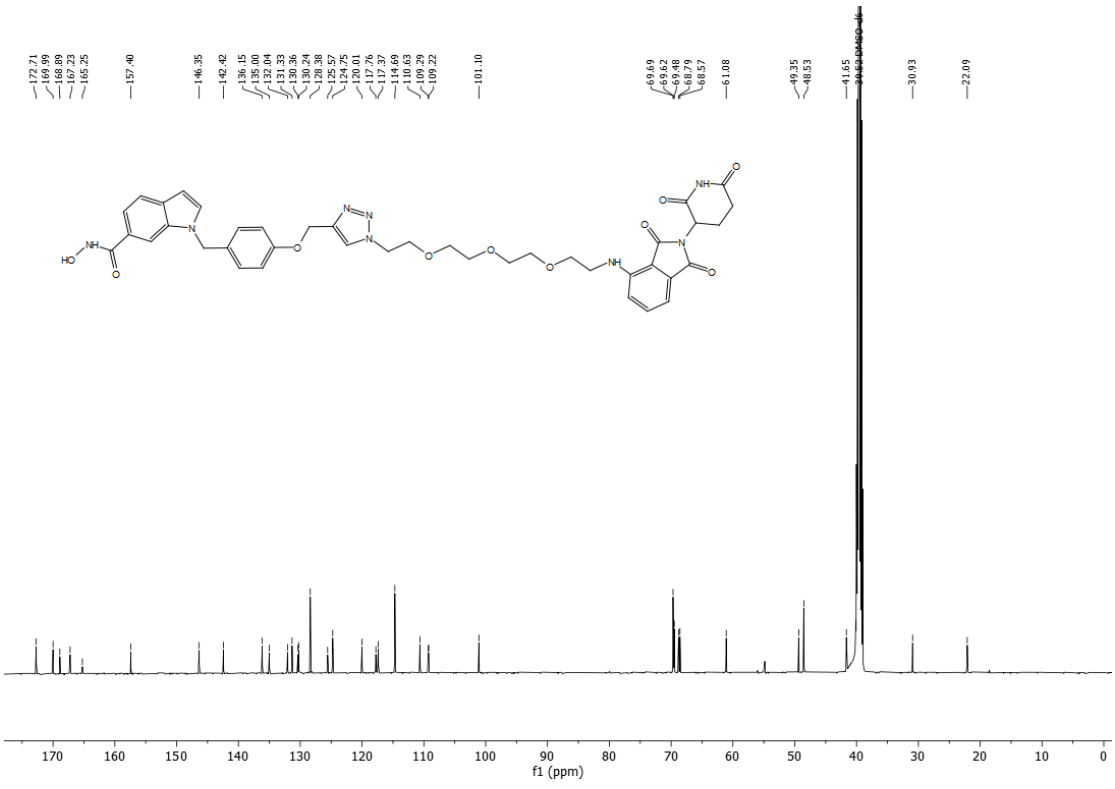

HR-MS spectrum of **BP2**

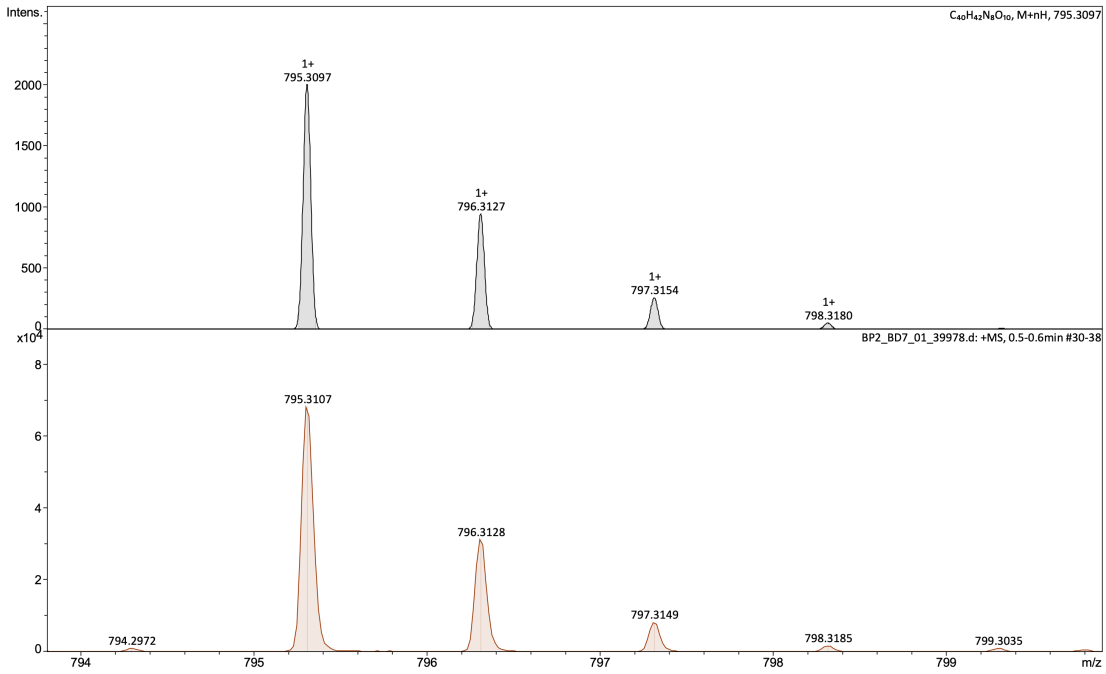

HPLC chromatogram of **BP2** (Purity: 97.6%)

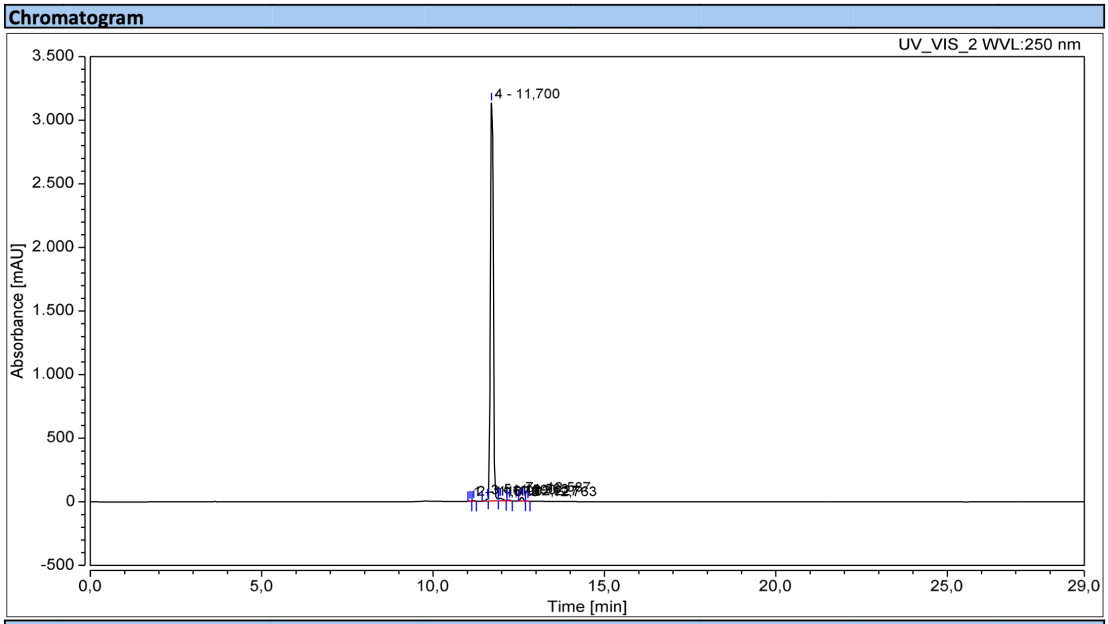

Integration Results

No.	Peak Name	Retention Time min	Area mAU*min	Height mAU	Relative Area %	Relative Height %	Amount n.a.
1		11,073	0,177	3,312	0,06	0,10	n.a.
2		11,190	0,412	6,700	0,13	0,21	n.a.
3		11,590	1,213	15,888	0,38	0,49	n.a.
4		11,700	309,517	3127,964	97,60	97,27	n.a.
5		11,963	2,609	19,559	0,82	0,61	n.a.
6		12,227	0,418	6,011	0,13	0,19	n.a.
7		12,587	2,622	34,179	0,83	1,06	n.a.
8		12,763	0,150	2,168	0,05	0,07	n.a.
Total:			**317,117**	**3215,781**	**100,00**	**100,00**	

^{1}H NMR spectrum of **BP3** (600 MHz, DMSO-d_6)

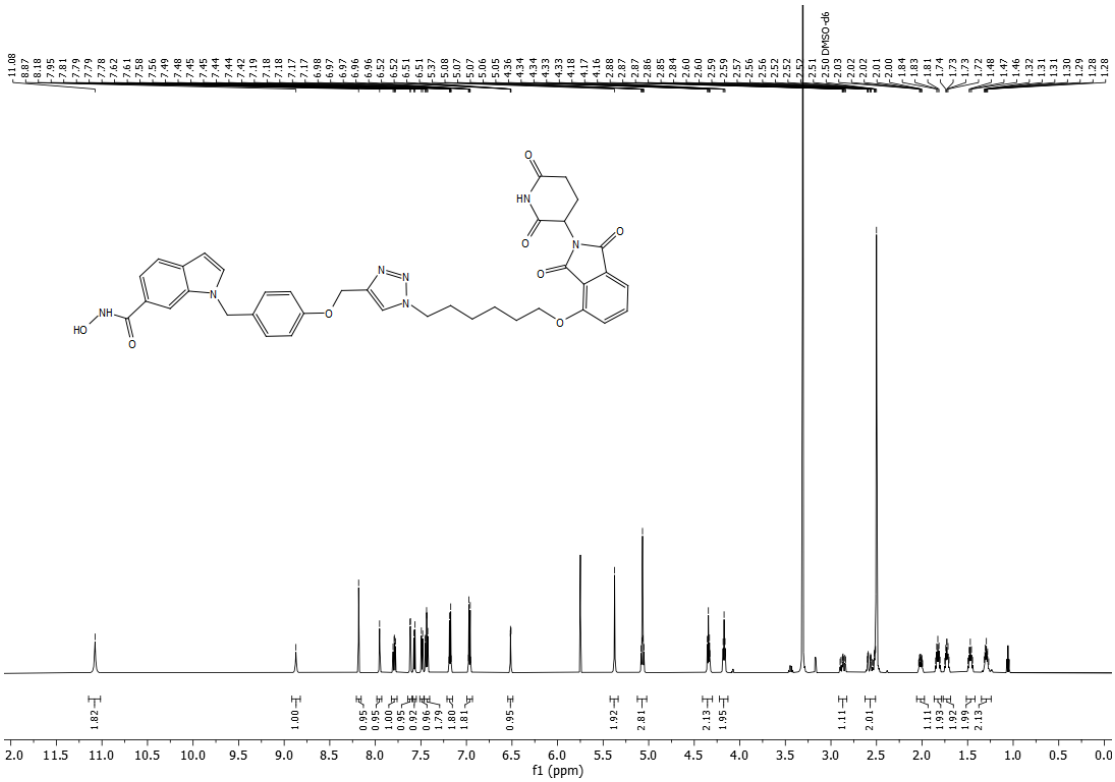

^{13}C NMR spectrum of **BP3** (600 MHz, DMSO-d_6)

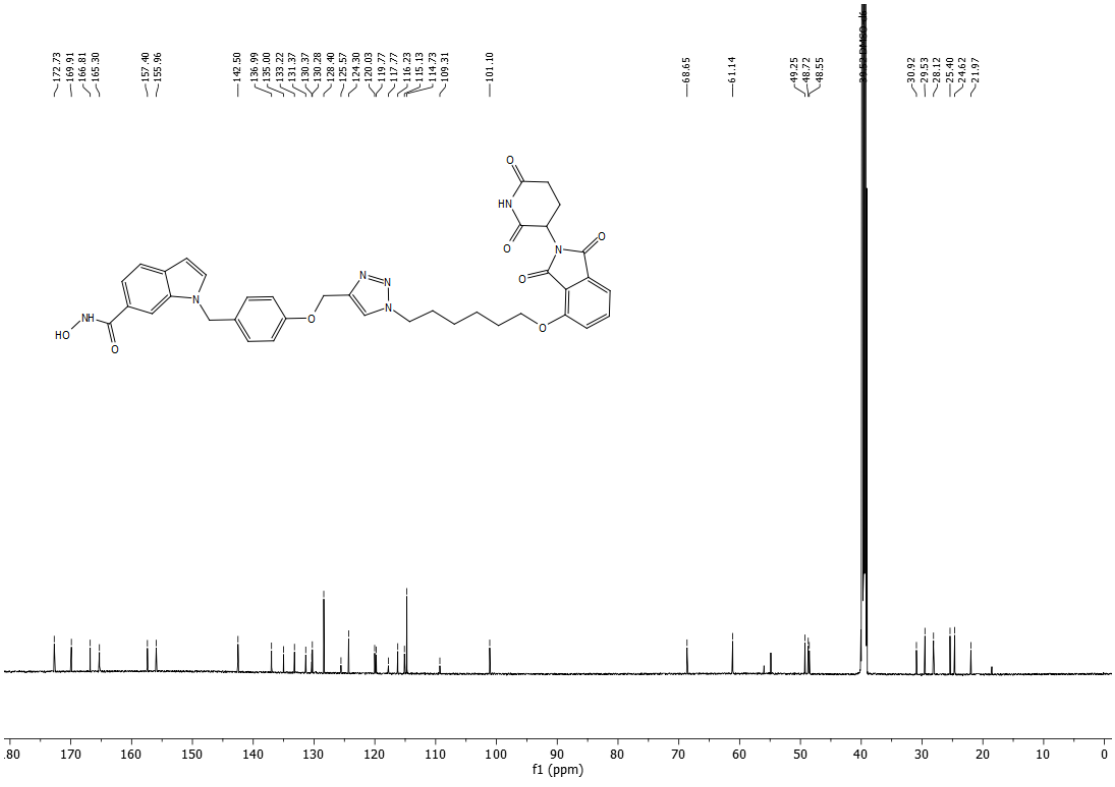

HR-MS spectrum of **BP3**

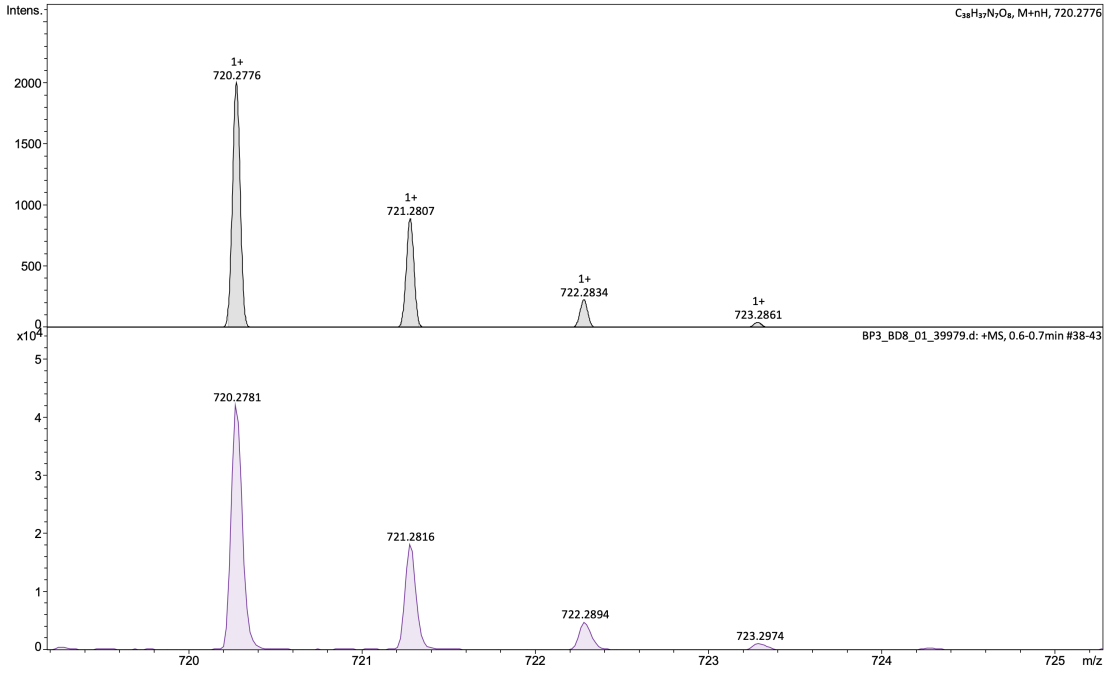

HPLC chromatogram of **BP3** (Purity: 99.7%)

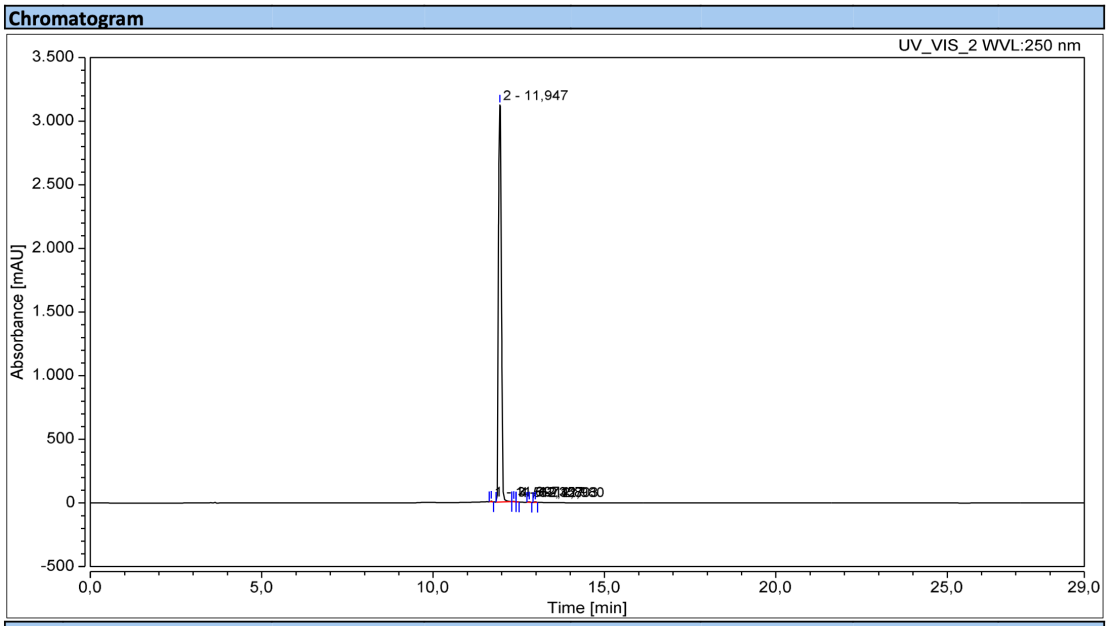

Integration Results

No.	Peak Name	Retention Time min	Area mAU*min	Height mAU	Relative Area %	Relative Height %	Amount n.a.
1		11,697	0,325	5,052	0,11	0,16	n.a.
2		11,947	302,388	3119,375	99,68	99,53	n.a.
3		12,357	0,129	2,216	0,04	0,07	n.a.
4		12,417	0,028	0,000	0,01	0,00	n.a.
5		12,803	0,235	3,467	0,08	0,11	n.a.
6		12,980	0,264	3,933	0,09	0,13	n.a.
Total:			**303,369**	**3134,044**	**100,00**	**100,00**	

^{1}H NMR spectrum of **BP4** (600 MHz, DMSO-d_6)

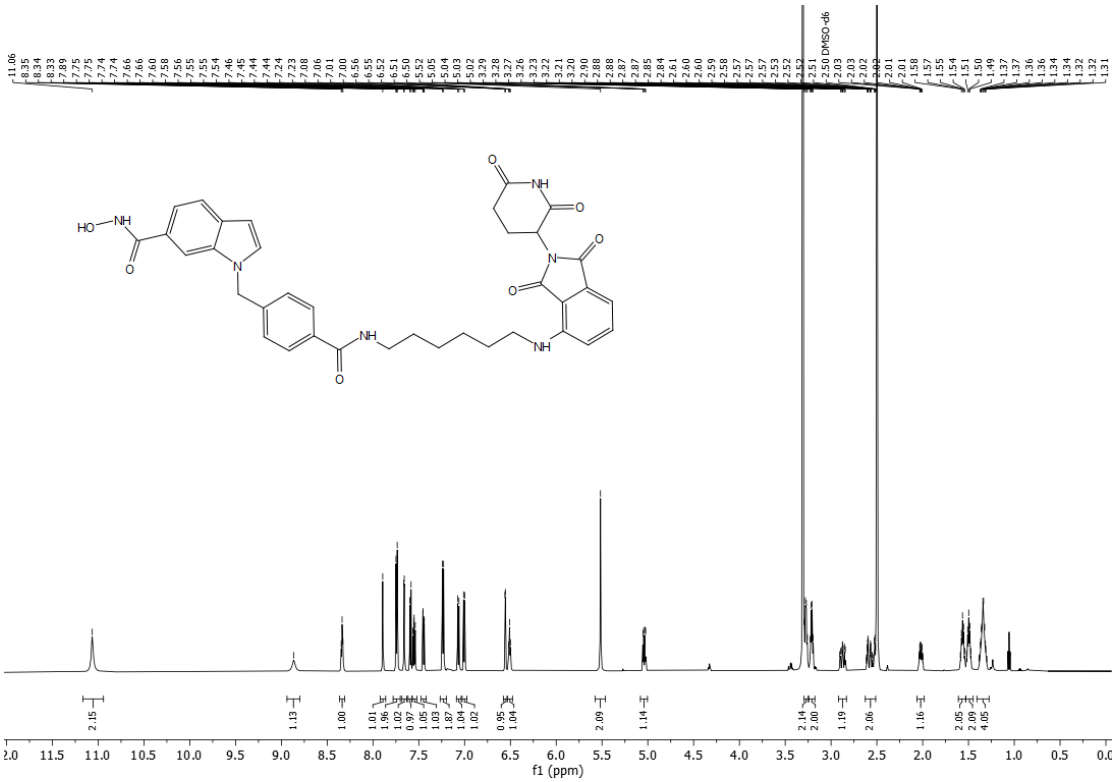

^{13}C NMR spectrum of **BP4** (600 MHz, DMSO-d_6)

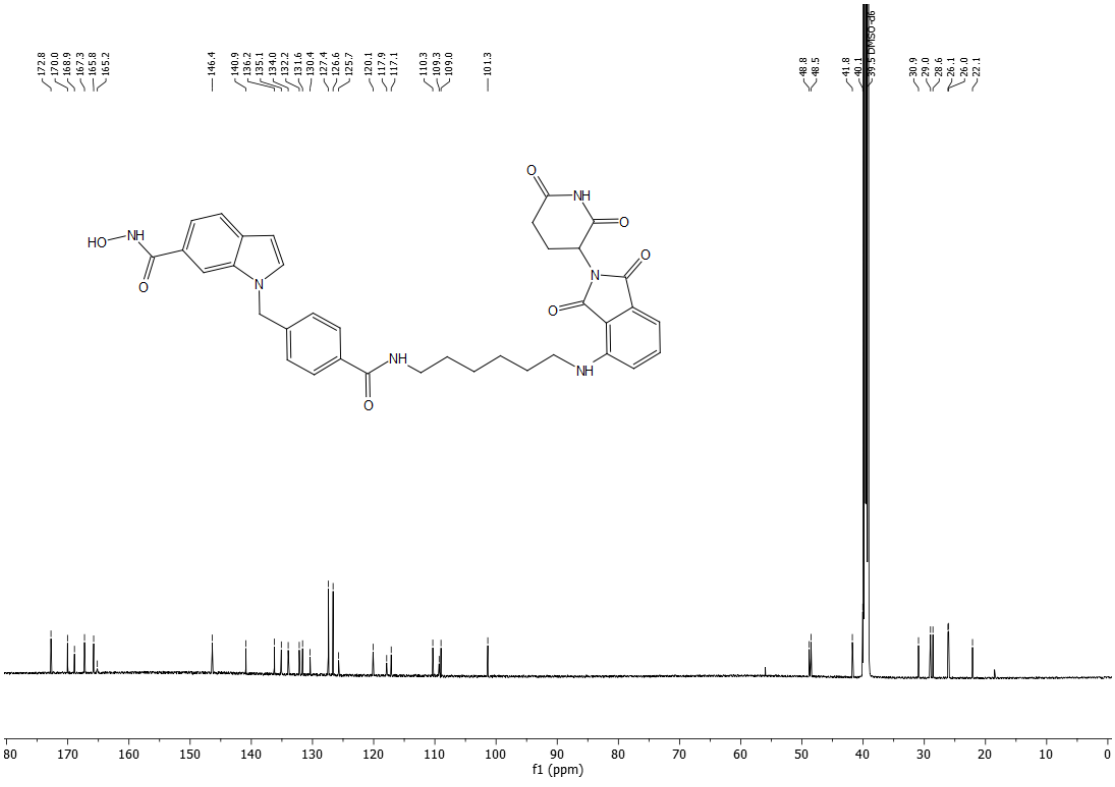

HR-MS spectrum of **BP4**

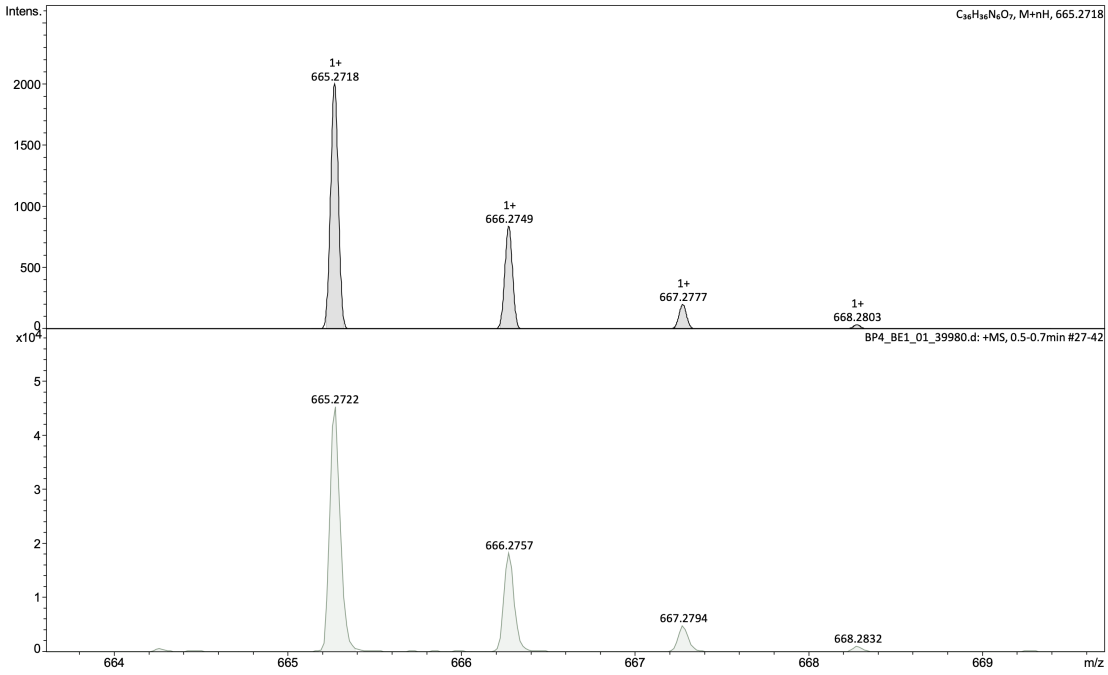

HPLC chromatogram of **BP4** (Purity: 99.4%)

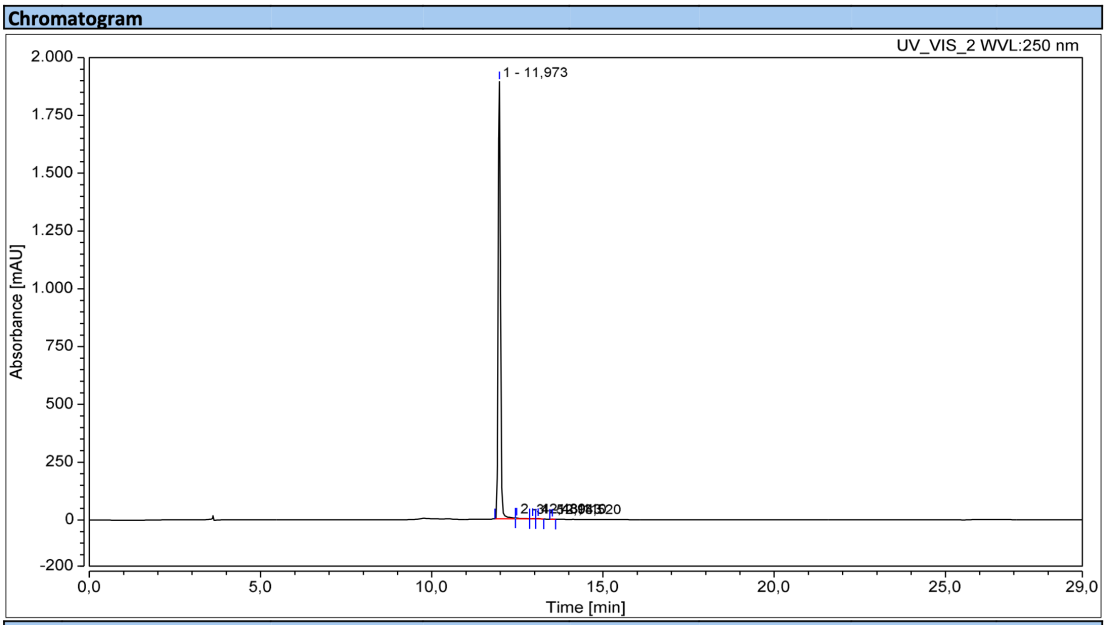

Integration Results

No.	Peak Name	Retention Time min	Area mAU*min	Height mAU	Relative Area %	Relative Height %	Amount n.a.
1		11,973	142,965	1890,421	99,38	99,62	n.a.
2		12,480	0,547	3,183	0,38	0,17	n.a.
3		12,943	0,082	1,091	0,06	0,06	n.a.
4		13,110	0,191	1,971	0,13	0,10	n.a.
5		13,520	0,075	1,013	0,05	0,05	n.a.
Total:			**143,860**	**1897,679**	**100,00**	**100,00**	

^{1}H NMR spectrum of **BP5** (600 MHz, DMSO-d_6)

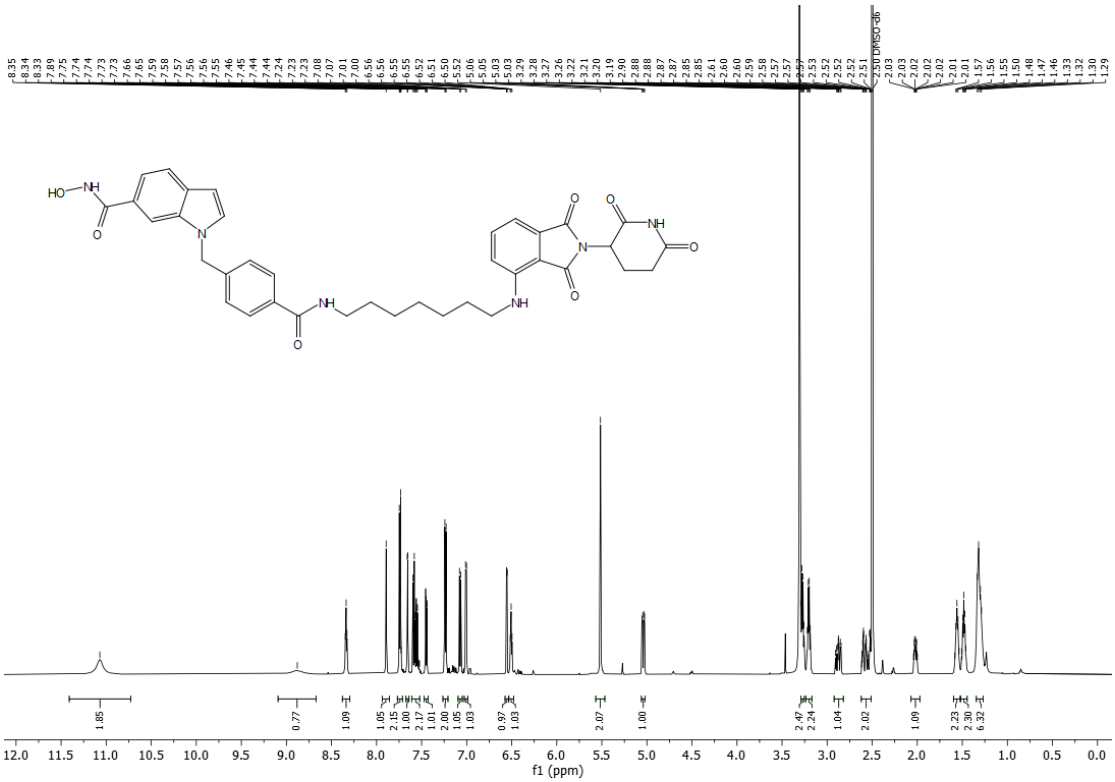

^{13}C NMR spectrum of **BP5** (600 MHz, DMSO-d_6)

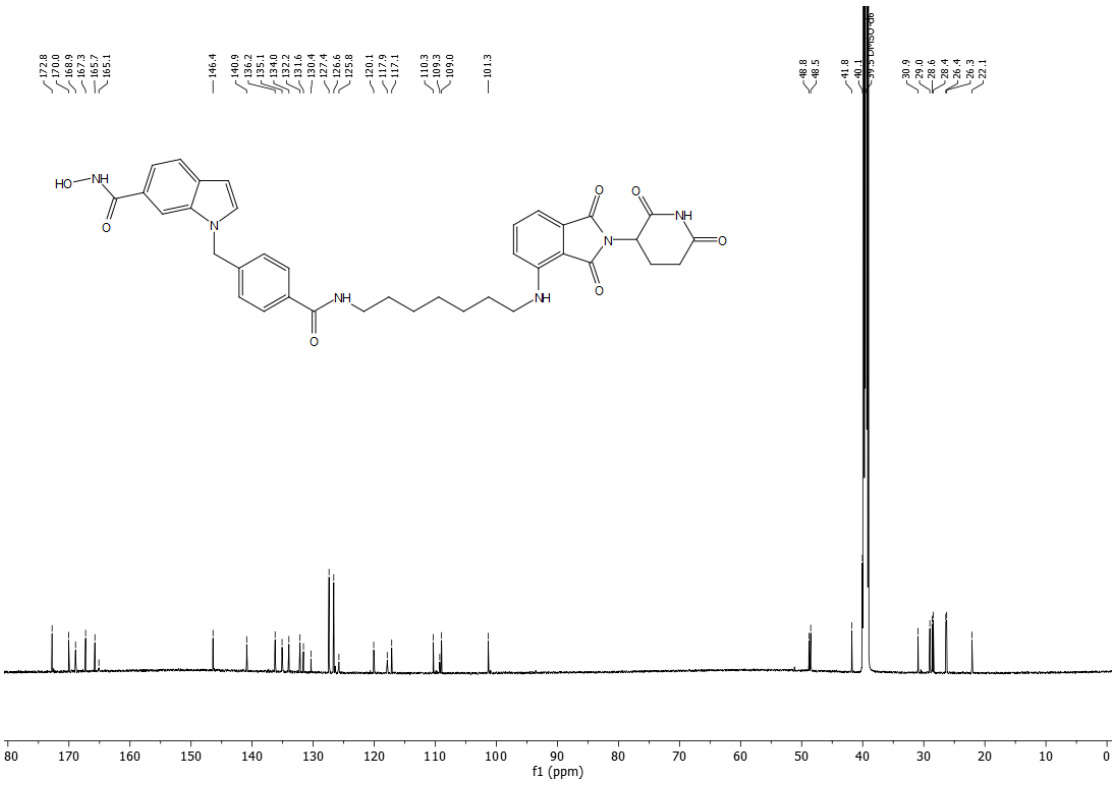

HR-MS spectrum of **BP5**

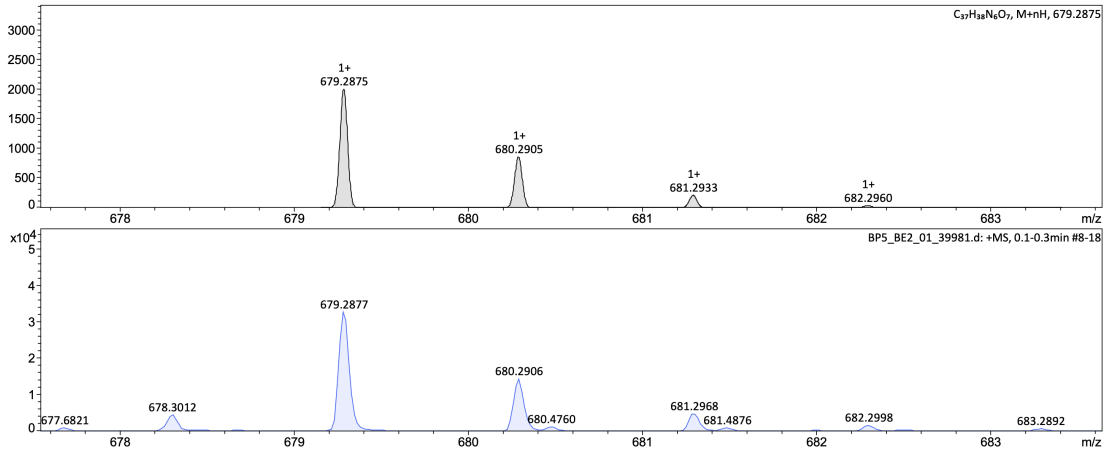

HPLC chromatogram of **BP5** (Purity: 98.1%)

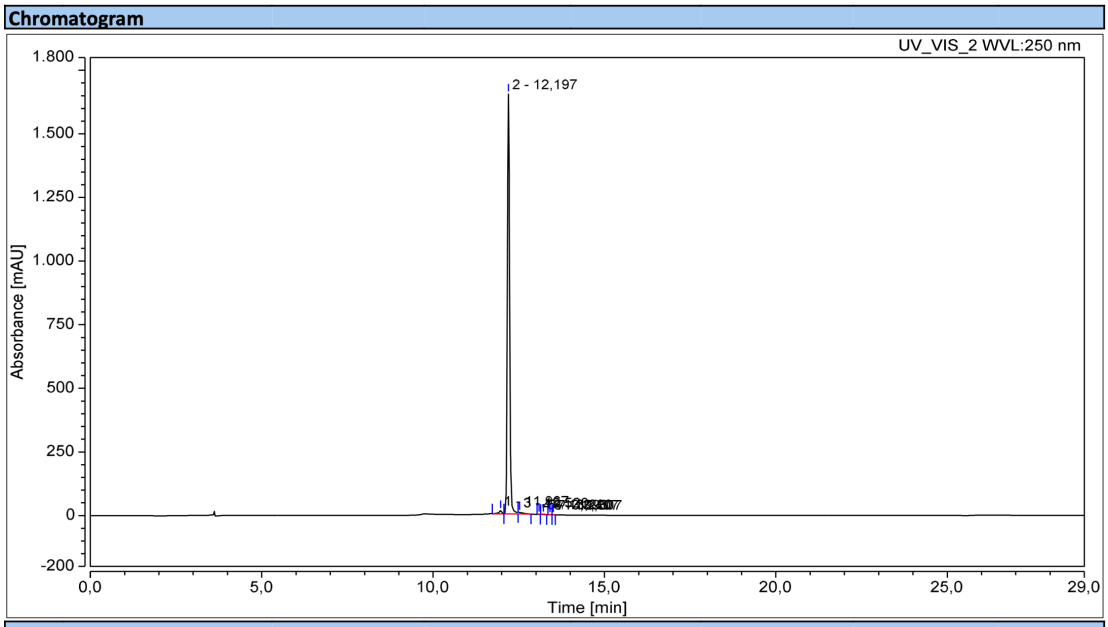

Integration Results

No.	Peak Name	Retention Time min	Area mAU*min	Height mAU	Relative Area %	Relative Height %	Amount n.a.
1		11,967	1,217	12,468	0,94	0,75	n.a.
2		12,197	126,703	1649,987	98,06	98,66	n.a.
3		12,520	1,061	6,421	0,82	0,38	n.a.
4		13,093	0,025	0,523	0,02	0,03	n.a.
5		13,220	0,135	1,764	0,10	0,11	n.a.
6		13,407	0,042	0,673	0,03	0,04	n.a.
7		13,507	0,027	0,507	0,02	0,03	n.a.
Total:			**129,210**	**1672,344**	**100,00**	**100,00**	

^{1}H NMR spectrum of **BP6** (600 MHz, DMSO-d_6)

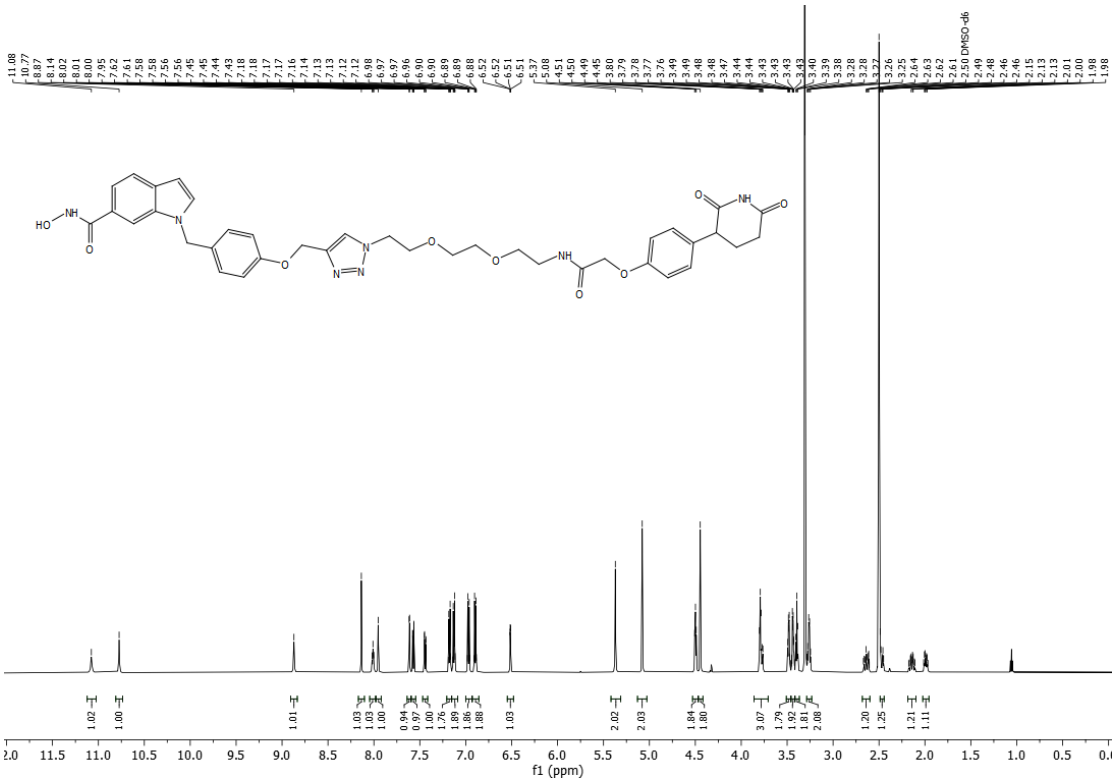

^{13}C NMR spectrum of **BP6** (600 MHz, DMSO-d_6)

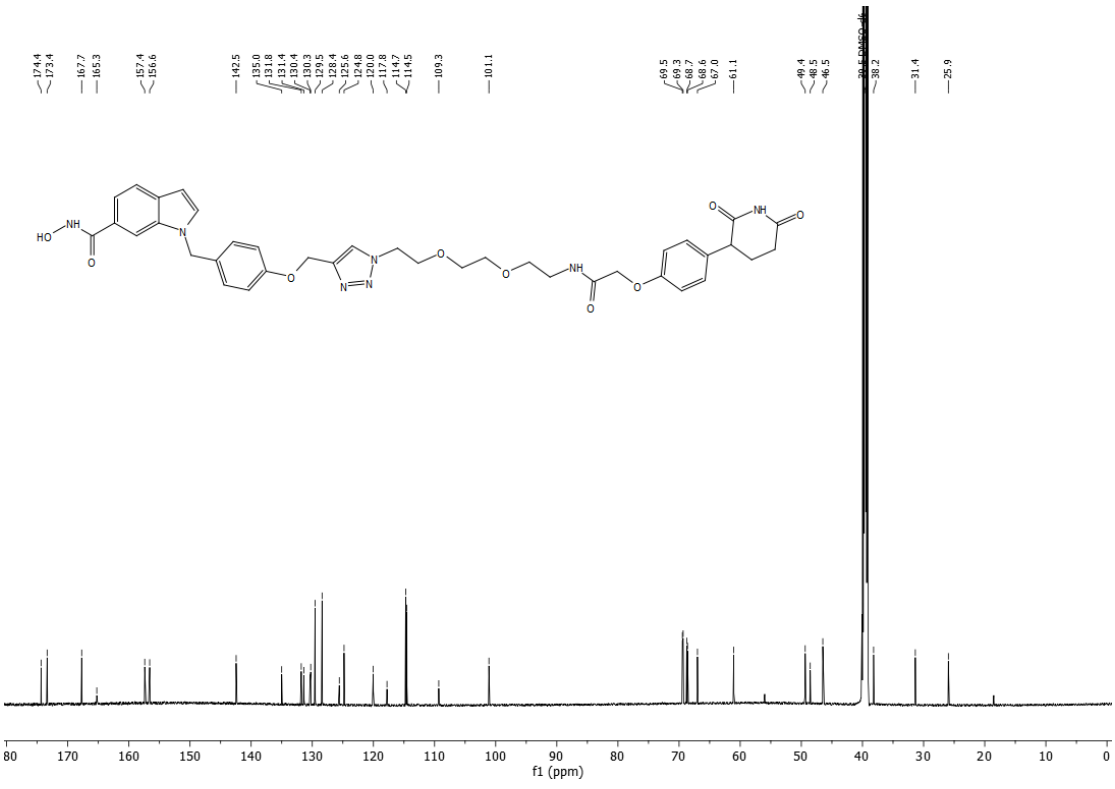

HR-MS spectrum of **BP6**

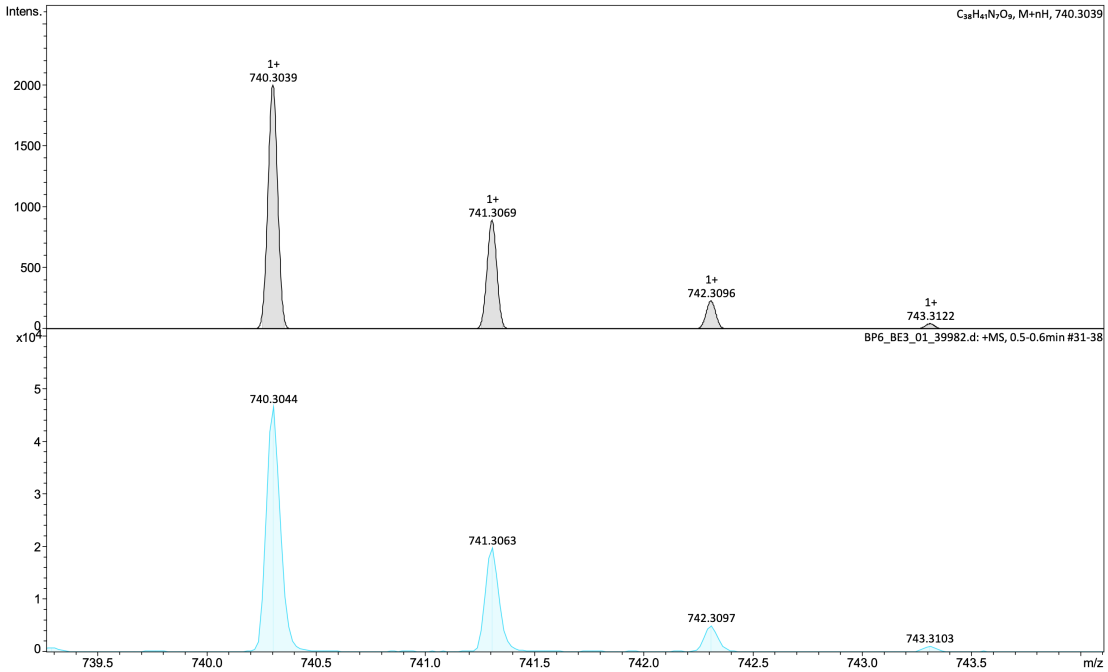

HPLC chromatogram of **BP6** (Purity: 99.5%)

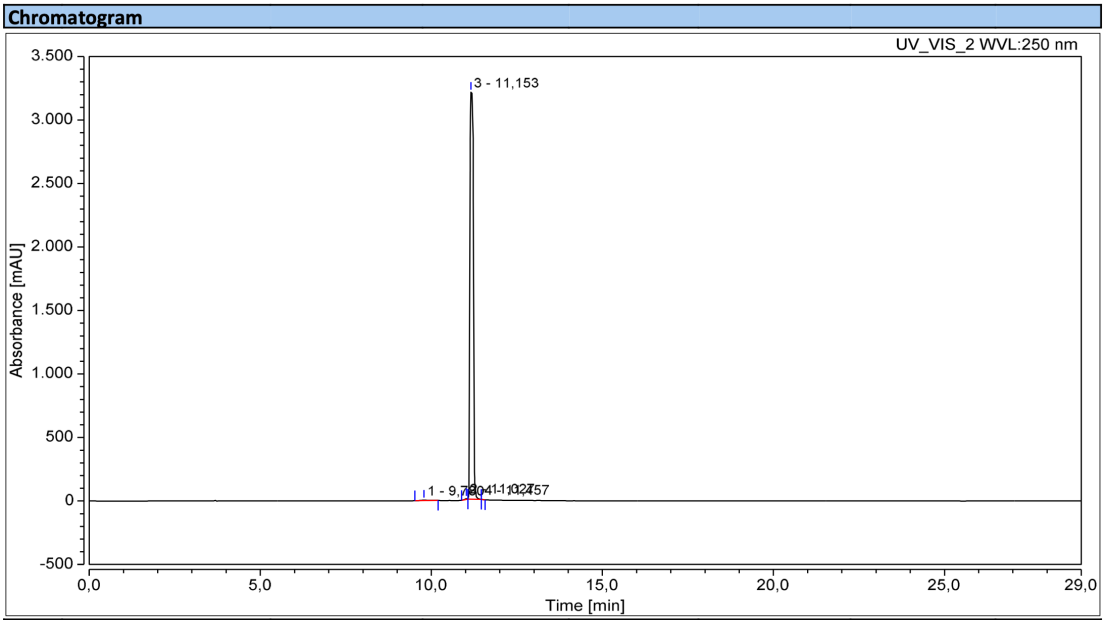

Integration Results

No.	Peak Name	Retention Time min	Area mAU*min	Height mAU	Relative Area %	Relative Height %	Amount n.a.
1		9,780	0,989	3,252	0,27	0,10	n.a.
2		11,027	0,679	8,924	0,18	0,28	n.a.
3		11,153	367,029	3204,680	99,54	99,62	n.a.
4		11,457	0,045	0,000	0,01	0,00	n.a.
Total:			**368,742**	**3216,856**	**100,00**	**100,00**	

^{1}H NMR spectrum of **BP7** (600 MHz, DMSO-d_6)

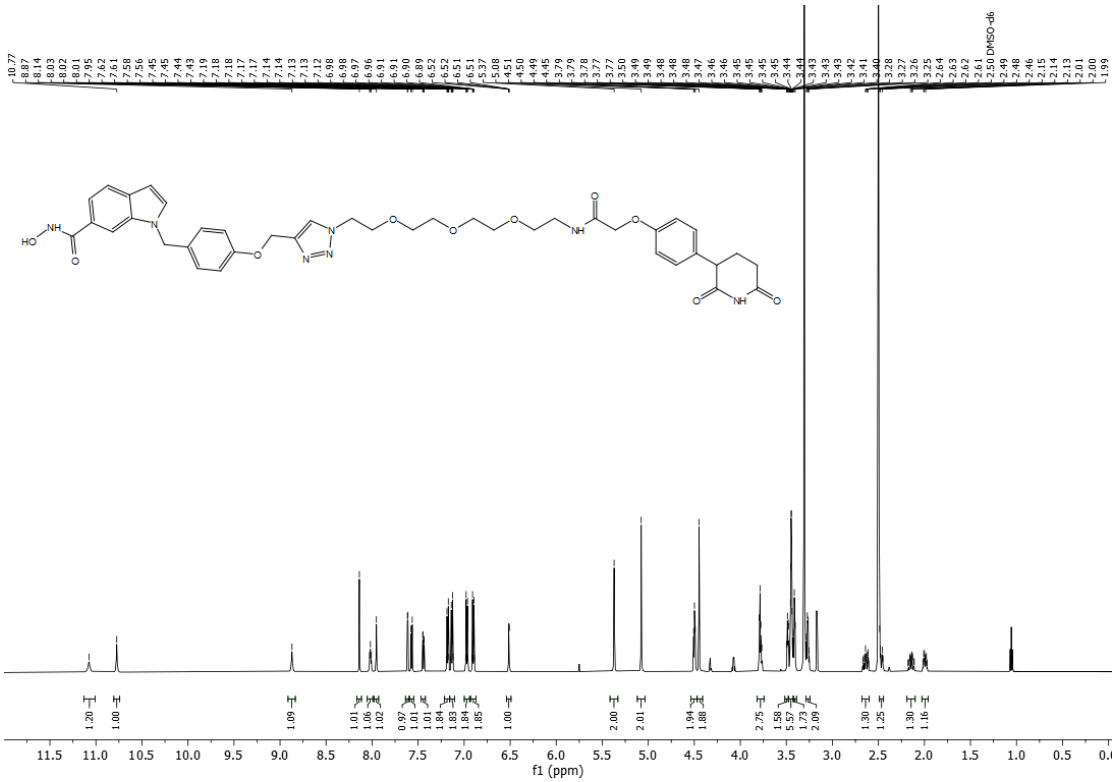

^{13}C NMR spectrum of **BP7** (600 MHz, DMSO-d_6)

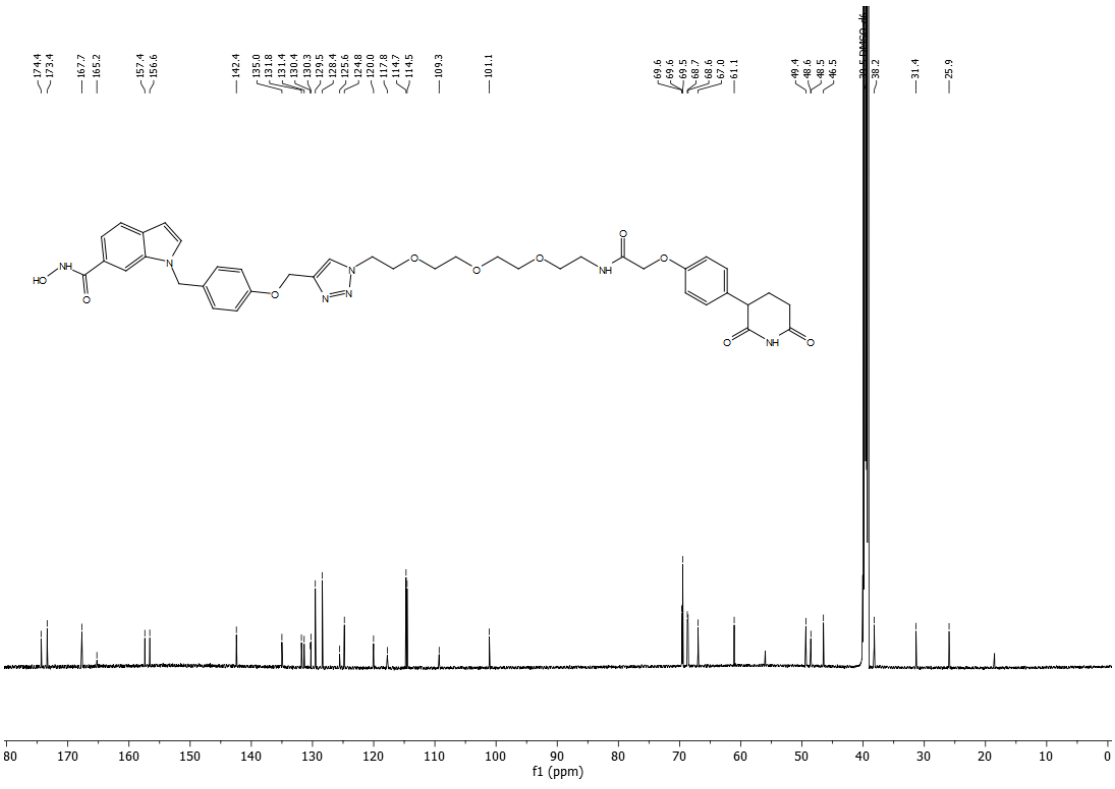

HR-MS spectrum of **BP7**

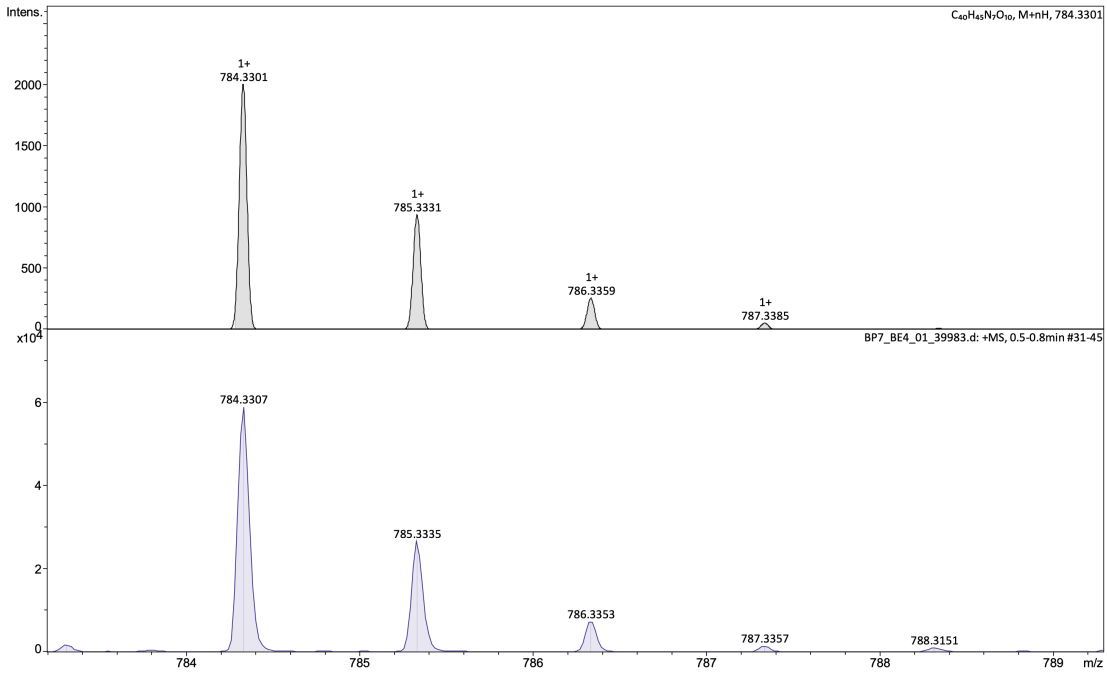

HPLC chromatogram of **BP7** (Purity: 97.7%)

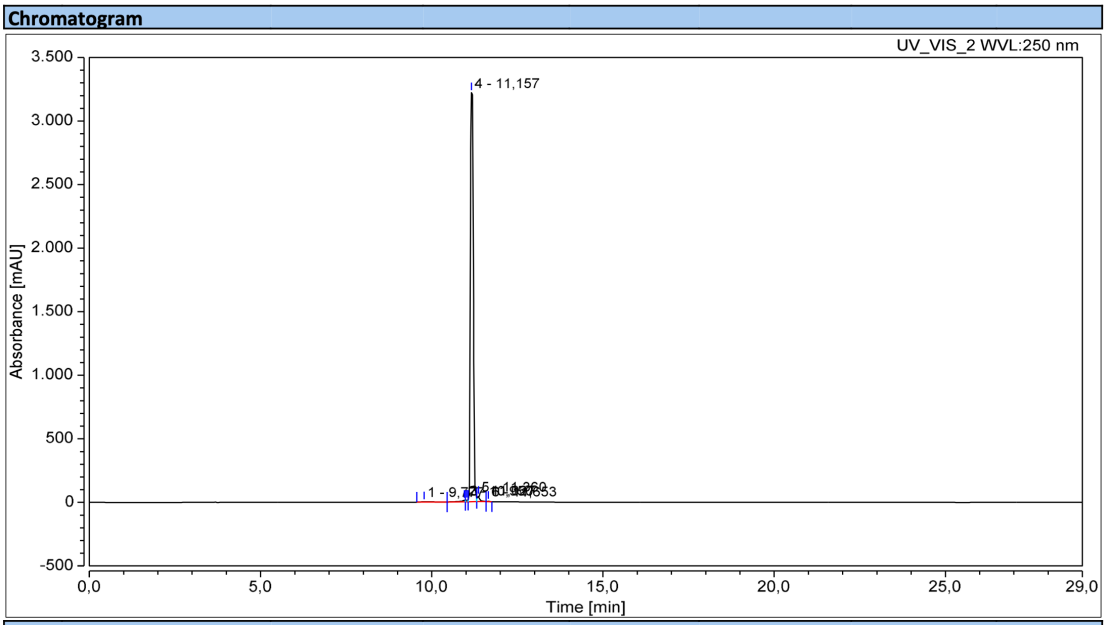

Integration Results

No.	Peak Name	Retention Time min	Area mAU*min	Height mAU	Relative Area %	Relative Height %	Amount n.a.
1		9,777	1,081	3,305	0,33	0,10	n.a.
2		10,950	1,529	11,291	0,47	0,34	n.a.
3		11,027	0,946	12,931	0,29	0,39	n.a.
4		11,157	320,789	3216,630	97,71	97,80	n.a.
5		11,360	3,717	41,433	1,13	1,26	n.a.
6		11,653	0,230	3,239	0,07	0,10	n.a.
Total:			**328,291**	**3288,829**	**100,00**	**100,00**	

^{1}H NMR spectrum of **BP8** (600 MHz, DMSO-d_6)

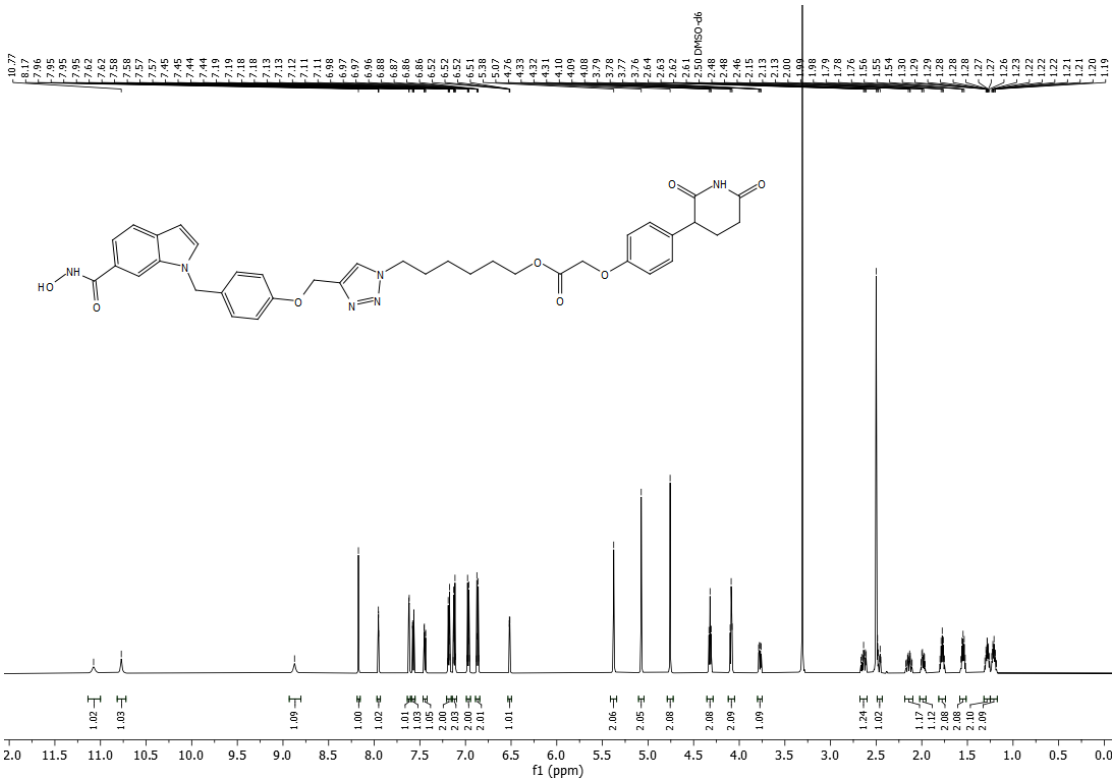

^{13}C NMR spectrum of **BP8** (600 MHz, DMSO-d_6)

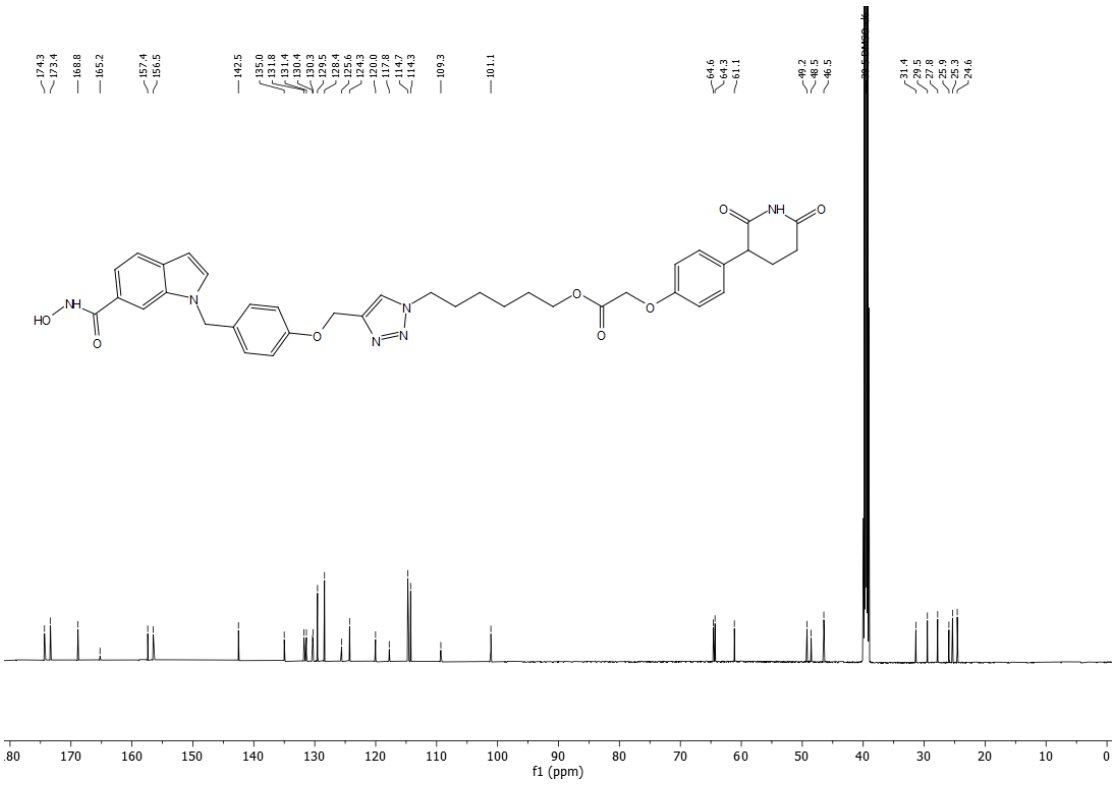

HR-MS spectrum of **BP8**

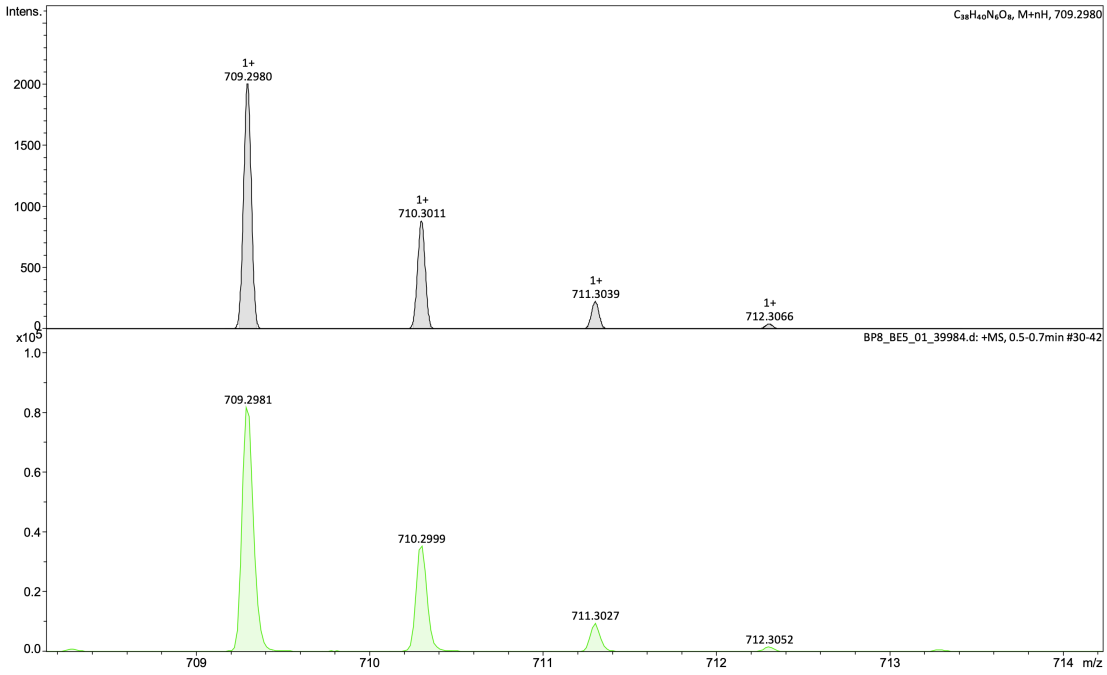

HPLC chromatogram of **BP8** (Purity: 99.3%)

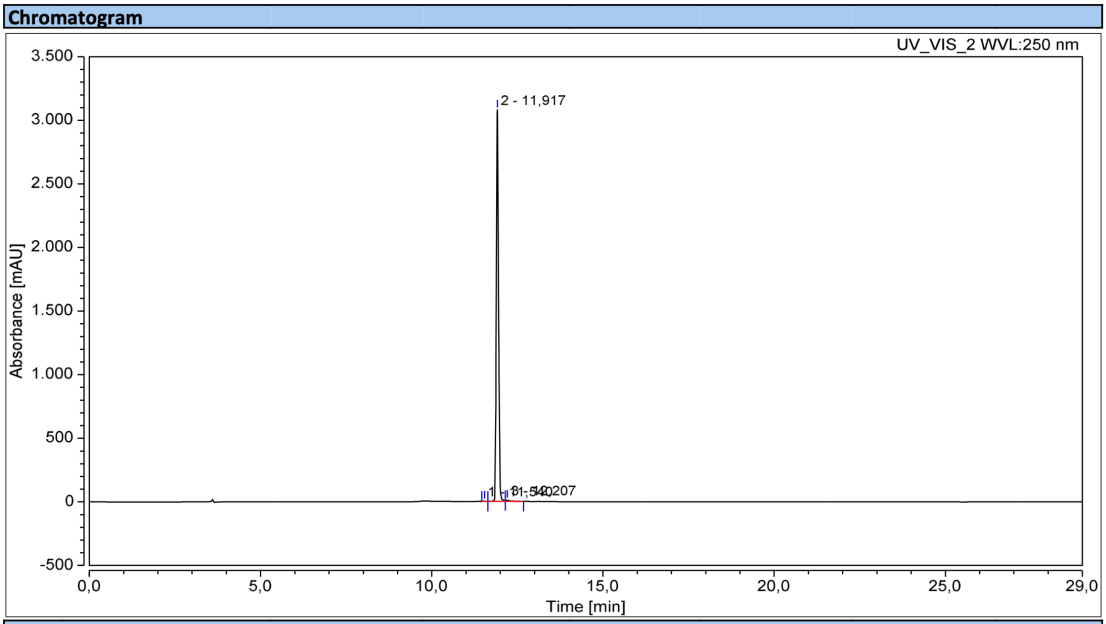

Integration Results

No.	Peak Name	Retention Time min	Area mAU*min	Height mAU	Relative Area %	Relative Height %	Amount n.a.
1		11,540	0,148	1,671	0,06	0,05	n.a.
2		11,917	232,525	3077,747	99,29	99,62	n.a.
3		12,207	1,511	10,055	0,65	0,33	n.a.
Total:			**234,184**	**3089,473**	**100,00**	**100,00**	

^{1}H NMR spectrum of **BP9** (600 MHz, DMSO-d_6)

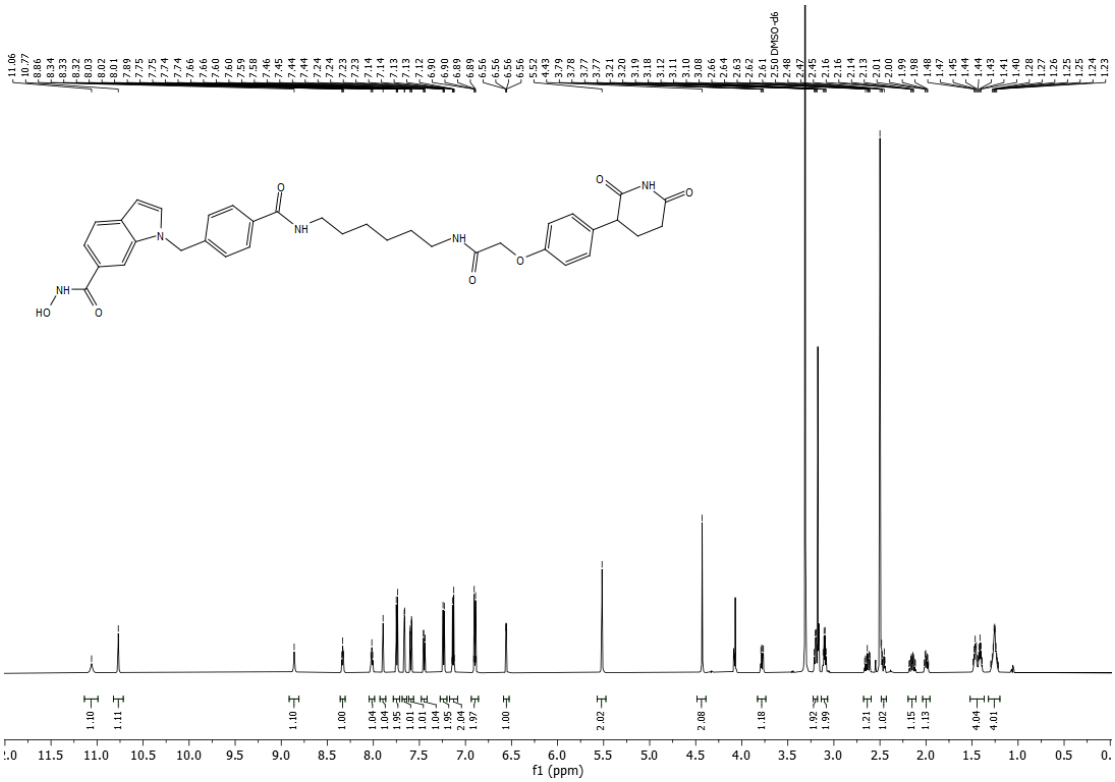

^{13}C NMR spectrum of **BP9** (600 MHz, DMSO-d_6)

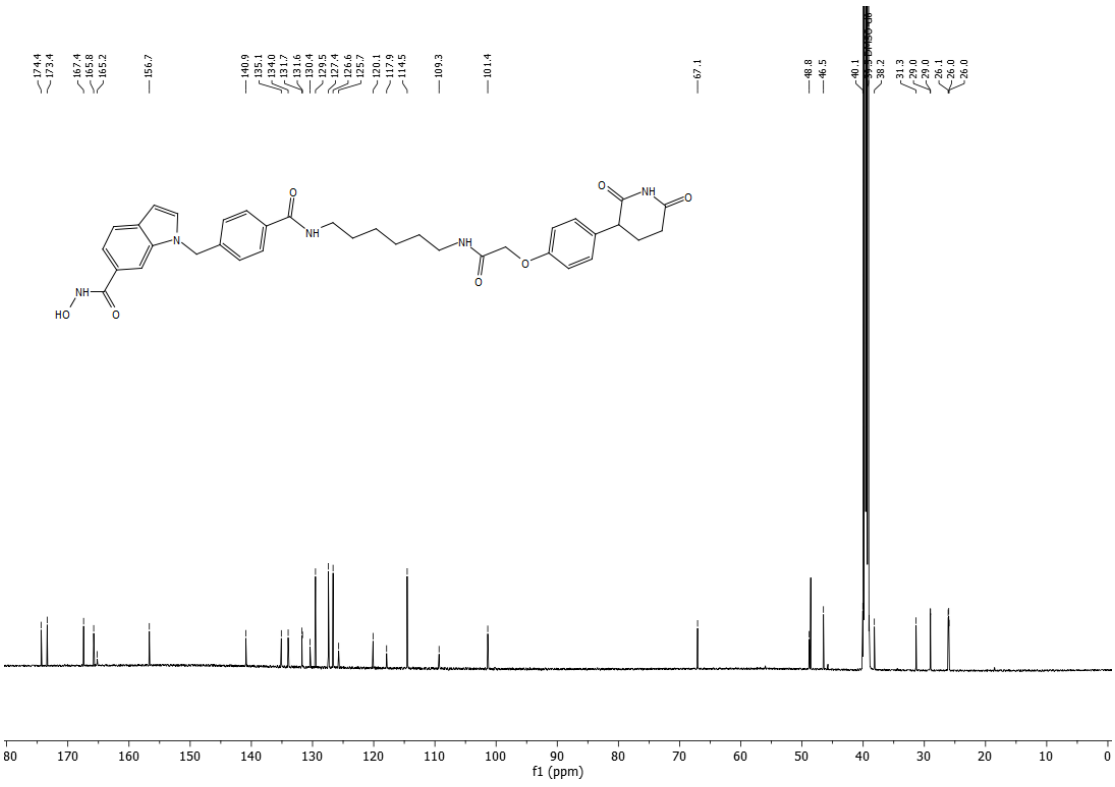

HR-MS spectrum of **BP9**

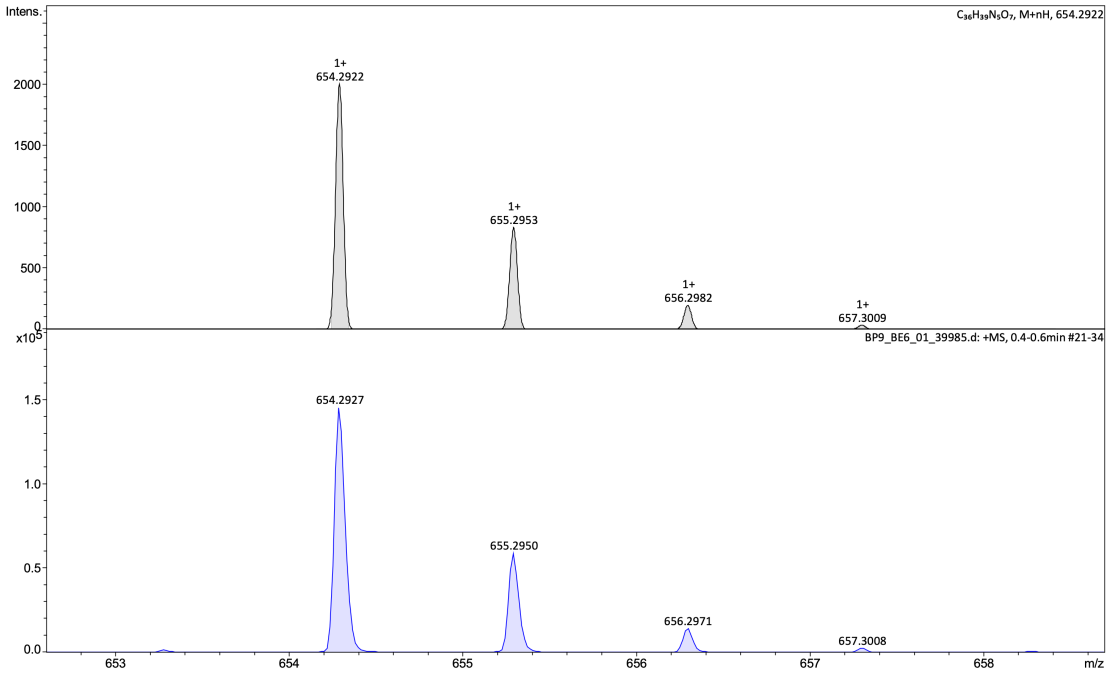

HPLC chromatogram of **BP9** (Purity: 96.8%)

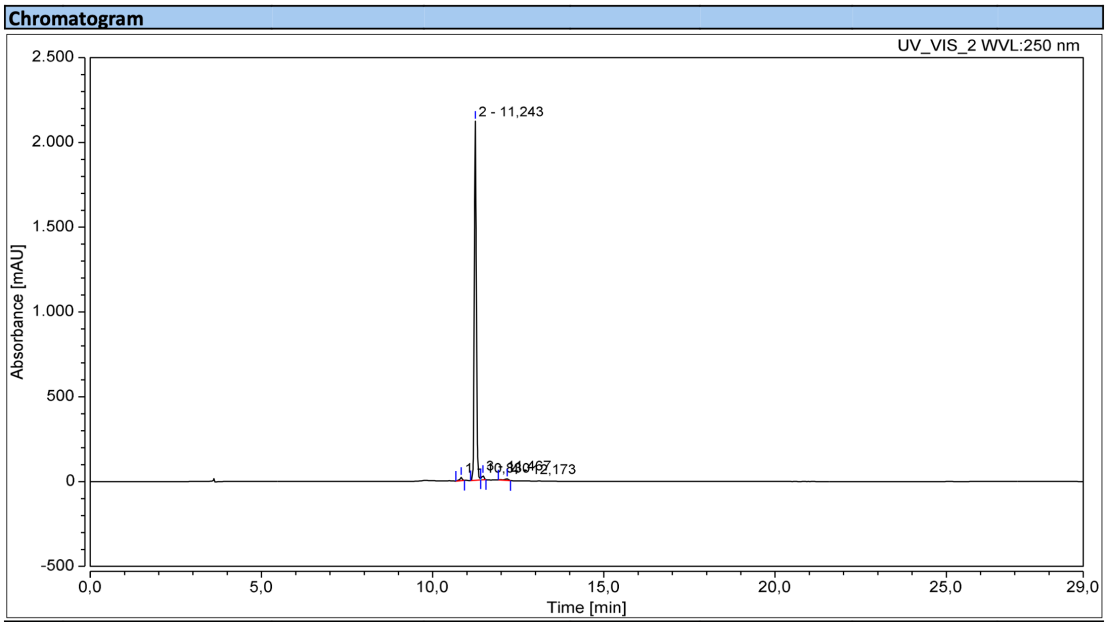

Integration Results

No.	Peak Name	Retention Time min	Area mAU*min	Height mAU	Relative Area %	Relative Height %	Amount n.a.
1		10,830	1,558	19,358	1,02	0,89	n.a.
2		11,243	147,543	2118,234	96,75	97,44	n.a.
3		11,467	2,025	26,608	1,33	1,22	n.a.
4		12,173	1,379	9,643	0,90	0,44	n.a.
Total:			**152,505**	**2173,843**	**100,00**	**100,00**	

^{1}H NMR spectrum of **BP10** (600 MHz, DMSO-d_6)

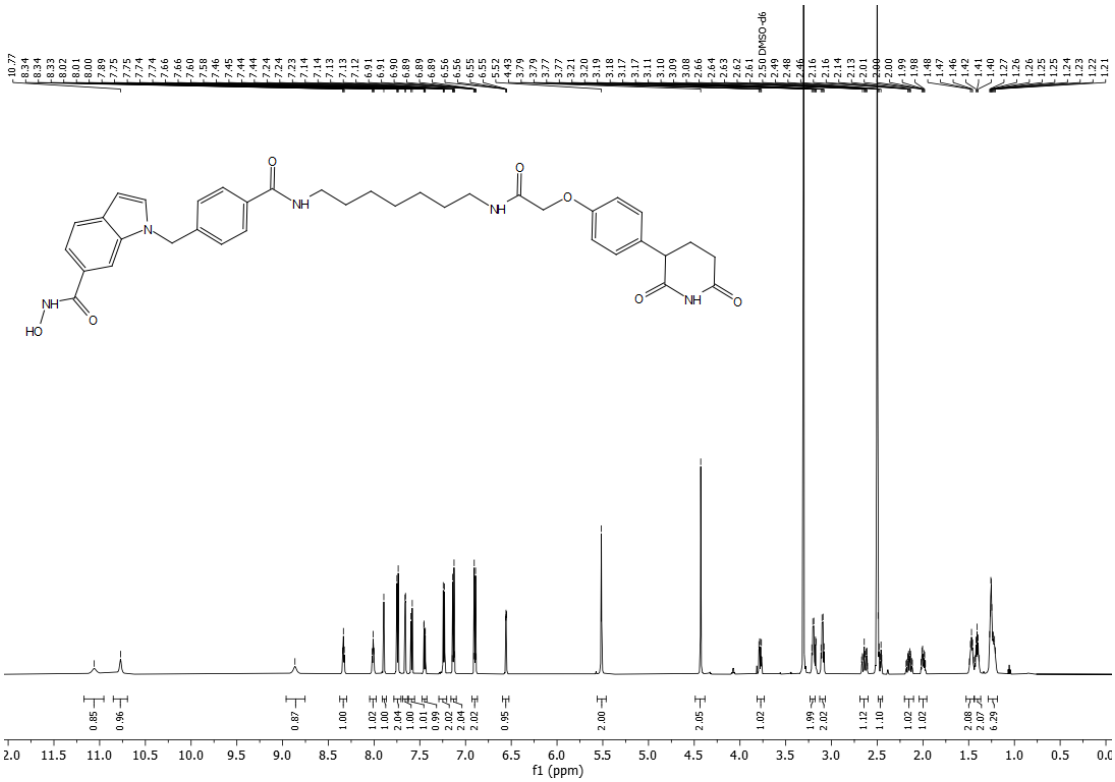

^{13}C NMR spectrum of **BP10** (600 MHz, DMSO-d_6)

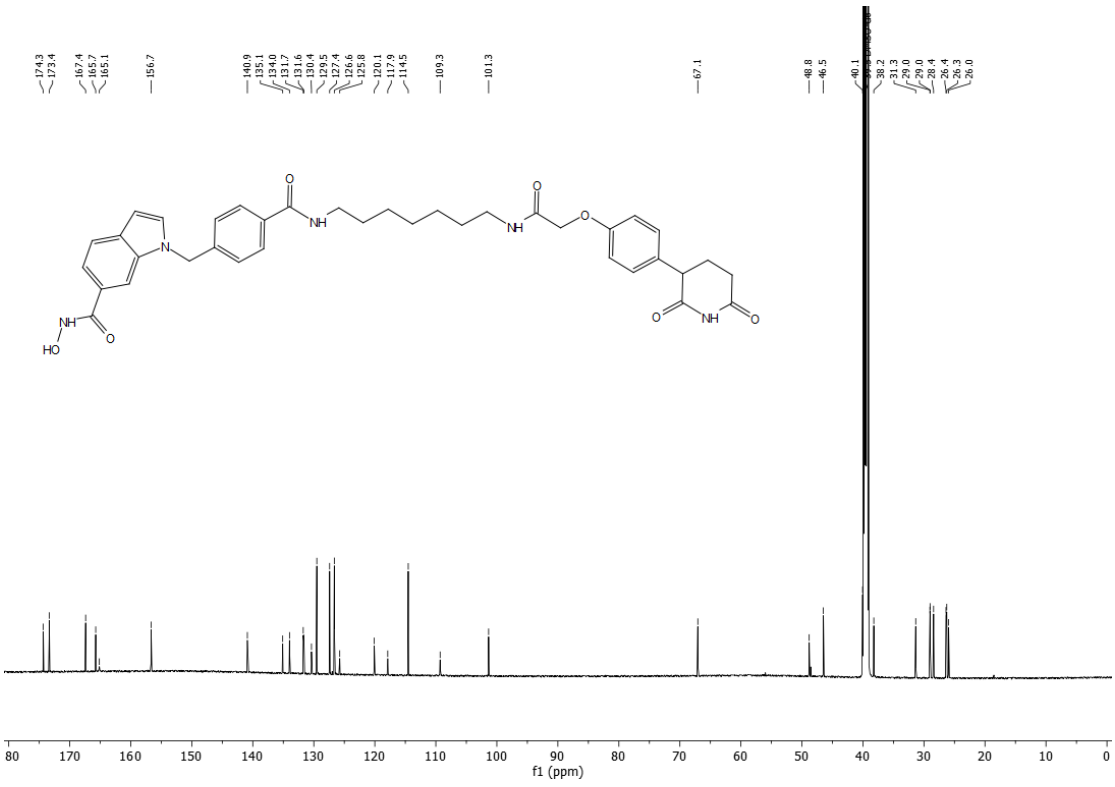

HR-MS spectrum of **BP10**

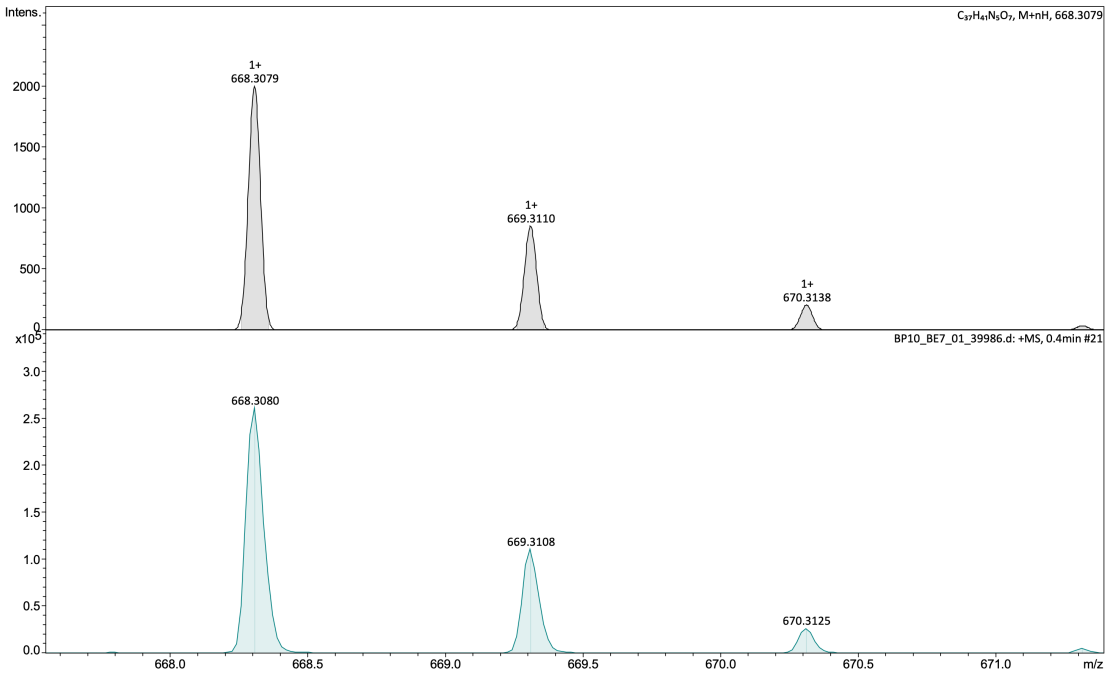

HPLC chromatogram of **BP10** (Purity: 96.1%)

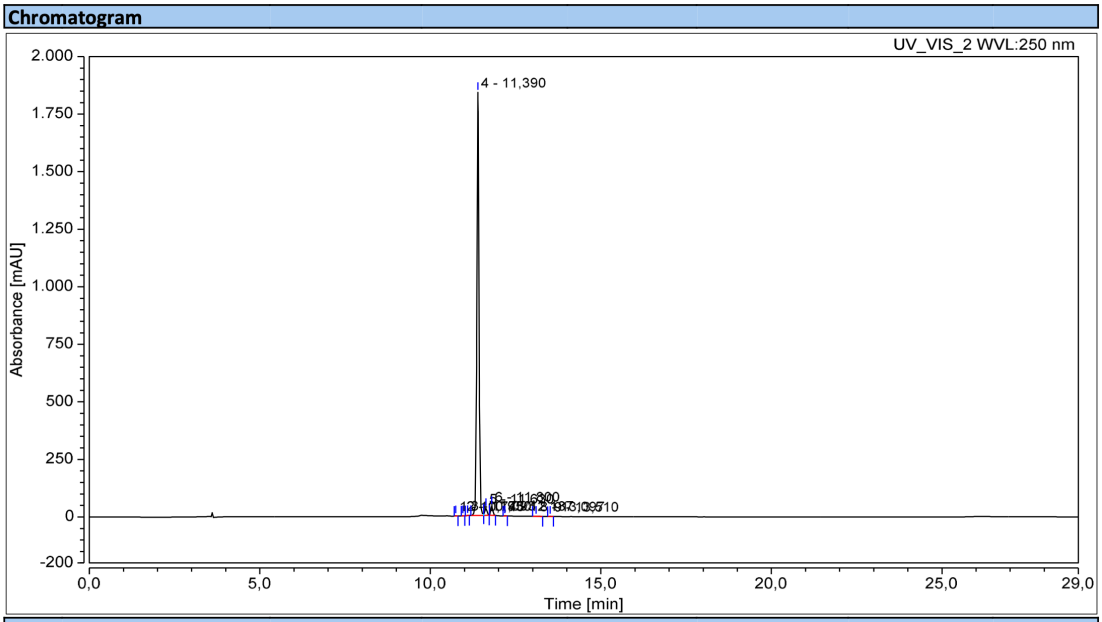

Integration Results

No.	Peak Name	Retention Time min	Area mAU*min	Height mAU	Relative Area %	Relative Height %	Amount n.a.
1		10,743	0,052	0,941	0,04	0,05	n.a.
2		10,950	0,054	0,911	0,04	0,05	n.a.
3		11,093	0,047	0,676	0,03	0,04	n.a.
4		11,390	131,394	1837,877	96,11	96,08	n.a.
5		11,630	2,248	30,290	1,64	1,58	n.a.
6		11,800	2,672	39,221	1,95	2,05	n.a.
7		12,187	0,082	1,228	0,06	0,06	n.a.
8		13,097	0,114	0,982	0,08	0,05	n.a.
9		13,510	0,054	0,809	0,04	0,04	n.a.
Total:			**136,716**	**1912,935**	**100,00**	**100,00**	

^{1}H NMR spectrum of **BP1-N** (600 MHz, DMSO-d_6)

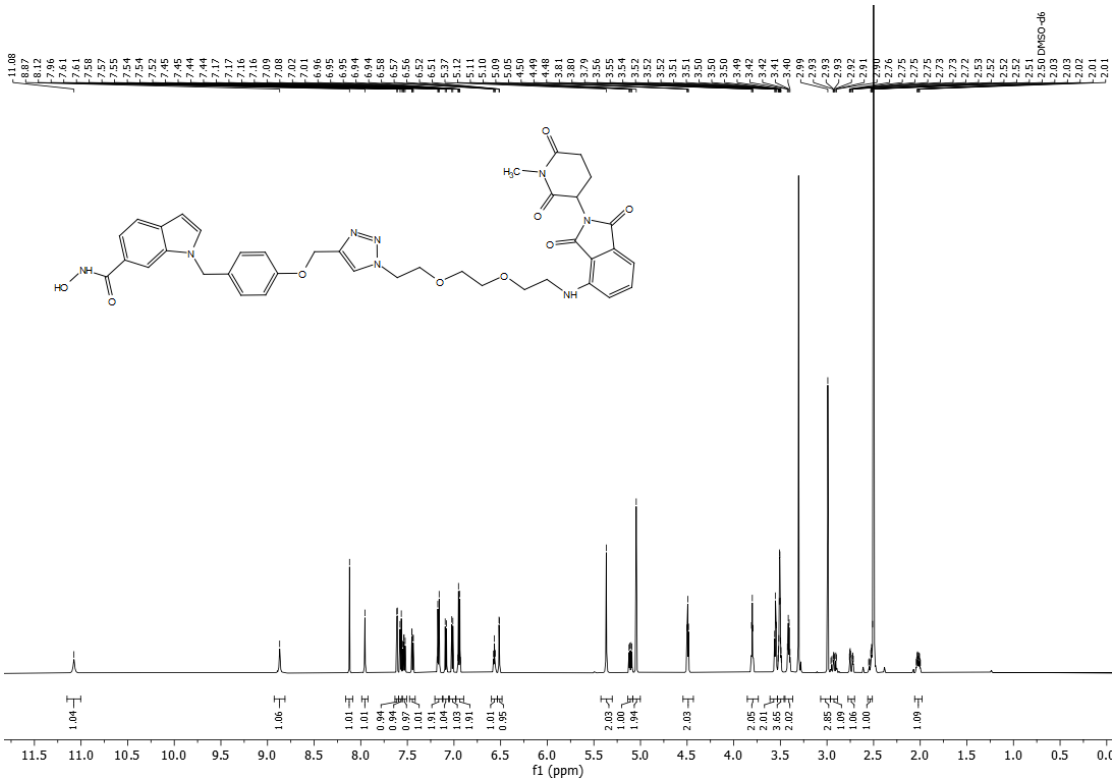

^{13}C NMR spectrum of **BP1-N** (600 MHz, DMSO-d_6)

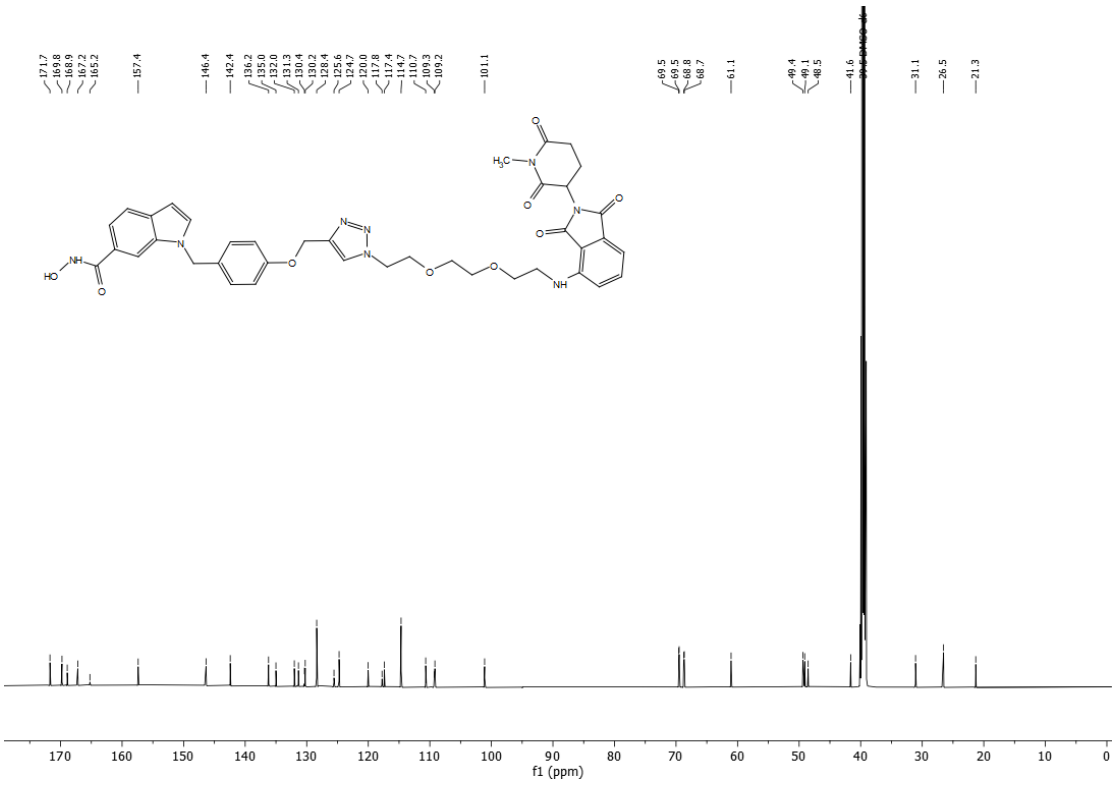

HR-MS spectrum of **BP1-N**

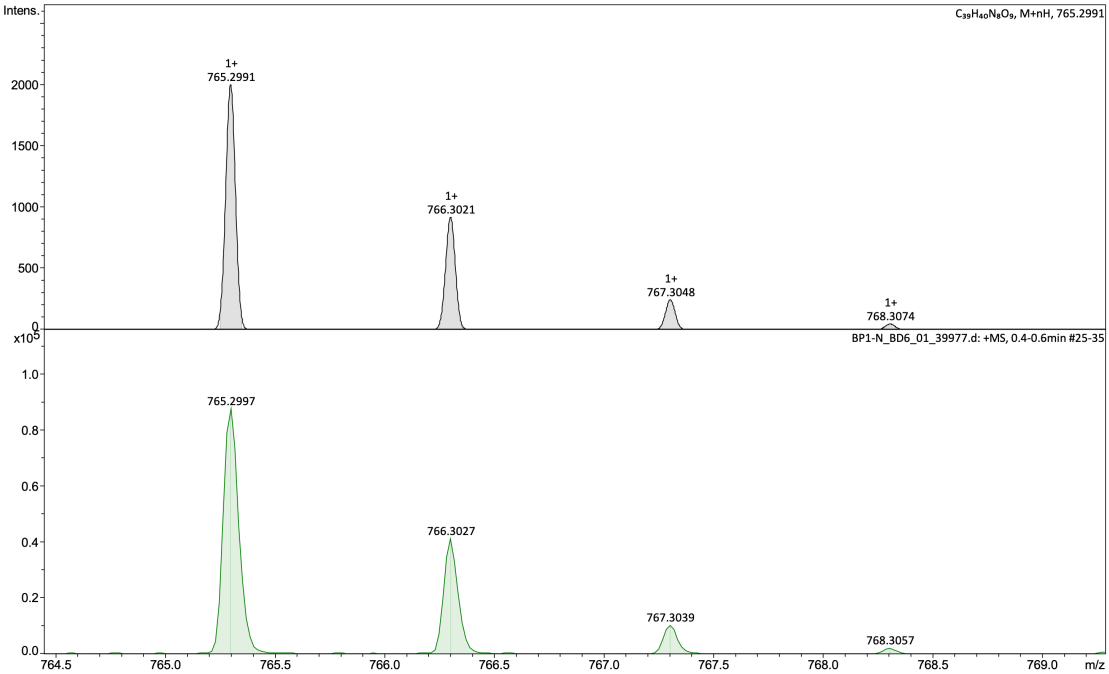

HPLC chromatogram of **BP1-N** (Purity: 98.6%)

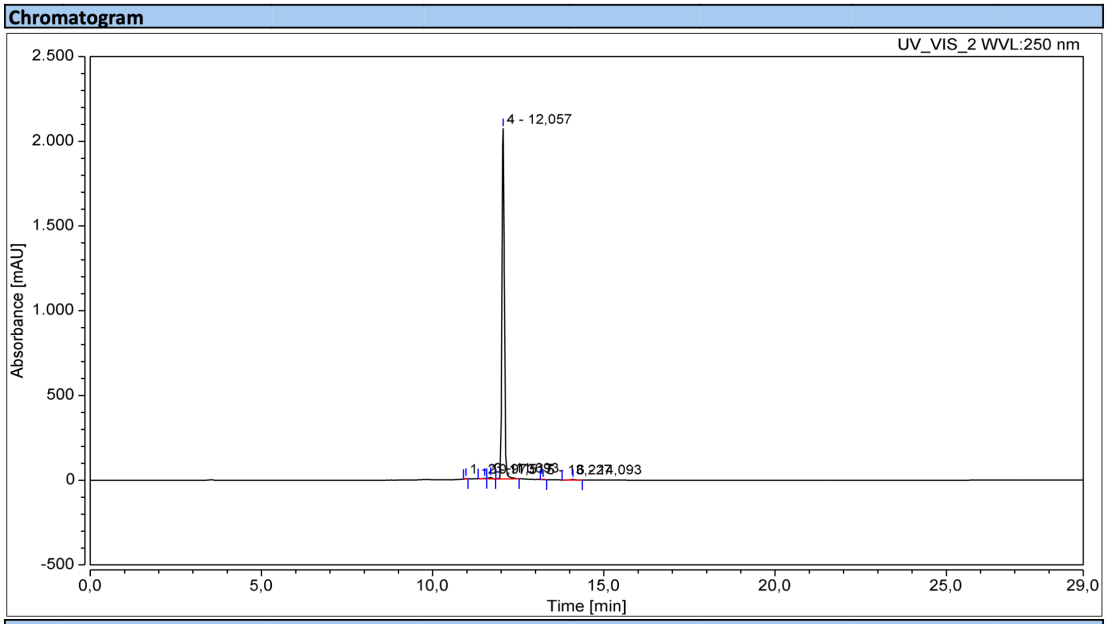

Integration Results

No.	Peak Name	Retention Time min	Area mAU*min	Height mAU	Relative Area %	Relative Height %	Amount n.a.
1		10,973	0,195	3,067	0,12	0,15	n.a.
2		11,517	0,398	3,360	0,24	0,16	n.a.
3		11,693	1,027	8,319	0,61	0,40	n.a.
4		12,057	165,479	2066,722	98,64	98,96	n.a.
5		13,227	0,188	2,450	0,11	0,12	n.a.
6		14,093	0,467	4,597	0,28	0,22	n.a.
Total:			**167,754**	**2088,516**	**100,00**	**100,00**	

4. References

(1) Bricelj, A.; Dora Ng, Y. L.; Ferber, D.; Kuchta, R.; Müller, S.; Monschke, M.; Wagner, K. G.; Krönke, J.; Sosič, I.; Gütschow, M.; Steinebach, C. Influence of Linker Attachment Points on the Stability and Neosubstrate Degradation of Cereblon Ligands. *ACS Med. Chem. Lett.* **2021**, *12* (11), 1733-1738.

7.4 Appendix IV. Publication III: Targeted histone deacetylase degradation via chemical induced proximity by direct recruitment of the CUL4 complex adaptor protein DDB1

The following pages include the article "Targeted histone deacetylase degradation via chemical induced proximity by direct recruitment of the CUL4 complex adaptor protein DDB1" as it was published in ACS Medicinal Chemistry Letters by the American Chemical Society.

The article is reprinted with the permission from:

Shiyang Zhai, Nicola Willemsen, Tao Sun, Mateo Malenica, Shixin Deng, Matthias Geyer, Finn K. Hansen

ACS Med. Chem. Lett. **2025**, 16, 2070–2077.

https://doi.org/10.1021/acsmedchemlett.5c00506

ACS Medicinal Chemistry Letters

pubs.acs.org/acsmedchemlett Letter

Targeted Histone Deacetylase Degradation via Chemical Induced Proximity by Direct Recruitment of the CUL4 Complex Adaptor Protein DDB1

Shiyang Zhai, Nicola Willemsen, Tao Sun, Mateo Malenica, Shixin Deng, Matthias Geyer, and Finn K. Hansen*

Cite This: ACS Med. Chem. Lett. 2025, 16, 2070−2077 Read Online

ACCESS | Metrics & More | Article Recommendations | Supporting Information

ABSTRACT: Targeted protein degradation using proteolysis-targeting chimeras (PROTACs) has emerged as a powerful strategy for disease treatment. By recruiting E3 ligases, these molecules enable selective degradation of pathogenic proteins. Cereblon (CRBN), a key component of the CUL4-DDB1-CRBN E3 ligase complex, is the most commonly recruited E3 ligase in PROTACs, including those targeting histone deacetylases (HDACs). In this study, we designed **SZ-2**, a bifunctional molecule derived from the DDB1 ligand MM-02-57 and the HDAC inhibitor vorinostat, to simultaneously bind DDB1 and HDACs. **SZ-2** effectively induced degradation of HDAC1 and HDAC2 and demonstrated potent anti-multiple myeloma activity, highlighting its potential as a novel therapeutic agent.

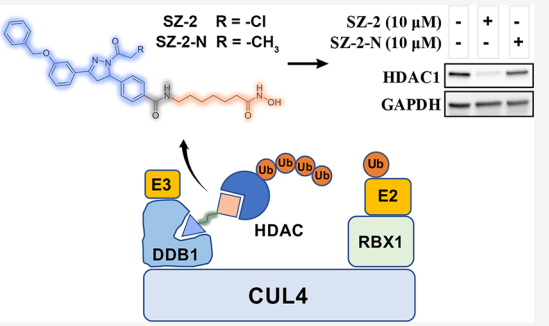

KEYWORDS: *Histone deacetylase (HDAC), Cancer, Damage-specific DNA binding protein 1 (DDB1), Proteolysis targeting chimeras (PROTACs), Targeted Protein Degradation (TPD)*

Histone deacetylases (HDACs), a protein family serving as a key factor for post-translational modifications, exert their functions by catalyzing acetyl group removal from histone and nonhistone proteins. As crucial epigenetic regulators, HDACs influence a wide range of cellular processes, such as DNA replication and repair, metabolism, cell cycle regulation, apoptosis, differentiation, and immune responses.[1,2] Mammalian HDACs are categorized into four classes, including class I (HDAC1, 2, 3 and 8), class II (HDAC4, 5, 7, 9, 6 and 10), class III (Sirt1−7) and class IV (HDAC11). Among these subtypes, class I, II, and IV are Zn^{2+}-dependent, while class III depends on NAD^{+}.[2,3] Given their critical role in the field of epigenetics, HDACs have emerged as important targets in the past decade for HDAC-associated diseases, such as cancer. Notably, extensive efforts to develop HDAC inhibitors (HDACis) have resulted in promising candidates for disease treatment, with four HDACis for Zn^{2+}-dependent subtypes having received FDA approval for cancer indications.[4,5] However, their use is limited by adverse effects, restriction to rare hematological cancers, lack of first-line approval, and the withdrawal of certain indications (e.g., panobinostat in relapsed/refractory multiple myeloma).[6] In addition to conventional use of small molecule inhibitors, the field of targeted HDAC degradation by proteolysis-targeting chimeras (PROTACs) is rapidly emerging.[7−15]

Damage-specific DNA binding protein 1 (DDB1) is a critical component of the cellular machinery, playing significant roles in DNA repair,[16] protein ubiquitination,[17−20] viral replication,[21−24] and cellular regulation.[25−27] In the context of protein ubiquitination, DDB1 functions as a part of the CUL4-DDB1 E3 ubiquitin ligase complex.[28,29] This complex plays a crucial role in the ubiquitination of various cellular proteins, which leads to their subsequent degradation by the proteasome. Thus, this process regulates the stability and activity of target proteins within cells.[17−19] Specifically, during this process, DDB1 acts as adaptor protein for different DDB1 and CUL4-associated factors (DCAFs), which serve as substrate receptors in the CUL4-DDB1 E3 ubiquitin ligase complex and mediate the specificity of substrate recognition.[30,31] To date, degradation for different targets has been achieved by direct recruitment of DCAF11[32−37] and DCAF16.[36,38] In contrast, cereblon (CRBN), the most commonly recruited E3 ligase in PROTACs, serves as a non-DCAF substrate receptor for the CRL4-DDB1 E3 ubiquitin ligase complex. In addition to E3 ligase-mediated induced proximity, a more direct strategy for recruiting DDB1 was recently reported. This approach

Received: August 20, 2025
Revised: September 8, 2025
Accepted: September 9, 2025
Published: September 16, 2025

https://doi.org/10.1021/acsmedchemlett.5c00506
ACS Med. Chem. Lett. 2025, 16, 2070−2077

facilitated the proteasomal degradation of BRD4, the androgen receptor, 3-phosphoglycerate dehydrogenase, EGFR, and CDK4.[18,19]

In this study, inspired by a reported DDB1 ligand[39] and the covalent DDB1 binder MM-02-57,[19] we developed small molecule, DDB1-recruiting HDAC degraders by simply merging the pharmacophores of DDB1 ligands and vorinostat. This strategy aimed to directly recruit HDACs to the adapter protein DDB1 without requiring an E3 ligase recruiter. This approach led to the discovery of compound **SZ-2** as a potent and preferential HDAC1 degrader with promising anti-multiple myeloma activity.

For the molecular design of DDB1-recruiting HDAC degraders (Figure 1), we selected both noncovalent and covalent DDB1 ligands as warheads to trigger CUL4-DDB1-based protein ubiquitination. Based on recent evidence supporting the efficacy of linker-less molecular glue-like degraders, we chose to exclude a linker moiety to minimize the molecular weight of the target compound.[40−42] Utilizing the molecular hybridization strategy, the hydroxamic acid along with the six-carbon unit were taken from the non-selective HDAC inhibitor vorinostat. The design of compounds **SZ-1** and **SZ-2** as potential DDB1-based HDAC degraders resulted from merging this fragment into the DDB1 ligands. Since the bromoacetyl group can efficiently undergo nucleophilic substitution reactions with cysteine residues,[43] compound **SZ-3** was also designed by replacing the chlorine atom in **SZ-2** with bromine. The synthesis of the target compounds was performed as summarized in Scheme 1 and Scheme 2.

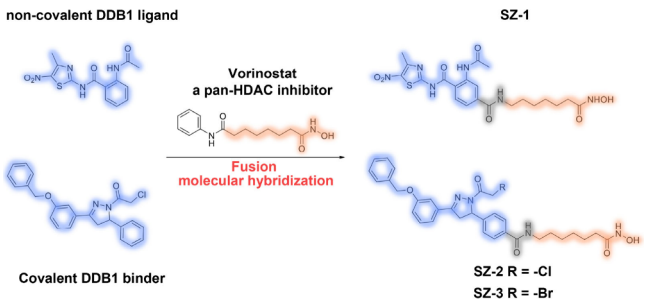

Figure 1. Molecular design of DDB1-based HDAC degraders.

As shown in Scheme 1, the synthesis of noncovalent degrader **SZ-1** started from the commercially available 2-aminoterephthalic acid. The carboxylic acid at the 2-position of benzene ring was protected to yield the monomethyl ester **1**. Afterward, cyclization with bis(trichloromethyl) carbonate occurred to generate the isatoic anhydride derivative **2**. This intermediate was then reacted with 4-methyl-5-nitrothiazol-2-amine hydrochloride (Scheme S1, Supporting Information) and DIPEA in THF to afford compound **3**. Next, the amino group was acetylated to form compound **4** (**F16**). Subsequently, compound **4** was hydrolyzed, followed by acidification with hydrochloric acid to yield the key intermediate **5**. Next, the amide coupling reaction of **5** and methyl 7-

Scheme 1. Synthesis of the Noncovalent Degrader SZ-1[a]

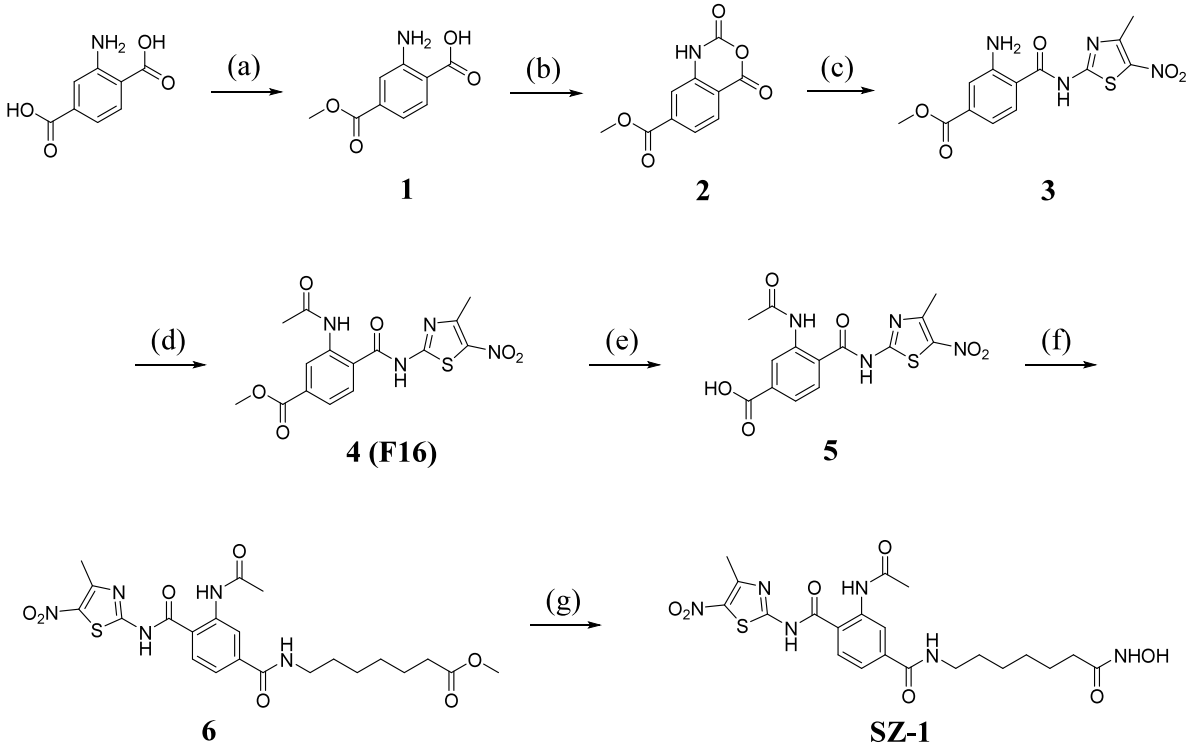

[a](a) TMSCl, MeOH, N_2, rt, 19 h, 85%; (b) bis(trichloromethyl) carbonate, THF, 60 °C, 4 h, 89%; (c) 4-methyl-5-nitrothiazol-2-amine hydrochloride, DIPEA, anhydrous DMF, rt, 6 h, 76%; (d) acetic acid, HATU, DIPEA, anhydrous DMF, rt, 43 h, 71%; (e) (i) LiOH × H_2O, THF/MeOH/H_2O, rt, 16.5 h; (ii) HCl (0.5 M in H_2O), two-step yield, 81%; (f) methyl 7-aminoheptanoate hydrochloride, HATU, DIPEA, anhydrous DMF, rt, 17 h, 45%; (g) (i) hydroxylamine (50 wt.% in water), NaOH, MeOH/DCM, 0 °C to rt, 1 h; (ii) HCl (0.5 M in H_2O), two-step yield, 10%.

https://doi.org/10.1021/acsmedchemlett.5c00506
ACS Med. Chem. Lett. 2025, 16, 2070−2077

Scheme 2. Synthesis of Covalent Degraders SZ-2 and SZ-3[a]

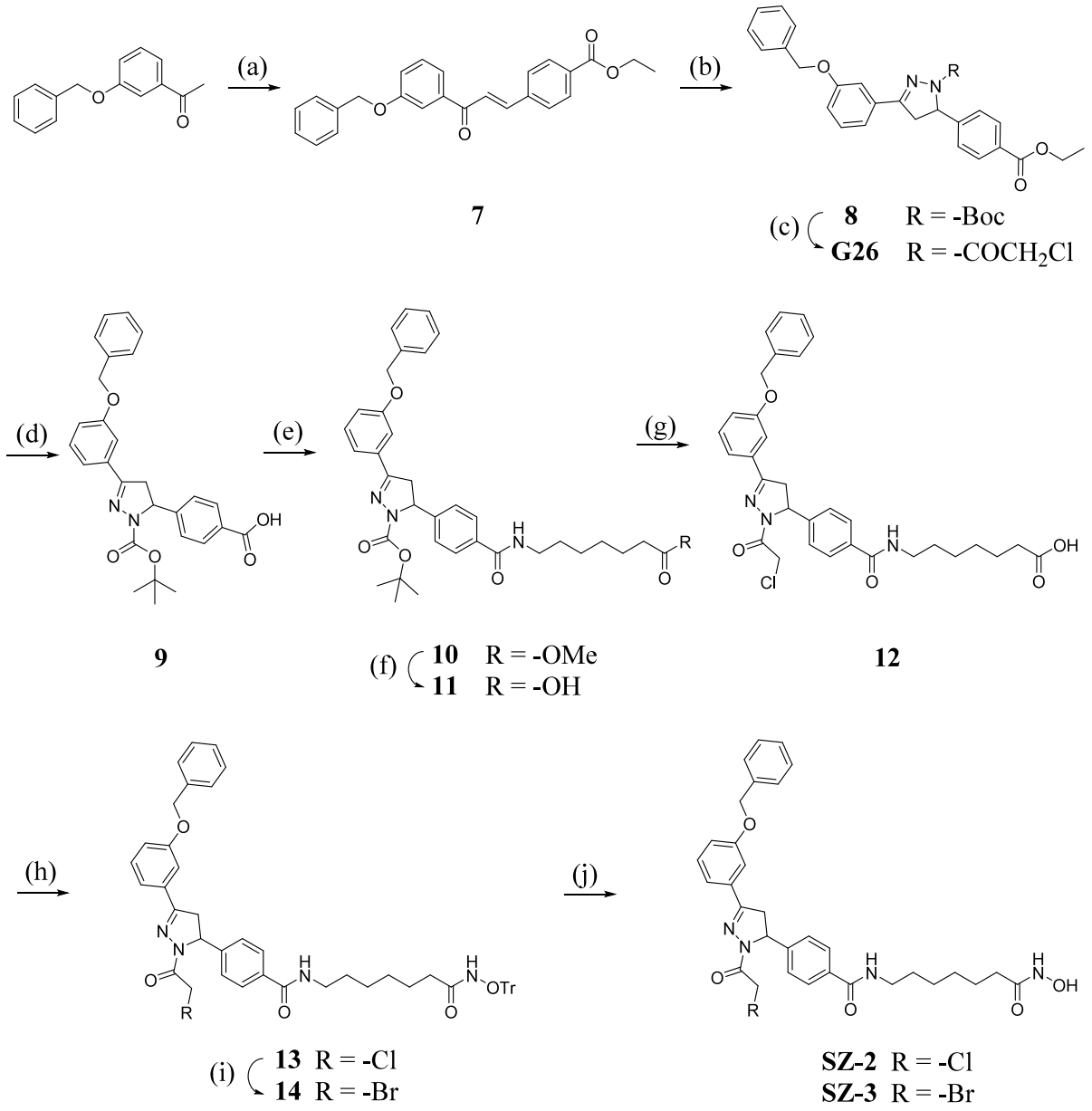

[a](a) Methyl 4-formylbenzoate, KOH, ethanol, rt, 15 h, > 78%; (b) *tert*-butyl hydrazinecarboxylate, 1,3,4,6,7,8-hexahydro-2*H*-pyrimido[1,2-*a*]pyrimidine, N_2, 60 °C, 22 h, > 66%; (c) (i) TFA, CH_2Cl_2, rt, 2 h; (ii) chloroacetyl chloride, Et_3N, 0 °C to rt, 17 h, two-step yield, 95%; (d) (i) LiOH·H_2O, THF/MeOH/H_2O, 50 °C, 23 h; (ii) HCl (0.5 M in H_2O), two-step yield, 93%; (e) methyl 7-aminoheptanoate hydrochloride, HATU, DIPEA, anhydrous DMF, rt, 18.5 h, 73%; (f) (i) LiOH × H_2O, THF/MeOH/H_2O, rt, 17 h; (ii) HCl (0.5 M in H_2O), two-step yield, 88%; (g) (i) TFA, CH_2Cl_2, rt, 2 h; (ii) chloroacetyl chloride, Et_3N, 0 °C to rt, 20 h, two-step yield, 70%; (h) *O*-tritylhydroxylamine, PyCloP, DIPEA, anhydrous DMF, rt, 18 h, 82%; (i) NaBr, acetone, reflux, 48 h, 42%; (j) triisopropylsilane, TFA, DCM, rt, 2 h, 30% (**SZ-2**), 18% (**SZ-3**).

aminoheptanoate resulted in the formation of compound **6**. Finally, the methyl ester group in compound **6** was converted into the hydroxamic acid by direct hydroxylaminolysis, resulting in the formation of the target compound **SZ-1**.

The synthesis of the covalent degrader **SZ-2** started with an aldol condensation reaction between the commercially available 1-(3-(benzyloxy)phenyl)ethan-1-one and methyl 4-formylbenzoate in the presence of potassium hydroxide in ethanol (Scheme 2). Compound **7** was then reacted with *tert*-butyl hydrazinecarboxylate using 1,3,4,6,7,8-hexahydro-2*H*-pyrimido[1,2-*a*]pyrimidine as the catalyst to yield **8**. Compound **G26** was obtained by first removing the Boc-protecting group from compound **8**, followed by the acylation reaction with chloroacetyl chloride. Compound **9** was synthesized by first hydrolyzing compound **8** with lithium hydroxide monohydrate, followed by acidification with hydrochloric acid. The product was subjected to a HATU-mediated amide coupling reaction in the presence of methyl 7-aminoheptanoate hydrochloride and DIPEA to produce compound **10**. The subsequent hydrolysis of **10** afforded the carboxylic acid **11**. After Boc-deprotection of compound **11**, compound **12** was synthesized by adding chloroacetyl chloride to the solution of deprotected **11** in the presence of triethylamine as a base. Subsequently, compound **12** did undergo a PyCloP-mediated amide coupling reaction with *O*-tritylhydroxylamine to yield compound **13**. The brominated

https://doi.org/10.1021/acsmedchemlett.5c00506
ACS Med. Chem. Lett. 2025, 16, 2070−2077

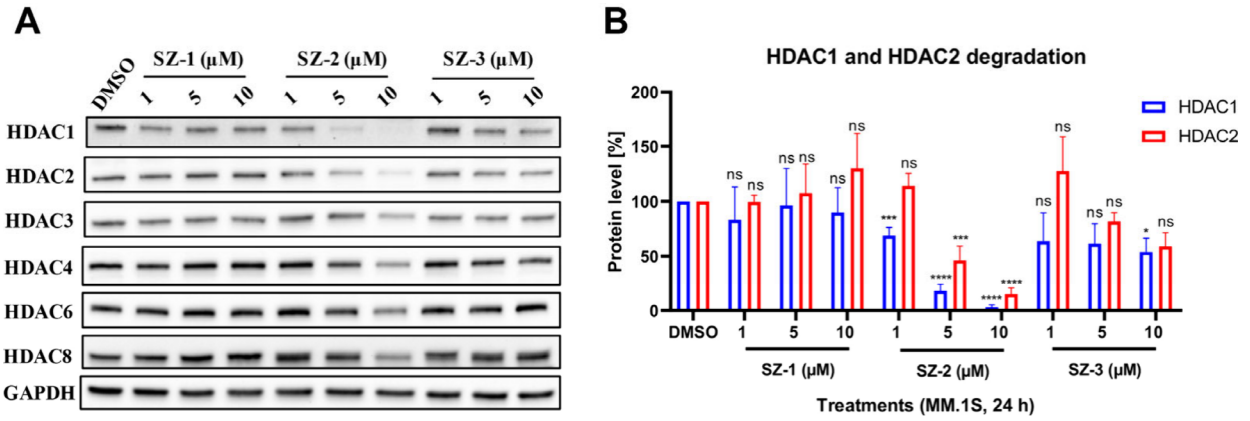

Figure 2. HDACs degradation induced by **SZ-1**, **SZ-2** and **SZ-3** in MM.1S cells. (A) Western blot analysis of HDAC1, 2, 3, 4, 6, and 8 degradation in MM.1S cells treated with **SZ-1**, **SZ-2** and **SZ-3** at different concentrations for 24 h. GAPDH was selected as loading control. Representative image of $n = 3$ replicates. (B) Statistical analysis of HDAC1 and HDAC2 degradation. Normalization was done on the transferred membrane against the total protein. Data from $n = 3$ replicates. Statistical analysis was performed by using one-way ANOVA in GraphPad Prism 8. Statistical significance was indicated with asterisks (ns = no significance; * = $p < 0.05$; *** = $p < 0.001$; **** = $p < 0.0001$).

Table 1. Cell Viability and HDAC Enzyme Inhibition Assay for the Synthesized Compounds

	IC_{50} (μM)		IC_{50} (μM)	
Cmpd.	MM.1S[a]	MCF-7[b]	HDAC1	HDAC6
SZ-1	n. e.	n. e.	0.107 ± 0.007	0.012 ± 0.001
SZ-2	3.28 ± 0.19	3.46 ± 1.51	6.41 ± 1.10	0.479 ± 0.063
SZ-3	11.9 ± 1.13	14.2 ± 0.61	1.23 ± 0.02	0.122 ± 0.006
F16	33.5 ± 0.17	n. e.	n. d.	n. d.
G26	6.81 ± 0.21	5.39 ± 0.54	n. d.	n. d.
Ricolinostat	2.59 ± 0.27	6.54 ± 4.00	0.160 ± 0.005[c]	0.018 ± 0.002[c]
Vorinostat	0.79 ± 0.13	4.51 ± 2.92	0.089 ± 0.013	0.026 ± 0.001

[a]Cell viability data in MM.1S cells were obtained using the CellTiterGlo 2.0 assay; [b]Cell viability data in MCF-7 cells were obtained using the MTT assay. [c]Data taken from the literature.[44]

compound **14** was produced by refluxing **13** in acetone with sodium bromide serving as the source of bromide ions. In the final step, triisopropylsilane and TFA were used to remove the protecting groups in compounds **13** and **14**, yielding the chloroacetyl-based covalent degrader **SZ-2** and bromoacetyl-based covalent degrader **SZ-3**, respectively.

After synthesizing these three compounds, we first tested their degradation efficiency on several HDAC subtypes in MM.1S cells, including HDAC1−3 and HDAC8 (class I), HDAC4 (class IIa), and HDAC6 (class IIb). Interestingly, significant degradation of HDAC1 and HDAC2 was observed in MM.1S cells under the treatment with the covalent ligand-based degrader **SZ-2**, while the noncovalent degrader **SZ-1** was inactive (Figure 2A, 2B, Figure S1, Supporting Information). For **SZ-3**, which contains a bromoacetyl group as its covalent warhead, significant degradation of HDAC1 was only achieved at a concentration of 10 μM (Figure 2B). Notably, the $D_{max,\ 24\ h}$ values of **SZ-2** for HDAC1 and HDAC2 reached 99% and 90%, respectively. Furthermore, no degradation of HDAC3, 4, 6, and 8 was observed at a concentration of 5 μM. However, a slight reduction in the levels of these proteins was observed after treatment with 10 μM of **SZ-2**.

In addition, HDAC1 and HDAC6 degradation was investigated in the MCF-7 breast cancer cell line using the same treatment settings as in the MM.1S cell line. As a result, only a significant degradation of HDAC1, but not HDAC6, was observed under **SZ-2** treatment at 10 μM, resulting in a $D_{max,\ 24\ h}$ value of 38% (Figure S2, Supporting Information).

In the next step, the antiproliferative activities of **SZ-1**, **SZ-2**, and **SZ-3** were evaluated in MM.1S and MCF-7 cells. For comparison, both the noncovalent (**F16**) and covalent (**G26**) warheads were included in the assay, together with ricolinostat and vorinostat as positive controls. Interestingly, the noncovalent degrader **SZ-1** did not show antiproliferative effects against both cell lines, and its noncovalent warhead **F16** only displayed a low antiproliferative activity with an IC_{50} of 33.5 ± 0.17 μM (Table 1, Figure S3, Supporting Information). For the covalent degraders, the chloroacetyl-based compound **SZ-2** exhibited relatively strong effects on both cell lines. In MM.1S cells, **SZ-2** exerted stronger antiproliferative activity than its covalent warhead **G26** and had a similar effect to that of ricolinostat. Among the investigated compounds, **SZ-2** showed the best antiproliferative activity in MCF-7 cells, with an IC_{50} of 3.46 ± 1.51 μM. The bromoacetyl-based compound **SZ-3** showed a moderate effect on both cell lines. Notably, cytotoxicity data for **SZ-2** and **G26** in both cell lines, along with the results from Western blot experiments, suggest that **SZ-2**'s antiproliferative effect is linked to HDAC knockdown and not solely to DDB1 binding.

Furthermore, biochemical HDAC1 and 6 enzyme inhibition assays were conducted with **SZ-1**, **SZ-2**, and **SZ-3**. All three degraders exhibited stronger inhibitory effects on HDAC6 than against HDAC1. Among them, **SZ-1** demonstrated comparable potency against HDAC1 and an even greater inhibitory effect on HDAC6 compared to vorinostat. Although **SZ-1** exhibited the highest HDAC inhibitory potency among the three

https://doi.org/10.1021/acsmedchemlett.5c00506
ACS Med. Chem. Lett. 2025, 16, 2070−2077

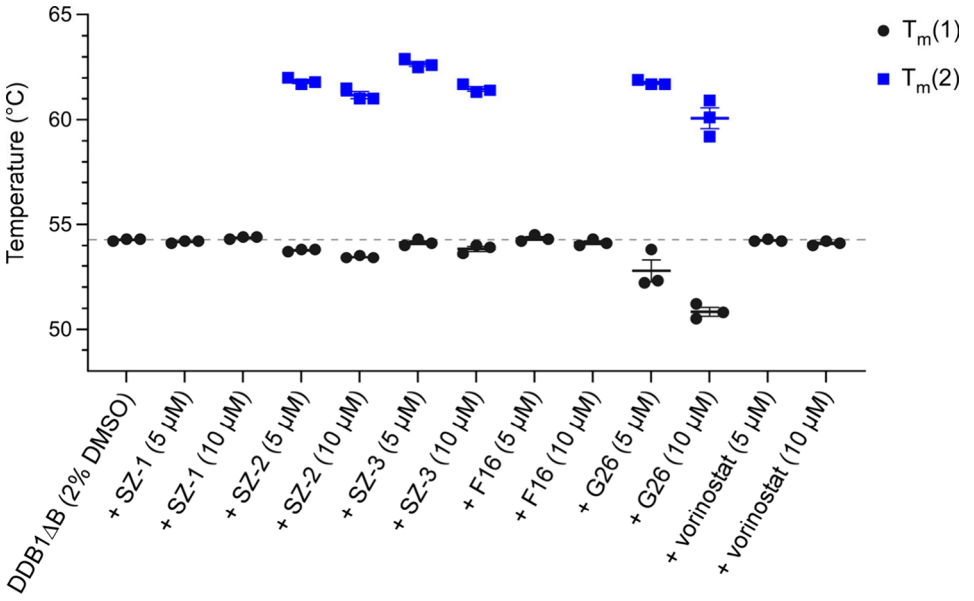

Figure 3. Thermal stability of DDB1ΔB in the presence and absence of compounds. The melting temperature (T_m) was determined by nanoDSF. For **SZ-2**, **SZ-3** and **G26**, a change in the fluorescence emission spectrum is observed with a second T_m at 60−62 °C, suggesting an interaction between the compound and the protein. Prior to the measurements, all samples were incubated for 10 min in DDB1ΔB SEC buffer supplemented with DMSO. Representative image of n = 3 replicates.

compounds, its low antiproliferative activity may result from limited cell permeability. Interestingly, **SZ-2** and **SZ-3** showed relatively low inhibitory potency, with **SZ-2** exhibiting the weakest activity against both HDAC subtypes, particularly HDAC1. Nevertheless, **SZ-2** exhibited the most potent HDAC1 degradation (Figure 2).

To analyze the DDB1 target engagement, we determined the thermal stability of DDB1 in the presence or absence of compounds **SZ-1**, **SZ-2**, **SZ-3**, **F16**, **G26** and vorinostat using recombinant protein. The thermal stability of DDB1ΔB protein was assessed by the nanodifferential scanning fluorimetry (nanoDSF) technique. Melting temperatures (T_m's) were determined with 2 μM DDB1ΔB, purified in crystallization grade quality,[17−20] adding either 5 or 10 μM of the test compounds, and compared to unligated protein (DMSO control). Prior to the measurements, all samples were incubated for 10 min in DDB1ΔB SEC buffer (50 mM HEPES pH 7.4, 200 mM NaCl, 1 mM TCEP) supplemented with DMSO, ensuring a final DMSO concentration of 2%. The resulting T_m's indicate structural changes in the protein induced by the ligands (Figure 3, Figure S4, Supporting Information). The DDB1ΔB reference measurement showed a single T_m around 54.3 °C (T_m 1). Addition of **SZ-1**, **F16** or vorinostat at increasing concentrations to DDB1ΔB did not change the proteins melting temperature (Figure S4). However, for **SZ-2**, **SZ-3**, and **G26**, a significant change in the fluorescence emission spectra was observed, leading to a shift and disappearance of T_m 1 and the appearance of a second peak (T_m 2) at around 60−62 °C as an indication for a potential interaction between the compound and the protein. This effect was concentration dependent and strongest for **G26** followed by **SZ-2** and **SZ-3** (Figure S4). The observations support the hypothesis that these compounds bind to DDB1.

After identifying **SZ-2** as the most effective degrader in this set, we determined its $DC_{50,\ 24\ h}$ value for the degradation of HDAC1, as well as analyzed its cellular target engagement. To this end, the degradation of HDAC1 was quantified after the treatment with several concentrations of **SZ-2** for 24 h. This resulted in a $DC_{50,\ 24\ h}$ value of 2.55 ± 0.38 μM for HDAC1 (Figure 4A, 4B). The cellular target engagement of **SZ-2** was investigated by analyzing acetylation levels of Ac-histone H3

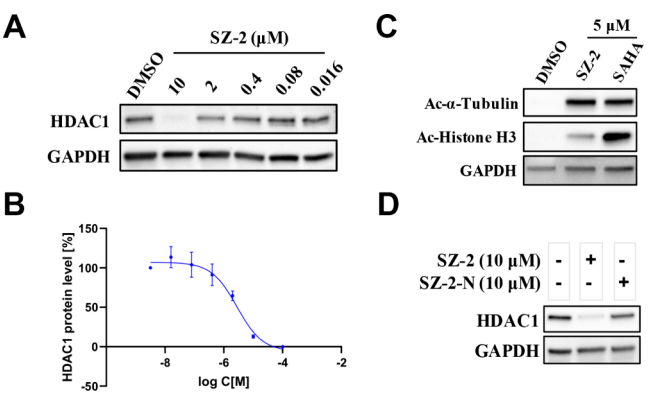

Figure 4. Determination of the DC_{50} value of **SZ-2** for HDAC1 degradation and its cellular target engagement in MM.1S cells. (A) Western blot analysis of HDAC1 degradation in MM.1S cells treated for 24 h with **SZ-2** at different concentrations. GAPDH was selected as loading control. Representative image of n = 2 biologically independent experiments, each performed in triplicates. (B) The DC_{50} value (2.55 ± 0.38 μM) for HDAC1 was obtained by fitting the D_{max} values to a variable slope response model (three parameters). Representative graph of n = 2 biologically independent experiments, each performed in triplicates. (C) Immunoblot analysis of acetylated α-tubulin and histone H3 levels in MM.1S cells. MM.1S cells were incubated for 24 h at a concentration of 5 μM of **SZ-2**. Vorinostat (SAHA, 5 μM) was used as positive control, and GAPDH was chosen as loading control. Representative image of n = 2 biologically independent experiments, each performed in triplicates. (D) Immunoblot analysis of HDAC1 levels in MM.1S cells. MM.1S cells were incubated for 24 h at a concentration of 10 μM of **SZ-2** and **SZ-2-N**, respectively. GAPDH was chosen as loading control. Representative image of n = 3 replicates.

https://doi.org/10.1021/acsmedchemlett.5c00506
ACS Med. Chem. Lett. 2025, 16, 2070−2077

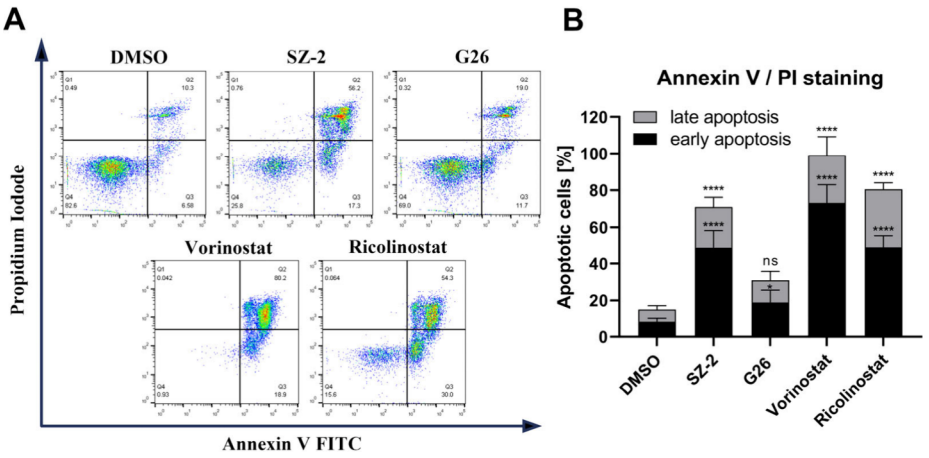

Figure 5. Apoptosis induction analysis. (A) Flow cytometry analysis of MM.1S cells treated with 5 μM of **SZ-2**, **G26**, vorinostat, ricolinostat, or vehicle (DMSO) for 48 h, followed by annexin V-FITC/PI staining. Representative images from $n = 3$ biologically independent experiments. (B) Quantification of early and late apoptotic cells. Cells with positive annexin V but negative PI signals were considered as early apoptotic cells, and cells with both positive annexin V and PI signals were considered to be late apoptotic cells. Statistical significance was indicated with asterisks (ns = no significance; * = $p < 0.05$; **** = $p < 0.0001$).

and Ac-α-tubulin. As shown in Figure 4C, **SZ-2** strongly upregulated Ac-α-tubulin, a known HDAC6 substrate, at a concentration of 5 μM, indicating strong HDAC6 inhibition. This result is consistent with the HDAC6 inhibition data. In addition, an upregulation of Ac-histone H3 was observed, confirming **SZ-2**'s ability to inactivate class I HDACs, including HDAC1 and HDAC2 (Figure 2A, Figure 4C).

To validate that the HDAC1 knockdown induced by **SZ-2** is DDB1-dependent, the negative control **SZ-2-N** was synthesized (Scheme S2, Supporting Information). In this molecule, a propionyl group was introduced to replace the chloroacetyl electrophile in **SZ-2**, which prohibits its covalent binding to DDB1. Immunoblot analysis confirmed that **SZ-2** caused a robust HDAC1 degradation at a concentration of 10 μM, whereas **SZ-2-N** did not induce any degradation at this concentration (Figure 4D).

Noticing the potent antiproliferative activity of **SZ-2** in the MM.1S and MCF-7 cell lines, we further investigated its ability to induce apoptosis. In this assay, MM.1S cells were treated with 5 μM of **SZ-2** and **G26**, as well as the two positive controls, vorinostat and ricolinostat, for 48 h. Subsequently, Annexin V-FITC/propidium iodide (PI) staining was performed, followed by flow cytometry analysis. As shown in Figure 5, **SZ-2** treatment significantly increased the number of early and late apoptotic MM.1S cells. In contrast, the covalent DDB1 ligand **G26** did not significantly induce apoptosis. Consistent with the results from the cell viability assay in MM.1S cells, **SZ-2** evoked comparable apoptosis induction as ricolinostat, though weaker than vorinostat (Table 1, Figure 5).

Taken together, we developed the covalent degrader **SZ-2**, which targets DDB1 and HDACs, by merging the pharmacophores of the reported parent molecules MM-02–57 and vorinostat. The identified hit compound **SZ-2** reduced HDAC1 protein levels *via* direct DDB1 recruitment, exhibiting a $DC_{50,\ 24\ h}$ value of 2.55 μM. In addition, **SZ-2** exerted potent antiproliferative effects against MM.1S (IC_{50} = 3.28 μM) and MCF-7 (IC_{50} = 3.46 μM) cells. Biochemical enzyme inhibition assays indicated its engagement of HDAC1 and HDAC6, which was further confirmed by the cellular target engagement analysis. Additionally, nanoDSF assays suggested that **SZ-2** binds to DDB1. Furthermore, **SZ-2** induced apoptosis in MM.1S cells, highlighting its potential as a promising anti-multiple myeloma agent. Following these successful proof-of-concept studies, we plan to further optimize **SZ-2**. Specifically, we aim to refine the DDB1 recruiter and generate both linker-less and linker-containing degrader libraries using our previously published HAIR approach,[13,45] which allows rapid library generation.

■ ASSOCIATED CONTENT

Supporting Information

The Supporting Information is available free of charge at https://pubs.acs.org/doi/10.1021/acsmedchemlett.5c00506.

Experimental procedures, Supplemental Figures and Schemes, ^{1}H NMR and ^{13}C NMR spectra for all synthesized compounds, and HPLC chromatograms of test compounds (PDF)

■ AUTHOR INFORMATION

Corresponding Author

Finn K. Hansen − *Department of Pharmaceutical and Cell Biological Chemistry, Pharmaceutical Institute, University of Bonn, 53121 Bonn, Germany;* orcid.org/0000-0001-9765-5975; Phone: (+49) 228 73 5213; Email: finn.hansen@uni-bonn.de; Fax: (+49) 228 73 7929

Authors

Shiyang Zhai − *Department of Pharmaceutical and Cell Biological Chemistry, Pharmaceutical Institute, University of Bonn, 53121 Bonn, Germany;* orcid.org/0009-0005-6840-3177

Nicola Willemsen − *Institute of Structural Biology, University of Bonn, 53127 Bonn, Germany*

Tao Sun − *Department of Pharmaceutical and Cell Biological Chemistry, Pharmaceutical Institute, University of Bonn, 53121 Bonn, Germany*

Mateo Malenica − *Department of Pharmaceutical and Cell Biological Chemistry, Pharmaceutical Institute, University of Bonn, 53121 Bonn, Germany*

Shixin Deng − *Department of Pharmaceutical and Cell Biological Chemistry, Pharmaceutical Institute, University of Bonn, 53121 Bonn, Germany*

https://doi.org/10.1021/acsmedchemlett.5c00506
ACS Med. Chem. Lett. 2025, 16, 2070−2077

Matthias Geyer − *Institute of Structural Biology, University of Bonn, 53127 Bonn, Germany*

Complete contact information is available at: https://pubs.acs.org/10.1021/acsmedchemlett.5c00506

Notes

The authors declare no competing financial interest.

No unexpected or unusually high safety hazards were encountered.

■ ACKNOWLEDGMENTS

S. Z. (grant no. 202106150022) and T. S. (grant no. 202107060004) are funded by the China Scholarship Council. The new NMR console for the 500 MHz NMR spectrometer used in this research was funded by the Deutsche Forschungsgemeinschaft (DFG, German Research Foundation) under project number 507275896. The work of M.M. and F.K.H. was funded by the Deutsche Forschungsgemeinschaft (DFG, German Research Foundation)−GRK2873 (494832089) and HA 7783/5-1. M.G. is supported by the Deutsche Forschungsgemeinschaft (DFG) under Germany's Excellence Strategy−EXC2151−390873048 and by the European Research Council (ERC Advanced Grant NalpACT).

■ ABBREVIATIONS

BRD4, bromodomain-containing protein 4; CDK4, cyclin-dependent kinase 4; CRBN, cereblon; CUL4, cullin-4; DCAF, DDB1-CUL4-associated factor; DCM, methylene chloride; DDB1, damaged DNA binding protein 1; DDB1ΔB, the human wild-type DNA damage-binding protein lacking the second beta-propeller domain; DIPEA, N, N-Diisopropylethylamine; DMF, dimethylformamide; EGFR, epidermal growth factor receptor; GAPDH, glyceraldehyde-3-phosphate dehydrogenase; HATU, (1- [Bis(dimethylamino)methylene]-1H-1,2,3-triazolo[4,5-*b*]pyridinium 3-oxide hexafluorophosphate); HDAC, histone deacetylases; HEPES, 4-(2-hydroxyethyl)-1-piperazineethanesulfonic acid; KOH, potassium hydroxide; nanoDSF, nanodifferential scanning fluorimetry; POI, protein of interest; PROTACs, proteolysis-targeting chimeras; PyCloP, chlor-tripyrrolidinophosphonium-hexafluorophosphat; RBX1, RING box protein-1; SEC, size exclusion chromatography; TCEP, tris(2-carboxyethyl)phosphine; THF, tetrahydrofuran; TFA, trifluoroacetic acid; VHL, von Hippel-Lindau

■ REFERENCES

(1) Biswas, S.; Rao, C. M. Epigenetic tools (The Writers, The Readers and The Erasers) and their implications in cancer therapy. *Eur. J. Pharmacol.* **2018**, *837*, 8−24.

(2) Porter, N. J.; Christianson, D. W. Structure, mechanism, and inhibition of the zinc-dependent histone deacetylases. *Curr. Opin. Struct. Biol.* **2019**, *59*, 9−18.

(3) Ho, T. C. S.; Chan, A. H. Y.; Ganesan, A. Thirty Years of HDAC Inhibitors: 2020 Insight and Hindsight. *J. Med. Chem.* **2020**, *63* (21), 12460−12484.

(4) Falkenberg, K. J.; Johnstone, R. W. Histone deacetylases and their inhibitors in cancer, neurological diseases and immune disorders. *Nat. Rev. Drug Discovery* **2014**, *13* (9), 673−691.

(5) West, A. C.; Johnstone, R. W. New and emerging HDAC inhibitors for cancer treatment. *J. Clin. Invest.* **2014**, *124* (1), 30−39.

(6) Pu, J.; Liu, T.; Wang, X.; Sharma, A.; Schmidt-Wolf, I. G. H.; Jiang, L.; Hou, J. Exploring the role of histone deacetylase and histone deacetylase inhibitors in the context of multiple myeloma: mechanisms, therapeutic implications, and future perspectives. *Exp Hematol. Oncol.* **2024**, *13* (1), 45.

(7) Pavan, A. R.; Smalley, J. P.; Patel, U.; Pytel, W. A.; Dos Santos, J. L.; Cowley, S. M.; Schwabe, J. W. R.; Hodgkinson, J. T. Cereblon-recruiting proteolysis targeting chimeras (PROTACs) can determine the selective degradation of HDAC1 over HDAC3. *Chem. Commun. (Camb.)* **2024**, *60* (94), 13879−13882.

(8) Xiao, Y.; Wang, J.; Zhao, L. Y.; Chen, X.; Zheng, G.; Zhang, X.; Liao, D. Discovery of histone deacetylase 3 (HDAC3)-specific PROTACs. *Chem. Commun. (Camb.)* **2020**, *56* (68), 9866−9869.

(9) Yang, K.; Song, Y.; Xie, H.; Wu, H.; Wu, Y. T.; Leisten, E. D.; Tang, W. Development of the first small molecule histone deacetylase 6 (HDAC6) degraders. *Bioorg. Med. Chem. Lett.* **2018**, *28* (14), 2493−2497.

(10) Kadier, K.; Niu, T.; Ding, B.; Chen, B.; Qi, X.; Chen, D.; Cheng, X.; Fang, Y.; Zhou, J.; Zhao, W.; Liu, Z.; Yuan, Y.; Zhou, Z.; Dong, X.; Yang, B.; He, Q.; Cao, J.; Jiang, L.; Zhu, C. L. PROTAC-Mediated HDAC7 Protein Degradation Unveils Its Deacetylase-Independent Proinflammatory Function in Macrophages. *Adv. Sci. (Weinh)* **2024**, *11* (36), No. e2309459.

(11) Chotitumnavee, J.; Yamashita, Y.; Takahashi, Y.; Takada, Y.; Iida, T.; Oba, M.; Itoh, Y.; Suzuki, T. Selective degradation of histone deacetylase 8 mediated by a proteolysis targeting chimera (PROTAC). *Chem. Commun. (Camb.)* **2022**, *58* (29), 4635−4638.

(12) Wurnig, S. L.; Hanl, M.; Geiger, T. M.; Zhai, S.; Dressel, I.; Pieńkowska, D. E.; Nowak, R. P.; Hansen, F. K. Light-activatable photochemically targeting chimeras (PHOTACs) enable the optical control of targeted protein degradation of HDAC6. *RSC Med. Chem.* **2025**, *16*, 2452.

(13) Sinatra, L.; Yang, J.; Schliehe-Diecks, J.; Dienstbier, N.; Vogt, M.; Gebing, P.; Bachmann, L. M.; Sönnichsen, M.; Lenz, T.; Stühler, K.; Schöler, A.; Borkhardt, A.; Bhatia, S.; Hansen, F. K. Solid-Phase Synthesis of Cereblon-Recruiting Selective Histone Deacetylase 6 Degraders (HDAC6 PROTACs) with Antileukemic Activity. *J. Med. Chem.* **2022**, *65* (24), 16860−16878.

(14) Stopper, D.; Honin, I.; Feller, F.; Hansen, F. K. Development of Ethyl-Hydrazide-Based Selective Histone Deacetylase 6 (HDAC6) PROTACs. *ACS Med. Chem. Lett.* **2025**, *16* (3), 487−495.

(15) Smalley, J. P.; Baker, I. M.; Pytel, W. A.; Lin, L. Y.; Bowman, K. J.; Schwabe, J. W. R.; Cowley, S. M.; Hodgkinson, J. T. Optimization of Class I Histone Deacetylase PROTACs Reveals that HDAC1/2 Degradation is Critical to Induce Apoptosis and Cell Arrest in Cancer Cells. *J. Med. Chem.* **2022**, *65* (7), 5642−5659.

(16) Iovine, B.; Iannella, M. L.; Bevilacqua, M. A. Damage-specific DNA binding protein 1 (DDB1): a protein with a wide range of functions. *Int. J. Biochem. Cell Biol.* **2011**, *43* (12), 1664−1667.

(17) Ghosh, P.; Schmitz, M.; Pandurangan, T.; Zeleke, S. T.; Chan, S. C.; Mosior, J.; Sun, L.; Palve, V.; Grassie, D.; Anand, K.; Frydman, S.; Roush, W. R.; Schönbrunn, E.; Geyer, M.; Duckett, D.; Monastyrskyi, A. Discovery and design of molecular glue enhancers of CDK12-DDB1 interactions for targeted degradation of cyclin K. *RSC Chem. Biol.* **2025**, *6* (1), 36−55.

(18) Huang, Z.; Zhang, K.; Jiang, Y.; Wang, M.; Li, M.; Guo, Y.; Gao, R.; Li, N.; Wang, C.; Chen, J.; Wang, J.; Liu, N.; Liu, X.; Liu, S.; Wei, M.; Yang, C.; Yang, G. Molecular glue triggers degradation of PHGDH by enhancing the interaction between DDB1 and PHGDH. *Acta Pharm. Sin. B* **2024**, *14* (9), 4001−4013.

(19) Meyers, M.; Cismoski, S.; Panidapu, A.; Chie-Leon, B.; Nomura, D. K. Targeted Protein Degradation through Recruitment of the CUL4 Complex Adaptor Protein DDB1. *ACS Chem. Biol.* **2024**, *19* (1), 58−68.

(20) Zhang, Z.; Li, Y.; Yang, J.; Li, J.; Lin, X.; Liu, T.; Yang, S.; Lin, J.; Xue, S.; Yu, J.; Tang, C.; Li, Z.; Liu, L.; Ye, Z.; Deng, Y.; Li, Z.; Chen, K.; Ding, H.; Luo, C.; Lin, H. Dual-site molecular glues for enhancing protein-protein interactions of the CDK12-DDB1 complex. *Nat. Commun.* **2024**, *15* (1), 6477.

(21) Tang, K. F.; Xie, J.; Chen, M.; Liu, Q.; Zhou, X. Y.; Zeng, W.; Huang, A. L.; Zuo, G. Q.; Wang, Y.; Xiang, R.; Ren, H. Knockdown of damage-specific DNA binding protein 1 (DDB1) enhances the HBx-siRNA-mediated inhibition of HBV replication. *Biologicals* **2008**, *36* (3), 177−183.

(22) Hodgson, A. J.; Hyser, J. M.; Keasler, V. V.; Cang, Y.; Slagle, B. L. Hepatitis B virus regulatory HBx protein binding to DDB1 is required but is not sufficient for maximal HBV replication. *Virology* **2012**, *426* (1), 73−82.
(23) Kang, X.; Chen, X.; He, Y.; Guo, D.; Guo, L.; Zhong, J.; Shu, H. B. DDB1 is a cellular substrate of NS3/4A protease and required for hepatitis C virus replication. *Virology* **2013**, *435* (2), 385−394.
(24) Wick, E. T.; Treadway, C. J.; Li, Z.; Nicely, N. I.; Ren, Z.; Baldwin, A. S.; Xiong, Y.; Harrison, J. S.; Brown, N. G. Insight into Viral Hijacking of CRL4 Ubiquitin Ligase through Structural Analysis of the pUL145-DDB1 Complex. *J. Virol.* **2022**, *96* (17), No. e0082622.
(25) Zhao, L.; Wang, X.; Pomlok, K.; Liao, H.; Yang, G.; Yang, X.; Chen, Y. G. DDB1 promotes the proliferation and hypertrophy of chondrocytes during mouse skeleton development. *Dev. Biol.* **2020**, *465* (2), 100−107.
(26) Xue, Z.; Guo, J.; Ma, R.; Zhou, L.; Guo, Y.; Cang, Y.; Fan, H.; Chen, J.; Qian, W.; Wang, L. The DDB1-DCAF2 complex is essential for B cell development because it regulates cell cycle progression. *Cell. Mol. Immunol.* **2021**, *18* (3), 758−760.
(27) Yang, L.; Chen, W.; Li, L.; Xiao, Y.; Fan, S.; Zhang, Q.; Xia, T.; Li, M.; Hong, Y.; Zhao, T.; Li, Q.; Liu, W. H.; Xiao, N. Ddb1 Is Essential for the Expansion of CD4(+) Helper T Cells by Regulating Cell Cycle Progression and Cell Death. *Front. Immunol.* **2021**, *12*, 722273.
(28) Angers, S.; Li, T.; Yi, X.; MacCoss, M. J.; Moon, R. T.; Zheng, N. Molecular architecture and assembly of the DDB1-CUL4A ubiquitin ligase machinery. *Nature* **2006**, *443* (7111), 590−593.
(29) Chamberlain, P. P.; Lopez-Girona, A.; Miller, K.; Carmel, G.; Pagarigan, B.; Chie-Leon, B.; Rychak, E.; Corral, L. G.; Ren, Y. J.; Wang, M.; Riley, M.; Delker, S. L.; Ito, T.; Ando, H.; Mori, T.; Hirano, Y.; Handa, H.; Hakoshima, T.; Daniel, T. O.; Cathers, B. E. Structure of the human Cereblon-DDB1-lenalidomide complex reveals basis for responsiveness to thalidomide analogs. *Nat. Struct. Mol. Biol.* **2014**, *21* (9), 803−809.
(30) Lee, J.; Zhou, P. DCAFs, the missing link of the CUL4-DDB1 ubiquitin ligase. *Mol. Cell* **2007**, *26* (6), 775−780.
(31) Raisch, J.; Dubois, M. L.; Groleau, M.; Lévesque, D.; Burger, T.; Jurkovic, C. M.; Brailly, R.; Marbach, G.; McKenna, A.; Barrette, C.; Jacques, P. E.; Boisvert, F. M. Pulse-SILAC and Interactomics Reveal Distinct DDB1-CUL4-Associated Factors, Cellular Functions, and Protein Substrates. *Mol. Cell. Proteomics* **2023**, *22* (10), 100644.
(32) Zhang, X.; Luukkonen, L. M.; Eissler, C. L.; Crowley, V. M.; Yamashita, Y.; Schafroth, M. A.; Kikuchi, S.; Weinstein, D. S.; Symons, K. T.; Nordin, B. E.; Rodriguez, J. L.; Wucherpfennig, T. G.; Bauer, L. G.; Dix, M. M.; Stamos, D.; Kinsella, T. M.; Simon, G. M.; Baltgalvis, K. A.; Cravatt, B. F. DCAF11 Supports Targeted Protein Degradation by Electrophilic Proteolysis-Targeting Chimeras. *J. Am. Chem. Soc.* **2021**, *143* (13), 5141−5149.
(33) Xue, G.; Xie, J.; Hinterndorfer, M.; Cigler, M.; Dötsch, L.; Imrichova, H.; Lampe, P.; Cheng, X.; Adariani, S. R.; Winter, G. E.; Waldmann, H. Discovery of a Drug-like, Natural Product-Inspired DCAF11 Ligand Chemotype. *Nat. Commun.* **2023**, *14* (1), 7908.
(34) Tin, G.; Cigler, M.; Hinterndorfer, M.; Dong, K. D.; Imrichova, H.; Gygi, S. P.; Winter, G. E. Discovery of a DCAF11-dependent cyanoacrylamide-containing covalent degrader of BET-proteins. *Bioorg. Med. Chem. Lett.* **2024**, *107*, 129779.
(35) Wang, Y.; Wei, T.; Zhao, M.; Huang, A.; Sun, F.; Chen, L.; Lin, R.; Xie, Y.; Zhang, M.; Xu, S.; Sun, Z.; Hong, L.; Wang, R.; Tian, R.; Li, G. Alkenyl oxindole is a novel PROTAC moiety that recruits the CRL4DCAF11 E3 ubiquitin ligase complex for targeted protein degradation. *PLoS Biol.* **2024**, *22* (5), No. e3002550.
(36) Sarott, R. C.; You, I.; Li, Y. D.; Toenjes, S. T.; Donovan, K. A.; Seo, P.; Ordonez, M.; Byun, W. S.; Hassan, M. M.; Wachter, F.; Chouchani, E. T.; Slabicki, M.; Fischer, E. S.; Ebert, B. L.; Hinshaw, S. M.; Gray, N. S. Chemical Specification of E3 Ubiquitin Ligase Engagement by Cysteine-Reactive Chemistry. *J. Am. Chem. Soc.* **2023**, *145* (40), 21937−21944.
(37) Feller, F.; Weber, H.; Miranda, M.; Honin, I.; Hanl, M.; Hansen, F. K. Replacing a Cereblon Ligand by a DDB1 and CUL4 Associated Factor 11 (DCAF11) Recruiter Converts a Selective Histone Deacetylase 6 PROTAC into a pan-degrader. *ChemMedChem.* **2025**, *20*, No. e202500035.
(38) Zhang, X.; Crowley, V. M.; Wucherpfennig, T. G.; Dix, M. M.; Cravatt, B. F. Electrophilic PROTACs that degrade nuclear proteins by engaging DCAF16. *Nat. Chem. Biol.* **2019**, *15* (7), 737−746.
(39) LIU, J.; PLEWE, M. B.; LEE, M. R.; HAN, X.; CHEN, L.; ZHANG, C.; WANG, J. MODIFIED PROTEINS AND PROTEIN DEGRADERS. WO 2021/239117, 2021.
(40) Lim, M.; Cong, T. D.; Orr, L. M.; Toriki, E. S.; Kile, A. C.; Papatzimas, J. W.; Lee, E.; Lin, Y.; Nomura, D. K. DCAF16-Based Covalent Handle for the Rational Design of Monovalent Degraders. *ACS Cent. Sci.* **2024**, *10* (7), 1318−1331.
(41) Toriki, E. S.; Papatzimas, J. W.; Nishikawa, K.; Dovala, D.; Frank, A. O.; Hesse, M. J.; Dankova, D.; Song, J. G.; Bruce-Smythe, M.; Struble, H.; Garcia, F. J.; Brittain, S. M.; Kile, A. C.; McGregor, L. M.; McKenna, J. M.; Tallarico, J. A.; Schirle, M.; Nomura, D. K. Rational Chemical Design of Molecular Glue Degraders. *ACS Cent. Sci.* **2023**, *9* (5), 915−926.
(42) Orr, L. M.; Tomlinson, S. J.; Grupe, H. R.; Lim, M.; Ho, E.; Yilmaz, H.; Zhou, G.; Leon, B.; Olzmann, J. A.; Nomura, D. K. DCAF16-Based Covalent Degradative Handles for the Modular Design of Degraders. *ACS Cent. Sci.* **2025**, *11* (7), 1207−1217.
(43) Hillebrand, L.; Liang, X. J.; Serafim, R. A. M.; Gehringer, M. Emerging and Re-emerging Warheads for Targeted Covalent Inhibitors: An Update. *J. Med. Chem.* **2024**, *67* (10), 7668−7758.
(44) Feller, F.; Honin, I.; Miranda, M.; Weber, H.; Henze, S.; Hanl, M.; Hansen, F. K. Development of the First-in-Class FEM1B-Recruiting Histone Deacetylase Degraders. *J. Med. Chem.* **2025**, *68* (2), 1824−1843.
(45) Sinatra, L.; Bandolik, J. J.; Roatsch, M.; Sönnichsen, M.; Schoeder, C. T.; Hamacher, A.; Schöler, A.; Borkhardt, A.; Meiler, J.; Bhatia, S.; Kassack, M. U.; Hansen, F. K. Hydroxamic Acids Immobilized on Resins (HAIRs): Synthesis of Dual-Targeting HDAC Inhibitors and HDAC Degraders (PROTACs). *Angew. Chem., Int. Ed.* **2020**, *59* (50), 22494−22499.

https://doi.org/10.1021/acsmedchemlett.5c00506
ACS Med. Chem. Lett. 2025, 16, 2070−2077

Supplementary Information

Targeted histone deacetylase degradation via chemical induced proximity by direct recruitment of the CUL4 complex adaptor protein DDB1

Shiyang Zhai,[a] Nicola Willemsen,[b] Tao Sun,[a] Mateo Malenica,[a] Shixen Deng,[a] Matthias Geyer,[b] Finn K. Hansen[a]*

[a]Department of Pharmaceutical and Cell Biological Chemistry, Pharmaceutical Institute, University of Bonn, 53121 Bonn, Germany.

[b]Institute of Structural Biology, University of Bonn, 53127 Bonn, Germany.

*Corresponding author:

Prof. Dr. Finn K. Hansen, Pharmaceutical and Cell Biological Chemistry, Pharmaceutical Institute, University of Bonn, An der Immenburg 4, 53121 Bonn, Germany. Tel.: (+49) 228 73 5213. Fax: (+49) 228 73 7929. E-mail: finn.hansen@uni-bonn.de.

Table of Contents

1. Supplementary Figures and Schemes S3

1.1. Figure S1-S4 ..... S3

1.2. Synthesis of 4-methyl-5-nitrothiazol-2-amine hydrochloride S6

1.3. Synthesis of compound **SZ-2-N** S6

2. Biological Experiments S6

2.1. Enzyme inhibition assays S6

2.2. DDB1 protein expression and purification S7

2.3. NanoDSF assay S7

2.4. Cell culture S8

2.5. CellTiterGlo® 2.0 assay in MM.1S cells S8

2.6. MTT assay in MCF-7 cells S9

2.7. Western blotting S9

2.8. Apoptosis assay S10

3. Chemical Experiments S11

3.1. General information S11

3.2. Compounds preparation S12

3.3. NMR, HR-MS and HPLC data of **SZ-1**, **SZ-2**, **SZ-3**, **SZ-2-N**, **F16** and **G26** S28

4. Immunoblot replicates S40

5. References S40

1. Supplementary Figures and Schemes

1.1. Figure S1-S4

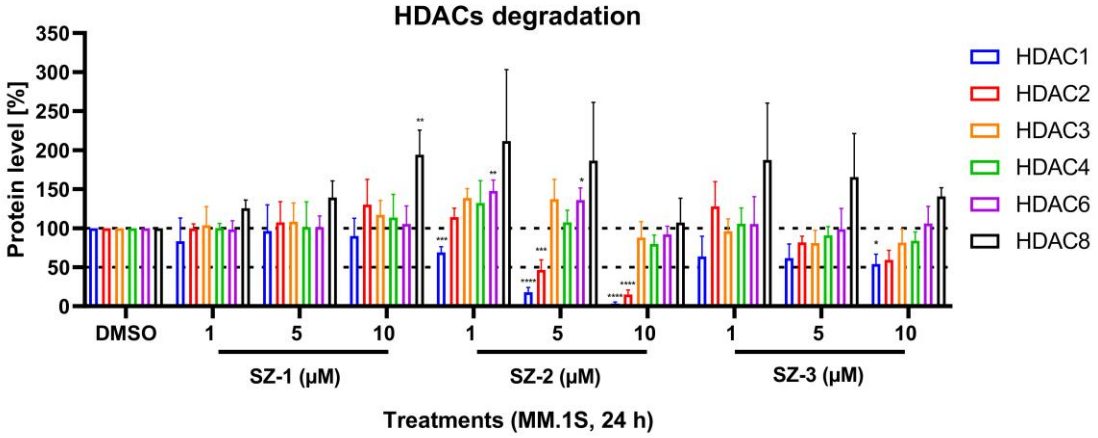

Figure S1. Statistical data for HDACs degradation in MM.1S cells after incubation with the indicated compounds at different concentrations for 24 h. Normalization was done on the transferred membrane against the total protein. Data from n = 3 replicates. Statistical analysis was performed by using one-way ANOVA in GraphPad Prism 8. Statistical significance was indicated with asterisks (ns = no significance; * = $p < 0.05$; ** = $p < 0.01$; *** = $p < 0.001$; **** = $p < 0.0001$).

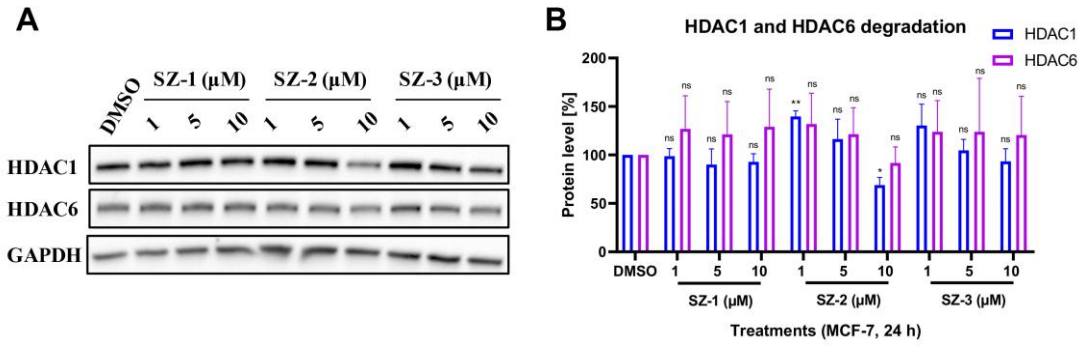

Figure S2. HDAC degradation induced by **SZ-1**, **SZ-2** and **SZ-3** in MCF-7 cells. (A) Western blot analysis of HDAC1 and HDAC6 degradation in MCF-7 cells treated with **SZ-1**, **SZ-2** and **SZ-3** at different concentrations for 24 h. GAPDH was selected as loading control. Representative image of n = 3 replicates. (B) Statistical data for HDAC1 and HDAC6 degradation. Normalization was done on the transferred membrane against the total protein. Data from n = 3 replicates. Statistical analysis was performed by using one-way ANOVA in

GraphPad Prism 8. Statistical significance was indicated with asterisks (ns = no significance; * = $p < 0.05$; ** = $p < 0.01$).

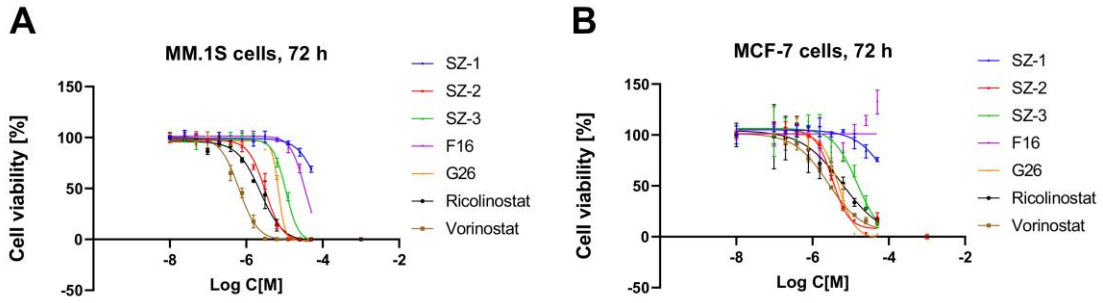

Figure S3. Viability assay on MM.1S and MCF-7 cells. (A) CellTiterGlo® 2.0 assay on MM.1S cells. Ricolinostat and vorinostat were taken as positive controls; (B) MTT assay on MCF-7 cells. Ricolinostat and vorinostat were taken as positive controls. Data are represented from n = 3 independent experiments.

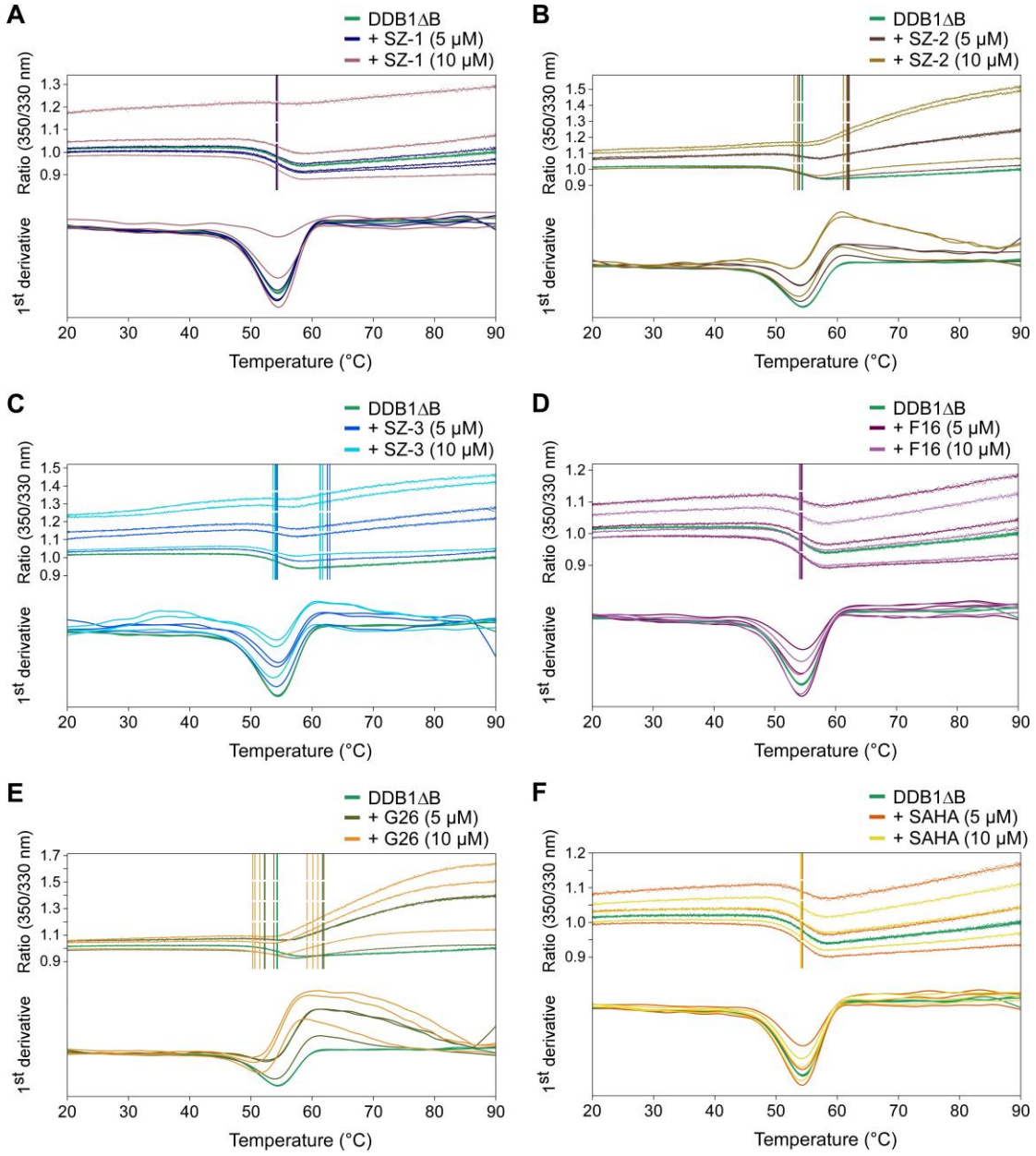

Figure S4. Thermal stability of DDB1ΔB in the presence and absence of compounds. (A-F) The melting temperatures (T_m's) were determined by nanoDSF within a range from 20 to 90°C. Shown is the ratio of the intrinsic fluorescence emission at 350 and 330 nm (top) and the first derivative thereof (bottom). Two different concentrations of compounds (5 µM and 10 µM) were each added to 2 µM DDB1ΔB protein. Addition of **SZ-2** (B), **SZ-3** (C) and **G26** (E) lead to changes in the fluorescence emission spectra in a concentration dependent manner.

1.2. Synthesis of 4-methyl-5-nitrothiazol-2-amine hydrochloride

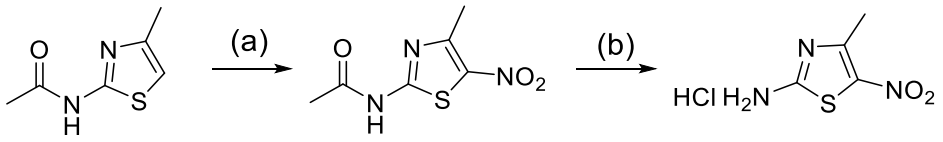

Scheme S1. (a) *N*-(4-methylthiazol-2-yl)acetamide, conc. H_2SO_4, KNO_3, 0 °C, 2.5 h, 86%; (b) conc. HCl (aq.), MeOH, 50 °C, 7 h, 97%.

1.3. Synthesis of compound SZ-2-N

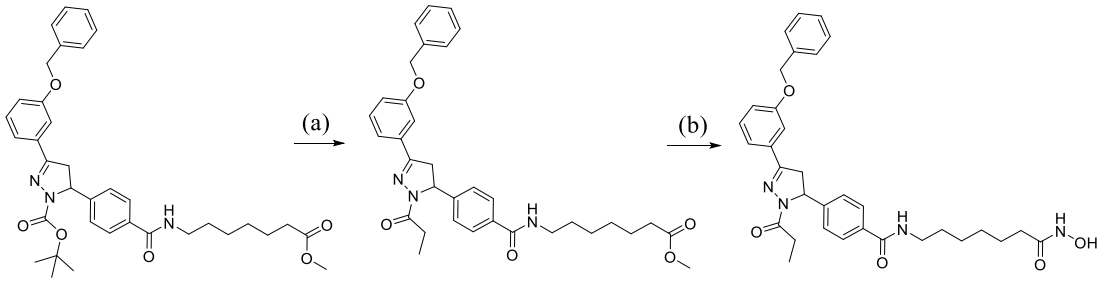

Scheme S2. (a) (i) TFA, DCM, 2 h; (ii) propionyl chloride, triethylamine, DCM, 0 °C to rt, 17 h, 59% (two-step yield); (b) (i) hydroxylamine (50 wt. % in water), NaOH, MeOH/DCM, 0 °C to rt, 2 h; (ii) HCl (0.5 M in H_2O), 79% (two-step yield).

2. Biological Experiments

2.1. Enzyme inhibition assays

Serial dilutions of the test compounds and controls were prepared from their respective stock DMSO solution in assay buffer (50 mM Tris-HCl, pH 8.0, 137 mM NaCl, 2.7 mM KCl, 1.0 mM $MgCl_2 \cdot 6H_2O$, 0.1 mg/mL BSA). 5.0 µL of this serial dilution were transferred to black OptiPlate-96 microplates (Revvity) along with 35 µL of the fluorogenic substrate ZMAL (Z-Lys(Ac)-AMC, 21.43 µM in assay buffer) and 10 µL of the enzyme solution,[1] using human recombinant HDAC1 (BPS Bioscience, Catalog#50051) and HDAC6 (BPS Bioscience, Catalog#50006). The assay with a total volume of 50 µL (HDAC1 max. 5% DMSO; HDAC6 max. 1% DMSO) was incubated at 37 °C for 90 minutes. Subsequently, 50 µL of trypsin (0.4 mg/mL) in trypsin buffer (50 mM Tris-HCl, pH 8.0, 100 mM NaCl) was added and incubated

for another 30 minutes at 37 °C. The IC_{50} values were determined by generating dose-response curves and performing a non-linear regression utilizing GraphPad Prism GraphPad Software, San Diego, CA, USA). Each compound was evaluated in at least two independent experiments in duplicates.[2-5]

2.2. DDB1 protein expression and purification

The protein purification was performed according to the protocol described by Ghosh and colleagues.[6] In short, the human wild-type DNA damage-binding protein (DDB1) lacking the second beta-propeller domain (UniProt accession number Q16531; residues 1–1140 Δ396–705), termed DDB1ΔB, was PCR-amplified from AddGene plasmid #124213 and inserted into a pACEBac1 vector, which had been modified with an His_6 affinity tag. The DDB1ΔB construct was expressed in *Sf*9 insect cells and subjected to affinity chromatography, anion exchange chromatography, and size exclusion chromatography (SEC). Following anion exchange chromatography, protein fractions containing DDB1ΔB protein were determined by SDS PAGE analysis, pooled, concentrated and loaded onto an ÄKTA pure FPLC system (Cytiva) equipped with a preparative Superdex 200 increase 10/300 GL column (Cytiva), pre-equilibrated in SEC buffer (50 mM Hepes pH 7.4, 200 mM NaCl, 1 mM TCEP). Peak fractions were monitored by SDS PAGE, and fractions containing homogenous DDB1DB protein were pooled, concentrated, aliquoted, snap frozen in liquid nitrogen, and stored at -80 °C for further applications.

2.3. NanoDSF assay

To evaluate the thermal stability of DDB1ΔB protein, nano-differential scanning fluorimetry (nanoDSF) was performed using a Prometheus NT.48 device (NanoTemper). In this method, thermal stability was measured between 20 °C and 90 °C with a temperature increase of 1.5 °C per minute. Thus, proteins are heated under a linear temperature gradient while the fluorescence of tyrosine and tryptophan residues is recorded at 330 nm and 350 nm. The protein starts to unfold and the aromatic residues become exposed to the solvent, so their fluorescence changes, allowing real-time tracking of the denaturation process. The melting temperature (T_m), shown as the inflection point of the 350/330 nm fluorescence ratio and determined from the maxima or minima of the first derivative, was calculated using the PR.ThermControl software (v. 2.1.6,

NanoTemper). Melting temperatures were examined with 2 µM DDB1ΔB protein with either 5 or 10 µM of the test compounds and compared to unligated protein (DMSO control) using Prometheus NT.48 Standard Capillaries (NanoTemper). Prior to the measurements, all samples were incubated for 10 minutes or 2 hours in DDB1ΔB SEC buffer (50 mM HEPES pH 7.4, 200 mM NaCl, 1 mM TCEP) supplemented with DMSO, ensuring a final DMSO concentration of 2 %.

2.4. Cell culture

MM.1S cells were obtained from the American Type Culture Collection (ATCC, Manassas, VA, USA). Cells were cultured in RPMI 1640 (Life Technologies, Darmstadt, Germany) supplemented with 10 % fetal bovine serum (PAN Biotech GmbH, Aidenbach, Germany), 100 IU/mL penicillin and 0.1 mg/mL streptomycin (PAN Biotech GmbH, Aidenbach, Germany) and 1 mM sodium pyruvate (ThermoFisher Scientific Inc.; Waltham, MA, USA) and were incubated at 37 °C under humidified air with 5% CO_2. MCF-7 cells were obtained from the American Type Culture Collection (ATCC, Manassas, VA, USA). Cells were cultured in Dulbecco's Modified Eagle's Medium (DMEM, Gibco) already containing L-glutamine and pyruvate, and supplemented with 10 % fetal bovine serum (PAN Biotech GmbH, Aidenbach, Germany), 100 IU/mL penicillin and 0.1 mg/mL streptomycin (PAN Biotech GmbH, Aidenbach, Germany), and were incubated at 37 °C under humidified air with 5% CO_2.

2.5. CellTiterGlo® 2.0 assay in MM.1S cells

Following a previously reported method,[7] 2,500 MM.1S cells/well were seeded in white 384-well plates (Greiner Bio-One, Kremsmuenster, Austria). The final assay volume was 25 µL. A 200-fold dilution series was prepared in DMSO and further diluted to 10-fold in medium and added to the cells. The final DMSO concentration was 0.5%. The toxicity of compounds was determined after 72 h using the CellTiter-Glo® 2.0 Cell Viability Assay (Promega, Madison, WI, USA, #G9242) according to the manufacturer's protocol. Subsequently, the luminescence was measured using a Tecan Spark (Tecan Group AG, Maennedorf, Swiss). Data was analyzed with the four-parameter logistic equation (GraphPad Prism 9.0, San Diego, CA, USA).

2.6. MTT assay in MCF-7 cells

MTT assay in MCF-7 cells. Assays were conducted following previously reported methods.[3] MTT (3-(4,5-dimethylthiazol-2-yl)-2,5-diphenyltetrazolium bromide; Catalog# A2231; BioChemica, Applichem GmbH, Darmstadt, Germany) was used to measure cell viability. A total of 2,500 MCF-7 cells were seeded in triplicates in 96-well plates (Starlab GmbH, Hamburg, Germany) with each well containing 200 µL of volume. These cells were subsequently treated with dilution series of different compounds. Following an incubation period of 72 hours, 20 µL of freshly prepared MTT solution (5 mg/mL) was added and the mixture was incubated for 1 hour at 37 °C and 5% CO_2. After removing the supernatant, the formazan dye was solubilized in 200 µL DMSO (Sigma-Aldrich, Steinheim, Germany). The absorbance was determined at 570 nm with background subtraction at 690 nm by a microplate photometer (Thermo Scientific Multiskan EX, Thermo Fisher Sceintific). The acquired data was normalized to DPBS, considering 100% viability, and the half-maximal inhibitory concentration (IC_{50}) was determined by plotting dose response curves and nonlinear regression with GraphPad Prism (GraphPad Software, San Diego, CA, USA).

2.7. Western blotting

Western blots on HDAC1, 2, 3, 4, 6, 8, acetylated histone H3, acetylated α-tubulin and GAPDH in MM.1S cells, as well as the HDAC1, 6 and GAPDH in MCF-7 cells were performed according to a previously published protocol.[8-10] In brief, the treated MM.1S or MCF-7 cells were collected and lysed with cell extraction buffer (ThermoFisher Scientific Inc.; Waltham, MA, USA), supplemented with 0.1 mM PMSF, Halt™ Protease Inhibitor (Thermo Fisher), and sodium orthovanadate (ThermoFisher Scientific Inc.; Waltham, MA, USA). Protein concentration was determined using a BCA kit (ThermoFisher Scientific Inc.; Waltham, MA, USA). Equal amounts of protein (25 µg) from the lysates was denatured by Laemmli 2× Concentrate (Catalog# S3401-10VL, Sigma-Aldrich, St. Louis, MO, USA), and Precision Plus Protein Unstained Standard was used as molecular weight marker (Catalog# 1610363, Bio-Rad, Hercules, CA, USA). SDS-PAGE was performed with precast gels with a polymerization degree of 4-15% (for ac-histone H3) and 10% or 12% for other proteins (Mini-PROTEAN® TGX™ Stain-Free™; Bio-Rad Laboratories GmbH, Germany). Afterward, proteins were

transferred to Trans-Blot Turbo®-PVDF membranes (Bio-Rad). The membrane was blocked with skimmed milk powder in Tris-buffered saline-Tween 20 (with 0.2% Tween 20) for 60 min, followed by three washing cycles of 10 min using Tris-buffered saline-Tween 20. Next, membranes were incubated with primary antibodies for a total of 60 min at room temperature under slight agitation and then incubated at 4 °C overnight. Membranes were rinsed again three times before applying the secondary anti-rabbit IgG HRP-conjugated mAbs (R&D Systems, Inc., Minneapolis, USA) or anti-mouse IgG HRP-conjugated mAbs (Santa Cruz Biotechnology, Texas, USA) for 90 min. After rinsing of the secondary antibody, membranes were detected using the ClarityECL Western Blotting Substrate (Bio-Rad). For quantitative determination, the StainFree technique was employed (Bio-Rad), which allows the imaging of whole lysates in SDS-PAGE before blotting and normalization on the transferred membrane against the total protein. Pixel density analysis was performed with the IMAGE LAB software (Bio-Rad). Primary antibodies were used as antibody solutions in 1:1000–1:20000 dilutions according to the manufacturer's indication. Anti-HDAC1 (Catalog#5356S, Cell Signaling Technology, Denver, MA, USA), anti-HDAC2 (Catalog# sc-9959, Santa Cruz Biotechnology, Dallas, TX, USA), anti-HDAC3 (Catalog#85057S, Cell Signaling Technology, Denver, MA, USA), anti-HDAC4 (Catalog#7628S, Cell Signaling Technology, Denver, MA, USA), anti-HDAC6 (Catalog#7558S, Cell Signaling Technology, Denver, MA, USA), anti-HDAC8 (Catalog#66042S, Cell Signaling Technology, Denver, MA, USA), anti-acetyl-histone H3 (Catalog#9677S, Cell Signaling Technology, Denver, MA, USA), anti-acetyl-α-tubulin (Catalog#5335, Cell Signaling Technology, Denver, MA, USA), anti-GAPDH (Catalog# T0004, Affinity Biosciences, Cincinnati, OH, USA).

2.8. Apoptosis assay

3×10^5 cells/well of MM.1S cells were seeded into 24-well plates and treated for 48 h with 5 μM of indicated compounds or vehicle (DMSO) under cell culture condition. Subsequently, washed the cells with staining buffer (HEPES 0.1 M, NaCl 1.4 M, $CaCl_2 \times 3\ H_2O$ 25 mM), resuspended in 300 μL and 150 μL was transferred into a 96-well plate, followed by adding 5 μL/well annexin V-FITC (catalog# 640945, BioLegend, San Diego, CA, USA) and 10μL/well propidium iodide (catalog# 421301, BioLegend, San Diego, CA, USA), incubated for 15 min

for staining. The analysis was performed by flow cytometry (Guava® easyCyteTM, Luminex, Austin, TX, USA). Normalization, statistical analysis and bar graph creation were done by GraphPad Prism (GraphPad Software, San Diego, CA, USA). Significance testing was performed with a one-way analysis of variance (ANOVA).

3. Chemical Experiments

3.1. General information

Chemicals and solvents are commercially available and used without further purification, if not stated otherwise. For all HPLC purposes, acetonitrile in HPLC-grade quality (HiPerSolv CHROMANORM, *VWR*) was used. Water was purified with a PURELAB flex® (*ELGA VEOLIA*). Air-sensitive reactions were carried out under nitrogen or argon atmosphere. Mixtures of two or more solvents are specified as "solvent A"/ "solvent B", 3/1, *v*/*v*; meaning that 100 mL of the respective mixture consists of 75 mL of "solvent A" and 25 mL of "solvent B". **Thin-layer chromatography (TLC)** was carried out on prefabricated plates (silica gel 60, F_{254}, *Merck*). Components were visualized either by irradiation with ultraviolet light (254 nm or 366 nm) or by staining appropriately. **Column Chromatography:** If not stated otherwise, column chromatography was carried out on silica gel (60 Å, 40-60 µm, *Acros Organics*). In addition, a flash column system (puriFlash® XS 520 Plus, Advion Interchim Scientific) was utilized for the purification of the synthesized compounds. **Nuclear Magnetic Resonance Spectroscopy (NMR):** Proton (^{1}H) and carbon (^{13}C) NMR spectra were recorded either on a *Bruker* AVANCE 500 MHz at a frequency of 500 MHz (^{1}H) and 126 MHz (^{13}C) or on a *Bruker* AVANCE III HD 600 MHz at a frequency of 600 MHz (^{1}H) and 151 MHz (^{13}C). The chemical shifts are given in parts per million (ppm). As solvents deuterated chloroform ($CDCl_3$) and deuterated dimethyl sulfoxide (DMSO-d_6) were used. The residual solvent signal ($CDCl_3$: ^{1}H NMR: 7.26 ppm, ^{13}C NMR: 77.1 ppm; DMSO-d_6: ^{1}H NMR: 2.50 ppm, ^{13}C NMR: 39.52 ppm) was used for calibration. The multiplicity of each signal is reported as singulet (s), doublet (d), triplet (t), quartet (q), pentet (p), sextet (sext), multiplet (m) or combinations thereof. Multiplicities and coupling constants are reported as measured and might disagree with the expected values. **Mass Spectrometry:** High resolution electrospray ionization mass spectra (HRMS-ESI) were acquired with *Bruker Daltonik GmbH* micrOTOF coupled to a an *LC*

Packings Ultimate HPLC system and controlled by micrOTOFControl3.4 and HyStar 3.2-LC/MS, with a *BrukerDaltonik GmbH* ESI-qTOF Impact II coupled to a *Dionex* UltiMateTM 3000 UHPLC system and controlled by micrOTOFControl 4.0 and HyStar 3.2-LC/MS or with a micrOTOF-Q mass spectrometer (*Bruker*) with ESI-source coupled with an HPLC Dionex UltiMate 3000 (*Thermo Scientific*). Low resolution electrospray ionisation mass spectra (LRMS-ESI) were acquired with an *Advion* expression® compact mass spectrometer (CMS) coupled with an automated TLC plate reader Plate Express® (*Advion*). **High Performance Liquid Chromatography (HPLC)**: A *Thermo Fisher Scientific* UltiMate™ 3000 UHPLC system with a Nucleodur 100-5 C18 (250 x 4.6 mm, *Macherey Nagel*) with a flow rate of 1 mL/min and a temperature of 25 °C or a 100-5 C18 (100 x 3 mm, *Macherey Nagel*) with a flow rate of 0.5 mL/min and a temperature of 25 °C with an appropriate gradient were used. For preparative purposes an AZURA Prep. 500/1000 gradient system (*Knauer*) with a Nucleodur 110-5 C18 HTec (150 x 32 mm, *Macherey Nagel*) column with 20 mL/min was used. Detection was implemented by UV absorption measurement at a wavelength of λ = 220 nm and λ = 250 nm. Bidest. H_2O (A) and ACN (B) were used as eluents with an addition of 0.1% TFA for eluent A. **Purity:** The purity of all final compounds was 95% or higher. Purity was determined *via* HPLC with the Nucleodur 100-5 C18 (250 x 4.6 mm, *Macherey Nagel*) at 250 nm. After column equilibration for 5 min, a linear gradient from 5% A to 95% B in 5 min followed by an isocratic regime of 95% B for 12 min was used.

3.2. Compounds preparation

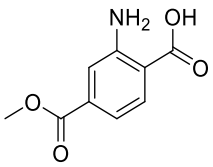

*2-Amino-4-(methoxycarbonyl)benzoic acid (**1**)*

Following a reported method,[11] TMSCl (2.10 mL, 16.6 mmol, 1.5 eq.) was added to the solution of 2-aminoterephthalic acid (2.00 g, 11.0 mmol, 1 eq.) in methanol (50 mL). The mixture was refluxed under nitrogen atmosphere for 19 h. The mixture was concentrated *in vacuo* and the crude was dissolved with saturated $NaHCO_3$ (aq.). The resulting mixture was washed with ethyl

acetate for three times. The aqueous layer was collected and acidified with AcOH to neutral pH. The resulting mixture was then extracted with ethyl acetate (3 x 50 mL) and the combined organic layer was washed with brine (50 mL) and dried over anhydrous Na_2SO_4. The solvent was removed *in vacuo* to generate compound **1** (1.82 g, 85%) without further purification. **^{1}H NMR** (600 MHz, DMSO-d_6) δ 7.79 (d, J = 8.3 Hz, 1H), 7.41 (d, J = 1.7 Hz, 1H), 7.02 (dd, J = 8.3, 1.7 Hz, 1H), 3.83 (s, 3H). **^{13}C NMR** (151 MHz, DMSO-d_6) δ 168.9, 166.0, 151.2, 133.9, 131.6, 117.3, 114.3, 112.9, 52.2. **LC-MS (ESI)**, $[M+H]^+$ *m/z*: 196.1.

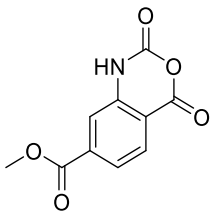

*Methyl 2,4-dioxo-1,4-dihydro-2H-benzo[d][1,3]oxazine-7-carboxylate (**2**)*

To a solution of compound **1** (1.70 g, 8.71 mmol, 1 eq.) in THF (50 mL) was added bis(trichloromethyl) carbonate (4.39 g, 14.8 mmol, 1.7 eq.). The mixture was stirred at 60 ℃ for 4 h. The mixture was cooled and poured into water, extracted with ethyl acetate (3 x 50 mL), the combined organic layer was washed with saturated $NaHCO_3$ (aq.) (30 mL) and then the brine (50 mL), dried over anhydrous Na_2SO_4 and the solvent was removed *in vacuo* to yield compound **2** (1.72 g, 89%) without further purification. **^{1}H NMR** (600 MHz, DMSO-d_6) δ 11.87 (s, 1H), 8.04 (d, J = 8.2 Hz, 1H), 7.72 (dd, J = 8.2, 1.5 Hz, 1H), 7.69 (s, 1H), 3.90 (s, 3H). **^{13}C NMR** (151 MHz, DMSO-d_6) δ 164.8, 159.3, 146.8, 141.5, 136.4, 129.6, 123.2, 115.9, 113.9, 52.8. **LC-MS (ESI)**, $[M+H]^+$ *m/z*: 222.2.

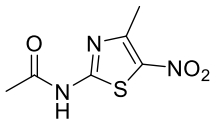

N-(4-methyl-5-nitrothiazol-2-yl)acetamide

To a solution of *N*-(4-methylthiazol-2-yl)acetamide (2.00 g, 12.8 mmol, 1 eq.) in conc. H_2SO_4 (8 ml) at 0 ℃ was added KNO_3 (1.68 g, 16.7 mmol, 1.3 eq.). The mixture was stirred for 2.5 h. Completion of the reaction was monitored by TLC. The resulting reaction mixture was poured into water slowly and neutralized with saturated $NaHCO_3$(aq.) until alkaline level. The mixture

was then extracted with ethyl acetate (3 x 50 mL), the combined organic phase was washed with water (50 mL), followed by brine (50 mL), dried over Na_2SO_4 and the solvent was removed *in vacuo*. The crude product was purified by flash chromatography (CyH/EtOAc, 0-66.6% EtOAc from 0-10 min, 66.6% EtOAc from 10-25 min) to gain the product as yellow solid (2.22 g, 86%). **^{1}H NMR** (600 MHz, DMSO-d_6) δ 12.94 (s, 1H), 2.65 (s, 3H), 2.22 (s, 3H). **^{13}C NMR** (151 MHz, DMSO-d_6) δ 170.3, 158.7, 154.0, 136.2, 22.5, 17.9. **LC-MS (ESI)**, $[M+H]^+$ *m/z*: 202.1.

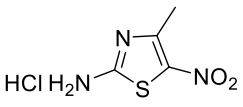

4-Methyl-5-nitrothiazol-2-amine hydrochloride

To a solution of *N*-(4-methyl-5-nitrothiazol-2-yl)acetamide (2.22 g, 11.0 mmol, 1 eq.) in MeOH (25 mL) was added conc. HCl (25 mL). The mixture was stirred at 50 °C for 7 h. The solvent was removed to afford the crude product (2.1 g, 97%) without further purification. **^{1}H NMR** (500 MHz, DMSO-d_6) δ 9.91 (s, 1H), 8.79 (s, 2H), 2.52 (s, 3H). **^{13}C NMR** (126 MHz, DMSO-d_6) δ 169.6, 159.4, 130.2, 18.2. **LC-MS (ESI)**, $[M+H]^+$ *m/z*: 160.1.

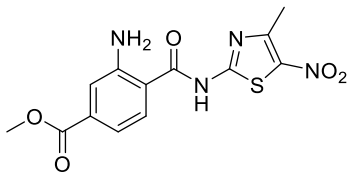

*Methyl 3-amino-4-((4-methyl-5-nitrothiazol-2-yl)carbamoyl)benzoate (**3**)*

To a solution of compound **2** (1.72 g, 7.78 mmol, 1 eq.) in anhydrous DMF (50 mL) was added 4-methyl-5-nitrothiazol-2-amine hydrochloride (1.67 g, 8.55 mmol, 1.1 eq.), followed by the addition of DIPEA (4.06 mL, 23.3 mmol, 3 eq.). The mixture was stirred at room temperature for 6 h. The mixture was poured into water, extracted with ethyl acetate (3 x 50 mL), the combined organic layer was washed with water (3 x 50 mL), followed by brine (50 mL), and dried over anhydrous Na_2SO_4. The solvent was removed *in vacuo* and the crude product was washed with MeOH, after which, the precipitate was collected *via* filtration to yield the desired compound **3** (1.99 g, 76%) without further purification. **^{1}H NMR** (500 MHz, DMSO-d_6) δ 9.02

(s, 2H), 7.99 (d, J = 8.4 Hz, 1H), 7.46 (d, J = 1.7 Hz, 1H), 7.05 (dd, J = 8.4, 1.7 Hz, 1H), 3.85 (s, 3H), 2.70 (s, 3H). **^{13}C NMR** (126 MHz, DMSO-d_6) δ 168.0, 165.8, 159.8, 153.6, 151.0, 136.1, 134.0, 129.9, 117.7, 114.2, 113.6, 52.3, 17.7. **LC-MS (ESI)**, $[M-H]^-$ *m/z*: 335.0.

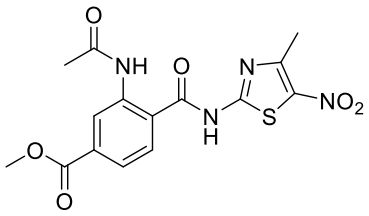

*Methyl 3-acetamido-4-((4-methyl-5-nitrothiazol-2-yl)carbamoyl)benzoate (**4/F16**)*

To a solution of compound **3** (1.78 g, 5.28 mmol, 1 eq.) in anhydrous DMF (50 mL) was added HATU (4.02 g, 10.6 mmol, 2 eq.), DIPEA (2.76 mL, 15.8 mmol, 3 eq.) and acetic acid (453 μL, 7.92 mmol, 1.5 eq.). The mixture was stirred at room temperature for 43 h. The completion of reaction was monitored by TLC. The resulting reaction mixture was poured into water, extracted with ethyl acetate (3 x 50 mL), the combined organic layer was washed with water (3 x 50 mL), followed by brine (50 mL), and dried over anhydrous Na_2SO_4. The solvent was removed *in vacuo* and the crude product was purified with silica column chromatography (DCM/MeOH 20:1 *v/v*) to generate compound **4** (1.42 g, 71%). **^{1}H NMR** (600 MHz, DMSO-d_6) δ 13.53 (s, 1H), 10.47 (s, 1H), 8.30 (s, 1H), 7.83 (d, J = 8.1 Hz, 1H), 7.77 (dd, J = 8.1, 1.7 Hz, 1H), 3.89 (s, 3H), 2.70 (s, 3H), 2.04 (s, 3H). **^{13}C NMR** (151 MHz, DMSO-d_6) δ 168.4, 167.2, 165.3, 160.1, 153.6, 137.0, 136.2, 132.6, 129.7, 128.4, 123.9, 123.1, 52.5, 23.7, 17.8. **HRMS (ESI)**: *m/z* $[M+H]^+$ calcd. for $C_{15}H_{14}N_4O_6S$ 379.0707, found: 379.0701.

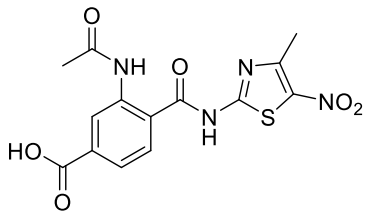

*3-Acetamido-4-((4-methyl-5-nitrothiazol-2-yl)carbamoyl)benzoic acid (**5**)*

To a solution of compound **4** (0.35 g, 0.925 mmol, 1 eq.) in a solvent mixture of THF/MeOH/H_2O (15 mL/ 3 mL/ 3 mL) was added $LiOH·H_2O$ (58 mg, 1.39 mmol, 1.5 eq.). The mixture was stirred at room temperature for 16.5 h, followed by stirring at 50 ℃ for extra

4 h. The completion of the reaction was monitored by HPLC. The solvent was removed and the crude product was dissolved with water and acidified by 0.5 M HCl (aq.) to neutral pH. The precipitate was then collected, washed with water and dried to afford compound **5** (0.272 g, 81%) without further purification. **^{1}H NMR** (600 MHz, DMSO-d_6) δ 13.50 (s, 1H), 13.32 (s, 1H), 10.41 (s, 1H), 8.25 (s, 1H), 7.80 (d, J = 8.1 Hz, 1H), 7.75 (dd, J = 8.0, 1.6 Hz, 1H), 2.70 (s, 3H), 2.04 (s, 3H). **^{13}C NMR** (151 MHz, DMSO-d_6) δ 168.4, 167.0, 166.3, 159.8, 153.7, 136.9, 136.2, 133.9, 129.5, 128.2, 124.1, 123.4, 23.7, 17.8. **LC-MS (ESI)**, $[M-H]^-$ *m/z*: 363.0.

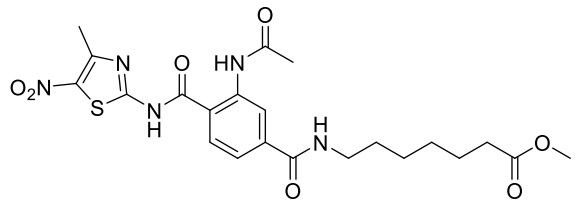

*Methyl 7-(3-acetamido-4-((4-methyl-5-nitrothiazol-2-yl)carbamoyl)benzamido)heptanoate (**6**)*

To a solution of compound **5** (0.250 g, 0.686 mmol, 1 eq.) in anhydrous DMF (5 mL) were added HATU (0.522 g, 1.37 mmol, 2 eq.) and DIPEA (359 µL, 2.06 mmol, 3 eq.). The mixture was stirred at room temperature for 0.5 h and methyl 7-aminoheptanoate hydrochloride (0.161 g, 0.823 mmol, 1.2 eq.) was then added to the system. Afterwards, the mixture was stirred at room temperature for 17 h. The mixture was poured into water, extracted with ethyl acetate (3 x 30 mL), the combined organic layer was washed with water (3 x 30 mL) and then with brine (30 mL), dried over anhydrous Na_2SO_4. The solvent was removed *in vacuo* and the crude product was purified with silica column chromatography (DCM/MeOH 10:1 *v/v*) to generate compound **6** (0.155 g, 45%). **^{1}H NMR** (600 MHz, DMSO-d_6) δ 13.45 (s, 1H), 10.32 (s, 1H), 8.58 (t, J = 5.6 Hz, 1H), 8.06 (s, 1H), 7.76 (d, J = 8.0 Hz, 1H), 7.66 (dd, J = 8.1, 1.7 Hz, 1H), 3.58 (s, 3H), 3.25 (q, J = 6.7 Hz, 2H), 2.70 (s, 3H), 2.30 (t, J = 7.4 Hz, 2H), 2.03 (s, 3H), 1.53 (h, J = 7.3 Hz, 4H), 1.31 (p, J = 3.1 Hz, 4H). **^{13}C NMR** (151 MHz, DMSO-d_6) δ 173.3, 168.3, 167.2, 165.0, 159.7, 153.7, 138.1, 136.7, 136.2, 129.1, 126.8, 122.1, 122.0, 51.1, 40.1, 33.2, 28.8, 28.2, 26.1, 24.4, 23.6, 17.8. **LC-MS (ESI)**, $[M+H]^+$ *m/z*: 506.2.

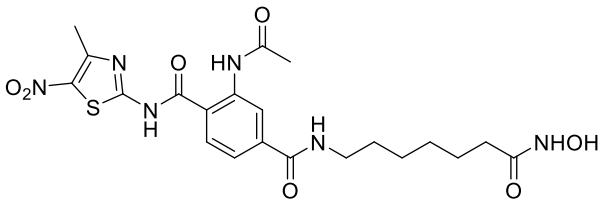

*2-Acetamido-N^4-(7-(hydroxyamino)-7-oxoheptyl)-N^1-(4-methyl-5-nitrothiazol-2-yl)terephthalamide (**SZ-1**)*

Compound **6** (0.150 g, 0.297 mmol, 1 eq.) was dissolved in a solvent mixture of MeOH/DCM (4 mL/2 mL) and the solution was cooled to 0 ℃. Hydroxylamine solution (1.18 g, 50 wt. % in water, 17.8 mmol, 60 eq.) was added and the mixture was stirred at 0 ℃ for 10 min. Subsequently, the prepared sodium hydroxide powder (0.119 g, 2.97 mmol, 10 eq.) was added into the reaction and the mixture was stirred for 1 h. Completion of the reaction was monitored by TLC. The solvent was removed and the crude product was dissolved with water and acidified with 0.5 M HCl (aq.) to neutral pH. The precipitate was then collected and subsequent purification was conducted by preparative HPLC to yield compound **SZ-1** (15 mg, 10%). **^{1}H NMR** (600 MHz, DMSO-d_6) δ 13.57 (s, 1H), 10.32 (s, 1H), 8.87 (s, 1H), 8.63 (s, 1H), 8.44 (t, J = 5.6 Hz, 1H), 8.21 (d, J = 8.0 Hz, 1H), 7.46 (d, J = 8.2 Hz, 1H), 3.23 (q, J = 6.7 Hz, 2H), 2.64 (s, 3H), 2.17 (s, 3H), 1.94 (t, J = 7.4 Hz, 2H), 1.50 (h, J = 7.1 Hz, 4H), 1.28 (td, J = 21.0, 19.4, 11.0 Hz, 4H). **^{13}C NMR** (151 MHz, DMSO-d_6) δ 171.8, 169.1, 168.0, 166.1, 160.9, 156.9, 139.8, 137.7, 132.9, 130.3, 124.9, 120.2, 118.5, 40.1, 32.2, 30.4, 28.9, 28.3, 26.2, 25.1, 18.8. **HRMS (ESI)**: *m/z* $[M+H]^+$ calcd. for $C_{21}H_{26}N_6O_7S$ 507.1656, found: 507.1638.

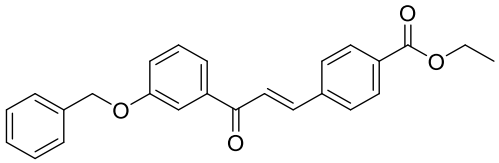

*Ethyl (E)-4-(3-(3-(benzyloxy)phenyl)-3-oxoprop-1-en-1-yl)benzoate (**7**)*

To a solution of 1-(3-(benzyloxy)phenyl)ethan-1-one (2.00 g, 8.84 mmol, 1 eq.) in ethanol (50 mL) was added methyl 4-formylbenzoate (1.45 g, 8.84 mmol, 1 eq.) and KOH (0.744 g, 13.3 mmol, 1.5 eq., aq. in 1.5 mL water). The mixture was stirred at room temperature for 15 h. The reaction mixture was poured into crushed ice and left for 1 h. To this suspension 1 M HCl (aq.) was added dropwise until the solution was acidic. The resulting crude solid precipitate was collected and dried, which was then dissolved by DCM and the purification was conducted

by flash chromatography (CyH/EtOAc, 0-20% EtOAc in cyclohexane, 0-10 min; 20% EtOAc in cyclohexane, 10-30 min) to the methyl ester and ethyl ester product mixture (2.66 g, >78%). The ethyl ester product (compound **7**) was further purified by silica column chromatography (CyH/EtOAc 4:1, *v/v*) for the analytical characterization. **^{1}H NMR** (600 MHz, $CDCl_3$) δ 8.12 – 8.05 (m, 2H), 7.81 (d, *J* = 15.7 Hz, 1H), 7.72 – 7.66 (m, 2H), 7.65 – 7.61 (m, 2H), 7.56 (d, *J* = 15.7 Hz, 1H), 7.49 – 7.38 (m, 5H), 7.38 – 7.32 (m, 1H), 7.22 (ddd, *J* = 8.2, 2.5, 1.1 Hz, 1H), 5.15 (s, 2H), 4.40 (q, *J* = 7.1 Hz, 2H), 1.42 (t, *J* = 7.1 Hz, 3H). **^{13}C NMR** (151 MHz, $CDCl_3$) δ 190.0, 166.1, 159.2, 143.5, 139.4, 139.1, 136.6, 132.1, 130.3, 129.9, 128.8, 128.4, 128.3, 127.7, 124.2, 121.5, 120.4, 114.3, 70.4, 61.4, 14.5. **LC-MS (ESI)**, $[M+H]^+$ *m/z*: 387.2.

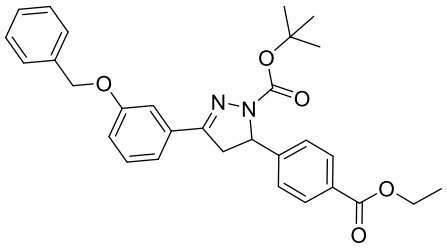

*tert-Butyl 3-(3-(benzyloxy)phenyl)-5-(4-(ethoxycarbonyl)phenyl)-4,5-dihydro-1H-pyrazole-1-carboxylate (**8**)*

In the process of compound **7** synthesis, the methyl ester was also obtained as a byproduct, which was also used here for the reaction. To a solution of methyl ester and ethyl ester product mixture from the last step (2.66 g, 1 eq.) in anhydrous ACN (60 mL) was added *tert*-butyl hydrazinecarboxylate (1.05 g, 7.92 mmol, 1.15 eq.) and 1,3,4,6,7,8-hexahydro-2*H*-pyrimido[1,2-*a*]pyrimidine (0.192 g, 1.38 mmol, 0.2 eq.). The mixture was then stirred at 60 °C for 22 h under nitrogen atmosphere. Completion of the reaction was monitored by TLC. The solvent was removed and the crude was dissolved with ethyl acetate, poured the mixture into water and extracted with ethyl acetate (3 x 50 mL). The combined organic layer was washed with brine (50 mL) and dried over anhydrous Na_2SO_4. The solvent was removed and the crude product was purified by silica chromatography (CyH/EtOAc 4:1, *v/v*) to provide the methyl ester and ethyl ester product mixture (2.28 g, > 66%). The ethyl ester product (compound **8**) was further purified by silica column chromatography (CyH/EtOAc 4:1, *v/v*) for the analytical characterization. **^{1}H NMR** (600 MHz, $CDCl_3$) δ 8.02 (d, *J* = 8.1 Hz, 2H), 7.50 (s, 1H), 7.44 (d, *J* = 7.4 Hz, 2H), 7.39 (t, *J* = 7.5 Hz, 2H), 7.31 (h, *J* = 7.9 Hz, 4H), 7.25 (d, *J* = 6.2 Hz, 1H),

7.04 – 7.00 (m, 1H), 5.39 (dd, *J* = 12.3, 5.6 Hz, 1H), 5.10 (s, 2H), 4.37 (q, *J* = 7.1 Hz, 2H), 3.77 (dd, *J* = 17.5, 12.2 Hz, 1H), 3.12 (dd, *J* = 17.5, 5.6 Hz, 1H), 1.39 (t, *J* = 7.1 Hz, 3H), 1.31 (s, 9H). **^{13}C NMR** (151 MHz, $CDCl_3$) δ 166.4, 159.1, 152.3, 151.7, 148.0, 136.8, 132.8, 130.3, 130.0, 129.7, 128.8, 128.2, 127.7, 125.7, 119.8, 117.5, 112.3, 81.8, 70.3, 61.7, 61.2, 42.9, 28.2, 14.5. **LC-MS (ESI)**, $[M-H]^-$ *m/z*: 499.1.

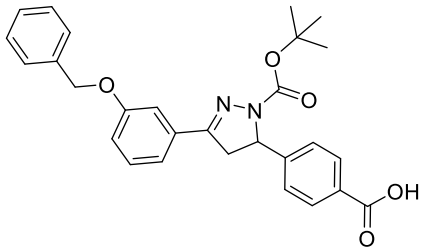

*4-(3-(3-(Benzyloxy)phenyl)-1-(tert-butoxycarbonyl)-4,5-dihydro-1H-pyrazol-5-yl)benzoic acid (**9**)*

To a solution of methyl ester and ethyl ester product mixture from last step (2.28 g, 1 eq.) in THF/MeOH/H_2O (20 mL/ 4 mL/ 4 mL) was added LiOH·H_2O (0.287 g, 1.5 eq.). The mixture was stirred at 50 °C for 23 h. The solvent was removed and the crude product was dissolved in water and acidified by 0.5 M HCl (aq.) to neutral pH. The precipitate was then collected, washed with water and dried to afford compound **9** (2.00 g, 93%) without further purification. **^{1}H NMR** (600 MHz, DMSO-d_6) δ 12.92 (s, 1H), 7.97 – 7.90 (m, 2H), 7.47 – 7.44 (m, 2H), 7.42 – 7.36 (m, 3H), 7.36 – 7.30 (m, 5H), 7.10 (ddd, *J* = 8.1, 2.7, 1.1 Hz, 1H), 5.44 (dd, *J* = 12.1, 5.3 Hz, 1H), 5.15 (s, 2H), 3.84 (dd, *J* = 17.9, 12.1 Hz, 1H), 3.15 (dd, *J* = 18.0, 5.4 Hz, 1H), 1.25 (s, 9H). **^{13}C NMR** (151 MHz, DMSO-d_6) δ 167.0, 158.5, 152.6, 150.7, 148.0, 136.9, 132.6, 129.9, 129.8, 128.4, 127.8, 127.7, 127.6, 125.7, 119.2, 116.7, 112.5, 80.2, 69.3, 61.1, 42.1, 27.7. **LC-MS (ESI)**, $[M-H]^-$ *m/z*: 471.1.

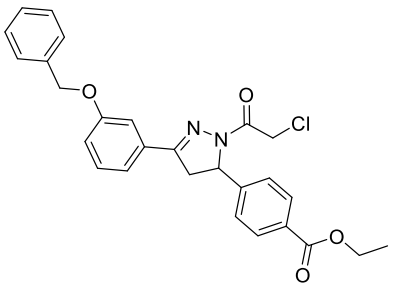

*Ethyl 4-(3-(3-(benzyloxy)phenyl)-1-(2-chloroacetyl)-4,5-dihydro-1H-pyrazol-5-yl)benzoate (**G26**)*

To a solution of compound **8** (0.100 g, 0.200 mmol, 1 eq.) in DCM (5 mL) was added TFA (2 mL), the mixture was stirred for 2 h at room temperature. The complete removal of the Boc-protecting group was monitored by HPLC. TFA and DCM were removed and the crude product was dried *in vacuo*. Subsequently, the crude product was re-dissolved in DCM (5 mL) and stirred at 0 °C for 10 min, followed by the addition of 2-chloroacetyl chloride (32 µL, 0.400 mmol, 2 eq.) dropwise and triethylamine (84 µL, 0.599 mmol, 3 eq.) dropwise. The mixture was stirred for 17 h. The crude product was obtained by removing the solvents *in vacuo* and further purified by silica column chromatography (CyH/EtOAc 2:1, *v/v*) to yield compound **G26** (0.09 g, 95%). **^{1}H NMR** (500 MHz, DMSO-d_6) δ 7.93 (d, J = 8.3 Hz, 2H), 7.50 – 7.44 (m, 3H), 7.43 – 7.36 (m, 6H), 7.34 (dd, J = 8.4, 6.2 Hz, 1H), 7.19 – 7.12 (m, 1H), 5.66 (dd, J = 11.9, 5.0 Hz, 1H), 5.16 (s, 2H), 4.79 (d, J = 13.9 Hz, 1H), 4.70 (d, J = 13.9 Hz, 1H), 4.31 (q, J = 7.1 Hz, 2H), 3.91 (dd, J = 18.3, 11.9 Hz, 1H), 3.23 (dd, J = 18.3, 5.1 Hz, 1H), 1.30 (t, J = 7.1 Hz, 3H). **^{13}C NMR** (126 MHz, DMSO-d_6) δ 165.4, 163.4, 158.5, 155.5, 146.6, 136.8, 131.8, 129.9, 129.6, 129.1, 128.4, 127.9, 127.8, 126.0, 119.6, 117.3, 113.1, 69.4, 60.6, 59.8, 42.3, 41.9, 14.1. **HRMS (ESI)**: *m/z* $[M+H]^+$ calcd. for $C_{27}H_{25}ClN_2O_4$ 477.1576, found: 477.1577.

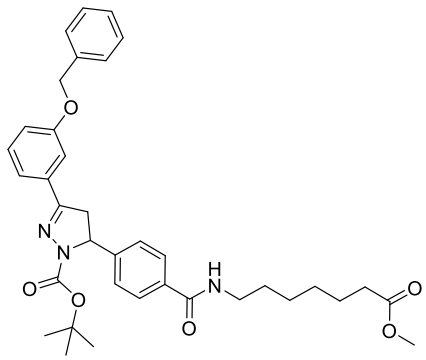

*tert-Butyl 3-(3-(benzyloxy)phenyl)-5-(4-((7-methoxy-7-oxoheptyl)carbamoyl)phenyl)-4,5-dihydro-1H-pyrazole-1-carboxylate (**10**)*

To a solution of compound **9** (2.50 g, 5.29 mmol, 1 eq.) in anhydrous DMF (15 mL) were added HATU (4.02 g, 10.6 mmol, 2 eq.) and DIPEA (2.76 mL, 15.9 mmol, 3 eq.). The solution was stirred for 30 min at room temperature followed by the addition of methyl 7-aminoheptanoate hydrochloride (1.24 g, 6.35 mmol, 1.2 eq.), and the mixture was stirred for 18.5 h at room

temperature. Completion of the reaction was monitored by HPLC. The mixture was poured into water and extracted with ethyl acetate (3 x 50 mL). The combined organic layers were then washed with water (3 x 50 mL), followed by brine (50 mL), dried over anhydrous Na_2SO_4, filtered, and concentrated *in vacuo* to yield the crude product, which was then purified by silica column chromatography (CyH/EtOAc 1:1, *v/v*) to afford compound **10** (2.38 g, 73%). **^{1}H NMR** (500 MHz, $CDCl_3$) δ 7.76 (d, *J* = 7.9 Hz, 2H), 7.50 – 7.45 (m, 1H), 7.45 – 7.41 (m, 2H), 7.41 – 7.36 (m, 2H), 7.36 – 7.32 (m, 1H), 7.32 – 7.26 (m, 3H), 7.24 (dt, *J* = 7.7, 1.3 Hz, 1H), 7.01 (ddd, *J* = 8.1, 2.6, 1.1 Hz, 1H), 6.30 (s, 1H), 5.38 (dd, *J* = 12.4, 5.3 Hz, 1H), 5.09 (s, 2H), 3.76 (dd, *J* = 17.5, 12.1 Hz, 1H), 3.65 (s, 3H), 3.50 – 3.38 (m, 2H), 3.09 (dd, *J* = 17.5, 5.4 Hz, 1H), 2.30 (t, *J* = 7.4 Hz, 2H), 1.70 – 1.57 (m, 4H), 1.45 – 1.22 (m, 13H). **^{13}C NMR** (126 MHz, $CDCl_3$) δ 174.3, 167.1, 159.1, 152.4, 151.8, 146.5, 136.8, 134.2, 132.8, 129.8, 128.7, 128.2, 127.7, 125.9, 119.8, 117.5, 112.3, 81.8, 70.3, 61.6, 51.6, 42.9, 40.1, 34.1, 29.6, 28.9, 28.2, 26.7, 24.9. **LC-MS (ESI)**, $[M+H]^+$ *m/z*: 614.3.

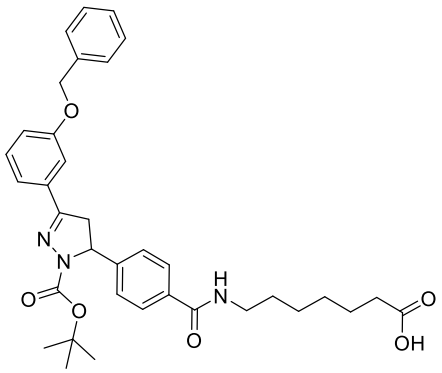

*7-(4-(3-(3-(Benzyloxy)phenyl)-1-(tert-butoxycarbonyl)-4,5-dihydro-1H-pyrazol-5-yl)benzamido)heptanoic acid (**11**)*

To a solution of compound **10** (2.37 g, 3.86 mmol, 1 eq.) in THF/MeOH/H_2O (60 mL /12 mL /12 mL), $LiOH·H_2O$ (0.324 g, 7.72 mmol, 2 eq.) was added. The mixture was stirred at room temperature for 17 h. Upon the completion of the hydrolysis (monitored by TLC), the solvents were removed *in vacuo*. The crude product was dissolved with water and acidified with HCl (0.5 M in water) until no more precipitate was formed. The resulting precipitate was collected *via* filtration, washed with water and dried *in vacuo*, to yield compound **11** (2.03 g, 88%) without further purification. **^{1}H NMR** (500 MHz, DMSO-d_6) δ 11.94 (s, 1H), 8.39 (t, *J* = 5.7 Hz, 1H), 7.82 (d, *J* = 8.3 Hz, 2H), 7.48 – 7.44 (m, 2H), 7.42 – 7.36 (m, 3H), 7.35 – 7.31 (m,

3H), 7.26 (d, *J* = 8.4 Hz, 2H), 7.10 (ddd, *J* = 8.0, 2.7, 1.2 Hz, 1H), 5.42 (dd, *J* = 12.0, 5.4 Hz, 1H), 5.15 (s, 2H), 3.83 (dd, *J* = 17.9, 12.1 Hz, 1H), 3.23 (q, *J* = 6.8 Hz, 2H), 3.12 (dd, *J* = 18.0, 5.4 Hz, 1H), 2.19 (t, *J* = 7.4 Hz, 2H), 1.49 (qt, *J* = 7.3, 3.8 Hz, 4H), 1.33 – 1.21 (m, 13H). **^{13}C NMR** (126 MHz, DMSO-d_6) δ 174.4, 165.6, 158.5, 152.5, 150.8, 146.0, 136.9, 133.7, 132.7, 129.8, 128.4, 127.8, 127.6, 127.5, 125.3, 119.2, 116.6, 112.5, 80.1, 69.3, 61.0, 42.1, 40.1, 33.6, 28.9, 28.2, 27.7, 26.2, 24.4. **LC-MS (ESI)**, $[M-H]^-$ *m/z*: 598.3.

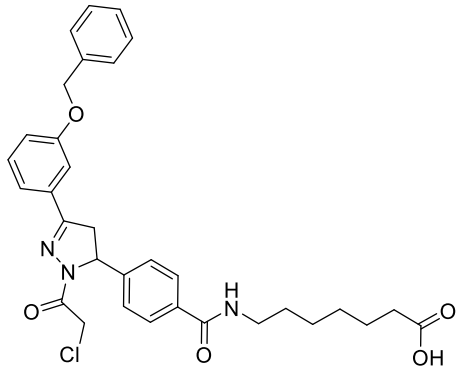

*7-(4-(3-(3-(Benzyloxy)phenyl)-1-(2-chloroacetyl)-4,5-dihydro-1H-pyrazol-5-yl)benzamido)-heptanoic acid (**12**)*

To a solution of compound **11** (0.500 g, 0.834 mmol, 1 eq.) in DCM (10 mL) was added TFA (2 mL). The mixture was stirred for 2 h at room temperature and the complete removal of the Boc-protecting group was monitored by HPLC. TFA and DCM were removed and the crude product was dried *in vacuo*. Subsequently, the crude product was re-dissolved with DCM (10 mL) and stirred at 0 °C for 10 min, followed by adding 2-chloroacetyl chloride (133 μL, 1.67 mmol, 2 eq.) dropwise and triethylamine (348 μL, 2.50 mmol, 3 eq.) dropwise. The mixture was stirred for 20 h. The crude product was obtained by removing the solvents *in vacuo* and purified by silica column chromatography (DCM/MeOH/AcOH 20:1:0.1, *v/v/v*) to yield compound **12** (0.337 g, 70%). **^{1}H NMR** (600 MHz, DMSO-d_6) δ 11.94 (s, 1H), 8.38 (t, *J* = 5.6 Hz, 1H), 7.79 (d, *J* = 8.2 Hz, 2H), 7.50 – 7.44 (m, 3H), 7.43 – 7.36 (m, 4H), 7.36 – 7.31 (m, 1H), 7.29 (d, *J* = 8.1 Hz, 2H), 7.15 (td, *J* = 4.7, 2.7 Hz, 1H), 5.62 (dd, *J* = 11.8, 4.9 Hz, 1H), 5.16 (s, 2H), 4.80 (d, *J* = 13.8 Hz, 1H), 4.70 (d, *J* = 13.8 Hz, 1H), 3.90 (dd, *J* = 18.2, 11.9 Hz, 1H), 3.25 – 3.22 (m, 2H), 3.22 – 3.19 (m, 1H), 2.19 (t, *J* = 7.4 Hz, 2H), 1.52-1.47 (m, 4H), 1.34 – 1.22 (m, 4H). **^{13}C NMR** (151 MHz, DMSO-d_6) δ 174.4, 165.7, 163.3, 158.5, 155.5, 144.3, 136.8, 134.0, 131.9, 129.9, 128.4, 127.9, 127.8, 127.6, 125.4, 119.6, 117.3, 113.0, 69.4, 59.8,

42.4, 42.0, 40.1, 33.6, 28.9, 28.3, 26.1, 24.4. **LC-MS (ESI)**, $[M-H]^-$ *m/z*: 574.2.

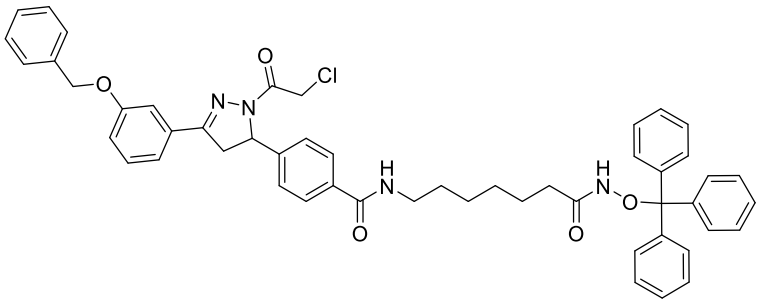

*4-(3-(3-(Benzyloxy)phenyl)-1-(2-chloroacetyl)-4,5-dihydro-1H-pyrazol-5-yl)-N-(7-oxo-7-((trityloxy)amino)heptyl)benzamide (**13**)*

To a solution of compound **12** (0.330 g, 0.573 mmol, 1 eq.) in anhydrous DMF (10 mL) were added PyCloP (0.483 g, 1.15 mmol, 2 eq.) and DIPEA (0.370 g, 2.86 mmol, 5 eq.). The solution was stirred for 30 min at room temperature followed by the addition of *O*-tritylhydroxylamine (0.473 g, 1.72 mmol, 3 eq.) and the mixture was stirred for 18 h at room temperature. Completion of the reaction was monitored by HPLC. The solvent was removed *in vacuo* directly and the crude product was purified by silica column chromatography (DCM/MeOH 20:1, *v/v*) to yield compound **13** (0.391 g, 82%). **^{1}H NMR** (600 MHz, DMSO-d_6) δ 10.13 (s, 1H), 8.36 (t, *J* = 5.4 Hz, 1H), 7.79 (d, *J* = 8.3 Hz, 2H), 7.46 (t, *J* = 7.6 Hz, 3H), 7.39 (q, *J* = 5.8, 4.3 Hz, 4H), 7.36 – 7.24 (m, 17H), 7.15 (tt, *J* = 5.5, 3.3 Hz, 1H), 5.63 (dd, *J* = 11.8, 4.9 Hz, 1H), 5.16 (s, 2H), 4.80 (d, *J* = 13.8 Hz, 1H), 4.70 (d, *J* = 13.8 Hz, 1H), 3.90 (dd, *J* = 18.2, 11.9 Hz, 1H), 3.24 – 3.21 (m, 1H), 3.18 (q, *J* = 6.7, 6.0 Hz, 2H), 1.78 (dt, *J* = 25.1, 6.6 Hz, 2H), 1.41 (p, *J* = 7.3 Hz, 2H), 1.19-1.12 (m, 4H), 0.99 (q, *J* = 8.3 Hz, 2H). **^{13}C NMR** (151 MHz, DMSO-d_6) δ 170.3, 165.7, 163.3, 158.5, 155.5, 144.3, 142.4, 136.8, 134.0, 131.9, 129.9, 128.9, 128.4, 127.9, 127.8, 127.6, 127.4, 127.3, 125.4, 119.6, 117.3, 113.0, 91.7, 69.4, 59.8, 42.4, 42.0, 40.1, 31.9, 28.9, 28.1, 26.1, 24.7. **LC-MS (ESI)**, $[M-H]^-$ *m/z*: 831.3.

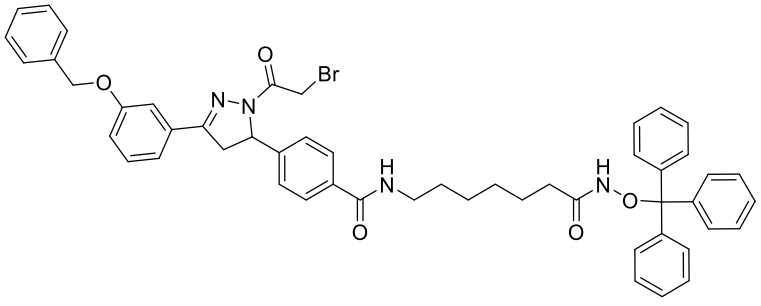

*4-(3-(3-(Benzyloxy)phenyl)-1-(2-bromoacetyl)-4,5-dihydro-1H-pyrazol-5-yl)-N-(7-oxo-7-((trityloxy)amino)heptyl)benzamide (**14**)*

To a solution of compound **13** (0.184 g, 0.221 mmol, 1 eq.) in acetone (5 mL) was added sodium bromide (0.227 g, 2.21 mmol, 10 eq.) and the mixture was refluxed for 48 h in the dark. The conversion of **13** to **14** was monitored by HPLC. The solvent was removed *in vacuo* and the crude product was re-dissolved in a mixture of methanol and acetonitrile, and filtered to remove the insoluble. The obtained crude product was subjected to purification by preparative HPLC to yield compound **14** (81 mg, 42%). **^{1}H NMR** (600 MHz, DMSO-d_6) δ 10.14 (s, 1H), 8.37 (q, J = 7.0, 5.7 Hz, 1H), 7.79 (d, J = 8.2 Hz, 2H), 7.50 – 7.42 (m, 3H), 7.42 – 7.36 (m, 4H), 7.35 – 7.18 (m, 17H), 7.18 – 7.12 (m, 1H), 5.62 (dt, J = 15.5, 7.8 Hz, 1H), 5.16 (s, 2H), 4.52 (t, J = 10.5 Hz, 1H), 4.42 (t, J = 12.9 Hz, 1H), 3.90 (dd, J = 18.2, 11.8 Hz, 1H), 3.22 (d, J = 4.7 Hz, 1H), 3.21 – 3.15 (m, 2H), 1.85 (dt, J = 98.8, 7.4 Hz, 2H), 1.52 – 1.37 (m, 2H), 1.32 – 1.06 (m, 4H), 0.99 (p, J = 7.7 Hz, 2H). **^{13}C NMR** (151 MHz, DMSO-d_6) δ 170.3, 165.7, 163.4, 158.5, 155.4, 147.7, 144.3, 142.5, 136.8, 134.0, 131.9, 130.0, 128.9, 128.4, 127.9, 127.8, 127.7, 127.6, 127.5, 127.4, 127.3, 126.6, 125.3, 119.6, 117.3, 113.1, 91.7, 69.4, 59.7, 42.4, 42.1, 40.1, 32.1, 28.9, 28.2, 26.1, 24.9. **LC-MS (ESI)**, $[M-H]^-$ *m/z*: 875.1.

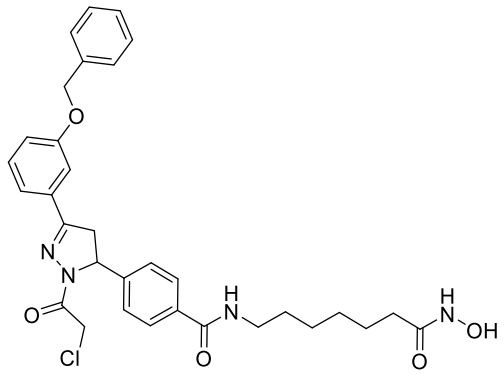

*4-(3-(3-(Benzyloxy)phenyl)-1-(2-chloroacetyl)-4,5-dihydro-1H-pyrazol-5-yl)-N-(7-(hydroxyamino)-7-oxoheptyl)benzamide (**SZ-2**)*

To a solution of compound **13** (0.2 g, 0.240 mmol) in DCM (5 mL) was added triisopropylsilane (0.5 mL) and, after stirring for 10 min, TFA (1 mL) was added. The mixture was stirred at room temperature for 2 h and the complete deprotection was monitored by HPLC. Subsequently, the solvent was removed *in vacuo* and the crude product was purified by flash column chromatography using a reverse phase C18 column to yield **SZ-2** (43 mg, 30%). **^{1}H NMR** (600

MHz, DMSO-d_6) δ 10.30 (s, 1H), 8.62 (s, 1H), 8.38 (t, *J* = 5.7 Hz, 1H), 7.84 – 7.75 (m, 2H), 7.46 (t, *J* = 7.4 Hz, 3H), 7.42 – 7.37 (m, 4H), 7.34 (dd, *J* = 8.3, 6.4 Hz, 1H), 7.31 – 7.27 (m, 2H), 7.15 (tq, *J* = 4.7, 2.9, 2.0 Hz, 1H), 5.62 (dd, *J* = 11.8, 4.9 Hz, 1H), 5.16 (s, 2H), 4.80 (dd, *J* = 13.8, 1.7 Hz, 1H), 4.70 (dd, *J* = 13.9, 1.7 Hz, 1H), 3.90 (dd, *J* = 18.2, 11.9 Hz, 1H), 3.23 (t, *J* = 5.2 Hz, 2H), 3.20 (d, *J* = 5.7 Hz, 1H), 1.93 (t, *J* = 7.4 Hz, 2H), 1.48 (h, *J* = 6.9 Hz, 4H), 1.31 – 1.25 (m, 4H). **^{13}C NMR** (151 MHz, DMSO-d_6) δ 169.1, 165.7, 163.3, 158.5, 155.5, 144.3, 136.8, 134.0, 131.9, 130.0, 128.4, 127.9, 127.8, 127.6, 125.4, 119.6, 117.3, 113.0, 69.4, 59.8, 42.4, 42.0, 40.1, 32.2, 29.0, 28.3, 26.1, 25.0. **HRMS (ESI)**: *m/z* $[M+H]^+$ calcd. for $C_{32}H_{35}ClN_4O_5$ 591.2369, found: 591.2356.

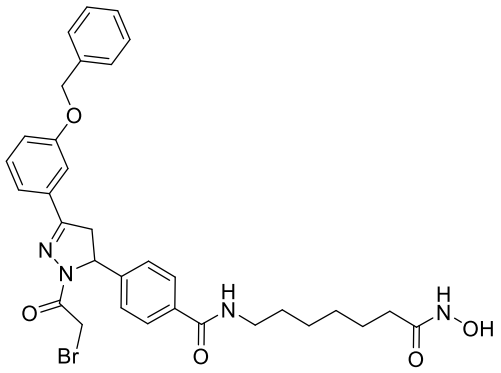

*4-(3-(3-(Benzyloxy)phenyl)-1-(2-bromoacetyl)-4,5-dihydro-1H-pyrazol-5-yl)-N-(7-(hydroxyamino)-7-oxoheptyl)benzamide (**SZ-3**)*

To a solution of compound **14** (71 mg, 0.081 mmol) in DCM (3 mL) was added triisopropylsilane (0.3 mL) and, after stirring for 10 min, TFA (0.6 mL) was added. The mixture was stirred at room temperature for 2 h and the complete deprotection was monitored by HPLC. Subsequently, the solvent was removed *in vacuo* and the crude was purified by preparative HPLC to yield **SZ-3** (9 mg, 18%). **^{1}H NMR** (600 MHz, DMSO-d_6) δ 10.30 (s, 1H), 8.62 (s, 1H), 8.38 (t, *J* = 5.6 Hz, 1H), 7.79 (d, *J* = 8.3 Hz, 2H), 7.49 – 7.43 (m, 3H), 7.42 – 7.37 (m, 4H), 7.33 (dd, *J* = 8.3, 6.3 Hz, 1H), 7.29 (d, *J* = 8.3 Hz, 2H), 7.18 – 7.13 (m, 1H), 5.62 (dd, *J* = 11.8, 4.8 Hz, 1H), 5.17 (s, 2H), 4.53 (d, *J* = 11.1 Hz, 1H), 4.41 (d, *J* = 11.1 Hz, 1H), 3.90 (dd, *J* = 18.2, 11.8 Hz, 1H), 3.24 – 3.22 (m, 2H), 3.20 (d, *J* = 5.0 Hz, 1H), 1.93 (t, *J* = 7.4 Hz, 2H), 1.48 (h, *J* = 6.9 Hz, 4H), 1.31 – 1.23 (m, 4H). **^{13}C NMR** (151 MHz, DMSO-d_6) δ 169.1, 165.7, 163.4, 158.5, 155.4, 144.3, 136.8, 134.0, 131.9, 130.0, 128.4, 127.9, 127.8, 127.6, 125.3, 119.6, 117.3, 113.1, 69.4, 59.7, 42.4, 42.1, 40.1, 32.2, 29.0, 28.3, 26.1, 25.0. **HRMS (ESI)**: *m/z*

$[M+H]^+$ calcd. for $C_{32}H_{35}BrN_4O_5$ 635.1864, found: 635.1845.

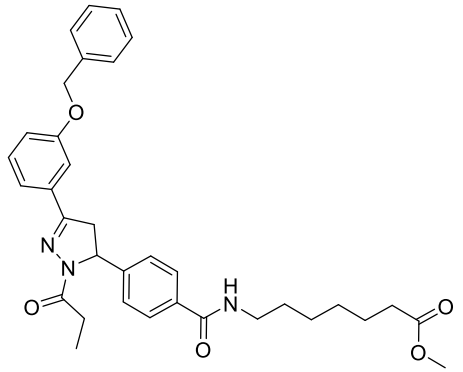

*Methyl 7-(4-(3-(3-(benzyloxy)phenyl)-1-propionyl-4,5-dihydro-1H-pyrazol-5-yl)benzamido)heptanoate (**S1**)*

To a solution of compound **10** (0.400 g, 0.652 mmol, 1 eq.) in DCM (10 mL) was added TFA (2 mL). The mixture was stirred for 2 h at room temperature and the complete removal of the Boc-protecting group was monitored by HPLC. TFA and DCM were removed and the crude product was dried *in vacuo*. Subsequently, the crude product was re-dissolved in DCM (10 mL) and stirred at 0 ℃ for 10 min, followed by the addition of propionyl chloride (114 μL, 1.30 mmol, 2 eq.) dropwise and triethylamine (272 μL, 1.96 mmol, 3 eq.) dropwise. The mixture was stirred for 17 h. The crude product was obtained by removing the solvents *in vacuo* and further purified by silica column chromatography (DCM/MeOH 50:1, *v/v*) to yield compound **S1** (0.219 g, 59%). **^{1}H NMR** (600 MHz, DMSO-d_6) δ 8.36 (t, J = 5.6 Hz, 1H), 7.78 (d, J = 8.0 Hz, 2H), 7.47 (d, J = 7.6 Hz, 2H), 7.40 (d, J = 7.4 Hz, 2H), 7.37 (d, J = 7.3 Hz, 2H), 7.34 (q, J = 8.0, 7.3 Hz, 1H), 7.24 (d, J = 8.0 Hz, 2H), 7.12 (d, J = 6.9 Hz, 1H), 5.57 (dd, J = 11.9, 4.8 Hz, 1H), 5.16 (s, 2H), 3.84 (dd, J = 18.1, 12.0 Hz, 1H), 3.57 (s, 3H), 3.22 (q, J = 6.6 Hz, 2H), 3.14 (dd, J = 18.1, 4.8 Hz, 1H), 2.74 (ddp, J = 23.4, 15.4, 7.5 Hz, 2H), 2.28 (t, J = 7.4 Hz, 2H), 1.50 (dt, J = 14.6, 7.1 Hz, 4H), 1.28 (s, 4H), 1.06 (t, J = 7.5 Hz, 3H). **^{13}C NMR** (151 MHz, DMSO-d_6) δ 173.3, 170.8, 165.8, 158.5, 153.8, 145.2, 136.9, 133.8, 132.4, 129.9, 128.4, 127.9, 127.7, 127.5, 125.3, 119.2, 116.8, 112.8, 69.3, 59.3, 51.1, 41.8, 40.1, 33.2, 28.9, 28.1, 26.8, 26.1, 24.3, 9.0. **LC-MS (ESI)**, $[M+H]^+$ *m/z*: 570.8.

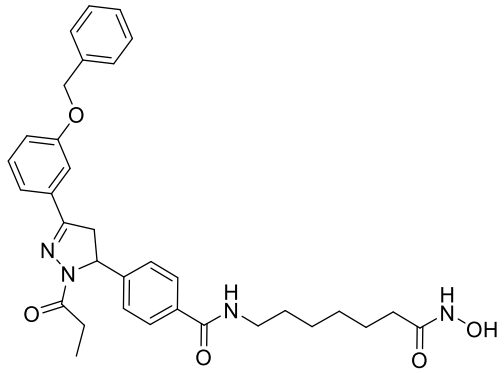

*4-(3-(3-(Benzyloxy)phenyl)-1-propionyl-4,5-dihydro-1H-pyrazol-5-yl)-N-(7-(hydroxyamino)-7-oxoheptyl)benzamide (**SZ-2-N**)*

Compound **S2** (0.100 g, 0.176 mmol, 1 eq.) was dissolved in a solvent mixture of MeOH/DCM (2 mL/2 mL) and the solution was cooled to 0 ℃. Hydroxylamine solution (699 μL, 50 wt. % in water, 11.4 mmol, 65 eq.) was added and the mixture was stirred at 0 ℃ for 10 min. Subsequently, the prepared sodium hydroxide powder (71 mg, 1.76 mmol, 10 eq.) was added into the reaction and the mixture was stirred for 2 h. Completion of the reaction was monitored by TLC. The solvent was removed and the crude product was dissolved in water and acidified with 0.5 M HCl (aq.) to neutral pH. The precipitate was then collected to yield compound **SZ-2-N** (79 mg, 79%). **^{1}H NMR** (600 MHz, DMSO-d_6) δ 10.31 (s, 1H), 10.21 (s, 1H), 8.62 (s, 1H), 8.37 (t, J = 5.5 Hz, 1H), 7.78 (d, J = 8.2 Hz, 2H), 7.46 (d, J = 7.3 Hz, 2H), 7.40 (d, J = 7.3 Hz, 2H), 7.37 (d, J = 7.2 Hz, 2H), 7.33 (t, J = 7.3 Hz, 1H), 7.24 (d, J = 8.3 Hz, 2H), 7.12 (dt, J = 7.1, 2.3 Hz, 1H), 5.57 (dd, J = 11.9, 4.8 Hz, 1H), 5.16 (s, 2H), 3.84 (dd, J = 18.1, 12.0 Hz, 1H), 3.22 (q, J = 6.6 Hz, 2H), 3.14 (dd, J = 18.1, 4.9 Hz, 1H), 2.74 (ddp, J = 23.4, 15.4, 7.5 Hz, 2H), 1.93 (t, J = 7.4 Hz, 2H), 1.48 (dt, J = 13.7, 6.7 Hz, 4H), 1.25 (dd, J = 12.1, 6.2 Hz, 4H), 1.06 (t, J = 7.5 Hz, 3H). **^{13}C NMR** (151 MHz, DMSO-d_6) δ 170.8, 169.1, 165.8, 158.5, 153.8, 145.2, 136.8, 133.8, 132.4, 129.9, 128.4, 127.9, 127.7, 127.5, 125.3, 119.2, 116.8, 112.8, 69.3, 59.4, 41.8, 40.1, 32.2, 29.0, 28.3, 26.8, 26.1, 25.0, 9.0. **HRMS (ESI)**: *m/z* $[M+H]^+$ calcd. for $C_{33}H_{38}N_4O_5$ 571.2915, found: 571.2938.

3.3. ^{1}H, ^{13}C NMR, HR-MS and HPLC data of SZ-1, SZ-2, SZ-3, SZ-2-N, F16 and G26

^{1}H NMR spectrum of **SZ-1** (600 MHz, DMSO-d_6)

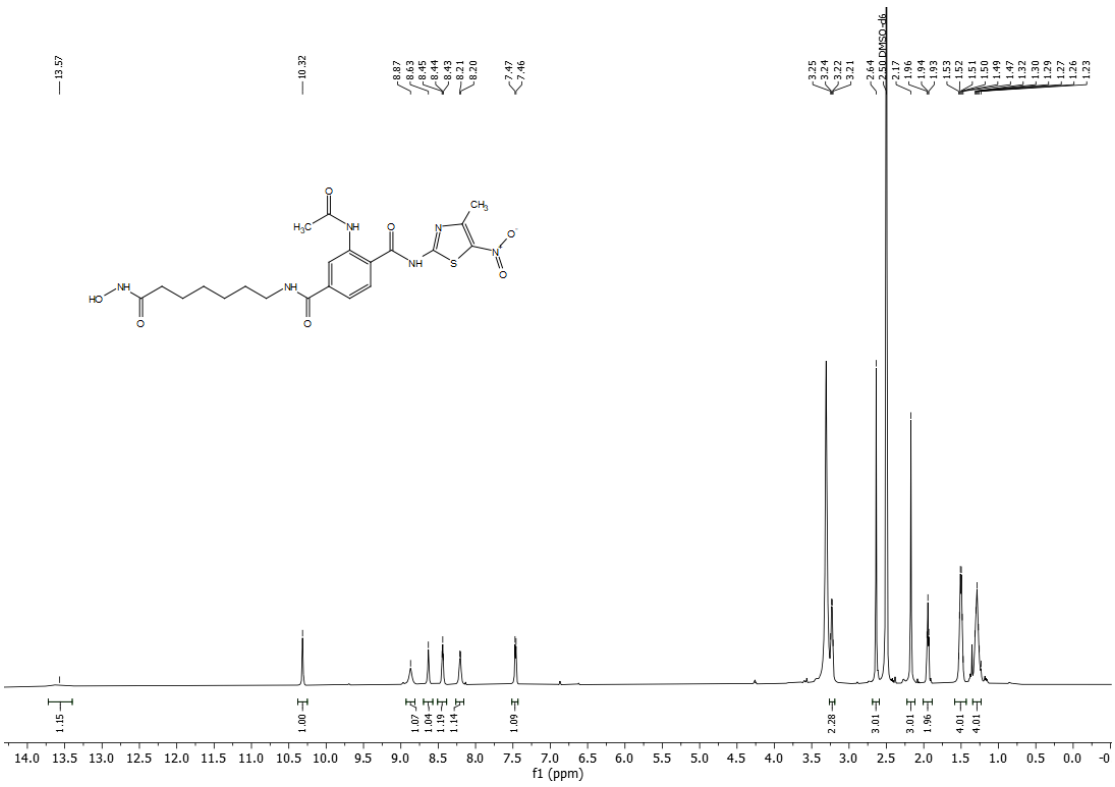

^{13}C NMR spectrum of **SZ-1** (151 MHz, DMSO-d_6)

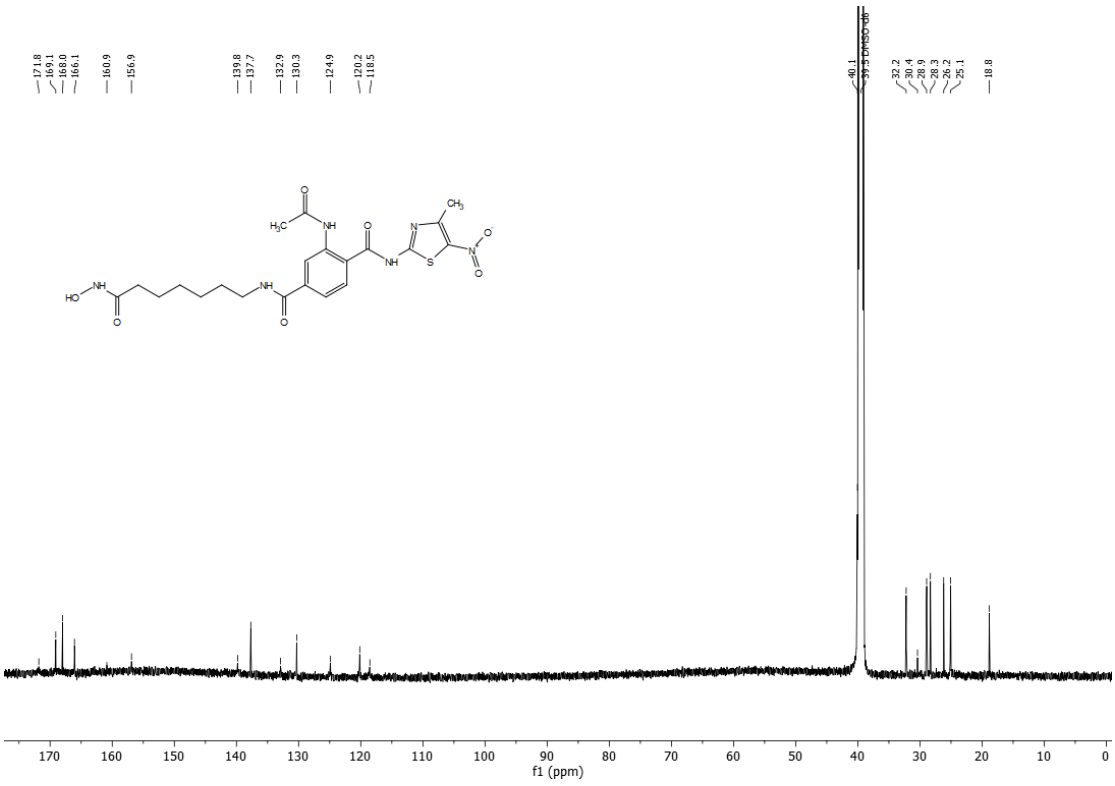

HR-MS spectrum of **SZ-1**

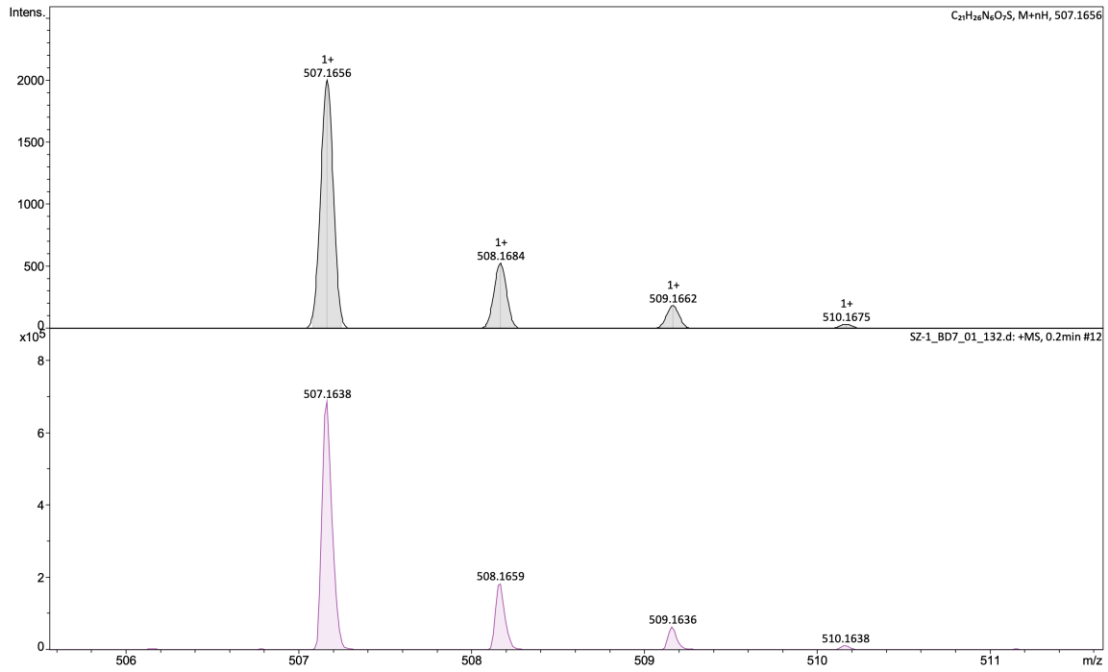

HPLC chromatogram of **SZ-1** (Purity: 97.9%)

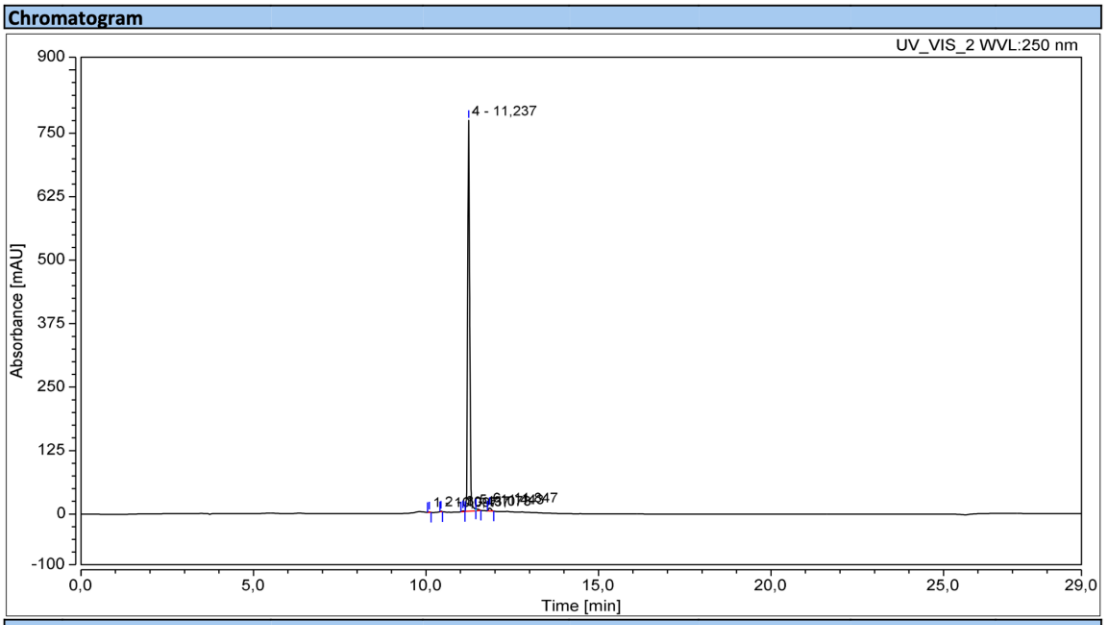

Integration Results

No.	Peak Name	Retention Time min	Area mAU*min	Height mAU	Relative Area %	Relative Height %	Amount n.a.
1		10,097	0,055	1,085	0,11	0,14	n.a.
2		10,437	0,052	1,367	0,10	0,17	n.a.
3		11,073	0,130	2,190	0,26	0,28	n.a.
4		11,237	49,655	770,096	97,87	98,06	n.a.
5		11,443	0,322	3,429	0,64	0,44	n.a.
6		11,847	0,520	7,190	1,02	0,92	n.a.
Total:			**50,735**	**785,356**	**100,00**	**100,00**	

^{1}H NMR spectrum of **SZ-2** (600 MHz, DMSO-d_6)

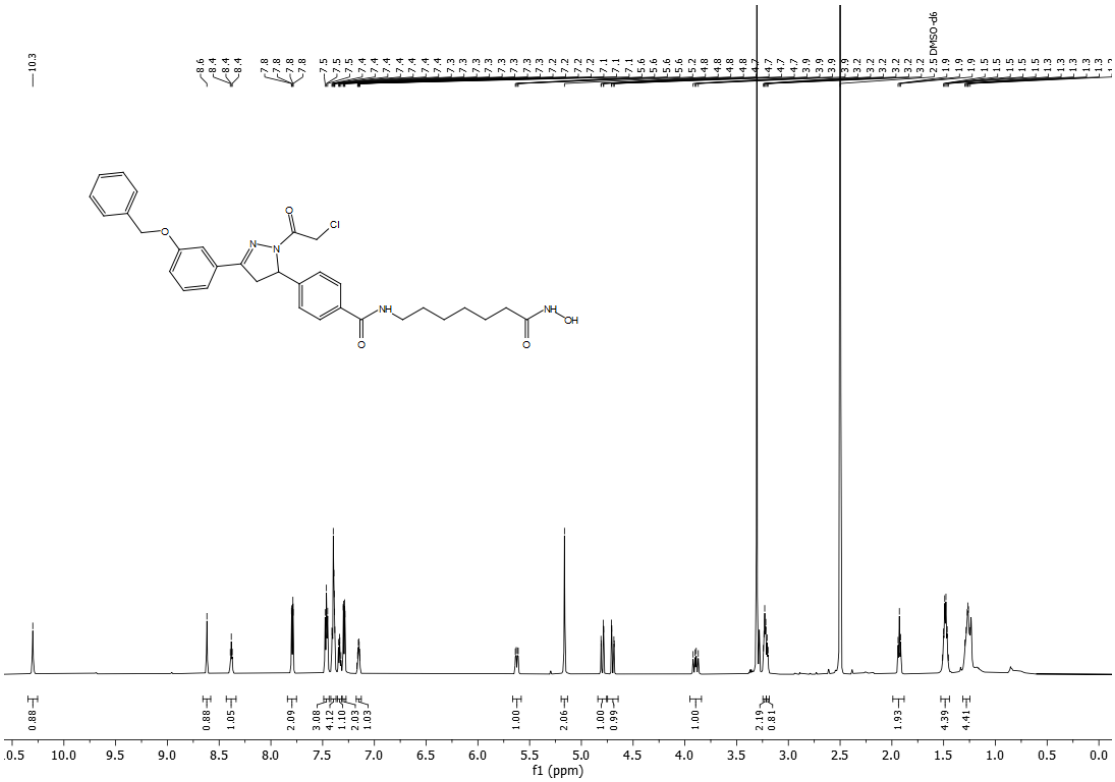

^{13}C NMR spectrum of **SZ-2** (151 MHz, DMSO-d_6)

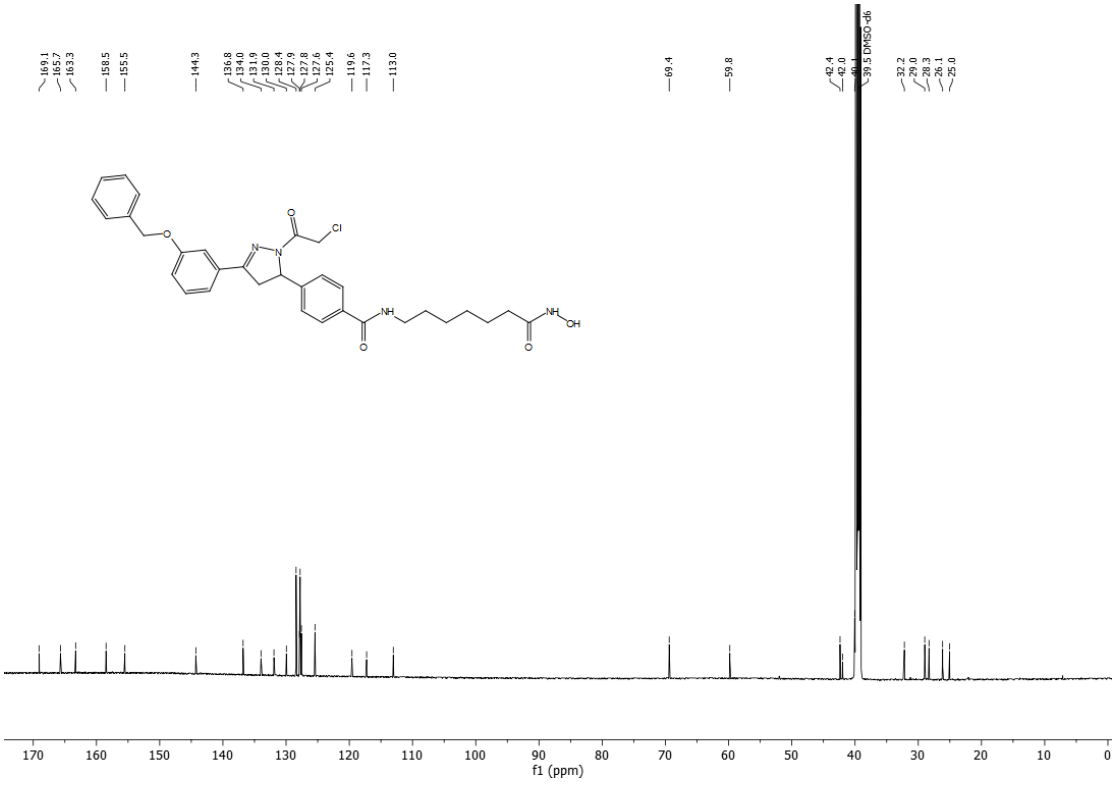

HR-MS spectrum of **SZ-2**

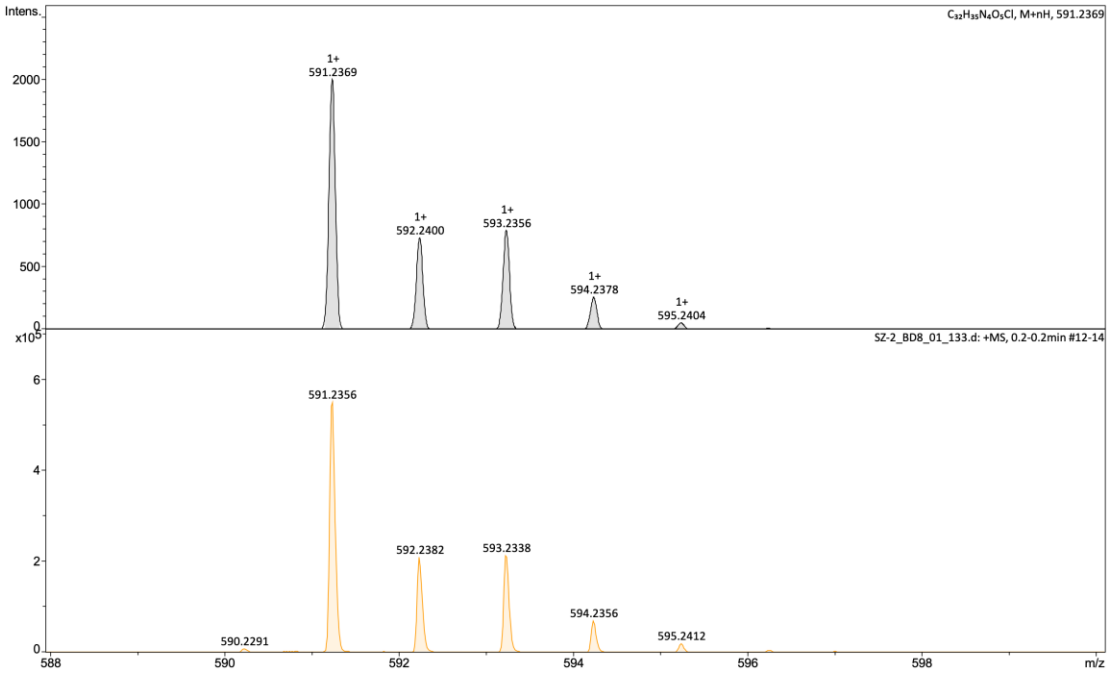

HPLC chromatogram of **SZ-2** (Purity: 98.3%)

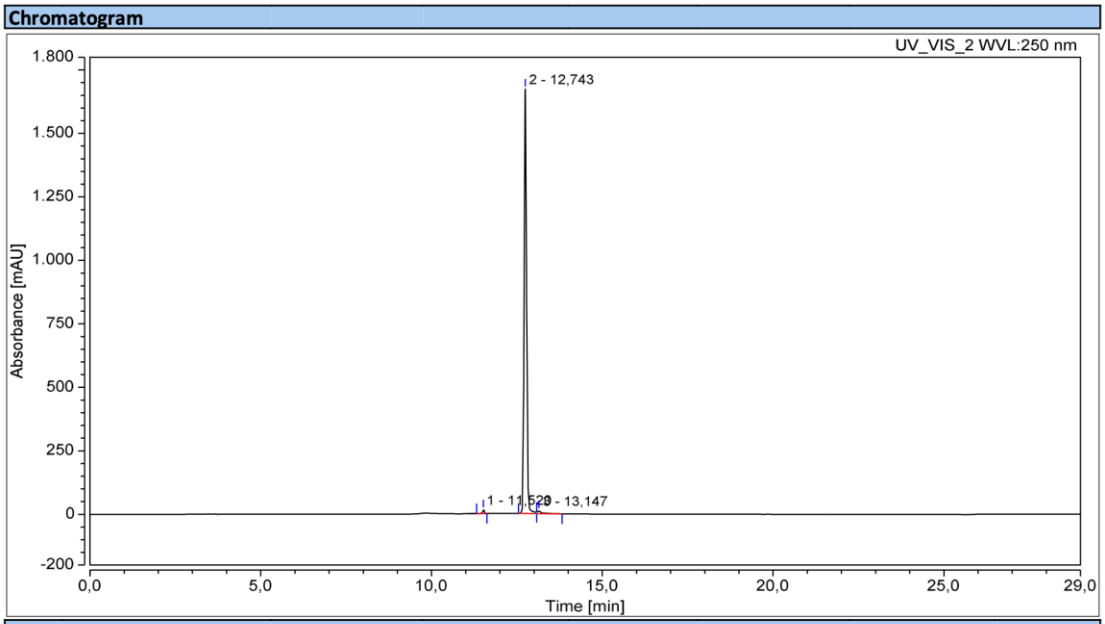

Integration Results

No.	Peak Name	Retention Time min	Area mAU*min	Height mAU	Relative Area %	Relative Height %	Amount n.a.
1		11,520	0,851	14,905	0,60	0,88	n.a.
2		12,743	138,554	1670,998	98,27	98,45	n.a.
3		13,147	1,581	11,358	1,12	0,67	n.a.
Total:			**140,986**	**1697,261**	**100,00**	**100,00**	

^{1}H NMR spectrum of **SZ-3** (600 MHz, DMSO-d_6)

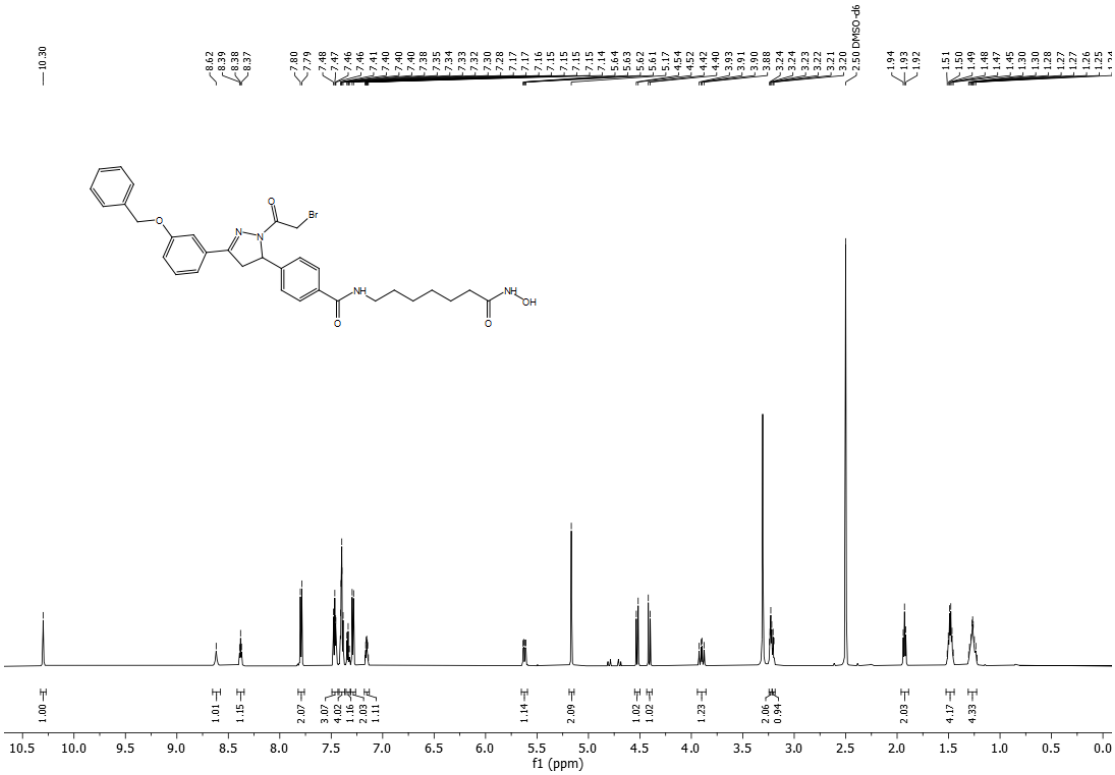

^{13}C NMR spectrum of **SZ-3** (151 MHz, DMSO-d_6)

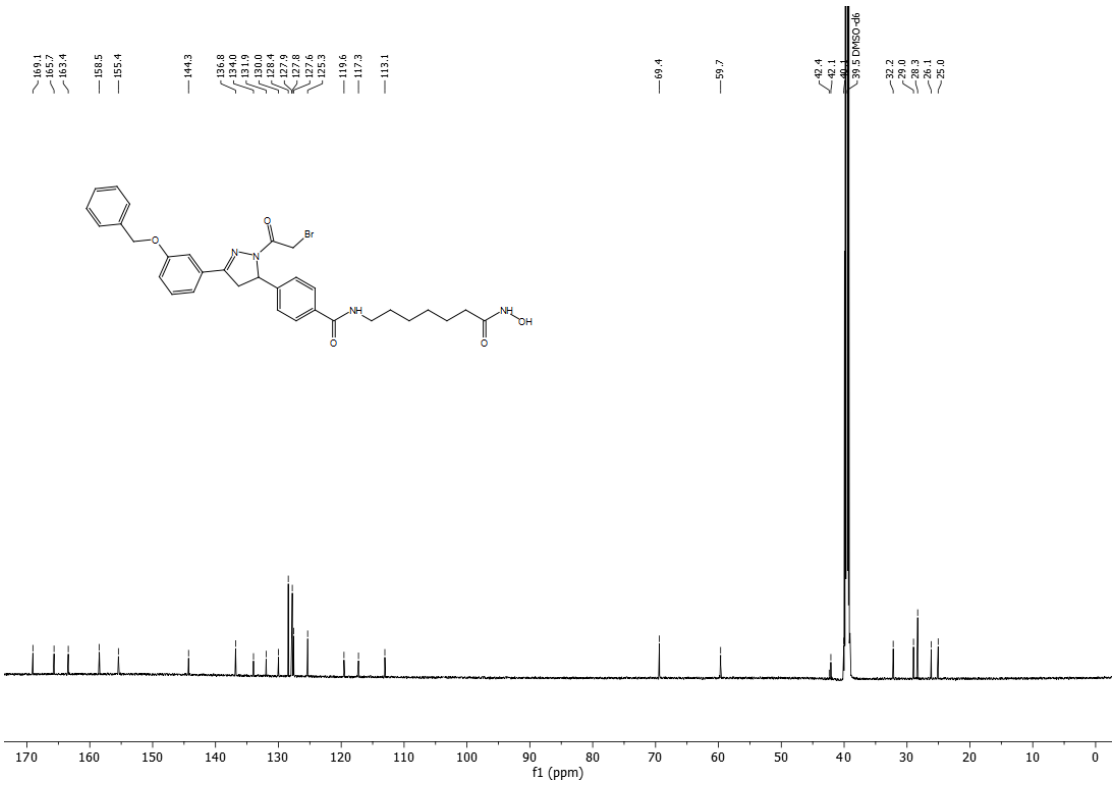

HR-MS spectrum of **SZ-3**

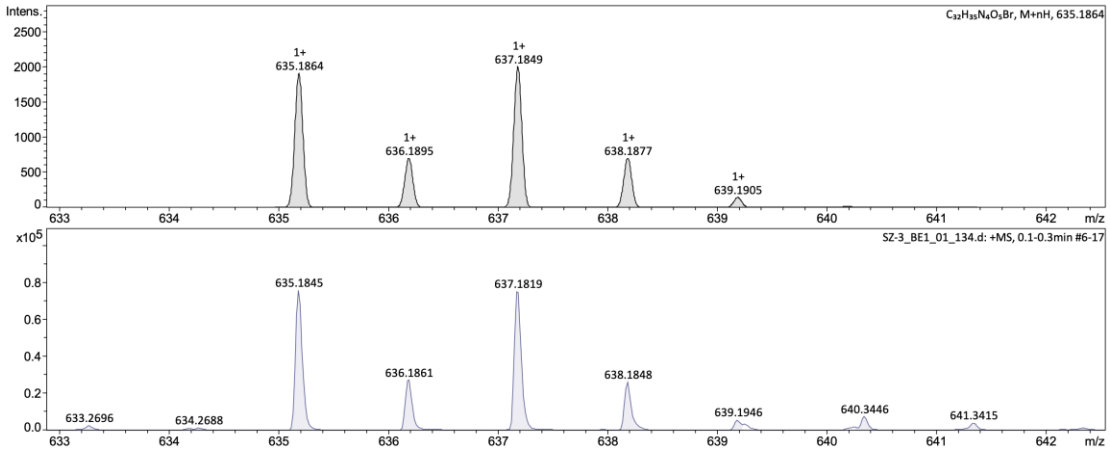

HPLC chromatogram of **SZ-3** (Purity: 95.8%)

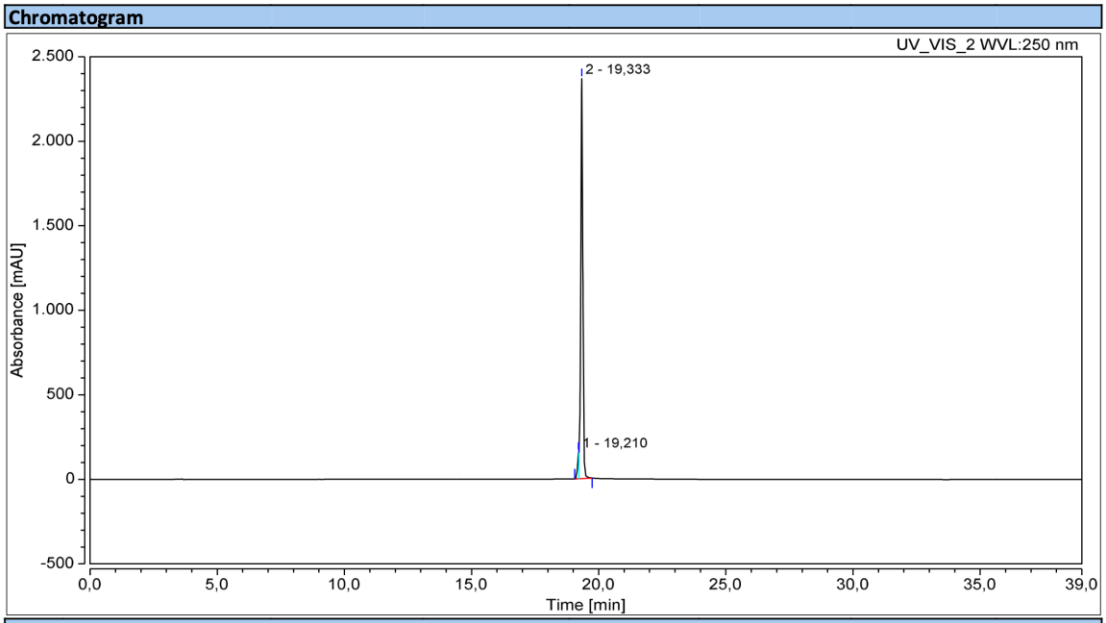

Integration Results

No.	Peak Name	Retention Time min	Area mAU*min	Height mAU	Relative Area %	Relative Height %	Amount n.a.
1		19,210	10,043	156,242	4,18	6,20	n.a.
2		19,333	230,044	2365,817	95,82	93,80	n.a.
Total:			**240,087**	**2522,060**	**100,00**	**100,00**	

^{1}H NMR spectrum of **SZ-2-N** (600 MHz, DMSO-d_6)

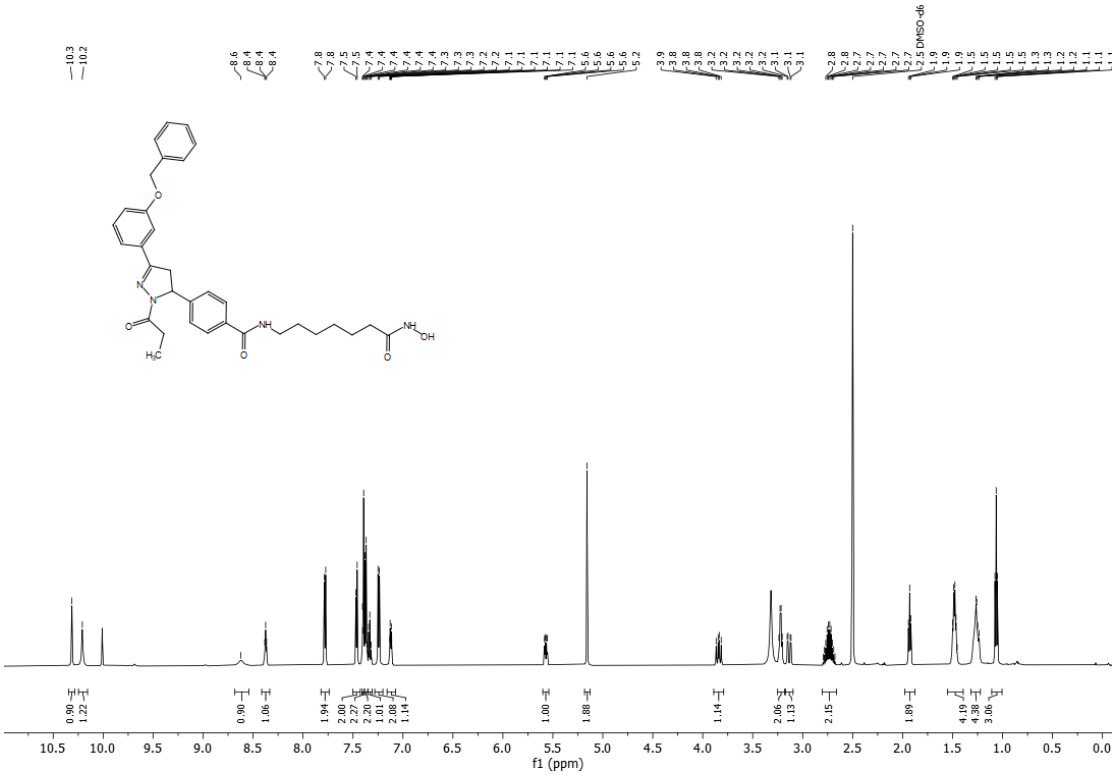

^{13}C NMR spectrum of **SZ-2-N** (151 MHz, DMSO-d_6)

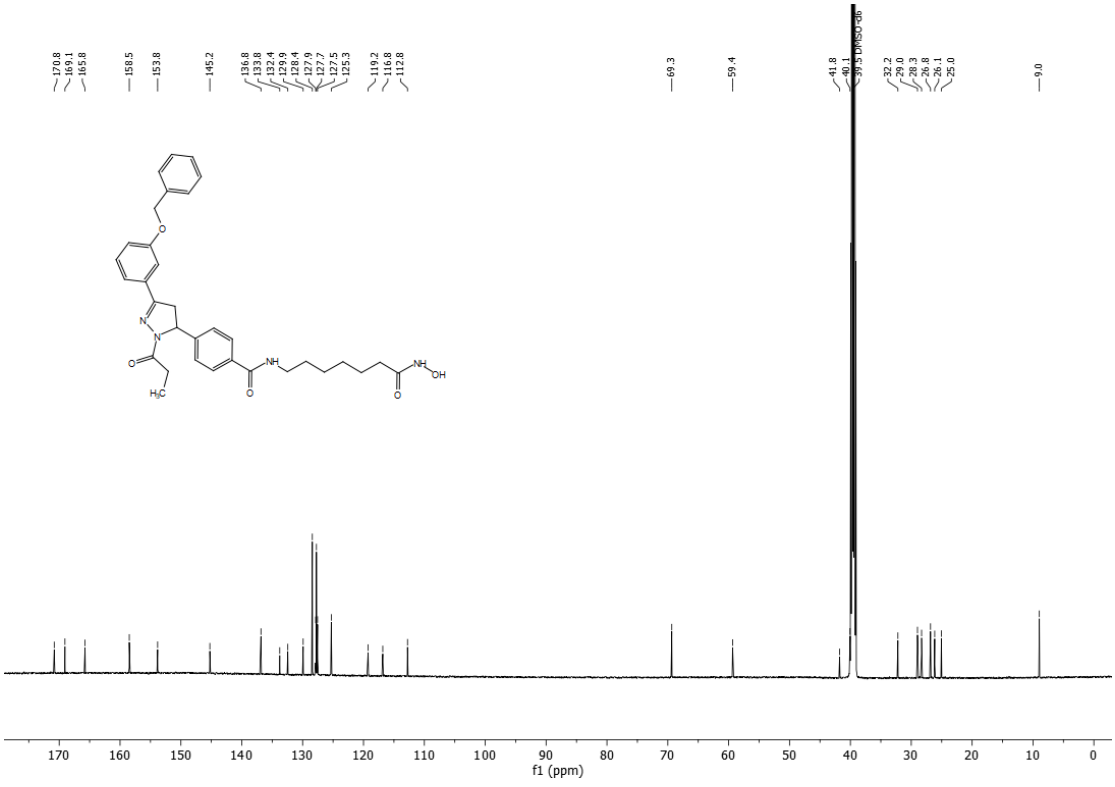

HR-MS spectrum of **SZ-2-N**

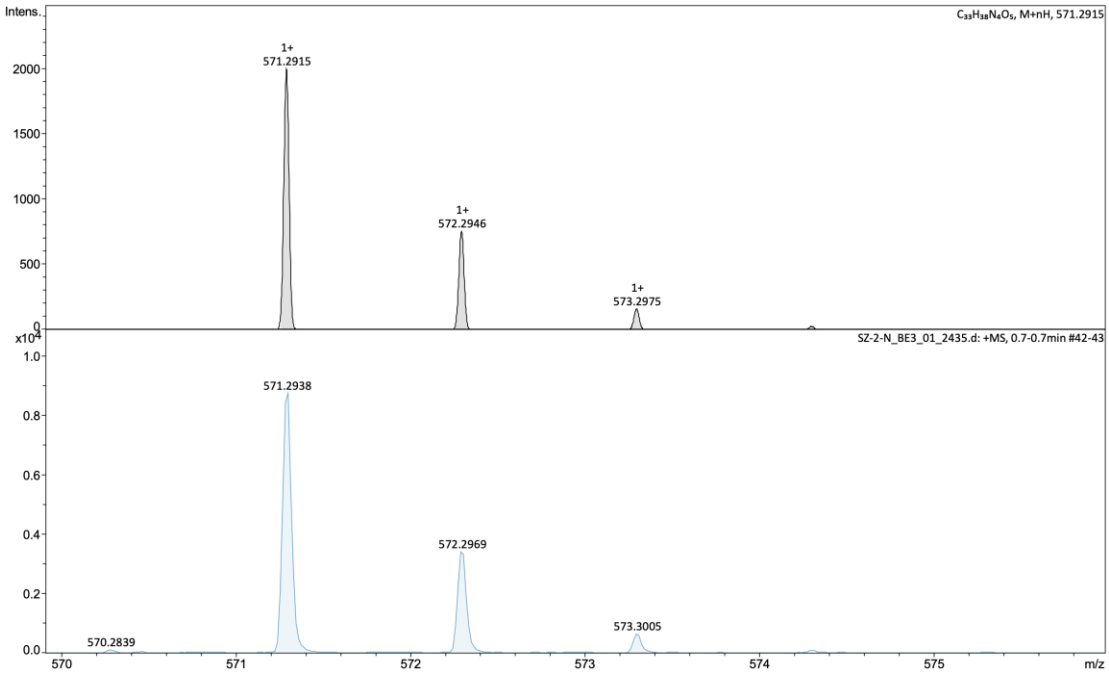

HPLC chromatogram of **SZ-2-N** (Purity: 95.3%)

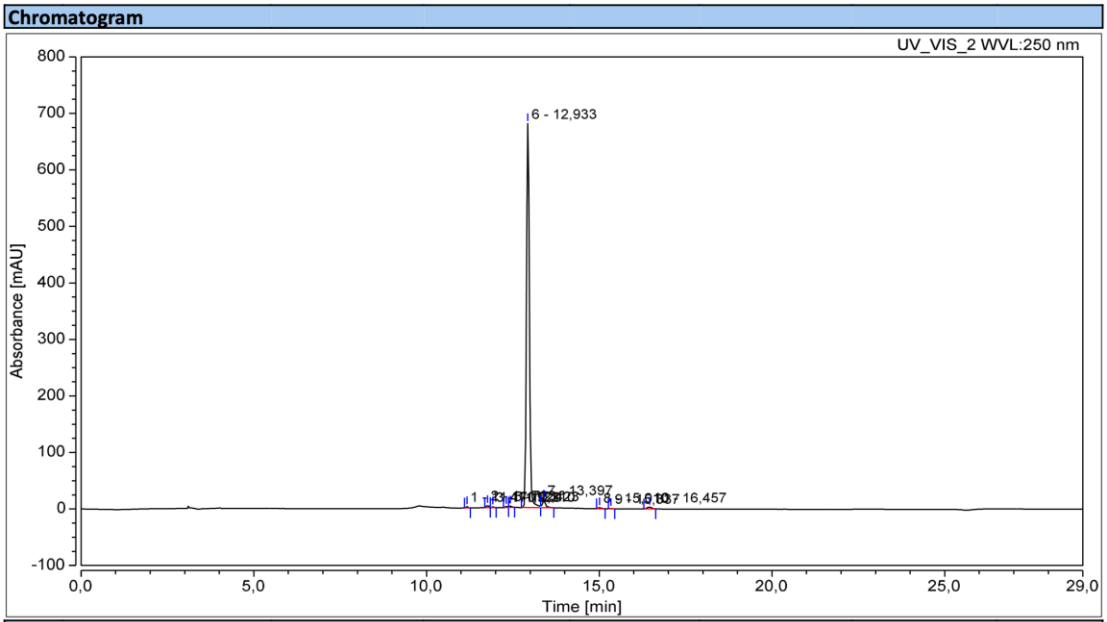

Integration Results

No.	Peak Name	Retention Time min	Area mAU*min	Height mAU	Relative Area %	Relative Height %	Amount n.a.
1		11,170	0,162	2,368	0,24	0,33	n.a.
2		11,763	0,336	4,249	0,49	0,60	n.a.
3		11,920	0,117	1,438	0,17	0,20	n.a.
4		12,310	0,157	1,836	0,23	0,26	n.a.
5		12,423	0,240	2,727	0,35	0,38	n.a.
6		12,933	64,637	679,410	95,32	95,58	n.a.
7		13,397	1,442	13,508	2,13	1,90	n.a.
8		15,010	0,187	1,880	0,28	0,26	n.a.
9		15,337	0,042	0,455	0,06	0,06	n.a.
10		16,457	0,488	2,951	0,72	0,42	n.a.
Total:			**67,808**	**710,823**	**100,00**	**100,00**	

^{1}H NMR spectrum of **F16** (600 MHz, DMSO-d_6)

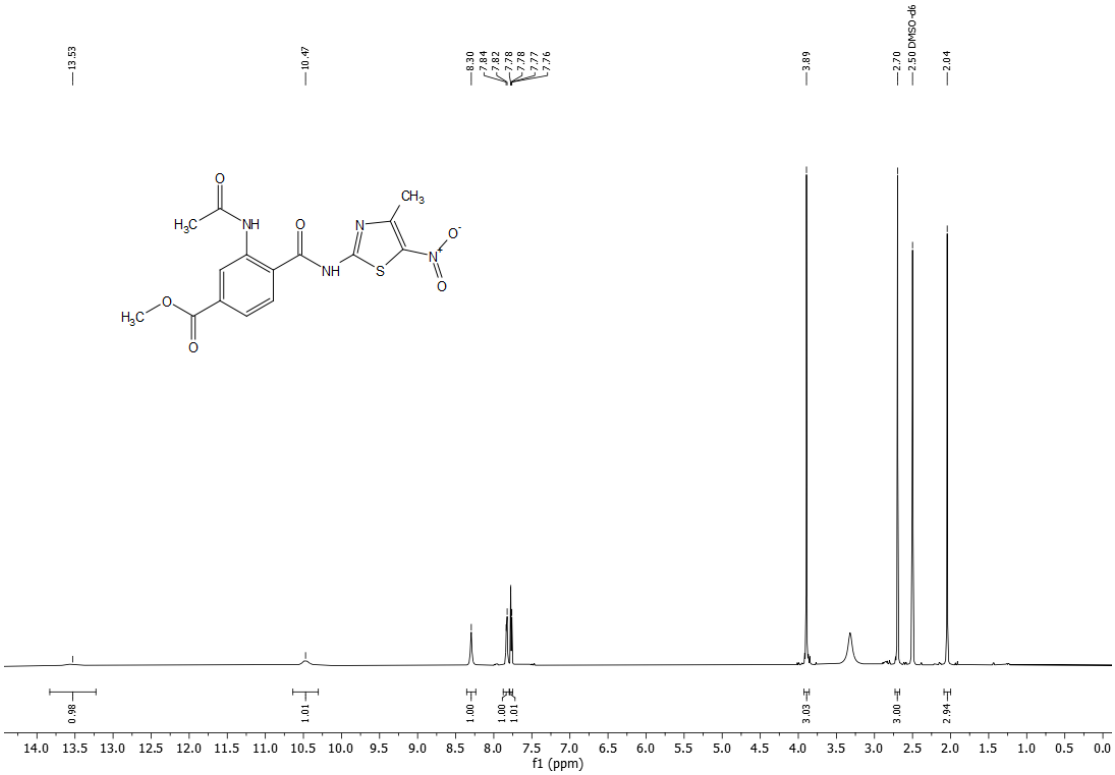

^{13}C NMR spectrum of **F16** (151 MHz, DMSO-d_6)

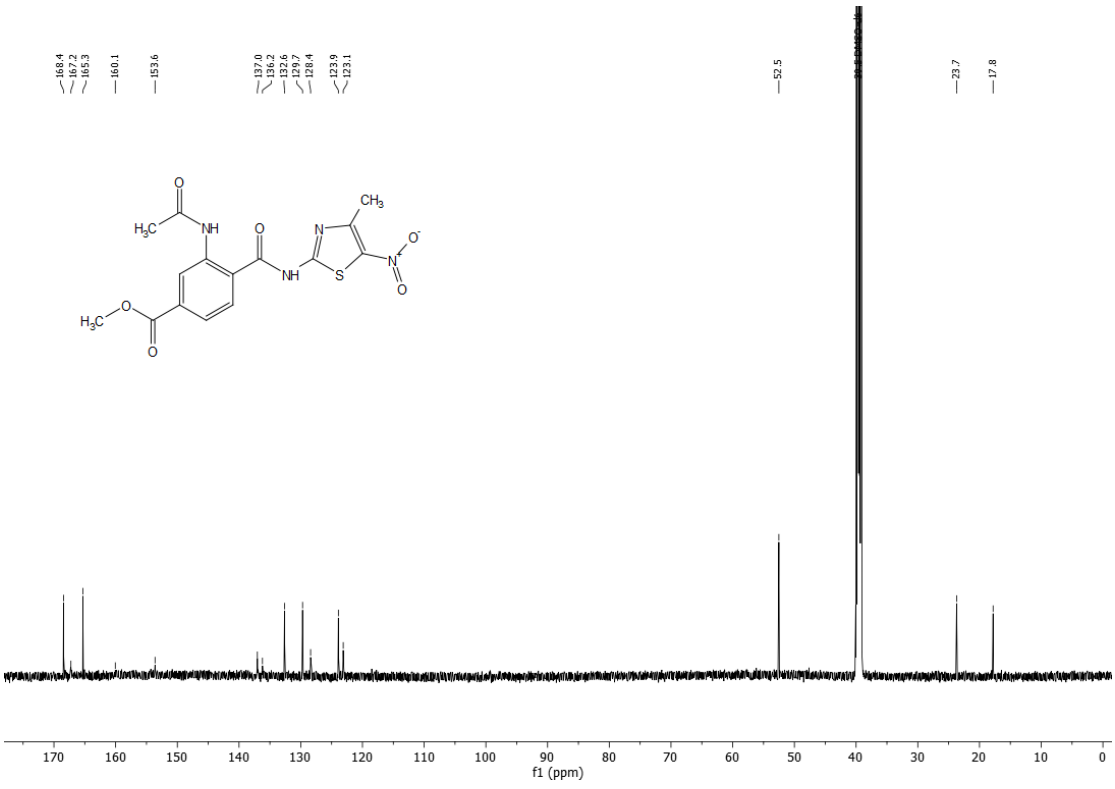

HR-MS spectrum of **F16**

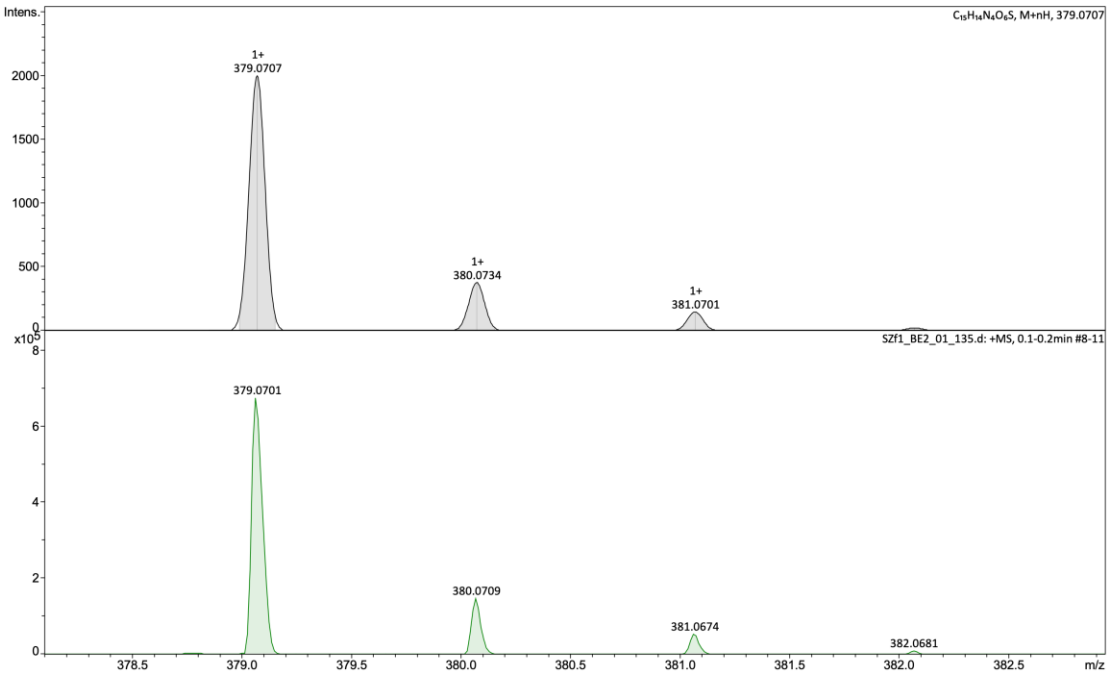

HPLC chromatogram of **F16** (Purity: 98.9%)

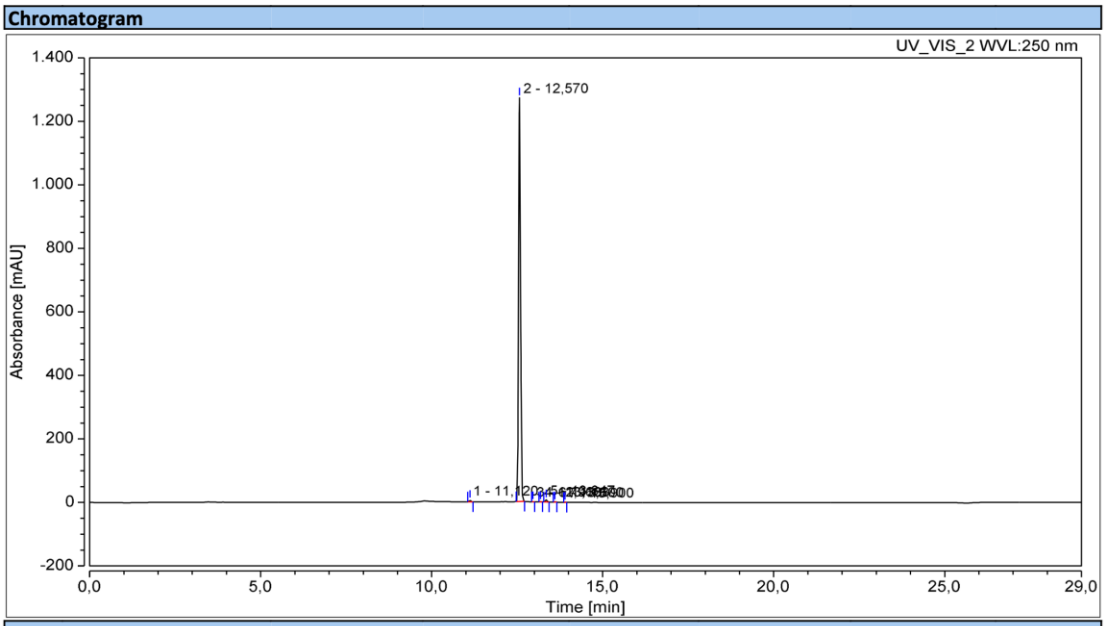

Integration Results

No.	Peak Name	Retention Time min	Area mAU*min	Height mAU	Relative Area %	Relative Height %	Amount n.a.
1		11,120	0,285	5,350	0,33	0,42	n.a.
2		12,570	85,094	1271,392	98,93	98,83	n.a.
3		12,960	0,028	0,542	0,03	0,04	n.a.
4		13,183	0,060	1,137	0,07	0,09	n.a.
5		13,347	0,460	6,510	0,53	0,51	n.a.
6		13,600	0,063	1,120	0,07	0,09	n.a.
7		13,900	0,021	0,407	0,02	0,03	n.a.
Total:			**86,012**	**1286,458**	**100,00**	**100,00**	

^{1}H NMR spectrum of **G26** (500 MHz, DMSO-d_6)

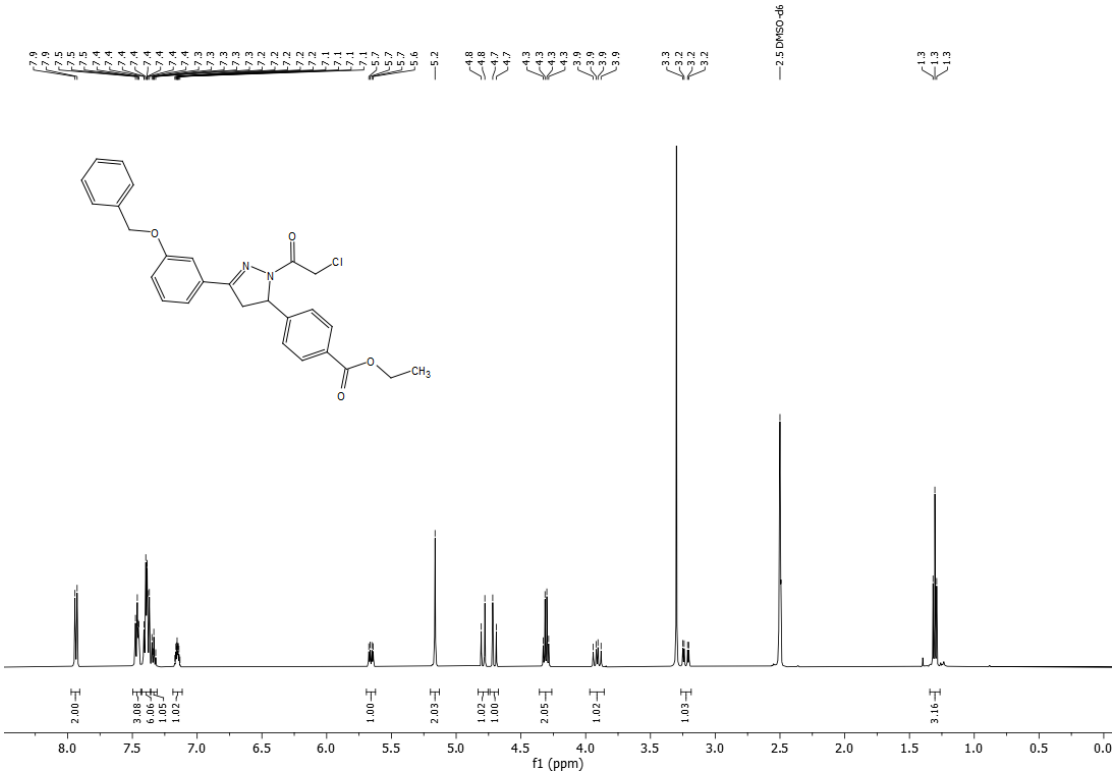

^{13}C NMR spectrum of **G26** (126 MHz, DMSO-d_6)

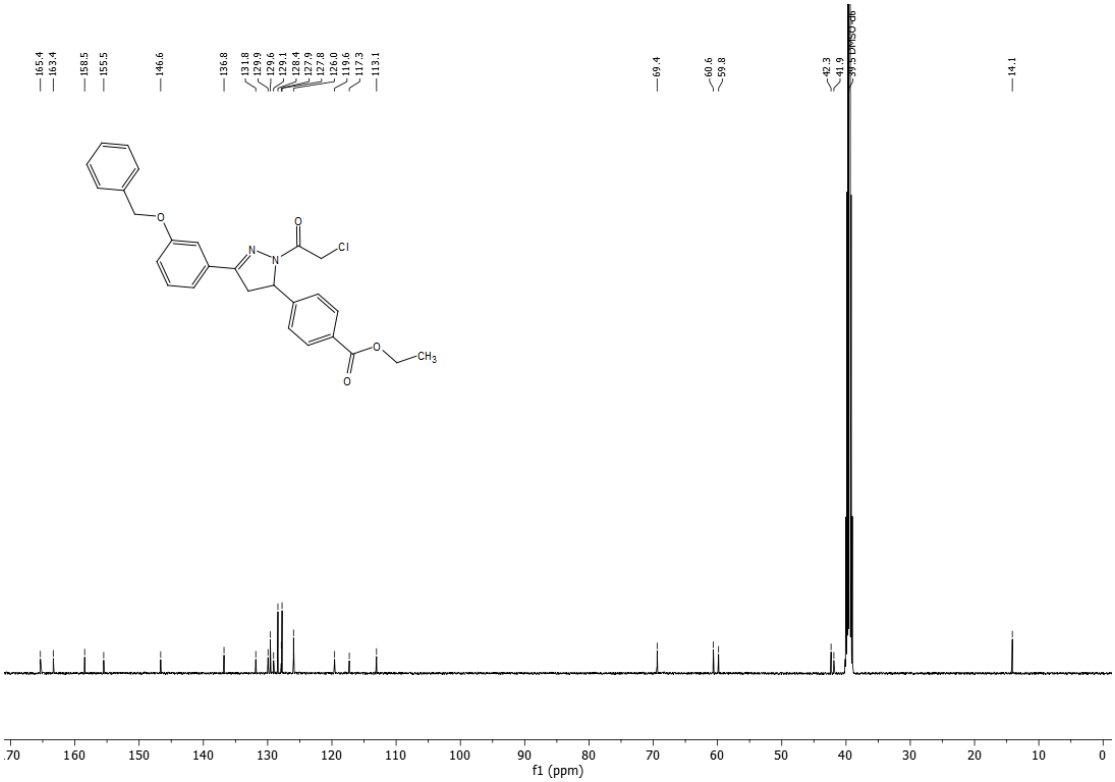

HR-MS spectrum of **G26**

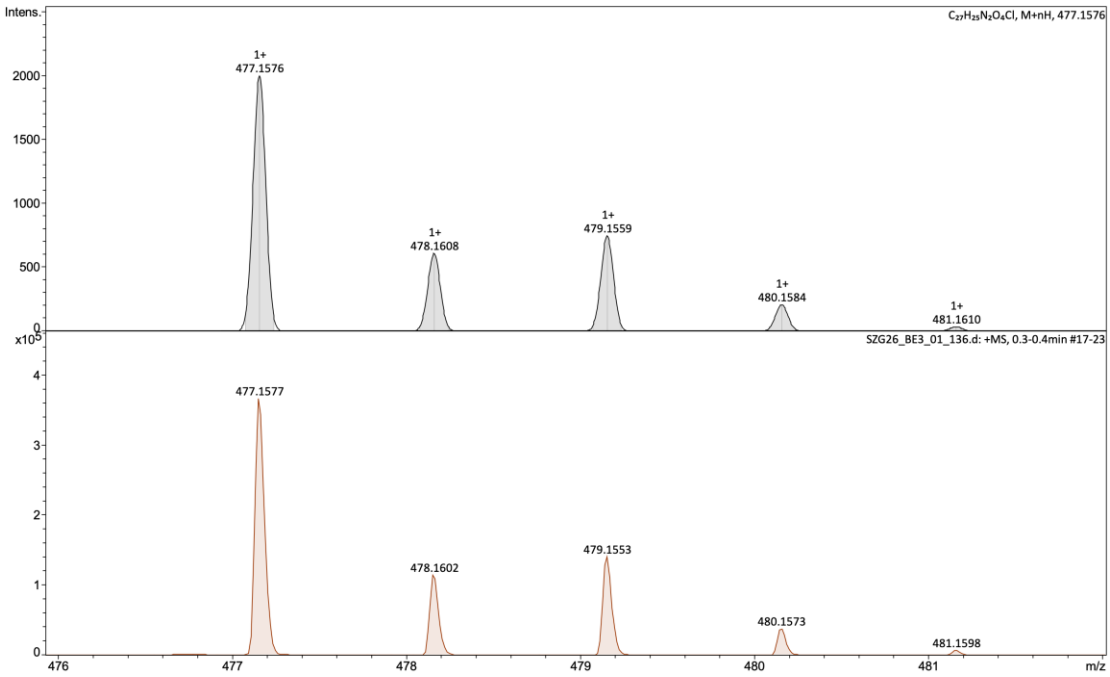

HPLC chromatogram of **G26** (Purity: 98.0%)

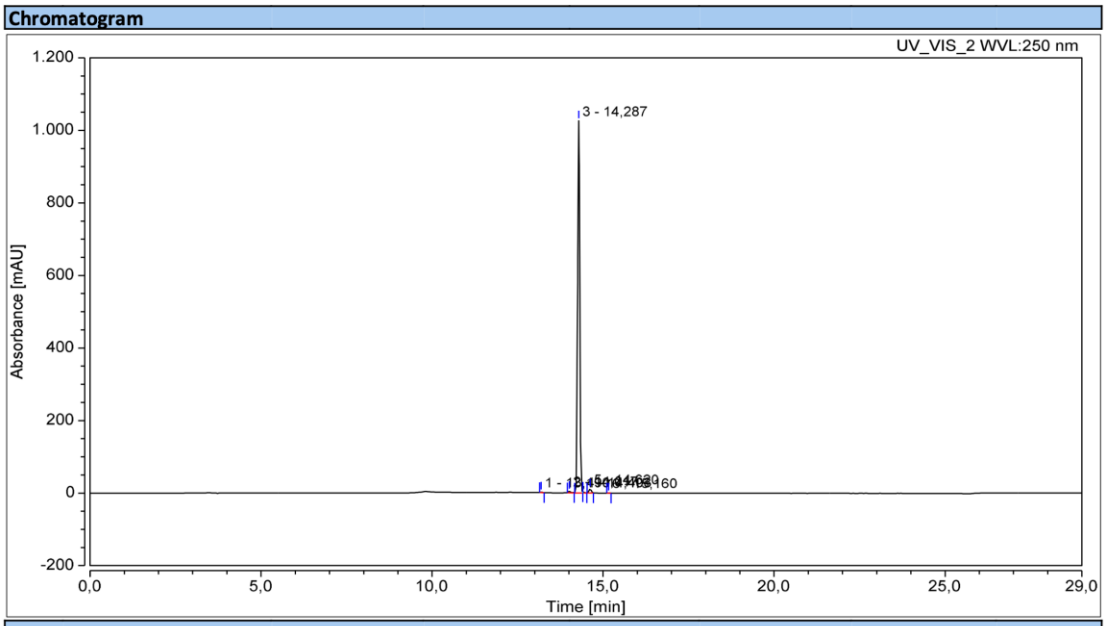

Integration Results

No.	Peak Name	Retention Time min	Area mAU*min	Height mAU	Relative Area %	Relative Height %	Amount n.a.
1		13,190	0,077	1,363	0,11	0,13	n.a.
2		14,017	0,358	4,786	0,49	0,46	n.a.
3		14,287	71,676	1025,786	98,01	98,11	n.a.
4		14,403	0,122	2,307	0,17	0,22	n.a.
5		14,620	0,864	10,875	1,18	1,04	n.a.
6		15,160	0,033	0,476	0,05	0,05	n.a.
Total:			**73,130**	**1045,593**	**100,00**	**100,00**	

4. Immunoblot replicates

Replicates for Figure 2A

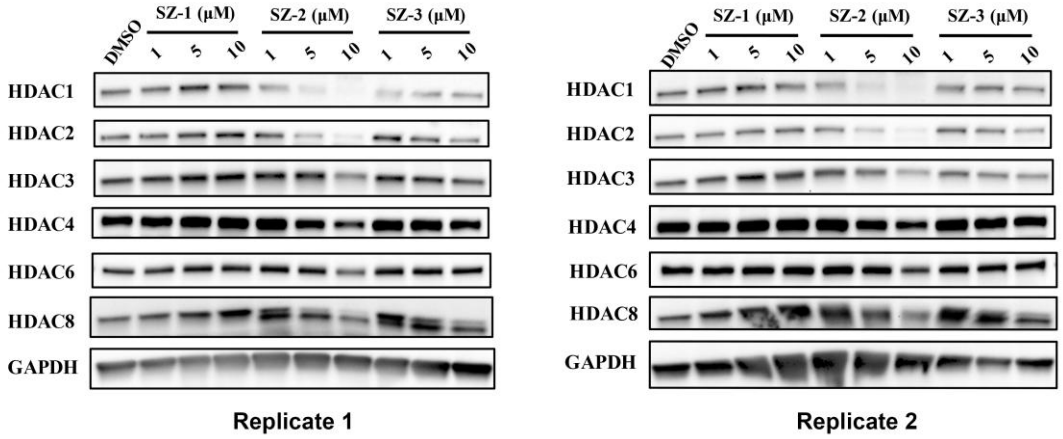

5. References

(1) Kraft, F. B.; Hanl, M.; Feller, F.; Schäker-Hübner, L.; Hansen, F. K. Photocaged Histone Deacetylase Inhibitors as Prodrugs in Targeted Cancer Therapy. *Pharmaceuticals (Basel)* **2023**, *16* (3).

(2) Reßing, N.; Schliehe-Diecks, J.; Watson, P. R.; Sönnichsen, M.; Cragin, A. D.; Scholer, A.; Yang, J.; Schäker-Hübner, L.; Borkhardt, A.; Christianson, D. W.; Bhatia, S.; Hansen, F. K. Development of Fluorinated Peptoid-Based Histone Deacetylase (HDAC) Inhibitors for Therapy-Resistant Acute Leukemia. *J. Med. Chem.* **2022**, *65* (22), 15457-15472.

(3) Kraft, F. B.; Enns, J.; Honin, I.; Engelhardt, J.; Schöler, A.; Smith, S. T.; Meiler, J.; Schäker-Hübner, L.; Weindl, G.; Hansen, F. K. Groebke Blackburn Bienayme-mediated multi-component synthesis of selective HDAC6 inhibitors with anti-inflammatory properties. *Bioorg. Chem.* **2024**, *143*, 107072.

(4) Schäker-Hübner, L.; Warstat, R.; Ahlert, H.; Mishra, P.; Kraft, F. B.; Schliehe-Diecks, J.; Schöler, A.; Borkhardt, A.; Breit, B.; Bhatia, S.; Hügle, M.; Gunther, S.; Hansen, F. K. 4-Acyl Pyrrole Capped HDAC Inhibitors: A New Scaffold for Hybrid Inhibitors of BET Proteins and Histone Deacetylases as Antileukemia Drug Leads. *J. Med. Chem.* **2021**, *64* (19), 14620-14646.

(5) König, B.; Watson, P. R.; Reßing, N.; Cragin, A. D.; Schäker-Hübner, L.; Christianson, D. W.; Hansen, F. K. Difluoromethyl-1,3,4-oxadiazoles Are Selective, Mechanism-Based, and Essentially Irreversible Inhibitors of Histone Deacetylase 6. *J. Med. Chem.* **2023**, *66* (19),

13821-13837.

(6) Ghosh, P.; Schmitz, M.; Pandurangan, T.; Zeleke, S. T.; Chan, S. C.; Mosior, J.; Sun, L.; Palve, V.; Grassie, D.; Anand, K.; Frydman, S.; Roush, W. R.; Schönbrunn, E.; Geyer, M.; Duckett, D.; Monastyrskyi, A. Discovery and design of molecular glue enhancers of CDK12-DDB1 interactions for targeted degradation of cyclin K. *RSC Chem. Biol.* **2024**, *6* (1), 36-55.

(7) Zhai, S.; Honin, I.; Schäker-Hübner, L.; Hanl, M.; Jacobi, L.; Dressler, F.; Pieńkowska, D. E.; König, P.; Gerhartz, J.; Voget, R.; Bendas, G.; Gütschow, M.; Meissner, F.; Burckhardt, B. B.; Nowak, R. P.; Steinebach, C.; Hansen, F. K. Development and Characterization of the First Selective Class IIb Histone Deacetylase Degraders. *J. Med. Chem.* **2025**, *68* (13), 13793-13821.

(8) Schäker-Hübner, L.; Haschemi, R.; Buch, T.; Kraft, F. B.; Brumme, B.; Schöler, A.; Jenke, R.; Meiler, J.; Aigner, A.; Bendas, G.; Hansen, F. K. Balancing Histone Deacetylase (HDAC) Inhibition and Drug-likeness: Biological and Physicochemical Evaluation of Class I Selective HDAC Inhibitors. *ChemMedChem* **2022**, *17* (9), e202100755.

(9) Sinatra, L.; Vogelmann, A.; Friedrich, F.; Tararina, M. A.; Neuwirt, E.; Colcerasa, A.; König, P.; Toy, L.; Yesiloglu, T. Z.; Hilscher, S.; Gaitzsch, L.; Papenkordt, N.; Zhai, S.; Zhang, L.; Romier, C.; Einsle, O.; Sippl, W.; Schutkowski, M.; Gross, O.; Bendas, G.; Christianson, D. W.; Hansen, F. K.; Jung, M.; Schiedel, M. Development of First-in-Class Dual Sirt2/HDAC6 Inhibitors as Molecular Tools for Dual Inhibition of Tubulin Deacetylation. *J. Med. Chem.* **2023**.

(10) Feller, F.; Hansen, F. K. Targeted Protein Degradation of Histone Deacetylases by Hydrophobically Tagged Inhibitors. *ACS Med. Chem. Lett.* **2023**, *14* (12), 1863-1868.

(11) Ursuegui, S.; Yougnia, R.; Moutin, S.; Burr, A.; Fossey, C.; Cailly, T.; Laayoun, A.; Laurent, A.; Fabis, F. A biotin-conjugated pyridine-based isatoic anhydride, a selective room temperature RNA-acylating agent for the nucleic acid separation. *Org. Biomol. Chem.* **2015**, *13* (12), 3625-3632.

Danksagung

As this thesis comes to an end, I reflect with deep appreciation on the past four years since I arrived in Germany in November 2021 to begin my PhD studies at the University of Bonn. This journey has been both challenging and rewarding, and it would not have been possible without the support of many people and institutions.

First and foremost, I would like to express my sincere and heartfelt gratitude to my supervisor, Prof. Dr. Finn K. Hansen, for his outstanding guidance throughout my doctoral studies. From shaping research questions and designing experiments to revising manuscripts, submissions, and responses to reviewers, his academic support has been invaluable. I am particularly grateful for his patience, encouragement, and attention to detail, which have greatly contributed to the quality of this dissertation. Beyond academic guidance, I also appreciate his genuine care and consideration in daily life, which provided constant encouragement throughout my PhD journey.

I would also like to sincerely thank my colleagues and group members for creating such a supportive and collaborative working environment. Their kindness and willingness to help greatly eased my transition to a new country and research setting. I am grateful for their assistance in experiments and discussions, as well as for the friendly atmosphere that made daily work enjoyable and motivating. My sincere thanks also go to the technical staff of the research group and the faculty, whose professional expertise and support were essential to the successful completion of my experimental work.

I gratefully acknowledge the financial support provided by the China Scholarship Council (CSC) and by my supervisor, which made my doctoral studies in Germany possible and allowed me to fully focus on my research and academic development.

Finally, I would like to express my heartfelt gratitude to my family and friends for their unwavering support, understanding, and encouragement throughout these years. Despite the physical distance, my family's unconditional love and trust have been a constant source of strength, while my friends' companionship and encouragement helped me maintain balance and positivity during my PhD journey.